



Q
57
P76
v. 57
1954
PER



Digitized by the Internet Archive
in 2024

KONINKLIJKE NEDERLANDSE AKADEMIE
VAN WETENSCHAPPEN

PROCEEDINGS OF THE
SECTION OF SCIENCES

VOLUME LVII

SERIES B
PHYSICAL SCIENCES

1954
NORTH-HOLLAND PUBLISHING COMPANY
(N.V. NOORD-HOLLANDSCHE UITGEVERS MAATSCHAPPIJ)
AMSTERDAM

The complete Proceedings consist of three Series, viz.:

SERIES A: MATHEMATICAL SCIENCES

SERIES B: PHYSICAL SCIENCES

SERIES C: BIOLOGICAL AND MEDICAL SCIENCES

Articles for these Series cannot be accepted unless formally communicated for publication by one of the members of the Royal Neth. Academy of Sciences.

CONTRIBUTIONS TO THE PROBLEM OF THE ASSOCIATION BETWEEN PROTEINS AND LIPIDS. VIA *)¹⁾

- a) *Further investigations on the coacervation of gelatin + K-oleate + salt at pH 9.2, using two gelatin preparations with different I.E.P. (9.2 and 5.7)*
- b) *The existence of two modes of binding of oleate to gelatin*

BY

H. G. BUNGENBERG DE JONG, C. R. VAN SOMEREN **) AND F. KLEIN ²⁾

(Communicated at the meeting of November 28, 1953)

1. Introduction

Two types of gelatin are known which can be made industrially from the parent protein collagen. These two types will be denoted in the following with A and B.

Type A: with an I.E.P. higher than 7; the charge is relatively small in the pH range from 6 to 9,

Type B: with a well-defined I.E.P. at the acid side of neutrality, as a rule in the neighbourhood of pH 5.

Gelatin preparations of type B were used throughout in the preceding publications of this series, e.g. in studying the coacervation of gelatin (I.E.P. 5.0) + oleate + K-tetraborate. The salt used serves a double function, namely, it provides for a sufficient K⁺-ion concentration and at the same time regulates the pH.

The present investigation concerns the analogous coacervation—always at pH 9.2—while the following gelatin preparations were used:

1. Pigskin-gelatin from unknown origin with an I.E.P. 9.2,
2. Gelatin 00000 from the "Lijm en Gelatinefabriek Delft" at Delft, Netherlands. This preparation also had an I.E.P. of 9.2,
3. A transformation product of Gelatin 00000, I.E.P. 5.7.

*) The term lipid is used here in a wide sense, including fatty acids and other long-chain electrolytes.

¹⁾ Part I appeared in these Proceedings, **45**, 601 (1942), the parts II (A, B, and C) III and IV in these Proceedings, Series **B 55**, 317, 329, 338, 347, 360 (1952) and Part V, *ibid.*, **56**, 203 (1953).

**) Aided by grants from the "Netherlands Organization for Pure Research (Z.W.O.)."

²⁾ Publication No. 24, of the Team for Fundamental Biochemical Research (under the direction of H. G. BUNGENBERG DE JONG, E. HAVINGA and H. L. BOOIJ).

The results will be compared with those obtained in Part III; for this purpose the mixing diagram of the results of Part III is reproduced in figure 1. According to data given in that publication, figure 2 has been drawn. It represents the mixing ratios at maximal coacervate volume as a function of the corresponding salt concentrations.

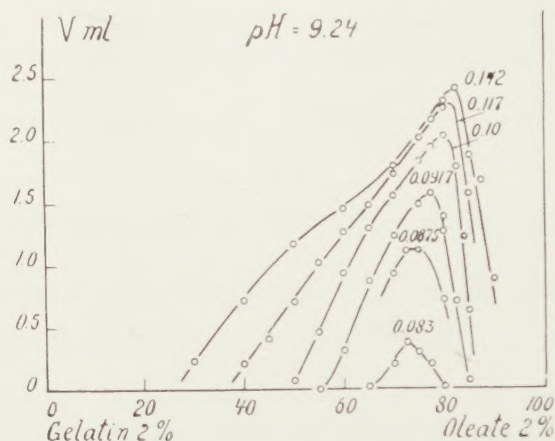


Fig. 1. The coacervate volume as a function of the mixing ratio of a gelatin solution (1.7 g dry gelatin/100 ml) and an oleate solution (65.8 millimoles/l). The concentrations of the K-tetraborate are given in moles/l.

I.E.P. of the gelatin is 5.0.

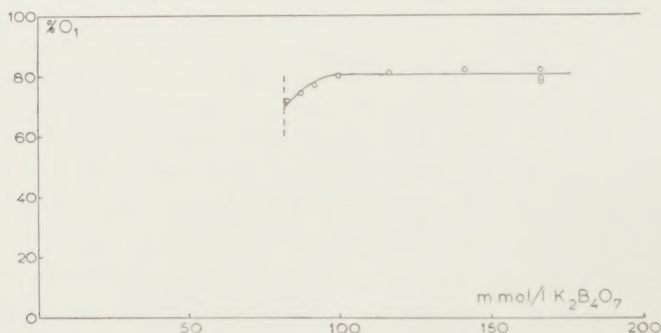


Fig. 2. Mixing ratios which correspond to the maxima in Fig. 1 and of other coacervate volume curves, not represented in Fig. 1. O_1 is the same oleate solution as denoted in Fig. 1 by Oleate 2 %.

2. Materials and methods

Potassium oleate was prepared from Oelsäure reinst, E. MERCK, Darmstadt, a stock solution of 0.1 mole/l being made by dissolving the required amount of oleic acid in the equivalent amount of KOH.

The iso-electric points of the above mentioned gelatin preparations and of the gelatin used in Part III were determined by micro-electrophoresis ³⁾ (Figs. 3 and 4 and in section 7, fig. 12).

³⁾ The electrophoretic measurements were carried out by means of a modified Northrop apparatus. Suspended SiO_2 particles served as an "electrophoretic indicator"

Both the pigskin gelatin and the gelatin 00000 proved to be fit for our experiments as a 2 % solution showed no calcium reaction with ammoniumoxalate ⁴⁾.

The stock solutions of the gelatin preparations were made in the usual way (30 min. swelling at 18°; thereafter dissolving 1 hr. at 40°).

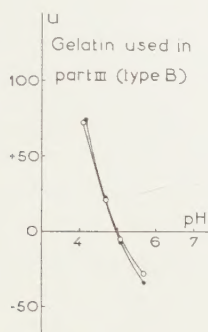


Fig. 3

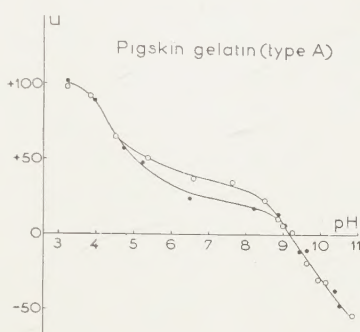


Fig. 4

Fig. 3. Determination of the I.E.P. of the gelatin used in the Figs. 1 and 2. The electrophoretic velocity is given in arbitrary units. White circles with diluted acetate buffers; black circles with diluted phosphate-citrate buffers.

Fig. 4. Determination of the I.E.P. of pigskin gelatin used in the following section. Variation of the pH by the addition of NaOH or HCl. White circle: determination in the presence of 0.5 millimoles/l K-tetraborate. Black circles: without K-tetraborate.

From the stock solution of gelatin (G) and of oleate (O) secondary stock solutions were prepared, denoted as G_1 (gelatin) and O_1 (oleate), which contain the same K-tetraborate concentration. Mixtures of G_1 and O_1 were then made in sedimentation tubes in the thermostat (40°):

$$a \text{ ml } O_1 + (20 - a) \text{ ml } G_1.$$

After thoroughly mixing, the tubes are left overnight in the thermostat. Next morning the volume of the coacervate layer is read off.

The same difficulties, as are described in part III, arose at higher K-tetraborate concentrations, namely, floating of the coacervate layer at higher mixing percentages of O_1 .

The method in reading off these systems is the same as is described in Part III.

A special difficulty in performing experiments with the type A gelatin at pH 9.2 is the occurrence of irreversible changes of the gelatin at this pH with the time. It is for this reason that the secondary stock solution (G_1) must be used immediately after preparation. If the gelatin remains in the thermostat for example during $\frac{1}{2}$ hr

(see KRUYT, H. R., in Colloid Science II, Elsevier Publishing Company, Amsterdam 1949, Chapter IX, § 2 and page 277).

The measurements were performed at room temperature. For the variation of the pH, very diluted buffers, NaOH or HCl were used. The pH of the mixtures was determined with the glass electrode, just before the measurements.

In performing these measurements we were helped by C. MALLEE and A. DE BAKKER, to whom we express our sincere thanks.

⁴⁾ Gelatin of type B may contain calcium, causing precipitation of Ca-oleate in the mixing series. In order to avoid this, the gelatin preparation must be free of calcium.

before using it, it was found that the coacervate volume of the mixtures of the left part of the mixing diagram decreased.

The nature of these changes will be discussed in the sections 6 and 7. For the preparation of the gelatin with I.E.P. 5.70, see section 8.

3. Coacervation in mixtures of "Pigskin gelatin" and K-oleate in dependence of the K-tetraborate concentration

Mixing series which contain a relatively high salt concentration (e.g. 188 and 165 millimoles/l K-tetraborate) show a coacervate volume curve with one maximum (fig. 5). The shape of the curve resembles those which are obtained in experiments reproduced in figure 1. The only difference is that the left branch of the curve shows a pronounced inflexion point.

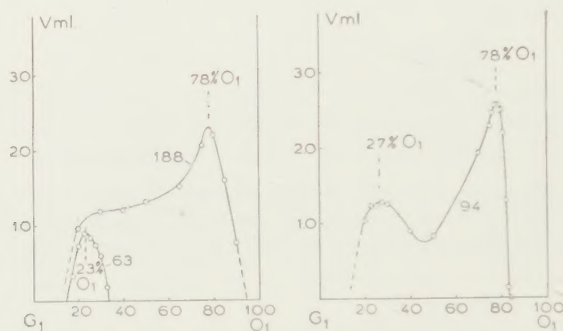


Fig. 5

Fig. 6

Figs. 5 and 6. Coacervate volumes, separated from the mixtures of O₁ (62.5 millimoles/l oleate) and G₁ (1.556 g dry pigskin gelatin/100 ml). The numbers indicate the concentrations of K-tetraborate in millimoles/l.

At somewhat lower salt concentrations, e.g. 125 and 109 millimoles/l K-tetraborate, already a minimum appears in the ascending branch of the curve, more or less in the middle of the mixing diagram. The curve now shows two maxima, one in the left part of the mixing diagram and another one in the right part. The minimum increases in depth as the salt concentration is lowered (fig. 6: the curve with 94 millimoles/l K-tetraborate).

To gain an insight into the nature of these two maxima, the refractive index (n) of the coacervate layers and of the equilibrium liquids was measured. The results of these measurements are given in figure 7. This diagram supports the idea that the coacervate volume curve (fig. 6) is composed of two different curves, each possessing a maximum and which partially overlap each other.

A strong indication is given by the n -curve of the equilibrium liquids (curve E in fig. 7). The two minima of this curve correspond approximately with the two maxima of the coacervate volume curve (fig. 6). This means that there are two mixing proportions at which the solubility of the

coacervate is minimal⁵⁾. One would also expect the n-curve of the coacervates (C in fig. 7) to show two maxima, their position corresponding with the maxima of the coacervate volume curve in fig. 6.

This does not come true at first sight as only the left maximum of the diagram is represented distinctly in the n-curve. The n-curve shows only a slight indication of a maximum corresponding with the right maximum of the mixing diagram (fig. 6). The shape of the curve C can be explained by considering this curve to be composed of two separate

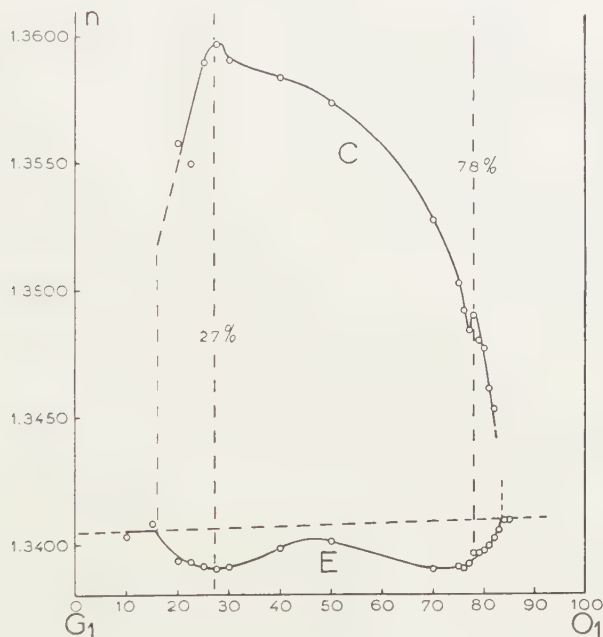


Fig. 7. The refractive index (n) of the coacervates (curve C) and of the equilibrium liquids (curve E), occurring in the mixing series which is represented in Fig. 6.

curves, both possessing a maximum, the left one much higher than the other.

A high value of the refractive index means that the coacervate is relatively rich in colloids. We may say now that, the coacervate of the left maximum contains relatively much more colloids than the coacervate of the right maximum.

This is supported by, *a*) that after tilting the tubes, the levelling of the interface coacervate/equilibrium liquid is much slower (high viscosity), and *b*) the maximal coacervate volume is much smaller.

The effects of a still further decrease of the K-tetraborate concentration is shown in fig. 8. The minimum increases and at about 85 millimoles/l

⁵⁾ For the use of the refractive index in studying coacervates, see BOOLJ, H. L., J. C. LYCKLAMA and C. J. VOGELSANG, these Proceedings, 52, 1006 (1949).

reaches the abscissa. From now on there exist two separate curves. The right curve shrinks very fast and disappears at about 83 millimoles l K-tetraborate, while the left curve is still vigorous at this and lower salt concentrations [compare also fig. 5] and disappears at last at a concentration between 47 and 50 millimoles/l.

The mixing proportions corresponding to the maxima of a number of coacervate volume curves (a.o. those represented in the figs. 5, 6 and 8) have been recorded in Table I⁶⁾, from which figure 9 has been drawn.

TABLE I

Mixing proportions of the left and the right maximum in fig. 8 as a function of the K-tetraborate concentration

K-tetraborate mmol/l	Left maximum % O ₁	K-tetraborate mmol/l	Left maximum % O ₁	Right maximum % O ₁
44	no coacervation	80	25	no coacervation
47	no coacervation	81.5	26	no coacervation
50	22	83	26	67.5
53	22.5	84.5	25	72.5
56	23	86	27	73.5
59	23	92	26	76
63	23	94	27	78
66	24	94	28	79
69	24	109	±30	78
72	26	125	±30	82
75	25	156	no maximum	78
78	26	188	no maximum	78

4. Comparison of the results with Part III; Composition of the characteristic associations

a) *The oleate-rich association*: When we compare fig. 8 and fig. 1, the very similar behaviour of the maximum of the right part of the mixing diagram in both cases is striking. The maximum shifts after its appearance in the direction of higher mixing proportions (expressed in %O₁) as the salt concentration is increased. It can be seen from fig. 2 and from the upper curve in fig. 9, that this shift is limited to a relatively small tract of salt concentrations (ascending part of the curve). At higher salt concentration the position of the maximum becomes independent of the K-tetraborate concentration (horizontal branch of the curve). The composition of this

⁶⁾ A graphical method was used to determine the position of the maxima. In the upper half of the curve, two or three horizontal lines are drawn, and the middle points of the parts cut off from these lines by the branches of the curve are connected (this connecting line most time is a straight line). The intersection point of this bisecting line and the curve is taken as the position of the maximum. This method has the advantage that several points of the curve are used. Without this method, the detection of the maximum is less reliable, as the highest point in the curve may only be highest point by chance (e.g. experimental error).

oleate-gelatin association can be calculated from the mixing ratio of G_1 and O_1 and the colloid concentration of the used solutions.

The mixing ratio of the horizontal branch of the upper curve in fig. 9 is calculated from the mean of the last six values of column 5 of Table I

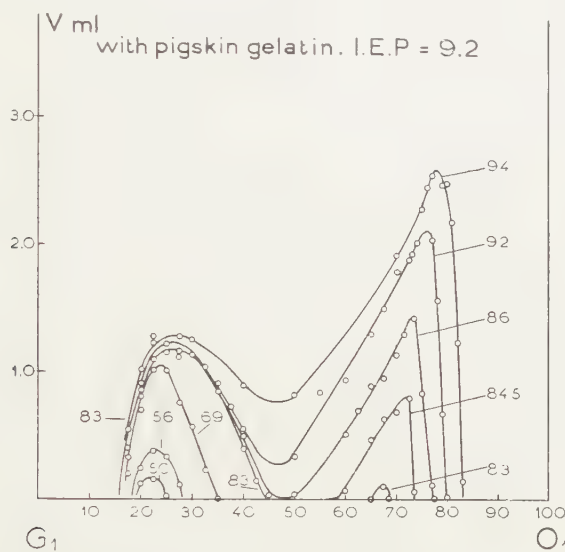


Fig. 8. Volume of the coacervate separated from mixtures of G_1 and O_1 at a number of K-tetraborate concentrations (mmol/l). The colloid concentrations of G_1 and O_1 as in figs. 5 and 6.

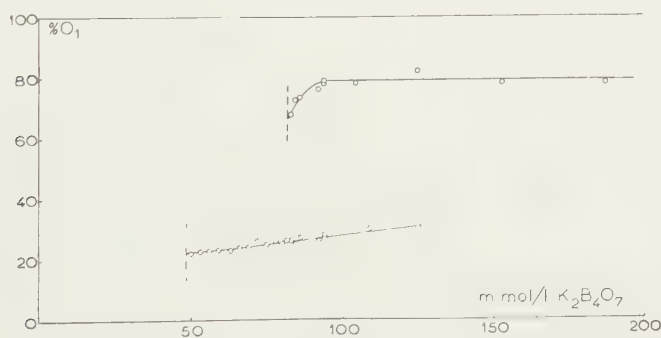


Fig. 9. Mixing ratios which correspond to the maxima of the curves in fig. 8 and in other coacervate volume curves which are not given here.

and is $78.8 \pm 0.7\%$ O_1 . The gelatin concentration (G_1) is $10/16 \times 2.49 = 1.556$ g dry gelatin/100 ml. The oleate concentration (O_1) is $10/16 \times 100 = 62.5$ millimoles/l oleate.

Calculation then shows that the composition of the characteristic oleate-gelatin association is:

$$14.9 \pm 0.6 \text{ millimoles oleate / g dry pigskin gelatin.}$$

About the same ratio is found for the association of the corresponding part of the curve in fig. 2. In Part III, we gave for the experimental points on the horizontal part of the curve the values 80 : 81 : 82 : 78 : 79 and 82 % O_1 , the mean of which is 80.3 ± 0.7 % O_1 .

As the colloid concentration of G_1 (1.76 gr dry gelatin 100 ml) and of O_1 (65.8 millimoles/l oleate) are known, it is possible to calculate the composition of the characteristic association, namely:

$$15.8 \pm 0.7 \text{ millimoles oleate / g dry gelatin.}$$

Analysis of the coacervates and of the equilibrium liquid gave

$$15.0 \text{ millimoles oleate / g gelatin.}$$

It is seen that not only qualitatively, but also quantitatively there exists a striking similarity between the coacervates represented in the right part of fig. 8 and of fig. 1. The same similarity is present in the shift of the maximum, occurring just after the coacervation sets in. At first appearance of the coacervation (fig. 8) the maximum lies at about 67.5 % O_1 (error about 1 %). This corresponds to a composition of

$$8.3 \pm 0.4 \text{ millimoles oleate / g dry pigskin gelatin.}$$

The value given in Part III was 70 % O_1 (error about 2 %). Calculation shows that the composition is:

$$9.0 \pm 0.9 \text{ millimoles oleate / g dry gelatin.}$$

It is striking that these values given as % of the maximum amount of oleate bound to 1 g gelatin are equal:

$$100 \times 8.3/14.9 = 56 \% \text{ and } 100 \times 9.0/15.8 = 57 \%.$$

Taking into account all the similarities, quantitative as well as qualitative, mentioned above, one cannot but conclude that the oleate-rich associations, indicated by the maxima of the right half of the mixing diagram in fig. 8 and the maxima in fig. 1 are nearly identical.

b) *The oleate-poor association*

We now direct our attention to the left part of the mixing diagram represented in the figs. 1 and 8, which show a great difference. In fig. 8 maxima are seen in the left half of the graph, which are not present in fig. 1.

In fig. 9, the lower line represents the mixing proportions of these maxima.

Increase of the salt concentration shifts the maximum towards higher mixing proportions (from about 22.5 to 30 % O_1), a shift which ends abruptly at higher salt concentration. This points to a trivial cause.

Both facts can be explained by assuming that the two curves in fig. 8 overlap each other up till the minimum in the coacervate volume curve disappears at last. Accordingly it seems safe to attach no real significance

to this gradual shift in the sense of an indication of a change in the composition of the characteristic oleate-gelatin association as a result of an increase of the salt concentration.

The most reliable determination of the composition of the association will be derived from the position of the maximum just after the coacervation has set in. For the position of this maximum, we will take the first three values of column 2 Table I; the mean is 22.5 % O_1 (error up to 1 mixing %).

Given the gelatin concentration G_1 (1.556 g / 100 ml) and the oleate concentration O_1 (62.5 millimoles/l), the composition of the association is calculated to be:

$$1.17 \pm 0.07 \text{ millimoles oleate / g dry pigskin gelatin.}$$

5. Discussion

a) Mode of binding of the oleate to the pigskin gelatin in the oleate-poor association

By means of a pH-titration curve, W. A. LOEVEN determined the total amount of basic groups of the pigskin gelatin ⁷⁾ used in the experiments of section 3. This proved to be 1.14 millimoles/g dry pigskin gelatin, a value which is about the same (taken into consideration the experimental error) as the ratio 1.17 ± 0.07 millimoles oleate / g dry pigskin gelatin, which was shown to be characteristic of the oleate-poor association (section 4).

We may now conclude that the maxima of the left half of the mixing diagram (fig. 8) indicate the binding of an equivalent amount of oleate anions to the basic groups of the pigskin gelatin.

b) Nature of the coacervate around the equivalent mixing proportion

The single fact that an equivalent amount of oleate anions is bound to the basic groups of the pigskin gelatin, will not yet lead to coacervation or flocculation. One must keep in mind that the experiments are performed at pH 9.2, i.e. at the I.E.P. of the pigskin gelatin. At this pH the positive and negative charges of the protein molecule compensate each other. The binding of an equivalent amount of oleate anions to the basic groups of the gelatin will cause a change of the charge equilibrium and the protein will acquire a negative charge which increases its solvability.

Indeed, no coacervation occurs when not at least 50 millimoles/l K-tetraborate is present in the system. The task of the salt is to diminish the effective charge of the liberated COO^- groups. This is done by the K^+ ion, either by screening off or by being bound to the COO^- group.

Summarizing the facts mentioned above, we may say that the coacervate

⁷⁾ Personal communication. The experiments are part of investigations which will be published shortly as Thesis (Leiden, 1953).

of the equivalent mixing proportions is to be considered as a tricomplex coacervation.

For a review of previous publications on tricomplex systems see H. G. BUNGENBERG DE JONG, in H. R. KRUYT, *Colloid Science II*, Amsterdam 1949; Chapter X, § 6.

c) On the non-existence of a maximum curve in the left part of the mixing diagram, fig. 1

There is no reason to believe that no binding occurs between oleate anions and the basic groups of the gelatin type B. The explanation must be sought for elsewhere, and is provided by the work on tricomplex coacervation.

Tricomplex coacervation is optimal when the experiments are performed at the I.E.P. of the protein. An increase of the working pH diminishes the tricomplex coacervate. A sufficient high pH at last, makes the appearance of a tricomplex coacervate altogether impossible.

With regard to this, the difference between the two mixing diagrams of fig. 1 and fig. 8 becomes much more clear.

In the experiments corresponding with fig. 8, the working pH and the I.E.P. of the gelatin are both 9.2. This situation provides optimal conditions for tricomplex coacervation, whereas in the experiments of fig. 1, which were also performed at pH 9.2, a gelatin preparation was used with I.E.P. 5.0. Obviously, this I.E.P. is too far from the pH at which the experiments are performed as no maximum is observable. The given explanation is supported by experiments with gelatin I.E.P. 5.7, which are described in section 8. In these experiments, the maximum in the left half of the mixing diagram just makes its appearance.

d) Nature of the oleate-rich association (corresponding to the maximum in the right half of the mixing diagram)

There is no need to repeat the arguments given in section 4. It was proved that the maximum, which occurs in the right half of the mixing diagram of fig. 8 is in principle the same as the maximum occurring in fig. 1. Accordingly, the characteristic oleate rich association consists of sandwich micelles of oleate anions, covered on both sides with a protein monolayer, which are bound to the surface of the sandwich micelle by means of ion-dipole interaction.

For further details on this type of associations, we refer to the preceeding parts of this series⁸).

⁸) The above hypothesis was put forward in Part II. It received support in the Parts III and IV, which deal with the coacervation of gelatin type B + oleate + salt. Part IV describes experiments, the results of which point to facts, in favour of ion-dipole binding and contradict the exclusive existence of a tricomplex binding of the protein to the soap anions in the soap rich association.

The insight gained in the present investigation — concerning the binding of an equivalent amount of oleate anions by the basic groups of the protein — makes a slight modification of the above interpretation necessary.

It seems quite reasonable to consider that in the systems corresponding to the right maximum of the mixing diagram, the equivalent binding persists. It then follows that from the total amount of oleate bound to one gram of gelatin about 14 millimoles/g is present in the sandwich micelles between the monolayer while the rest, about 1.2 millimoles, is bound by the basic groups on the exterior surface of the protein monolayer.

It was already mentioned in Part II of this series, that salt ions, which are absolutely indispensable for coacervation, serve a double task.

These are:

- a) formation of precursors of sandwich micelles (the main function) and,
- b) a sufficient screening off, of the ionized groups of the protein, which emerge from the exterior surface of the monolayer towards the surrounding medium. [This promotes the actual separation into coacervate layer and equilibrium liquid.]

As we know now, that the emerging positive groups of the gelatin are bound by an equivalent amount of oleate, the second function is then limited. The salt only has to screen off the negative groups of the protein with its cations. A scheme of this situation is given in fig. 10, in which the

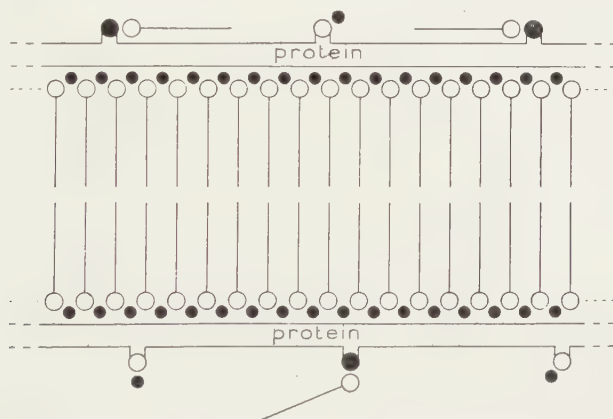


Fig. 10. Scheme for the oleate rich association. Explanation see text.

emerging ionized groups of the monolayer are represented by circles (white = negative groups ; black = positive groups). The carbon chains of the oleate ions on the outside may eventually contribute to the relatively high viscosity of the coacervate by adhering to analogous carbon chains of oleate ions of other association units in the surrounding.

The scheme has further been brought up to date by uniting the negative heads (white) of the oleate anions by cations (black). We may conclude, from

Part IV of this series and from recent investigations ⁹⁾ that ions with opposite charge in regard to the soap ions actually take part in the formation of the sandwich micelles. As to the details, concerning the polypeptide chains in the monolayer, no definite pronouncement can be made at the present ¹⁰⁾.

(to be continued)

⁹⁾ H. G. BUNGENBERG DE JONG and A. RECOURT, these Proceedings, Series B 56, 303, 315 (1953).

¹⁰⁾ We still hold that the protein molecule must lie flat against the sandwich micelle. In this situation, the negative heads of the soap anions—which form a pattern of charges on the surface of the sandwich micelle—can interact with the peptide groups of the protein by ion-dipole binding. The original idea that the side chains lie flat in the plane of the monolayer (apart from the ionized groups which are tilted out) cannot be maintained, as the polypeptide chain of the gelatin is probably built in another way. The former scheme has another disadvantage, namely, that the side of the monolayer against the sandwich micelle, has the same properties as the side which is turned towards the medium. This would promote the formation of a three-dimensional association in which the sandwich micelles are separated by only one protein monolayer. If this would be the case, one should certainly not expect the formation of coacervates, relatively rich in water.

It is therefore believed, that the protein monolayer, covering the sandwich micelle, must have different properties on both sides. A number of newer ideas on the configuration of polypeptide chains in the protein monolayer open possibilities to satisfy the above requirements (compare the articles of L. PAULING and B. COREY in the Proceedings of the National Academy of Science, 37, (New York, 1951).

CONTRIBUTIONS TO THE PROBLEM OF THE ASSOCIATION
BETWEEN PROTEINS AND LIPIDS. VI_B *)¹⁾

- a) *Further investigations on the coacervation of gelatin + K-oleate + salt at pH 9.2, using two gelatin preparations with different I.E.P. (9.2 and 5.7)*
- b. *The existence of two modes of binding of oleate to gelatin*

BY

H. G. BUNGENBERG DE JONG, C. R. VAN SOMEREN **) AND F. KLEIN ²⁾

(Communicated at the meeting of November 28, 1953)

6. *On the influence of irreversible changes, on the coacervation of gelatin type A + oleate + K-tetraborate, which take place at pH 9.2*

As the stock of Pigskin gelatin was used up, we continued these investigations with gelatin 00000, which behaves itself, in principle the same as the former. The I.E.P. proved to be 9.2, the same value as the other preparation, and in experiments with oleate, the mixing diagram is quite similar too (compare fig. 16), and section 8. Our next aim was to study the irreversible changes with time, which proceed in a gelatin solution, type A at pH 9.2. As is already mentioned in section 2, this fact necessitates a very fast performing of the experiments with Pigskin gelatin. Two mixtures of gelatin and oleate, 30 % and 70 % O₁ respectively, were made. They contained K-tetraborate in a concentration too low, for coacervation. Both the mixtures were stored at 40° in a thermostate.

After various intervals of time (1, 19.5, 25, 47, 73 and 140 hours), samples were taken from which the coacervation as a function of the tetraborate concentration was investigated. This was done as follows: two series of sedimentation tubes were prepared, containing: a ml K₂B₄O₇ 0.5 moles/l + + (5.5—a) ml H₂O. To the first series we then added 10 ml of the 30 % O₁ mixture and to the second series the same amount of the 70 % O₁ mixture. The results are shown in fig. 11.

*) The term lipid is used here in a wide sense, including fatty acids and other long-chain electrolytes.

¹⁾ Part I appeared in these Proceedings, 45, 601 (1942), the parts II (A, B and C), III and IV in these Proceedings, Series B 55, 317, 329, 338, 347, 360 (1952) and Part V, *ibid.*, 56, 203 (1953).

**) Aided by grants from the "Netherlands Organization for Pure Research (Z.W.O.)."

²⁾ Publication No. 24, of the Team for Fundamental Biochemical Research (under the direction of H. G. BUNGENBERG DE JONG, E. HAVINGA and H. L. BOOIJ).

These graphs show that the footpoints of the two curves shift gradually to the right (i.e. to higher salt concentrations). This means that the coacervates become more soluble.

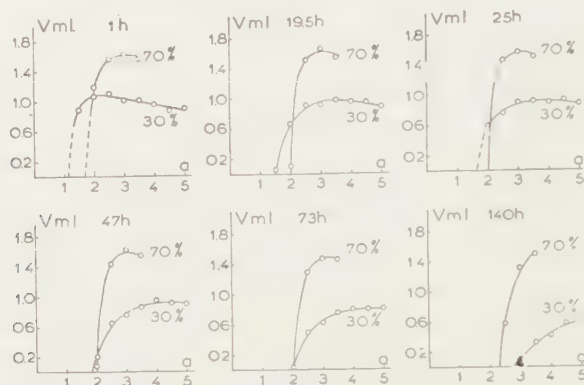


Fig. 11. Coacervate volumes obtained at 30 % and 70 % O₁, as a function of the K-tetraborate concentration (for a see text), after 1, 19.5, 25, 47, 73 and 144 hrs. exposure to 40°.

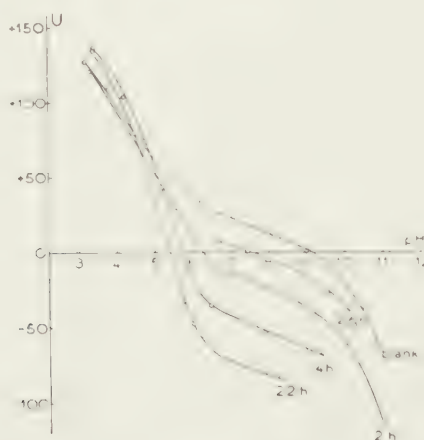


Fig. 12. Shift of the I.E.P. of Gelatin 00000 after exposure of the solution (pH 9.2) to 66°, during the times indicated in the figure. The electrophoretic velocity (U) in arbitrary units.

The most interesting point is, however, that the footpoint of the 30 % O₁ curve after 73 hours coincides with the footpoint of the 70 % O₁ curve and after 140 hours lies distinctly to the right of this curve. This suggests strongly, that prolonged exposure of the gelatin type A. to a temperature of 40°, changes the I.E.P. of the gelatin in a way, that the conditions for tricomplex coacervation become more and more unfavourable (see section 5, sub C).

For this reason it was necessary, to study the effect of prolonged exposure of the gelatin to heat, on the I.E.P.

7. *Transformation of gelatin type A into gelatin type B (by prolonged exposure of the solution to higher temperatures at pH 9.2)¹¹⁾*

Three series of experiments on the effect of prolonged exposure to higher temperatures, on the I.E.P. of gelatin 00000 at pH 9.2, have been performed at 30, 40 and 66° respectively. A mixture of 200 ml gelatin solution 3 % (6 g air-dry/200 ml) and 10 ml K-tetraborate 0.5 moles/l was placed in the thermostat. At certain intervals, samples were taken, which were cooled off and stored in the refrigerator, or used instantly for the electrophoretic measurements, carried out at room temperature. One ml gelatine solution was added to 10 ml of a suspension of SiO₂ particles + a ml HCl or NaOH + (39 - a) ml H₂O.

Figure 12 shows several of the curves (experiment at 66°). It is seen that the lower part of the curve is shifted downwards but approximately preserves its shape. As a result of this shift, the I.E.P. is shifted to lower pH values.

The results of all the experiments have been collected in Table II from

TABLE II

Temperature ° C	Time of exposure (hours)	I.E.P.	I.E.P.-5.65	log(I.E.P.-5.65)
66	—	9.2	3.55	0.55
	0.33	8.0	2.35	0.37
	0.67	7.5	1.85	0.28
	1	7.0	1.35	0.13
	2	6.25	0.60	0.78-1
	4	5.75	0.10	0.00-1
	6	5.65	—	—
	8	5.65	—	—
	10	5.65	—	—
	22	(5.40)	—	—
40	0.5	8.78	3.13	0.495
	1	8.40	2.75	0.44
	1.5	8.10	2.45	0.39
	6	6.85	1.20	0.08
30	0.5	9.18	3.53	0.55
	1	9.05	3.40	0.53
	4	8.50	2.85	0.455
	7.5	8.23	2.58	0.41

which fig. 13 was drawn. From it appears that the rate of displacement of the I.E.P. is strongly increased by an increase of the temperature. This points to the fact that the shift is the result of a chemical reaction.

The shift comes at 66° in a reasonable time to completion, whereby the gelatin of type A has been transformed into type B with an I.E.P. of

¹¹⁾ The experiments of this section have been performed by A. DE BAKKER and C. MALLEE, to whom we express our sincere thanks, for their valuable help.

5.65. The slightly lower I.E.P. after 22 hours heating may be due to another slow process. When we consider the curve for 66° in fig. 13, it appears that the rate of the displacement of the I.E.P. is fast at first, then gradually slows down and has reached almost its end after about 6 hours.

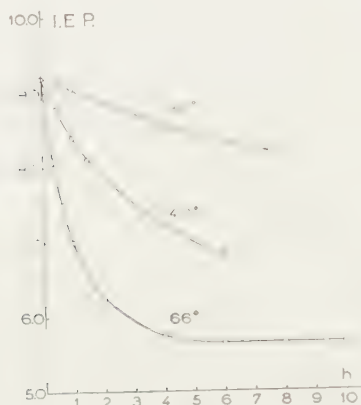


Fig. 13

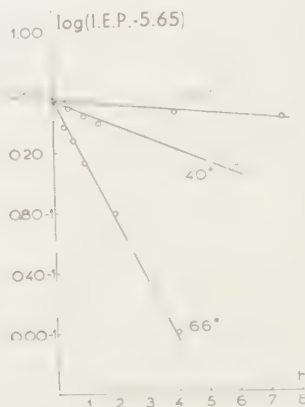


Fig. 14

Fig. 13. Shift of the I.E.P. with time; at three temperatures.

Fig. 14. Shift of the I.E.P. considered as a chemical reaction of the first order

This reminds of the reaction velocity of a first order reaction. It indeed appears, that by a formula of a first order reaction, the rate of the displacement of the I.E.P. can be satisfactorily described, when we take I.E.P. 5.65 as the endpoint of the reaction (see fig. 14 where a straight line is obtained when $\log (\text{I.E.P.} - 5.65)$ is plotted against the time of exposure to heat.

Taking into account that the U—pH curves shift downwards while approximately preserving their shape, the rate of the displacement of the I.E.P. is an approximate measure of the rate of displacement of the curve downwards in fig. 12. The latter rate, therefore, also follows the formula of a first order reaction.

It is known that collagen and gelatin of type A, contain much more amide-groups than gelatin of type B. Further it is known that in alkaline media, NH_3 is split off.

The chemical reaction which takes place in the experiments described, is believed to be a hydrolysis of the amide-groups (first order reaction!). Thus, COOH -groups of the gelatin are set free, the U—pH curve in fig. 12 is displaced downwards and the I.E.P. is shifted in the direction of lower pH values.

8. *Mixing diagrams with curves, intermediate between those of fig. 8 and fig. 1*

In § 5 sub c, we attached great importance to the difference between the I.E.P. of the protein and the pH at which the experiments are performed.

The optimal conditions for the tricomplex coacervation, around the equivalent binding, exists when the I.E.P. and the working pH are the same (fig. 8). The absence of maxima in the left part of fig. 1 is explained by the distance between the working pH and the I.E.P., namely $9.2 - 5.0 = 4.2$, which is already far too great for tricomplex coacervation.

It then follows, that mixing diagrams intermediate in character may be obtained, when gelatin preparations with an I.E.P. between 5.0 and 9.2 are available ¹²⁾.

As we have found in section 7, that prolonged exposure to heat of gelatin type A shifts the I.E.P. gradually from 9.2 towards 5.65, the results in section 6 (fig. 11) from experiments with a 30 % and a 70 % O_1 mixture, may already be seen as an indirect proof of the existence of the above mentioned intermediate mixing diagrams.

We decided nevertheless to investigate a complete mixing diagram with gelatin 00000, which has been transformed into type B, I.E.P. 5.7, by heating the solution (containing K-tetraborate) previously during 5 hours at 66°. Figure 15 shows the mixing diagram obtained with this gelatin preparation after treatment; for comparison see fig. 16 which shows a mixing diagram obtained with untreated gelatin 00000 ¹³⁾.

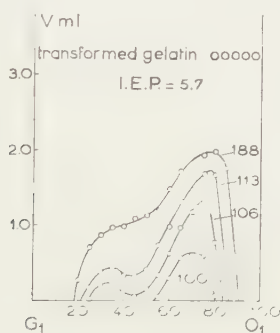


Fig. 15

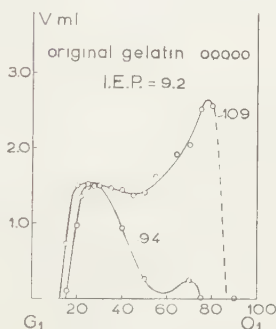


Fig. 16

Fig. 15. Coacervation in mixtures of heat exposed gelatin 00000 and oleate at pH 9.2 and at a number of K-tetraborate concentrations (millimoles/l).

Fig. 16. Coacervation in mixtures of gelatin 00000 and oleate at pH 9.2 at two K-tetraborate concentrations (millimoles/l).

Fig. 16 has only two coacervate volume curves, but this is enough to show that the untreated gelatin 00000, I.E.P. 9.2, behaves in the same way as the formerly used Pigskin gelatin, I.E.P. 9.2. Both in the figures 16

¹²⁾ Another way to lessen the distance between the I.E.P. and the working pH, is to work with gelatin I.E.P. 5.0 at pH values lower than 9.2. But this way is impossible in experiments with oleate because of complications (protein-acid soap association). Compare Part III, section 5 and Part V of this series.

¹³⁾ In determining the mixing diagram Fig. 15, help was given by C. MALLEE, to whom we express our sincere thanks.

and 8, the coacervation in the right half of the mixing diagram disappears first, at decrease of the K-tetraborate concentration and the coacervation in the left half of the mixing diagram remains. The mixing diagram (fig. 15) obtained from transformed gelatin 00000 (I.E.P. 5.7, after exposure to higher temperature) is clearly of intermediate character. It resembles strongly the mixing diagram of fig. 1 namely, that at decrease of the K-tetraborate concentration the coacervation disappears last in the right half of the mixing diagram. It differs from fig. 1 in that shallow maxima appear in the left part of the mixing diagram just before the coacervation disappears here altogether. The tricomplex relations are just able to show their presence in the left half of the mixing diagram, whereas this is no longer the case in fig. 1. This can be explained by the lesser distance from I.E.P. to the working pH (3.5 units in stead of 4.2 units in fig. 1), but still the conditions for tricomplex coacervation are unfavourable.

The results of this section confirm the discussion in section 5 sub *c*, in which it was argued that:

- a) equivalent binding of oleate to the basic groups takes place with both the types of gelatin, and
- b) the distance between the I.E.P. and the pH at which the experiments are performed, determines whether or not the equivalent binding can manifest itself in the curves of the mixing diagram.

9. Summary

1. The coacervation of pigskin gelatin (I.E.P. 9.2) + K-oleate + K-tetraborate has been investigated at pH 9.2.

2. It is shown that two oleate-gelatin associations exist, an oleate rich association with a composition of about 15 millimoles oleate/g dry gelatin, and an oleate poor association with a composition of about 1.2 millimoles/g dry gelatin.

3. The amount of oleate bound to the gelatin in the oleate poor association is equivalent to the content of basic groups in the gelatin. The nature of the coacervation around the equivalent mixing proportion in the mixing diagram is that of a tricomplex coacervation.

4. In the analogous coacervation of the system: gelatin (I.E.P. 5.0) + oleate + K-tetraborate, studied in Part III, the mixing diagram only shows the oleate rich association with a composition of about 15 millimoles/g dry gelatin. The oleate poor association cannot manifest itself here as the conditions for tricomplex coacervation are very unfavourable. The difference between the I.E.P. of the protein and the pH at which the experiments are performed is too great.

5. A gelatin I.E.P. 9.2 can be transformed into a gelatin with I.E.P. 5.65. The shift is the consequence of a chemical reaction of the first order which is assumed to be a hydrolysis of the amide groups.

6. In the mixing diagram of the transformed gelatin, a slight indication of the oleate poor association is present, which is explained by the fact that the difference between the I.E.P. and the pH at which the experiments are carried out is less.

7. It is assumed that in the oleate rich association the equivalent binding is still present. From the about 15 millimoles/g dry gelatin, about 14 are present in the sandwich micelles enclosed between the two protein monolayers and about 1.2 millimoles/g dry gelatin is bound to the basic groups of the gelatin situated at the exterior surface of the monolayers.

*Department of Medical Chemistry
University of Leyden.*

INTUITIVE AND DISCURSIVE THOUGHT, A COMPARISON

BY

J. CLAY

(Communicated at the meeting of November 28, 1953)

I have requested the permission of the Academy to lay before you the present argument wherein I will have the opportunity of offering a few problems for your consideration.

As of late various facts induced me to occupy myself with the problems I wish to pose, the cause of my request is threefold:

First of all at the Congress „Les troisièmes Entretiens de Zürich" (1948) a number of members was invited to indicate the relation between theory and experience. This led to a lively discussion especially between mathematicians, as to which form of thought is primary, the intuitive or the discursive.

In the second place, in the past summer at the School for Philosophy in Amersfoort a general philosophical congress in Hawaii was mentioned where thinkers of oriental and occidental schools of thought came together. There an effort was made to make a comparative study of intuitive eastern thought and logical discursive western thought, to bring these methods closer together and if possible to form a synthesis. The Hawaiian congress stressed the possibility that intuitive thought which western thinkers take to be pre-logical may be supra-logical.

In the third place I myself became clearly aware that in the solution of all problems of a psychological, ethical, aesthetic, religious and philosophical nature the result depends not only on the logical treatment, but that a value-judgment, a preference, sympathy or antipathy always plays a decisive role, thereby more often than not prohibiting the achieving of a final conclusion. That is the reason why these problems always re-appear without ever being definitely settled.

In the case of scientific problems, on the contrary, a final judgment can often be arrived at, because valuation is kept in the background or shut out altogether and the logical discriminating faculty plays the leading part.

Most of the different conceptions of the truth-criterium of a judgment were formerly based firstly on the agreement of thought and reality, secondly on the absence of contradiction (formal truth); thirdly the pragmatistical conception is "truth is that which promotes acting well (good action)" and Nietzsche's sceptical relativistic version hereof "Wahr-

heit ist der zweckmässigste Irrtum", "Truth is the most efficient error". However, I wish to launch a different view.

I think evidence should just as well be rejected as a criterium of truth. To my opinion it is only a subjective attendant circumstance of feeling or belief of truth, but one which gives no further motivation and therefore cannot carry general conviction. Nothing guarantees that an evidence may not be seeming or superficial. How many centuries has it taken to conquer the evidence of the earth's surface being a plane. How long and how hotly controversy has raged before mankind accepted that the sun does not circle around the earth. The existence of a God, governing the world with infinite goodness is just as evident to many as the impossibility thereof is to many others. Just as evident as it is to great numbers of citizens that the only right form of society is the democratic one, as evident is it to others that that form is far from being ideal. No, evidence can never be the firmest support of truth.

The criterium of truth which I should like to apply is the following: True or right is a judgment or a whole of judgments, which is independent of the postulates (starting point of the reasoning) and independent of the line followed in reasoning, as well as of the point of time upon which the judgment has been pronounced and of the subject who pronounced it.

First of all be taken the case of formal judgments as they are arrived at in mathematics. Whoever executes an addition, will be perfectly aware that he may not stop before the result of counting upwards and downwards is the same. If only rough results are wanted, the grouping of the numbers may be changed, the result will be independent of the moment of the manipulation and finally also independent of the person who carried out the manipulation.

Mathematically worded the demand is: that the result of a judgment should be invariant for starting-point (postulates) and line of reasoning, for time and for reasoning subject.

To mathematicians this definition may appear almost self-evident and perhaps even trivial. Yet it may be established that this very formulation has been given by the author 30 years ago in a paper read at the University in Batavia and as far as he knows had never been given before and is not to be found among the many truth-criteria in the Dictionaries of Philosophy of R. EISLER, BALDWIN, LALANDE or MAUTHNER, although a few times mention has been made of the requirement that the judgment must apply to all subjects.

The author has since made use of this wording in many lectures, but has never yet published it and according to his knowledge, it has not been taken over yet either by philosophers or other workers. The author had been inspired to this definition by the graphs, which he made at the time for the physical constants e/m , the specific charge of the electron e , the elementary electric quantum and h , Planck's constant. It is evident that in 1915 for e/m a high degree of agreement was reached starting from

very different points and along different lines. The first value to be arrived at was the one found in 1896, by computation, from the Zeeman-effect the second one from the parabolic method of J. J. THOMSON etc. Every kind of sign in the graph indicates a different method. In the upper

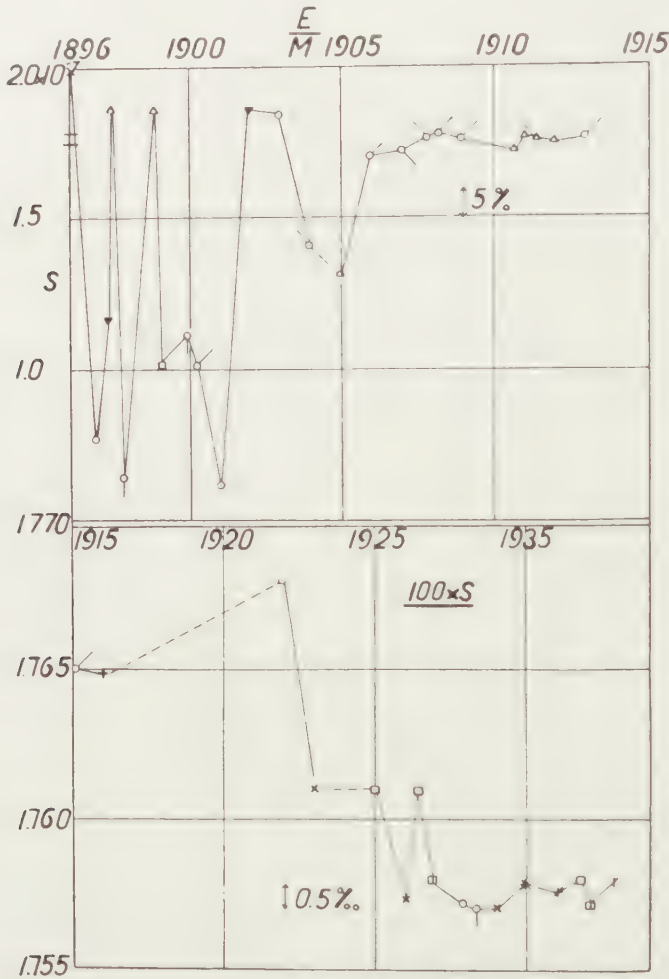


FIG. 1

graph 10 different methods are indicated. Since that fine convergency had been reached in 1915, the methods have been considerably perfected. On a one hundred times larger scale the results of measurements made from 1915–1938 are given, always showing the same tendency.

For the electric elementary quantum e the same obtains. As to h , the convergency of the values have been given from the start of the research, because already the first computed value did not differ more than $1.5 \frac{0}{100}$ from the later convergent value.

Of course it is not possible in other domains to point out similar agreements which apply also quantitatively, but the analogous qualitative agreement applies there as well.

Cf. Tijdschr. v. Wijsbegeerte, to appear in 1954.

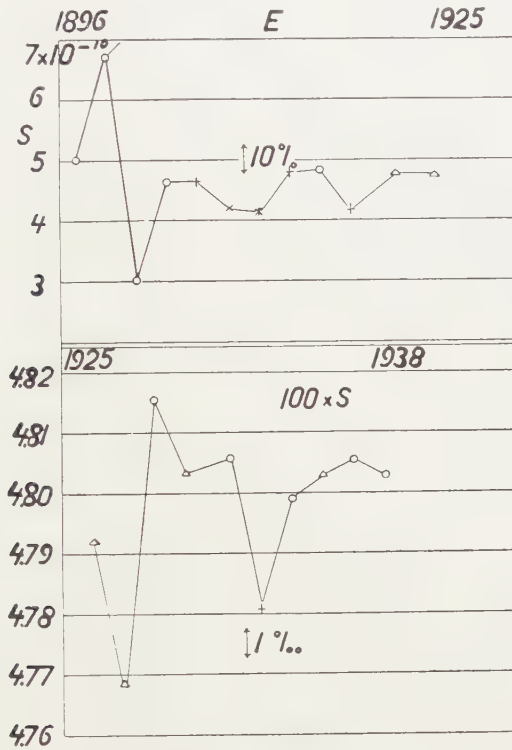


Fig. 2

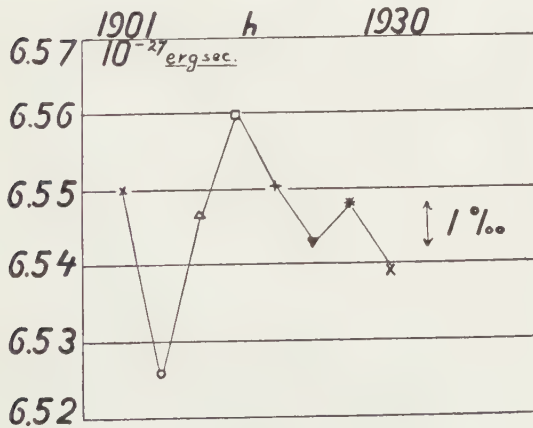


Fig. 3

Dependence on time and subject is of course very important for judgments of perception, which notoriously depend very often on the moment and likewise on the disposition of the observer.

In my opinion the criterium of truth given before applies to all kinds of judgments (judgments of perception, semantic, logical, formal, theoretic, pragmatic and creative judgments). It gives a direct basis for a value-judgment of intuitive and discursive thought. For practically all authors discussing intuitive thought do describe it as appearing instantaneously and in its entirety, unexpectedly. There is no saying how and from where it arises or along what line it travels, so that with regard to the criterium established it lags far behind discursive thought. Moreover it manifests itself in one single moment and there is no possibility of calling forth a reiteration. Besides, the activity of the intuitive notion concerns only one person. It is not possible for others to share it or to have a simultaneous, analogous experience.

All this does nowise mean that the function of intuitive thought should not be highly appreciated by many investigators and scholars. But they think it an important predecessor of a form of judgment, requiring confirmation by discursive thought.

Examples of this abound. The brilliant chemist VAN 'T HOFF e.g. had a pronounced preference for phantasy, a special form of intuition, but he owned that though phantasy might represent the building material, logical truth represented the building itself (E. COHEN, J. H. v. 'T HOFF p. 1954). His famous contemporary KÉKULÉ describes minutely his well-known dream about the discovery of the benzene ring and tells how he saw the atoms of carbon dancing about with the other atoms. And suddenly one of the rows of atoms arranged itself into a ring. Immediately after waking up, however, he went to work to formulate his thoughts logically after this intuitive find. He says:

"Let us learn to dream, perhaps it may aid us to find truth. But let us take care not to publish our dreams before they have been verified by our waking mind" (E. COHEN idem p. 62)".

The biologist and philosopher HANS DRIESCH says (*Ordnungslehre* pag. 351) "Contrary to discursive thought intuitive thought is abbreviated thought (*das abgekürzte Denken*). In his "Wissen und Denken" (Knowledge and Thought) he agrees with Spinoza's opinion (with its *scientia intuitiva*) that mental activity (*Schauen*) can liberate man from his affections for this can only be done by mental intuition (*unmittelbares Schauen*). I will revert to this in course of time.

Before proceeding I want to state here that probably many of us, scientific thinkers, hold discursive thought, advancing step by step, superior to intuitive thought, although indeed we do not repudiate the latter form of understanding.

And that is exactly the reason why this part of my argument is submitted to you, together with the second part following hereafter, which serves the same purpose although its contents differ.

In my opinion the character of intuitive thinking is extremely important for the advancement of science. Therefore I should like to hear

the direct personal experience of many people schooled in productive thinking and to compile these experiences. An exchange of thought between 2 of our members during the visit of our Academy to Brussels induced me to make the present effort. Having cognizance of this experience would doubtless profit us all. Think only how HELMHOLTZ, at the celebration of his 70th birthday related in his magisterial oration the way in which the most important of his brain-waves had reached him. He says: "Often the intuition steals into our minds quite unnoticed, its purport not having been seen through at the start. Sometimes a coincidence helps afterwards to fix as yet how and under what circumstances they came. Otherwise they are just there, one knows not wherefrom. In other cases they arise suddenly, effortless as an inspiration. As far as my experience reaches, they never arose in tired brains or at the writing desk.

I had always to consider my problem so thoroughly from every angle that I knew each turn and entanglement thereof by heart and could survey the whole of it without written aid. More often than not this was only possible after prolonged preliminary labour. When the fatigue caused thereby had subsided, a moment of perfect bodily freshness and quiet content had to set in, before the happy thoughts came. Sometimes they were there in the morning at the awakening. This has also been observed by Gauss. Very easily however they arose during a light climb in wooded mountains in sunny weather. The smallest amount of alcohol seemed to chase them away".

This is a fine description containing a careful account of his experiences, by one of the most favoured among scientific investigators.

It is a matter of fact that but very little is known about intuitive thought. How useful might it be if on this subject there were more inter-communication. Just imagine that a neuro-physiologist was able to prepare a substance stimulating the activity. This is not inconceivable at all and how much might that profit us.

The foregoing is intended to encourage you to answer some questions, drawn up with a view to a preliminary investigation, namely to find out if there is any sense in these questions being put on a larger scale. It is only an encouragement, in the event that you yourself would be interested. I would of course not think of insisting.

The rest of my argument has another aspect, however. In the introduction I mentioned the difference, which, according to Indian thinkers, exists between occidental and oriental thought. In their opinion as far as Indian and Chinese thinkers are concerned, intuitive thought dominates discursive thought in the Orient; and consequently their order of consequence ought to be reversed, and intuitive thought ought to be considered as supra-logical or supra-discursive. Further they advance that the intuitive element has been neglected in the occident. This is also the opinion of KWEE SWAN LIAT, though reached by another argument, as appears from his recent thesis for his doctorate.

As far as philosophical thought is concerned, this must be contested. Truly, our thought comprises a number of activities, which, without being separable with precision, are yet separable. I have made an attempt to do this in my book: "De Ontwikkeling van het Denken" "The development of Thought". There a discrimination is made between awareness, directed attention, perception, feeling, observation, imagination, understanding, belief, judgment, reason (Vernunft) and knowledge. Even here the question presents itself, if e.g. synthesizing reason does not already overlap understanding and might therefore be equalised to intuition, because both try by the synthetizing element to reach a compromise or synthesis across unsurmountable contradictions.

When passing in review the value attributed to intuitive thought by the principal occidental schools of thought the observer will first of all be met by the fact that in his philosophy NICOLAUS CUSANUS accords the greatest value to the intuitive element, a statement, to which the four forms of knowledge he indicates bear witness namely perception, understanding, the unity-seeking intellect and mystical contemplation. By his phenomenology CUSANUS has become the founder of European thought.

In GIORDANO BRUNO's work the triality is premised of perception, understanding and reason (Vernunft), a grouping which afterwards is met again in the work of KANT and HEGEL.

SPINOZA always speaks of three forms of thought and as the highest thereof he estimates the scientia intuitiva through which we possess the knowledge of God, from which all other knowledge issues.

As basis of all knowledge naturalistic DESCARTES takes the lumen naturale which ought to be mentioned in connection with intuition.

The formulation of lumen naturale by AUGUSTINUS reads as follows:

"Man in his variable and transient existence cannot institute the eternal being of the pure ideas. He can only accept them as a gift out of the hands of God. The cause of our being able to attain to pure knowledge irrespective of the senses and of experience is that in the moment of our turning to this divine wisdom the light of the one universal and eternal reason is present and is being clarified in us. The divine "word" is the hidden sun which reveals the eternal truth to the inner sight of the mind; it remains the only and infallible teacher for all human knowledge".

This insight has been taken over by all thinkers in the initial period of modern philosophy.

After that comes the idealistic period of KANT, FICHTE, SCHELLING and HEGEL. Here the discrimination is found between sensory perception, understanding (Verstand) and the synthetic reason (Vernunft), which overlaps contradictions. Of recent times HUSSERL may be added hereto, with his "Wesensschau" and the existentialistic philosophy evolving therefrom. The latter neither denies nor evades the irrational in the least. Further DRIESCH with his vitalistic doctrine and above all BERGSON with his special preference for intuition. He says that every philosopher is

characterized by one single intuitive basic idea. With BERGSON himself this is the "durée" the conception of duration, perception of time. How could a western philosopher let himself be persuaded that western philosophy has neglected intuitive thinking? And intuition itself has been represented here in more varieties than in eastern philosophy. Partly its character is the same, namely the immediateness of the conception of the intuitive concepts, their synthetic character, their endeavour to be all-embracing and to have antitheses united in them. Thus in western philosophy the concepts arise of HUSSERL's *Wesensschau*, of reason and idea in idealistic philosophy and of the durée with BERGSON. All these concepts are correlatives to the Chinese Tao and the Indian Atman, wherein a great number of contradictions are united. These concepts are admitted without objections, just like the Hegelian idea which comprises subject and object. The system of SCHELLING is self-styled an identity-philosophy.

It is not only philosophy that has an eye for intuition; science and especially mathematics have repeatedly directed their attention thereto. Sciences based on the observation of nature have done this of course to a lesser degree than the others. POINCARÉ e.g. in his *Valeur de la Science* p. 11 has written a very important discourse on "L'Intuition et la Logique en Mathématique". It is on account of his work, that an extensive and interesting exchange of thoughts has taken place chiefly in France. Many quotations herefrom are cited by the mathematician CARMICHAEL in his book: *The logic of Discovery* (p. 206 and following). In this book the role of intuition is very much stressed and it is shown how it plays a very prominent part in all mathematical discoveries.

Also POINCARÉ does point out the immediateness and the insight in the totality of the problem, which intuition proves to give.

Let us take an excessive case of the difference of both ways of thought. A geologist is going to make a thorough study of the Alpine mountains. If he is an analysing discursive thinker, his intention will be to investigate with a microscope every square inch of the chosen territory for its phenomena and mutual relations.

If he is an intuitionist, he will get aboard an aeroplane and take literally speaking a bird's eye view of the territory. This latter kind of survey, rendering impossible the obtrusion of too many details, particularly suits an explorer, who wants to determine direction. A mind tending to microscopic investigation does not have a wide enough range of view, and therefore is not able to see the general line. He cannot see far enough in advance to decide what the direction of his investigation will have to be. "It is therefore" says POINCARÉ "that the discoverer wants first and foremost intuition, although afterwards the discursive logical element will be just as indispensable".

If one should ask now: "this intuitive thought, which leads to such, often blurred, concepts, is it at the same time supra-rational and infra-rational?" an affirmative answer might at once be given. But it is surely

TABLE I

Number of events ABC-D₁D₂ per hour which were accompanied by a discharge of two or more of the counters E

Coincidences	Rate of 2-f	Rate of 3-f	Rate of 4-f	Rate of 5-f
0 cm Pb in Q 0 cm Pb in P	1.19 ± 0.19	0.29 ± 0.11	0.10 ± 0.05	0.05 ± 0.14
1 cm Pb in Q 0 cm Pb in P	2.07 ± 0.09	0.40 ± 0.05	0.11 ± 0.02	0.04 ± 0.01
1 cm Pb in Q 10 cm Pb in P	1.06 ± 0.14	0.18 ± 0.10	0.09 ± 0.05	0.04 ± 0.01
2.5 cm Pb in Q 0 cm Pb in P	2.08 ± 0.08	0.40 ± 0.02	0.10 ± 0.02	0.03 ± 0.01
5 cm Pb in Q 0 cm Pb in P	1.85 ± 0.11	0.41 ± 0.05	0.10 ± 0.03	0.03 ± 0.01
10 cm Pb in Q 0 cm Pb in P	1.51 ± 0.10	0.38 ± 0.05	0.11 ± 0.01	0.02 ± 0.01
15 cm Pb in Q 0 cm Pb in P	1.50 ± 0.08	0.22 ± 0.03	0.08 ± 0.01	0.02 ± 0.01
15 cm Pb in Q 10 cm Pb in P	1.10 ± 0.05	0.30 ± 0.05	0.14 ± 0.01	0.04 ± 0.01
17.5 cm Pb in Q 0 cm Pb in P	1.62 ± 0.05	0.29 ± 0.01	0.10 ± 0.01	0.01 ± 0.01
17.5 cm Pb in Q 10 cm Pb in P	0.81 ± 0.06	0.45 ± 0.04	0.11 ± 0.01	0.02 ± 0.01
20 cm Pb in Q 0 cm Pb in P	1.46 ± 0.06	0.22 ± 0.03	0.06 ± 0.01	0.01 ± 0.01
2.5 cm Pb in Q 0 cm Pb in P	1.62 ± 0.10	0.27 ± 0.04	0.03 ± 0.01	0.02 ± 0.01

We also determined the number of times per hour that one of the counters I through V had been singly hit with either 1 or 17.5 cm of lead in Q.

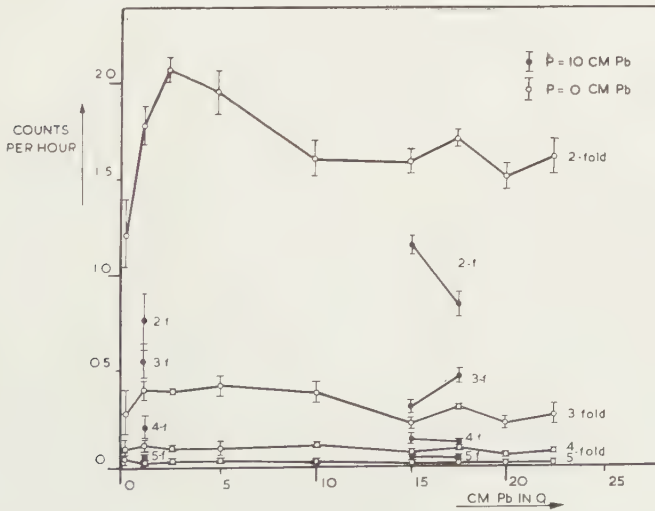


Fig. 3. Coincidences ABC-D₁D₂ per hour for cases in which two or more counters E had been hit.

These figures are collected in table II. As the number of processes in which these secondary cascade particles are produced constitute about 1/1000 of the total number of cases and as the distribution of the secondaries for various directions appears to be rather isotropic we may conclude that the minimum value of the energies involved in these processes is about 30 times the energy a meson has at sea level, i.e. in total about 10^{11} eV. This appears to be a reasonable value.

TABLE II

Events ABC-D₁D₂ per hour in which one of the counters E has been singly struck

cm Pb in Q	Counter	Rate with 0 cm Pb in P	Rate with 10 cm Pb in P
1	I	1.5 ± 0.1	2.0 ± 0.1
	II	1.3 ± 0.1	2.9 ± 0.2
	III	1.1 ± 0.1	2.7 ± 0.2
	IV	0.7 ± 0.1	2.4 ± 0.1
	V	1.1 ± 0.1	3.0 ± 0.2
17.5	I	2.55 ± 0.06	2.0 ± 0.2
	II	4.5 ± 0.1	2.0 ± 0.2
	III	4.3 ± 0.1	1.6 ± 0.2
	IV	4.2 ± 0.1	1.6 ± 0.2
	V	4.5 ± 0.1	1.9 ± 0.2

From the 4th column it is obvious that the hard secondaries produced in Q have given showers in the 10 cm Pb in P.

In conclusion we wish to thank Mr L. ROELAND for his help in performing the measurements.

REFERENCES

1. CLAY, J. and W. SCHEEN, Physica 14, 489 (1948).
CLAY, J., C. WANSDRONK and TH. J. DEKKER, Physica 18, 582 (1952).

ON THE NEUTRAL HORIZONTAL COMPONENT OF COSMIC RADIATION

BY

J. CLAY AND M. BRUIN

(*Natuurkundig Laboratorium der Universiteit van Amsterdam, Nederland*)

(Communicated at the meeting of November 28, 1953)

SUMMARY. An experiment was performed in which effects due to the neutral horizontal component of the cosmic radiation were measured at sea level. The results seem to indicate that apart from photons energetic neutrons play an important part as producers of charged secondary particles in lead, aluminium, paraffin and water.

1. *Introduction.* In 1948 ROGOZINSKY [1] concluded from his experiments that a penetrating neutral horizontal component existed in the cosmic radiation. In his opinion there were three possibilities: the non-ionizing radiation might consist of neutral mesons, of neutrons, or of hitherto unknown particles.

Our measurements were performed in the years 1949–1952 in order to study more in detail the nature of the events reported by ROGOZINSKY due to neutral, mainly horizontal, particles. We investigated the effect of screens of lead, aluminium, paraffin and water on the radiation concerned. In the following we shall describe the experiments and put forward our opinion that a soft electronic part and a more penetrating component, mainly consisting of energetic neutrons, might be responsible for the effects measured.

2. *Experimental arrangement.* The set-up used is shown in figure 1. It consists of a horizontal telescope formed by the counter sets B and E. The counter sets A and G are connected in anticoincidence with the counters B, C, D and E. We shall refer to events A_BCDEG_ (indicating the fact that the counter concerned is not discharged) as anticoincidences and to events BCDEG_ as coincidences. The counters F could be connected either in coincidence or in anticoincidence with the other counters. Whenever use has been made of such a combination this will be explicitly mentioned in the following. The counters G served to prevent air showers from being registered as horizontal rays passing through the telescope.

We used only .6 mm thick glass wall Geiger counters coated with aquadag. The counters A, G and F had an effective length of 70 cm and a diameter of 3.6 cm. The effective length of the counters B, C and D was

30 cm, their diameter also being 3.6 cm. Conventional coincidence and anti-coincidence circuits were used. The resolving time was measured to be 6 microseconds. Proper functioning of counters and circuits was checked at short intervals. The mains supply voltage was stabilized.

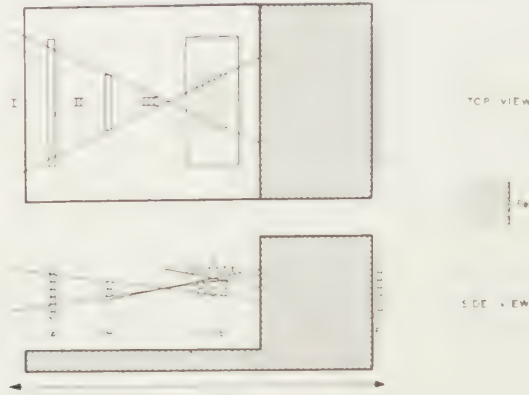


Fig. 1. Experimental arrangement

We wanted to examine properties of the neutral horizontal radiation and compare these as far as possible with those of the ionizing particles in the same direction. If one places materials in space II, the non-ionizing rays will have a certain chance of producing charged secondaries. These need not have the direction of the neutral primary, but it may be shown (section 3g) that the geometry of the set-up is favouring the recording of secondaries from neutral primaries making small angles to the horizontal.

TABLE I

Coincidences	Layer of material in			Interpretation
	I	II	III	
A-BCDEG-	0	variable	0	Production of ionizing secondaries by neutral primaries
	0	fixed	variable	Absorption of charged secondaries from neutral primaries
	variable	fixed	0	Absorption of neutral primaries through production of charged secondaries ¹⁾
BCDEG-	0	0	variable	Absorption of charged primaries
	variable	fixed	0	Absorption of charged primaries, production of ionizing secondaries by neutral primaries

¹⁾ In this case charged particles might produce in material in space I non-ionizing particles of the same kind as already present in the air. These might again give rise to charged secondaries in space II and thus be registered. An estimate of this effect will be given later-on (section 3c).

Therefore we will very roughly assume the cone of incoming neutral particles which are measured also to be determined by the counters B and E.

Various amounts of material were placed in the spaces I, II and III. Some of the simple experimental set-ups we used and the interpretation we want to give of the results are given in table I. The absorption and production processes occurring in the counter walls and the wooden boxes have in this table been neglected for the sake of simplicity. Results obtained from measurements performed according to this scheme are given in the next sections.

3. Measurements

a) Production of charged secondaries by non-ionizing primaries

In case no material was present in any of the spaces I, II and III a zero effect existed of $4.3 \pm .1$ events A_BCDEG_ per hour. As this effect was extremely constant even when up to 50 cm of lead was placed in I, it was assumed that apart from some non-ionizing rays producing charged

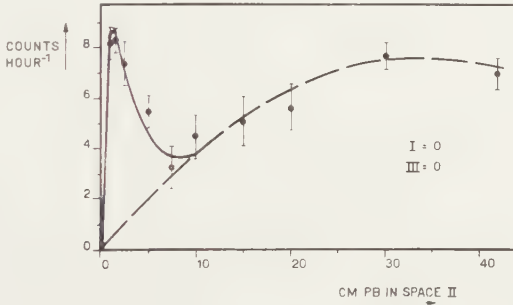


Fig. 2. Rate of events A_BCDEG_ as a function of the thickness of lead in space II with I = 0 and III = 0

secondaries in the material continually present between the counters A and B (less than $.5 \text{ gcm}^{-2}$), this relatively large effect could mainly be attributed to leakage of charged particles (presumably muons) through the anticoincidence counters and to inefficiency of the electronic apparatus. Indeed we found that it was possible to reduce this zero rate to about 2 per hour by using a double layer of anticoincidence counters A. The counting rates reported have been corrected for the zero effect.

The rate of events A_BCDEG_(counts/hour) as a function of the thickness of the lead layer in space II and nothing in spaces I and III is given in table II and plotted in figure 2.

It will be noticed that a sharp maximum occurs in the counting rate near 1.5 cm of lead, followed by a fast decrease. The form and the place of this maximum indicate that this part of the curve results from photons materializing in the lead. The tail of the curve amounting to about 90 % of the maximum value is due to a second kind of process, the initiating particles of which must obviously also have been present in the air. We

tried to separate these two components as far as possible, the drawn and dashed curve of figure 2 representing the contribution arising from photons and other neutral particles. The transition curve of the latter is much flatter and shows only little absorption for large thicknesses of lead. A plausible explanation of this effect might be given by assuming that it is due to energetic neutrons which produce the registered charged secondaries in nuclear processes in lead. Neutral secondaries of lower energy might again give rise to charged particles, but often the latter will not even have enough energy to pass the counter walls. Whether or not any neutral particles are produced in the lead in II by ionizing primaries from the air cannot be concluded from this measurement. It is in principle possible to decide this by comparing these results with those from measurements in which lead is placed in space I. This will be discussed in section 3c.

TABLE II

Number of events A_BCDEG_ as a function of the thickness of lead in space II with I = 0 and III = 0

Cm Pb in II	A_BCDEG_ total	Hours	Rate/hour	Corr. rate/hour
0	1819	421.6	$4.3 \pm .1$	$- \pm .1$
1	438	35.0	$12.5 \pm .6$	$8.2 \pm .7$
1.5	1227	97.5	$12.6 \pm .4$	$8.3 \pm .5$
2.5	230	19.7	$11.7 \pm .8$	$7.4 \pm .9$
5	387	39.5	$9.8 \pm .5$	$5.5 \pm .6$
7.5	109	14.4	$7.6 \pm .7$	$3.3 \pm .8$
10	160	18.2	$8.8 \pm .7$	$4.5 \pm .8$
15	111	11.8	$9.4 \pm .9$	5.1 ± 1.0
20	177	17.7	$10.0 \pm .8$	$5.7 \pm .9$
30	632	54.0	$11.7 \pm .5$	$7.6 \pm .6$
40	466	42.0	$11.1 \pm .5$	$7.0 \pm .6$

If the radiation considered would consist of neutrons, the cross section for production of secondaries might be taken to be about one half of the geometrical cross section [2]. We made a rough estimate of the intensity for particles with that cross section. To this end it was assumed that the particles of which secondaries were registered were incident in a cone of the same order of magnitude as the one determined by the counters B and E (see section 3g). The intensity then found is $2 \cdot 10^{-4} \text{ sec}^{-1} \text{ cm}^{-2} \text{ sterad}^{-1}$ for the horizontal direction. BARTON [3] detected neutral particles capable of penetrating 10 cm of lead by means of an anticoincidence arrangement in a *vertical* set-up at sea-level as well as at mountain altitudes. When measuring the anticoincidence rate as a function of the zenith angle of the telescope he still observed an appreciable number of events when the telescope had a horizontal direction. As the radiation he detected in the vertical direction was explained to consist of high energy neutrons, he suggested that the rate for the horizontal direction might likewise be

due to these particles. BARTON measured a vertical intensity at sea-level about twenty times as large as the horizontal one we calculated here on the assumption that the radiation would also consist of neutrons. In a horizontal direction he still had an intensity of about one quarter of the vertical intensity. However, his apparatus selected relatively more particles from various directions as may be seen from the dependence of his events on the zenith angle. An intensity of the order of magnitude we found might indeed be well explained by assuming that the radiation consists of neutrons [3, 4]. As far as the intensity is concerned it is therefore not necessary to explain the effects found by an unknown radiation.

In light materials the production of secondary electrons by photons is not important [5, 6]. Several layers consisting of aluminium, paraffin and water were placed in space II. The corrected results are given in table III.

TABLE III

Number of events A_{BCDEG} as a function of a layer of material in space II with I = 0 and III = 0

Material	Thickness cm	Rate/hour	Corrected rate/hour
paraffin	8	$5.1 \pm .3$	$.8 \pm .4$
	17	$6.4 \pm .1$	$2.1 \pm .2$
	24	$6.7 \pm .4$	$2.4 \pm .5$
	30	$6.8 \pm .2$	$2.5 \pm .3$
water	30	$7.2 \pm .2$	$2.9 \pm .3$
aluminium	5	$6.7 \pm .2$	$2.4 \pm .3$
	10	$7.8 \pm .2$	$3.5 \pm .3$
	20	$7.6 \pm .3$	$3.3 \pm .4$

If the neutral radiation responsible for the production of secondaries consisted of neutrons, one would expect the cross section for this process to be proportional to $A^{2/3}$, A being the atomic number of the absorber. The number of anticoincidences to be expected per unit time in equal masses of different materials would then be proportional to $A^{-1/3}$, if the multiplicity of the secondaries plays no important part in the registration of the process (see section 3f). In figure 3 the production rates as a function

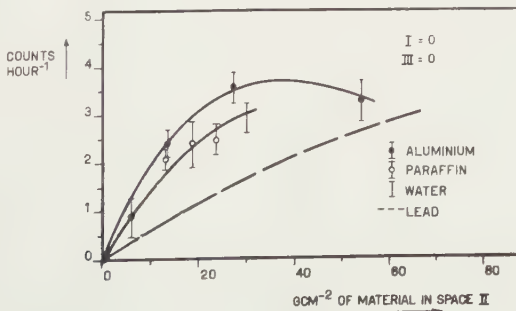


Fig. 3. Number of events A_{BCDEG} as a function of the thickness of a layer of material in space II with I = 0 and III = 0

of the mass of material in space II has been plotted. For comparison the dashed curve from figure 2 has been included, representing events due to the production of secondaries in lead by the radiation considered. Although the inaccuracy is large, below the maximum of the curves the rates for the lighter materials appear to have definitely larger values than those for lead. If one multiplies the values plotted on the y-axis with $A^{1/3}$ for the elements aluminium and lead the results fit reasonably well. They are therefore not inconsistent with the assumption that the neutral radiation consists of neutrons. It is remarkable that the figures for paraffin and water are lying below those for aluminium.

b) *Penetrating power of charged secondaries produced by neutral primaries in lead*

The penetrating power of charged secondaries produced by neutral incident rays may be measured by placing different thicknesses of absorber in space III while a fixed amount of material is present in space II. Measurements were performed with 1.5 cm of lead in II as producing material in order to have mainly secondaries from photons, and with 10 cm of lead in II as producing material, thus selecting mainly secondaries from the non-photon neutral component. The results are collected in tables IV and V. For easy comparison they have been plotted on different scales in

TABLE IV

Absorption of secondaries produced in 1.5 cm of lead in II, with I = 0

Cm Pb in III	A_BCDEG_ total	Hours	Rate/hour	Corr. rate/hour
0	1227	97.5	$12.6 \pm .4$	$8.3 \pm .5$
1	464	42.5	$10.9 \pm .5$	$6.6 \pm .6$
2	258	30.0	$8.6 \pm .5$	$4.3 \pm .6$
5	164	25.6	$6.4 \pm .6$	$2.1 \pm .7$
10	106	24.0	$4.4 \pm .4$	$.1 \pm .5$

TABLE V

Absorption of secondaries produced in 10 cm of lead in II, with I = 0

Cm Pb in III	A_BCDEG_ total	Hours	Rate/hour	Corr. rate/hour
0	160	18.2	$8.8 \pm .7$	$4.5 \pm .8$
1	770	105.2	$7.3 \pm .3$	$3.0 \pm .3$
2	451	82.5	$5.5 \pm .2$	$1.2 \pm .3$
5	431	93.7	$4.6 \pm .2$	$.3 \pm .3$
10	323	75.2	$4.3 \pm .2$	$- \pm .3$

figure 4. The secondaries produced by the neutral particles other than photons appear to be more readily absorbed. Secondaries produced in 20 cm of lead in II showed, within the statistical uncertainties, the same absorption curve as those produced in 10 cm of lead.

c) *Absorption of neutral primaries through production of charged secondaries.*

We now consider measurements with varying lead thickness in I (up to 40 cm), a fixed amount of lead in II (1.5 cm) and no material in III. The obtained figures are given in table VI and plotted in figure 5.

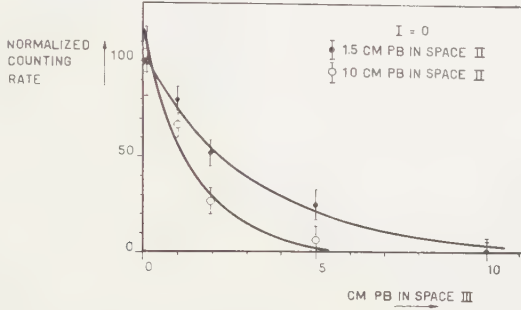


Fig. 4. Absorption of secondaries produced in 1.5 and 10 cm of lead in space II, with $I = 0$

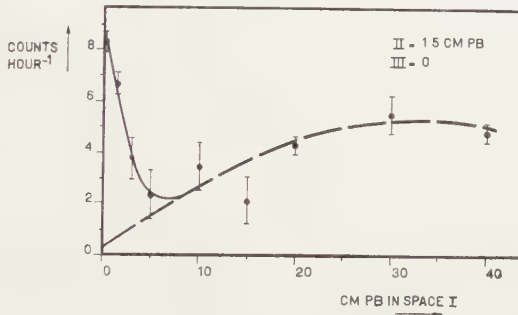


Fig. 5. Counting rate A_{BCDEG} as a function of the lead thickness in I, with $II = 1.5$ cm of lead, $III = 0$

TABLE VI

Events A_{BCDEG} as a function of the lead thickness in I, with $II = 1.5$ cm of lead and $III = 0$

Cm Pb in I	A_{BCDEG} total	Hours	Rate/hour	Corr. rate/hour
0	1227	97.5	$12.6 \pm .4$	$8.3 \pm .5$
1.5	991	90.5	$11.0 \pm .3$	$6.7 \pm .4$
3	125	15.4	$8.1 \pm .7$	$3.8 \pm .8$
5	74	11.2	$6.6 \pm .8$	$2.3 \pm .9$
10	105	13.4	$7.8 \pm .8$	$3.5 \pm .9$
15	63	9.8	$6.4 \pm .8$	$2.1 \pm .9$
20	1202	140.3	$8.6 \pm .2$	$4.3 \pm .3$
30	124	12.6	$9.8 \pm .9$	5.5 ± 1.0
40	760	83.4	$9.1 \pm .3$	$4.8 \pm .4$

When no material is present in space I, a number of neutral particles passing A will produce charged secondaries in II. When lead is placed in I

the same processes will take place in I and the rate $A_BCDEG_$ decreases due to charged particles produced in I hitting the anticoincidence counters. The fast decrease with the first few centimeters of lead will again be due to photons, but apart from this effect we notice (compare with section 3a) that other neutral particles are able to pass through a thick layer of lead in A before producing ionizing secondaries. In figure 5 the two components are separated which is indicated by the drawn and the dashed curve. The dashed curve has a good resemblance to the one in figure 2, the ratio of the heights of the two curves being 1.5. In section 3b the penetrating power of the secondaries was measured. For the mean range of these secondaries one may obtain a value of 1.6 cm Pb from the lower curve of figure 4. Using this value, the calculated ratio of the heights of the two curves of figures 2 and 5 is 1.6. This is in good agreement with the above one of 1.5, which was directly obtained from the curves of figures 2 and 5.

From this result one may draw another conclusion. If neutral particles of the kind considered had been produced in I by charged incoming particles, the dashed curve of figure 5 would be too high as a result of this and the ratio of the heights of the two curves would have been too small. As this value is however consistent with the value calculated from section 3b, it may be concluded that no serious error has been made ignoring the local production of neutral particles in the lead of space I. One may estimate that certainly less than 10 % of the neutral particles were produced in the lead in space I.

d) *Absorption of charged particles.* When measuring coincidences $BCDEG_$ the zero-effect will be due to all charged particles. We shall ignore those soft particles stopping in the counter walls and the wooden boxes, together forming an 'absorber' of less than 1 gcm^{-2} . As hardly any events $BCDEG_F$ are registered one may safely assume that the counting rate of events $BCDEG_$ is due to ionizing rays passing through the telescope in the direction B-E and not the other way round, the thick iron shielding absorbing all but the ionizing rays coming in that way. The decrease of the events $BCDEG_$ as a function of the thickness of lead absorber in space III is shown in figure 6. The counting rates are given in table VII.

TABLE VII
Absorption of charged particles, I = 0, II = 0

Cm Pb in III	BCDEG_ total	Hours	Rate/hour
0	953	55.3	$17.2 \pm .6$
1	341	20.1	$17.0 \pm .9$
2	920	60.2	$15.3 \pm .5$
5	384	24.0	$16.0 \pm .8$
10	341	22.4	$15.2 \pm .8$
15	442	28.5	$15.5 \pm .7$

It will be noticed that about 90 % of the ionizing horizontal radiation measured belongs to the hard component, thus presumably consisting of muons.

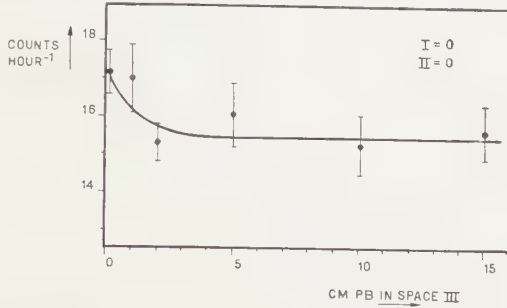


Fig. 6. Coincidences BCDEG_ as a function of the thickness of lead in space III

e) *Effects due to neutral and charged incoming primaries.* The number of coincidences BCDEG_ as a function of the amount of lead in space II was measured with no material in the spaces I and III. Apart from the rate due to effects of neutral particles (section 3a) one thus measures coincidences caused by charged primaries. The data obtained have been collected in table VIII and plotted in figure 7. For a large thickness of

TABLE VIII

Number of events BCDEG_ as a function of the thickness of lead in space II, with
I = 0 and III / = 0

Cm Pb in I	BCDEG_ total	Hours	Rate/hour
0	953	55.3	$17.2 \pm .6$
1.5	937	40.4	$23.2 \pm .8$
3	2939	112.4	$26.1 \pm .5$
4.5	1360	62.9	$21.6 \pm .6$
7.5	238	11.2	21.4 ± 1.4
10	261	13.0	20.1 ± 1.2
15	513	23.0	22.3 ± 1.0
20	303	14.0	21.6 ± 1.5
40	710	30.6	$23.2 \pm .8$
40	546	23.8	22.9 ± 1.0

lead all incoming soft charged particles will have been absorbed. If one takes e.g. the value of the coincidence rate obtained with a thickness of 20 cm of lead one may obtain the number of hard charged particles by subtracting the effect due to neutral primaries given in table II, which yields a rate of 15.9 ± 2.4 . For zero thickness of the material soft as well as hard charged particles are counted, therefore the ratio of the number of hard charged particles to the total number of charged particles is $.92 \pm .17$, in agreement with the value found in section 3d, where we concluded that the charged particles mainly consisted of muons.

f) *Effect of multiplicity of secondary particles.* It is difficult to estimate the influence of multiple secondaries emitted in one process initiated by a neutral particle. In order to look for an effect we first distinguished between cases in which the upper or the lower counter B had been struck.

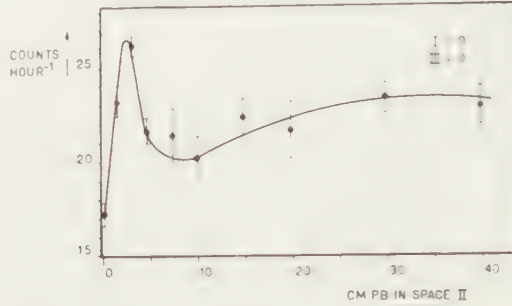


Fig. 7. Number of events BCDEG_ as a function of the thickness of lead in II with $I = 0$ and $III = 0$

The material in space II was 1.5 and later on 15 cm of lead. We had about equal numbers of anticoincidence rates in which the upper and in which the lower counter were hit, and moreover this rate was one half of the normal total A_BCDEG_-rate, which indicated that we did not register an observable number of cases in which B and C had each simultaneously been struck by a charged particle. We further used an additional counter K in anticoincidence with the counters B. This counter was placed at various distances above the counters B (2.5–20 cm). Again 1.5 and 15 cm of lead was placed in space II (nothing in spaces I and III) and the normal anticoincidence rate was compared with the one obtained when K was connected in anticoincidence with the other counters. If only one charged particle were emitted in each process one would expect no difference between the rates with or without K. In the case of a low multiplicity the rate should decrease if K was switched on. When many secondaries would be emitted one might again expect only little influence on the rate, as in many of those cases one of the secondaries might have struck one of the counters A anyway. With 1.5 cm of lead in II we noticed no change of the coincidence rate. As in this case the production of electrons by photons predominates, this is in agreement with expectation, since for an electron pair generated by a photon the angle between the particles will generally be a small one. For a thickness of 15 cm of lead in space II where the photon component has disappeared, an effect of a few percent was found, but the accuracy was too low to indicate whether the effect was real or not.

The muons present in the horizontal cone will only seldom produce electrons in the lead making a large angle with the primary. Thus if the anticoincidence counters A are switched off and the rate BCDEG_ is

measured with and without the additional counter K in anticoincidence, an increase of the rate should be mainly attributed to multiplicity of secondary particles produced by neutral primaries. The maximum effect on the rate BCDEG₋ was found to be $(10 \pm 5) \%$ for the case where 15 cm of lead was placed in space II. This seems an indication that multiple processes did occur.

g) *Geometrical considerations.* It goes not without saying that only neutral particles within a narrow, nearly horizontal cone gave rise to the measured effects. It is likely that in general the charged secondaries produced do not have the direction of the incoming neutral particle. Besides one has to consider the possibility that charged particles from outside the horizontal cone either produce in the material in space II charged secondaries which have a horizontal direction, or are themselves scattered in that direction. In order to evaluate the influence of production by or scattering of charged particles a large area of anticoincidence counters was placed over the material in space II. The number of anticoincidences A₋BCDEG₋ did not change, from which it results that there was no undesired influence of charged particles.

We then covered the anticoincidence counters above the producing material with lead layers which had a thickness of 1.5, 5 and 20 cm respectively, in order to evaluate the influence of neutral particles which struck the apparatus and which were mainly coming in from directions making large angles to the horizontal direction. The largest possible influence on the coincidence rate now proved to be 4 %. This effect could therefore not be of much importance in the results obtained. From these measurements we may therefore conclude that disturbing effects due to particles deviating appreciably from the horizontal direction occurred only to a negligible extent in the results.

The fact that the measured secondaries were apparently caused by neutral particles entering the set-up in rather a small cone around the horizontal need not necessarily imply that these secondaries show a preference for the direction of their primaries. The geometry of the arrangement may play an important part. As on the average only secondaries produced in the last 2 cm of lead were registered it is apparent that the effective surface of the material is largest in a direction nearly perpendicular to the horizontal.

In order to evaluate the effect due to air showers the anticoincidence counters G above the counters C, D and E were switched off. The influence on the coincidence and anticoincidence rates proved to be about 1 per hour, independent of the materials present in the spaces I, II and III. This indicates that the tray G indeed mainly discriminated against air showers, and shows that there was no large decrease of the counting rates due to one of the multiple secondaries hitting these counters. Large multiplicities therefore apparently occurred very infrequently.

4. *Conclusions.* In the foregoing we have investigated several properties of the horizontal cosmic radiation. From the results we think we may derive the following conclusions:

1. In the neutral horizontal radiation a soft component is present which is completely absorbed in a thickness of about 10 cm of lead; this radiation most probably consists of photons.

2. A neutral component having a much larger mean free path in lead and producing a much flatter transition effect is also present in the horizontal radiation.

3. The intensity of the latter radiation is of the order of magnitude as the intensity one may expect of energetic neutrons.

4. The cross section for the production of secondaries in lead and aluminium by this radiation is proportional to $A^{-1/3}$, A being the atomic number of the absorber.

5. The secondaries from photons are absorbed more slowly than those produced by the other neutral component.

6. For photons no multiplicity of secondaries was found. The remaining neutral radiation showed an effect of multiple secondaries in some cases.

7. Of the above properties none seems inconsistent with the hypothesis that the non-electronic neutral horizontal particles are neutrons. As other known neutral particles which might be considered would give rise to results different from the ones measured, we think that indeed fast neutrons are present in the neutral horizontal radiation at sea-level.

8. The neutrons which may give rise to the measured effects are mostly present in the air, as in lead certainly less than 10 % of the measured intensity is locally produced.

9. About 90 % of the charged incident particles in the horizontal direction are not absorbed in 15 cm of lead. This is a strong indication that the charged radiation consists mainly of muons.

This work represents part of the research program of the Foundation for Fundamental Research of Matter (F.O.M.) made possible by financial aid of the Netherlands Organization for Pure Research (Z.W.O.).

The authors wish to thank Prof. Dr G. W. RATHENAU, Dr H. DEN HARTOG and Dr H. F. JONGEN for helpful discussions.

REFERENCES

1. ROGOZINSKY, A., C. R. Ac. Sci. (Paris) 227, 628 (1948).
2. DE JUREN, J., Phys. Rev. 80, 27 (1950).
3. BARTON, J. C., Proc. Phys. Soc. A64, 1042 (1951).
4. COCCONI, V., Phys. Rev. 76, 517 (1949).
5. CLAY, J. and G. KLEIN, Physica 17, 858 (1951).
6. BRUIN, M. and J. CLAY, Physica 19, 719 (1953).

HYDRO- AND AERODYNAMICS

ON THE COALESCENCE OF WAVE LIKE SOLUTIONS OF A SIMPLE NON-LINEAR PARTIAL DIFFERENTIAL EQUATION. I

BY

J. M. BURGERS

(*Mededeling No. 76 uit het Laboratorium voor Aero- en Hydrodynamica der Technische Hogeschool te Delft*)

(Communicated at the meeting of November 28, 1953)

1. *Introduction.* — The object of the following pages is to consider the wave like solutions of the non-linear partial differential equation

$$(1) \quad \frac{\partial v}{\partial t} + v \frac{\partial v}{\partial y} - \nu \frac{\partial^2 v}{\partial y^2},$$

which appear when positive “impulses” are introduced at the origin $y=0$ at a series of successive instants t_1, t_2, t_3, \dots . The coefficient ν is supposed to be a very small quantity. The impulses in this case give rise to a type of waves with steep fronts (“*shock waves*”), propagating themselves in the positive direction along the y -axis. If the impulses are of varying strengths, the wave originating from a strong impulse can overtake a preceding wave produced by a weaker impulse; when this happens the two waves merge into a single one and in this way a gradual decrease of the number of waves will result. It is intended to study some features of this decrease.

Although the problem is a mathematical one, it may serve as a primitive illustration of what can happen in a semi-infinite column of gas, when a series of compression and expansion waves is produced by means of a piston at the bottom of the column. The compression waves develop into shock waves; since the speed of propagation of shock waves is dependent on their strength, the possibility of overtaking is found also here. The analogy would be closer if we consider a gas of extremely low temperature and if we could prevent that the energy dissipated in the shock waves will heat the gas. The energy might perhaps be radiated away by processes of the nature of those considered by ZANSTRA in his theory of condensation phenomena in a nebula¹). The shock waves would then

¹) H. ZANSTRA, On the Formation of Condensations in a Gaseous Nebula, to be published in the Proceedings of the “Second Symposium on Gas Dynamics of the Interstellar Clouds”, Cambridge (England), July 6–11, 1953, and in a more extended form in the “Journal of Atmospheric and Terrestrial Physics”.

The subject of compressible turbulence had already been considered at the First Symposium on Cosmical Aerodynamics (Paris, 1949). At the Second Symposium

present very high Mach numbers and in the equation of gas dynamics

$$\frac{\partial u}{\partial t} + u \frac{\partial u}{\partial x} = - \frac{1}{\rho} \frac{\partial p}{\partial x} + \frac{4}{3} \frac{\eta}{\rho} \frac{\partial^2 u}{\partial x^2}$$

(η being the coefficient of viscosity, which like ν in eq. (1), plays a subordinate part in the treatment of the motion), the term depending on the pressure gradient becomes almost negligible. The equation then approaches the same form as eq. (1). There will remain, however, strong compressions at every shock wave front, followed by expansions; hence the density distribution will be disturbed.

It should be observed that in so far as we touch here upon problems of "compressible turbulence", we have to do with a form of turbulence provoked by a certain degree of randomness in the boundary conditions, in this particular case in the amplitudes or in the timing of the waves produced in the system. The degree of randomness admitted in the boundary conditions (for instance, the mean square deviation of the amplitudes of the waves from their mean value) is an important parameter, which remains visible in the final result. The non-linear properties of the equation governing the system prevent that this randomness is smoothed out and act as a kind of selective mechanism. In this respect there is great difference with the central problem of incompressible turbulence, as it is found *e.g.* in the case of the flow through a tube with smooth walls, where the boundary conditions are given in a mathematically exact form and where turbulence, according to the prevailing views, develops spontaneously in consequence of some form of instability. In that case the intensity of the turbulence and its spectrum are functions of the Reynolds number characterizing the flow and do not bear any reference to the magnitude of random impulses or to random irregularities of the wall.

With acoustical waves, where the Mach number is not very high, the problem of wave propagation is more complicated. In that case there is a "sound velocity", depending on the state of the medium in which the propagation takes place, and there is both forward and backward propagation with respect to the moving gas. Interference between two shock

M. J. LIGHTHILL read a paper on "Effects of Compressibility on Turbulence" and in the later discussions of the Symposium the subject returned several times, with the attention directed in particular to the case of high Mach numbers and to the rôle played by shock waves. The turbulence of the interstellar gas probably for the most important part is caused by the heating of the gas by the ultraviolet radiation of very hot young stars, and it is to be expected that shock waves will be generated, moving outwards from these stars. The randomness in the distribution of these stars and in the epochs of their births, together with the irregularities in the distribution of the density of the gas, lead to a peculiar form of turbulence.

In so far as one can speak about "energy" in the mathematical system described by eq. (1), there is a "dissipation of energy" of amount $(v_- - v_+)^3/12$ in every steep front of the wave system, where v_- is the value of v just on the left hand side and v_+ the value just on the right hand side (with $v_- > v_+$). Compare the paper quoted in footnote 3, end of section 5 (p. 253) and section 9. III (p. 258).

waves overtaking each other will then lead to the appearance of waves moving in two directions. A number of cases has been treated in the literature²⁾. The formulation of a general statistical problem for such waves, as might be produced by random motions of a piston at the end of the column, will be very difficult. With decreasing temperature of the gas, the "sound velocity" decreases more and more, so that the distinction between forward and backward going waves becomes less effective. With zero "sound velocity" we return to the case described by eq. (1): here propagation is due exclusively to the presence of the non-linear term in the equation and thus depends directly on the value of v itself; consequently when v nowhere is negative, there will be forward propagation only.

To come back to the problem stated in the opening paragraph of this section, the circumstance that we wish to consider waves generated by separate impulses, and not by some continuously acting "impressed force" at the origin, is not of intrinsic importance. In principle the considerations to be developed will also apply to the continuous case, since owing to the nature of the differential equation, waves with steep fronts automatically arise out of any arbitrary system of waves. However, the detailed analysis of what will happen in the system becomes more complicated. Since the problem is already difficult enough with discrete impulses, it was thought advisable to restrict the analysis to the latter case.

In the case where the series of impulses has started at a given instant, there is a "first" wave in the system. The front of this first wave has a smaller speed of propagation than its successors, so that even when all impulses are exactly of the same magnitude and are regularly spaced in time, the successive waves will gradually overtake the first wave and merge with it. This likewise leads to a decrease of the number of waves in the field, but in a less interesting way than what happens when there is a random distribution of strengths. We shall therefore leave the "first" wave out of the picture and consider a statistically stationary state.

We shall first (in section 2) give a descriptive treatment of the solution in which we are interested, based on the results of a former publication³⁾.

²⁾ See K. O. FRIEDRICHS, Formation and Decay of Shock Waves, Commun. on Applied Mathem. 1, 211–257 (1948), and W. CHESTER, The Decay of Shock Waves, Quart. Journ. of Mech. and Applied Mathem. 5, 408–421 (1952). In these papers shock waves are considered the strength of which is not large, so that entropy variations can be neglected.

³⁾ J. M. BURGERS, Correlation Problems in a One-dimensional Model of Turbulence, these Proceedings 53, 247–260, 393–406, 718–742 (1950). In that paper attention was focused on the development in time of a wave system given at $t = 0$ as a statistical function of y (homogenous with respect to y in its statistical properties). In the present lines we consider the development with increasing y of a system of waves generated at $y = 0$, with statistical character homogeneous in time. It is probable that the method developed in the present paper can also be applied to the other problem.

In sections 3 and 4 this will be followed by a more rigorous treatment, starting from an exact solution of eq. (1) which has been given by other authors ⁴⁾. These methods give the rules governing the merging of successive waves. We must then attempt to deduce expressions for the chance that merging occurs, when the impulses follow each other in a random way and the only datum available is a frequency curve for their magnitudes.

The main problem is to find the mean interval between the remaining waves at a great distance from the origin. This is treated in sections 7–11 and it is attempted to construct an approximate solution. — Section 12 brings some additional details.

2. *Description of the system of waves produced by a series of successive impulses.* — We start from a result given in section 4 of reference 3) (*l.c.* p. 250), where a solution of eq. (1) is presented corresponding to a single impulse of magnitude $A^2/2$ introduced at the point y_0 at the instant t_0 . The resulting course of v with great approximation is given by a triangular wave, the triangle having base length $A(t-t_0)^{1/2}$, front height $A(t-t_0)^{-1/2}$ and constant area $A^2/2$ (see fig. 1). The steepness of the front

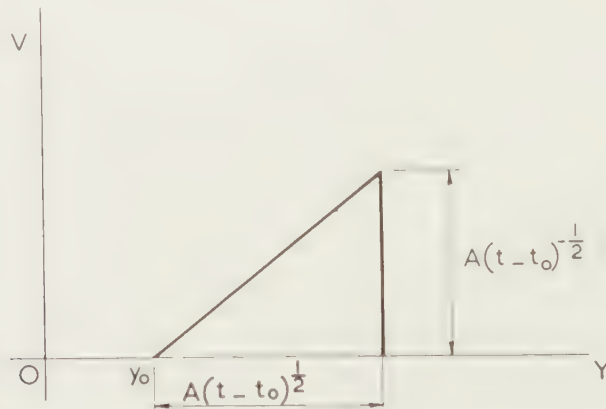


Fig. 1

is determined by the ratio A^2/v and the closeness of the approximation becomes greater as this ratio increases. As is easily seen the velocity of advance of the front is equal to one half the front height.

When a series of successive impulses of magnitudes $\bar{\omega}_1, \bar{\omega}_2, \bar{\omega}_3, \dots$ is introduced at the point $y=0$, at instants t_1, t_2, t_3, \dots , each impulse will lead to the appearance of a triangular wave and the various triangles are superposed on each other in the way indicated in fig. 2. For any given

⁴⁾ E. HOFF, Commun. on Pure and Applied Mathem. 3, 201–230 (1950), in particular p. 203. — J. D. COLE, Calif. Institute of Technology, private communication (1949).

instant t this figure is constructed by drawing a set of straight lines originating from $y=0$ and having slopes given by $1/(t-t_i)$; between these lines we draw vertical segments in such a way that a triangle with area

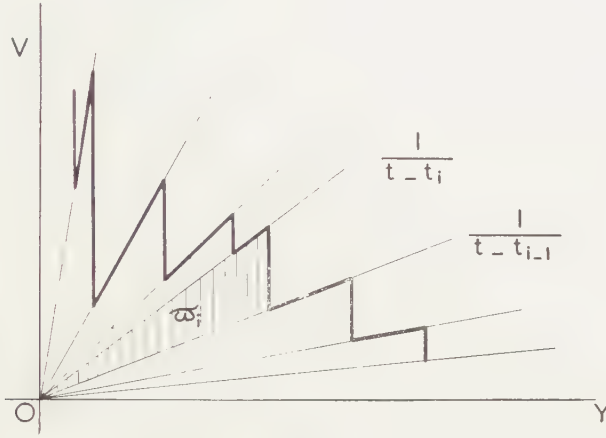


Fig. 2

$\tilde{\omega}_i$ is formed between the lines with slopes $1/(t-t_i)$ and $1/(t-t_{i-1})$. We denote the position of the corresponding vertical segment by ξ_i and have:

$$(2) \quad \xi_i = \left\{ \frac{2 \tilde{\omega}_i}{t_i - t_{i-1}} (t - t_i) (t - t_{i-1}) \right\}^{1/2}.$$

If it happens that all ξ_i thus determined satisfy the condition

$$(3) \quad \xi_i < \xi_{i-1},$$

as was assumed in fig. 2, the result is all right. The value of v at a point y satisfying

$$\xi_i < y < \xi_{i-1}$$

is then given by:

$$(4) \quad v = \frac{y}{t - t_{i-1}}.$$

If condition (3) is violated in one or more cases, a correction is necessary to which we shall come back below.

The diagram obtained gives a representation of the course of v at the instant t , as indicated by the broken heavy line. The development of the picture in course of time is determined by the rules: (1) all inclined lines turn to the right in conformity with the expression $1/(t-t_i)$ for their slopes; (2) every triangle must retain a constant area $\tilde{\omega}_i$.

We assume that new impulses are continually introduced at $y=0$ as time advances, which will give rise to new triangles, to be superposed at the left end of the curve. It will be supposed that these impulses follow each other in a random manner, but so that there is some statistical

pattern in their succession. An important special case is that in which the instants t_i follow each other with constant intervals T , while the magnitudes of the $\tilde{\omega}_i$ are random, subjected to a distribution to be specified afterwards.

We now come back to condition (3), which in general will not be satisfied everywhere. The velocities of advance of the various fronts will be unequal and there will appear cases in which the value of some $d\xi_i/dt$ exceeds that of $d\xi_{i-1}/dt$. In such a case the distance $\xi_{i-1} - \xi_i$ between the consecutive fronts decreases. It will become zero at the instant t given by:

$$(5) \quad t - t_i = (t_i - t_{i-2}) \frac{\tilde{\omega}_{i-1}/(t_{i-1} - t_{i-2})}{\tilde{\omega}_i/(t_i - t_{i-1}) - \tilde{\omega}_{i-1}/(t_{i-1} - t_{i-2})}.$$

It is convenient to write:

$$(6) \quad \tau_i = t_i - t_{i-1}; \quad \psi_i = \tilde{\omega}_i/\tau_i.$$

We then find:

$$(5a) \quad t - t_i = (\tau_i + \tau_{i-1}) \frac{\psi_{i-1}}{\psi_i - \psi_{i-1}},$$

and further, from (2):

$$(7) \quad \xi_i = \xi_{i-1} = \frac{1}{\psi_i - \psi_{i-1}} \left\{ 2 \tilde{\omega}_i \tilde{\omega}_{i-1} (\tilde{\omega}_i + \tilde{\omega}_{i-1}) \frac{\tau_i + \tau_{i-1}}{\tau_i \tau_{i-1}} \right\}^{1/2}.$$

The result will have sense only when $t - t_i$ is positive, which requires:

$$(8) \quad \psi_i > \psi_{i-1}.$$

In the general case of variable intervals it is, therefore, not the strength of the impulses alone which determines whether overtaking will occur, but strength divided by the preceding time interval, as represented by ψ_i . With constant intervals $\tau_i = T$ for all i formulae (5) and (7) simplify to:

$$(5b) \quad t - t_i = 2T \frac{\tilde{\omega}_{i-1}}{\tilde{\omega}_i - \tilde{\omega}_{i-1}}$$

$$(7a) \quad \xi_i = \xi_{i-1} = \frac{2 \{ \tilde{\omega}_i \tilde{\omega}_{i-1} (\tilde{\omega}_i + \tilde{\omega}_{i-1}) T \}^{1/2}}{\tilde{\omega}_i - \tilde{\omega}_{i-1}},$$

and the condition for overtaking becomes $\tilde{\omega}_i > \tilde{\omega}_{i-1}$.

As soon as two fronts have overtaken each other, we must count these two fronts as a single one; they will never separate again. From that instant onward we must leave out the instant t_{i-1} in our construction and no longer use the inclined line with the slope $1/(t - t_{i-1})$. We now work as if an impulse of strength $\tilde{\omega}_i + \tilde{\omega}_{i-1}$ had been introduced at the instant t_i , so that it succeeds the impulse $\tilde{\omega}_{i-2}$ introduced at t_{i-2} . The time interval corresponding to the combined impulse then is $\tau_i + \tau_{i-1}$.

A combined impulse after some time can merge with another impulse, and so on. This process will lead to a gradual decrease of the number of fronts.

We now summarize the rule for the construction of the diagram which

shall give the course of v at a given instant t . We proceed as has been indicated before; however, wherever we find a case with $\xi_i > \xi_{i-1}$, we take out the instant t_{i-1} and combine $\tilde{\omega}_i$ and $\tilde{\omega}_{i-1}$ into a single impulse, supposed to be introduced at the instant t_i . If we should find that the new value calculated for ξ_i would exceed ξ_{i-2} , or else, if it would be smaller than ξ_{i+1} , the process has to be repeated, until all cases which violated condition (3) have been eliminated. It can be shown that the result of this elimination is independent of the order in which it is carried out.

The following observation is of interest. We define time mean values of ψ_i and ψ_i^2 by means of:

$$(9a) \quad \bar{\psi} = (\sum \psi_i \tau_i) / (\sum \tau_i) = (\sum \tilde{\omega}_i) / (\sum \tau_i)$$

$$(9b) \quad \bar{\psi}^2 = (\sum \psi_i^2 \tau_i) / (\sum \tau_i).$$

In the process of merging the values of the $\tilde{\omega}_i$ and also those of the corresponding time intervals τ_i are added. Instead of ψ_i and ψ_{i-1} a new value of ψ_i is obtained, given by:

$$(10) \quad (\psi_i)_{\text{new}} = \frac{\psi_i \tau_i + \psi_{i-1} \tau_{i-1}}{\tau_i + \tau_{i-1}}.$$

It is easily seen that the mean value $\bar{\psi}$ is not affected by this process. However, it follows from the relation

$$(\psi_i)_{\text{new}}^2 (\tau_i + \tau_{i-1}) = \psi_i^2 \tau_i + \psi_{i-1}^2 \tau_{i-1} - (\psi_i - \psi_{i-1})^2 \frac{\tau_i \tau_{i-1}}{\tau_i + \tau_{i-1}},$$

that the mean value $\bar{\psi}^2$ decreases in consequence of each merging process. Hence the dispersion in the values of the ψ_i must decrease.

3. *Exact solution of equation (1).* — It has been shown independently by E. HOPF and by J. D. COLE⁴⁾ that eq. (1) can be reduced to a linear equation by means of the substitution:

$$(11) \quad v = -2\nu \frac{\partial}{\partial y} (\ln u).$$

Since the value of v given by this formula is not influenced by the multiplication of u with a factor depending on t alone, it is possible to determine u so that it satisfies the equation for heat flow or diffusion:

$$(12) \quad \frac{\partial u}{\partial t} = \nu \frac{\partial^2 u}{\partial y^2}.$$

A solution of eq. (12) adapted to our case is:

$$(13) \quad u = u_0 + \int_{t_0}^t d\theta \frac{1}{\sqrt{t-\theta}} \exp \left\{ \frac{-y^2}{4\nu(t-\theta)} + \frac{1}{2\nu} \int_{t_0}^{\theta} A(\theta') d\theta' \right\},$$

where u_0 is a (small) positive constant, while $A(\theta')$ is an arbitrary function of the auxiliary variable θ' . The lower limit of both integrals, t_0 , denotes

the instant since which the impulses have been introduced at $y=0$. In order to obtain an expression corresponding to the series of discontinuous impulses considered before, we must replace the integral with respect to θ' in the exponent by a "step function":

$$(14) \quad \sum_{t_0}^{\theta} \tilde{\omega}_i(t_i),$$

the summation to be extended over all t_i satisfying $t_0 < t_i < \theta$.

It will be evident that when ν is made smaller and smaller, the exponential function in (13) can become either excessively large (when the exponent is positive) or excessively small (when the exponent is negative). It follows that in the calculation of v with the aid of (11) we need only to consider the immediate neighbourhood of that value θ_m of θ , for which the expression

$$(15) \quad Z = \frac{-y^2}{2(t-\theta)} + \int_{t_0}^{\theta} A(\theta') d\theta'$$

in which y and t are given, has its largest maximum, provided that this maximum is positive ⁵⁾. The resulting value of v will then be:

$$(16) \quad v = -\frac{2}{u} \frac{\partial u}{\partial y} = \frac{y}{t-\theta_m}.$$

If all maxima of Z happen to be negative, the value of u will reduce to u_0 , that of $\partial u / \partial y$ to zero and we obtain $v=0$.

The correctness of the result given by (16) depends on the rate of change of the exponential function near the maximum. In general one can say that when the second derivative of Z at the largest maximum has a finite (that is, non-zero, and necessarily negative) value, the rate of decrease of the exponential function on both sides of the maximum will be so rapid, that no other value of θ than θ_m will give an appreciable contribution to the integral for u . However, when this second derivative would become very small, which can happen for large values of y (see below, section 12. B), the behaviour of the exponential function will be different and formula (16) must be replaced by a corrected expression in which neighbouring values of θ play a certain part.

It will easily be seen that even in the case of a continuous function $A(\theta')$ the value obtained for θ_m , when considered as a function of y for constant t (or as a function of t for constant y) can be *discontinuous* for certain values of y (or of t). This will occur when the maximum of Z which was the largest one for a given y , does not remain the largest maximum

⁵⁾ It may be that there are found two maxima of equal height for some value of y . A small change of y will then usually be sufficient to produce a difference. To avoid the necessity of considering cases with two equal maxima, we can assume that such a change is introduced. But we shall have to give attention to maxima of equal height in section 4, and in sections 7 and following.

when y changes, but at a certain instant is superseded by another maximum which from then onward will be the largest one. This will have the result that also v becomes discontinuous, so that a steep front will have developed in a certain portion of the v -curve.

When the integral in the expression (15) for Z is replaced by a step function as indicated by (14), a discontinuous behaviour of θ_m is always obtained and it is found that θ_m itself becomes a step function. Between any two successive points of discontinuity on the y -scale the value of θ_m will be constant and will be equal to the instant t_j at which the last impulse $\tilde{\omega}_j$ admitted into the sum (14) is introduced. Indeed, for values of θ_m slightly larger than t_j but below t_{j+1} , the sum does not change, but the term $-y^2/(t-\theta_m)$ becomes more negative, so that Z decreases and one drifts away from the maximum. One cannot expect, however, that the consecutive values of θ_m will completely reproduce the series of values t_j ; it is possible that certain t_j will not occur in the series of values of θ_m . As we shall see below, this indicates that two or more fronts have merged, in the way as described in section 2.

4. *Properties of the relation between θ_m and y .* — It can be shown that with increasing y (t being kept constant) the value of θ_m pertaining to the maximum of Z cannot increase, but must either remain constant or decrease. This holds both for an integral with a continuous function $A(\theta')$ and for the step function (14). In the latter case the proof is as follows.

According to the definition of θ_m we have:

$$(17) \quad \frac{-y^2}{2(t-\theta_m)} + \sum_{t_0}^{\theta_m} \tilde{\omega}_i > \frac{-y^2}{2(t-\theta')} + \sum_{t_0}^{\theta'} \tilde{\omega}_i,$$

for all $\theta' \neq \theta_m$. We take $\theta' > \theta_m$. The inequality (17) then is equivalent to:

$$(17a) \quad \frac{y^2(\theta' - \theta_m)}{2(t - \theta_m)(t - \theta')} > \sum_{\theta_m}^{\theta'} \tilde{\omega}_i.$$

When y increases and θ_m and θ' are kept constant, the latter inequality becomes stronger. Hence with increasing y and constant θ_m and θ' , the inequality (17) will remain valid for all $\theta' > \theta_m$. It follows that there can be no largest value of Z for any θ exceeding θ_m when y increases; the largest value of Z must occur either for the same θ_m or for a smaller value.

— It can be proved in a similar manner that when y decreases, the corresponding value of θ_m must either remain constant or must increase.

As a corollary we find that the height of the maximum decreases with increasing y . Let θ' , θ'' be the values of θ_m corresponding to y' , y'' , respectively, with $y'' > y'$ and consequently $\theta'' < \theta'$. We then have:

$$\frac{-y'^2}{2(t-\theta')} + \sum_{t_0}^{\theta'} \tilde{\omega}_i \geq \frac{-y'^2}{2(t-\theta'')} + \sum_{t_0}^{\theta''} \tilde{\omega}_i > \frac{-y''^2}{2(t-\theta'')} + \sum_t^{\theta''} \tilde{\omega}_i,$$

or:

$$(18) \quad Z' > Z''.$$

The converse naturally also holds.

With constant y it is possible to consider θ_m as a function of t . It is then found that with increasing t the value of θ_m must either remain constant or increase; with decreasing t the value of θ_m must remain constant or decrease.

We shall now prove that in the case where the step function (14) is used, the result given by (16) coincides with that obtained according to the procedure described in section 2. For this purpose we consider the step function which is found for θ_m as a function of y (t being kept constant). Let y' and y'' ($>y'$) be two consecutive points where θ_m changes discontinuously: at y' from $\theta_m=t_h$ to $\theta_m=t_k$; at y'' from $\theta_m=t_k$ to $\theta_m=t_l$; where $t_h > t_k > t_l$ (and thus $h > k > l$). We then have just to the left of y' :

$$(19a) \quad \frac{-y^2}{2(t-t_h)} + \sum_{t_0}^{t_h} \tilde{\omega}_i > \frac{-y^2}{2(t-t_k)} + \sum_{t_0}^{t_k} \tilde{\omega}_i;$$

and just to the right of y' :

$$(19b) \quad \frac{-y^2}{2(t-t_h)} + \sum_{t_0}^{t_h} \tilde{\omega}_i < \frac{-y^2}{2(t-t_k)} + \sum_{t_0}^{t_k} \tilde{\omega}_i.$$

Since the expressions occurring here are continuous functions of y , in which all other quantities are constants, it follows that:

$$(19c) \quad \frac{-y'^2}{2(t-t_h)} + \sum_{t_0}^{t_h} \tilde{\omega}_i = \frac{-y'^2}{2(t-t_k)} + \sum_{t_0}^{t_k} \tilde{\omega}_i.$$

and consequently:

$$(20) \quad y' = \left\{ \frac{2(\tilde{\omega}_{k+1} + \tilde{\omega}_{k+2} + \dots + \tilde{\omega}_h)}{t_h - t_k} (t - t_h) (t - t_k) \right\}^{1/2}.$$

Similarly:

$$(20a) \quad y'' = \left\{ \frac{2(\tilde{\omega}_{l+1} + \tilde{\omega}_{l+2} + \dots + \tilde{\omega}_k)}{t_k - t_l} (t - t_k) (t - t_l) \right\}^{1/2}.$$

These expressions are identical with the one given by (2) for ξ_i , provided we consider the impulses $(\tilde{\omega}_{k+1} + \dots + \tilde{\omega}_h)$ as merged into a single one, introduced at the instant t_h ; and the impulses $(\tilde{\omega}_{l+1} + \dots + \tilde{\omega}_k)$ as merged into a single one, introduced at the instant t_k , while the predecessor of this latter impulse was introduced at t_l . In the notation of section 2 we should write $\xi_h = y'$; $\xi_k = y''$ and the condition (3) will be satisfied, since we have $\xi_h < \xi_k$ with $h > k$.

To prove that no ξ_i is left out from the series which remains after the cases violating condition (3) have been eliminated by the procedure indicated in section 2, we start from the other side and assume that the proper series of values of the ξ_i has been constructed according to that procedure. Now choose a value of y satisfying $\xi_i < y < \xi_{i-1}$. Since (2) can be written (with j as general index):

$$\tilde{\omega}_j = \frac{\xi_j^2}{2(t-t_j)} - \frac{\xi_j^2}{2(t-t_{j-1})} \quad (\text{for all } j),$$

we have, for any $j < i$ ($j = i-1, i-2, \dots$, for which $\xi_j \geq \xi_{i-1} > y$):

$$\tilde{\omega}_j - \frac{y^2}{2(t-t_j)} + \frac{y^2}{2(t-t_{j-1})} > 0;$$

and for any $j \geq i$ ($j = i, i+1, i+2, \dots$, for which $\xi_j \leq \xi_i < y$):

$$\tilde{\omega}_j - \frac{y^2}{2(t-t_j)} + \frac{y^2}{2(t-t_{j-1})} < 0.$$

It follows that

$$(21) \quad (\tilde{\omega}_0 + \dots + \tilde{\omega}_{i-1}) - \frac{y^2}{2(t-t_{i-1})} > (\tilde{\omega}_0 + \dots + \tilde{\omega}_j) - \frac{y^2}{2(t-t_j)}$$

for all $j \neq i-1$. This proves that the quantity Z , calculated for the chosen value of y , has its largest value when $\theta_m = t_{i-1}$. According to (16) the value of v for this value of y will be equal to: $y/(t-t_{i-1})$, which is the same result as is found by the construction of section 2 (formula 4).

5. *Chance for the coalescence of two consecutive fronts, when the original impulses are introduced at constant time intervals.* — We suppose that impulses ω_i are introduced at $y=0$ at the instants $t=iT$, T being a constant. The magnitude of the impulses are subjected to a frequency function:

$$(22) \quad \varphi(\omega) d\omega$$

with integral equal to unity. There shall be no correlation between the magnitudes of consecutive impulses. When the impulse ω_i is larger than ω_{i-1} , the wave produced by it will overtake the preceding wave at the instant t determined by (5b). It appears from this expression that $t-t_i$ will be of the same order as T if the difference $\omega_i - \omega_{i-1}$ is of the same order as ω_i . Overtaking in this case would occur quite rapidly after the introduction of the impulse. The problem will be more interesting, however, when the process of overtaking and merging is dispersed over a much longer period. This requires the difference $\omega_i - \omega_{i-1}$ to be small; we shall therefore suppose that the frequency function (22) gives a distribution of values strongly concentrated around a mean value Ω ⁶⁾.

The point at which two waves will merge is given by (7a). With sufficient approximation we can replace the various ω_i occurring in the numerator by the mean value Ω , so that we obtain:

$$(23) \quad \xi_i = \xi_{i-1} = \frac{\sqrt{(2\Omega)^3 T}}{\omega_i - \omega_{i-1}}.$$

⁶⁾ If we do not start with impulses ω_i all closely concentrated about the mean value Ω , the merging process itself will finally lead to a situation in which the values of the ψ_i , defined in (6), will show only very slight fluctuations around the mean value Ω/T . Hence in a more general treatment, such a case might be taken as a starting point. It is, however, more convenient to start from the case defined in the text.

The merging will occur before a prescribed point y is reached, if $\xi_i < y$. This requires:

$$(24) \quad \omega_i - \omega_{i-1} > g,$$

where

$$(25) \quad g = \frac{1}{y} \frac{(\overline{2\Omega})^3 T}{y}.$$

If ω_i is given, the chance for an ω_{i-1} satisfying this condition will be:

$$\int_0^{\omega_i - g} d\omega' \varphi(\omega').$$

Since ω_i can have any value, the total chance for finding a pair ω_i, ω_{i-1} satisfying (24) is:⁷⁾

$$(26) \quad F = \int_0^\infty d\omega \varphi(\omega) \int_0^{\omega - g} d\omega' \varphi(\omega').$$

For infinite y , which makes $g \rightarrow 0$, the value of the double integral is $\frac{1}{2}$, whichever distribution function is chosen.

By way of example we take:

$$(27) \quad \varphi(\omega) = \frac{1}{\sigma\sqrt{2\pi}} \exp\left\{-\frac{(\omega - \Omega)^2}{2\sigma^2}\right\},$$

where σ^2 is the mean square deviation of ω from the mean value Ω . The value of F is then found to be:

$$F = \frac{1}{2} \left(1 - \operatorname{Erf} \frac{g}{2\sigma}\right).$$

In this case F becomes practically zero as soon as $g > 5\sigma$, or, having regard to (25), for values of y satisfying:

$$(28) \quad y < \frac{1}{5\sigma} \frac{(\overline{2\Omega})^3 T}{y}.$$

Almost no merging will occur before this limit is passed.

With the process of merging considered here we shall never come further than the elimination of half of the original waves. In reality the number of waves is further reduced by the merging of double waves with other single or with double waves; and in general by the merging of combined waves.

(to be continued)

⁷⁾ The supposition of a distribution function strongly concentrated around the mean value Ω ensures that $\varphi(\omega)$ will be practically zero already before ω itself is zero. Hence it is not necessary to be more precise in the lower limit of the first integral (which properly written should be g , instead of zero).

ON THE COALESCENCE OF WAVE LIKE SOLUTIONS OF A
SIMPLE NON-LINEAR PARTIAL DIFFERENTIAL EQUATION. II

BY

J. M. BURGERS

*(Mededeling No. 76 uit het Laboratorium voor Aero- en Hydrodynamica der Technische
Hogeschool te Delft)*

(Communicated at the meeting of November 28, 1953)

6. *Merging of three consecutive waves.* — Assume that three consecutive impulses satisfy the relation:

$$(29) \quad \omega_{i+1} > \omega_i + g > \omega_{i-1} + 2g,$$

with g given by (25). We know that this condition is sufficient to ensure that the wave produced by ω_i will overtake ω_{i-1} , and that ω_{i+1} will overtake ω_i , before the point y is reached. One of these two processes will occur first; let this be the first mentioned one. We then have in the field the wave ω_{i+1} with a corresponding time interval T , and the combined wave $\omega_i + \omega_{i-1}$ with the time interval $2T$. Since $\omega_{i+1} > \frac{1}{2}(\omega_i + \omega_{i-1})$, it follows that the wave ω_{i+1} will overtake the combined wave $\omega_i + \omega_{i-1}$; from (5) it can be found that this will occur at the instant:

$$t^* = iT + T \frac{3(\omega_i + \omega_{i-1})}{2\omega_{i+1} - \omega_i - \omega_{i-1}},$$

while the place where it occurs is determined by (7), which gives, with sufficient accuracy:

$$(30) \quad \xi^* = \frac{3\sqrt{(2\Omega)^3 T}}{2\omega_{i+1} - \omega_i - \omega_{i-1}}.$$

Since the denominator of the fraction exceeds $3g$, we find $\xi^* < y$. Hence the merging of ω_{i+1} with $\omega_i + \omega_{i-1}$ takes place before the point y is reached. — The same result is found when the merging of ω_{i+1} and ω_i would occur first, the combined wave then overtaking ω_{i-1} . Thus when three consecutive impulses satisfy the relation (29), the two smaller ones will be eliminated before the point y is reached, and no change is brought about in the calculation of the chance for the process of elimination as given in the preceding section.

However, it will be seen from (30) that in the case where $\omega_i > \omega_{i-1} + g$, but $\omega_{i+1} < \omega_i + g$, so that (29) does not fully hold, there is still the possibility that the wave ω_{i+1} will overtake the combined wave $\omega_i + \omega_{i-1}$ before the point y is reached. This will occur if:

$$(31a) \quad \omega_{i+1} > \frac{1}{2}(\omega_i + \omega_{i-1}) + \frac{3}{2}g.$$

A similar calculation shows that in the case where $\omega_{i+1} > \omega_i + g$, but $\omega_i < \omega_{i-1} + g$, so that (29) fails on the other side, the combined wave $\omega_{i+1} + \omega_i$ can overtake the single wave ω_{i-1} if

$$(31b) \quad \omega_{i-1} < \frac{1}{2}(\omega_i + \omega_{i+1}) - \frac{3}{2}g.$$

These two possibilities give a chance for the elimination of fronts, which is not covered by the formulae of the preceding section. To take account of them we must add to F the amount:

$$(32) \quad \left\{ \begin{aligned} F_1 = & \int_0^\infty d\omega \varphi(\omega) \int_0^{\omega-g} d\omega' \varphi(\omega') \int_{\omega_I}^{\omega+g} d\omega'' \varphi(\omega'') + \\ & + \int_0^\infty d\omega \varphi(\omega) \int_{\omega+g}^\infty d\omega' \varphi(\omega') \int_{\omega-g}^{\omega_{II}} d\omega'' \varphi(\omega''), \end{aligned} \right.$$

where $\omega_I = \frac{1}{2}(\omega + \omega') + 3/2g$, $\omega_{II} = \frac{1}{2}(\omega + \omega') - 3/2g$.

It will be evident, that to proceed in this way to more complicated cases, will require a difficult investigation of the various relations that can present themselves in groups of 4, 5, ... and more waves. This will not lead to a speedy method of calculation for the total chance for coalescence.

7. Reduction of the problem concerning the merging of successive waves to a geometrical problem. We consider a fixed point y and are interested in the waves which pass this point. We consequently shall treat θ_m as a step function of the variable t .

Let t' be a point where θ_m changes discontinuously from t_h to t_k with increasing t . It follows from section 4 that now $t_k > t_h$ and $k - h = m > 0$. We are interested in the values of m for the various steps.

Similarly to (19a) and (19c) we have:

$$(33) \quad \frac{-y^2}{2(t' - t_h)} + \sum_{t_h}^{t_h} \omega_i \geq \frac{-y^2}{2(t' - t_{h+n})} + \sum_{t_h}^{t_{h+n}} \omega_i,$$

with equality for $n = m$, and inequality for all other positive or negative values of n .

We put:

$$(34) \quad \omega_i = \Omega + \gamma_i,$$

where the γ_i are subjected to a distribution function with a mean spread small in comparison with the constant amount Ω . A convenient assumption is given by the distribution function

$$(35) \quad \varphi(\gamma) d\gamma = \frac{1}{\sigma \sqrt{2\pi}} \exp(-\gamma^2/2\sigma^2) d\gamma,$$

with $\sigma \ll \Omega$. We construct the "summation curve":

$$(36) \quad S_n = \sum_1^n \gamma_{h+i},$$

with $S_0=0$, and $S_j=-\gamma_h-\gamma_{h-1}-\dots-\gamma_{h+j+1}$ for $j<0$. We shall not apply the notation defined in (6), but will write:

$$(37) \quad t' - t_h = \tau, \text{ so that } t' - t_{h+n} = \tau - nT,$$

and we put

$$(38) \quad \frac{g^2 T}{2 \tau^2} = \Omega + \varepsilon.$$

The condition (33) can then be brought into the form:

$$(39) \quad Q(n) \equiv n\varepsilon + \frac{1}{2}n^2g \left(1 + \frac{\varepsilon}{\Omega}\right)^{3/2} \left(1 - \frac{nT}{\tau}\right)^{-1} \geq S_n,$$

with g given by (25). Again equality holds for $n=m$; for all other values of n the inequality is valid.

Evidently ε must be of the order of σ (or smaller). In general each point of discontinuity t' will have its own τ and ε . When these are known, $Q(n)$ is a known function of the integer n . The value of n can become very large, but it is probable nevertheless that $nT \ll \tau$. For most purposes we can then replace (39) by the approximation:

$$(40) \quad Q(n) \cong n\varepsilon + \frac{1}{2}n^2g \geq S_n.$$

In this form the condition requires that the parabola $Q(n)$ shall make contact with the "summation curve" in two points, one corresponding to $n=0$, the other one corresponding to $n=m$; and shall be situated above it everywhere else. Since the γ_i follow each other at random it must be expected that the summation curve will gradually deviate more and more from its mean value zero; the deviation can be expected to increase with the square root of $|n|$. However, if $|n|$ is large enough, the parabola will always reach higher than the summation curve.

The relations implied in the condition (40) can be illustrated by imagining that a parabola $Q(n)=\frac{1}{2}n^2g$ is cut out from a sheet of paper and is superposed on the plane in which the "summation curve" is drawn. We move the parabola, starting from a sufficient height and shifting it downward, until it contacts the summation curve in a single point and remains above it everywhere else. We then displace the parabola further, in such a way that it continually passes through the point of contact, until a second point of contact is obtained, while everywhere else the parabola still remains above the summation curve (see fig. 3a). This is always possible, for it is easily seen that if the displacement of the parabola, after the first point of contact had been made, occurred to the right, its right hand branch will come down, while the left hand branch will rise; hence contact on the left hand side will not be made, but a new point of contact will be obtained to the right of the first point.

We can then repeat the process, moving the parabola (its axis must always remain vertical) in such a way that it continually passes through the second point of contact, until a new point of contact, still further

to the right, is obtained. Then we take this point as fixed point and again go further to the right. In a similar way we can displace the parabola towards the left of the first point of contact. By this process we arrive at an infinite series of points which can be contacted by the parabola (see fig. 3b). These points are those where the maximum condition for the



Fig. 3a



Fig. 3b

quantity Z is fulfilled [accepting the approximation involved in making use of condition (40) instead of the rigorous condition (39)]. The distances between the successive points of contact obtained by this construction, give the values m indicating the number of waves which have merged together between the successive maxima.

In every case where twofold contact has been established in this way, the equation:

$$m\varepsilon + \frac{1}{2} m^2 g = S_k - S_h,$$

S_k here being the ordinate of the summation curve in the right hand point of contact and S_h the ordinate in the left hand point of contact, while $m=k-h$, determines the value of ε for that case. Then (38) gives τ for that same case.

The problem before us is to find the mean value of m for a given value of y . It is to be expected that with increasing y , which leads to smaller values of g and thus to flatter parabolas, the mean distance between the points of contact will become larger. A rough estimate can be obtained as follows. The two points of contact in general will be tops on approximately the same height above the mean level of the "summation curve" and the form of the parabola requires that this height shall be of the order $H = m^2 g / 8$. Now the probability to reach this height in $m/2$ steps γ_i , each step being subjected to the distribution function (35), is found to be:

$$\frac{1}{\sigma\sqrt{\pi m}} \exp\left(-\frac{H^2}{m\sigma^2}\right) = \frac{1}{\sigma\sqrt{\pi m}} \exp\left(-\frac{m^3 g^2}{64\sigma^2}\right).$$

Hence we may expect the mean value of m to be proportional to $(\sigma/g)^{2/3}$. The picture is too crude to lead to a satisfactory estimate of the numerical coefficient, but the appearance of the factor $(\sigma/g)^{2/3}$ is the basis of the similarity transformation given by eqs. (50) below.

8. *Expression for the probability of double contact in points with a given distance m .* — It is convenient to shift the picture in every case where twofold contact has been established, in such a way that the left hand point of contact is brought back to the origin. We shall then construct the “summation curve” always from this origin. By this procedure we shall arrive at an ensemble of possible summation curves, and our datum is not the shape of a particular curve, but a frequency function for all possible curves starting from the origin. The relevant frequency function must be deduced from the distribution function for γ_i , for which we use the expression (35).

We take a particular value of m and will investigate the possibility of contact in the points S_0 and S_m , where $S_0 = 0$, while S_m is situated between limits S_m and $S_m + dS_m$. We construct the parabola:

$$(41) \quad S_n = n\varepsilon + \frac{1}{2} n^2 g, \text{ with } \varepsilon = S_m/m - \frac{1}{2} mg,$$

passing through these points. We require that all points S_n of the summation curve, other than S_0 and S_m , shall lie below this parabola. A measure must be obtained for the probability of this situation.

It is of importance to observe that not every point of the “summation curve” can be a point of contact. Hence if we consider all possible summation curves starting from the same point as origin, there will be many cases in which a second contact point cannot be found, because the origin was no contact point. It follows that if we denote by $P(m)$ the probability for second contact at a given distance m from the origin, this probability will be small and also its sum with respect to all values of m from 1 to infinity will remain small compared with unity. Evidently this sum measures the probability that the origin shall be a contact point, so that we must have:

$$(42) \quad \sum_1^{\infty} P(m) = 1/\bar{m},$$

where \bar{m} is the mean distance between two successive contact points.

A second formula to find \bar{m} is:

$$(43) \quad \bar{m} = \left\{ \sum_1^{\infty} m P(m) \right\} / \left\{ \sum_1^{\infty} P(m) \right\}.$$

It follows that we must have:

$$(44) \quad \sum_1^{\infty} m P(m) = 1.$$

This equation can be used as a check on the calculations, at least as a check on the order of magnitude. It will be seen that in the further work

certain approximations must be introduced with the aid of adjustable factors; eq. (44) gives a condition which must be satisfied by these factors.

To attack our problem we first need an expression for the probability of any possible situation of the whole system of points provided one point is fixed at the origin. To avoid infinities we shall provisionally limit our system to $-N \leq n \leq +N$; further we shall write s_n for the ordinate of an arbitrary point, reserving capital letters S_n for the points on the parabola as determined by (41). The simultaneous distribution function for the whole system, assuming the distribution function (35) for the $\gamma_n = s_n - s_{n-1}$, can then be written in the form:

$$(45) \quad \frac{E}{(\sigma\sqrt{2\pi})^{2N}} ds_{-N} \dots ds_{-1} ds_{+1} \dots ds_N,$$

in which:

$$(45a) \quad E = \exp \left\{ -\frac{1}{2\sigma^2} \sum_{n=-N+1}^N (s_n - s_{n-1})^2 \right\},$$

with $s_0 = 0$.

In order to obtain a probability measure for all situations satisfying the condition $s_n \leq S_n$ with $n \neq 0$, $n \neq m$, we must integrate the expression (45) with respect to all s_n , with the exception of s_0 (which is zero) and of s_m (for which the value S_m has to be inserted), from $-\infty$ until S_n . We then arrive at a quantity depending exclusively on the value chosen for S_m and which has dS_m as a factor. The problem is to evaluate the integral and to obtain its limit for indefinitely increasing values of N .

The circumstance that no integration has to be effected with respect to s_0 and s_m and that these variables have fixed values, makes it possible to decompose E into three factors which can be integrated independently. These factors are defined as follows:

$$(45b) \quad E_I = \exp \left\{ -\frac{1}{2\sigma^2} \sum_1^m (s_n - s_{n-1})^2 \right\}$$

$$(45c) \quad E_{II} = \exp \left\{ -\frac{1}{2\sigma^2} \sum_{m+1}^N (s_n - s_{n-1})^2 \right\}$$

$$(45d) \quad E_{III} = \exp \left\{ -\frac{1}{2\sigma^2} \sum_{-N+1}^0 (s_n - s_{n-1})^2 \right\}.$$

9. *Investigation of the integral depending on E_{II} .* — We have to find the integral:

$$(46) \quad \int \dots \int \frac{ds_{m+1} \dots ds_N}{(\sigma\sqrt{2\pi})^{N-m}} \exp \frac{-\{(s_{m+1} - S_m)^2 + (s_{m+2} - s_{m+1})^2 + \dots + (s_N - s_{N-1})^2\}}{2\sigma^2}.$$

This integral can be obtained by means of the following procedure. We define a function $\psi_{m+1}(s_{m+1})$ by the conditions:

$$(47) \quad \psi_{m+1} = \begin{cases} \frac{1}{\sigma\sqrt{2\pi}} \exp \frac{-(s_{m+1} - S_m)^2}{2\sigma^2} \dots s_{m+1} < S_{m+1} \\ 0 \dots s_{m+1} > S_{m+1} \end{cases}$$

Next we define a series of functions $\psi_n(s_n)$, with $n=m+2, \dots, N$, by the algorithm:

$$(48) \quad \psi_n(s_n) = \begin{cases} \frac{1}{\sigma\sqrt{2\pi}} \int_{-\infty}^{+\infty} ds_{n-1} \psi_{n-1}(s_{n-1}) \exp \frac{-(s_n - s_{n-1})^2}{2\sigma^2} \dots s_n < S_n \\ 0 \dots s_n > S_n. \end{cases}$$

Finally we must calculate:

$$(49) \quad \int_{-\infty}^{s_n} ds_N \psi_N(s_N).$$

A direct calculation according to this procedure may be carried through for small values of m , although the work will be cumbersome. Since we are interested in the case where m takes large values, a more effective method must be sought, which, however, will involve some approximations.

It is convenient first to introduce a similarity transformation which will help us to obtain a proper picture of the order of magnitude of the various quantities. We write:

$$n = [n]n^* \quad ; \quad s = [s]s^*,$$

with similar expressions for m and S . The exponent of the e -function in (48) induces us to introduce the following relation between the factors $[n]$ and $[s]$:

$$[n] = [s]^2/\sigma^2,$$

while formula (41) for the parabolic boundary leads to the relation:

$$[s] = g[n]^2.$$

Solving we find:

$$[n] = \sigma^{2/3} g^{-2/3} \quad ; \quad [s] = \sigma^{4/3} g^{-1/3}.$$

For shortness we write:

$$(50a) \quad f = \left(\frac{g}{\sigma}\right)^{1/3} = \frac{(2\Omega)^{1/2} T^{1/6}}{(\sigma y)^{1/3}},$$

where use has been made of (25); we can make f as small as we please by choosing y sufficiently large (f is dimensionless, as will be seen when it is noticed that the dimensions of Ω and σ are $L^2 T^{-1}$). This has the consequence that the steps in the new variable n^* , which are equal to f^2 , will become very small.

The complete transformation, including that of ε , is now given by the formulae:

$$(50b) \quad \begin{cases} n = n^*/f^2 & ; & m = m^*/f^2 \\ s = s^*\sigma/f & ; & S_n = S_n^*\sigma/f & ; & \varepsilon = \varepsilon^*\sigma f. \end{cases}$$

Equation (41) then takes the form:

$$(41a) \quad S_{n^*}^* = n^* \varepsilon^* + \frac{1}{2} n^{*2},$$

while formula (48) becomes:

$$(51) \quad \psi_{n^*} = \begin{cases} \frac{1}{f\sqrt{2\pi}} \int_{-\infty}^{+\infty} ds' \psi_{n'}(s') \exp \frac{-(s^* - s')^2}{2f^2} \dots s^* < S_{n^*}^* \\ 0 \dots \dots \dots s^* > S_{n^*}^* \end{cases}$$

where we have written s^* for $s_{n^*}^*$, n' for $n^* - f^2$ and s' for the variable corresponding to n' .

The smallness of f has the consequence that the difference between the functions ψ_{n^*} and $\psi_{n'}$ will be small. Hence if we write down the relation:

$$(51a) \quad \psi_{n^*}(s^*) - \psi_{n'}(s^*) = \frac{1}{f\sqrt{2\pi}} \int_{-\infty}^{+\infty} ds' \{\psi_{n'}(s') - \psi_{n'}(s^*)\} \exp \frac{-(s^* - s')^2}{2f^2},$$

it is attractive to construct an approximation by making use of the method proposed by KOLMOGOROFF⁸⁾. We consider ψ as a function of two continuous variables n^* and s^* , and put:

$$\begin{aligned} \psi_{n^*}(s^*) - \psi_{n'}(s^*) &= f^2 \frac{\partial \psi}{\partial n^*}; \\ \psi_{n'}(s') - \psi_{n'}(s^*) &= (s' - s^*) \frac{\partial \psi}{\partial s^*} + \frac{(s' - s^*)^2}{2} \frac{\partial^2 \psi}{\partial s^{*2}}. \end{aligned}$$

Relation (51a) is then transformed into the following partial differential equation:

$$(52) \quad \frac{\partial \psi}{\partial n^*} = \frac{1}{2} \frac{\partial^2 \psi}{\partial s^{*2}}.$$

This equation must be used in conjunction with the boundary conditions:

$$(53a) \quad \psi(n^*, s^*) = 0 \text{ for } s^* \text{ reaching the limit determined by (41a);}$$

$$(53b) \quad \psi = \frac{1}{\sigma\sqrt{2\pi}} \exp \frac{-(s^* - S_{m^*}^*)^2}{2f^2} \text{ for } n^* = m^* + f^2.$$

Properly speaking the algorithm defined by (51) does not give a value zero for ψ on the boundary itself, at least not at points near the beginning. The immediate application of the "diffusion equation" (52) from the start will give too large a loss of "material" and cause an unwarranted loss of probability in the final result. It would be more correct to work out a number of steps (say, five) with the aid of the original formula (51) and to use the diffusion equation (52) afterwards. Since the evaluation of the integrals required by (51) already becomes troublesome with the second step, this has been omitted and it is attempted to make up for the inaccuracy by introducing a slight change in the second boundary condition, for which the form (55b) will be taken instead of (53b). In (55b) the quantity n_0 is supposed to be equal to a few times f^2 , so that the boundary condition is applied, not at the first step, but at a later one; the

⁸⁾ A. KOLMOGOROFF, Ueber die analytischen Methoden in der Wahrscheinlichkeitsrechnung, Mathem. Annalen **104**, 415-458 (1931).

coefficient before the exponential function in (55b) has been chosen so that until that step there is no loss of "material through the boundary" and thus no loss of probability. It is assumed that the value of n_0 can be adjusted later on.

In the following lines we shall drop the asterisk with the transformed variables. It is convenient to change the signs of s and S and to consider the field between the (reflected) boundary and $+\infty$. Finally we shall diminish the values of S by S_m and those of n by m . The differential equation is not affected and will now be written:

$$(54) \quad \frac{\partial \psi}{\partial n} = \frac{1}{2} \frac{\partial^2 \psi}{\partial s^2},$$

while the boundary conditions are taken in the forms:

$$(55a) \quad \psi = 0 \text{ for } s = -(m + \varepsilon) n - \frac{1}{2} n^2;$$

$$(55b) \quad \psi = \frac{f}{\sigma \sqrt{2\pi n_0}} \exp \frac{-s^2}{2n_0} \text{ for } n = n_0.$$

Having arrived so far we still have in front of us a technical difficulty connected with the circumstance that the boundary condition (55a) refers to a curved line in the n, s -plane. We shall therefore introduce a further approximation and replace the curved line by a straight line $s = -an$. The value of a likewise will be adjusted later ⁹⁾.

⁹⁾ It does not make much difference if the boundary is approximated by a chain of several straight segments. This can be shown as follows:

From eq. (48) we deduce the relation:

$$\int_{-\infty}^{+\infty} ds_n \psi_n < \int_{-\infty}^{+\infty} ds_{n-1} \psi_{n-1}.$$

The same result is obtained from the diffusion equation, since there is always a loss of "material" at the boundary. Hence we can calculate an upper limit for the integral (57) by applying (56) with a value of n corresponding to the first corner of the chain. Since moreover:

$$\text{Erf} \frac{(s+an)\sqrt{n_0}}{\sqrt{2n(n-n_0)}} < \frac{2}{\sqrt{\pi}} \frac{(s+an)\sqrt{n_0}}{\sqrt{2n(n-n_0)}} \cong \frac{\sqrt{2n_0}}{\sqrt{\pi}} \frac{s+an}{n},$$

we find:

$$\begin{aligned} \int_{-an}^{\infty} ds \frac{\sigma}{f} \psi(s) &< \frac{\sqrt{n_0}}{\pi n^{3/2}} \int_{-an}^{\infty} ds (s+an) \exp\left(-\frac{s^2}{2n}\right) = \\ &= \frac{\sqrt{n_0}}{\pi n^{3/2}} \left\{ n \exp\left(-\frac{a^2 n}{2}\right) + \sqrt{\frac{\pi}{2}} a n^{3/2} \left(1 + \text{Erf} a \sqrt{\frac{n}{2}}\right) \right\}, \end{aligned}$$

which in its turn is smaller than:

$$\frac{2\sqrt{n_0}}{\sqrt{2\pi}} \left\{ a + \frac{1}{\sqrt{2\pi n}} \exp\left(-\frac{a^2 n}{2}\right) \right\}.$$

This does not differ much from the result given by (58), which can be approximated by

$$2a \sqrt{n_0/2\pi}.$$

The solution of eq. (54) with the proposed boundary condition is:

$$(56) \quad \psi = \frac{f}{\sigma\sqrt{2\pi n}} \exp \frac{-s^2}{2n} \operatorname{Erf} \frac{(s+an)\sqrt{n_0}}{\sqrt{2n(n-n_0)}}.$$

In this expression we must substitute $n=Nf^2$ and calculate the integral (49). In consequence of the similarity transformation this integral takes the form:

$$(57) \quad \int_{-an}^{\infty} ds \frac{\sigma}{f} \psi(s) = \frac{1}{\sqrt{2\pi n}} \int_{-an}^{\infty} ds \exp \frac{-s^2}{2n} \operatorname{Erf} \frac{(s+an)\sqrt{n_0}}{\sqrt{2n(n-n_0)}}.$$

A large value of N will also make n rather large. It is evident that the domain in which the exponential function gives a contribution extends to values of s of the order $n^{\frac{1}{2}}$. It is possible, therefore, to replace the Error-function by $\operatorname{Erf} a\sqrt{n_0}/2$, and it follows that the value of the integral becomes:

$$(58) \quad \operatorname{Erf} a \sqrt{n_0}/2.$$

Since this result is independent of n , it at once represents the limiting value for $N \rightarrow \infty$.

It will be evident that a similar procedure can be applied for the calculation of the integral depending on E_{III} . If we change the signs of s and S , and also that of n , the boundary of the domain will be:

$$(59) \quad s = \varepsilon n - \frac{1}{2}n^2,$$

In the more important cases we can expect ε to be negative. We shall replace the parabola by the straight line $s = -a'n$. The result of the integration will then be:

$$(60) \quad \operatorname{Erf} a' \sqrt{n_0}/2.$$

The approximations applied here are based on the assumption that a and a' are positive quantities, so that the boundary in both cases is a "receding" one.

(to be continued)

HYDRO- AND AERODYNAMICS

ON THE COALESCENCE OF WAVE LIKE SOLUTIONS OF A SIMPLE NON-LINEAR PARTIAL DIFFERENTIAL EQUATION. III

BY

J. M. BURGERS

(Mededeling No. 76 uit het Laboratorium voor Aero- en Hydrodynamica der Technische Hogeschool te Delft)

(Communicated at the meeting of November 28, 1953)

10. *Investigation of the integral depending on E_I .* — Provisionally it will be supposed that the similarity transformation has not yet been carried out. The integral to be calculated can be written:

$$(61) \quad \int \dots \int \frac{ds_1 \dots ds_{m-1}}{(\sigma\sqrt{2\pi})^m} \exp \left\{ -\frac{1}{2\sigma^2} \sum_1^m (s_n - s_{n-1})^2 \right\},$$

in which $s_0=0$ and $s_m=S_m$. We introduce new variables x_n defined by:

$$(62) \quad s_n = x_n + (n/m)S_m;$$

we then obtain $x_0=x_m=0$ and the boundary of the field is determined by $X_n = -\frac{1}{2}n(m-n)g$. We further have:

$$\begin{aligned} \sum (s_n - s_{n-1})^2 &= \sum (x_n - x_{n-1})^2 + S_m^2/m = \\ &= \{x_1^2 + (x_2 - x_1)^2 + \dots + (x_{m-1} - x_{m-2})^2 + x_{m-1}^2\} + S_m^2/m. \end{aligned}$$

The factor $\exp(-S_m^2/2m\sigma^2)$ can be taken before the integral signs. Again we define:

$$(63) \quad \psi_1(x_1) = \begin{cases} \frac{1}{\sigma\sqrt{2\pi}} \exp \frac{-x_1^2}{2\sigma^2} & \dots x_1 < X_1 \\ 0 & \dots x_1 > X_1, \end{cases}$$

and

$$(64) \quad \psi_n(x_n) = \begin{cases} \frac{1}{\sigma\sqrt{2\pi}} \int_{-\infty}^{+\infty} dx_{n-1} \psi_{n-1}(x_{n-1}) \exp \frac{-(x_n - x_{n-1})^2}{2\sigma^2} & \dots x_n < X_n \\ 0 & \dots x_n > X_n. \end{cases}$$

The last function to be calculated in this way will be $\psi_{m-1}(x_{m-1})$; having obtained this function we must find the integral:

$$(65) \quad \frac{\exp(-S_m^2/2m\sigma^2)}{\sigma\sqrt{2\pi}} \int dx_{m-1} \psi_{m-1}(x_{m-1}) \exp \frac{-x_{m-1}^2}{2\sigma^2}.$$

Owing to the symmetrical character of the exponential function and the boundary conditions with respect to the x_n we may, however, proceed

in a slightly different way and work from both ends towards the centre. Assuming for convenience that m (which in the important cases is a large number) is odd and writing $m = 2M + 1$, we work from the left hand side until $\psi_M(x_M)$:¹⁰⁾

$$\psi_M(x_M) = \frac{1}{\sigma\sqrt{2\pi}} \int dx_{M-1} \psi_{M-1}(x_{M-1}) \exp \frac{-(x_M - x_{M-1})^2}{2\sigma^2}.$$

On the right hand side we start from:

$$\psi_{2M}(x_{2M}) = \frac{1}{\sigma\sqrt{2\pi}} \exp \frac{-x_{2M}^2}{2\sigma^2},$$

and work backwards until the function:

$$\psi_{M+1}(x_{M+1}) = \frac{1}{\sigma\sqrt{2\pi}} \int dx_{M+2} \psi_{M+2}(x_{M+2}) \exp \frac{-(x_{M+1} - x_{M+2})^2}{2\sigma^2}.$$

Evidently ψ_{M+1} will be the same function of x_{M+1} as ψ_M is of x_M ; we shall write $\psi(x')$, $\psi(x)$ for these functions, respectively. We then still must calculate the double integral:

$$(66) \quad \frac{\exp(-S_m^2/2m\sigma^2)}{\sigma\sqrt{2\pi}} \int dx \int dx' \psi(x) \psi(x') \exp \frac{-(x-x')^2}{2\sigma^2}.$$

We now introduce the similarity transformation and the approximation by means of the diffusion equation in order to obtain the function $\psi(x)$. We also change the signs of x and X , so that—in the new variables—the boundary is given by:

$$(67) \quad X_n = +\frac{1}{2}n(m-n).$$

Instead of this curved boundary, which we need only in the domain $0 < n < M$, we use the straight line $x = bn$ (the parabola thus is replaced by an isosceles triangle). The diffusion equation has the form (54) and we arrive at:

$$(68) \quad \psi(x) = \frac{f}{\sigma\sqrt{2\pi M}} \exp \frac{-x^2}{2M} \operatorname{Erf} \frac{(x-bM)\sqrt{n_0}}{\sqrt{2M(M-n_0)}}.$$

In this expression x and M are of normal order of magnitude, whereas n_0 is of the order of f^2 and thus is very small. We shall approximate the Error-function and write:

$$(68a) \quad \psi(x) = \frac{f\sqrt{n_0}}{\pi\sigma M^{3/2}} (x-bM) \exp \frac{-x^2}{2M}.$$

It is then necessary to calculate the following integral (in which also S_m and m occurring in the exponential function before the integral signs have

¹⁰⁾ To save space the domain in which $\psi = 0$ has not been indicated in the following formulae.

been subjected to the similarity transformation: $S_m = \sigma f^{-1} S^*$, $m = f^{-2} m^*$, the asterisks afterwards being omitted):

$$(69) \quad \frac{1}{\sigma \sqrt{2\pi}} \exp\left(\frac{-S^2}{2m}\right) \cdot \frac{n_0}{\pi^2 M^3} \int_{bM}^{\infty} dx \int_{bM}^{\infty} dx' (x - bM) (x' - bM) \exp\left\{ -\frac{x^2 + x'^2}{2M} - \frac{(x - x')^2}{2f^2} \right\}.$$

Since the quantity $(x - x')^2$ in the exponential function is divided by the small quantity $2f^2$, the difference between x and x' must be small in order to give an appreciable contribution. The following transformation is convenient:

$$x = bM + r \cos\left(\frac{\pi}{4} + \vartheta\right) \quad ; \quad x' = bM + r \sin\left(\frac{\pi}{4} + \vartheta\right);$$

we then use r and ϑ as integration variables. It will be seen that ϑ can take values of order f only; hence in the less sensitive terms it can be considered as a constant (equal to zero) and the integration with respect to ϑ can be carried out immediately. This leaves us with:

$$\frac{1}{\sigma \sqrt{2\pi}} \exp\left(\frac{-S^2}{2m}\right) \cdot \frac{fn_0}{2\pi^{3/2} M^3} \int_0^{\infty} dr r^2 \exp\left(-\frac{(r + \varrho)^2}{2M}\right),$$

where ϱ has been written for $bM/\sqrt{2}$. The final result is ¹¹⁾:

$$(70) \quad \frac{1}{\sigma \sqrt{2\pi}} \exp\left(\frac{-S^2}{2m}\right) \frac{fn_0}{\pi(2M)^{3/2}} B,$$

where we have written:

$$(71) \quad B = (1 + 2\beta^2) (1 - \text{Erf } \beta) - \frac{2}{\sqrt{\pi}} \beta \exp(-\beta^2),$$

with $\beta = b\sqrt{M}$, while M is practically equal to $m/2$.

11. The frequency function for m . — The results of the integrations carried out in sections 9 and 10 make it possible to write down a measure for the probability that there shall be twofold contact with a distance m between the contact points, the value of S_m being situated between prescribed limits S and $S + dS$, while all other points of the summation curve are situated below the parabola determined by the contact points. This quantity is given by the product of the expressions (58), (60) and (70), multiplied by the differential dS_m or dS , which in the transformed variables must be expressed as $\sigma f^{-1} dS$. We obtain:

$$(72) \quad \frac{dS}{\sqrt{2\pi}} \exp\left(\frac{-S^2}{2m}\right) \frac{n_0}{\pi m^{3/2}} B (\text{Erf } a \sqrt{n_0/2}) (\text{Erf } a' \sqrt{n_0/2}).$$

¹¹⁾ It has been checked that almost the same result is obtained by working exclusively from the left hand side, having regard to the circumstance that the boundary of the domain consists of two straight segments, and calculating the integral (65). The only difference is that fn_0 in (70) is replaced by $f^2 n_0^\dagger$. The two quantities would be the same if $n_0 = f^2$. I do not, however, consider this as a valid argument for the determination of n_0 , in view of the several approximations introduced. The calculation carried out in section 11 leads to $n_0 = 3.8 f^2$.

In this formula a is the inclination of the straight line replacing the parabola (55a), which, if we express ε with the aid of S ($S = m\varepsilon + \frac{1}{2}m^2$), can be written: $s = -(\frac{1}{2}m + S/m)n - \frac{1}{2}n^2$;

a' is the inclination of the straight line replacing the parabola (59), which in the same way can be written: $s = -(\frac{1}{2}m - S/m)n - \frac{1}{2}n^2$;

b (which occurs in B) is the inclination of the straight line replacing one half of the parabola (67), which is independent of S . — All quantities in (72) are transformed variables: the true value of the distance between the contact points in these variables is given by m/f^2 .

We now must integrate over S . We have no exact expressions for a and a' , but we assume

$$(73) \quad a = \chi \cdot (\frac{1}{2}m + S/m) \quad ; \quad a' = \chi \cdot (\frac{1}{2}m - S/m),$$

where χ can be adjusted later. The exponential factor in (72) makes it unnecessary for S to take large values; moreover, the approximations used in section 9 were based on the supposition that both a and a' are positive quantities. It follows that we must take as integration limits: $S = -\frac{1}{2}m^2$, $S = +\frac{1}{2}m^2$; and that we can approximate the product of the two Error-functions by $(2n_0/\pi)\chi^2 (\frac{1}{4}m^2 - S^2/m^2)$. The result of the integration gives us the quantity $P(m)$ defined in section 8:

$$(74) \quad P(m) = \frac{2\chi^2}{\pi^2} n_0^2 B \cdot B_0/m^2,$$

where

$$(75) \quad B_0 = (2\beta_0^2 - 1) \operatorname{Erf} \beta_0 + \frac{2}{\sqrt{\pi}} \beta_0 \exp(-\beta_0^2),$$

with $\beta_0 = (m/2)^{3/2} = 0,353 m^{3/2}$.

The order of magnitude of P is determined by the factor n_0^2 , which is of the order f^4 . Since, as mentioned before, the true value of m is equal to mf^{-2} , when expressed in the variables used here, equation (43) takes the form:

$$(76) \quad \bar{m} = \frac{1}{f^2} \frac{\int_0^\infty dm B \cdot B_0/m}{\int_0^\infty dm B \cdot B_0/m^2}.$$

Equation (44) becomes

$$(77) \quad \frac{2\chi^2}{\pi^2} \frac{n_0^2}{f^4} \int_0^\infty dm B \cdot B_0/m = 1.$$

As adjustable numerical quantities we had introduced $n_0 f^2$: the ratio of b to $\frac{1}{2}m$ (compare 67); and χ . A plausible value for b would seem to be $b = m/3$, which makes $\beta = m^{3/2}/3\sqrt{2} = 0,235 m^{3/2}$. A somewhat crude numerical calculation then gives:

$$\int_0^\infty dm B \cdot B_0/m = 0,192 \quad ; \quad \int_0^\infty dm B \cdot B_0/m^2 = 0,106.$$

A plausible assumption for χ may be $\chi=4/3$. Equation (77) can now be used to fix a value for n_0/f^2 ; this comes out as:

$$n_0/f^2 = 3,8,$$

which is not unreasonable.

The mean value \bar{m} as given by (76) is independent of our choice for χ and n_0 . One finds:¹²⁾

$$(78) \quad \bar{m} = 1,8 f^{-2} = 0,9 \frac{(\sigma y)^{2/3}}{\Omega T^{1/3}}.$$

12. *The fluctuations in the value of v and the influence of the coefficient ν in eq. (1). Final remarks.* — Now that the main result has been obtained, it may be of interest to make two observations on the course of the function v .

A. — According to formula (16) the value of v is given by:

$$v = \frac{y}{t - \theta_m}.$$

Sudden jumps in the value of v occur whenever θ_m changes discontinuously. As was mentioned in the beginning of section 7, these changes are from a value t_h to a value t_k , differing by $(k-h)T = mT$. Since in general mT can be considered as small in comparison with $t - t_h$, the mean amplitude of the resulting jumps in v will be determined by:

$$\Delta v \cong \frac{yT}{(t - t_h)^2} \bar{m}.$$

For $t - t_h$ we use the approximate value determined by (37) and (38); we then obtain:

$$(79) \quad \Delta v \cong \frac{2\Omega}{y} \bar{m}.$$

Having regard to formula (78) it follows that the amplitude of the jumps decreases proportionally with $y^{-1/3}$.

B. — In all our considerations the value of the coefficient ν in eq. (1) did not play a part, save that it had to be extremely small. However, once a definite value of ν has been chosen, it is possible to find values of y for which the approximation (16) does not hold. Indeed, this approximation is based on the supposition that the second derivative of Z is not a very small quantity. The second derivative of Z in a region where no term is added to or taken away from the sum over the $\tilde{\omega}_i$, is given by:

$$\frac{d^2 Z}{d\theta^2} = \frac{y^2}{2(t - \theta)^3},$$

¹²⁾ It may be observed that if we insert the limiting value (28) for y , below which practically no merging should occur, we find $\bar{m} = 0,6$. This indeed means that practically no merging will have occurred, although it must be kept in mind that the calculations leading to (78) are valid only when \bar{m} is large compared with unity.

or, when again use is made of (37) and (38):

$$(80) \quad \frac{d^2 Z}{d\theta^2} \sim \frac{1}{y} \left| \frac{\partial \bar{G}}{\partial T^3} \right|.$$

This quantity can be made as small as we like by increasing y sufficiently. It follows that the variation of Z may become too slow to permit us to concentrate on the single value θ_{cr} . The resulting value of r must then be obtained from a more complicated expression. We must expect that in such cases the value of r will not show the discontinuities we had found before, but a gradual change instead.

The scale for y appearing here is of the order $\Omega^{2+T^{1-r-1}}$. This scale is wholly independent of the scale which determines the merging of waves as considered in sections 5-11 and which depends on $\Omega^2 = T^{1-\sigma^{-1}}$. Hence by playing around with σ and r (which have the same dimensions, *viz.* $L^2 T^{-1}$) we can make either the merging process, or the viscous friction preponderant.

C. — If one replaces the system of discrete impulses by the action of a continuous "impressed force" at the origin, the analysis must start from a consideration of the exponent in formula (13). It is to be expected that this will lead us to the problem of a parabola tangent to the integral curve

$$\int_{\theta_0}^{\theta} A(\theta') d\theta'$$

in two points, the mean distance between these points again being the quantity to be found. We shall then need certain statistical data concerning the function $A(\theta')$, for instance its mean value

$$\overline{A(\theta')}$$

and the correlation function for the fluctuations:

$$\overline{\{A(\theta') - \bar{A}\} \{A(\theta' + \tau) - \bar{A}\}}.$$

D. — A problem of interest might be to study the gradual decrease of $\overline{\psi^2}$ with increasing y , according to what has been mentioned at the end of section 2, where ψ is the quantity defined in (6). Also the "spectrum" of the remaining waves could be investigated.

OCCURRENCE OF PREFERRED ORIENTATIONS ON DECOMPOSITION OF KCl-NaCl MIX-CRYSTALS

BY

W. G. BURGERS AND G. W. TICHELAAR

(Laboratory for Physical Chemistry, Technical University, Delft, Holland)

(Communicated at the meeting of November 28, 1953)

Summary

As appeared from an X-ray investigation, the ageing of single crystals of supersaturated KCl-NaCl solid solutions gives rise to preferred orientations of the lattice of the equilibrium phases. Some of the diffraction patterns are described and the relation of the preferred orientation to the orientation of the parent single crystal is indicated.

§ 1. *Introduction*

A continuous series of substitutional mix-crystals crystallises from the melt in the system KCl-NaCl. These mix-crystals decompose at lower temperatures into a KCl-rich- and a NaCl-rich phase. This behaviour is described in the phase-diagram of fig. 1; the solubility gap was determined

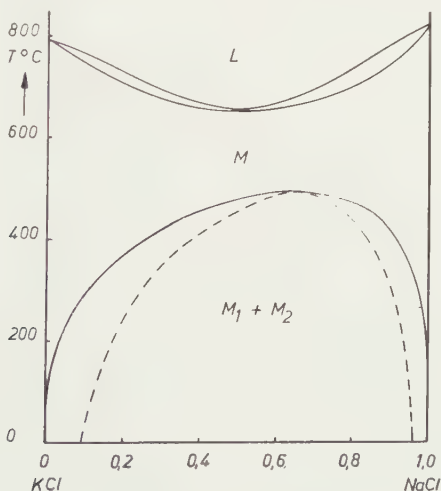


Fig. 1. Phase-diagram of the system KCl-NaCl.

by NACKEN (1918) and again recently in this laboratory by BUNK (1953). The upper consolute temperature is about 500° C; at room temperature the equilibrium phases are pure KCl and pure NaCl.

Single crystals can be grown by slowly cooling the melt. If kept in a dry atmosphere, the mix-crystals remain homogeneous almost indefinitely at room temperature; in a humid atmosphere, however, they decompose quickly into the component phases, as is shown by the misty appearance of the originally lucid crystals. Thermal decomposition can be brought about by heating at temperatures below the solubility curve for various times. The process can be followed optically by observing the progressing opaqueness under the ultramicroscope (EITEL (1918)) or by measurement of the extinction of incident light (SCHEIL and STADELMAIER (1952)). Although the latter investigation yields data about the rate of decomposition as a function of temperature and composition, it gives only some general indication about the atomic processes causing the decomposition. SCHEIL and STADELMAIER concluded, from a comparison of the activation energy for decomposition, as deduced from their measurements, with that found for the ionic conductivity of KCl and NaCl that the necessary diffusion takes place via defect lattice points only, by displacement of the cations. HYVÖNEN (1952) measured the evolution of heat during the ageing of KCl-NaCl solid solutions at room temperature and slightly higher temperatures. From the time dependence of the effect he concluded that two superposed ageing processes occur: a relaxation process obeying an exponential law of decay, probably due to re-arrangement of short range order, followed by a slowly increasing process, probably due to nucleation.

§ 2. *Experimental*

In the course of the investigation of the system KCl-NaCl carried out in this laboratory, we studied the decomposition of metastable single crystals by means of X-rays. It appeared that, depending on the way the decomposition was brought about, either at room temperature by the influence of water vapour, or by heat treatment, various pronounced and reproducible preferred orientations of the terminal phases could be produced. Also, however, less pronounced orientations were observed, intermediate between the orientations mentioned before. Although at this moment the investigation is still in progress, we like to show a few preliminary results.

Single crystals were grown by slowly cooling the melt in a porcelain crucible. After keeping the solidified mass at 600° C for at least 10 hours (to remove possible coring by diffusion), the homogeneous solid solution was quenched by taking the crucible out of the oven and removing the crystal as quickly as possible. It usually broke up into parts, some of which contained single crystals, from which thin platelets could be split off easily. With these plates (about $3 \cdot 3 \cdot 0.5$ mm) the X-ray investigation was made. Fig. 3, which is a Laue-photograph of such a metastable mix-crystal, shows that good single crystals could be obtained in this way.

Most of our work has been carried out with crystals containing 60 mole %

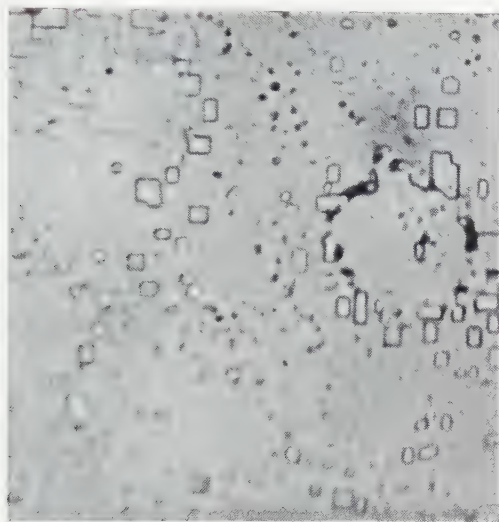


Fig. 2. Microphotograph of a cube face of a metastable mix-crystal (20 % NaCl) kept under normal atmospheric conditions ($\times 300$).

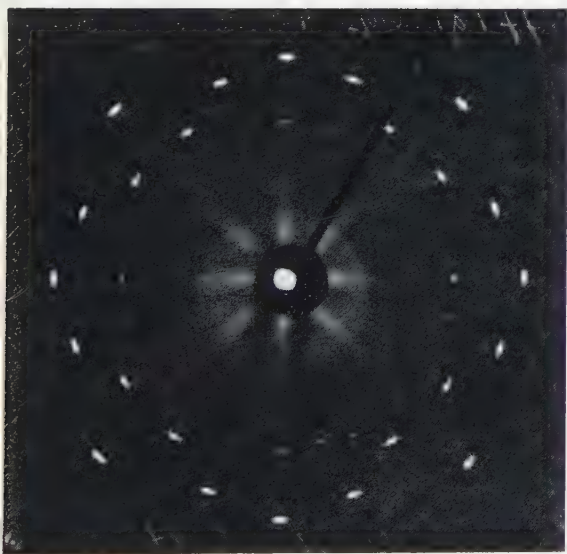


Fig. 3. Kept at room temperature in a dry atmosphere, W radiation.

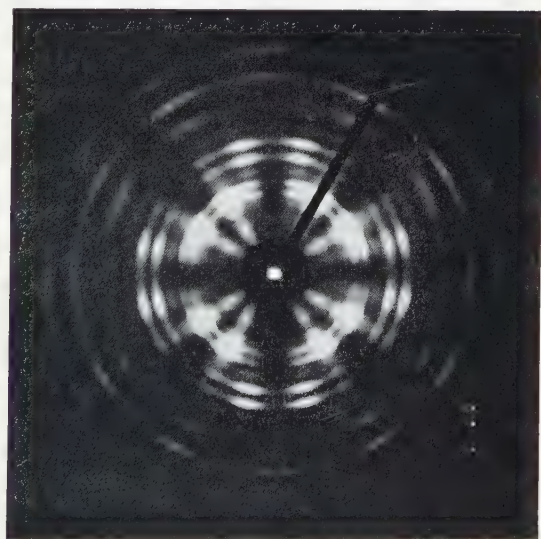


Fig. 4. Kept at room temperature under normal atmospheric conditions, Mo-K radiation.

Fig. 3-8. Laue-photographs of metastable mix-crystals (60 % NaCl) quenched to room-temperature and kept under different conditions. Incident beam parallel to a cube-axis.

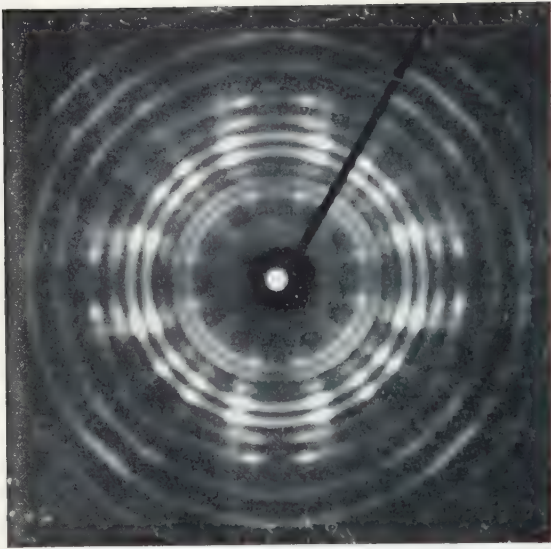


Fig. 5. Aged at 240° C. Mo-K radiation.



Fig. 6. Aged at 240° C. W radiation.

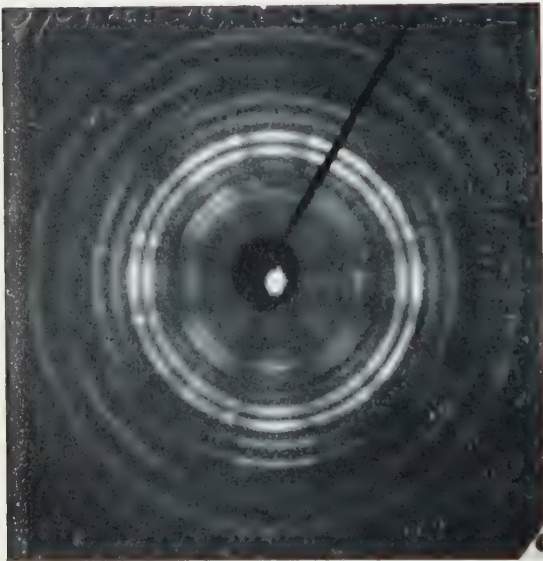


Fig. 7. Aged at 340° C. Mo-K radiation.



Fig. 8. Aged at 430° C. Mo-K radiation.

NaCl; in *all cases described here* the crystals were quenched from about 550° C to room temperature before ageing. Up till now the following results have been obtained:

A. Photographs of the decomposed crystals, taken with Mo-K radiation, showed "double" Debye-Scherrer rings corresponding to the parameters of the two equilibrium phases¹⁾.

B. In case preferred orientations of the terminal phases occur, they were the same for both. This followed from the corresponding positions of the intensity maxima on the Debye-Scherrer rings (cf. figs. 4, 5, 7, 8).

C. Depending on the way the decomposition was brought about, different orientation relationships were observed:

1. Due to the influence of water vapour at room temperature, oriented overgrowth on the surface of the single crystal took place, the lattice of the crystallites being parallel to that of the single crystal. This effect is more pronounced on crystals with compositions near the pure compounds; it is shown by fig. 2, which is a microphotograph of a cube face of a 20 % NaCl mix-crystal kept under normal atmospheric conditions.

2. The orientation of the terminal phases inside a crystal kept in the room-atmosphere is more complicated as is shown by a Laue-photograph with Mo-K radiation with the incident beam parallel to a cube-axis of the original single crystal (fig. 4; 60 % NaCl). The complete determination of this texture did not show a simple orientation relationship with the parent lattice.

3. Ageing of a 60 % NaCl mix-crystal at 170° C and at 240° C gave rise to a texture that could be deduced from the parent lattice by rotations about each of the four [111]-directions (the normals to the octahedral planes)²⁾. Actually there is a preference for the 60°-180°-300° rotations (twin positions), this preference being more pronounced for ageing at 240° C than for ageing at 170° C. This texture gives rise to remarkable patterns of spots and striae as shown in fig. 5 and particularly in fig. 6 which are Laue-photographs taken with resp. Mo- and W-radiation with the incident beam parallel to a cube-axis of the original single crystal.

4. The texture of the precipitate crystallites after ageing at 430° C

¹⁾ This holds for ageing after quenching to room-temperature. If, however, the crystals were quenched from 550° C to the ageing temperature directly, the photographs were more complicated.

²⁾ In some experiments also another texture was observed with crystals aged at 170° C. This texture could be deduced from the parent lattice by 35°-55° rotations about [100]-directions. (The same orientation-relationship was found by JONES, LEECH and SYKES (1942) on ageing of a silver-rich Ag-Cu single crystal). With polychromatic radiation this gave rise to striae which had a strong resemblance to those observed by GEISLER and HILL (1948) in an ageing Al-Mg-Si alloy. These authors ascribe the latter to a precipitate of one- and two-dimensional crystallites. As yet we have no indication whether this interpretation holds also in our case, as the intensity-maxima on the striae on photographs taken with Mo-K radiation were always falling on the Debye-Scherrer rings.

cannot be given in such an unambiguous way as was possible for the textures after ageing at 170°C and 240°C . We may put it that it can be approximated by twinning on $\{111\}$ and a small rotation either about a $[110]$ -axis or a $[112]$ -axis of the parent lattice. Fig. 8 shows a Laue-photograph of a single crystal (60° , NaCl) decomposed at this temperature: this texture-type is easily recognised by the appearance of twelve intensity-maxima on the (220) -interference circles (the intensive "doublets" on the photograph).

5. Ageing of a 60 % NaCl mix-crystal at 340°C gives a combination of the textures observed at 240°C and at 430°C , which can be seen in fig. 7 in comparison with figs. 5 and 8.

§ 3. Discussion of texture

The diffraction patterns, described in par. 2 under $C3$ and shown in figs. 5 and 6, can be easily explained with the aid of a representation of the texture in reciprocal space. The position of a crystallographic plane is found in reciprocal space as a point at a distance $\lambda R/d$ from the origin in the direction perpendicular to the plane, λ being the wave-length, d the spacing of the plane and R the radius of the sphere of reflection. In this way positions of (220) -planes of a cubic lattice are indicated in fig. 9 by black circles. For a continuous series of wave-lengths and a constant value of R , the positions of these planes are given by lines going from the origin through the black circles (see JAMES (1948) and GEISLER and HILL (1948)). Rotations of these lines about each of the four

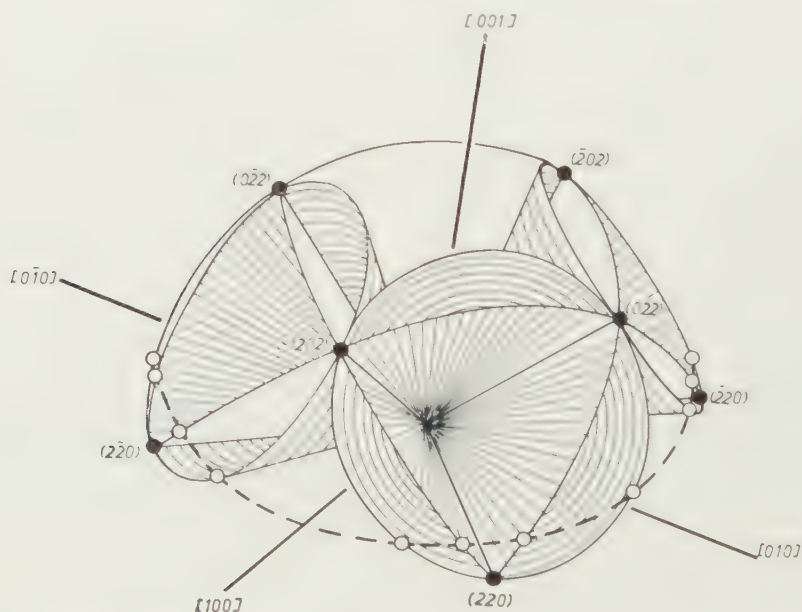


Fig. 9. Representation of $[111]$ -rotated texture in reciprocal space for polychromatic radiation. (Cf. text).

[111]-directions of the lattice give rise to a system of planes and cones as is shown by fig. 9. This represents the texture in reciprocal space for polychromatic radiation and a constant value of the radius of the sphere of reflection. The diffraction pattern is found as the projection, from the centre of the sphere on the plane of the film, of the curves of intersection of this sphere with the texture representation. The sphere passes through the origin of the reciprocal space, its centre lying on the direction of the incident X-ray beam.

The projection was brought about optically with the aid of a spherically shaped glass container representing the sphere of reflection. The lines of intersection were scratched out on the blackened surface and were projected on a screen with the aid of a small lamp in the centre of the sphere (see *BURGERS and TAN KOEN HIOK (1946)*). Fig. 10 is a drawing after this

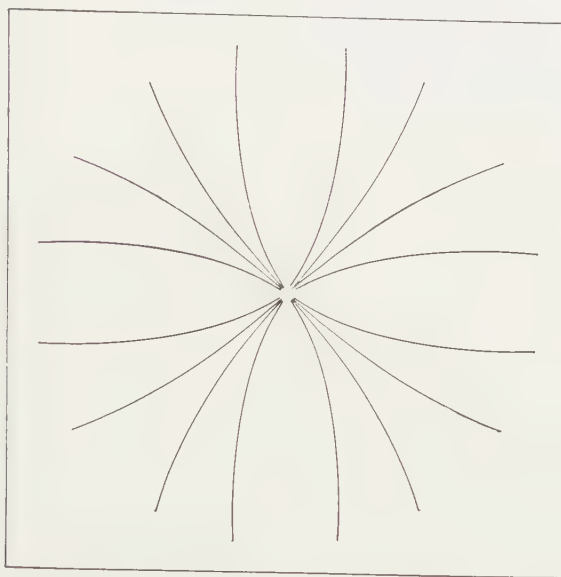


Fig. 10. Optical illustration of the corresponding Laue-photograph, fig. 6.

projection for a direction of the incident X-ray beam perpendicular to a cube-face of the original lattice. It can be compared with the Laue-photograph shown in fig. 6.

Actually, λ has a minimum value and the planes and cones of fig. 9 do not reach the origin of reciprocal space. Because of this the streaks do not reach the centre of the photograph.¹⁾

For *one* wave-length the texture is represented by rotations of the (220)-points only, which give rise to a system of great and small circles, as shown in fig. 9. The intersections of these circles with the sphere of reflection for the incident X-ray beam perpendicular to a cube face are

¹⁾ Moreover, the photograph shows also weak striae due to other planes than the (220)-planes considered here.

indicated with open circles. From this it is clear that on a Laue-photograph taken with characteristic radiation there must be four intensity maxima on each quadrant of the Debye Scherrer circle corresponding with the (220)-planes. Moreover, the streaks from the polychromatic radiation must pass through these maxima. This can be clearly seen in fig. 5.

In the foregoing we have only given a description of various textures formed on ageing of undercooled KCl-NaCl mix-crystals. The question as to the mechanism of the atomic processes involved in the decomposition has been left open. The occurrence of definite preferred orientations can be taken as an indication that the atomic displacements bringing about the decomposition favour definite crystallographic planes and directions. In the continuation of this investigation, applying both X-ray and microscopic methods, we hope to be able to get more information on the crystallographic mechanism of the process.

Delft, November 1953.

REFERENCES

- BUNK, A. J. H. and G. W. TICHELAAR, *Proc. Kon. Ned. Akad. v. Wet.* **B56**, 375 (1953).
 BURGERS, W. G. and TAN KOEN HIOK, *Physica* **11**, 353 (1946).
 EITEL, W., *Z. Mineral.* 173 (1919).
 GEISLER, A. H. and J. K. HILL, *Acta Cryst.* **1**, 238 (1948).
 HYVÖNEN, L. J., *Soc. Scient. Fenn. Comment. Phys.-Math.* **16**, No. 15 (1952).
 JAMES, R. W., "The optical principles of the diffraction of X-rays", p. 245 (London, 1948).
 JONES, F. W., P. LEECH and C. SYKES, *Proc. Roy. Soc.* **A181**, 154 (1942).
 NACKEN, R., *Sitz. Ber. preuss. Akad. Wiss.* 192, (1918).
 SCHEIL, E. and H. STADELMAIER, *Z. Metallk.* **43**, 227 (1952).

FORMATION OF COMPACT PIECES OF GRAY TIN

BY

L. J. GROEN AND W. G. BURGERS

(Laboratory for Physical Chemistry, Technical University, Delft, Holland)

(Communicated at the meeting of November 28, 1953)

To the best of our knowledge gray tin so far has only been obtained in powder-form (see e.g. BUSCH *et al.* (1951)). In this connection it seems of interest to communicate that we succeeded in obtaining compact pieces of gray tin, about 1 mm thick and with a surface-area of about 25 mm².

These pieces were obtained in the following way: Thin sheets of white tin (impurity content no more than 0.01 %), about 1 mm thick, were kept in a refrigerator at about -8°C , after part of their surface had been rubbed briskly with gray tin powder, in order to cause rapid inoculation. After an incubation-period, varying from one to three days, the white tin appeared to be infected, and a spot of gray tin became visible. In the following days, the gray tin nucleus grew with a linear velocity of about 0.015 cm/h. The gray tin formed in this way did not split into small particles, as is usually the result of the transformation, due to the accompanying increase in volume and the brittleness of the material. It appeared to be quite coherent. With continued growth of the gray phase, bursts and cracks appear and pieces of the above-mentioned size split off (*cf.* figs. 1 and 2). An X-ray rotation-photograph of a small piece only showed the line-pattern of the gray modification.

If such a piece is heated to 40°C , it becomes retransformed into a compact, ductile, piece of white tin. Compact pieces of gray tin were obtained starting with polycrystalline material as well as with single-crystals. In one case, starting from a single crystal, we got a Laue-transmission-photograph, which showed the formation of a gray single crystal (*fig.* 3).

In this stage the experiments suggest three conditions to be essential for the formation of this compact gray tin:

- a. the use of thin sheets,
- b. a slow rate of transition and
- c. the growth of only one nucleus.

The use of thin sheets enables the gray tin to extend in volume without splitting too soon by the stresses due to its extension. Slow growth,

attained by cooling to -8°C instead of the usual -50°C and starting at one point in the white tin, may favour a uniform formation of the gray phase. Apart from these points, perhaps also the purity of the material has an influence.

We intend to obtain more detailed information on these questions and on the physical properties of compact gray tin.

Delft, November 1953.

REFERENCES

- BUSCH, G., Z. Physik. Chemie **198**, 23 (1951).
———, J. WIELAND and H. ZOLLER, Helv. Physica Acta **24**, 49 (1951); "Semi-conducting materials", p. 188 (London, Butterworth, 1951).

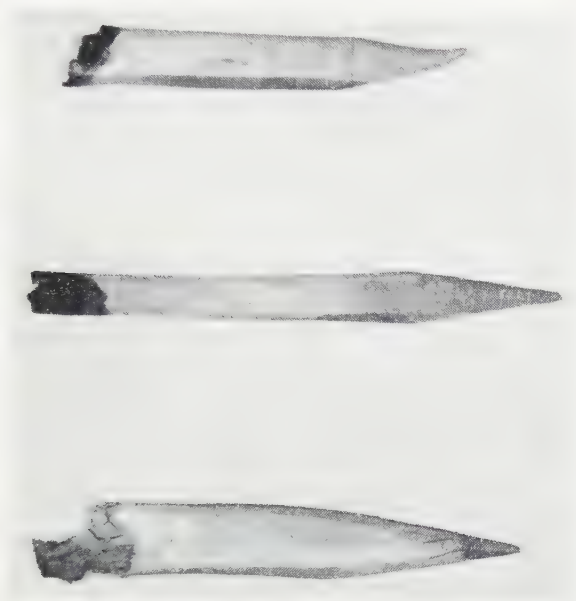


Fig. 1. Transformation of white tin into compact gray tin. (Natural size).



Fig. 2. Compact pieces of gray tin ($\times 1\frac{1}{2}$).



Fig. 3. Laue-photograph of single crystal of gray tin.

or

$$(2) \quad v_H = K_{H \text{ obs.}} [\text{E.T.A.}]$$

with the observed pseudo first order hydrolysis constant

$$(3) \quad K_{H \text{ obs.}} = K_H [\text{OH}^-]$$

The results of our measurements dealing with the alkaline hydrolysis of E.T.A. are summarized in table 1 and fig. 1.

TABLE 1

Hydrolysis at 37° C of a solution of 0.0025 m E.T.A. in 0.2 molar borate buffers of various pH. For the calculations of $[\text{OH}^-]$ K_{water} at 37° C was taken as 2.4×10^{-14} .

Exp. No.	pH	OH^- (mol. ml ⁻¹)	$K_{H \text{ obs.}} \times 10^6$ (sec. ⁻¹)	$K_H \times 10^{-2}$ (ml. mol. ⁻¹ sec. ⁻¹)
1	8.33	5.13×10^{-9}	8.1	15.8
4	8.71	1.23×10^{-8}	16.5	13.4
16	8.92	2.00×10^{-8}	22.9	11.5
19	9.67	1.12×10^{-7}	61.4	5.5

From these data it can be seen that the reaction involving OH^- ions seems to cease from being the rate controlling one at $\text{pH} > 8.7$.

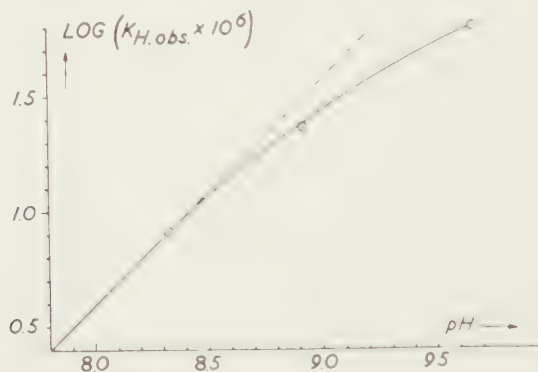


Fig. 1. Observed pseudo first order hydrolysis constants plotted against the pH. The experimental conditions are described in table 1. The dotted line is the theoretical one, derived according to equation (3) with $K_H = 15.8 \times 10^2$ ml. mol.⁻¹ sec.⁻¹

Obviously, a stepwise mechanism is involved and a reaction scheme of the following general type might be assumed:



Similar schemes have been rejected by SCHAEFFGEN [1] but accepted by NODA *et al.* [5] the sequence of the first two reactions being also still open to discussion. In our opinion the second or third step could be rate controlling at low pH whereas at higher pH the first step would become rate controlling, causing the reaction to be independent of pH.

3. Influence of oxygen on the breakdown of E.T.A.

We found an overwhelming effect of oxygen on the breakdown of E.T.A. in aqueous solutions. During all measurements of reactions with low velocity, the reaction rate began to increase considerably after four or more hours of incubation. This is not a case of simple autocatalysis, as addition of acetate or ethyl mercaptane had no effect at all on the reaction velocity. When, however, a stream of oxygen was bubbled slowly through the solution during a hydrolysis experiment the effect was striking as is illustrated in fig. 2 where the course of the concentration of E.T.A. is plotted against the time of incubation during similar hydrolysis experiments in the presence and absence of oxygen.

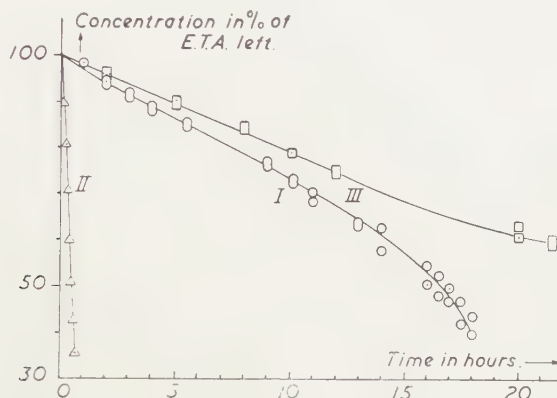


Fig. 2. Course of the concentration of E.T.A. with the time of incubation during the hydrolysis of 0.0025 m E.T.A. solutions in borate buffer at pH 8.3. I. Under normal conditions without complete exclusion of oxygen. II. When oxygen is bubbled slowly through the solution. III. In deaerated buffer under nitrogen atmosphere.

Further investigation on this phenomenon is still in progress.

4. Isolation of acetyl glycine

A check through literature failed to reveal satisfactory data about the isolation of compounds obtained by aminolysis of E.T.A. Furthermore, the statement by SCHWYZER [4] that E.T.A. would not yield any aminolysis products at all made it quite desirable to try to isolate acetyl glycine in a reasonable yield after aminolysis of E.T.A. by glycine. To this end 3 ml of freshly distilled E.T.A. was added to 70 ml of a 1 molar glycine solution in deaerated borate buffer at pH 8.4. The reaction mixture was stirred vigorously and kept at a temperature of 37° C under nitrogen atmosphere for 12 hours. During this time the pH was measured every thirty minutes and kept between 8.3 and 8.6 by addition of a solution of 10 N NaOH. Then the reaction mixture was brought to pH 5.2 by addition of a few drops of 5 N sulphuric acid and evaporated to dryness in vacuum at a temperature of about 35° C. The crystalline residue was redissolved

in 20 ml of distilled water, brought to pH 3 by addition of 5 N sulphuric acid solution and put in the refrigerator overnight. The next morning 1.2 gr. of precipitate (M.P. 204° C) was filtered off, this quantity of crude acetyl glycine being sufficient for our purpose. After four recrystallizations from hot water the white crystalline compound had a constant melting point of 208° C (corr.) (Lit.: 207–208° C for acetyl glycine [8]).

Micro-analysis ¹⁾:

	Calc.	Found
C	41.03	41.54
H	6.00	6.02
N	11.97	11.76

Our kinetic data on the simultaneous hydrolysis and aminolysis of E.T.A. in alkaline aqueous solutions are rather complicated. As the measurements are still continued these data will be published later. The authors wish to thank Dr. C. A. SALEMINK for providing the E.T.A. and Mr. E. M. DUYVIS and Mr. P. H. WIERSEMA for carrying out the reaction velocity measurements.

5. Summary

The rate of the alkaline hydrolysis of ethylthioacetate (E.T.A.) has been determined and proved to be of first order in E.T.A. and of an order varying between one and zero in the OH⁻ ions. Oxygen has been shown to lead to rapid decomposition of E.T.A. Acetyl glycine has been isolated in good yield and high purity from the reaction between E.T.A. and glycine at pH 8.4.

¹⁾ The micro-analysis was carried out at the Organic-Chemical Institute T.N.O., Utrecht.

BIBLIOGRAPHY

1. SCHAEFGEN, J. R., J. Am. Chem. Soc. **70**, 1308 (1948).
2. RYLANDER, P. N., D. S. TARBELL, J. Am. Chem. Soc. **72**, 3021 (1950).
3. HAWKINS, P. J., D. S. TARBELL, J. Am. Chem. Soc. **75**, 2982 (1953).
4. SCHWYZER, H., Helv. Chim. Acta **36**, 414 (1953).
5. NODA, L. H., S. A. KUBY, H. A. LARDY, J. Am. Chem. Soc. **75**, 913 (1953).
6. LIPMANN, F., C. TUTTLE, J. Biol. Chem. **159**, 21 (1945).
7. KONINGSBERGER, V. V., J. TH. G. OVERBEEK, Proc. Kon. Nederl. Akad. v. Wetenschap. Series B, **56**, 248 (1953).
8. HERBST, R. M., D. SHEMIN, Org. Synth. **19**, 4 (1939).

THE AUSTRALOPITHECINAE AND PITHECANTHROPUS. III

BY

G. H. R. VON KOENIGSWALD

(Communicated at the meeting of October 31, 1953)

How close the javanese *Pithecanthropi* resemble in certain points the *Australopithecinae*, is most spectacularly demonstrated by the robust jaw of *Meganthropus*, which comes astonishingly close to the conditions found in *Paranthropus*. Our javanese species is unfortunately poorly represented, but a jaw fragment recently described by MARKS (1953) exhibits the same robustness of the corpus mandibulae which proves that this characteristic is typical and not pathological.

According to ROBINSON (1953) a mental spine is also indicated in three *Paranthropus* mandibles. We must wait for the publication to see how they compare with the conditions observed in *Meganthropus*. The outline and pattern of the lower premolars and first molar in both species is, however, not as similar as ROBINSON, judging from casts only, is inclined to assume. The molar of *Meganthropus* has a fovea anterior closed by a trigonid crest which is still completely preserved, and also the second deciduous herver molar is of a decidedly more primitive pattern. We will discuss this question in a separate paper. In spite of a great similarity *Meganthropus* cannot be regarded as an *Australopithecinae* of south-african type.

We agree with ROBINSON that *Meganthropus africanus*, collected by KOHL-LARSEN in East Africa has nothing to do with our javanese form and rather belongs to the *Australopithecinae*. Of this species only the fragment of an upper jaw containing the two premolars is known (a molar of normal size referred to the same species had better be excluded); because of the large size WEINERT attached the name *Meganthropus* to this find, but of the type species no upper premolars are known. The view that the specimen in question might belong to an *Australopithecinae*, has already been expressed earlier: first by W. ABEL (vide: L. KOHL-LARSEN, 1943), later by TEILHARD DE CHARDIN (1952, p. 347) and the present author (VON KOENIGSWALD 1953, p. 132). In this case a decision might be possible, as all *Australopithecinae* have only two roots on the first upper premolar, while in *Pithecanthropus modjokertensis* the same tooth still has its original three roots and we might expect the same condition in *Meganthropus s. str.*

For a definition of the relationship between the *Australopithecinae* and

the Pithecanthropi we have to rely mainly on *Paranthropus crassidens* and *Pithecanthropus modjokertensis*, which are the best known members of each group. The first question we might ask is: in which respect are the Australopithecinae more primitive? At the present stage of our knowledge there is little to be said: with respect to the low brain capacity the Australopithecinae might be transitional between *Pithecanthropus* and the big apes, but the brain-molar coefficient seems to put them in one group with the anthropoids—also: ASHTON's calculations of the absolute brain capacity—. Regarding the entrance to the nose they are also mainly on the anthropoid side, and only in the formation of the fossa glenoidalis they seem to represent an intermediate stage.

Pithecanthropus modjokertensis differs from modern Man in the possession of a simian gap, three roots on the anterior upper premolar, the relative size proportions for the upper and lower molars, and the trigonid-talonid division of the lower first deciduous molar. The simian gap, being a real primitive characteristic, has already disappeared from the permanent dentition of the Australopithecinae: the first upper premolar has only two roots, and only in the relative size proportions of the molars, (which however are absolutely much bigger than in the Hominidae) and the general topography of the lower first milk molar they agree with the Pithecanthropi.

The Australopithecinae disagree with the Pithecanthropi and exceed modern Man *and* in the reduction of the front teeth—incisivi, canini and first premolars—*and* in the molarisation of the deciduous dentition. Both these processes are irreversible, and so they already exclude the Australopithecinae from a direct ancestorship of the Pithecanthropi and modern Man as well.

That is nothing new and has been stated by several authors. Reviewing the Australopithecinae, ROBINSON recently has declared: "It seems improbable that those known at present should be human ancestors" (1952, p. 200).

Even if we do not agree with WEIDENREICH, who regarded *Sinanthropus* as a true early Mongolian and *Pithecanthropus* as a direct ancestor of the Australian aboriginal, there is no reason to regard the Pithecanthropi as the representatives of a side branch of modern Mankind, as certain authors are inclined to do. But if the Pithecanthropi would still not fulfil the conditions what have we to expect in a form directly ancestral to *Homo sapiens*?

What kind of characteristics might we expect—or must we expect—in an early human ancestor? If we only would take the dentition, the front teeth would be less reduced than in the Australopithecinae, not only the incisors, but especially the anterior premolars. The first upper premolar might have had three roots; one is lost in the Australopithecinae already by the extreme shortening of the face. Then we certainly might expect a diastema; not only is such a diastema present in *Pithecanthropus*

modjokertensis, but it is also found in the juvenile skull of *Australopithecus africanus*, where it measures 3.5 mm on each side. This must be regarded as a sign, that it was developed in the older, ancestral forms, even if it seems to have been suppressed in all adult specimens of the *Australopithecinae*. Probably the high lower canine of *Plesianthropus* is still an adaptation to these conditions.

Such an early human ancestor — and it most probably will be an ancestor we have in common with the *Australopithecinae* — could, according to definition, never be an *Australopithecus* s.str., but a form, unknown till now, which might have had more in common with the *Pithecanthropi* than with the *Australopithecinae*.

Therefore the *Australopithecus*-“stage”, as we know it, is not simply a stage (or level) *below* the *Pithecanthropus*-stage, as has been assumed by certain german authors, but something different.

We have already seen that the tendencies we can distinguish within the *Australopithecinae* are different from those we observe in the *Hominidae* s.str. In spite of all apparently human affinities, they remain anthropoids in some very essential points. We are here not only referring to the brain molar coefficient and the brain capacity, but to a fact, not yet mentioned: the development of a sagittal crest (*crista saggitalis*) in *Paranthropus crassidens*, which has been observed in two skulls (BROOM and ROBINSON 1952, figs. 10, 11, 13). Both specimen, probably

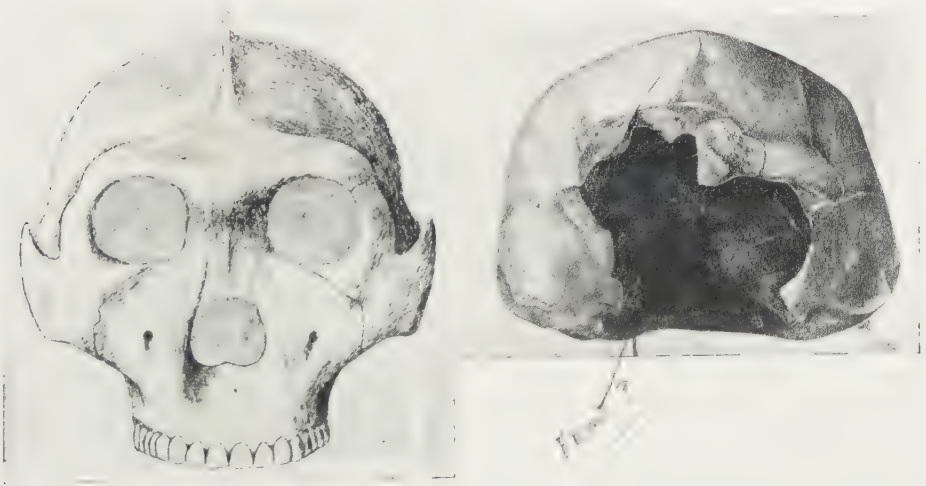


Fig. 10. *Front view (norma frontalis) of skulls. Paranthropus crassidens* (reconstruction) left, and *Pithecanthropus erectus*. — Not same scale. (After BROOM and ROBINSON (1952) and v. KOENIGSWALD (1941)).

because of their relative low brain capacity, have been referred to female individuals; this seems, in view of the conditions observed in recent anthropoids, quite improbable.

In the small gibbons such a crista never develops, nor did it develop in the female chimpanzee, some males being an exception. In the male orang the crista is mostly, in the big male gorilla nearly always present, and often in the females. There is a clear relation between the size of the species and the occurrence of that crista. It cannot be an accident, that we find this specialisation just in *Paranthropus crassidens*—as far as we know the largest of all Australopithecinae!

The crista is also a sign of a limited brain capacity. Our brain molar index, as well as ASHTON's calculations, show that in this respect we are here not above the anthropoids. *The Australopithecinae might be regarded as specialised Hominidae on an anthropoid level.*

Did the Australopithecinae originate in Africa, or are they confined to this region? Most probably not. In Europe *Anchitherium*, (the Miocene horse), the Pliocene horse *Hipparion* and *Equus*, which appear with the beginning of the Pleistocene, are not direct descendants from each other, but branches from a common american stock. The earliest Proboscideans occur in the Lower Tertiary of North Africa—together with *Parapithecus* and *Propliopithecus*, the first anthropoids—but the transition from *Mastodon* via *Stegodon* into *Elephas* took place in Asia. It is not necessary, that the Australopithecinae should be descendants of *Proconsul* from the Lower Miocene in Kenya only because both have been found in Africa; nothing is known about the Upper-Miocene and Pliocene Primates of Africa; even the direct forerunners of chimpanzee and the gorilla have remained unknown till now. In view of the many higher Primates in the Siwaliks of the Himalaya, India might have been an important center for the development of higher Primates.

If we search for possible traces of Australopithecinae in Asia, we first might look at the canine from the Pleistocene of Southern China, mentioned in connection with *Plesianthropus*. BROOM himself was so impressed by this (and other) specimen, that he wrote: "We can, I think, feel fairly confident that a large Australopithecine, and probably two, inhabited China in Upper Pliocene or Lower or Middle Pleistocene times. And if this should prove to be the case it may be that they will prove to be even nearer to man's ancestor than the South African Australopithecinae" (1946, p. 66)—As I have already mentioned, there are *Australopithecus*-like forms in China, which will be described before long.

BROOM also mentioned in this connection *Gigantopithecus* from the same layers of Southern China: "unfortunately it is only known by a few teeth, but these seem to me so nearly allied to those of *Paranthropus* that I consider *Gigantopithecus* to be probably a giant Australopithecine, and not an "anthropoid" in the narrow sense" (1946, p. 138).

Gigantopithecus has been regarded by WEIDENREICH as a giant Hominid: but a closer study has revealed that although the molars share

with modern Man the trend towards hypsodonty, they are certainly overspecialised, and not in the common line (v. KOENIGSWALD 1952). They also differ by the "block pattern" from the molars of the Australopithecinae: *Gigantopithecus* is a Hominid in a wide sense in the same way as the Australopithecinae.

From our limited knowledge it becomes evident, that in the Lower Pleistocene there must have existed at least three different branches of "human-like types", besides the Early Hominidae themselves. Such a differentiation is typical of an explosive phase of evolution, and therefore I am personally inclined to regard the Pliocene, most probably the Lower Pliocene, as the most critical phase in the evolution of Man.

In putting the Australopithecinae (and other related forms) on side branches, and regarding the human branch as the normal line of evolution, we certainly underestimate the unique position of Man. Man is the product of certain evolutionary processes, which are characteristic only of him, and which probably quite late lifted him out of his animal existence and transferred him into a human being. The animal stage is a "normal" stage, and the Australopithecinae are on the main branch. Unable of changing their evolutionary course, maintaining a powerful dentition—in spite of the trend to reduce their frontteeth in which they resemble and surpass Man—, and a limited brain capacity, *the Australopithecinae, Hominidae in a wide sense, are representing the animal equivalent of Man.* At the time they lived in South Africa and China, the Pithecanthropi were already real Hominids, reducing their jaws (v. KOENIGSWALD 1940, 49, WEIDENREICH 1943), and—probably by a process connected with it as a compensation—receiving the benefit of a special increase in brain volume, which at the same time is the base of the intellectual and spiritual capacities, by which the Hominidae s. str. developed into human beings.

L I T E R A T U R E

- ABEL, W., Kritische Untersuchungen über *Australopithecus africanus* DART. — Morph. Jb. 165, 539–640 (1931).
- ADLOFF, P., Das Gebiss des Menschen und der Anthropomorphen. (Berlin, 1908).
- ASHTON, E. H., The endocranial capacities of the Australopithecinae. — Proc. Zool. Soc. London, 120, 715–721 (1950).
- BENNEJEANT, CH., Anomalies et variations dentaires chez les Primates; 1–258, (Clermont-Ferrand, 1936).
- BROOM, R., Finding the Missing Link, 1–104 (London, 1950).
- , The genera and species of the south african fossil ape-man. — J. Am. Phys. Anthropol., n.s. 8, 1–14 (1950).
- BROOM, R. and G. H. W. SCHEPERS, The South African Ape-Man: The Australopithecinae. — Transv. Mus. Mem. 2, 1–272 (1948).
- BROOM, R., J. T. ROBINSON and G. W. H. SCHEPERS, Sterkfontein Ape-Man: *Plesianthropus*. — Transv. Mus. Mem. 4, 1–117 (1950).
- BROOM, R. and J. T. ROBINSON, Swartkrans Ape-Man: *Paranthropus crassidens*. — Transv. Mus. Mem. 6, 1–123 (1952).

- LE GROS CLARK, W. E., New palaeontological evidence bearing on the evolution of the Hominoidea. — *Quart. J. Geol. Soc. London*, **105**, 225-264 (1950).
- , Hominid characters of the Australopithecine dentition. — *J. Roy. Anthropol. Inst.* **80**, 37-54 (1952).
- COOKE, H. B. S., Mammals, Ape-Men and Stone Age Man in Southern Africa. — *S. Afr. Arch. Bull.* **3**, 59-69 (1952).
- DART, A. R., The pedatory implemental technique of Australopithecus. — *Am. J. Phys. Anthropol.* n.s. **7**, 1-38 (1949).
- , A second adult palate of Australopithecus prometheus. — *Am. J. Phys. Anthropol.* n.s. **7**, 335-338 (1949).
- EHGARTNER, W., Fossile Menschenaffen aus Südafrika. — *Mitt. Anthropol. Ges. Wien*, **80**, 157-212 (1950).
- ELBERT, E., in: *Die Pithecanthropus-Schichten auf Java* (Leipzig, 1911).
- GLAESSNER, M. F., Neue Zähne von Menschenaffen aus dem Miozän des Wiener Beckens. — *An. Nat. Hist. Mus. Wien*, 15-27 (1931).
- GREGORY, W. K., M. HELLMAN and G. E. LEWIS, Fossil Anthropoids of the Yale-Cambridge India Expedition of 1935. — *Carnegie Inst. Washington publ.* nr. 495, 1-27 (1938).
- HOOIJER, D. A., Prehistoric teeth of Man and of the orang-utan from Central Sumatra. — *Zool. Mededeel. Leiden*, **29**, 175-301 (1948).
- HÜRZELER, J., Neubeschreibung von Oreopithecus bambolii. — *Schweiz. Pal. Abh.* **66**, 3-20 (1949).
- DE JONGE-COHEN, TH. E., Maximal, Minimal- und Mittelwerte der mesiodistalen Dimensionen der postkaninen Zähne des menschlichen Gebisses. — *Z. Anat. & Entwgesch.* **99**, 324-337 (1932).
- KOENIGSWALD, G. H. R. VON, Neue Pithecanthropus-Funde 1936-38. — *Wetensch. Mededeel. Dienst v. d. Mijnb. Nederl.-Indië* nr. **28**, 1-233 (1940).
- , The south african Man-Apes and Pithecanthropus. — *Carnegie Inst. Washington publ.* nr. 530, 205-222 (1942).
- , Remarks on the lower canine of Plesianthropus. — *R. Broom Commemorative Vol.*, 159-164 (1948).
- , Gigantopithecus blacki, a giant fossil Hominoid from the Pleistocene of Southern China. — *Anthropol. Pap. Am. Mus. Nat. Hist. New York*, **43**, 295-325 (1952).
- , Die Phylogenie des Menschen. — *Die Naturwissenschaften* **40**, 128-137 (1953).
- KOHL-LARSEN, L., *Auf den Spuren des Vormenschen* (Stuttgart, 1943).
- RIET LOWE, C. VAN, The Vaal River Chronology. — *S. Afr. Arch. Bull.* **7**, 1-15 (1952).
- MARKS, P., Preliminary note on the discovery of a new jaw of Meganthropus VON KOENIGSWALD in the Lower Middle Pleistocene of Sangiran, Central Java. — *Madjalah Ilum Alam Untuk Indonesia*, **109**, 26-33 (1953).
- MIJSBERG-VAN ROYEN, J. H. N. and W. A. MIJSBERG, Over geslachtsverschillen in het gebit der Javanen. — *Ge. Tijdschr. Nederl.-Indië*, **72**, 277-283 (1932).
- PEDERSEN, P. O., The East Greenland Eskimo Dentition. — *Meddel. om Grønland* **142**, nr. 3, 1-250 (1949).
- REMANE, A., Beiträge zur Morphologie des Anthropoidengebisses. — *Arch. f. Natgesch.* **11**, (1921).
- , Die Zähne des Meganthropus africanus. — *Z. Morph. & Anthropol.* **42**, 311-329 (1951).
- , Der vordere Premolar von Australopithecus prometheus und die Morphologie des Australopithecinegebisses. — *idem*, **43**, 288-310 (1952).

- ROBINSON, J. T., The Australopithecine-bearing deposits of the Sterkfontein-area. — *An. Transv. Mus.* **22**, 1–19 (1952).
- , The Australopithecines and their evolutionary significance. — *Proc. Lin. Soc. London*, **163**, 196–200 (1952).
- , The nature of *Telanthropus capensis*. — *Nature* **171**, 33 (1953).
- , *Meganthropus*, *Australopithecines* and *hominids*. — *Am. J. Phys. Anthropol.* n.s. **11**, 1–38 (1953).
- SCHULTZ, A. H., The relative size of the cranial capacity in *Primates*. — *Am. J. Phys. Anthropol.* **28**, 273–287 (1941).
- SELENKA, E., *Menschenaffen*, 1–160 Wiesbaden, (1898).
- TEILHARD DE CHARDIN, P., *Australopithèques, Pithecanthropus et structure phyletique des Hominiens*. — *Comp. rend. seances Acad. Sciences*, Paris, **234**, 377–379 (1952).
- TERRA, M. DE, *Beiträge zu einer Odontografie der Menschenrassen*, (Berlin, 1905).
- TOERIEN, M. J., The fossil Hyenas of the Makapansgat Valley. — *Afr. J. Sc.* **48**, 293–300 (1952).
- WEIDENREICH, F., The dentition of *Sinanthropus pekinensis*. — *Pal. Sinica* **101**, 1–180 (1937).
- , The skull of *Sinanthropus pekinensis*. — *Pal. Sinica*, **127**, 1–485 (1943).
- , Giant Early Man from Java and South China. — *Anthrop. Pap. Am. Mus. Nat. Hist. New York*, **40**, 1–134 (1945).
- ZAPFE, H., *Lebensspuren der eiszeitlichen Höhlenhyäne*. — *Palaeobiologica* **7**, 111–146 (1938).

ENTROPY AND MOBILITY OF ADSORBED MOLECULES

V. CO, CO₂ AND CS₂ ON CHARCOAL ¹⁾

BY

J. H. DE BOER AND S. KRUYER

(Communicated at the meeting of December 19, 1953)

1. INTRODUCTION

Various investigators studied the adsorption of CO on charcoal and many publications deal with the adsorption of CO₂ on charcoal. In the course of our investigations of the thermodynamic behaviour of adsorbed gases we have used these data, and also those of the adsorption of CS₂ on charcoal, to calculate the differential heat of adsorption, ΔH and the differential adsorption entropy, ΔS . The procedure is described in article I of this series, where two models were introduced. The experimental figures of ΔS are used to calculate ΔS^0 for the standard states of these two models, viz. the model of the "entropically ideal site adsorption", ΔS_i^0 , and the model of the "entropically ideal mobile adsorption", ΔS_m^0 . These figures are then compared with theoretical figures, namely the total translation entropy of the gas in the standard state at the given temperature, ${}_gS_{tr}^0$, and the difference between this entropy and the entropy of the ideal two-dimensional gas in its standard state at the same temperature, ${}_gS_{tr}^0 - {}_aS_{tr}^0$. This procedure enables us to derive conclusions with respect to the mobility of the adsorbed molecules.

2. CARBON MONOXIDE ON CHARCOAL AT HIGHER TEMPERATURES

RAY and BOX ²⁾ studied the adsorption of CO on the same charcoal as used by them for all other gases. Their data on the adsorption of nitrogen have been used in article II, those on hydrogen in article III and the numerous data on hydrocarbons in article IV of this series. The specific area of their charcoal is given as 1152 m²/g. The data are assembled in table I.

Table II gives data published by Miss HOMFRAY ³⁾, who used the same charcoal as for her measurements of the adsorption of argon (article I), nitrogen (article II) and methane (article IV of this series). In article II

¹⁾ I. J. H. DE BOER and S. KRUYER, Proc. Kon. Ned. Ak. v. Wet. **B55**, 451 (1952); II. J. H. DE BOER and S. KRUYER, Proc. Kon. Ned. Ak. v. Wet. **B56**, 67 (1953); III. J. H. DE BOER and S. KRUYER, Proc. Kon. Ned. Ak. v. Wet. **B56**, 236 (1953); IV. J. H. DE BOER and S. KRUYER, Proc. Kon. Ned. Ak. v. Wet. **B56**, 415 (1953).

²⁾ G. C. RAY and E. O. BOX, Ind. Eng. Chem. **42**, 1315 (1950).

³⁾ I. F. HOMFRAY, Z. physik. Chem. **74**, 129 (1910).

TABLE I
CO on charcoal; data from G. C. RAY and E. O. BOX

T_1 and T_2 °C	T °K	θ	$-\Delta H$ kcal/mol	$-\Delta S_i^0$ e.u.	${}_gS_{tr}^0$ e.u.	$-\Delta S_m^0$ e.u.	${}_gS_{tr}^0 - {}_aS_{tr}^0$ e.u.
37.8 and 93.3	339	0.012	4.1	19.4	36.6	10.7	11.4
		0.019	3.0	16.1		7.4	
93.3 and 148.9	394	0.10	2.9	16.9	37.3	8.5	11.5
148.9 and 204.4	450	0.19	4.0	16.2	38.0	7.2	11.7

TABLE II
CO on charcoal; data from I. F. HOMFRAY

T_1 and T_2 °C	T °K	θ	$-\Delta H$ kcal/mol	$-\Delta S_i^0$ e.u.	${}_gS_{tr}^0$ e.u.	$-\Delta S_m^0$ e.u.	${}_gS_{tr}^0 - {}_aS_{tr}^0$ e.u.
-34 and 0	256	0.13	4.6	19.2	35.2	11.4	11.1
		0.24	4.6	19.3		11.8	
0 and 20	283	0.035	4.8	19.4	35.7	10.9	11.2
		0.075	4.9	20.0		11.6	
		0.13	4.7	19.2		11.2	
		0.16	4.6	18.9		11.7	
20 and 46	306	0.035	4.6	18.9	36.1	10.1	11.3
		0.07	4.8	19.9		11.1	
		0.09	4.7	19.5		10.9	

we derived the figure 303 m²/g for the specific area of her charcoal. This figure is also used here.

All entropy figures indicate a mobile adsorption. Comparing $-\Delta S_m^0$ with $({}_gS_{tr}^0 - {}_aS_{tr}^0)$ leads to the conclusion that at temperatures higher than room temperature (table I) some "super-mobility" (see article I) is shown. In studying the adsorption of N₂ a similar picture was found (article II). The physical adsorption of CO closely resembles that of N₂; the heat of adsorption is slightly higher.

3. CARBON MONOXIDE AT LOW TEMPERATURES

VAN ITTERBEEK and VAN DINGENEN ⁴⁾ used two different charcoals for their study of the adsorption of CO, viz. an active charcoal called "Carbotox", which was also used for their measurements of the adsorption of helium (article I) and of hydrogen and deuterium (article III) and another activated charcoal, called "Desorex B", which they used for the study of the adsorption of oxygen (article III).

In article III of this series we estimated the specific area of their sample of "Carbotox" from their measurements of argon and of hydrogen and deuterium. The figures varied between 1160 m²/g and 1220 m²/g and we used 1200 m²/g. However, their isotherms of CO on this charcoal of

⁴⁾ A. VAN ITTERBEEK and W. VAN DINGENEN, *Physica* 4, 1169 (1937).

TABLE III

CO on charcoal; data from A. VAN ITTERBEEK and W. VAN DINGENEN

T_1 and T_2 °K	T °K	θ	$-\Delta H$ kcal/mol	$-\Delta S_i^0$ e.u.	${}_g S_{tr}^0$ e.u.	$-\Delta S_m^0$ e.u.	${}_g S_{tr}^0 - a S_{tr}^0$ e.u.
"Carbotox"							
54.85 and 58.04	56.45	0.95	2.46	19.9	27.7	19.8	9.6
58.04 and 60.13	59.2	0.81	3.04	28.7	27.9	26.6	9.6
		0.92	2.28	17.0		17.6	
		0.985	2.44	18.0		21.1	
60.13 and 65.36	62.75	0.60	3.85	35.2	28.2	31.5	9.7
		0.81	2.75	20.9		18.7	
		0.88	2.54	21.5		20.2	
"Desorex B"							
54.50 and 57.85	56.2	0.70	2.62	22.0	27.6	19.7	9.6
		0.79	2.11	14.4		12.9	
		0.89	2.07	14.4		14.1	
57.85 and 60.50	59.2	0.56	3.50	34.5	27.9	30.8	9.6
		0.65	3.32	33.2		30.1	
		0.74	3.18	32.4		29.8	
		0.84	3.09	31.6		29.9	
60.50 and 64.55	62.5	0.52	2.49	17.0	28.2	13.0	9.7
		0.65	2.50	19.7		16.4	
		0.75	2.51	21.2		18.5	
		0.84	2.53	22.4		20.6	
64.55 and 75.25	69.9	0.51	1.96	8.3	28.7	4.0	9.8
		0.68	2.16	14.3		9.6	
75.25 and 85.05	80.15	0.51	3.00	22.0	29.4	18.1	10.0
85.05 and 90.03	87.5	0.24	2.53	11.8	29.8	6.2	10.0
		0.43	1.83	7.3		2.2	

54.85° K, 58.04° K and 60.13° K when plotted according to the method of BRUNAUER, EMMETT and TELLER, give - all three - a figure of 1400 m²/g. We, therefore, use this latter figure for our calculations with their data on the adsorption of CO.

Using the method of BRUNAUER, EMMETT and TELLER with VAN ITTERBEEK and VAN DINGENEN's data on the adsorption isotherms of CO on "Desorex B" at 54.15° K and 57.95° K, we find a specific area of 1050 m²/g. In article III of this series we estimated the figure 1370 m²/g from the data on the adsorption of oxygen. For our calculations of the adsorption data of CO we shall consider the specific surface area available for CO to be 1050 m²/g. The data are assembled in table III.

The results obtained from the data relating to "Desorex B" vary

considerably from temperature to temperature; the results gained with "Carbotox" seem to be somewhat more reliable. All figures lead to the conclusion that at temperatures lower than 63° K the mobility of the adsorbed CO molecules is seriously hindered. The results which we obtained for temperatures between 69° K and 88° K are such that no conclusion seems to be justified.

4. CARBON DIOXIDE ON CHARCOAL

All available data which could be used for our calculations have been assembled in table IV. In this table, therefore, data of various authors are used.

TABLE IV
CO₂ on charcoal

T_1 and T_2 °C	T °K	θ	$-\Delta H$ kcal/mol	$-\Delta S_i^0$ e.u.	${}_gS_{tr}^0$ e.u.	$-\Delta S_m^0$ e.u.	${}_gS_{tr}^0 - {}_aS_{tr}^0$ e.u.	Authors
0 and 20	283	0.068	6.0	23.1	37.0	15.5	11.6	5)
		0.135	6.0	22.5		14.7		
0 and 25	285.5	0.017	7.79	22.3	37.1	14.3	11.65	6)
		0.33	7.26	21.8		14.6		
		0.37	7.19	21.6		14.5		
		0.60	6.96	21.2		14.9		
		0.73	6.91	20.8		15.0		
25 and 50	310.5	0.014	6.52	20.7	37.5	12.3	11.7	
		0.05	6.52	21.3		13.0		
		0.07	6.51	21.3		13.0		
		0.13	6.48	21.4		13.2		
		0.17	6.33	21.1		13.0		
0 and 30	288	0.53	6.4	18.4	37.1	13.1	11.7	7)
		0.75	6.3	18.6		12.0		
30 and 80	328	0.19	6.9	20.2	37.8	12.3	11.8	
		0.38	6.9	20.0		13.1		
20 and 46	306	0.10	6.5	20.0	37.4	11.9	11.7	3)
		0.19	6.3	19.5		11.6		
		0.32	6.5	20.0		12.5		
		0.39	6.3	19.4		12.0		
		0.47	6.3	19.6		12.6		
37.8 and 65.6	325	0.09	5.8	20.9	37.7	12.7	11.8	2)
		0.11	6.1	21.9		13.7		
65.6 and 93.3	353	0.034	5.6	20.2	38.1	11.8	11.9	
		0.045	6.2	21.6		13.2		
		0.068	7.4	25.3		16.9		
93.3 and 121.1	380	0.045	6.2	21.7	38.5	13.2	11.95	

CARMAN and RAAL ⁵⁾ published data on adsorption isotherms of CO₂

⁵⁾ P. C. CARMAN and F. A. RAAL, Proc. Roy Soc. (London) **A209**, 38 (1951).

on charcoal at 0° and 20° C; they indicate that the specific area of their charcoal was 960 m²/g.

MAGNUS and KRATZ ⁶⁾ give isotherms at 0°, 25° and 50° C. We used a Langmuir plot of their isotherm of 0° C to find the amount of CO₂ adsorbed in a unimolecular layer, from which amount the degree of occupation, θ , could be found. If the molecular area of a CO₂ molecule is taken to be 19.5 Å², the specific area of their charcoal was 350 m²/g.

TITOFF ⁷⁾ studied the adsorption of CO₂ on the same charcoal as used by him for the adsorption of nitrogen. These latter data are incorporated in our article II where we estimated 290 m² g to be the specific area of his charcoal. This figure is also used here.

MISS HOMERAY ³⁾ measured the adsorption of CO₂ on the same charcoal as used for CO (see section 2 of this article). A Langmuir plot of her isotherm of 0° C gives the amount of CO₂ adsorbed in a unimolecular layer: with 19.5 Å² for the molecular area of CO₂ this gives 346 m²/g for the specific area, which is in good agreement with the figure 303 m²/g, which we used in article II of this series and in section 2 of the present article.

RAY and BOX ²⁾ studied the adsorption of CO₂ at somewhat higher temperatures, using the same charcoal (specific area 1152 m² g) as for the other gases.

The heat of adsorption, calculated from the data of the various authors is practically the same. Comparing the entropy data we may conclude that they all point to a mobile adsorption of CO₂. At the lower end of the temperature range of table IV the free movement of the two-dimensional CO₂ gas seems to be slightly hindered, whilst at the higher temperatures this hindering seems to be less, at least at the lower degrees of occupation, θ .

Even at room temperature, however, the difference between $-AS_m^0$ and $({}_o S_{tr}^0 - {}_a S_{tr}^0)$ is only about 3 e.u. As at 283° K the rotation entropy of CO₂ gas, ${}_o S_{rot} = 13.0$ e.u. (${}_o S_{rot} = 13.6$ e.u. at 380° K), this difference cannot be ascribed to the loss of one of the free rotations ($\frac{1}{2} {}_o S_{rot}$). In article II of this series, in the discussion of the free movements of adsorbed argon and nitrogen, we pointed out that a hindering of the free movement means a hindering of the free translation and not of the rotation. We may conclude that CO₂ is adsorbed as a mobile two-dimensional gas, the molecules of which show a slightly hindered translatory movement over the surface, whereas their rotation is not hindered.

5. CARBON DISULPHIDE ON CHARCOAL

GOLDMANN and POLANYI ⁸⁾ measured the adsorption of CS₂ on the same charcoal as used by them for the adsorption of *n*-pentane (article IV). A BRUNAUER, EMMETT and TELLER plot from their isotherms at 0° C

⁶⁾ A. MAGNUS and H. KRATZ, Z. anorg. Chem. **184**, 241 (1929).

⁷⁾ A. TITOFF, Z. physik. Chem. **74**, 641 (1910).

⁸⁾ F. GOLDMANN and M. POLANYI, Z. physik. Chem. **132**, 321 (1928).

and 20.5° C gives the amount of CS₂ just filling a unimolecular layer as $v_m = 0.445$ grams per gram of charcoal. The degrees of occupation, θ , are calculated with that figure. The data are assembled in table V.

TABLE V
CS₂ on charcoal; data from F. GOLDMANN and M. POLANYI

T_1 and T_2 °C	T K	θ	$-1H$ kcal/mol	$-\Delta S_i^0$ e.u.	${}_gS_{tr}^0$ e.u.	$-\Delta S_m^0$ e.u.	${}_gS_{tr}^0 - {}_aS_{tr}^0$ e.u.
0 and 20.5	283	0.17	12.7	29.6	38.7	22.0	12.2
		0.32	11.1	25.9		18.8	
		0.48	10.2	23.5		16.9	

The difference between $-\Delta S_m^0$ and $({}_gS_{tr}^0 - {}_aS_{tr}^0)$ is greater than with CO₂. The entropy figures, nevertheless, point rather to a restricted mobile adsorption than to a localized adsorption. The question arises here whether the extra loss of entropy has to be ascribed to a hindering of the translation movement or to the rotation of the molecules or to both. The rotation entropy ${}_gS_{rot}$ of the CS₂ gas at 283° K is 15.5 e.u., which means that, if any, only a small part of the rotation entropy is lost. A study of the molecular area, similar to that described in article IV of this series in relation to *n*-pentane and *n*-heptane, reveals that we have to do with rotating molecules. As stated in article IV, the specific area of the charcoal of GOLDMANN and POLANYI was 885 m²/g. With the figure of v_m , mentioned above, the molecular area of a CS₂ molecule is calculated to be 25.2 Å². This figure is comparable with that of the two-dimensional VAN DER WAALS' constant b_2 , viz. 23.5 Å², which means that the molecules are not lying flat on the surface, but that they rotate. LIVINGSTON⁹⁾ gives a molecular area for CS₂ from the adsorption data of CS₂ on zinc dust, the figure being 37.9 Å². In this latter case, apparently, the CS₂ molecules lie flat on the surface.

6. DISCUSSION

The direct results of our calculations have been discussed already in the various sections. The adsorption of the three gases, investigated in the present article, on charcoal and at room temperature, is again a case of mobile adsorption. The molecules of CO move freely, the movements of the CO₂ molecules are slightly hindered, the movements of the CS₂ molecules are more severely hindered. The molecules of all three gases, however, rotate freely.

The latter conclusion is rather important for the understanding of the picture of physical adsorption. CO has a very small dipole—the dipole moment is roughly 0.1 Debye—and the contribution of this rotating dipole towards the binding energy, hence to the heat of adsorption is negligibly small. The slightly higher polarizability of CO ($\alpha = 1.99 \times 10^{-24}$ cm³) with

⁹⁾ H. K. LIVINGSTON, J. Colloid Sci. **4**, 447 (1949).

respect to the figure of N_2 ($\alpha = 1.74 \times 10^{-24} \text{ cm}^3$) causes the heat of adsorption of CO to be somewhat higher than that of N_2 .

CO_2 and CS_2 possess quadrupole moments of appreciable magnitude. These rotating quadrupoles contribute appreciably to the strength of the bond of the physical adsorption by polarizing the adsorbing surface. The polarizability of CO_2 ($\alpha = 2.65 \times 10^{-24} \text{ cm}^3$) is not large enough to explain its rather high heat of adsorption.

The two-dimensional constants b_2 for CH_4 (16.4 \AA^2) and for CO_2 (16.5 \AA^2) are practically the same. We may, therefore, consider the distance between the centre of a rotating CO_2 molecule and the adsorbing surface to be the same as the similar distance for CH_4 . The contributions of the non-polar VAN DER WAALS' forces of these two gases toward their heats of adsorption may then be expected to be in ratio to their polarizabilities. The polarizability of CO_2 being $\alpha = 2.65 \times 10^{-24} \text{ cm}^3$ and that of CH_4 $\alpha = 2.60 \times 10^{-24} \text{ cm}^3$, we should, therefore, expect the contribution of the non-polar VAN DER WAALS' forces toward the heat of adsorption of CO_2 to be roughly 5 kcal mol. The higher figures of table IV indicate that the rotating quadrupole contributes appreciably.

MAGNUS¹⁰) using the picture of rotating quadrupoles derived a theoretical expression for the heat of adsorption, according to which the heat of adsorption decreases with increasing temperature. He proved this to be the case. The figures of table IV, though derived from various authors, using different charcoals, indicate a similar decrease.

SUMMARY

1. CO, CO_2 and CS_2 , when adsorbed on charcoal at temperatures in the neighbourhood of room temperature, behave as two-dimensional gases.
2. Adsorbed CO at temperatures higher than room temperature, is "super mobile", whilst at temperatures lower than 63°K its movements are strongly hindered.
3. The adsorbed molecules of all three gases rotate freely.

*Central Laboratory of the
Netherlands State Mines*

Geleen (L.), Dec. 1953

¹⁰) A. MAGNUS, Z. physik. Chem. A142, 401 (1929).

OPTICAL ROTATION OF ORGANIC LIQUIDS

BY

P. VAN DER LEEDEN

(Communicated at the meeting of December 19, 1953)

Summary. A simple phenomenological formula for the molecular optical rotatory power of organic substances is given. It is shown that it is not in contradiction with practice. It might be valuable in determining the geometrical configuration.

1. *A simple phenomenological formula for the optical rotation*

In physical chemistry some phenomenological rules are of much use. Some of them might be called additivity rules. Their most essential feature is that they reduce the number of necessary data by claiming that the quantity considered may be derived from the data of certain groups of atoms, ions, etc. from which the molecule may be supposed to be built up. Usually the mathematical procedure consists of adding up the contributions of these groups. These rules usually have a more or less well founded approximative theoretical basis. Such rules are known and used f.i. for the index of refraction, dispersion, diamagnetism, faraday-effect and surface tension [1].

For the optical rotation there does not exist any general simple rule. The only phenomenological rule in existence, as far as the author is aware of, is the saturation rule. It states that, if one of the groups bound to an asymmetrical carbon atom is increased in length by inserting a number of CH_2 -groups, the molecular rotatory power approximates to a limiting value. This rule may, however, not be compared with those mentioned above as its application is far more restricted.

It may be seen immediately that in the case of optical rotation no additivity rule can exist. This would be contrary to the notion of the asymmetrical carbon atom. This does however not imply that no simple phenomenological rule, making use of *characteristic constants* for certain groups of atoms, may be found. The only conclusion allowed here is that the rule must involve other mathematical operations than additions only. In fact the optical rotation is relatively a rather complicated differential property of these groups. We will show that, if we restrict ourselves to simple algebraic formulae and make use of the known symmetry properties, the formula to be chosen is unique but for a certain factor.

Any formula describing the molecular rotatory power with the aid of "characteristic group constants" will have to fulfil the following conditions. Let the groups, bound to the carbon atom considered, be denoted by I, II, III and IV in a certain geometrical order.

a. The formula must reduce to zero if any two of the groups I, II, III, IV are identical.

b. If any two of the groups I, II, III, IV are interchanged, the formula must change sign only.

c. On replacing one of these groups by a group V (at the identical geometrical position) the rotatory power must be able to change its sign.

d. Moreover we will ask for as simple a formula as possible.

Let a_1, a_2, a_3 and a_4 denote the "characteristic constants" of the groups I, II, III and IV. The values of a_j will depend on the wavelength. Then the mathematical formula fulfilling the above conditions best is:

$$(1) \quad M_{D,\lambda} = M \cdot \alpha_\lambda = (a_1 - a_2)(a_2 - a_3)(a_1 - a_4)(a_2 - a_3)(a_2 - a_4)(a_3 - a_4).$$

Of course there is no certainty a priori that (1) will do. It might f.i. well be that this function will have to be multiplied by a function $f(n_\lambda)$ of the index of refraction n_λ at the wave length considered. This seems most likely indeed. However the optical rotation being a *differential* property and the index of refraction being an additive one, the influence of the latter might be relatively very small. For the time being we will accept this point of view and put $f(n_\lambda) = C$, a constant, provisionally.

In trying to find out whether (1) suits its purpose, one meets with more difficulties than is usual with additivity rules. This is due to the following:

a. The formula always contains four different a 's (or $\alpha = 0$).

b. Each characteristic constant occurs to the third power.

c. The expression is of the sixth power in all a 's together.

d. The experimental data don't give the sign of α .

Thus one is not able to determine the a -values from a suitable amount of data by just solving some linear equations.

The following arguments, however, make some simplifications possible.

a. A constant added to all the a 's does not make any difference, thus one of them can be made zero, say for the CH_3 -group.

b. The ratios of the α 's do not change if all a 's are multiplied by the same factor.

c. The saturation rule which may be extended to state that the influence of any "far away" substitution, not giving rise to a new center of optical activity, will be small.

2. A preliminary numerical test

The amount of numerical data available is extensive. For this preliminary test the more frequently occurring substitution groups will be selected. We will restrict ourselves to liquids only. Mixing up data for liquids and gases seems unwise in connexion with our neglect of (n_λ) . Moreover the data for gases, which we would have preferred otherwise, are rare. All data used are from the International Critical Tables. The sequence $\text{H}_1, \text{CH}_3, \text{C}_2\text{H}_5$ etc. forms the basis for the characteristic constants. It proved easiest to take CH_3 as zero point and $C = 100$. The values used are given in table 1.

TABLE 1

H	OH	Cl	Br	J	CH ₃	C ₂ H ₅	C ₃ H ₇	C ₄ H ₉	C ₆ H ₁₃	(C ₂ O ₂ H ₃) ¹⁾
-3	-2.93	-2.85	-2.65	-2.4	0	1	1.15	1.25	1.30	1.42

As an illustration we give some calculated values for the halogenides in table 2.

TABLE 2

Substance	Group ²⁾	M	α_D	$M_{D, \text{exp.}} \cdot 10^{-2}$	$M_{D, \text{calc.}} \cdot 10^{-2}$
C ₄ H ₉ J	H/CH ₃ /C ₂ H ₅ /J	184	32	59	62
C ₅ H ₁₁ J	H/CH ₃ /C ₃ H ₇ /J	198	37	74	76
C ₆ H ₁₃ J	H/CH ₃ /C ₄ H ₉ /J	212	38	81	84
C ₆ H ₁₇ J	H/CH ₃ /C ₆ H ₁₃ /J	240	40.5	99	90
C ₉ H ₁₉ J	H/C ₂ H ₅ /C ₆ H ₁₃ /J	254	17.6	44	51
C ₈ H ₁₇ Br	H/CH ₃ /C ₆ H ₁₃ /Br	193	29 ± .2	57 ± 4	61
C ₉ H ₁₉ Br	H/C ₂ H ₅ /C ₆ H ₁₃ /Br	207	13.1 ± .3	27 ± 1	27
C ₈ H ₁₇ Cl	H/CH ₃ /C ₆ H ₁₃ /Cl	148 ⁵	20.4	30	29
C ₉ H ₁₉ Cl	H/C ₂ H ₅ /C ₆ H ₁₃ /Cl	162 ⁵	7.9 ± .2	12.5 ± .5	12.5

¹⁾ The same value may be taken for the propionate and butyrate groups approximately.

²⁾ All alkylgroups are normal ones.

A graphical illustration for the methylcarbinols, the iodides, the chlorides, the acetates and the propionates is given in fig. 1. It may be seen from this figure that a formula of the form chosen may well represent the change of the molar optical rotation in a series of homologous substances.

3. Discussion

The author wants to warn the reader that not too much worth must be ascribed to the fairness of the representation. It is in part due to the adaptation of the constants. In part it may be due to the sign of the rotation being unknown. In fact the values for H, CH₃ and C₂H₅ might well have been chosen somewhat different; the accepted values are round numbers for the sake of convenience. On the other hand, if the sign of the rotation were known, nothing would go wrong. If this happened f.i. for the alcohols the characteristic constant for the OH-group might be replaced by -3.07. This would practically give the same results, except for the sign.

The geometrical order might in future well be correlated with such a formula. For instance replacing an acetate-group by a J, Br or Cl-atom or by the OH-group will normally give no change in sign of the rotation, according to the above.

As a special point of interest we may note that as the "saturation" values for the acetates and propionates lie very close, the rotation should be the same for all of them. That this happens indeed is shown by fig. 1.

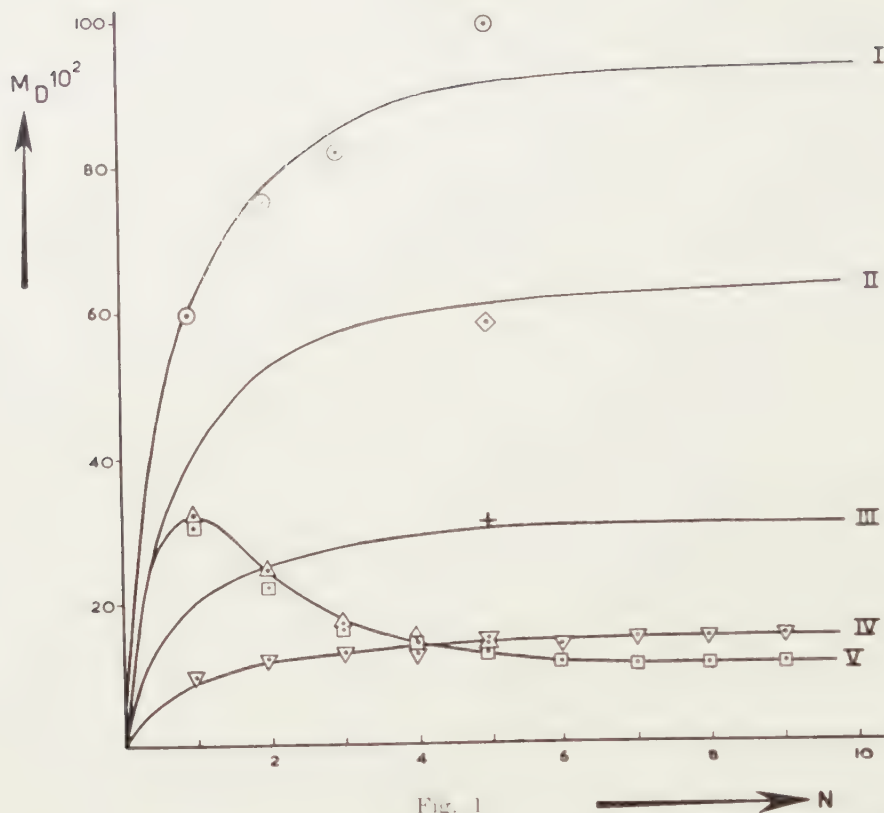


Fig. 1

Molar rotation of some organic compounds as a function the length of the alkyl-group (n)

I	jodides	$C-H/CH_3/C_nH_{2n+1}/J$	○
II	bromides	$C-H/CH_3/C_nH_{2n+1}/Br$	◇
III	chlorides	$C-H/CH_3/C_nH_{2n+1}/Cl$	+
IV	methylalcohols	$C-H/CH_3/C_nH_{2n+1}/OH$	△
V	acetates	$C-H/CH_3/C_nH_{2n+1}/C_2O_2H_3$	□
"	propionates	$C-H/CH_3/C_nH_{2n+1}/C_3O_2H_5$	▽

4. Conclusions and Outlook

It may be concluded that a formula of the type given seems suitable for a phenomenological description of the molar rotatory power.

It is quite unsatisfactory that no adequate theoretical derivation is given. There seems however little doubt that such a derivation is possible.

*Bosscha Laboratory for Physics
University of Indonesia*

Bandung, Java

REFERENCES

1. J. P. WIBAUT c.s. *Rec. Trav. Chim.* **58**, 329 (1939), **59**, 1220 (1940).
R. DE MALLEMAN, *J. Phys. et le Radium* **7**, 295, 368 (1926).
- A. J. WATERMAN, VLUGTER, VAN WESTEN and LEENDERTSE, *J. Inst. Petr. Techn.* **21**, 661, 701 (1935), **24**, 16 (1938).
- S. BROERSMA, J. H. WATERMAN, J. B. WESTERDIJK and E. C. WIERSMA, *Physica* **10**, 97 (1943).

ON THE USE OF GLASS GLOBULES AS MICROSCOPE-LENSES

BY

P. H. VAN CITTERT

(Communicated by Prof. M. W. WOERDEMAN on behalf of Prof. E. J. DIJKSTERHUIS at the meeting of December 19, 1953)

P. VAN DER STAR [1] recently again drew attention to the possibility of using a small glass globule as a lens for a simple microscope. This use already dates from the time of van Leeuwenhoek. A globule was melted to a glass thread and then this globule, mostly without its being melted off the thread (the latter nearly always causing tensions in the glass) was mounted before a metal plate provided with a small aperture or between two metal plates. This method has remained in use a very long time and rightly: the images observed through such a glass globule are remarkably good, much better than those of the compound microscopes made before 1830. They are very little influenced by spherical and chromatic aberration, the depth of focus is also very slight. Curiously enough van Leeuwenhoek always used little lenses ground by himself, though as regards spherical as well as chromatic aberration they were less practicable (see below). In the third part of his famous standard work on the microscope [2] P. HARTING even propagated the use of such glass globules as late as 1850 and even then extensively indicated a new method of making such glass globules. Unlike before, HARTING melted his globules off the thread and then melted them down in a small hole in a platinum tin. HARTING used these globules in a microscope after WOLLASTON [3] constructed especially in accordance with his instructions, which, together with a number of HARTING globules is preserved in the University museum of Utrecht. In 1933 the present author [4], together with a number of microphotographs made with the microscope of van Leeuwenhoek at Utrecht, also published some photographs made by means of a home-made glass globule, while in 1941 T. Y. KINGMA BOLTJES [5] in an extensive study entitled "Some experiments with blown glasses" again drew attention to the surprisingly good quality of the images obtained by means of such a glass globule ¹⁾.

For a not too great divergence of the light-rays for a symmetric biconvex

¹⁾ In figure 1 of his publication KINGMA BOLTJES plots the resolving powers measured by himself and by HARTING a century earlier in the graph published by the present author in his "Descriptive Catalogue" [3c]. This, however, gives too favourable a picture of the resolving powers of the globules, as both KINGMA BOLTJES and HARTING used a condenser, while the data in [3c] referred to illumination with parallel light.

lens with radii of curvature R mm, refractive index n and thickness t mm the formula (fig. 1)

$$x_1 x_2 = f^2 \text{ resp. } \frac{1}{v} + \frac{1}{b} = \frac{1}{f},$$

obtains, in which

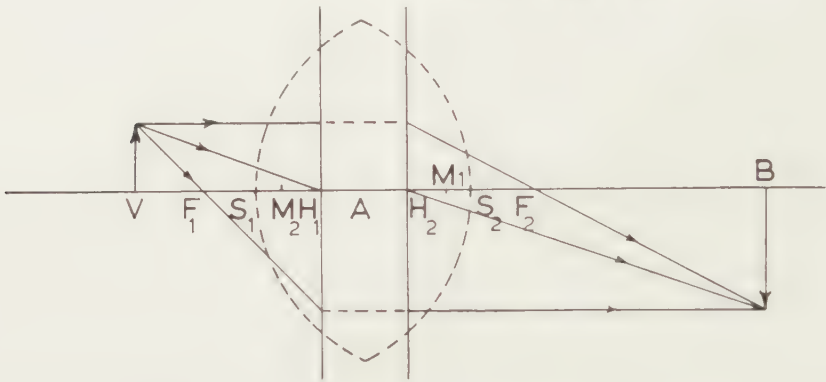
$$f = \frac{nR^2}{N} \quad N = (n-1) \{2Rn - t(n-1)\}.$$

The magnification is

$$M = \frac{f}{x_1} = \frac{x_2}{f} = \frac{b}{v},$$

while further

$$S_1 H_1 = S_2 H_2 = \psi = \frac{(n-1)lt}{N} \text{ and } \frac{AF_1}{AH_1} = \frac{AF_2}{AH_2} = f + \frac{1}{2}t = \psi \text{ en}$$



$$\begin{array}{lll} M_1 S_1 = M_2 S_2 = R & F_1 H_1 = F_2 H_2 = f & S_1 H_1 = S_2 H_2 = \psi \quad S_1 S_2 = t \\ V F_1 = x_1 & B F_2 = x_2 & V H_1 = v \quad B H_2 = b \end{array}$$

Fig. 1

For an infinitely thin lens ($t = 0$)

$$N = Rn(n-1) \text{ and so } f = \frac{R}{2(n-1)}$$

and the points H_1 and H_2 coincide with A . For a spherical lens ($t = 2R$) however,

$$N = 2(n-1)R \text{ and so } \frac{nR}{2(n-1)},$$

while, as ψ becomes $= R$ the points H_1 and H_2 now coincide with the centre of the sphere. So for a spherical lens the formula

$$\frac{1}{b} + \frac{1}{v} = \frac{2(n-1)}{nR}$$

holds good. For $n = 1.5$ the local distance $f = 1.5 R$. So a non-accommodated eye sharply observes an object placed at a distance $\frac{1}{2}R$ from the surface

of the globule. The angular magnification is then

$$M = \frac{250}{1,5 R}.$$

Aberrations arise for larger values of the divergence.

In table 1 for various values of i (cf. fig. 2), so for various magnitudes of the aperture of the diaphragm $QQ' = 2R \sin i$ a number of data have

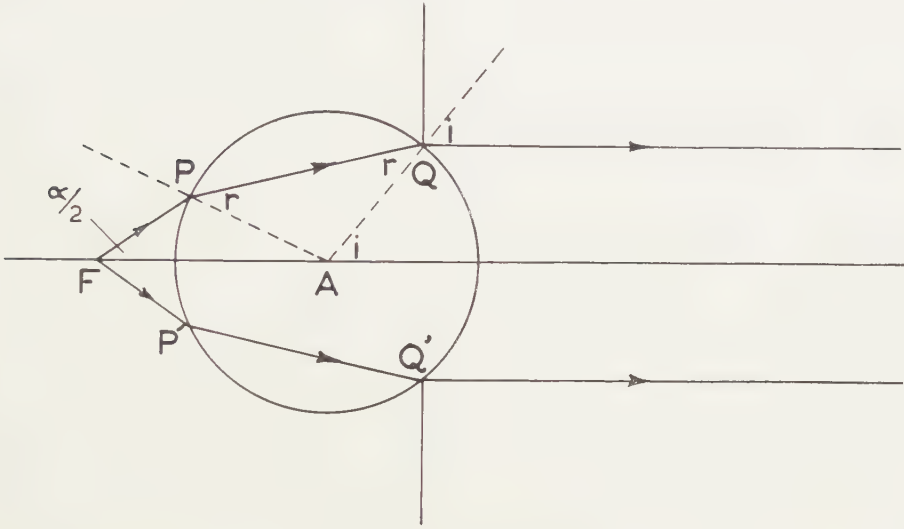


Fig. 2

been brought together, viz. half the aperture $\frac{1}{2}\alpha = 2(i - r)$, the numerical aperture $A = \sin \frac{1}{2}\alpha$, the resolving power $d = \lambda/A$ for $\lambda = 0,54 \mu$ and the focal distance $f = FA$ (the angles have been rounded off to multiples of $20'$).

TABLE 1

i	$\frac{1}{2}\alpha$	A	d	f
0°	0°	0	—	$1,500 R$
5°	$3^\circ 20'$	0,058	$9,27 \mu$	$1,499 R$
10°	$6^\circ 40'$	0,116	$4,65 \mu$	$1,496 R$
15°	10°	0,174	$3,11 \mu$	$1,490 R$
20°	$13^\circ 40'$	0,236	$2,29 \mu$	$1,448 R$
25°	$17^\circ 20'$	0,298	$1,81 \mu$	$1,418 R$
30°	21°	0,358	$1,51 \mu$	$1,395 R$
35°	25°	0,423	$1,28 \mu$	$1,357 R$
40°	$29^\circ 20'$	0,590	$1,11 \mu$	$1,312 R$
45°	$33^\circ 40'$	0,544	$1,00 \mu$	$1,247 R$

As the path of the light-rays through glass globules is entirely independent of the diameter of these globules, provided that the same relative part of the globule is diaphragmed, the numerical aperture of all glass

globules with the same relative aperture is completely identical and so they *all have the same resolving power*. So as the resolving power d is independent of the magnification M , the product $D = Md$, which VAN DER STAR in his booklet plots against M , should be represented by a straight line I through the zero (fig. 3). Only for a very small magnification the

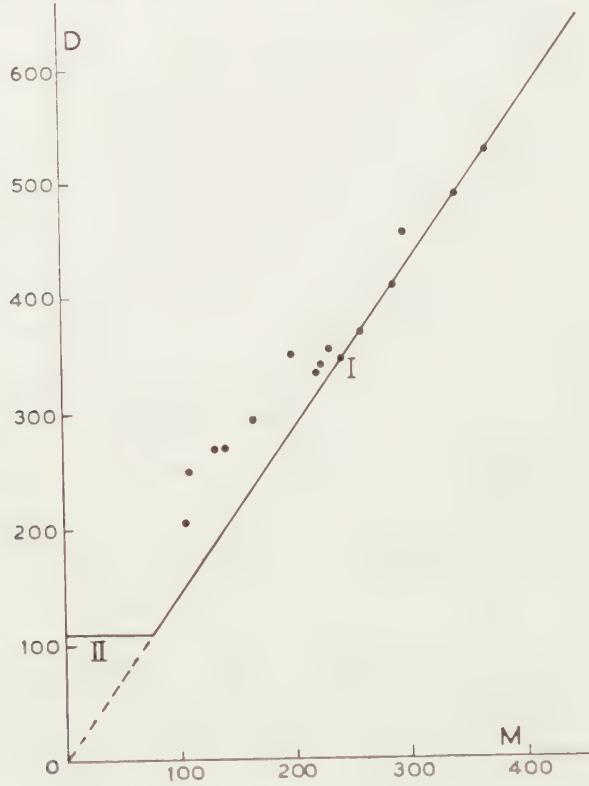


Fig. 3

condition must be fulfilled that two points can only then be seen separately by an average eye, at least if they are seen radially under an angle of about $1\frac{1}{2}' = 0,000437$. Then

$$\frac{Md}{250} = \text{about } 0,000437, \text{ so } D = Md = \text{constant} = \text{about } 109 \mu$$

holds good, with which the experimental value 115μ found by VAN DER STAR corresponds well ¹⁾. So for small magnifications the line II, parallel to the M -axis, holds good. So the theoretical curve representing the connection between the D and M consists of two straight lines, viz. the line I through the zero and the line II through a point $D = \text{about } 110 \mu$.

¹⁾ The size of the pupil of the eye plays no part; with globules with such a big radius of curvature that the active aperture would be bigger than that of the pupil of the eye, the resolving power has been limited for a long time by the above-mentioned $1\frac{1}{2}'$ condition.

The line I drawn in fig. 3 has been connected as well as possible to the five best globules measured by VAN DER STAR. These five globules give points which lie almost exactly on this line, that corresponds to $d = 1,43 \mu$. The other points point to a somewhat smaller resolving power, which, if the quality is the same, shows that the aperture is somewhat smaller. (The points given by VAN DER STAR in his fig. 1 have been indicated in fig. 3) It follows from $d = 1,43 \mu$ that about half of the globules were diaphragmed ($i = 31\frac{1}{2}^\circ$). It is a pity that VAN DER STAR does not state the aperture of his globules, but he informed me that it was indeed about 30° ¹⁾.

The point F , which is about $1\frac{1}{2} R$ mm removed from the centre A of the globule, is observed sharply by a non-accommodated eye. If the aperture of the globule is α , a point P , removed at a very little distance

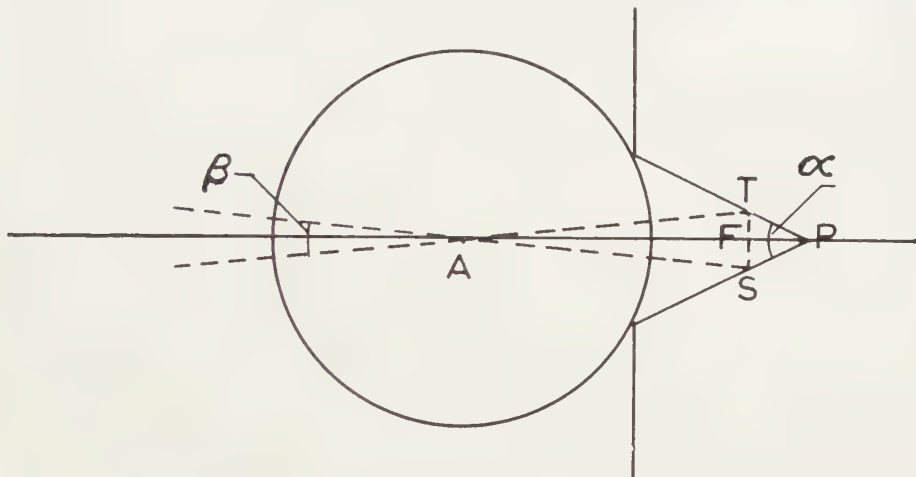


Fig. 4

$FP = p$ mm from the focus causes in the focal plane a light-patch ST with a diameter $2p \operatorname{tg} \frac{1}{2}\alpha$ (fig. 4). Now this light-patch is observed via the globule under an angle β , determined by

$$\operatorname{tg} \frac{1}{2}\beta = \frac{p}{1,5R} \operatorname{tg} \frac{1}{2}\alpha.$$

When the angle $\beta < 1\frac{1}{2}'$, this light-patch is still observed as one sharp point. So it is required:

$$\operatorname{tg} \frac{1}{2}\beta = \frac{1}{2}\beta = \frac{p}{1,5R} \operatorname{tg} \frac{1}{2}\alpha < 0,75' = 0,000218$$

or $p < 0,000327 R \operatorname{ctg} \frac{1}{2}\alpha$.

For $R = 1$ mm and $\frac{1}{2}\alpha = 30^\circ$ p becomes $< 0,57 \mu$. So only points situated within this distance from the focal plane can be observed sharply. So the depth of focus is very good.

¹⁾ The line $D = 1,05 M + 115$ indicated by VAN DER STAR has no physical significance at all; the conclusion that the resolving power even for the strongest globules could never exceed the value $1,05 \mu$ is wrong.

In order to get an impression of the influence of the chromatic aberration we are going to suppose that the refractive indices for the wave-lengths, corresponding to the Fraunhofer-lines F , C and E are $n_F = 1,506$, $n_E = 1,503$ and $n_C = 1,499$ respectively (borosilicate crown I)¹⁾. As all light-rays through the centre A (fig. 5) of the globule continue unbrokenly,

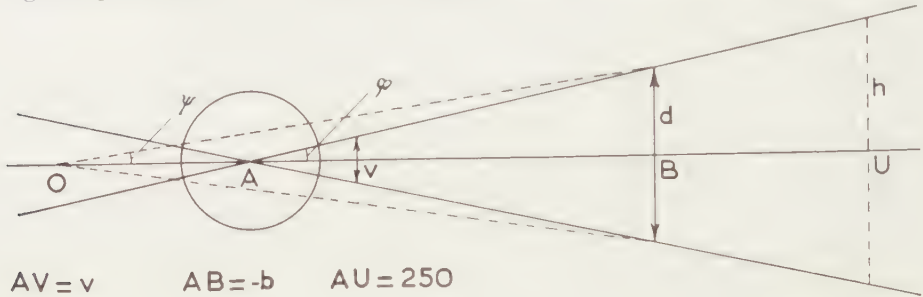


Fig. 5

the images B_F , B_E and B_C for the wave-lengths F , E and C will be seen from A under the same angle φ and fall *completely* behind one another. So, seen from A , the images will completely cover themselves and will therefore not at all be influenced by chromatic aberration. However, the eye cannot be placed in A , but the globule must be held a little before the eye. If we assume that the distance from the optical centre O of the eye to the point A is, for instance, 10 mm, further, that the radius of the diameter of the cone at a distance of 250 mm from A is h mm and that the distance AB from A to one of the virtual images is $-b$, this image becomes, seen from O under the angle

$$\psi = \frac{-bh}{(-b+10)250} \text{ instead of under } \varphi = \frac{h}{250}.$$

We now consider a globule with $R = 1$ mm and place the object V at such a distance from the globule that for the wave-length E the image is observed at 250 mm before the lens ($b_E = -250$). The formula

$$\frac{1}{c} + \frac{1}{b} = \frac{2(n-1)}{nR}$$

then teaches us that $v = 1,49$ mm, $b_C = -143$ mm and $b_F = -1000$ mm, while the magnifications for E , C and F are 168 , 96 and $672 \times$ respectively. Though the images for the different colours are very divergent, the angles under which they are seen from the point O are:

$$\psi_E = \frac{h}{260} = 0,00385 h$$

$$\psi_C = \frac{143 h}{153 \times 250} = 0,00374 h$$

$$\psi_F = \frac{1000 h}{1010 \times 250} = 0,00396 h.$$

¹⁾ The influence of the wave character of the light, the chromatic and the spherical aberration should really be treated simultaneously. This leads to very great mathematical difficulties, however.

The sensitivity of the eye for E is great as compared with that for C and F , the sensitivity of the eye outside the field CF is rather small.

Now, if the angles $\psi_E - \psi_C = 0,00011 h$ and $\psi_F - \psi_E = 0,00011 h$ are smaller than $1\frac{1}{2}' = 0,000437$, so $h < 4$ mm, the colours E and C or E and F are not observed separately. So for an image-field of 8 mm the field of view is completely achromatic. In practice this is even better. If we suppose that the image-forming light-beam is bounded on the side of the eye by a diaphragm with a diameter of 1 mm ($i = 30^\circ$, table 1), the resolving power is about $1,5 \mu$. Therefore, the object distance being $v = 1,49$ mm, two points, as regards the resolving power, must be seen at least under an angle of 0,001 radial, so as to be observed separately. This angle is still about twice as large as the $1\frac{1}{2}'$ required by the eye. So the field of view may be about twice as large before the chromatic aberration becomes troublesome, for when the angles are smaller the diffraction images for the wave-lengths C and F are largely covered by that of the wave-length E which acts much more strongly upon the eye. When the aperture is larger, this gets worse of course. As regards magnification a globule with $R = 0,6$ mm corresponds very well with the lens of van Leeuwenhoek at Utrecht. The magnification for the wave-length E is then about 279 times. The differences in the angles $\psi_E - \psi_C$ and $\psi_F - \psi_E$ are now on an average 0,00016 h .

For the lens of van Leeuwenhoek at Utrecht ($R_1 = R_2 = 0,75$ mm, $d = 1,1$ mm) in case the virtual image for the wave-length E lies 250 mm from the centre A , one finds for $\psi_E - \psi_C$ and $\psi_F - \psi_E$ 0,00018 h on an average. So with the lens of van Leeuwenhoek the influence of the chromatic aberration is somewhat greater than that with a glass globule of about the same strength.

Fig. 6 gives an impression of the magnitude of the spherical aberration of a glass globule. The path of the emerging rays has been drawn in the case that a parallel light-beam with a diameter $\frac{1}{2}R$ ($i = 30^\circ$) falls on the globule. In the coaxial focus a light-patch then arises with a radius of about $1/500 R$, surrounded by a halo about $18 \times$ as large, the average intensity of which is only about $1/400$ of that of the coaxial light-patch (computed graphically, supposing that the spherical aberration is the only defect of the image). VAN ALBADA [6] computed the spherical aberration for several shapes of lenses. He found that the distance between the coaxial focus and the focus of the marginal rays, for a lens of exactly the same shape and aperture as the lens of van Leeuwenhoek at Utrecht ($d = 1,68$; $R_1 = R_2 = 1,145$; $f = 1,45$; $n = 1,523$, radius of the lens aperture on the side of the eye 0,58, everything expressed in any given measure), was 0,182, while this distance is only 0,137 for a glass globule with the same aperture and the same focal distance. This is in complete agreement with results of VAN HEEL (private communication). It follows from the latter's computations that as regards the spherical aberration the spherical shape is more favourable than any other shape. For a lens aperture identical

with that of the microscope of van Leeuwenhoek at Utrecht he found that in the coaxial focus the proportion of the radii of the light-patches due to spherical aberration of the lens of van Leeuwenhoek and of an equally strong globule was about 50 : 37.

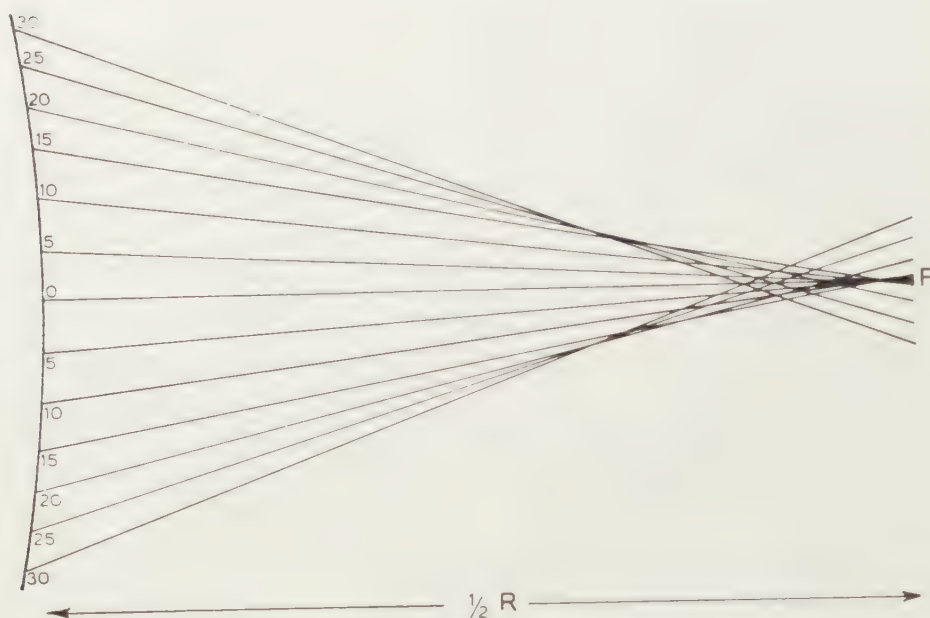


Fig. 6

The chromatic as well as the spherical aberration of the lens of van Leeuwenhoek being greater than that of an equally strong globule, it remains a mystery why van Leeuwenhoek preferred ground lenses. VAN DER STAR's explanation that the field of view of a globule is only 1 to $1\frac{1}{2}$ cm seems to me untenable. The microphotograph of an object micrometer given by VAN DER STAR in fig. 11 of [1] is indeed only sharp for $1\frac{1}{2}$ cm, but outside this $1\frac{1}{2}$ cm the lines of the micrometer become double, which in my opinion cannot be the consequence of a spherical or chromatic aberration, but must be due to the quality of the globule. In fig. 7 a microphotograph of a NOBERT's test plate is shown, made about 20 years ago by the present author by means of a glass globule with a magnification $320\times$, that had been selected as the best from more than a hundred globules. The photograph gives 4 groups, running from a line distance 2.66μ to one of 2.02μ , taken with a magnification $225\times$ which is sharp for the whole photograph, i.e. for 7 cm. So with $320\times$ this would be for about 8.5 cm. The diameter of the globule was 1.1 mm and on the side of the image it had an aperture of 0.5 mm (other photographs made by means of this globule are to be found in [4]). By way of comparison fig. 8 gives the same object shown by means of the microscope of van Leeuwenhoek at Utrecht. When we judge this photograph, the fact should be taken

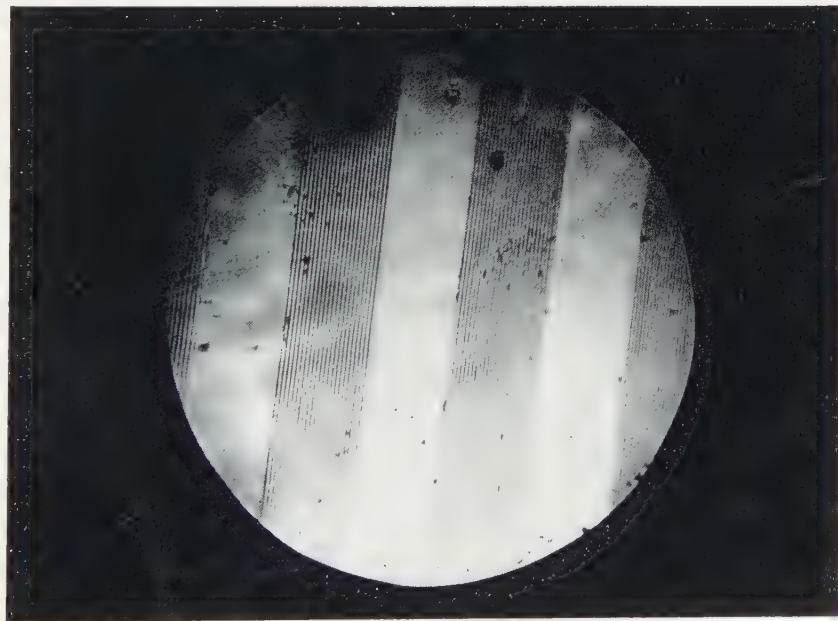


Fig. 7

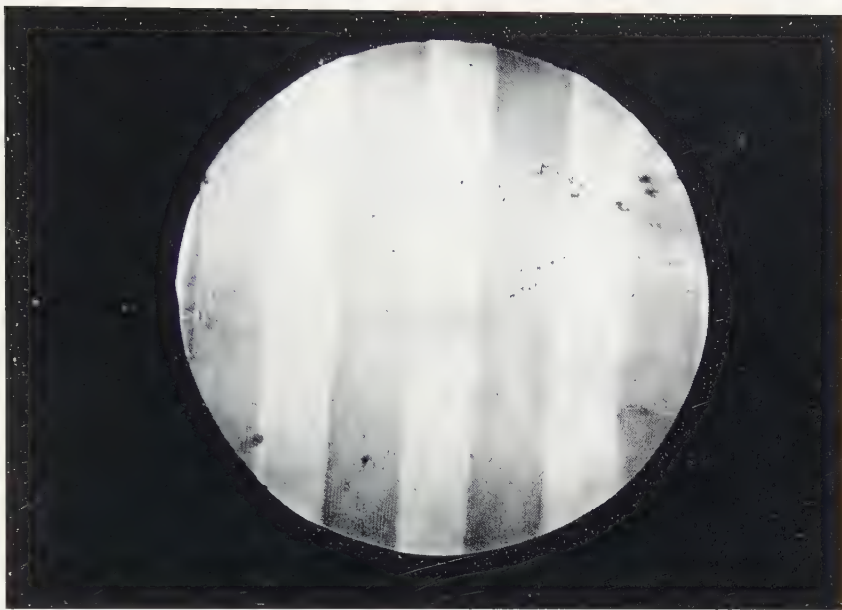


Fig. 8

into account that the front side of the lens of van Leeuwenhoek is strongly scratched, so that, the object lying very close to this scratched front side, the image has become less sharp. The image distances are identical for the two photographs. So it is certainly possible to observe images with a large field of view by means of a glass globule. But it may be, of course, that in view of the defective resources formerly available, a better result could be achieved by means of ground and polished lenses than with molten glass globules.

Utrecht University Museum

REFERENCES

1. STAR, P. VAN DER, Descriptive catalogue of the simple microscopes in the "Rijksmuseum voor de Geschiedenis der Natuurwetenschappen" at Leyden (1953).
2. HARTING, P., *Het mikroskoop* III p. 55 e.v. (1850).
- 3a. ———, l.c. p. 78–79 footnote.
- b. ———, *Bulletin de Sc. phys. et nat.* **1**, 354 (1839).
- c. CITTERT, P. H. VAN, Descriptive catalogue of the collection of microscopes in charge of the Utrecht University Museum. (Noordhoff, Groningen, 1934).
4. ———, *Natuur en Mensch* **53**, 136 (1933).
5. KINGMA BOLTJES, T. Y., *Antoni van Leeuwenhoek* **7**, 61 (1940/41).
6. ALBADA, L. E. W. VAN, *Natuur en Mensch* **54**, 140 (1934).

REVERSALS OF THE MAIN GEOMAGNETIC FIELD. III

BY

J. HOSPERS

(Communicated by Prof. F. A. VENING MEINESZ at the meeting of Sept. 26, 1953)

CONTENTS

	page
§ 5. Repeated reversals of the main geomagnetic field	112
§ 6. The apparent disagreement with other work	114
§ 7. Applications of rock magnetism	116
Acknowledgements	118
Summary	119
References	120

§ 5. *Repeated reversals of the main geomagnetic field*

The reversals take place, as the observations show, through 180°. This suggests that it is not a local phenomenon, but that the whole earth's field has been reversed, so that we are in fact dealing with reversals of the main geomagnetic field. The manner in which these reversals occur is difficult to ascertain, as each lava flow only fossilizes the external field at the time of cooling and the record therefore is discontinuous. It seems advisable to postpone any conclusions as to the mode of reversal until sediments, which may provide a more continuous record, have been studied with a view to this question.

The time scale as provided by the geological observations is necessarily rather uncertain. The only available yard-stick is the average time interval between successive lava flows. HAWKES (1916) has estimated this as 1,000 years. This figure represents, in fact, the minimum length of time required to produce the observed degree of weathering and sedimentation between successive flows in the Tertiary series. On the other hand, tillites and fluvioglacial beds occur between flows in the Early Quaternary series. These beds of glacial and fluvioglacial origin are sometimes covered by pillow lavas which are thought to have originated when lava came into contact with the ice cap, but in most cases they are overlaid by normal, subaerially formed flows. A tillite represents in all probability at least several thousands of years. One thousand years seems therefore to be an underestimate for the average time interval in the Early Quaternary series. The same is concluded from the number of flows (24) in the Early Quaternary series of Mt. Esja in S.W. Iceland. The time taken for the formation of this series is more likely to be 240,000 than 24,000 years,

especially as two presumably glacial beds occur in it. For the Early Quaternary flows the average time interval between successive flows is therefore 1,000–10,000 years, and this figure is thought to apply to the Tertiary series as well.

Combining the observations of the number of flows in each N or R zone in all sections, it appears that up to 24 flows may occur in an R zone and up to 25 flows in an N zone. A normal or reversed geomagnetic field therefore persists over periods of 25,000 to 250,000 years. Considering the evidence shown in the stratigraphic column (Table VI), it appears that there is no evidence of reverse magnetization in rocks younger than those of the Early Quaternary formation. This suggests that the Quaternary period comprises one R and one N period, and the period of time over which a normal or reversed field persists may therefore be as much as 500,000 years. The best figure for the average length of time over which the earth's magnetic polarity remains unchanged is therefore 250,000–500,000 years.

The time taken by the actual reversal is infinitesimal if one considers the reversal as due to a decrease in field strength and a subsequent increase in the opposite direction. If the change is actually a change in direction, there is more point in discussing the rate of reversing. The observations show that in lava flows the reversal occurs within at most two average time intervals between successive flows; the reversal therefore occurs within 2,000–20,000 years. A figure of about $1/50$ of the period over which the same polarity persists is therefore suggested.

The number of periods with R fields is, as shown in Table VI, at least four. The geological record on which this table is based is, of course, very far from complete, but the fact that the N and R zones alternate in comparable thicknesses suggests that the phenomenon is periodic and that N and R fields occur with equal frequency. The observations therefore suggest that the main geomagnetic field reverses every $\frac{1}{4} - \frac{1}{2} \times 10^6$ years and that this has been happening at least since Miocene times, i.e. for the last $12 - 26 \times 10^6$ years.

In the Introduction reference has already been made to the many instances of reverse magnetization in igneous rocks. The two best known examples are the Pilansberg dyke system in Southern Transvaal (GELLERTICH 1937, discussed in CHAPMAN & BARTELS 1940, pp. 156–7) and the tholeiite dykes of Northern England (BRUCKSHAW & ROBERTSON 1949). These interesting observations have been tentatively explained by their authors as due to a reversed geomagnetic field at the time of solidification of the rock. The same explanation has been advanced for the reverse magnetization found in the igneous complex of Mull (BRUCKSHAW 1953) and for that found in the volcanic system of Gergovie, France (ROCHE 1950, 1951, 1953). ROCHE made several observations which have a direct bearing on the origin of the reverse magnetization. This author compared the intensity of permanent magnetization (per gram) and the susceptibility

(per gram) of N and R igneous rocks from the volcanic system of Gergovie and found the mean values shown in Table XV. This agrees completely

TABLE XV

Group	Intensity of permanent magnetization in e.m.u./gm.	Susceptibility times present field strength in e.m.u.
Normal magnetization	1.20×10^{-3}	0.32×10^{-3}
Reverse magnetization	1.14×10^{-3}	0.31×10^{-3}

with our findings. ROCHE also heated some specimens with natural reverse magnetization and found that the permanent magnetization was lost without a change in sign and that on cooling a thermo-remanence was acquired in the direction of the external field. This is also in complete agreement with our observations. In addition ROCHE (1953) has reported some very interesting field observations. He found that clay, baked by overlying reversely magnetized lava flows was invariably reversely magnetized in the same direction. In two cases he was able to show that these clays were not derived from rocks of volcanic origin but from the Archaean basement. He further observed that a marly limestone, which had been baked by a reversely magnetized dyke, was also reversely magnetized in practically the same direction. ROCHE therefore explains the observed reverse magnetization as acquired in a reversed field.

It may be significant that reverse magnetization has never been found in igneous rocks younger than Early Quaternary; in all instances where Late Quaternary igneous rocks (lava flows) were investigated the magnetization proved to be normal.

§ 6. *The apparent disagreement with other work*

a. The conclusion that the geomagnetic field in Iceland has been repeatedly reversed and that these reversals probably were worldwide, is seemingly contradicted by investigations on sedimentary rocks by TORRESON, MURPHY and GRAHAM (1949). These authors concluded from their measurements that for the last 50 million years the geomagnetic field centred on the earth's geographic axis and that the results are consistent with the idea that no reversal of magnetic polarity occurred during that period. This conclusion is based on investigations of sedimentary rocks mainly of Tertiary (Eocene-Pliocene) age (from 50–60 million to 5–10 million years old) and some of Jurassic age (125, — 150,000,000 years old). This work has been a great step forward in the study of rock magnetism and constitutes the first systematic investigation of the natural permanent magnetization of sediments of pre-Quaternary age. However, more recent work in this field shows that the permanent magnetization of a sediment, acquired on deposition, is often unstable (personal communication of Mr E. IRVING, Cambridge University; cf. also GRAHAM

1949 and below). The stability of the magnetization must therefore be established before definite conclusions can be drawn and this has not been done in the case of the sediments under discussion. It may be of interest to note that of the 99 samples on which the above conclusion is based, 7 were actually found to possess R magnetization.

b. In Silurian sediments in the U.S.A. anomalous magnetization has also been found. In West Virginia there are a series of beds, 30 or more metres thick, which are magnetized as if they had been laid down in the southern magnetic hemisphere. The beds are enclosed above and below by beds having normal magnetization. (TUVÉ 1950, pp. 62–3.) This author, however, believes that the most straightforward explanations of the observed anomalous magnetization — a reversal of the earth's magnetic field or a drifting of the continents — are not satisfactory, as at Clinton, New York, beds bearing the same unusual fossil (a rare ostracod) as the West Virginia deposits and thus presumably of the same age as these beds, do not show anomalous magnetization. In the present author's opinion the validity of this argument cannot be admitted, as the figure of 100,000 years quoted as the period of time this rare ostracod could have lived is quite arbitrary. If this period of time is assumed to be 500,000 or 1,000,000 years, sufficient time is available for one period of N and one of R polarity of the earth's magnetization. Moreover, there is no evidence that the normal magnetization of the Clinton beds was acquired on deposition.

It should be added, however, that a reversal of the earth's magnetic field through 180° in Silurian times cannot account for the anomalous magnetization found in West Virginia either, as compared with the present field direction only the vertical and not the horizontal component is reversed.

c. KAWAI (1951) has investigated sediments in Japan ranging in age from Miocene to Quaternary. These sediments were formed by nearly continuous deposition in a shallow sea, the only break being situated between Miocene and Pliocene. The total thickness is more than 6,000 metres; the series was sampled at intervals of 30 metres. The bulk of this series of sediments is normally magnetized, except some Late Tertiary marine andesitic tuffs and some andesitic lava flows of the same age. This seems at first sight to contradict the hypothesis of repeated reversals, as the total thickness of R sediments is very small compared with that of the N sediments. However, no tests of stability of the magnetization were carried out.

In a later typewritten communication N. KAWAI and S. KUME discuss in some detail the stability of the magnetization of these sediments. They show that by repeated heating and cooling between 0 and 40°C in a constant field of 0.4 gauss sedimentary specimens acquire a permanent magnetization of the same order of intensity as the original natural magnetization of the specimens. They therefore conclude that sedimentary

specimens may acquire a secondary magnetization in the direction of the present field through diurnal or seasonal changes in temperature, a secondary magnetization which is superimposed on the primary magnetization which originated during deposition. The natural permanent magnetization of these sediments is therefore the resultant of the primary and the secondary magnetization. The intensity of the secondary magnetization may vary and cause a large scatter in the directions of natural permanent magnetization in the same bed. Occasionally this secondary magnetization can be so large that it swamps the primary magnetization; this is illustrated by a conglomerate of which the pebbles show directions of magnetization which are perfectly lined up in the direction of the present field. By means of an ingenious geometrical consideration KAWAI and KUME find that for Upper Miocene sediments the primary magnetization is reverse (Declination S 19.3° W, Inclination -54.3°). Similarly reversed primary magnetizations were thus found by these authors in sediments of Pliocene and Plio-Pleistocene age in Japan.

This illustrates the importance of stability tests being carried out on sediments before valid conclusions can be drawn.

d. JOHNSON, MURPHY and TORRESON (1948) have described measurements on Pacific ocean cores. From these measurements it is concluded that the direction and intensity of the earth's magnetic field have remained substantially constant during the last million years. These results are given with some reserve by the authors as the ferromagnetic material responsible for the permanent magnetization has not been identified and as stability tests, as used in other sediments, cannot be applied. The possibility therefore exists that the magnetization of these cores is unstable.

e. It has been endeavoured in the past to find the orientation of bore hole samples of sedimentary rocks by measuring their permanent magnetization. The underlying assumption is that the samples are magnetized in the direction of the present field. The released information is scarce and often only the horizontal component has been measured (LYNTON 1938, REICH 1941). On the whole it seems that the partial success of this method does not so much prove that no reversely magnetized sediments have been encountered as that the magnetization in most sediments is unstable.

The apparent disagreement of previous work on the magnetization of sediments with the repeated reversals of the earth's magnetization suggested in this paper is therefore not so serious as may seem at first sight. It results that for all work on the magnetization of sediments the stability is of paramount importance.

§ 7. *Applications of rock magnetism*

Apart from suggesting the interesting phenomenon of repeated reversals of the main geomagnetic field, the study of rock magnetism has several other applications. In the first place the reversely magnetized zones,

whatever their explanation, seem to be confined to definite stratigraphic levels and may be useful for correlation over comparatively short distances between different sections in series of lava flows. Secondly, rock magnetism may be a new tool in the study of problems such as continental drift and polar wandering.

The idea that studies of rock magnetism might make a new approach of the problem of polar wandering and continental drift possible was first expressed by MERCANTON (1926). In later years it was again put forward by GRAHAM (1949, p. 160) and by GUTENBERG (1951, p. 204). Mr E. IRVING of the Department of Geodesy and Geophysics, Cambridge, has recently independently realised the importance of this approach and is at present studying the problem. A formidable difficulty in these researches is the proved instability of the permanent magnetization in many sedimentary rocks.

Polar wandering and continental drift can be distinguished from each other if data from several continents are available for the same geological formation. If polar wandering has occurred (it is assumed that in that case the magnetic pole wanders with the geographic pole, as for the last thousands of years the magnetic pole has centred on the geographic pole) a certain geological formation gives in each continent a mean direction of magnetization which is significantly different from the present and the dipole field and these mean directions will agree as to the position of the pole. If continental drift has occurred, the mean direction of magnetization of a certain geological formation will in each continent be significantly different from present and dipole field, but these mean directions will not agree as to the position of the pole.

We have already seen that for nearly all groups of Tertiary specimens there is no significant difference between the dipole field and the mean direction of magnetization. This points to the conclusion that Iceland has not suffered appreciable rotation or changes in latitude since Tertiary (at least Miocene) times. Changes in longitude can of course, not be detected by this method. A more satisfactory procedure is to mean all observations on Tertiary lava flows, the R specimens taken in the opposite direction. This involves a combination of specimens from S.W. and N. Iceland, where the dip of the theoretical dipole field is $+76.7^\circ$ and $+77.2^\circ$ respectively. The mean of these values is therefore used. In Table XVI the comparison is made. Using FISHER's treatment of dispersion on a sphere (FISHER 1953) it can be calculated (number of unit vectors

TABLE XVI

	Declination	Inclination	Angle with mean direction
Mean direction of permanent magnetization	N 1.5° E	$+77.8^\circ$	0°
Dipole field	N 0° E	$+77.0^\circ$	0.8°

$= N = 102$, length of the resultant vector $= R = 88.37$, radius of the circle of confidence for $P = 0.05$ amounting to 5.5°) that the probability is only 5 % that the true direction of magnetization makes an angle of more than 5.5° with the mean direction of magnetization as calculated. This enables us to qualify the earlier statement that no appreciable rotation or change in latitude has occurred. Taking the 5 % probability level as certainty, the direction of the dipole field in Tertiary times must lie inside a cone with a semi-angle of 5.5° around the mean direction of magnetization. The maximum possible rotation which Iceland can have suffered since Tertiary times is therefore 25° and the maximum possible change in magnetic dip is approximately 5° , the latter corresponding to a maximum possible change in latitude of 9° . (It should be noted that the two possible maximum changes cannot occur simultaneously.) This shows that within the limits of accuracy stated above, Iceland has suffered no rotation or changes in latitude since Tertiary (Miocene) times, i.e. since at least 20 million years.

The same result can be used to express the limits within which the magnetic and geographic poles must have been situated. It can thus be shown that the position of the pole in Miocene times, as given by KÖPPEN and others (cf. GUTENBERG 1951, p. 202) is definitely outside the range of possible positions. These measurements therefore contradict the theory of polar wandering, and do not support the theory of continental drift as proposed by WEGENER, though it must be said that Iceland plays no significant role in WEGENER's theory and is not suitable as a testing ground (cf. WEGENER, 1924).

Acknowledgments

The work described above has involved assistance from several persons and organisations to whom the author is greatly indebted. He wishes to tender his sincere thanks to Professors M. G. RUTTEN and R. W. VAN BEMMELEN of Utrecht University, who introduced him to Iceland and its many geological and geophysical problems; to Professor W. NIEUWENKAMP of Utrecht University who suggested the investigation of the natural permanent magnetization of Icelandic lava flows; to Professor P. M. S. BLACKETT, Dr J. McG. BRUCKSHAW and Dr S. A. A. S. VINCENZ, all of London University, for permission to use their magnetometers; to Dr S. K. RUNCORN, Professor Sir RONALD A. FISHER and Mr B. C. BROWNE, all of Cambridge University for much help and encouragement; to Mr TH. SIGURGEIRSSON and Dr S. THORARINSSON, both at Reykjavik, Iceland, for valuable assistance during the actual field work, and to Mr J. H. PARRY of this Department for his able assistance in the laboratory experiments.

The author also wishes to thank the "Netherlands Organisation for Pure Scientific Research" (Z.W.O.), the "N.V. Bataafse Petroleum Maatschappij" both at The Hague, and the Royal Society of London for financial aid.

Summary

a. The normal natural permanent magnetization of the lava flows in Iceland originated when they cooled down for the first time after their formation. This magnetization was acquired in the direction of the local geomagnetic field at that time. This magnetization (thermo-remanent magnetization) has been stable in direction over periods of millions of years.

b. Normally magnetized sediments have been studied. Their permanent magnetization has an intensity which is about one-hundredth of that of the lava flows (per cc.). This magnetization originated when the sediment was deposited; its direction is that of the local field.

c. The measurements show that taken over periods of several thousands of years the magnetic pole centres on the geographic pole. This has been so since Miocene times (approximately 20×10^6 years ago).

d. Reversely magnetized igneous and sedimentary rocks have also been found. The reversely magnetized lava flows presumably occupy definite stratigraphic levels and can be traced as far as geological correlation permits. Zones of flows with normal and reverse magnetization alternate in comparable thicknesses. There are no significant differences in susceptibility and intensity of permanent magnetization between zones with normal and reverse magnetization. The large body of field evidence suggests that these zones are similar in every respect, except that they cooled down in fields of opposite directions but of similar strength. The same conclusion is indicated by the reversely magnetized sediments.

e. Of the four different mechanisms proposed by NÉEL which can produce reverse magnetization in a normal field, the two involving chemical action must be eliminated as they cannot be reconciled with the field evidence. On the other hand the reverse magnetization of sediments can only be explained by chemical action. The mechanism which assumes the interaction of two substances of different Curie points can also be eliminated, as the laboratory experiments show that this mechanism, though in itself perhaps possible, cannot account for the reverse magnetization of the Icelandic rocks. The laboratory experiments also practically exclude the possibility of NÉEL's remaining explanation, which assumes the presence of a self-reversing mineral, being responsible for the natural reverse magnetization of the lava flows.

f. It is therefore suggested, though not without some reserve, that the Icelandic rocks have preserved a record of a repeatedly reversing main geomagnetic field. As the reversal is through 180° , it seems that this reversal is world-wide and is, in fact, a reversal of the polarity of the earth's magnetization. The manner in which the reversal takes place is still unknown, but it appears that the field changes to the opposite direction within one-fiftieth of the period over which a normal or a reversed field persists. This period is thought to be 250,000–500,000 years. The number of actually observed periods of reversed fields is 4, but the observations

suggest that it is a recurrent phenomenon that has been taking place at least since Miocene times (approximately 20×10^6 years ago).

g. Within the limits of experimental accuracy Iceland has suffered no rotation and no changes in latitude since Miocene times. The position of the geographic pole in Miocene times as suggested by workers on polar wandering is definitely outside the possible range of positions and the theory of polar wandering is therefore not supported.

REFERENCES

- BRUCKSHAW, J. MCG. and ROBERTSON, E. I., The magnetic properties of the tholeiite dykes of north England. *Mont. Not. R. Astr. Soc., Geoph. Suppl.* **5**, 308–20 (1949).
- , Magnetic properties of rocks. *Nature* **171**, 500–2 (1953).
- CHAPMAN, S. and BARTELS, J., *Geomagnetism*. 2 vol. (Oxford, 1940 (reprinted 1951)).
- , The main geomagnetic field. *Nature* **161**, 462–4 (1948).
- CHEVALLIER, R., L'aimantation des laves de l'Etna. *Ann. de Phys., Paris, série 10*, **4**, 5–162 (1925).
- COLLOQUE INTERNATIONAL DE FERROMAGNÉTISME ET D'ANTIFERROMAGNÉTISME DE GRENOBLE, 3 au 7 juillet 1950. *J. de Phys.* **12**, no. 3, 149–508 (1951).
- FISHER, R. A., *Statistical methods for research workers*. (Edinburgh and London, 1950).
- , Dispersion on a sphere. *Proc. Roy. Soc., A*, **217**, 295–305 (1953).
- FLEMING, J. A. (ed.), *Terrestrial Magnetism and Electricity*. (New York, 1949).
- GELLETICH, H., Über magnetitführende eruptive Gänge und Gangsysteme im mittleren Teil des südlichen Transvaals. *Beitr. angew. Geophys.* **6**, 337–406 (1937).
- GRAHAM, J. W., The stability and significance of magnetism in sedimentary rocks. *J. Geoph. Res.*, **54**, 131–67 (1949).
- , Note on the significance of inverse magnetizations of rocks. *J. Geoph. Res.*, **57**, 429–31 (1952).
- GUTENBERG, B. (ed.), *Internal constitution of the Earth*. (New York, 1951).
- HAALCK, H., *Der Gesteinsmagnetismus*. (Leipzig, 1942).
- HAWKES, L., The building up of the North Atlantic Tertiary volcanic plateau. *Geol. Mag.*, **53**, 385–95 (1916).
- HEILAND, C. A., Possible causes of abnormal polarization of magnetic formations. *Zeitschr. f. Geophysik*, **6**, 228–35 (1930).
- HOLMES, A., The construction of a geological time-scale. *Trans. Geol. Soc. Glasgow*, **21**, 117–52 (1947).
- HOSPERS, J., Remanent magnetism of rocks and the history of the geomagnetic field. *Nature*, **168**, 1111–2 (1951).
- JOHNSON, E. A., MURPHY, T. and TORRESON, O. W., Pre-history of the earth's magnetic field. *J. Terr. Mag. Atmos. Elec.*, **53**, 349–72 (1948).
- KAWAI, N., Magnetic polarization of Tertiary rocks in Japan. *J. Geoph. Res.*, **56**, 73–9 (1951).
- KJARTANSSON, G., *Hekla. Árbók Ferðhafélags Islands*, Reykjavík. 167 pp. with map. (1945).
- KOENIGSBERGER, J. G., Natural residual magnetism of eruptive rocks. *J. Terr. Mag. Atmos. Elec.*, **43**, 119–30, 299–320 (1938).
- LIBBY, W. F., *Chicago radiocarbon dates III*. (Chicago, 1952).
- LYNTON, E. D., Recent developments in laboratory orientation of cores by their magnetic polarity. *Geophysics*, **3**, 122–9 (1938).

- MERCANTON, P. L., Aimantation des basaltes groenlandais. C-R. Acad. Sci. Paris, 182, 859-60 (1926).
- MINAKAMI, T., Magnetization of the new lava flows of Miyakesima Island. Tokyo Imp. Univ. Earthquake Res. Inst. Bulletin, 19, 612-8 (1941).
- NAGATA, T., Reverse thermo-remanent magnetism. Nature, 169, 704-5 (1952).
- , AKIMOTO, S. and UYEDA, S., Reverse thermo-remanent magnetism. Proc. Imp. Acad. Japan, 27, 643-5 (1951).
- , ——— and ———, Reverse thermoremanent magnetism II. Proc. Imp. Acad. Japan, 28, 277-81 (1952).
- NÉEL, L., Propriétés magnétiques des ferrites; ferrimagnétisme et antiferromagnétisme. Ann. de Phys., Paris, 3, 137-98 (1948).
- , Preuves expérimentales du ferrimagnétisme et de l'antiferromagnétisme. Ann. de l'Institut Fourier, 1, 163-83 (1949).
- , L'inversion de l'aimantation permanente des roches. Ann. Géophys., 7, 90-102 (1951).
- , Confirmation expérimentale d'un mécanisme d'inversion de l'aimantation thermorémanente. C. R. Acad. Sci. Paris, 234, 1991-3 (1952).
- PJETURSS, H., Island. Handbuch der Regionalen Geologie, 4, 1. (Heidelberg, 1910).
- REICH, H., Über die Grundlage der magnetischen Bohrkernorientierung. Öl und Kohle, 37, 213-7 (1941).
- ROCHE, A., Sur les caractères magnétiques du système éruptif de Gergovie. C. R. Acad. Sci. Paris, 230, 113-5 (1950).
- , Sur les inversions de l'aimantation rémanente des roches volcaniques dans les monts d'Auvergne. C. R. Acad. Sci. Paris, 233, 1132-4 (1951).
- , Sur l'origine des inversions d'aimantation constatées dans les roches d'Auvergne. C. R. Acad. Sci. Paris, 236, 107-9 (1953).
- STREET, R., Antiferromagnetism. Science Progress, 39, 258-82 (1951).
- THORARINSSON, S., Tefrokronologiske studier på Island. Geografiska Annaler, (Stockholm, 1944).
- , The eruption of Mt. Hekla, 1947-1948. Bulletin Volcanologique, série 2, 10, 157-68 (1950).
- , Laxárgljúfur and Laxárhraun. Geografiska Annaler, (Stockholm, 1951).
- TORRESON, O. W., MURPHY, TH. and GRAHAM, J. W., Magnetic polarization of sedimentary rocks and the Earth's magnetic history. J. Geoph. Res., 54, 111-29 (1949).
- TUVE, M. A., Annual report of the director of the Department of Terrestrial Magnetism. Carnegie Institution of Washington. Year Book No. 49, for 1949-1950. (1950).
- VESTINE, E. H., LAPORTE, L., LANGE, I., COOPER, C. and HENDRIX, W. C., Description of the Earth's main magnetic field and its secular change, 1905-1945. Carnegie Institution of Washington, Publication 578. (1947).
- WEGENER, A., The origin of continents and oceans. (transl. 3rd German ed. London, 1924).
- ZEUNER, F. E., Dating the past. (2nd ed., London, 1950).

*Department of Geodesy and Geophysics
Cambridge University, England*

ON THE ACCELERATING INFLUENCE OF TIN-IONS ON THE
TRANSITION OF WHITE INTO GRAY TIN

BY

L. J. GROEN

(Laboratory for Physical Chemistry, Technical University, Delft, Holland)

(Communicated by Prof. W. G. BURGERS at the meeting of November 28, 1953)

1. By the work of COHEN (1899) it has become well-known that the transition of white into gray tin is accelerated by immersion into a solution containing tin-ions. In his experiments he used a solution of pinksalt ($(\text{NH}_4)_2\text{SnCl}_6$). COHEN ascribes this positive influence to the formation of local elements white tin/solution/gray tin. Below the transition point ($13,2^\circ\text{C}$), the unstable white modification is dissolved and the stable gray modification precipitated, due to the electromotive force of the element. If a bar or a sheet or small particles of white tin are immersed into a pinksalt solution, and the temperature is lowered down to -50°C , small, invisible, nuclei of gray tin are produced in some spots of the material; as a result local elements of the above-mentioned type are formed, thus causing a quicker transformation into the gray form.

2. On the basis of Cohen's electrochemical theory of the accelerating effect, one might conclude that gray tin is formed when a solution containing tin-ions is electrolyzed at a temperature under the transition point. In order to test this expectation, electrolyses were carried out at -50°C , the electrolysis-cell being cooled by a dry ice-spirit mixture. On account of the low solubility of pinksalt in alcohol at -50°C (crystals were precipitated by cooling a solution from room-temperature to -50°C), a 0,5 % SnCl_2 -solution in alcohol was used as electrolyte¹⁾. As it was found (cf. par. 4) that both SnCl_6^{--} - and Sn^{++} -ions exert an accelerating influence on the transition, this variation with regard to Cohen's experiments is not essential.

In all cases a sheet of white tin was used as anode; the cathode consisted of resp. white tin, copper, gray tin and germanium. Since the resistance of the solution is fairly high, a high voltage had to be applied, 110 V; the current-density was about 0,1 A/cm². During the electrolysis the contents of the beaker were stirred with an electrical stirrer. The time of electrolysis varied from 1-2 hours.

First, two electrolyses with resp. a white tin and a copper cathode were

¹⁾ The solution was 0,2 n with respect to HCl.

carried out under the conditions described. In both cases a gray deposit was formed. Removed from the cathode and rinsed with water, alcohol and acetone (care being taken that the temperature of these liquids was below the transition point), the deposit appeared to consist of a very fine powder.

To identify its composition, X-ray powder-diagrams were made at room-temperature. They showed in both cases only the line-pattern of white tin. Similar powder-diagrams of gray tin prepared in a "normal" way (by immersing white tin-powder into a 0,6 % $(\text{NH}_4)_2\text{SnCl}_6$ -solution in ethyl-alcohol and maintaining a temperature of -50°C for several days) showed the line-pattern of gray tin very intensively and only a weak indication of the strongest white tin-lines. Therefore the amount of white tin which is formed during X-ray exposure is so small that the conclusion seems justified that the products of the electrolysis consisted of white tin.

Since copper and white tin might be unsuitable for depositing the diamond-structure of the gray tin-modification, in two other electrolyses resp. gray tin and germanium were used as cathode. The structure of germanium is the same as that of gray tin, the lattice constants being resp. 5,36 and 6,46 Å. According to ROGERS and FYDELL (1953), germanium has a positive influence on the rate of transition, due to its corresponding structure. As gray tin was available only as powder and not in compact form ¹⁾, it was prepared for use as cathode by pressing it into tablet-form, care being taken that the pressure was not too high in order to prevent transition into the white state. Germanium was available in the form of a small disc.

However, also in these two cases, on electrolysis at -50°C X-ray powder-diagrams showed that only white tin was formed.

3. The formation of white tin instead of gray tin on electrolysis of a tin-salt solution at a temperature below the transition point, as shown by the above experiments, seems inconsistent with Cohen's theory of the accelerating influence of tin-ions on the rate of transition of gray into white tin. This seems still more likely as we observed that on a boundary between white and gray tin-powder, immersed into a solution of a tin-salt, no faster transition takes place than in the white tin mass itself. This conflicts with what one might expect because on such a boundary "local" elements white tin/solution/gray tin are accumulated.

With regard to this question it may be remarked that the work of BUSCH and co-workers (1951) has established the fact that gray tin is no metal but a semi-conductor. Therefore the equilibrium between the potential determining ions existing at the interface white tin/tin salt-solution cannot exist at the interface gray tin/tin salt-solution. In this connection

¹⁾ Recently we have succeeded in preparing compact pieces, measuring several mm across. They were obtained by slow transition of white tin sheet. Details of this process will be published later.

it seems also of interest to point out that COHEN (1899), DOUWES DEKKER (1927) and BRØNSTED (1914) had various difficulties with the so-called "transition-element" gray tin/tin-ions in solution/white tin, by means of which they tried to measure the transition-point, indicated by zero-value of the electromotive force.

4. In conclusion a few preliminary measurements may be mentioned which were undertaken to obtain more information on the influence of metal-ions on the rate of the transition-process. For this purpose samples of "pure" white tin-powder (Kahlbaum) were kept at -50°C while immersed into a solution of various salts in 96 %-alcohol. The process of the transition has been followed by observing the difference in colour between gray and white tin. The measurements therefore merely give an impression of the amount transformed.

The following results were obtained:

1. There is no visible difference in accelerating action between Sn^{++-} , Sn^{++++-} or SnCl_6^{--} -ions.
2. The rate of transition increases with the concentration of the tin-ions.
3. Even a 0,0006 % $(\text{NH}_4)_2\text{SnCl}_6$ -solution has an accelerating effect.
4. HCl , H_2SO_4 and NaOH act as accelerators, their effect being most probably due to the formation of resp. Sn^{++-} and SnO_2^{--} -ions, as was evident from the positive reaction on tin with cacotheline.
5. Zn^{++-} , Fe^{++++-} and GeO_2^{--} -ions have no influence, although Zn , Fe and Ge act as accelerators when alloyed with tin (COHEN (1936); ROGERS and FYDELL (1953)).

Summary

Tin, deposited by electrolysis from a tin-salt-solution at a temperature of -50°C , i.e. below the transition-point of white tin into gray tin ($13,2^{\circ}\text{C}$), is white tin. This seems inconsistent with Cohen's theory, according to which the accelerating effect of tin-ions in solution on the rate of transition of white into gray tin can be ascribed to internal electrolysis in local elements white tin/solution/gray tin.

It is further shown that only tin-ions, independent of valency or complex-form, even in very small quantities, have an accelerating influence on the transition of white into gray tin.

Delft, November 1953.

REFERENCES

- BRØNSTED, J. N., *Z. Physik. Chem.* **88**, 479 (1914).
 BUSCH, G., J. WIELAND and H. ZOLLER, *Helv. Physica Acta* **24**, 49 (1951); also: "Semi-conducting Materials", (London, Butterworth, 1951).
 COHEN, E., *Z. Physik. Chem.* **30**, 601, 625 (1899).
 ——— and A. K. W. VAN LIESHOUT, *Z. Physik. Chem.* **A177**, 331 (1936).
 DOUWES DEKKER, K., Thesis Utrecht (1927).
 ROGERS, R. R. and J. F. FYDELL, *J. Electrochem. Soc.* **100**, 161 (1953).

PHYSICS

THEORY AND APPLICATION OF HIGH RESOLUTION INTERFEROMETERS

BY

F. BRUIN

(Zeeman Laboratory, University of Amsterdam, the Netherlands)

Part III

LIMITATIONS TO RESOLUTION

(Communicated by Prof. C. J. BAKKER at the meeting of November 28, 1953)

Summary

In part III it will be investigated which effects limit the operation of an interferometer with multifold reflection and how the highest sensitivity may be obtained.

5. *Improving the properties of the etalon*

The compound interferometer. If for some purpose, e.g. the resolution of the hyperfinestructure of an optical emission line, the resolving power as well as the dispersion ratio of the interferometer should be increased this might be done by placing two interferometers behind one another with their plates parallel. The set-up of two etalons in cascade is called a compound interferometer. Because a number of fringes is suppressed the spectral range is considerably extended. The angle-dispersion, however, which is independent of L is not influenced by this cascade arrangement. So the dispersion ratio $D = \sigma_D / \Delta\sigma_0$ is *greatly increased*. This was observed first by HOUSTON [14] in 1927. The shape of the resonance curve of radiation which has traversed both interferometers is given by the product of the single intensities (27). An example is given in figure 9a for $L' = 4/5 L$.

The application of optical interferometers, as said before, offers great difficulties and can sometimes only be favourably applied if the source radiation has a large intensity. To prevent undesired "coupling" between the two systems the facing surfaces of the interferometers should make a small angle. As the radiation between the orders of one interferometer is not suppressed completely by the other one the intermediate orders of the combined system will not completely disappear. In optics this means that weak satellites of atomic spectral lines will be recognized with great difficulty or not at all. In the microwave region the intensity mostly offers no difficulty, as here monochromatic sources of high power exist. Also the technical difficulties are far smaller than in the optical case.

Figure 9b gives an example of a waveguide cascade interferometer for which the coupling is performed by small circular holes. Suppose for this case that $L=10$ meter and $\lambda=10$ mm. If the first guide is at resonance we will have resonance again if λ is changed by 0.5% . This means that each 15 Mc/s energy will be transmitted within a narrow frequency band. If the Q -factor of each system is 5000 then the total Q_t is approximately 7500. The dispersion ratio of the first interferometer is $D=Q/n_0=2.5$ and of the total system $D_t=5 Q_t/n_0=19$. Here we have a very effective method to suppress undesired modes in the second resonator.

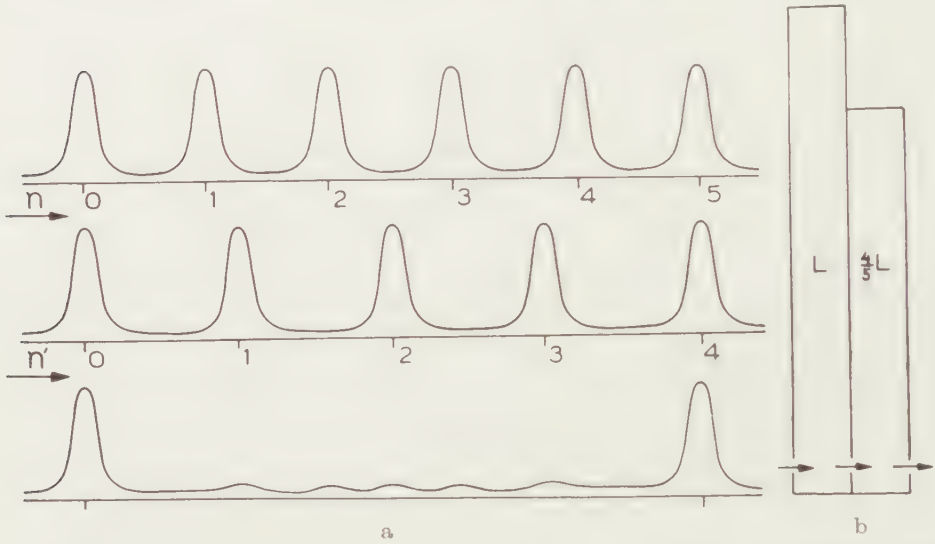


Fig. 9a. Resonance curves of two interferometers having different length L and resulting pattern of the two systems in cascade. Fig. 9b. Schematic cross section of a microwave compound interferometer.

High-reflecting multilayers. The reflectivity of the plates may be greatly increased, without excessive losses due to absorption, by coating the surface of the boundaries instead of with a silver film with a transparent layer having a thickness of a quarter wavelength and a high refractive index. When describing the experiment of POWLES [8] (part II) it was already pointed out that high reflectivity may be obtained by using a low loss medium of high refractive index, the reflectivity (fringe factor) being given by the FRESNEL equation

$$(52) \quad R^2 = f = \left[\frac{N' - 1}{N' + 1} \right]^2.$$

In this equation N' is the refractive index between the boundaries whereas outside these boundaries there is assumed to be vacuo. From (52) it follows that a single transparent layer of high refractive index may act as a multiple beam interferometer having a reasonable Q -factor and dispersion ratio. The first maximum in transmitted intensity will occur

at approximately $L = \lambda/4N'$ whereas the transmission according to (24) is given by

$$(24) \quad I_0 = \left[\frac{aT^2}{R} \right]^2 \frac{f}{(1-f)^2}.$$

Really high resolution is obtained when quite a number of layers are used, each having an effective thickness of a quarter wavelength, alternatively having high and low refractive index. Each layer will act as an etalon and the resulting resonance curve will be the product of all individual resonance curves of these interferometers in cascade. Neglecting losses the total reflectivity of k equal $\lambda/4$ -sheets at a mutual distance of $\lambda/4$ in free space is equal to that of a single $\lambda/4$ -sheet having a refractive index of N'^{2k} . With the present materials for the visible range not much seems to be gained by the use of multilayers as a silver coating may have very high reflectivity in this region. It is true a silver film has the disadvantage that only a freshly made surface has high reflectivity, but multilayers only have a very restricted wavelength range in which they are effective, whereas it is difficult to make many layers of uniform thickness. At both ends of the visible spectrum, i.e. in the red and the violet where silver has a rather poor reflectivity the multilayer is certainly superior. It was pointed out by TOLANSKY [24] that the multilayer technique may also open new fields of research in ultraviolet interferometry. The best results with this technique have been obtained in the microwave region where one may dispose of low loss materials of high refractive index. CULSHAW [22] using for each plate eight $\lambda/4$ -sheets of polystyrene, spaced $\lambda/4$ apart in air, obtained a fringe factor of $f = 0.9954$, corresponding to a dispersion ratio of $D \approx 700$, at a wavelength of 8 mm.

6. Other limits to resolving power

The losses due to reflections can be made very small. In optics a Q -factor of several times 10^6 is no exception and the same values have also been obtained with superconducting cavities [15]. Next to the energy losses which arise from multifold reflections the resolving power of the interferometer is also limited by a number of other factors which we will consider now.

Limitations by the transmitted intensity. In optics as well as in the microwave region for a given source intensity a final increase of the Q -factor of the interferometer is always associated with a decrease in transmitted power. Therefore, in order to observe sharp HAIDINGER fringes an extensive source of high intensity should be used, whereas FIZEAU fringes would even need a higher intensity, as a small aperture would be necessary to obtain a collimated beam of plane waves. For microwaves a very definite coupling between source, interferometer and detector may be obtained by means of small carefully located coupling holes. The power transmission is proportional to the energy density of the field near the holes and to the sixth power of the hole diameter d , whereas

the relative frequency shift of the resonance frequency due to the presence of holes is proportional to the third power of d . At present little is known yet about the properties of holes.

In order to obtain high resolving power in optics, i.e. a fringe factor which nearly equals unity, the plates should have high reflectivity. Only until recently this was achieved by applying a silver coating of optimum thickness, which resulted in a very poor intensity of the transmitted beam. It may be seen from the formulae developed in part I (24), (45), that the *absorption* in the coating only influences the intensity of the transmitted radiation and that neither the dispersion ratio D nor the so-called *contrast* $(1+f)^2/(1-f)^2$ (see figure 2 part I) is dependent on it. The absorption being the main handicap in keeping reasonable transmitted power while increasing the reflectivity, it is clear that far higher resolution may be obtained once the problem of absorption is overcome. This important conclusion was made by TOLANSKY in 1946 and its consequences are well illustrated in a paper by JACQUINOT and DUFOUR [24]. It is because of this that low-loss multilayers at least in some parts of the optical region have led to an improvement in resolution which would have seemed impossible ten years ago.

It is not difficult to find the conditions for optimum transmissivity of the plates. Let us assume for a moment that plate I and plate II are not identical. Then according to (24) the transmission may be given by

$$(89) \quad I_0 = \frac{|aT_I T_{II}|^2}{R_I R_{II}} \cdot \frac{1}{(1-f)^2}.$$

The transmission of the plates or of the coupling holes may be described [21] by the quality factors $Q_I = \pi n_0 R_I / T_I^2$ and $Q_{II} = \pi n_0 R_{II} / T_{II}^2$. As I_0 is symmetric in Q_I and Q_{II} and can have only one maximum value it follows that the first step to maximize I_0 should be to take Q_I equal to Q_{II} . This means that the plates should have equal properties, a fact which was assumed early in part I.

If we call the quality factor of the empty interferometer $Q_e = \pi n_0 |f| / (1-f)$ and the one for the same interferometer but being not transparent Q_0 then according to (51)

$$(90) \quad \frac{1}{Q_e} = \frac{1}{Q_0} + \frac{1}{Q_I} + \frac{1}{Q_{II}} = \frac{1}{Q_0} + \frac{2}{Q_I}.$$

By putting $\partial/\partial Q_I I_0 = \partial/\partial Q_I (\pi^2 Q_e^2 Q_I^2) = 0$, which is a condition for optimum transmission one obtains with (90)

$$(91) \quad Q_I = 2Q_0 = 4Q_e$$

So for optimum transmission we find that the interferometer should have plates with equal properties, the losses due to absorption should be equal to those due to transmission, and the power transmission should be 6.25 %.

Flatness of the plates. The limit of inaccuracy for optical grinding is nearly the natural one of atomic dimensions namely about 10^{-3} micron.

Because of this for a very good optical instrument the dispersion ratio, which may be approximated by $D \approx \lambda/\Delta L$, cannot be made much better than 50. For rocksalt plates, which are applied in the infrared region, this is little less than a micron [16], resulting in a possible dispersion ratio of about 5. For microwaves this ratio is much higher. If the plates are flat and parallel to 1 micron and if we take $\lambda = 10$ mm we find $D = 10^4$.

Temperature changes. The parts which determine the distance between the plates of an optical interferometer and also of many cavity resonators in microwave technics are made of invar. As a rule the influence of temperature on the apparatus can be made sufficiently small. This is different for the waveguide interferometer for which the temperature effect is large and difficult to control because of its length. Keeping λ fixed we find by differentiating formula (62) after substitution of $1/\lambda_g = n/2L$

$$(92) \quad \frac{dn}{n} = \left[\frac{2L}{n\lambda_c} \right]^2 \frac{d\lambda_c}{\lambda_c} + \left[\frac{2L}{n\lambda} \right]^2 N' dN' + \frac{dL}{L}.$$

If $d\lambda_c/dT$, dN'/dT and dL/dT are known one can evaluate dn/dT from (92). If one wishes to measure the influence of the temperature T on the refractive index, one may eliminate the temperature dependence of the waveguide interferometer in the wavelength region under consideration by putting equal the first and third term in (92) so that

$$(93) \quad \frac{dL}{d\lambda_c} = - \frac{4}{n^2} \left[\frac{L}{\lambda_c} \right]^3.$$

For a cavity one can satisfy this relation by taking materials having different coefficients of expansion for the plunger shaft and the cavity cylinder [13]. For the optical etalon compensation in this way is impossible because in this case $\lambda_c \rightarrow \infty$ and so the first right hand term of (92) becomes zero. However, under normal circumstances it has been found that for this etalon a thermal expansion of the invar distance pieces is practically compensated by the reduced density of an air medium.

Variations of the radiation source. Already FIZEAU noticed that the number of properly interfering reflections is limited by the finite length of the wave trains. If the wave packet is used from head to tail this natural uncertainty in wavelength determines the resolving power to be obtained by the interferometer. For light waves this limit is actually reached and amounts to approximately 10^7 . For microwaves this is quite different. Here the radiation is not generated by a large number of *independent* oscillators, but by *one* system of very closely *coupled* oscillators [23]. As a matter of fact these are the only characteristics which make possible a distinction between optical and technical sources of radiation. In the latter case the uncertainty in wavelength is no longer determined by the lengths of the individual wavetrains but by the total intensity of the radiation. This may be shown in the following way.

If we assume that on the average the wave of the macroscopic oscillator

is built up by an assembly of m photons per unit of time the total momentum of the wave will be mh/λ . As these photons are closely correlated we may consider them to have a regular phase relation. Applying HEISENBERG's principle $\Delta\lambda\Delta p \approx h$ to this system of photons we find $\Delta\lambda/\lambda \approx 1/m$. Thus a high power flux will give rise to a small uncertainty in wavelength, i.e. a 'macroscopic' stationary electromagnetic wave. For a wave having a wavelength of 10 mm and an intensity of only 1 microwatt the number m is about 10^{17} , so that the wavelength could be measured in 17 decimals if no other disturbances would exist. These other irregularities are mainly due to shot noise from the electron beam in the cavity of the klystron-oscillator and variations of its electric power supply. For cm-waves this leads to wavetrains having a coherent length which is of the same order as for an optical source namely about 10^7 wavelengths. Considerable improvement in the long time frequency stability is achieved by feeding back the output of the interferometer to the oscillator and so supply the latter with the resolving power of the interferometer. By doing this only the much smaller thermal fluctuations of the electrons in the metal of the interferometer will give rise to frequency variations. In this way a long time stability of one part in 10^9 has been reached. We conclude that in the microwave region it is advantageous to choose an 'optical' source as an *absolute* frequency standard but to use for *relative* frequency measurements a technical oscillator with feedback on an interferometer.

7. Thermal and other disturbances in the interferometer

If all uncertainties in the determination of a wavelength or intensity, mentioned in the foregoing sections, would be eliminated, finally still the fluctuations of the interfering system itself remain. Even if no source radiation is incident on the instrument there is always the interaction between the electrons in the metal of the interferometer and the statistically distributed radiation field. This radiation is partly superimposed on the tops of the resonance peaks and puts a limit to e.g. the smallest observable wavenumber difference $\Delta\sigma_{\min}$. This quantity depends on what part of a resonance curve is used for observation and reaches its smallest value at the steepest parts of the curve [18]. Yet we will confine our calculations to a top of the resonance curve, where $\Delta\sigma_{\min}$ has its most unfavourable (maximum) value, as the observation of other parts of the curve mostly introduces extra uncertainties if no complicated technique of detection is used.

Although in optics the usual way to determine an intensity maximum of a fringe is still the putting of a cob thread across it while looking at it through a microscope, it was pointed out by GEHRCKE [4] as early as 1906 that this is certainly *not* the most accurate way. By following this procedure only a small fraction is used of the information contained in the image. It is clear that one should instead make a statistical analysis of the total picture.

It is perhaps not superfluous to mention that the minimum detectable physical quantity is exclusively and always determined by the fact that either the number of observations or the time of observation is limited. If there were no slow changes in the apparatus during an experiment and if the time scale of the research program could be chosen arbitrarily the problem of finding the minimum detectable signal would not exist. A well founded theory of optimum detectability originates from the observation of radar pulses and its first application in pure physics is found in the fields of radioastronomy, microwave spectroscopy and nuclear magnetic resonance (1946-48). Of this theory, which will form the basis of future experimental physics, we will only very roughly sketch the main features. The theory for resonant as well as non-resonant microwave systems was given by HERSHBERGER, by JEN and by TOWNES and GESCHWIND [19]. It may be applied immediately to observations with an interferometer.

As the absolute value of the transmitted resonance curve is a quantity of little interest, the main problem which we wish to solve is not, like e.g. in the transmission of radar pulses, the determination of the *absolute* value of the minimum detectable signal power ΔI . For the interferometer as a measuring device the sensitivity is set by the dependence of the minimum *relative* change $\Delta I/I_0$ in received source power I_0 on the ratio $\Delta I_n/I_0$ of the received noise power ΔI_n to this source power.

The mathematical analysis of threshold signals from a system which is nearly in thermal equilibrium follows two schemes, which are equivalent from the theoretical point of view but which differ by the order of succession of the operations involved. As a good experimental technique should follow this analysis as closely as possible it is not surprising that also two types of observation have been developed. In one type a FOURIER analysis is followed by taking the mean value of the squared signal while in the other type the FOURIER analysis is preceded by this operation. Especially when slow fluctuations predominate it is advantageous to apply the first method, so that the corresponding large FOURIER components may be eliminated.

In microwave spectroscopy this is done by sweeping periodically through a small part of the microwave spectrum at a repetition frequency ν (relatively high compared to the main fluctuations), after which only a very narrow band $\Delta\nu$ around ν is amplified and detected. One calls $\Delta\nu$ the *equivalent bandwidth* of the detecting system. If this modulation is due to gas absorption in an interferometer, all information about this absorption will be present in the side bands of the received signal. If we call the power in the side bands ΔI_s , this being equal to the mean value of the difference in received power due to modulation, and ΔI the mean power absorbed by the gas due to sine wave amplitude modulation, then it is easily shown that these quantities are related by

$$(94) \quad \Delta I_s = \frac{\Delta I^2}{4I_0}$$

in which I_0 is the output power of the interferometer. As a criterion for the minimum absorption which may be observed it is convenient (though not necessary) to put the observed side band power ΔI_s equal to the detected noise power $\Delta I_n = FkT\Delta\nu$ at the side band frequencies, in which F is the overall noise figure of the system, k BOLTZMANN'S constant, T the absolute temperature and $\Delta\nu$, as before, the equivalent bandwidth of the receiver. In this way we find for the minimum detectable relative absorption of power by the gas

$$(95) \quad q_{\min} = \frac{\Delta I_{\min}}{I_0} = 2 \sqrt{\frac{FkT\Delta\nu}{I_0}}$$

in which I_0 should have its maximum value, as derived in § 6. Usually q_{\min} is a very small quantity. If we take the following characteristic values for the microwave region: $F=50$, $T=300^\circ$ K, $\Delta\nu=10^3$ c/s, $I_0=10^{-2}$ Watt then we find $q_{\min} \approx 10^{-10}$.

From the foregoing it might seem as if q_{\min} is not ultimately determined by the previously mentioned condition of a finite time of observation. Yet it may be shown that the so-called response time of the detecting apparatus is inversely proportional to its equivalent bandwidth $\Delta\nu$. As an observation should be much longer than the response time it is clear that the minimum value of q_{\min} is set by the longest time of meaningful observation.

Also from the above reasoning it follows that the product of the detecting sensitivity and signal information will be approximately constant, i.e. by gaining much information about the shape of the signal (using a broad spectrum) one increases q_{\min} (shortens the available time of observation). This uncertainty principle for observation originates from the same FOURIER analysis as HEISENBERG'S principle in quantum mechanics.

In microwave techniques the FOURIER analysis may precede the squaring and averaging because here one disposes of a crystal diode being a detector with an extremely short response time. When in optics the photographic plate is used, which integrates intensity, the opposite order of succession may be applied only. It is clear that in this case the time of exposure is limited by slow irregular changes which cannot be interpreted as thermal noise. The intensity curves of the interferometer may now be obtained by photometric tracing of the developed plate after which the analysis again will lead to formula (95). The right hand term in (95) may now be considered as the minimum root-mean-square error in the relative change in output power.

In order to find the value of the minimum observable attenuation constant α_m'' of a gaseous medium we consider like before the intensity I_0 transmitted at resonance before and after a gas is let in an interferometer. According to (56) we then find a decrease in intensity

$$(96) \quad \Delta I = I_e - I = \left[1 - \frac{Q^2}{Q_e^2} \right] I_0.$$

Following the notation of page 528 part II and assuming that Q_m is much larger than Q_e it follows from (51) that

$$(97) \quad Q \approx Q_e \left[1 - \frac{Q_e}{Q_m} \right]$$

so that now ΔI may be approximated by

$$(98) \quad \Delta I = 2 \frac{Q_e}{Q_m} I_0.$$

Applying (95) we find for the minimum detectable $1/Q_m$

$$(99) \quad \left(\frac{1}{Q_m} \right)_{\min} = \frac{1}{2Q_e} q_{\min}$$

or with (54), (63) and (66)

$$(100) \quad \alpha''_{m \min} = \frac{\pi \sigma_0 N' \cos^2 \varphi_1}{2Q_e} q_{\min} \quad \text{and} \quad \alpha''_{g \min} = \frac{\pi}{2\lambda_g Q_e} q_{\min}.$$

This indicates in order of magnitude the lowest attenuation constant of a gas which may be detected by an interferometer at resonance, assuming that the resonance curve is not shifted by the introduction of the gas and that the receiver is linear in detecting intensity. In the same way one may indicate the order of magnitude of the smallest change of wavenumber which can be detected by a change in intensity at the top of an interferometer resonance curve. According to formula (57) this top part may be approximated by the parabola

$$\Delta I = 4Q_e^2 I_0 \left(\frac{\Delta \sigma}{\sigma_0} \right)^2.$$

The minimum detectable value of $\Delta \sigma$ at once follows from (57) and (95)

$$(101) \quad \Delta \sigma_{\min} = \frac{\sigma_0}{2Q_e} \sqrt{q_{\min}}.$$

Formulae (100) and (101) make it clear that one should strive for an optimum value of Q_e in order to be able to measure the smallest values of $\alpha''_{m \min}$ and $\Delta \sigma_{\min}$ due to the introduction of a gas. As the quality factor of an interferometer is proportional to the ratio of the effective volume to the surface which determines this volume, the classical etalon — having no guiding boundaries — from this point of view apparently represents the most sensitive instrument to measure these quantities.

The effective volume to surface ratio is increased with the distance L between the plates and therefore L should be made as large as possible. When a classical etalon is used, the plates having dimensions comparable with the wavelength of the radiation source, it will be found that due to diffraction the losses will increase with L , so that one might expect some optimum quality factor for a finite L . Also diffraction will result in a wavelength which is larger than the free space value. For a typical set-up at 8 mm wavelength CULSHAW [22] found deviations of a few parts in 10^4 .

Finally we will try to find the best conditions for the measurement of

refractive indices if frequency measurements are impossible. Differentiating (62), putting N' equal to 1 and substituting (62) again we find

$$(102) \quad (N'^2 - 1) = \frac{\Delta\sigma}{\sigma_0} + \left(\frac{\lambda}{\lambda_g}\right)^2 \left[\frac{\Delta L}{L} - \frac{\Delta\lambda_c}{\lambda_c}\right] + \frac{\Delta\lambda_c}{\lambda_c}.$$

According to (101) we can not measure a $\Delta\sigma/\sigma_0$ smaller than $\Delta\sigma_{\min}/\sigma_0$, so that

$$(103) \quad (N'^2 - 1)_{\min} = \frac{\sigma_0}{2Q_e} \sqrt{q_{\min}} + \left(\frac{\lambda}{\lambda_g}\right)^2 \left[\frac{\Delta L}{L} - \frac{\Delta\lambda_c}{\lambda_c}\right] + \frac{\Delta\lambda_c}{\lambda_c}.$$

In this formula ΔL and $\Delta\lambda_c$ are fixed quantities of the order of a micron. In order to find the conditions for minimum detectable refractive index we put $\partial/\partial\lambda_c \Delta(N'^2 - 1)_{\min} = 0$ and $\partial/\partial\lambda_g \Delta(N'^2 - 1)_{\min} = 0$. Then we obtain

$$(104) \quad \lambda_g = \lambda, \quad \frac{\Delta\lambda_c}{\lambda_c} = \frac{\Delta L}{L}.$$

From the first condition it follows that the classical etalon is again most sensitive for measuring a small refractive index. After this we may conclude from the second condition that the accuracy will increase with the distance L between the plates. Substituting the results (104) in (103) we find that at optimum performance

$$(105) \quad \Delta(N'^2 - 1)_{\min} = \frac{\sigma_0}{2Q_e} \sqrt{q_{\min}} + \frac{\Delta L_{\min}}{L}.$$

8. Concluding remarks

In this paper we have tried to give a survey of the widely scattered literature on the properties of interferometers with multifold reflections. Special emphasis has been given to microwave interferometers as at present these instruments form a field of greater interest. We have considered their properties with respect to the measurement of the phase and attenuation constants of gases by means of simple experiments. It was found that the classical etalon is unique among these resonating systems not only because of its simplicity, but also because of its superior qualities in measuring the phase constant α'_m and the attenuation constant α''_m of a medium. If one is forced by practical difficulties to supply the etalon with a guiding boundary one should make its cross section as large as possible in order to reduce the influence of this boundary to a minimum. As such a waveguide is certainly not necessary for waves having a wavelength shorter than a few millimeters we conclude that among the systems considered the etalon is the most accurate and sensitive device for measuring or comparing wavelengths in gases or in vacuo in the whole wavelength region from 0.4 micron to a few millimeters. This implies that, when the wavelength of a sharp spectral line is chosen as the standard of length, the etalon will form an ideal ruler. If this spectral line lies in the microwave region one may dispose of a single physical resonance phenomenon which constitutes both the standard of length (wavelength) and time (frequency). From the simultaneous and independent measurement of wave length

and frequency the velocity of electromagnetic waves may be determined. In this way one may reach accuracies far higher than were obtained by the earlier optical "long distance" experiments. The application of cavity resonators or high reflecting multilayers will increase the accuracy of length measurement so that it may become comparable to the high accuracy of time measurement. Also a search for an ether drift or rather a check on the theory of relativity by means of a microwave etalon or cavity can be carried out more accurately than the classical experiments by MICHELSON, MORLEY and MILLER [17].

Symbols which are frequently used in this paper have been collected in the following list. For many quantities no generally accepted notation and denomination seems to exist. The recent linking up of the radio field with optics by means of the microwave technique on one hand made the situation more confusing but on the other hand stresses the necessity of adopting a unified notation which is adequate for the whole field. The properties of the etalon, which make it a most valuable tool in the spectrum from ultraviolet to microwaves, seem to offer an excellent opportunity to define satisfactorily quite a number of physical quantities. Probably due to historical development not only the symbolism but also the definitions of some quantities differ for different authors. The refractive index for instance is often found to be defined by SNELLIUS' law or by the ratio of the phase velocity and the free space velocity, no provision being made for a definition when the medium exhibits losses. Especially in experiments with radiowaves the square of the refractive index or the permittivity of a medium is often confused with the static dielectric constant, whereas probably because of careless or obsolete definition most authors fail to state how losses were taken into account in their measurements. We wish to remark that, due to the symmetry in the occurrence of ϵ and μ in the foregoing formulae, all results that have been derived may be applied without any restriction to measure either the permittivity or permeability of gases as long as only one of these quantities affects the experiments. It is realized that the notation used in this paper is not completely satisfying but it is hoped that this attempt may stimulate others so that a consistent set of definitions and symbols for both the optician and the electrical engineer may be decided upon in the near future.

Acknowledgements. This work represents part of the research program of the Foundation for Fundamental Research of Matter (F.O.M.) made possible by financial aid of the Netherlands Organization for Pure Research (Z.W.O.).

The author wishes to thank Prof. Dr C. J. BAKKER and Dr J. C. VAN DEN BOSCH for their stimulating interest and valuable comments, Dr M. BRUIN, F. W. HEINEKEN and P. F. A. KLINKENBERG for reading the text and checking most of the formulae and Mrs C. WESSENDORP for typewriting the manuscript.

LIST OF SYMBOLS

A	amplitude transmitted wave
AA^*	I , intensity transmitted wave
a	amplitude incident wave, height of waveguide cross section
B	amplitude reflected wave
b	width of waveguide cross section (large dimension)
c	$= 1/\sqrt{\epsilon_0\mu_0} = 2.998 \cdot 10^8$ m/sec, free space velocity of light in vacuo
D	$\approx \pi/(1-f)$ dispersion ratio
f	$= R^2 e^{-2\alpha'' L_1}$, fringe constant
F	noise factor
I	intensity
I_0	$= [aT^2/R]^2 [f/(1-f)^2]$, maximum transmitted intensity
j	$= \sqrt{-1}$
k	positive integer, Boltzmann's constant
L	plate distance, L_0 plate distance at resonance
L_1	$= L/\cos \varphi_1$, $L_2 = L \cos \varphi_1$
L_e	$= N'L/\cos \varphi_1 = N'L_1$, effective optical plate distance
m	D , effective number of beams
n	number of interfering waves
n_0	order number
N	$N' - jN'' = c\sqrt{\epsilon\mu}$, complex refractive index
N'	refractive index
N''	absorption index
Q	$\approx \pi n_0/(1-f)$, quality factor, Q -factor
Q_e	idem for empty interferometer, Q_m idem with gas medium
q_{\min}	$(\Delta I_n/I_0)^{1/2}$
R	$\approx e^{-\varrho''}$, reflectivity of boundary layer
r	$e^{-j\varrho}$, reflection coefficient of boundary layer
s_e	$= e^{-j\alpha(x_1 + y_1)}$, propagation coefficient of medium
T	$e^{-\tau''}$, transmissivity of boundary layer, temperature
t	$e^{-j\tau}$, transmission coefficient of boundary layer
x, y	cartesian coordinates
x_0	$x/\cos \varphi_0$, $x_1 = x/\cos \varphi_1$
α_0	$\omega\sqrt{\epsilon_0\mu_0}$, $j\alpha_0$ propagation constant in vacuo
α	$= \omega\sqrt{\epsilon\mu} = \alpha' - j\alpha''$, $j\alpha$ propagation constant of medium
α'	$= 2\pi/\lambda$, phase constant of medium
α''	attenuation constant of medium
α_g	$\alpha'_g - j\alpha''_g$, $j\alpha_g$ propagation constant in waveguide
α_{micr}	$= 2\alpha''/N'$, power absorption coefficient of medium
ΔI_n	$FkT\Delta\nu$
$\Delta n, \Delta\nu$, etc.	difference in n, ν etc.
Δn_0	$\approx (1-f)/\pi\sqrt{f}$, half-value width. Also $\Delta\lambda_0, \Delta\nu_0, \Delta\sigma_0$
ϵ	$\epsilon' - j\epsilon''$, permittivity of medium

ε_0	= $10^7/4\pi c^2$ farad per meter, permittivity of vacuo
λ	= $2\pi/\alpha'$, free space wavelength in vacuo
λ_0, ν_0 , etc.,	resonance wavelength, resonance frequency, etc.
λ_g	wavelength in guide
μ	= $\mu' - j\mu''$, permeability of medium
μ_0	= $4\pi 10^{-7}$ henry per meter, permeability of vacuo
Ψ	electromagnetic wave
π	= 3.1416
ϱ	= $\varrho' - j\varrho''$, $j\varrho$ reflection constant of boundary layer
σ	= $1/\lambda$, free space wavenumber in vacuo
σ_D	= $\sigma(n_0) - \sigma(n_0 - 1)$, spectral range
τ	= $\tau' - j\tau''$, $j\tau$ transmission constant of boundary layer
φ_0	incident angle, φ_1 angle in medium
ω	angular frequency

REFERENCES

1. AIRY, G. B., Math. Tracts, 301 (2 ed., 1831).
2. WOODMAN, L. E., A. W. WEBB, Phys. Rev. **30**, 561 (1910).
3. KURAKAWA, K., J.I.E.E. Japan, No. 12 (1926).
4. GEHRCKE, E., Die Wissenschaft, Heft 17 (Braunschweig, 1906).
5. FABRY, C. and A. PEROT, Ann. Chim. (7) **12**, 459 (1897).
6. PIERCE, G. W., Proc. Am. Acad. Arts Sci. **60**, 271 (1925).
7. TOLANSKY, S., High Resolution Spectroscopy (London, 1945).
8. POWLES, J. G., Nature **161**, 25 (1948).
9. BLEANEY, B. and R. P. PENROSE, Proc. Roy. Soc. **A89**, 358 (1947);
Proc. Phys. Soc. **59**, 418 (1947).
10. GOZZINI, A., Nuovo Cimento **8**, 361 (1951).
11. BIRNBAUM, G., Rev. Sc. Instr. **21**, 169 (1950).
12. BOSCH, J. C. VAN DEN and F. BRUIN, Nuovo Cimento Suppl. **9**, 238 and 245 (1952).
13. BOSCH, J. C. VAN DEN and F. BRUIN, Physica **19**, 705 (1953).
14. HOUSTON, W. V., Phys. Rev. **29**, 478 (1927).
15. PIPPARD, A. B., J. Sc. Instr. **26**, 296 (1949).
16. WHITE, J. U., Rev. Sc. Instr. **21**, 629 (1950).
17. FÜRTH, H., Nature **173**, 80 (1954).
18. LYONS, H., N.Y. Ac. Sc. **55**, 831 (1952).
19. GORDY, W., Rev. Mod. Phys. **20**, 668 (1948).
20. GEHRCKE, E., Handbuch d. Phys. Optik I (Leipzig, 1927).
21. SLATER, J. C., Rev. Mod. Phys. **18**, 441 (1946).
22. CULSHAW, W., Proc. Phys. Soc. **66 B**, 597 (1953).
23. FÜRTH, R., Physica **17**, 259 (1951).
24. Coll. sur les propr. optiques des lames minces, J. Phys. Rad. **11**, 303-480 (1950).
25. Techn. of Microwave Measurements, part 11, chapter 10 (R. M. REDHEFFER,
Ed. C. G. MONTGOMERY (McGraw Hill, 1947).

Excellent surveys of and literature about optical interferometers may be found in references [7], [4] and [20]. For microwaves we refer to [25]. Recent work on microwave etalons has been carried out by E. S. DAYHOFF, Nat. Bur. of Standards, Washington (private communication) and J. O. ARTMAN, Rev. Sc. Instr. **24**, 873 (1953).

THE RELATION BETWEEN THE TEMPERATURE COEFFICIENT OF ISOTHERMAL CELLS AND THE THERMOPOTENTIALS OF THE CORRESPONDING THERMOCELLS ¹⁾

BY

HANS HOLTAN JR ²⁾

(*Institute for Theoretical Physics, The University, Utrecht, Netherlands*)

(Communicated by Prof. J. M. BIJVOET at the meeting of October 31, 1953)

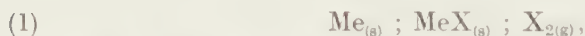
Abstract

REINHOLD [1] found experimentally that there is a correspondence between the temperature coefficient of an isothermal cell and the thermopotentials of the corresponding thermocells when the electrolyte is a solid salt. The exact relation is derived here and it is shown that the correspondence is actually only approximate.

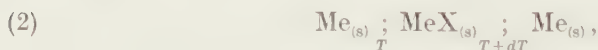
A similar correspondence between isothermal cells and corresponding thermocells is shown to be valid also for thermocells containing electrolytic solutions.

Cells containing solid electrolyte

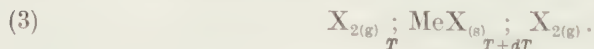
REINHOLD [1] has shown experimentally that the temperature coefficient of the isothermal cell



where $\text{Me}_{(s)}$, $\text{MeX}_{(s)}$ and $\text{X}_{2(g)}$ stand for solid metal, solid halide salt and halogen gas respectively, equals the differential thermopotential of the thermocell



minus the differential thermopotential of the thermocell



The temperature coefficient of the isothermal cell (1) is given by

$$(4) \quad (d\Delta\varphi/dT)_{is} = (S_{\text{Me}} + S_{\text{X}_2}/2 - S_{\text{MeX}})/F,$$

where S stands for molar entropy and F is Faraday's number.

¹⁾ Abstracted from the author's thesis, presented to the University, Utrecht (April 1953).

²⁾ Present address: Det Norske Zinkkompani A/S, Eitheim pr. Odda, Norway.

The thermopotential for a thermocell with solid electrodes and solid electrolyte is given by [2] [3] [4]

$$(5) \quad F \Delta\varphi/\Delta T = -S_a^*/z_a - S_{el}^* - \Delta S + S_a/z_a + S_{el},$$

no matter what the conventional transference numbers for the solid salt are. In equation (5) S_a^* and S_{el}^* are the molar entropy of transfer of the anion in the solid salt and of the electrons in the metallic phase, respectively, ΔS is the change of entropy during the heterogeneous electrode reaction, when one Faraday of electricity passes the interface, S_a and z_a the molar entropy and charge of the anion in the solid salt, respectively, and S_{el} the molar entropy of the electrons in the metallic phase.

The thermopotential of cell (2) is therefore given by

$$(6) \quad (\Delta\varphi/\Delta T)_1 = (S_{X-}^* - {}_1S_{el}^* - S_{MeX} + S_{Me})/F,$$

${}_1S_{el}$ being the molar entropy of transfer of the electrons in metal Me.

For thermocells with gas electrodes and solid electrolyte the thermopotential is given by [2] [4]

$$(7) \quad (\Delta\varphi/\Delta T)_2 = (S_{X-}^* - S_{el}^* - S_{X_2}/2)/F,$$

no matter what the conventional transference numbers for the solid salt are.

The thermopotential for cell (3) is therefore given by

$$(8) \quad (\Delta\varphi/\Delta T)_2 = (S_{X-}^* - {}_2S_{el}^* - S_{X_2}/2)/F,$$

where ${}_2S_{el}$ is the molar entropy of transfer of the electrons in the solid substance in which the gas in cell (3) is absorbed.

By subtracting (8) from (6) we obtain

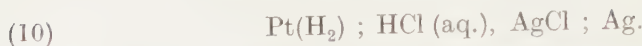
$$(9) \quad (\Delta\varphi/\Delta T)_1 - (\Delta\varphi/\Delta T)_2 = ({}_2S_{el}^* - {}_1S_{el}^* + S_{Me} + S_{X_2}/2 - S_{MeX})/F.$$

In the general case S_{el}^* is not the same in the two cells (2) and (3), *i.e.* the gas X_2 in cell (3) is not absorbed in metal Me of cell (2). The difference between the two electron entropies of transfer in equation (9) just equals the thermoelectric force of a thermocouple constructed of the metal Me of cell (2) and of the metal in which the halogen gas of cell (3) is absorbed [2] [5]. Since the thermoelectric force of metallic thermocouples is usually of the order of magnitude 10^{-5} volts degree $^{-1}$, while the thermopotentials in electrolytic thermocells are of the order of magnitude 10^{-3} volts degree $^{-1}$, we realise that the difference between the electron entropies of transfer in equation (9) may be neglected compared to the other terms. This explains why REINHOLD found the correspondence between thermocells and isothermal cells described in the beginning of this section.

Cells containing electrolytic solutions

One could expect a similar correspondence for cells containing electrolytic solutions.

Consider for instance the isothermal cell



The temperature coefficient of the potential difference of this cell is given by

$$(11) \quad (d\Delta\varphi/dT)_{\text{is}} = (\frac{1}{2}S_{\text{H}_2} + S_{\text{AgCl}} - S_{\text{Ag}} - S_{\text{HCl}})/F.$$

Consider then the thermocell



a cell which has not yet been investigated experimentally.

The general thermocell equation for a thermocell containing an electrolytic solution is given by the following expression when the Soret effect is hindered [2] [6]

$$(13) \quad \left\{ \begin{aligned} F \frac{\Delta\varphi}{\Delta T} = & -\frac{t^-}{z^-} {}_cS_{\text{a}}^* - \frac{t^+}{z^+} {}_cS_{\text{c}}^* - S_{\text{el}}^* - \Delta S + \frac{t^+}{z^+} S_{\text{c}} + \frac{t^-}{z^-} S_{\text{a}} \\ & + \left(\frac{t^+}{z^+} N_{\text{c}} + \frac{t^-}{z^-} N_{\text{a}} \right) S_{\text{H}_2\text{O}} + S_{\text{el}} \end{aligned} \right.$$

where t^- , z^- , t^+ and z^+ are transference numbers and charge for the anion and cation, respectively (the electrolyte is supposed to consist of only two kinds of charged particles), ${}_cS_{\text{a}}^*$ and ${}_cS_{\text{c}}^*$ the entropies of transfer of the hydrated anion and cation complexes, respectively, S_{c} , S_{a} , $S_{\text{H}_2\text{O}}$ and S_{el} the partial molar entropies of the cation and anion in the solution, of the solvent (water) and of the electrons in the metallic phase, respectively. N_{c} and N_{a} are the number of mols of solvent bound to one mol of cation and anion respectively.

The thermopotential of the thermocell (12) is then according to (13) given by

$$(14) \quad F(\Delta\varphi/\Delta T)_1 = t^- {}_cS_{\text{Cl}^-}^* - t^+ {}_cS_{\text{H}^+}^* - {}_{\text{Pt}}S_{\text{el}}^* + \frac{1}{2}S_{\text{H}_2} - t^- S_{\text{HCl}} + \Delta N S_{\text{H}_2\text{O}},$$

where ΔN is the number of mols of water carried from anode to cathode compartment when one Faraday of electricity has passed through the solution in the isothermal state, and ${}_{\text{Pt}}S_{\text{el}}^*$ is the molar entropy of transfer of the electrons in the platinum metal.

Then we consider the thermocell



a cell which has been investigated experimentally by BERNHARDT and CROCKFORD [7] and CROCKFORD and HALL [8]. According to (13) the thermopotential of this cell is given by

$$(16) \quad F(\Delta\varphi/\Delta T)_2 = t^- {}_cS_{\text{Cl}^-}^* - t^+ {}_cS_{\text{H}^+}^* - {}_{\text{Ag}}S_{\text{el}}^* + S_{\text{Ag}} - S_{\text{AgCl}} + t^+ S_{\text{HCl}} + \Delta N S_{\text{H}_2\text{O}}.$$

If we subtract (16) from (14), we get

$$(17) \quad (\Delta\varphi/\Delta T)_{\text{resultant}} = (1/F) ({}_{\text{Ag}}S_{\text{el}}^* - {}_{\text{Pt}}S_{\text{el}}^* + \frac{1}{2}S_{\text{H}_2} - S_{\text{HCl}} - S_{\text{Ag}} + S_{\text{AgCl}}).$$

As $_{Ag}S_{el}^* - _{Pt}S_{el}^*$ is the differential thermoelectric force for the thermocouple silver-platinum, it can be neglected compared with the other terms, and (17) then will be identical with (11). We therefore find the same correspondence between the temperature coefficient of an isothermal cell with solution and its corresponding thermocells as we found for cells containing solid electrolyte.

REFERENCES

1. REINHOLD, H., Z. anorg. Chem. **171**, 181 (1928).
2. HOLTAN jr., H., "Electric Potentials in Thermocouples and Thermocells", Thesis, Utrecht (1953).
3. ———, P. MAZUR and S. R. DE GROOT, Physica (in press).
4. ——— Proc. Kon. Ned. Ak. v. Wet., Amsterdam, **B 56**, 498 (1953).
5. GROOT, S. R. DE, "Thermodynamics of Irreversible Processes", (North Holland Publ. Comp., Amsterdam and Intersc. Publ., New York, 1951).
6. HOLTAN jr., H., Proc. Kon. Ned. Ak. v. Wet., Amsterdam, **B 56**, 510 (1953).
7. BERNHARDT, H. A. and H. D. CROCKFORD, J. Phys. Chem. **46**, 473 (1942).
8. CROCKFORD, H. D. and J. L. HALL, J. Phys. chem. **54**, 731 (1950).

EARTH-CRUST MOVEMENTS IN THE NETHERLANDS RESULTING FROM FENNOSCANDIAN POSTGLACIAL ISOSTATIC READJUSTMENT AND ALPINE FORELAND RISING

BY

F. A. VENING MEINESZ

(Communicated at the meeting of January 30, 1954)

For the study of the crustal movements in the Netherlands two great phenomena are important, the postglacial rising of Fennoscandia which may be expected to bring about a sinking in the surrounding area and the rising of the Alpine foreland which has given a recent upward movement in the Rhineland, the Ardennes and Limburg. We shall consecutively deal with both phenomena.

The evidence about the postglacial rising of Fennoscandia is generally interpreted as a proof of its being caused by the readjustment of isostasy after the crust's floating equilibrium had been disturbed by the relatively quick removal of the ice. It is likely that about two thirds of the original deviation has already disappeared. The evidence in favor of this hypothesis is the way the rising in the central area of Angermanland has occurred which could fairly accurately be derived from shore-lines and varves (DALY, 1925 [5], 1934 [6], 1940 [7], NANSEN, 1927 [14], LIDÉN, 1938 [13] and SAURAMO, 1939 [17]); as we shall see this time-curve strongly points to isostatic readjustment. The results of repeated precise levellings giving the rising in the present time are likewise in harmony with it and the same is true for the observed gravity anomalies from which we can deduce the amount of deviation from isostatic equilibrium which is still left. So the hypothesis seems well founded. For North America where a similar phenomenon may be expected the data now available are yet insufficient for coming to conclusions but what is present is not contradictory to it.

The best agreement with the data about the rising in Fennoscandia is obtained if we assume that at the time before the ice melted away the crust had entirely adjusted its isostatic equilibrium. This implies that at the time the ice had vanished—which we shall indicate by $t=0$ —only a depressed area was left behind; the loading effect of the melting water distributed over the water surface of the whole earth can for this purpose be neglected. The isostatic equilibrium of the depressed area is disturbed and so it may be expected to rise for readjusting its balance.

NISKANEN [15] has made the most successful approach for dealing

with this phenomenon. Simplifying it by supposing it two-dimensional, he has assumed the depression to have the shape

$$(1) \quad \zeta^0 = d^0 e^{-f^2 x^2}$$

in which ζ^0 is the depression at the time $t=0$, x the horizontal coordinate, z the vertical one, positive downward and d^0 the value of ζ^0 for $x=0$. The quantity f is inversely proportional to the horizontal dimensions of the phenomenon. The curve is given by fig. 1.

NISKANEN assumes the movement of the plastic substratum to obey the laws of hydrodynamics of viscous Newtonian fluids which is not likely to be quite true; probably the substratum has a small strength up to which stress-differences cause elastic deformation and only for greater values flow begins to occur. As this strength, however, is not likely to be larger than about 10–15 kg/cm², Niskanen's assumption is probably close enough to the real behavior of the substratum for allowing valid conclusions. It is easy to prove that the rigid earthcrust floating on the substratum is too weak to affect the phenomenon; its thickness of 30–40 km is too small with regard to the horizontal dimensions of the depression of about 1500 km for its elastic reaction to deformation to play a perceptible part.

NISKANEN puts the components v_x and v_z of the flow velocity in the substratum in the shape of a double Fourier integral

$$(2a) \quad v_x = -i \frac{k}{\pi} d^0 \int_{-\infty}^{+\infty} e^{-\alpha^2} d\alpha \int_0^{\infty} \lambda^2 \left[\cos \lambda (fx - \alpha) + i \frac{m}{f} e^{\lambda(f-m)z} \sin \lambda (fx - \alpha) \right] e^{-\lambda f z - \lambda^2 k t} d\lambda$$

$$(2b) \quad v_z = -\frac{k}{\pi} d^0 \int_{-\infty}^{\infty} e^{-\alpha^2} d\alpha \int_0^{\infty} \lambda^2 [\cos \lambda (fx - \alpha) + i e^{\lambda(f-m)z} \sin \lambda (fx - \alpha)] e^{-\lambda f z - \lambda^2 k t} d\lambda$$

which fulfill the hydrodynamic equations. The quantities α and λ disappear when carrying out the two integrations. The quantity m differs very little from f ; its value is given by

$$(2c) \quad m^2 = f^2 - \frac{k\varrho}{\eta}$$

where η is the pseudo-viscosity of the substratum and k a constant determined by the damping of the phenomenon; its value is approximately given by

$$(2d) \quad k = \frac{\varrho g}{2\eta f}.$$

The second term of the right member of (2c) is of the order of 10^{-34} and the first of the order of 10^{-18} ; for most purposes we can, therefore, neglect the difference of m and f .

The assumptions given by the formulas (2) lead to the following formulas

for the depression of the surface

$$(3a) \quad \zeta = \frac{d^0}{\sqrt{1+4kt}} e^{-\frac{f^2 x^2}{1+4kt}}$$

which for $t=0$ coincides with (1).

By differentiating this equation with regard to t we obtain the rising velocity at the surface which we shall denote by ω and in the center of the depressed area ($x=0$) by w

$$(3b) \quad \omega = \frac{2kf^0}{(1+4kt)^{3/2}} \left(1 - \frac{2f^2 x^2}{1+4kt}\right) e^{-\frac{f^2 x^2}{1+4kt}}.$$

For the center we get

$$(4a) \quad d = d^0(1+4kt)^{-1/2}$$

$$(4b) \quad w = -2kd^0(1+4kt)^{-3/2}$$

It is interesting to see that the rate of rising and the total uplift in the center are independent of f and, therefore, of the horizontal dimensions of the depression.

Examining (3b) we see that only the central part of the depression is rising; for a value of x given by

$$(5a) \quad x_b^2 = \frac{1-4kt}{2f^2}$$

the velocity w is zero and for greater values of x we find sinking. Combining (5a) with (3a) and (4a) we obtain for $x=x_b$

$$(5b) \quad \zeta_b = 0.607 d = 0.429 \frac{d^0}{fx_b}.$$

The sinking of the belt outside this boundary x_b is also clearly demonstrated by the fact that the integral of ζ is independent of time

$$(6) \quad \int_{-\infty}^{\infty} \zeta dx = \frac{d^0}{f} \int_{-\infty}^{\infty} f(1+4kt)^{-1/2} e^{-\frac{f^2 x^2}{1+4kt}} dx = \frac{\sqrt{\pi}}{f} d^0.$$

So the total volume of the depression remains the same. It flattens out, getting shallower and broader, till after infinite time the surface will be flat. So the rising area as well as the surrounding sinking belt are getting broader but the velocities diminish; according to formula (5a) the boundary between rising and sinking is increasing proportional to $\sqrt{1+4kt}$. This whole behavior is clearly shown by fig. 1 which gives the cross-section of the depression in Fennoscandia at the beginning ($t=0$) and at the present time ($t=9650$ years) and also the rising and sinking velocities for both periods. We see that incidentally the breadth of the present area of rising is roughly coinciding with that of the original depression and this has given rise to the erroneous idea that the rising is occurring over the whole depressed area.

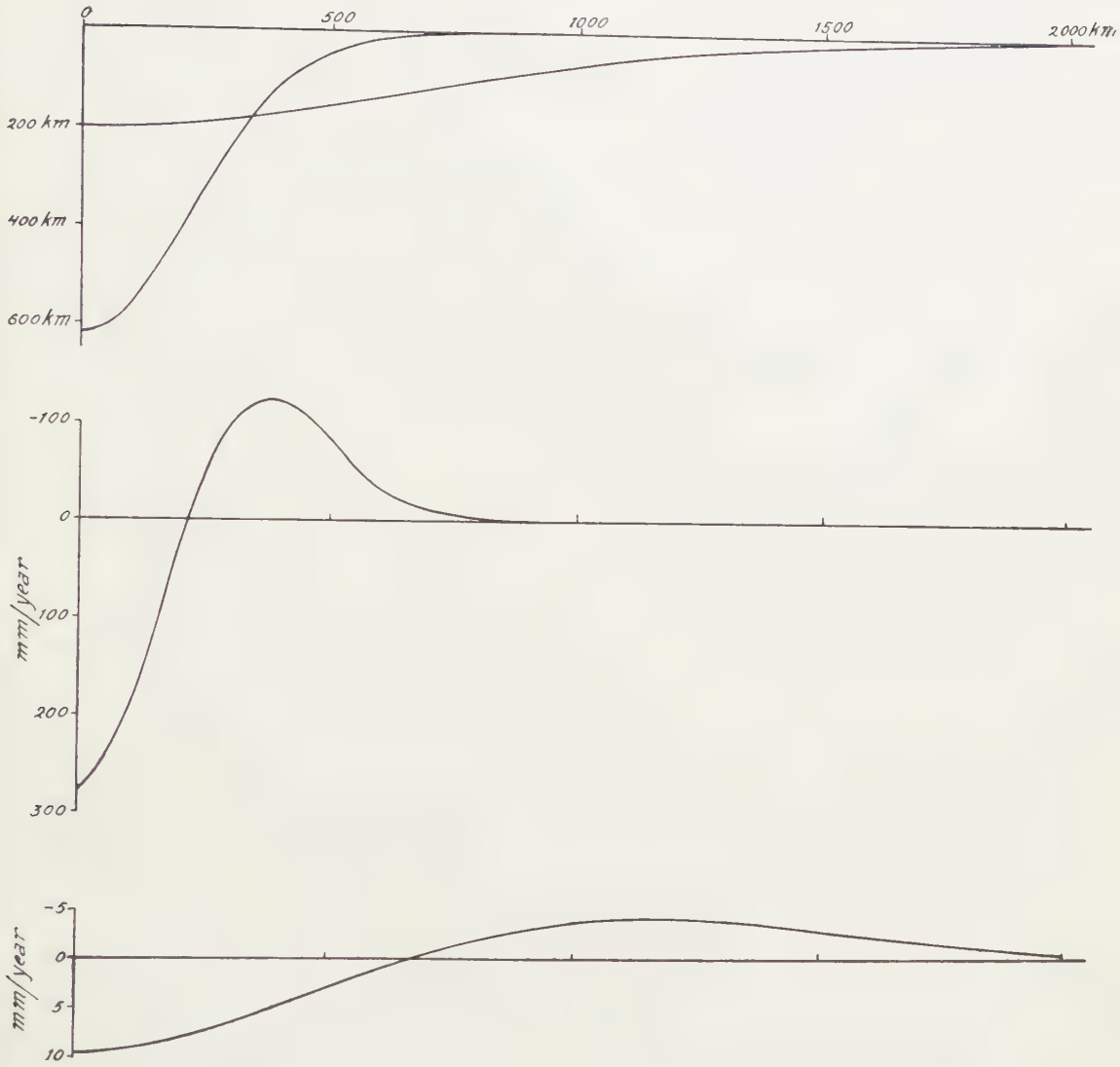


Fig. 1. Upper curves: Cross-sections of depressions for $t = 7700$ B.C. and for $t = 1950$ A.D. Middle curve: Rising velocity for $t = 7700$ B.C. Lower curve: Rising velocity for $t = 1950$ A.D.

In this treatment of the problem we have neglected the Earth's curvature and we have assumed infinite depth of the subcrustal area. As this may probably be considered to be the whole mantle and in view of the dimensions of the Fennoscandian phenomenon we can not expect these effects to be larger than that of the error of supposing it to be two-dimensional. If we assume the depression to have an elliptical shape with axis L_a and L_b and if we put $\pi/L_a = f_a$ and $\pi/L_b = f_b$ we can approximately take this shape into account by putting the value of f of our formulas at a value given by

$$(7) \quad f^2 = f_a^2 + f_b^2.$$

As we may further assume the volume of the three-dimensional depression to remain likewise constant with time we may probably suppose the sinking at greater distances from the center to be smaller than the formulas 3a and 3b give in a ratio about inversely proportional to these distances.

We shall now examine how the evidence in Fennoscandia checks with Niskanen's solution; we shall especially consider the data for the central area in Angermanland which seems the best and most consistent material. The next table gives the values provided by NANSSEN for the depression d of this area in meters increased by 200 m for the deviation from equilibrium still present there. This last figure has been derived from the mean gravity anomaly estimated at -27 mgal. The oldest value of 620 m has been found by diminishing Nansen's figure of 270 m for the depression before the year 6800 B.C. (Ref. 14, 1927, p. 63) by 100 m for the elastic rebound (DALY [6], 1934, p. 129-135; GUTENBERG [10], 1941, p. 752) and increasing it by Nansen's figure of 250 m for the rise from 6800 B.C. up to the present time and by the above figure of 200 m. The time $t = 0$ for this oldest figure will be derived below by supposing the ice to have disappeared suddenly at that moment. This is obviously a theoretical conception as it no doubt took some time for the ice to vanish. We shall find 7700 B.C. The second column of our table lists the rates of rising w in cm/year as it has been derived from the curve for d . The third column gives the ratio $d/w^{1/2}$ computed from the data of the first two columns, which we shall use for deriving the damping constant k ; according to the formulas (4a) and (4b) this quotient must be equal to $(d^{(0)} / 2k)^{1/2}$. Examining this column we are struck by the remarkable way these values are in harmony with each other which strongly points to the formulas (4a) and (4b) being right. The mean value is 205 and so we find for k

$$(8) \quad k = \frac{620^2}{2 \times 205^3} \times 10 = 0.223 \text{ per 1000 years.}$$

Introducing this value in (4a) and likewise the present value of d of 200 m and the initial value of 620 m we obtain the value t_p of t at the present moment. We get

$$(9) \quad t_p = 9650 \text{ years}$$

and so the moment $t=0$ corresponds to 7700 B.C.

By means of the formulas (4a) and (4b) we can now derive the value of d and w for the whole period elapsed since 7700 B.C. The 4th and 5th columns give the results for the same times to which Nansen's data of the first two columns refer.

Examining this table we see how remarkably well the figures of the first two columns given by NANSSEN and those of the last two derived from Niskanen's formulas check with each other. The most convincing agreement is evidently that of the 1st and 4th columns; the figures of the 2nd column are derived from the curve given by those of the 1st and so their

agreement to the figure of the 5th column may be expected. The exceptional good fitting of the formulas to the observational data is rather convincing for the truth of Niskanen's hypothesis; it seems unlikely that it should be incidental. It may be stated that in none of the figures there can be any adaptation. Other suppositions which have been made show much less satisfactory results (see e.g. GUTENBERG [10] 1941, p. 759 e.s.).

TABLE
Total depression d and rate of uplift w for the central area

Year	As given by NANSEN (1927, 1938)			As derived from (4a) and (4b)	
	$d(N)$ meters	$w(N)$ cm/year	d/w	$d(4a)$ meters	$w(4b)$ cm/year
7700 B.C.	620			620	
6800 B.C.	450	13.7	192	462	11.4
6000 B.C.	380	6.7	201	391	6.9
5000 B.C.	327	3.9	208	336	4.4
4000 B.C.	298	2.7	214	299	3.0
3000 B.C.	274	2.2	211	272	2.3
2000 B.C.	254	1.8	209	251	1.8
1000 B.C.	237	1.5	207	235	1.5
0	222	1.3	203	221	1.3
1000 A.D.	210	1.1	204	210	1.1
1950 A.D.	200	1.0	200	200	0.9
Mean			205		

A last point may be mentioned which is also checking; the last figure of the column for the rising velocity is exactly agreeing to the figures found by repeated precise levellings in the present period. We may e.g. refer to the accurate levelling carried out in Finland in the years 1892–1910 and repeated with still higher precision by KUKKAMÄKI c.s. since 1933 (KÄÄRIÄNEN [12], App. 1). It gives 0.9 cm rising on the east-side of the Bothnian Gulf and it shows the line of zero rising to run over Leningrad.

We shall now examine the consequences of the hypothesis for the Netherlands which are situated at about 1800 km distance from the center of the phenomenon in Ångermanland. For this purpose we have to discuss the horizontal dimensions of the phenomenon. Good indications can be derived from the above-mentioned Finnish results about the line of zero rising. Its distance to the axis of the depression is about 730 km and if we introduce this figure for x_b in (5a) and also the values of k and t given by (8) and (9) we obtain $f = 3 \times 10^{-8}$. As the whole depression has had an elliptical shape with a ratio of the two axis L_a and L_b of about 2 (see e.g. the map given by SAURAMO [17], p. 6), and as the short axis L_b is in the direction of Leningrad, (7) gives a value of f of the corresponding two-dimensional phenomenon of

$$(10) \quad f = \sqrt{1.25} \times f_b = 1.1 \times 3 \times 10^{-8} = 3.3 \times 10^{-8}$$

We can use this value for deriving the viscosity of the substratum η ;

introducing it in (2d) and likewise $k = 0.71 \times 10^{-11}$ per sec. and $q = 3.27$ we obtain

$$(11) \quad \eta = 0.7 \times 10^{22}$$

This value is less than has formerly been derived from the Fennoscandian data, e.g. by the writer (VENING MEINESZ [22]) who found $\eta = 3 \times 10^{22}$. This is caused by the approximation which for the sake of simpler mathematical treatment he assumed of an initial harmonic distribution of depressions and elevations in stead of the better supposition here made. In the harmonic case the depression can be filled from near-by elevations but this is not the case if initially only a depression is present; this requires a smaller viscosity for achieving the same rate of rising.

Applying the value of (10) for f and the assumptions about the elliptical shape and the Niskanen curve of formula (1) for the initial depression with the approximation implied in (7) to the Netherlands which are situated on the periphery of the phenomenon we get in much greater uncertainties. The crustal behavior must be influenced by the shape and depth of the initial depression in that area and this is practically unknown: between the Netherlands and Fennoscandia the North Sea constitutes an area where data are lacking. A gravity survey in that area would be important but it is difficult to make it as the risk of mines is still present. It may also be emphasized that for the Netherlands the applying of (7) for reducing the phenomenon to a two dimensional one is more hazardous as they are situated at large distance in the direction of the long axis of the ellipse. So we must remain conscious of the uncertainty of our deductions.

In order to derive the distance x from the center of the depression for the two-dimensional case for the long axe direction of the Netherlands we have to divide the distance of 1800 km by $\sqrt{5}$ and we get

$$(12a) \quad x = 800 \text{ km}$$

and

$$(12b) \quad fx = 2.64$$

By means of formula (5a) for x_b we can derive the way the boundary between the rising and sinking areas is travelling outward: it is represented by the upper curve of fig. 2. The value of the depression ζ_b at that point represents the maximum sinking which that station undergoes: according to formula (5b) it is inversely proportional to x_b and so we can easily derive from this curve how this maximum sinking diminishes with the distance from the center of the phenomenon. For the Netherlands we see that the maximum depression must occur at 6800 A.D. and from formula (5b) it follows that it will have a value of 100.7 m.

The other two curves of fig. 2 represent the depression ζ_{800} and the sinking velocity ω_{800} of the Netherlands which are listed in the following table as given by the formulas (3a) and (3b).

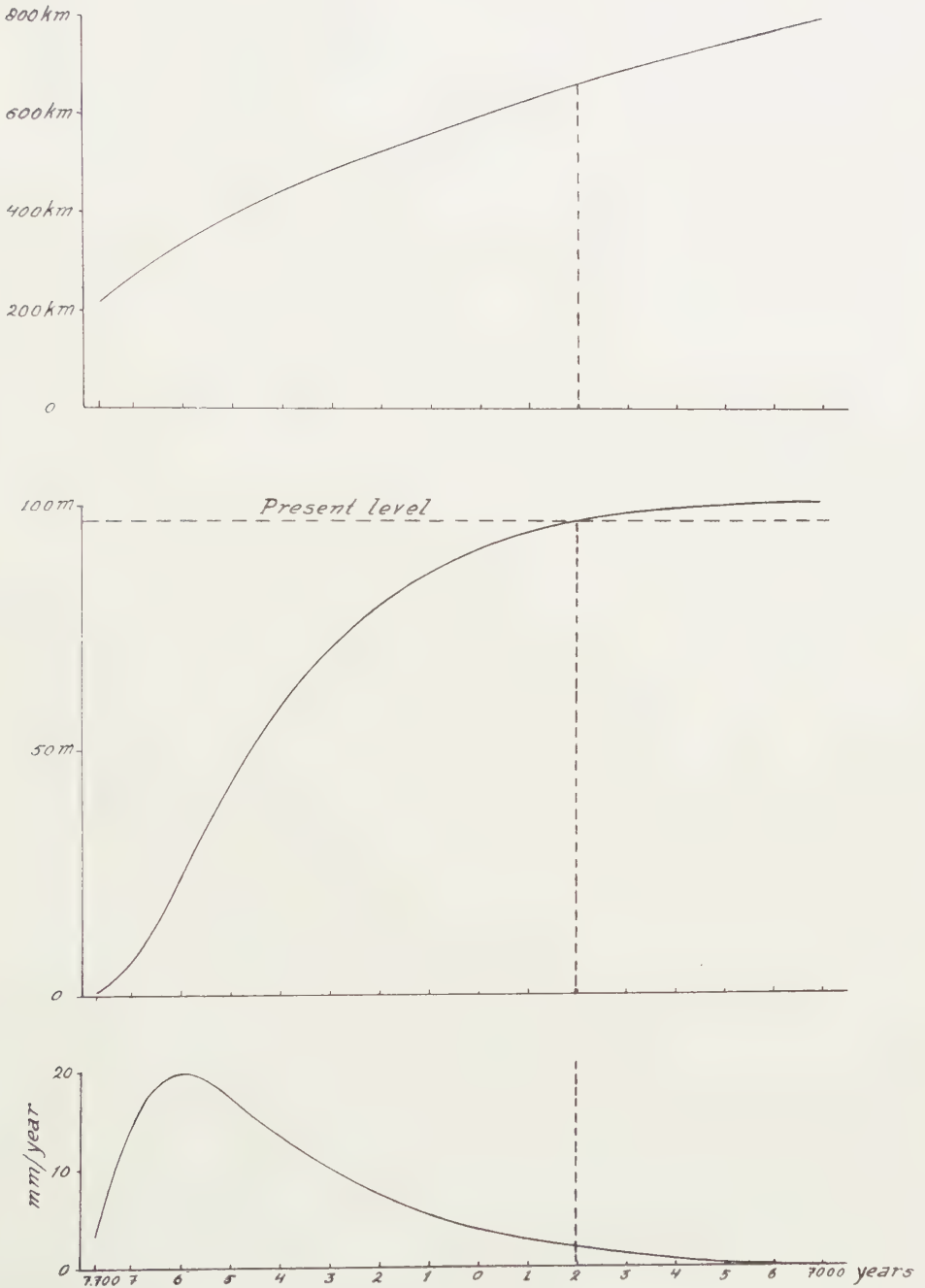


Fig. 2. Upper curve: Distance between center and point of zero sinking during the interval from 7700 B.C. to 7000 A.D. Middle curve: Position of the Netherlands below the original level. Lower curve: velocity of sinking of the Netherlands (middle and lower curve also for the interval from 7700 B.C. to 7000 A.D.)

Table of the depression ζ_{800} and the sinking velocity ω_{800} of the Netherlands

Time years B.C.	Depression m	Sinking mm/year	Time years A.D.	Depression m	Sinking mm/year
7700	0.6	3.35	0	91.0	3.98
6800	9.7	16.10	1000	94.7	2.86
6000	24.5	19.72	1950	96.9	2.02
5000	43.5	17.59	3000	98.6	1.34
4000	59.2	13.72	4000	99.7	0.85
3000	71.1	10.30	5000	100.4	0.47
2000	79.9	7.56	6000	100.6	0.18
1000	86.6	5.53	7000	100.7	-0.04
0	91.0	3.98	8000	100.5	-0.21

For the present period the rate is found to be 2 mm/year and this checks remarkably well with the amount found in the northern part of our country. We shall not go into details here about the great number of available observation data which are mainly provided by waterlevel-gauges and by the two precise levellings at a mean time interval of about 50 years. Both groups of data are much affected by ground settling and, as far as Limburg is concerned, by the consequences of mining activities. This makes it difficult to draw conclusions about movements of the earth-crust. Still the great number of available figures allows some provisional views and the result here derived of a sinking of 2 mm/year seems acceptable for the northern part of the Netherlands.

If we might consider this agreement as an indication that our deductions may be right, the second result may have value; it shows that the total sinking is 96.9 m. This would imply that we may expect a gravity anomaly of about -13 mgal and this does not appear to badly checking with the observed anomalies in the northern provinces.

The value of 96.9 m differs only 3.8 m from the maximum which may be expected in 6800 A.D. The sinking velocity shown by fig. 2 and by the table diminishes from 2.02 mm/year to 1.34 mm/year in 3000 A.D., 0.85 mm/year in 4000 A.D., 0.47 mm/year in 5000 A.D. and 0.18 mm/year in 6000 A.D. We need hardly say that after 6800 A.D. a rising will set in which, though slow in the beginning, will eventually lead to a rise of about 100 m making the deviation from isostatic balance disappear again. So the future of the Netherlands does not look too hopeless.

It appears to the writer that the second effect, the rising of the Alpine foreland, warrants a still more optimistic outlook for the faraway future of our country. It is hardly doubtful that these upward movements have already had a profound influence for the southern part of our country as well as of the greatest part of Belgium (CHARLIER [3], ESCHER [8], JONES [11], STEVENS [18], TESCH [21] and many other authors) and for great areas farther south; according to fig. 1 the sinking ought to have taken place for a broad belt of northern Europa and we find it only on the northern and northwestern margin of it.

The writer believes that this rising will not only remain present but that it will go on and spread farther northward. It seems to him that there is much evidence in favor of the hypothesis that it is caused by the melting of the deeper crustal root of the Alps—which, therefore, is lighter than the substratum—and its spreading northward below the European crust, causing this crust to rise and thus bringing about the European „Mittelgebirge”. We shall shortly consider the arguments leading to this hypothesis and examine the basis of the following two suppositions:

- 1^o the assumption that mountain formation in a geosyncline starts by the development of a root by the downbuckling of the crust under the effect of lateral compression.
- 2^o the assumption that this root gradually melts and spreads along the lower boundary of the crust.

It can be shown that the crust is not strong enough to maintain belts of strong negative gravity anomalies accompanied by positive belts on both sides as have been found in the East and West Indies and in other active geosyncline areas unless it is subject to strong lateral compression; these belts would otherwise by up- and downbending disappear in less than 100,000 years. This conclusion coincides with the views of most geologists that folding and overthrusting must have been caused by such compression. It can likewise be shown that a compression which is strong enough to bring about plastic deformation must lead to crustal downbuckling (BYLAARD [2] 1936, VENING MEINESZ [23] 1950).

It depends on the strength and character of the surface layers how they will react on this phenomenon. Probably sedimental layers will in most cases not, or not entirely, be carried down but will form folds and overthrusts at the surface as happened e.g. in the Alps, or will only partially be swallowed up and show scales at the surface as they occur e.g. in the Pyrennees. In case of an ocean crust with practically no sediments a deep trench develops.

BYERLY [1] and RICHTER-CHAKRABARTY [16] have both found seismic confirmation of the presence of a large root of crustal matter below the crust under the Sierra Nevada in California. There has likewise been obtained an extensive material of gravity data pointing to such roots below a great many mountain ranges.

In two ways recent seismic research in ocean-areas (EWING [9] and his collaborators) has given strong support to the buckling hypothesis. It has shown the ocean-crust in the deeper basins to consist of a thin layer of sediments of usually less than a kilometer in thickness, a layer of 3–5 km of a density of basalt and then ultrabasic matter of a density of about 3.3. This leads to the conclusion that the normal ocean-basin can not be deeper than about 6200 m for which depth the isostatic equilibrium would be fulfilled if on top of the ultrabasic layer no other layer were present. This depth-limit is in remarkable agreement with the ocean-sounding results;

nowhere greater depths of broad basins have been found. The deep ocean troughs must, therefore, be regarded as deviations from isostatic equilibrium and so in this regard they are exactly similar to the above mentioned belts of strong negative anomalies in the island arc areas: we have to assume the presence of forces for keeping them stable. These ocean trenches may thus be regarded as places where the crustal downbuckling is visible at the earth's surface.

A second confirmation is given by the seismic results found by REVELLE and RAITT *c.s.* over the Tonga trench. These results have not yet been published but a personal communication allows me to mention that the basaltic layer on both sides of the trench has the normal thickness of 3-5 km but that below the trench it is much thicker. This points strongly to downbuckling and not to sinking caused by subcrustal phenomena.

We shall not go into detail about the rising and isostatic readjustment we may in a later stage of the phenomenon expect in the downbuckled area when the tectonic compression of the crust has lessened sufficiently for this area to be able to detach itself from the neighboring crust on both sides; we know that mature folded mountain ranges only show small deviations from isostatic equilibrium.

There are two arguments for assuming that the downbuckled root of crustal matter gradually melts and flattens, thus spreading out below the crust. In the first place the crustal matter has by the downbuckling been transferred to a much lower level where a higher temperature is present than is compatible with a rigid state. In view of the fact that the lower boundary of the rigid crust under the oceans is no chemical discontinuity, we are sure that here this transition in physical properties is entirely determined by the temperature of the ultrabasic matter of which the main part of the crust as well as the plastic substratum consists. It seems likely that the same is true for the rigid continental crust and that here too its lower boundary is determined by temperature. In any case it appears impossible that the crustal matter of the downbuckled mountain root would continue to remain rigid at a depth of 20 km or more below the boundary of the rigid crust on both sides.

A second strong argument for its melting and horizontal spreading is provided by mountain-ranges like the Alps where the folding and overthrusting at the surface allows to make an estimate of the total shortening of the crust. For the Alps this estimate varies from 200 km to 400 km; it has developed in the course of about 150 million years. If the enormous amount of crustal matter thus concentrated would by erosion have been reduced to what is now present in the shape of the present mountain-system combined with the crust and the root below it as it is indicated by the gravity data, the eroded material ought to have been enormous and besides the difficulty to explain how this gigantic erosion could have taken place we also have to account for where the eroded matter got to. By studying this matter we arrive at the conclusion that this is entirely

impossible and that we, therefore, have to suppose another way for disposing of the matter that disappeared. Melting and partly flowing away of the root seems the only solution.

If melting of the root has taken place, it is clear that according to the hydrodynamics of viscous fluids it must have flattened in a similar way as the depression of Fennoscandia. We shall not go here into the equations and formulas for this phenomenon; we may reserve this for a future occasion.

There is much geologic evidence pointing to such an outward flow to the north, north-west and west; the rising of the European "Mittelgebirge" can be explained by the melted crustal matter spreading along the lower boundary of the crust and the isostatic equilibrium position of the crust thus having been lifted up. There is much less evidence of this also having occurred on the south side of the Alps. Perhaps this can be explained by assuming that a small strength of the substratum of about 10 kg/cm^2 prevents such a current to come into being when already a northward current has broken through this limit. A similar argument based on the same assumption has formerly been given by the writer for explaining that normally convection in the substratum seems to develop on one side only.

The rising of the European Mittelgebirge has been in many ways proven; we shall not go into details about it. We may refer e.g. to publications of STILLE [20], STEVENS [18], JONES [11] and many other authors. We may especially mention the studies of HANS CLOOS [4] who showed that many important features can be explained by the upward doming over a diameter of 350 km of a great area north of Switzerland, thus causing the Rhein-graben to sink down and bringing about the volcanism in the Eifel, the Neuwieder Becken, the Siebengebirge, the Westerwald, the Vogelsberg etc., the Rhön, near Hildburghausen, near Bayreuth, the Kaiserstuhl, the Hegauvolcanoes, the Uracher Maar area, and the Nördlinger Ries. This upward doming may be understood as a consequence of a northward current of root-matter below the crust in this area; the supposition that the root-spreading assumes the shape of more or less different currents flowing out beside each other seems acceptable. The frictional forces exerted by them on the crust may be expected to have caused the recent revival of tectonic activity in southern Belgium and northern Germany and the seismicity in these areas. The energy must evidently be too small to cause important orogeny with folding and overthrusting.

It appears rather likely that the frontal edge of these currents is not thinning out like a wedge but that it has a certain thickness. Because it is improbable the crust breaks above the edge this must be expected to cause a belt of moderate positive gravity anomalies in front of the edges and of similar negative anomalies behind them. This view may help us to find out how far the flow has advanced. In the Netherlands the positive anomalies may perhaps be identified with the E—W belt through the middle of the country which otherwise is difficult to understand. The edge

would then be marked by the depression through which the Rhine and the Waal take their western course. This seems to be one lobe of advance, while in Belgium another one appears to cause the rising in the direction of Thourout (STEVENS [19] p. 236). Between the two we find the depression of the Schelde and the Demer valleys which is likewise marked by positive anomalies. A systematic study of the boundary between the rising and sinking combined with our knowledge about the sinking caused by the Fennoscandian phenomenon may perhaps give data for the velocity of advance of the subcrustal flow.

We have still to prove that our hypothesis can give a solution for the problem where the crustal matter disappeared which was concentrated during the shortening of 200–400 km of the crust. For a rough estimate we shall adopt a breadth of the "Mittelgebirge" of 600 km and of the high Alps of 150 km and assume a double length of the first area with regard to the second. We may conclude to an excess cross-section caused by a shortening by 300 km of a 30 km crust of 9000 km² of which 1/5.45th part, equal to 1650 km², must show up at the surface, partly as mountain-mass and partly as eroded matter. If we assume the main range of the Alps to have a mean elevation of 2.5 km and the Mittelgebirge of 0.6 km, we get a total cross-section of the mountain-masses above sea-level of

$$F = 150 \times 2.5 + 2 \times 600 \times 0.6 = 1095 \text{ km}^2$$

and this would imply that in 150 million years 55.5 km² has disappeared by erosion, i.e. about 50 % of the actual mountain ranges. This figure does not appear extravagant and so our hypothesis seems to cover the difficulty.

We shall not discuss here other questions connected with our hypothesis; they may better be dealt with elsewhere. One is worth while mentioning, the possibility offered by the melting of the root of crustal matter, its spreading and its afterwards solidifying again, of the originating on a large scale of granite. The high temperature and pressure the crustal matter is subject to seem exactly to constitute the conditions needed for such a process.

Resuming our considerations regarding the two great phenomena the Netherlands are subject to, our conclusion may be that the future of our country does not seem too unfavorable, though far ahead of us, let us roughly say towards 3000–4000 A.D., probably great efforts will be needed for maintaining its whole territory safe against inundation. We must, however, emphasize the uncertainty of the figures and discussions given in our paper.

REFERENCES

1. BYERLY, P., The Sierra Nevada in the Light of Isostasy, *Bull. Geol. Soc. Am.* **48**, 2025–2031 (1938).
2. BYLAARD, P. P., Théorie des déformations plastiques et locales par rapport aux anomalies négatives de la gravitation, aux fosses océaniques, aux géosynclinaux, etc. Rapport Congrès d'Edinbourg de l'Union Géodésique et Géophysique (1936).

3. CHARLIER, CH. and L. JONES, L'apport de la Séismologie, de la Gravimétrie et de la Géodésie dans la connaissance de l'écorce terrestre en Belgique, *Bull. Acad. Roy. de Belgique, Cl. Sc.* 50 Sér. 37, 780-783 (1951).
4. CLOOS, H., Hebung-Spaltung-Vulkanismus, *Geol. Rundschau* 30, 405-527 (1939).
5. DALY, R. A., Pleistocene Changes of Level, *Am. Journ. o. Sc.* 10, 281-313 (1925).
6. ———, The Changing World of the Ice-age, (Yale Univ. Press, Newhaven, 1934).
7. ———, Strength and Structure of the Earth. (Prentice-Hall, New York, 1940).
8. ESCHER, B. G., Het vraagstuk van de daling van de bodem van Nederland, *Geol. en Mijnb.* 2, 173-196 (1940).
9. EWING, M. and J. LAMAR WORZEL, Gravity anomalies and Structure of the West Indies, *Bull. Geol. Soc. Am.* 65 (Feb. 1954).
10. GUTENBERG, B., Changes in sea-level, postglacial uplift, and mobility of the Earth's interior, *Bull. Geol. Soc. Am.* 52, 721-772 (1941).
11. JONES, L., Les premiers résultats de la comparaison du Deuxième Nivellement Général (1948) avec les nivellements anciens, *Bull. Soc. Belge Géol.* 59, 156-162 (1950).
12. KÄÄRIÄINEN, E., On the recent uplift of the earth's crust in Finland, *Veröff. Finn. Geod. Inst.* 42 (Helsinki, 1953).
13. LIDÉN, R., Den senkvartära strandförskjutningens förlopp och kronologi i Ångermanland, *Geol. Fören. Förhandl.* 60, H. 3 (1938).
14. NANSEN, FR., The Earth's crust, Its Surface forms and Isostatic Adjustment, *Avhandl. utgitt. av Det Norske Videnskaps-Akad. i. Oslo, I, Mat. Nat. Kl.* 12 (1927).
15. NISKANEN, E., On the Upheaval of Land in Fennoscandia, *Publ. Isost. Inst.* 6 (Helsinki, 1939).
16. RICHTER, C. F., and S. K. CHAKRABARTY, The Walker Pass earthquakes and Structure of the southern Sierra Nevada, *Bull. Seismol. Soc. Am.* 39, 93-107 (1949).
17. SAURAMO, M., The mode of the Land Upheaval in Fennoscandia during late-quaternary time, *Cptes Rendus Soc. Géol. de Finlande* 13, 1-26 (1939).
18. STEVENS, CH., L'étude des relations tectoniques du relief ardennais et ses difficultés, *Bull. Soc. Roy. Belge de Géographie* 1-11, (1943-1945).
19. ———, Les gauchissements épirogéniques du sol belge, *Rev. d. Quest.* (1945), *Scient.* 1947, 225-249 (1947).
20. STILLE, H., Oro- und epirogenetische Bewegungen der Erdkruste im Zusammenhang mit der Seismizität Zentralasiens und Norddeutschlands, *Acad. d. Sc. de l'U.R.S.S.* 32, 97-115 (1932).
21. TESCH, P., De schiervlakte van Eifel en Ardennen vóór de opheffing tot bergland, *Tijdschr. Kon. Ned. Aardrijksk. Gen.* 18, 2^o ser. 63-71 (1941).
22. VENING MEINESZ, F. A., The determination of the Earth's plasticity from the postglacial uplift of Scandinavia; Isostatic adjustment, *Proc. Kon. Akad. v. Wetens.* 40, 654-662 (1937).
23. ———, Earth's crust deformations in geosynclines, *Proc. Kon. Ned. Akad. v. Wetens.* 53, 27-46 (1950).

HENRI GEORGE DEXX †

(14 SEPTEMBER 1894–15 AUGUSTUS 1953)

BY

L. G. M. BAAS BECKING

(Summary of a contribution published in Series C, 57, No 2 of these Proceedings)

His career was, over a wide range of disciplines, that of a “master of all trades”. Born from a line of colonial servants, DEXX spent his boyhood in Java and remained inspired, until his death, by the greatness of tropical nature. His studies at the Technical University of Delft made him into a first rate organic chemist. Inspired by his teacher, Professor J. BÖESEKEN, he became the discoverer, in 1922, of the spatial structure of cyclic ring systems. After his marriage to CLAIRE TROUBAT from Pau, France, DEXX accepted a position as industrial chemist at Calvé, Delft. In this period, collaborating with A. J. KLUYVER and C. B. VAN NIEL, he found himself as a biologist. He clarified the mechanism of the oxidative breakdown of fats by moulds, he took part in the discovery of diacetyl in the butter aroma. He was the discoverer of heterothallism in *Penicillium* and developed methods for the isolation of the “ballistic yeasts”; the *Sporobolomycetes*. After the fusion of Calvé with Lever Brothers (later Unilever) DEXX had little chance for scientific work outside the technical realm. He started to grow and to study Orchids and became an authority in this field. Especially the symbiosis with *Corticium* drew his attention. In 1939–1940 he served as captain in the Regiment Grenadiers. During the war he performed much biochemical work on foodprocessing, on oxidative enzymes, on the production of Provitamin A and on the nutritive value of palmitates and stearates. He was imprisoned, for a short time, by the German police but fortunately returned safe and sound. After the war he was put in charge of a specialist-Nutrition Team of the Netherlands Red Cross and worked for nine months in Java. Apart from much organisatory work he prepared a successful baby food from milkpowder and developed various biochemical methods. After a short period with Unilever in Holland the “call of the east” became too strong and DEXX joined the staff of the Buitenzorg Gardens as Head of the Treub Laboratory. Amongst many things he did there, a most outstanding discovery is that of an acid resistant, nitrogen-fixing aerobe, *Beijerinckia*, which organism, strangely enough, seems to occur exclusively in the tropics. In 1948 he became a correspondent of the Royal Netherlands Academy of Sciences. Repatriated in 1950, he worked for a few happy years on microbiological problems, as advisor for the Royal Dutch Shell Co.

In his organo-chemical preparations, in the growing of plants and microbes, DERX had "catalytic fingers". The extreme range of his interest never detracted from the thoroughness and originality with which he attacked the problems. He remained faithful, throughout his life, to these problems. In his last years he studied cyclic compounds again the "Schardinger dextrins", produced by *Bacillus macerans*. In Buitenzorg he discovered that diacetyl is a component of the flower scent of a *Fagraea*. With his penetrating eyes, with his fertile mind, he must have had many wonderful experiences. As a scientist he remained comparatively unknown, and he received little public acclaim. But well he may have quoted his beloved PAUL VALÉRY:

"si on est quelqu'un, on n'a pas besoin d'être quelque chose"

FURTHER STATISTICAL PROBLEMS CONNECTED WITH THE
SOLUTION OF A SIMPLE NON-LINEAR PARTIAL
DIFFERENTIAL EQUATION

BY

J. M. BURGERS

(*Mededeling No. 77 uit het Laboratorium voor Aero- en Hydrodynamica der
Technische Hogeschool te Delft*)

(Communicated at the meeting of January 30, 1954)

1. *Introduction.* — The present paper is an attempt to apply the method developed in a communication “On the coalescence of wave-like solutions of a simple non-linear partial differential equation” ¹⁾ to questions raised in an earlier investigation concerning correlation problems in a one-dimensional model of turbulence ²⁾. The application of the exact solution of the non-linear equation as given by HOPF and by COLE ³⁾ makes it possible to discuss the state of the system at any given instant, without being obliged to go through the whole preceding history. This brings a great advantage over the older method, the outcome of which had been a more or less historical description of the development of the solution, starting from certain initial conditions, which necessitated the consideration of intermediate stages in proper order ⁴⁾ and made it difficult to arrive at a statistical picture of the ultimate behaviour. The result was that a considerable number of mean values and distribution functions had to be introduced, which functions could not be related to each other in such a way that a satisfactory system of statistical equations was obtained. It is to be expected that the new method will provide means for solving several questions which remained open in the former investigation. It is not intended to attack all these questions in the following lines; the object of the present paper is to sketch the method in general and to point to a few results and to further problems.

¹⁾ These Proceedings B57, 45–72 (1954).

²⁾ These Proceedings 53, 247–260, 393–406, 718–742 (1950).

³⁾ E. HOPF, *Commun. on Pure and Applied Mathem.* 3, 201–230 (1950), in particular p. 203. — J. D. COLE, *Calif. Instit. of Technology*, private communication (1949).

⁴⁾ The method used in sections 5–7 of the paper referred to in footnote 2) (*i.e.* pp. 252–256) was based on the behaviour of a particular solution of the first order equation obtained from eq. (1) by making $\nu = 0$. This method is equivalent to that of solving the first order equation by means of its characteristics. It is then necessary to consider all cases of intersection of characteristics in the order of their occurrence.

Whereas the paper mentioned in footnote 1) considered the behaviour produced by the action of some agency at the origin, in particular by periodic "impulses" which gave rise to the appearance of wave-like solutions propagating themselves in the direction of the positive y -axis, the present paper is concerned with solutions deriving from a given initial state along the entire y -axis and developing in the course of time.

2. *The solution of the partial differential equation.* — The equation is the same as before:

$$(1) \quad \frac{\partial v}{\partial t} + v \frac{\partial v}{\partial y} = \nu \frac{\partial^2 v}{\partial y^2}.$$

Again we make use of the transformation:

$$(2) \quad v = -2\nu \frac{\partial}{\partial y} (\ln u),$$

where the auxiliary variable u can be determined in such a way that it satisfies the equation:

$$(3) \quad \frac{\partial u}{\partial t} = \nu \frac{\partial^2 u}{\partial y^2}.$$

The solution for the case considered here (given initial state along the whole y -axis) can be written:

$$(4) \quad u = \frac{1}{\sqrt{t-t_0}} \int_{-\infty}^{+\infty} d\xi \exp \left\{ \frac{-\xi^2}{4\nu(t-t_0)} + \frac{1}{2\nu} \int_0^{\nu+\xi} a(\xi') d\xi' \right\},$$

where t_0 is the initial instant, while $a(\xi')$ is an arbitrary function of the auxiliary variable ξ' . For $t \rightarrow t_0$ this reduces to:

$$(5) \quad u = \sqrt{2\pi\nu} \exp \left\{ \frac{1}{2\nu} \int_0^{\nu} a(\xi') d\xi' \right\},$$

from which:

$$(6) \quad v_0(y) = v(t_0, y) = -a(y).$$

Hence the auxiliary function $a(y)$ represents the negative of the initial course of v . It is assumed that the value of $|a(y)|$ is bounded.

When ν is sufficiently small, the value of u and consequently that of v will be defined completely by that value ξ_m of ξ for which the expression

$$(7) \quad Z(\xi) = \frac{-\xi^2}{2(t-t_0)} + \int_0^{\nu+\xi} a(\xi') d\xi'$$

has an absolute maximum. We then find:

$$(8) \quad v(t, y) = -a(y + \xi_m).$$

Since the absolute maximum of $Z(\xi)$ must be an analytic maximum

when compared with the values of Z in its immediate neighbourhood, differentiation of (7) gives:

$$-\xi_m/(t-t_0) + a(y+\xi_m) = 0.$$

Hence we obtain:

$$\xi_m = a(y+\xi_m) \cdot (t-t_0) = -v(t, y) \cdot (t-t_0),$$

and consequently:

$$(9) \quad v(t, y) = v_0(y - v \cdot [t - t_0]).$$

This is the solution of the first order equation:

$$(10) \quad \frac{\partial v}{\partial t} + v \frac{\partial v}{\partial y} = 0,$$

to which (1) reduces when v is taken zero. However, it is well known that this solution is not always uniquely determined. An unambiguous determination is obtained only when the first order equation (10) is considered as a limiting case of the original equation (1) with the uniquely determined solution given by (2) in combination with (4); in that case the limit for $v \rightarrow 0$ is found from the maximum condition for Z .

The maximum condition can be interpreted geometrically as follows. It is assumed that y and t have given values and we put:

$$(11) \quad y + \xi = \eta.$$

With a change of sign the condition can then be written:

$$(12) \quad \frac{(\eta - y)^2}{2(t - t_0)} - \int_0^\eta a(\xi') d\xi' \geq \text{absolute minimum.}$$

We construct a curve $S(\eta)$ determined by:

$$(13) \quad S(\eta) = \int_0^\eta a(\xi') d\xi'$$

(for convenience again to be called "summation curve") and prepare a parabola

$$(\eta - y)^2 / 2(t - t_0),$$

which can be shifted in the plane of the drawing. The axis of the parabola is vertical and passes through the abscissa $\eta = y$. Assuming that the parabola originally is situated rather high in the field and then is moved downward, with a given value of y , we determine the moment at which for the first time it makes contact with the summation curve, while remaining above this curve everywhere else. If the abscis of the point of contact is denoted by η_m (compare the left hand part of fig. 1), the value ξ_m characterizing the absolute maximum of Z for the given value of y is obtained from:

$$(14) \quad \xi_m = \eta_m - y,$$

and (8) becomes:

$$(8a) \quad v(t, y) = -a(\eta_m).$$

When the value of y is increased (that of t being kept fixed) the contacting parabola glides over the summation curve. Evidently the value of η_m will move in the same direction as that of y (see the right hand part of fig. 1). The possibility exists that from time to time a double contact

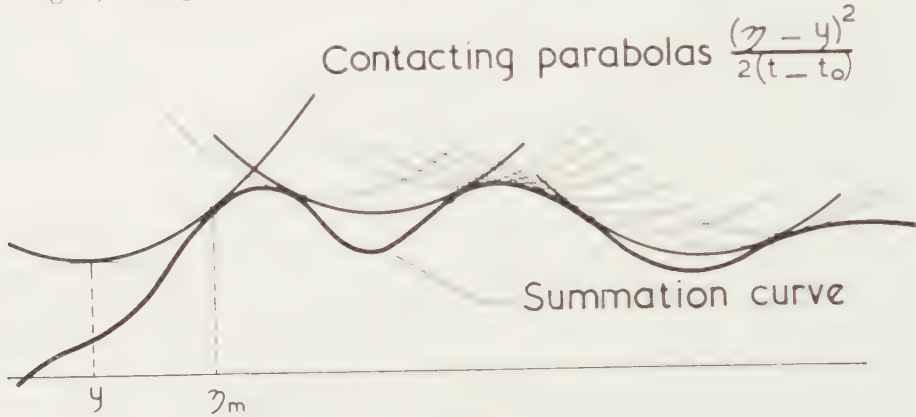


Fig. 1

is made (heavily drawn parabolas in the right hand part of fig. 1); in such a case the value of η_m changes discontinuously, which entails a discontinuous change of the value of v at the abscissa determined by the position of the axis of the parabola making the double contact ⁵⁾.

It is thus seen that the problem of the appearance of steep fronts ("shock waves", or "N-waves", as they have been called by FRIEDRICHS ⁶⁾) in the curve for v as a function of y , depends on the construction of parabolas touching the summation curve in two points. When a larger value of t is taken, the parabola becomes flatter and it can be expected that the mean distance between the contact points will increase. In a similar way as in the problem treated in the preceding communication this means that the number of shock wave fronts in the field decreases with increasing t , a consequence of the merging of successive fronts.

If the summation curve is of a rather regular type, it can be expected

⁵⁾ From condition (12) it follows that at the point of contact:

$$\frac{1}{t - t_0} - \left(\frac{da}{d\xi'} \right)_{\xi' = \eta_m} > 0.$$

If the derivative $da/d\xi'$ has an upper bound A , every point of the summation curve may become a contact point so long as $t - t_0 < 1/A$. As soon as $t - t_0 > 1/A$, there will be points of the summation curve for which the inequality is not satisfied, so that these points cannot be a contact point. Discontinuous jumps of η_m will then necessarily occur.

⁶⁾ Compare K. O. FRIEDRICHS, Formation and Decay of Shock Waves, Commun. on Applied Mathem. 1, 211-245 (1948), in particular p. 216.

for large values of t that the short arcs of the summation curve which admit a continuous change of η_m , approximately will present a parabolic form with the top directed upwards. Assume that such an arc can be described by:

$$S(\eta) = S_0 - \frac{1}{2}\alpha(\eta - \eta_0)^2,$$

S_0 being a constant for that arc; condition (12) then becomes:

$$\frac{(\eta - y)^2}{2(t - t_0)} - S_0 + \frac{1}{2}\alpha(\eta - \eta_0)^2 \geq \text{minimum}.$$

Hence along this arc we shall find:

$$\frac{\eta_m - y}{t - t_0} + \alpha(\eta_m - \eta_0) = 0,$$

from which:

$$\eta_m = \frac{y + \alpha(t - t_0)\eta_0}{\alpha(t - t_0) + 1}; \quad \eta_m - \eta_0 = \frac{y - \eta_0}{\alpha(t - t_0) + 1}.$$

Since along this arc: $a = -\alpha(\eta - \eta_0)$, equation (8a) gives:

$$(8b) \quad v(t, y) = \frac{y - \eta_0}{t - t_0 + 1/\alpha}.$$

Hence for large t the course of v between two steep fronts becomes a linear function of y , with a slope almost equal to $1/t$. This confirms the result of the paper mentioned in footnote 2), *l.c.* p. 254.

3. *Application to an initial course of $v_0(y)$ described by a chain of parallel straight segments.* — We assume that the initial course of v is given by a chain of parallel straight segments, alternating with vertical segments (shock fronts), in the way as was indicated in section 6 of the paper mentioned in footnote 2) (*l.c.* pp. 254–255), from which we reproduce fig. 4 as our present fig. 2. With a slight extension of the notation used there we put:

$$(15) \quad \begin{cases} \text{initial abscissae of the steep fronts (at } t=t_0): \xi_i = iL + \sum_1^i \varepsilon_j; \\ \text{initial abscissae of the points where } v_0 = 0: \sigma_i = \frac{1}{2}(\xi_{i+1} + \xi_i) + \theta_i. \end{cases}$$

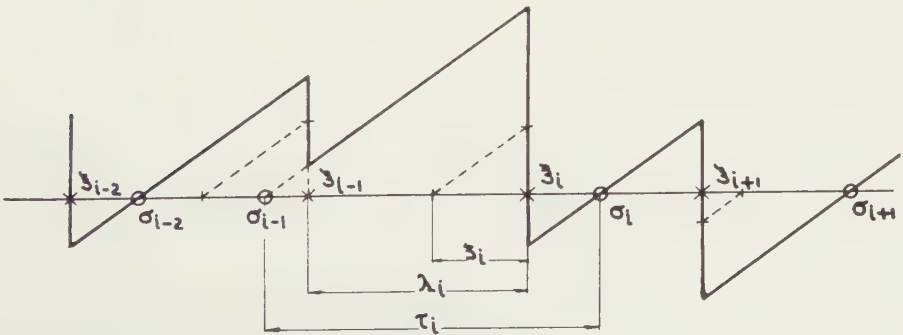


Fig. 2

Here L is the value of l (mean value of the segments λ_i , as defined *l.c.* p. 256, eq. 27), at $t = t_0$. The quantities ε_i and θ_i are random variables, assumed to be all independent of each other. Although both sets of quantities have the dimensions of a length, the part played by the θ 's is somewhat different from that played by the ε 's. It will be supposed that all θ 's have the same mean square value σ_θ^2 and that all ε 's have the same mean square value σ_ε^2 .

From the expressions for ξ_i and σ_i we deduce:

$$(16) \left\{ \begin{array}{l} \text{length of the segment} \\ \text{between two successive} \\ \text{steep fronts: } \lambda_i = \xi_i - \xi_{i-1} = L + \varepsilon_i; \\ \text{distance between two} \\ \text{successive points where} \\ v_0 = 0: \tau_i = \sigma_i - \sigma_{i-1} = L + \theta_i - \theta_{i-1} + \frac{1}{2}(\varepsilon_{i+1} + \varepsilon_i); \\ \text{jump of } v_0 \text{ at the cor-} \\ \text{responding steep front: } v_- - v_+ = \tau_i/t_0; \\ \text{value of the parameter } \zeta_i = \xi_i - \frac{1}{2}(\sigma_i + \sigma_{i-1}): \\ \zeta_i = -\frac{1}{2}(\theta_i + \theta_{i-1}) - \frac{1}{4}(\varepsilon_{i+1} - \varepsilon_i), \end{array} \right.$$

all for $t = t_0$.⁷⁾ It is necessary that all λ_i shall be positive; this requires that the ε_i shall not have negative values exceeding $-L$. Although it was assumed in the paper quoted that all τ_i likewise should be positive, this condition is not so important at $t = t_0$, and it will not bring about a great disturbance if there would be some negative τ_i in the initial state.

The summation curve now becomes a chain of parabolic arcs, each parabola having the same curvature at the top. It can be obtained as follows. We have:

$$(17) \quad v_0(y) = \frac{y - \sigma_i}{t_0} \text{ for } \xi_i < y < \xi_{i+1};$$

from which:

$$(17a) \quad a(\xi') = -\frac{\xi' - \sigma_i}{t_0} \text{ for } \xi_i < \xi' < \xi_{i+1}.$$

Hence by integration:

$$(18) \quad \left\{ \begin{array}{l} S(\eta) = \text{const.} - \frac{(\eta - \sigma_i)^2}{2t_0} + \frac{(\xi_i - \sigma_i)^2}{2t_0} + \\ + \frac{1}{2t_0} \sum_1^i \{ -(\xi_j - \sigma_{j-1})^2 + (\xi_{j-1} - \sigma_{j-1})^2 \} \text{ for } \xi_i < \eta < \xi_{i+1}. \end{array} \right.$$

From (15) we obtain:

$$\xi_j - \sigma_{j-1} = \frac{1}{2}L + \frac{1}{2}\varepsilon_j - \theta_{j-1}; \quad \xi_{j-1} - \sigma_{j-1} = -\frac{1}{2}L - \frac{1}{2}\varepsilon_j - \theta_{j-1}.$$

If for shortness we write:

$$(19) \quad \theta_j = \theta_j + \frac{1}{2}\varepsilon_{j+1},$$

⁷⁾ In the paper quoted the letter β was used for $1/t$; at the initial instant $\beta = 1/t_0$.

the expression for S can be brought into the form:

$$(18a) \quad \left\{ \begin{aligned} S(\eta) = \text{const.} - \frac{(\eta - \sigma_i)^2}{2t_0} + \frac{L\vartheta_i + \vartheta_i^2}{2t_0} + \frac{1}{t_0} \sum_1^i (L + \varepsilon_j) \theta_{j-1} \\ \text{for } \xi_i < \eta < \xi_{i+1}. \end{aligned} \right.$$

A special case, in which all ε_i have been taken zero, so that all segments λ_i have the same length L , has been sketched in fig. 3, where also a parabola making double contact has been represented.⁸⁾

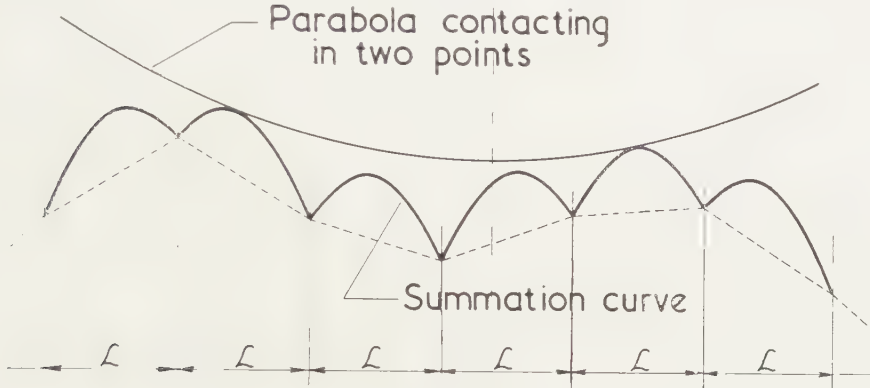


Fig. 3

The problem of constructing a parabola making double contact with the present type of summation curve is more difficult than the problem considered in sections 7 and 8 of the preceding paper (mentioned in footnote 1). However, when $t - t_0$ is a very large quantity (large compared with t_0), the parabola becomes very flat and the points of contact can never be far away from tops of the parabolic arcs of the summation curve. Hence for large values of t we can approximately replace the continuous summation curve by a set of points, determined by the tops of its parabolic segments. These points have ordinates:

$$(20) \quad S_n = \text{const.} + \frac{L\vartheta_n + \vartheta_n^2}{2t_0} + \frac{1}{t_0} \sum_1^n (L + \varepsilon_j) \theta_{j-1};$$

and abscissae:

$$\sigma_n = \text{const.} + \vartheta_n + \sum_1^n (L + \varepsilon_j).$$

The statistical problem appearing in connection with the construction of parabolas making double contact is still complicated by the circumstance that the abscissae of the points are not equidistant, and also by the somewhat complex form of the expressions for S_n and σ_n . But a further simpli-

⁸⁾ This case, which has a certain analogy to the case considered in the paper quoted in footnote 1) (impulses introduced with constant intervals of time), is too special for the problems of the paper quoted in footnote 2), since it would lead to a correlation function $v_1 v_2$ which would periodically repeat itself.

fication is possible since we are interested only in the large scale statistics of the summation curve. This allows us to omit the non-cumulative terms

$$(L\vartheta_n + \vartheta_n^2)/2t_0 \text{ in } S_n, \text{ and } \vartheta_n \text{ in } \sigma_n;$$

and to consider the expressions:

$$(21a) \quad S'_n = \text{const.} + \sum_1^n \gamma_j,$$

$$(21b) \quad \sigma'_n = \text{const.} + nL + \sum_1^n \varepsilon_j,$$

with:

$$\gamma_j = \frac{1}{t_0} (L + \varepsilon_j) \theta_{j-1}.$$

The terms omitted from (21a) and (21b) would be of interest only when the micro-statistics must be considered; for the problem of double contact at large intervals they are unimportant.

All γ_j are independent of each other, and so are all ε_j . The presence of a term $\varepsilon_j \theta_{j-1}$ in the expression for γ_j probably is of no consequence, since the θ 's are independent of the ε 's; moreover this term becomes small when σ_{II} is supposed to be small compared with L . We shall write:

$$\sigma^2 = \sigma_I^2(1 + \sigma_{II}^2/L^2);$$

this makes:

$$\overline{\gamma^2} = L^2 \sigma^2 / t_0^2.$$

We can imagine that an arbitrary summation curve is built up, starting from a given point (the first contact point), by making steps in the horizontal direction of magnitude $L + \varepsilon_j$, combined with purely random steps γ_j in the vertical direction. An ensemble of summation curves can be obtained, all starting from the same point, and we must find a measure for the probability that there will be curves passing through the second contact point, without ever crossing the parabola determined by the two contact points. This ensemble of summation curves again can be compared with the diffusion of material, released at the starting point, carried along by a convection current in steps of constant length L in the direction of the horizontal axis (v -axis) and subjected at the same time to random displacements, of magnitude ε_j , in the direction of the x -axis and γ_j in the direction of the vertical or s -axis.

This diffusion process can approximately be described by a partial differential equation of the form:

$$(22) \quad L \frac{\partial \psi}{\partial x} = \frac{L^2 \sigma^2}{2 t_0^2} \frac{\partial^2 \psi}{\partial s^2} + \frac{\sigma_{II}^2}{2} \frac{\partial^2 \psi}{\partial x^2}.$$

In an analogous way as was done in the preceding paper we imagine that the field in which the diffusion takes place, is bounded by the parabola destined to make double contact with the summation curve. All material

which passes this boundary is lost and causes a decrease of the probability for obtaining a summation curve reaching the contacting parabola in the second prescribed point and remaining below it everywhere else. Such a limiting parabola can be described by an equation of the form:

$$(23) \quad S = \frac{(\eta - \text{const.})^2}{2(t - t_0)}.$$

We make use of the following similarity transformation, in which n^* and s^* are the new dimensionless variables:

$$(24) \quad \begin{cases} x = n^* \sigma^{2/3} L^{1/3} (t - t_0)^{2/3} t_0^{-2/3} \\ s = s^* \sigma^{4/3} L^{2/3} (t - t_0)^{1/3} t_0^{-4/3}. \end{cases}$$

The diffusion equation then takes the form:

$$(25) \quad \frac{\partial \psi}{\partial n^*} = \frac{1}{2} \frac{\partial^2 \psi}{\partial s^{*2}} + \frac{\mu^2}{2} \frac{\partial^2 \psi}{\partial n^{*2}},$$

where

$$(26) \quad \mu^2 = \sigma_{II}^2 \sigma^{-2/3} L^{-4/3} (t - t_0)^{-2/3} t_0^{2/3}.$$

Since we must transform S in the same way as s , and η in the same way as x , the parabola making double contact with the summation curve and limiting the field in which the diffusion takes place, will obtain an equation of the form:

$$(27) \quad S^* = \frac{1}{2} (n^* - \text{const.})^2.$$

Now it is of importance to observe that the dimensionless coefficient μ^2 occurring before the second term on the right hand side of (25) can be made as small as we please by increasing $t - t_0$ indefinitely. It follows that for large values of t we approach to the same problem as was considered in sections 9–11 of the preceding paper. In particular we refer to eq. (52) of that paper, which is the limiting form of the present equation (25), and to eq. (41a), which corresponds to our present (27). The quantity which had been denoted by f^{-2} in that paper now is replaced by:

$$\sigma^{2/3} L^{-2/3} (t - t_0)^{2/3} t_0^{-2/3}.$$

Hence, referring to the result $\bar{m} = 1,8 f^{-2}$ of that paper (*l.c.* p. 71, eq. 78), we arrive at the following value for the mean distance between two contact points:

$$(28) \quad \bar{m}L = 1,8 \sigma^{2/3} L^{1/3} (t - t_0)^{2/3} t_0^{-2/3}.$$

According to (8a) the mean distance between two contact points, $\eta'' - \eta'$, gives the jump in the value of v :

$$\frac{\tau_i}{t} = (v_- - v_+)_i = -a(\eta') + a(\eta'') = \frac{\eta'' - \eta'}{t - t_0} \cong \frac{\eta'' - \eta'}{t}.$$

It follows that mL determines the mean value of τ_i . According to eq. (27)

of the paper mentioned in footnote 2) (*l.c.* p. 256), this mean value is equal to l , so that asymptotically:

$$(29) \quad l \cong 1,8 \sigma^{2/3} L^{1/3} (t/t_0)^{2/3}.$$

This result furnishes a proof of formula (91) of the paper mentioned in footnote 2) (*l.c.* p. 726), which originally had been derived from the assumption that a similarity rule would hold for the statistical arrangement of the segments λ_i and τ_i . The present proof does not need the a priori introduction of such an assumption; on the contrary it is pretty certain that the similarity property will be an asymptotic result of the statistical relations to which the system is subject.

4. *Further problems.* — The present method opens a way of approach to several questions connected with the correlation problems studied in the paper quoted in footnote 2). In the first place it is possible to obtain an expression for the probability of the various values of m , which will enable us to find the distribution function for the τ_i . It will further be necessary to consider the positions of the axes of the doubly contacting parabolas, since these positions determine the abscissae of the steep fronts in the course of v , and thus the lengths of the segments λ_i . While the mean value of the λ_i is the same as that of the τ_i , *viz.* the quantity denoted by l , the distribution function for the λ_i may be different. The distribution of the λ_i played an important part in certain deductions of the paper quoted, needed in the calculation of the correlation function $\overline{v_1 v_2}$; compare the definition of the functions $f_1(\lambda)$, $f_k(\lambda)$, *l.c.* p. 394, which moreover involved the problem whether there exist correlations between the τ_i and the λ_i .

The method applied in the present paper gives an answer to a problem left open in the older paper (*l.c.* p. 393), *viz.* to find a satisfactory basis for the description of the ensemble of states possible for the system of "shock waves" or "N-waves". Since we have obtained a method for deducing the statistical properties of the state of the system at any instant t directly from the initial state given for t_0 , it seems that a sufficiently general ensemble can be constructed by starting from an ensemble of initial states with a random distribution of the quantities ε_i and θ_i introduced in (15). As mentioned these quantities can be supposed to be wholly independent of each other; the only condition to be observed is that $L + \varepsilon_i$ may not become negative.

Incidentally the present method can lead to the solution of the statistical problem for the molecular analogue mentioned in footnote 3) of the older paper (*l.c.* p. 256). That problem referred to an assembly of molecules of various masses, moving with arbitrary velocities along a single line, while it was assumed that every time two molecules collide, they would combine with conservation of mass and of momentum. The ultimate form of the mass distribution function was asked. Since the masses in this analogue correspond to the τ_i of the wave problem, the solution of the latter case will lead to that of the molecular problem.

On the other hand there remain many problems concerning the principles of the method applied in this paper and in its immediate predecessor which deserve further analysis. Several details connected with the introduction of the diffusion equation for the probability must be worked out with greater precision.

Moreover, thus far we have considered a "summation curve" determined by discrete points and we have assumed that there should be no correlation between successive steps. The problem becomes much more difficult when the successive steps are not independent, but are correlated. It has been shown by GOLDSTEIN that this can lead to a more complicated equation for the probability function ⁹⁾. It is probable that as soon as a continuous summation curve is considered, similar complications will present themselves. Nevertheless it seems probable that for the large scale effects we shall always approach to a diffusion process asymptotically governed by an equation of the form:

$$(30) \quad \frac{\partial \psi}{\partial x} = J_0 \frac{\partial^2 \psi}{\partial x^2},$$

where ¹⁰⁾

$$(30a) \quad J_0 = \int_0^\infty \overline{v(y) v(y + \eta)} d\eta.$$

⁹⁾ S. GOLDSTEIN, On Diffusion by Discontinuous Movements, and on the Telegraph Equation, Quart. Journ. Mech. and Applied Mathem. **4**, 129-156 (1951).

¹⁰⁾ As proved in the paper quoted in footnote 2) (*l.c.* p. 249) the quantity J_0 is independent of the time. It can be calculated according to formula (35), *l.c.* p. 259. With the following values for the initial instant $t = t_0$:

$$\tau_i \zeta_i = -\frac{1}{2} L (\theta_i + \theta_{i-1} + \frac{1}{2} \varepsilon_{i+1} - \frac{1}{2} \varepsilon_i) - \\ - \frac{1}{2} (\theta_i^2 - \theta_{i-1}^2 + \theta_i \varepsilon_{i+1} + \theta_{i-1} \varepsilon_i + \frac{1}{4} \varepsilon_{i+1}^2 - \frac{1}{4} \varepsilon_i^2);$$

and

$$\sum \tau_i \zeta_i \cong - \sum (L + \varepsilon_{i+1}) \theta_i,$$

this formula gives:

$$J_0 = \frac{L^2 \overline{\theta^2} + \overline{\varepsilon^2} \overline{\theta^2}}{2L t_0^2} = \frac{L \sigma^2}{2 t_0^2}.$$

This is the coefficient of the preponderant term on the right hand side of equation (22) when divided by L .

THE DEHYDRATION OF ALUMINA HYDRATES

BY

J. H. DE BOER, J. M. H. FORTUIN AND J. J. STEGGERDA

(Communicated at the meeting of December 19, 1953)

1. *Introduction and nomenclature*

During the last ten years many research workers have tried to explain the complex nature of the dehydration of the alumina hydrates and numerous communications on this problem have appeared in American, French and English literature.

Unfortunately, different systems of nomenclature are in use; here we shall use the mineralogical names of the hydrates, viz. for the trihydrates, $\text{Al}_2\text{O}_3 \cdot 3\text{H}_2\text{O}$:

gibbsite (hydrargillite, α -alumina trihydrate, γ -trihydrate)

bayerite (β -alumina trihydrate),

and for the monohydrates, $\text{Al}_2\text{O}_3 \cdot \text{H}_2\text{O}$:

boehmite (γ -alumina monohydrate, α -alumina monohydrate)

diaspore (α -alumina monohydrate, β -alumina monohydrate).

The names which we shall use are in italics, the nomenclature in other systems is given in parentheses.

For the nearly anhydrous alumina with the spinel structure (described by VERWEY ¹⁾) we shall use the name $\gamma\text{-Al}_2\text{O}_3$ ($\eta\text{-Al}_2\text{O}_3$). For the nearly anhydrous alumina which is formed by dehydration of gibbsite, we shall use the name $\chi\text{-Al}_2\text{O}_3$ (in accordance with most other nomenclature systems, sometimes $\kappa'\text{-Al}_2\text{O}_3$ is used).

2. *The dehydration schemes*

Our experiments have led us to the following assumptions about the dehydration of gibbsite, bayerite and boehmite:

1) Dehydrations under normal conditions of H_2O pressure:



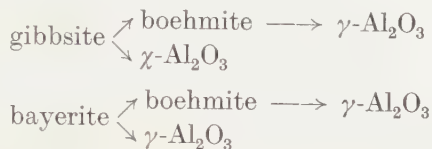
2) Dehydration under hydrothermal conditions, so under a water pressure which corresponds to the saturation pressure of water:



¹⁾ E. J. W. VERWEY, J. Chem. Phys. 3, 592 (1935).

Our experiments are completely in accordance with those of LAUBENGAYER and WEISZ²⁾ on the hydrothermal dehydration. We have not studied the hydrothermal decomposition of boehmite, as this was not important in our work.

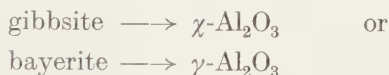
Many specimens of gibbsite and bayerite, however, give the following, apparently strange, picture of the dehydration:



3. *A suggested explanation*

To understand these phenomena we must realize that at the beginning of the dehydration, very high water pressures may exist inside the crystals, because of the difficulty for the water molecules to escape out of the interior of the crystals. Under these intragranular hydrothermal conditions boehmite will be the product formed.

The porosity of the product, will, however, increase during further dehydration and the internal water pressure will rapidly fall off. Below a certain water pressure a further transition of gibbsite (bayerite) to boehmite will not be possible. At increasing temperature the dehydration will begin again but now under much lower pressures; the reaction proceeds now as follows:



Obviously the first dehydration reaction to boehmite will not occur if the original gibbsite or bayerite consists of very small crystals. This fact was already observed by TERTIAN and PAPÉE³⁾ for gibbsite. We have studied two bayerites; one, consisting of small crystals, gives only $\gamma\text{-Al}_2\text{O}_3$ on dehydration, another, well-crystallized, bayerite gives both boehmite and $\gamma\text{-Al}_2\text{O}_3$ on dehydration.

4. *Experiments on the dehydration of gibbsite*

a) We have investigated gibbsite produced by Peter Spence and Sons Ltd *). Water content 53 % (calculated on anhydrous Al_2O_3). X-ray analysis shows it to be a well-crystallized gibbsite. The grain size (about 100 μ) remains constant on heating, even to a temperature of 750° C,

²⁾ A. LAUBENGAYER and R. WEISZ, J. Am. Chem. Soc. **65**, 247 (1943).

³⁾ R. TERTIAN and D. PAPÉE, Compt. rend. **236**, 1565 (1953); **236**, 1668 (1953).

*) We wish to thank Mr J. H. HARWOOD of Peter Spence and Sons Ltd, Widnes (Lancs.), England for his kindness to supply us with this gibbsite.

where the original product has lost 34 % of its weight (i.e. practically all its water).

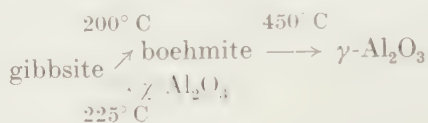
b) X-ray analysis

Samples of this gibbsite, heated during 7–10 hours at different temperatures, were investigated with $\text{CuK}\alpha$ -radiation, using a camera with a diameter of 57.4 mm. Up to 190°C the gibbsite remains, seemingly, unaltered. Above this temperature the pattern of well crystallized boehmite appears besides the pattern of gibbsite. Between 200 and 225°C the ratio boehmite: gibbsite seems to be constant, it is evident that the formation of boehmite has stopped.

Above 225°C the gibbsite disappears rather quickly and the X-ray diffraction shows that here gibbsite is transformed into a very poorly crystalline alumina, which we shall call $\chi\text{-Al}_2\text{O}_3$, according to the usual nomenclature. The pattern of $\chi\text{-Al}_2\text{O}_3$ contains only two broad and vague diffractions with spacings of 2.11 and 1.40 Å.

From 250 to about 450°C the pattern remains unchanged. At 450°C the boehmite decomposes, forming $\gamma\text{-Al}_2\text{O}_3$. So, the final product of dehydration at 500°C is a mixture of $\chi\text{-Al}_2\text{O}_3$ and $\gamma\text{-Al}_2\text{O}_3$. (See fig. 1a, 1b).

Summarizing we may say that the decomposition of our gibbsite proceeds through the following reactions:



This representation is analogous to that of BROWN and coworkers⁴⁾.

The only way to make boehmite as well crystallized as it is when formed at the dehydration of gibbsite, is autoclaving a hydrate (or any other alumina not heated above 800°C). We assume that the formation of well-crystallized boehmite by heating gibbsite is possible only because intragranular hydrothermal conditions exist.

c) Dehydration curve of gibbsite

Samples of gibbsite were heated at temperatures between 100 and 1000°C in air, with a partial water vapour pressure of 4.6 mm. To get reproducible results it is important to have the speed of heating of the samples nearly constant. Therefore, the samples were heated to the required temperature in about 1 hour, after which the temperature was kept constant for about 6 hours. After the heating the samples were cooled in small, rubber stoppered bottles; the water content was determined from the loss of weight on heating at 1200°C in a platinum crucible.

Figure 2 shows the water content (calculated on dry Al_2O_3) as a function of the temperature. Figure 3 shows the change in water content per $^\circ\text{C}$ as a function of the temperature.

⁴⁾ J. F. BROWN, D. CLARK and W. W. ELLIOT, J. Chem. Soc. p. 84 (1953).

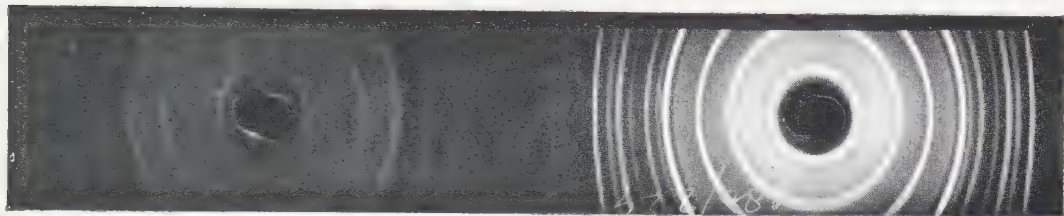


Fig. 1a. X-ray pattern of pure boehmite;

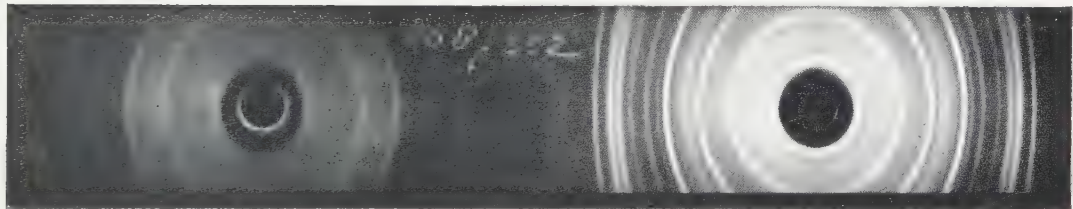


Fig. 1b. X-ray pattern of boehmite + α Al_2O_3 (gibbsite heated at 300° C);

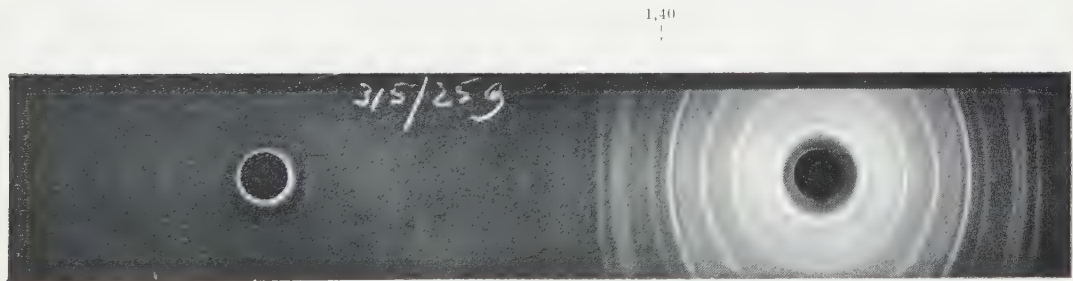


Fig. 1c. X-ray pattern of boehmite + γ - Al_2O_3 (bayerite 2, heated at 300° C.)

The curves of fig. 2 and 3 make it evident that the dehydration proceeds through 3 reactions:

- 1) At 165° C the sudden decrease of the water content is caused by the reaction gibbsite \longrightarrow boehmite.

The reaction stops when the internal water pressure has fallen off because of the increase in the porosity.

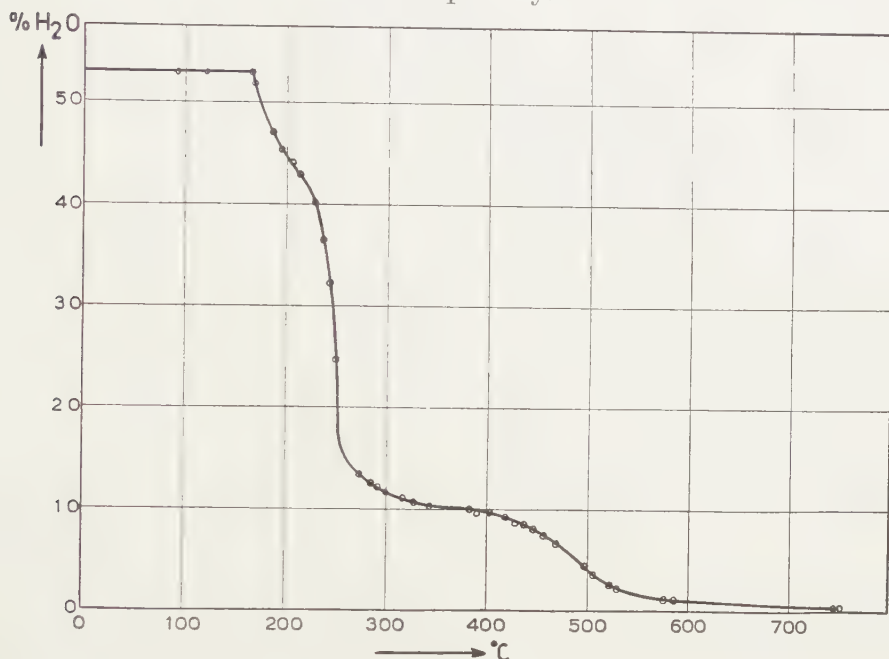


Fig. 2. Water content as a function of the temperature to which gibbsite is heated (calculated on anhydrous Al_2O_3).

- 2) At 200–225° C the dehydration starts again, according to the reaction gibbsite $\longrightarrow \chi\text{-Al}_2\text{O}_3$.

Between 300 and 400° C the water percentage is nearly constant at about 10 % (calculated on anhydrous Al_2O_3), which corresponds to a mixture of boehmite and $\chi\text{-Al}_2\text{O}_3$. This dehydration product is described as a non-stoichiometric boehmite by some French investigators ⁵). Quite recently, however, PRETTRE, IMELIK, BLANCHIN and PETITJEAN realize that this product may contain an anhydrous constituent ⁶).

- 3) At 450–500° C boehmite $\longrightarrow \gamma\text{-Al}_2\text{O}_3$.

From fig. 2 we can calculate $\frac{1}{3}$ of the gibbsite to be decomposed to boehmite and $\frac{2}{3}$ to $\chi\text{-Al}_2\text{O}_3$.

d) Differential thermal analysis

With a heating speed of 5° C per minute we get for our gibbsite a curve

⁵) J. TRAMBOUZE and M. PERRIN, *Compt. rend.* p. 1261 (1953); L. BLANCHIN, B. IMELIK and M. PRETTRE, *Compt. rend.* p. 1025 (1953).

⁶) M. PRETTRE, B. IMELIK, L. BLANCHIN and M. PETITJEAN, *Angew. Chem.* **65**, 549 (1953).

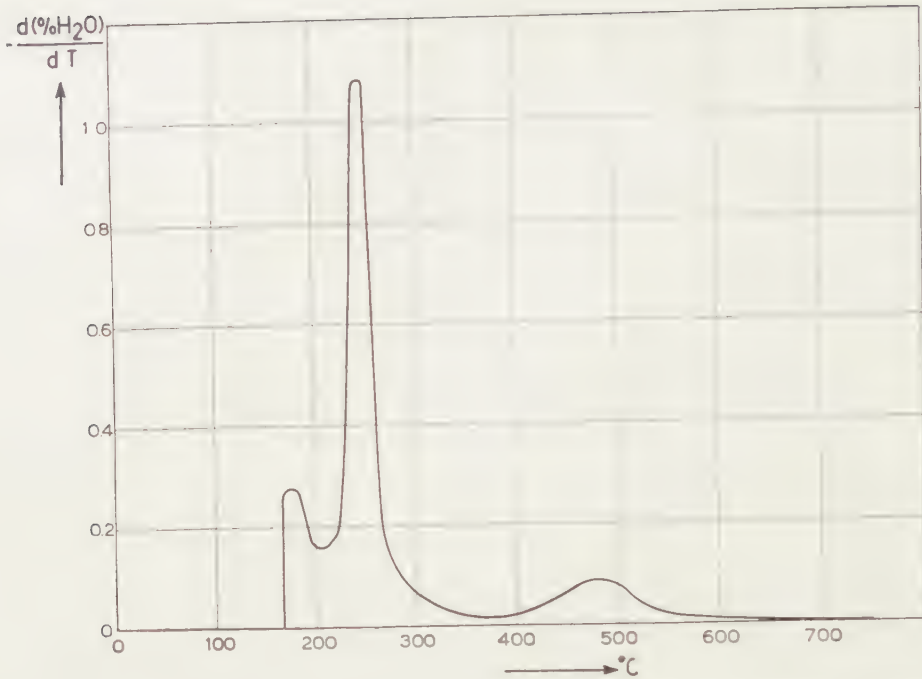


Fig. 3. — $d(\% \text{H}_2\text{O})/dT$ as a function of the temperature to which gibbsite is heated. as given in fig. 4. These results are completely in accordance with the work of BROWN c.s. ⁴⁾.

The differential thermal analysis confirms the results of the dehydration curve, especially if we compare fig. 3 and 4.

The three endothermic reactions do not agree in the decomposition diagram, given by DAY and HILL ⁷⁾:

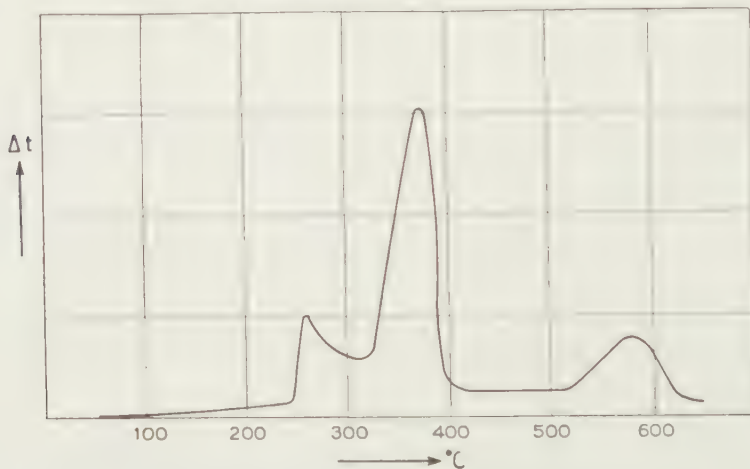


Fig. 4. Differential thermal analysis of gibbsite. (The temperatures which are indicated here, are, as a consequence of the method of heating, far higher than those which correspond with the transitions. The real temperatures are found in figs. 2 and 3).

⁷⁾ M. K. B. DAY and V. J. HILL, *Nature* **170**, 539 (1952).



for it is very improbable that the rehydration of $\chi\text{-Al}_2\text{O}_3$ to boehmite should be an endothermic reaction.

e) Lauric acid surface area determinations

The surface area of gibbsite as a function of the temperature of heating was determined by adsorption of lauric acid, dissolved in pentane, according to HOUBEN⁸⁾. The results are shown in fig. 5.

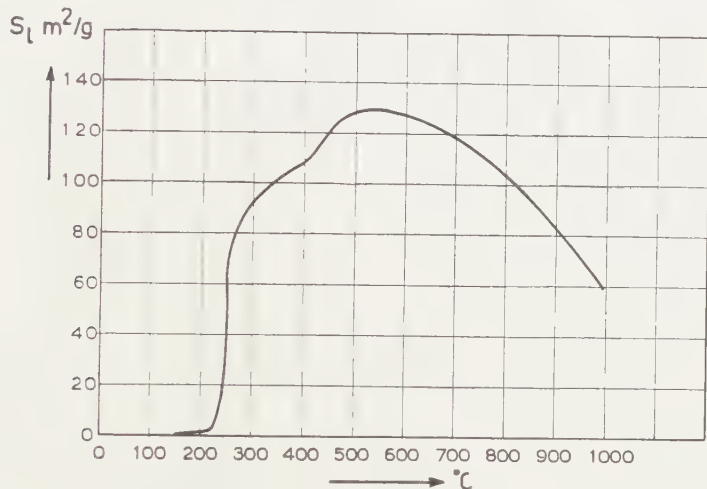


Fig. 5. Lauric acid surface area of gibbsite, pre-heated to the temperatures, indicated on the horizontal axis.

Below 220° C the surface area remains less than 2 m²/g, although the water content has already decreased to 42 % (calculated on anhydrous Al_2O_3). This small porosity makes possible the existence of intragranular hydrothermal conditions.

Above 225° C the surface area increases rapidly, the internal water pressure falls off and now the reaction $\text{gibbsite} \longrightarrow \chi\text{-Al}_2\text{O}_3$ takes place.

At 400° C the surface area increases again by the formation of $\gamma\text{-Al}_2\text{O}_3$ from boehmite.

Above 500° C the surface decreases because of the sintering of the pores.

5. Experiments on the dehydration of bayerite

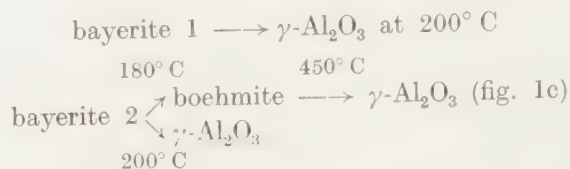
a) We have investigated two bayerites; one, prepared by the amalgam method described by SCHMÄH⁹⁾, we shall indicate as bayerite 1. Another sample of bayerite was made by very slow action of CO_2 (three weeks' exposure to the air) on an alkaline solution of sodium aluminate at room temperature. This bayerite, called bayerite 2, consists of comparatively big crystals.

⁸⁾ G. M. M. HOUBEN, thesis Delft (1951).

⁹⁾ H. SCHMÄH, Z. Naturforsch. 1, 323 (1946).

b) X-ray analysis

The two bayerites give different dehydration products:



The $\gamma\text{-Al}_2\text{O}_3$ formed by decomposition of bayerite is very poorly crystallized.

The dehydration diagram for bayerite 2 is analogous to that for gibbsite. Bayerite 1, giving only $\gamma\text{-Al}_2\text{O}_3$ on heating, behaves as the gibbsite described by TERTIAN and PAPÉE³⁾, which consists of very small crystals and gives only $\chi\text{-Al}_2\text{O}_3$ on dehydration.

The assumption that intragranular hydrothermal conditions cannot exist with too small crystals, provides a satisfactory explanation for the difference observed between the two bayerites.

c) Dehydration curve

Figure 6 gives the water content of bayerite 1 as a function of the temperature. It is evident that the dehydration proceeds in only one step.

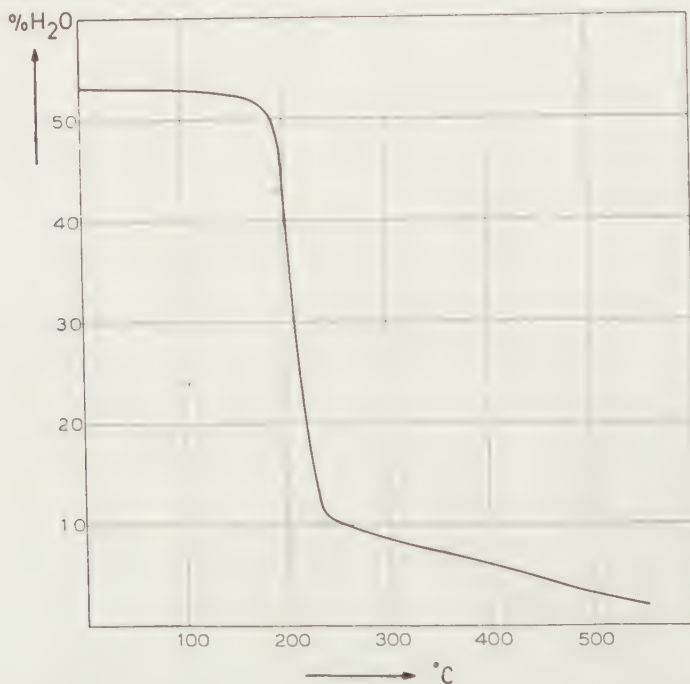


Fig. 6. Water content of bayerite 1 as a function of the temperature.

d) Differential thermal analysis

In figure 7 the differential thermal analyses of bayerite 1 and 2 are given.

The results are completely in accordance with the decomposition diagram assumed for the two bayerites. For bayerite 1 there is only one endothermic peak corresponding to:

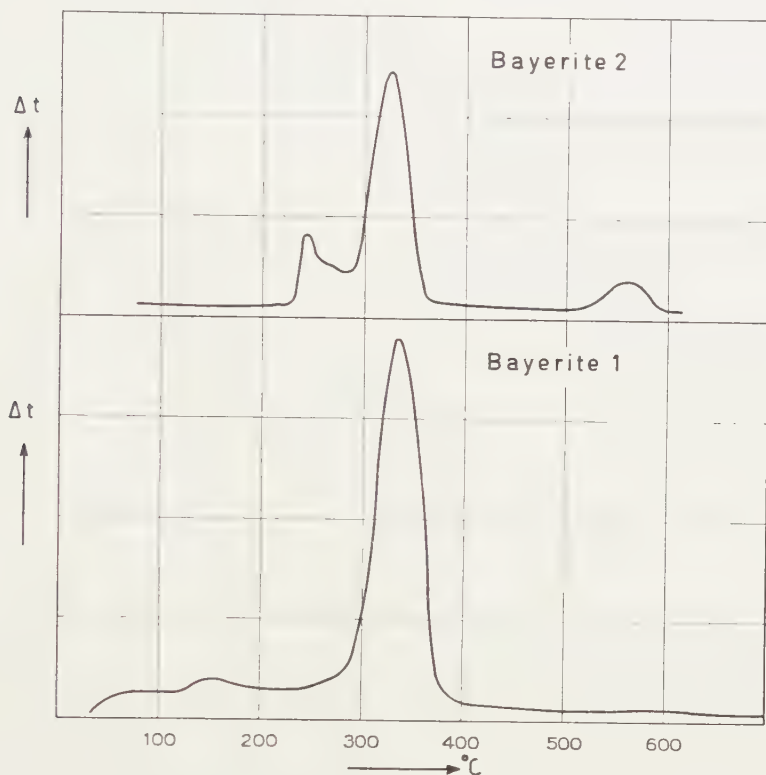
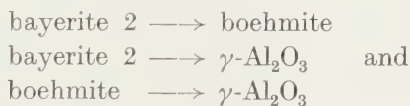


Fig. 7. Differential thermal analysis of a) bayerite 1; b) bayerite 2.

For bayerite 2 there are three endothermic reactions, viz.:



6. Experiments on the dehydration of boehmite

We have investigated two boehmites *). One sample was prepared by hydrolysis of highly pure aluminium isopropoxide; this very poorly crystallized product is called boehmite 1.

The second sample was made by autoclaving boehmite 1 at 275° C and about 50 at water vapour pressure. This well-crystallized product is called boehmite 2. The initial water contents of boehmite 1 and 2 are 38 % and 17.7 % respectively (calculated on anhydrous alumina).

*) We wish to thank Mr K. A. NATER for carrying out part of the experimental work.

The difference in water content arises from the water adsorbed on the surface of two samples. Therefore, in addition to the stoichiometric water content of 17.7 %, (calculated on anhydrous alumina) boehmite 1, with an extensive surface area (lauric acid surface area about 200 m²/g), contains an extra amount of 20.3 % of water as adsorbed water.

The dehydration curves, the differential thermal analyses and the surface areas (determined by the lauric acid method) as a function of temperature are given in figs. 8, 9 and 10. We obtained results similar to those of IMELIK, PETITJEAN and PRETTRE¹⁰).

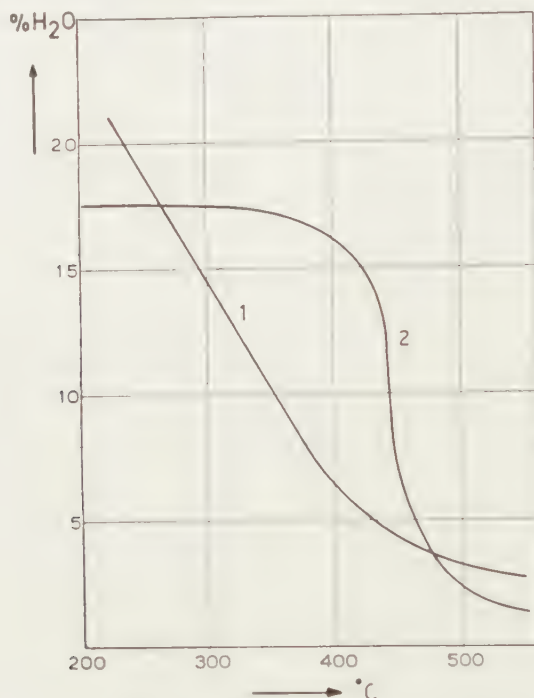


Fig. 8. Dehydration curves for boehmite 1 and 2. The water percentage is calculated on dry Al₂O₃.

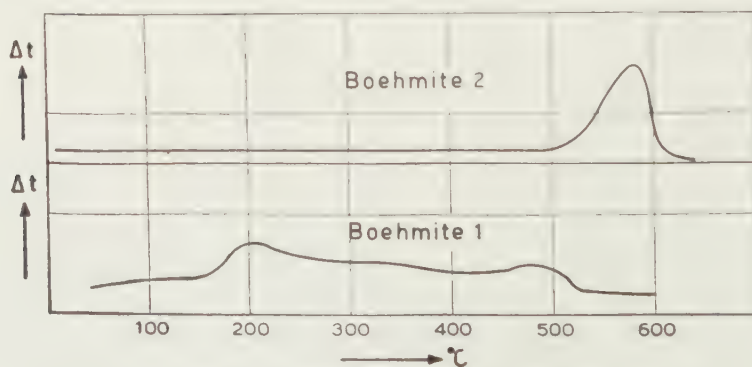


Fig. 9. Differential thermal analysis of boehmite 1 and 2.

¹⁰) B. IMELIK, M. PETITJEAN and M. PRETTRE, *Compt. rend.* p. 1278 (1953).

The difference between boehmite 1 (lauric acid surface area about 200 m²/g) and boehmite 2 is clearly shown: boehmite 1 gives a continuous dehydration, boehmite 2 has a rather sharp transition temperature.

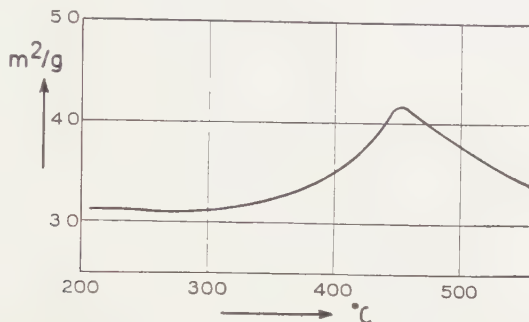


Fig. 10. Lauric acid surface of boehmite 2 as a function of the ignition temperature.

However, the two boehmites form the same γ -Al₂O₃ on ignition, the γ -Al₂O₃ from boehmite 1 being very badly crystallized.

7. The "non-stoichiometric boehmite"

The dehydration product of well-crystallized gibbsite with approximately 10 % H₂O (calculated on anhydrous Al₂O₃) is sometimes called a "non-stoichiometric boehmite" or a boehmite with a deficiency of water ("Defizitär-Böhmite"⁸) in German). According to our view it is a mixture of relatively well-crystallized boehmite which is formed by the intragranular hydrothermal dehydration of gibbsite crystals and of χ -alumina which is formed after the intragranular hydrothermal conditions cease to exist. We suggest that this dehydration product consists of grains of the same size as the original gibbsite grains, the inner part of each crystal having been converted into boehmite, whilst the outer part of each individual crystal has been dehydrated to χ -Al₂O₃. An electron diffraction pattern will reveal an anhydrous structure as is reported by PRETTE⁸ *et al.*⁸). A product as described here will—in accordance with the views developed in this article—show two sorts of pores, viz. capillaries with a small cross section in the inner part of the individual converted crystals and capillaries with a larger cross section in the outer part. This pore distribution may even be maintained after the boehmite inner parts have been dehydrated to γ -Al₂O₃. It is remarkable in this respect that ZWIETERING¹¹) found that Al₂O₃ prepared by dehydration of bayerite—where similar phenomena occur on dehydration (see section 5 of this article)—shows two groups of capillaries, one group with an average radius of just over 20 Å and another group with an average radius of, roughly, 40 Å.

Acknowledgment

One of us (J. M. H. FORTUIN) gratefully acknowledges a grant from the Delfts Hogeschoolfonds enabling him to contribute to these investigations.

¹¹) P. ZWIETERING, *De Ingenieur* **65**, O, 1 (1953).

Summary

A reaction mechanism for the dehydration of the alumina hydrates gibbsite, bayerite and boehmite is given.

The conception of intragranular hydrothermal conditions gives a satisfactory explanation of our own experiments and also of those of the numerous other investigators in this field. Our own experiments concern X-ray analysis, dehydration curves, differential thermal analysis, the study of the surface area during dehydration and the dehydration of the hydrates under hydrothermal conditions in autoclaves.

*Geleen, Central Laboratory of the Neth. State Mines
and Delft, Laboratory for Chemical Engineering of
the Technological University*

November 1953

PHYSICAL CHEMISTRY

GRAPHITIC OXIDE

I. THE FORMULA AND THE SPECIFIC VOLUMES OF THE HYDRATES

BY

J. H. DE BOER AND A. B. C. VAN DOORN

(Communicated at the meeting of January 30, 1954)

I. GRAPHITIC OXIDE (Graphitic acid)

Graphitic oxide is a lamellar graphite compound the chemical constitution of which has not been quite elucidated until now.

HOFMANN and coworkers ¹⁾ held the opinion that graphitic oxide could not be represented by one single formula; in their opinion the atomic C : O ratio determines how far the oxidation process has proceeded in each sample of graphitic oxide. The atomic ratio in "ideal" graphitic oxide was supposed to be C : O = 2. This would mean that all C valencies are saturated, each of the two valencies of an O-atom saturating a valency of a C-atom. Their atomic C : O ratio, determined experimentally (from elementary analyses), was about three.

THIELE ²⁾ proposed the gross-formula $\{C_6(OH)_3\}_n$, based on the results of elementary analysis. RUESS ³⁾, however, showed that the mode of purification, as applied by THIELE, was very incomplete. The graphitic oxide was purified by washing with glacial acetic acid in which 10 % acetic anhydride was dissolved. The adsorbed acetic acid (and acetic anhydride) was removed by washing with dry ether and finally the ether was removed by drying the sample at 70° C in high vacuum. With two samples purified in this manner, RUESS ³⁾ found 19.7 and 24.6 % ash.

The hygroscopical behaviour of graphitic oxide appeared to present many difficulties. HOFMANN ¹⁾ c.s. thought it not well possible to fully remove the physically adsorbed water; not even when drying in vacuo at higher temperatures (70–100° C).

It appeared to us, therefore, essential to investigate the behaviour of graphitic oxide with respect to water, apart from trying to elucidate the chemical constitution of graphitic oxide.

II. OUTLINE OF THE METHOD

a. *Oxidation of graphite*

It was not certain whether graphite need only be oxidized once in order to obtain a reproducible graphitic oxide. Therefore we subjected each of

¹⁾ U. HOFMANN, *Erg. exakt. Naturw.* **18**, 229 (1939).

²⁾ H. THIELE, *Z. anorg. Chem.* **190**, 145 (1930).

³⁾ G. RUESS, *Kolloid Z.* **110**, 17 (1945).

three portions of the same sample of graphite to an oxidation treatment. After purifying all three products one portion was oxidized once more and the third portion was oxidized as many as seven times. The experiments described were performed with the twice and with the seven times oxidized samples, the samples which were only treated once proved to be only partially oxidized (see IVa).

b. *Water vapour isobar*

If graphitic oxide with a certain (but unknown) water content is heated at different temperatures, the remaining water content of the sample is dependent on the water vapour pressure during the heating process. In most of our experiments the samples were heated in an atmosphere, having a partial water vapour pressure of 4.57 mm (this being the water vapour pressure of melting ice). In order to follow the variations in the water content of different samples conditioned in this manner the water content was estimated in two different ways, whilst also the density of the samples was determined. As it was not necessary to know the "true" density of every sample we determined it by imbibition with liquids. In order to find the best imbibition liquid various liquids were tried as described in III. Water proved to give the most satisfactory results.

c. *Water vapour isotherm*

Apart from these experiments at various temperatures and a constant water vapour pressure, five samples of graphitic oxide were conditioned at different water vapour pressures and constant temperature (20° C). The original samples were dried over P_2O_5 in high vacuum at 20° C.

d. *Elementary analysis*

We carried out elementary analyses (C-H) of all samples conditioned by one of the two methods described above. The oxygen content was found by subtraction.

III. EXPERIMENTAL PART

a. *Oxidation of graphite and purification of the graphitic oxide obtained*

The graphite used was Madagascar graphite, containing about 10 % ash (mainly iron and silicon). By a treatment at room temperature with concentrated hydrochloric acid, followed by a treatment with 35 % hydrofluoric acid and subsequently with concentrated hydrochloric acid again, each time during two days, the ash content could be reduced to 0.2 % (silicon dioxide). After washing with large quantities of distilled water, the graphite was dried at 120° C in a dry nitrogen atmosphere.

The STAUDENMAIER⁴⁾ method was used for the preparation of the graphitic oxide. 15 gms of graphite are suspended in a cold mixture of 130 ml nitric acid (63 %) and 265 ml concentrated sulphuric acid. During

⁴⁾ L. STAUDENMAIER, Ber. 31, 1481 (1898).

four days 190 gms potassium chlorate are added in portions. When adding the potassium chlorate, the temperature of the reaction mixture should not rise above 50°C , to avoid the danger of explosions by the formation of chlorine dioxide (ClO_2). As the temperature rises quite rapidly when the first portions of potassium chlorate are added, it is advisable to add not more than four grams of potassium chlorate at a time. The mixture, stirred occasionally, is left to cool to room temperature. After adding about 30 gms, the remaining potassium chlorate can be added in portions of about 6 gms an hour. The reaction mixture is allowed to stand, with occasional stirrings, during 14 days at room temperature under a hood with strong suction. During this oxidation the colour changes from black to green. If the oxidation process is repeated a few times with the same sample, the reaction mixture becomes yellow.

After completion of the oxidation a sufficient quantity of ice is added to the reaction mixture, so that after melting, the total liquid volume is twice as large as the original volume of the oxidation mixture.

This diluted mixture is passed through a glass suction filter. The precipitate is suspended in 400 ml nitric acid (1 : 1); then the suspension is thoroughly stirred after which the graphitic oxide settles and the supernatant liquid is decanted. The graphitic oxide is suspended in 200 ml warm (about 50°C) dilute nitric acid (1 : 2). After the graphitic oxide has settled, the supernatant liquid is decanted. This treatment with warm dilute nitric acid is repeated three times. The last treatment forms an essential part of the purification. Insufficient washing with dilute warm nitric acid leaves the ash content of the graphitic oxide samples at 5 % and higher. The ash content can be reduced to less than 1 % by washing with warm dilute nitric acid as described above. The reason must probably be sought in the formation of the potassium salt of graphitic acid. (The excess of sulphuric and nitric acid is indeed removed by washing with ice-water; the excess of potassium salts, however, is not.).

The nitric acid is removed by washing with large quantities of warm (50°C) distilled water until the filtrate is acid-free and free from sulphate-, nitrate- and chlorate ions. During these washings with warm water the graphitic oxide settles more and more slowly, and eventually peptisation occurs. Filtering through a glass filter becomes quite difficult then; by repeated centrifuging, decantation of the supernatant liquid, addition of warm water (about 50°C) whilst stirring, and centrifuging again, the process is notably accelerated.

After the washings with warm water, the graphitic oxide resembles wet clay. It is partially dried at room temperature in a desiccator over silicagel. During the drying process it has to be tried at various stages whether it is already possible to pulverize the graphitic oxide in an agate mortar. When drying is carried out too rigorously the graphitic oxide forms almost unpulverisable lumps. These dry graphitic oxide lumps decompose sometimes with a flame which is however limited to the spot where the pestle

exerts a large pressure. Experience teaches that graphitic oxide is best pulverisable at a water content of about 20 %. The pulverized graphitic oxide is eventually sieved through a 60 mesh sieve. It is stored in bottles (with a tightly-fitting rubber stopper) in a dry nitrogen atmosphere.

b. *Drying of graphitic oxide at room temperature*

As it seemed quite probable that graphitic oxide would decompose at elevated temperature, the graphitic oxide was dried at room temperature in high vacuum over P_2O_5 . Using a sample containing about 20 % water, this drying process required about two months. The criterion was that no change in weight of the sample should occur during seven consecutive days. In order to obtain a completely dry sample it was necessary to renew the P_2O_5 each day during the last fourteen days of the drying process. Great care had to be taken to ensure that only completely dried air could enter the desiccator. This was achieved by passing the air through drying tubes filled with soda-lime and P_2O_5 . The samples were weighed very rapidly in a well-closed weighing-bottle.

c. *Water vapour isobar*

The saturated vapour pressure of water at 0° C, i.e. 4.57 mm Hg, was chosen as the constant water vapour pressure. This water vapour pressure was obtained by passing a purified, oxygen-free current of nitrogen first through a wash-bottle filled with water at room temperature, and then through a wash-bottle filled with water and kept at 0° C in an ice-filled Dewar vessel. This moist stream of nitrogen was passed over the sample in a weighing-bottle. The weighing-bottle, which was occasionally stirred, stood in a beaker which was placed in an oil bath. The temperature was read from a thermometer placed just over the sample. The samples were kept at the chosen temperature till no change in weight was observed (5 to 7 days).

d. *Water vapour isotherm*

The relative water vapour pressure could be varied by using saturated solutions of different inorganic salts. In these tests a saturated lead-nitrate solution, kept at 20° C, was used to obtain a relative humidity of 98 %. Similarly, potassium carbonate, calcium chloride and lithium chloride give relative humidities of 44 %, 32 % and 15 % resp. The attainment of the adsorption equilibrium took 20 to 30 days. The criterion was that during three consecutive days no change in weight should be observed.

e. *Density measurements*

The density was determined at 25° C ($\pm 0.05^\circ$ C) in a 2 ml pycnometer. The graphitic oxide was placed in the pycnometer and entirely immersed in the imbibition liquid. Then, the graphitic oxide was degassed by evacuating the pycnometer to 18 mm Hg. Owing to variations in temperature, the attained vacuum etc., the accuracy of the determination was 0.3 %.

When using toluene, heptane and water, the measured densities appeared to increase in the order given. The water molecule is very small and strongly polar; therefore it will completely wet the graphitic oxide. It is obvious that all further determinations were carried out using water as imbibition liquid.

The determination proved to be independent of time, so that no reaction between water and graphitic oxide occurs at this temperature.

f. *Elementary analysis*

The C-H analyses were carried out in the usual macro-apparatus. In view of the decomposition (sometimes even explosive) of graphitic oxide at elevated temperatures, we had to take some special precautions. This very violent decomposition can only be prevented by heating the sample of graphitic oxide very slowly from room temperature to 180° C (one hour). The sample is then kept at 180° C for two hours, after which the temperature is raised again and combustion started. The length of the platinum combustion boat was sufficient (about 4 cm) to allow the weighed sample of graphitic oxide to be divided into several small portions.

IV. RESULTS AND DISCUSSION

a. *Oxidation*

The treatment described in IIIa has to be repeated a number of times in order to obtain complete oxidation.

This number depends on:

- 1) the time during which the graphite is left in the oxidizing solution;
- 2) the quantity of starting material, i.e. the quantity of graphite.

Doubling the amount of graphite to be oxidized—and of course also doubling the amount of oxidants used—results in a much less advanced degree of oxidation after one treatment. This may be understood if we have a proper insight into the oxidation mechanism.

According to HOFMANN and FRENZEL ⁵⁾ graphite swells when immersed in concentrated nitric acid (to which some concentrated sulphuric acid is added). This enables the chlorine dioxide, formed by the interaction between potassium chlorate and sulphuric acid, to penetrate between the hexagon layers of graphite where it acts as the oxidant proper. The potassium chlorate does not fully dissolve in the acid mixture and stays, partially undissolved, on the bottom of the beaker. The chlorine dioxide formed near the surface of the solid potassium chlorate has to diffuse between the graphite particles and between the hexagon layers of the graphite. This diffusion process may well be the rate determining step. The oxidation of larger quantities will then proceed much more slowly.

Elementary analyses showed that a once oxidized sample contains more carbon and less oxygen than a twice oxidized sample (using the quantities

⁵⁾ U. HOFMANN, A. FRENZEL, Ber. 63, 1248 (1930).

mentioned in the experimental part). Repeating the oxidation process up to seven times did not appear to bring about any further changes in the carbon- and oxygen-contents of the sample.

The experiments described hereafter were carried out partly with a twice, partly with a seven-times-oxidized sample.

b. *Water vapour isobar*

Eight portions from a seven times oxidized sample (original water content unknown) were conditioned at constant water vapour pressure and at different temperatures. A ninth sample (7 B) was heated in a dry stream of nitrogen to find out whether a fully waterfree graphitic oxide could be obtained in this manner.

TABLE 1
Densities of 9 portions of one graphitic oxide sample

Sample	Conditioning temperature °C	P _{H₂O} in mm Hg during conditioning	d_4^{25} (H ₂ O)
7 B	116	0	2.24
7 C	109	4.57	2.29
7 D	92	4.57	2.33
7 Y	86	4.57	2.33
7 X	76	4.57	2.31
7 E	64	4.57	2.25
7 F	54	4.57	2.17
7 G	44	4.57	2.13
7 H	35	4.57	2.08

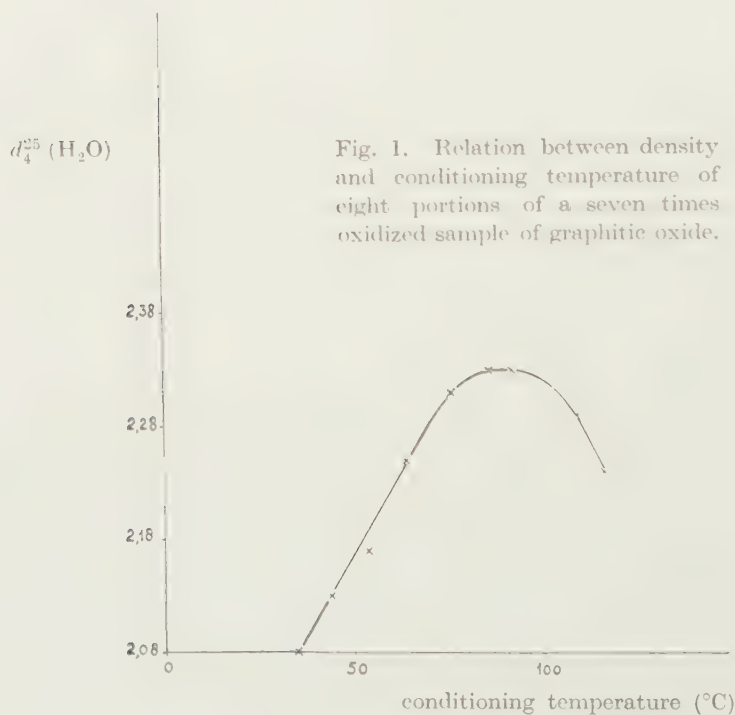


Fig. 1. Relation between density and conditioning temperature of eight portions of a seven times oxidized sample of graphitic oxide.

Fig. 1 graphically illustrates the change in density with the temperature. It is evident that the density values of the samples 7 X up to and including 7 H lie on a straight line. The density value increases with temperature, i.e. with decreasing water content. These samples have not been heated to a temperature higher than 76° C.

The density values of the samples 7 B, 7 C, 7 D and 7 Y, which have been heated to a temperature higher than 76° C, deviate much from this straight line. Probably, this must be ascribed to a decomposition of the samples.

HOFMANN, FRENZEL and CSALAN⁶⁾ showed that the transition from graphitic oxide to graphite, caused by thermal decomposition, is a continuous process. However, the decomposition, described above, proceeded in an atmosphere containing water vapour and a reaction between the decomposition product and water vapour, or an adsorption of water vapour should not be considered impossible. A reaction between the decomposition product and water is indicated by the behaviour of the samples 7 Y up to and including 7 B during the density measurements. In wetting these samples with the imbibition liquid, in our case with water, a considerable heat effect was observed. During the density measurements of the other samples (7 X down to and including 7 H) no such heat effect was observed.

c. *Water vapour isotherm and elementary analyses*

A sample of graphitic oxide (oxidized twice) was freed from water by drying at room temperature over P₂O₅ in high vacuum. Five portions (2 A, 2 B, 2 C, 2 D and 2 E) of this sample were conditioned at room temperature at different—though constant—water vapour pressures. The water content of the five portions was calculated from the increase in weight. The measured density values are summarized in table 2.

TABLE 2
Densities of 5 samples of graphitic oxide with a known water content

Sample	Relative humidity %	% water calculated from the increase in weight	d_4^{25} (H ₂ O)
2 A	10	6.46	2.18
2 B	15	7.11	2.15
2 C	32	12.13	2.03
2 D	44	14.20	1.97
2 E	98	27.65	1.72

The graph shown in Fig. 2 gives the correlation between the specific volume and the water content. This linear relation can be represented by

$$y = ax + b$$

⁶⁾ U. HOFMANN, A. FRENZEL and E. CSALAN, *Liebig's Ann.* **510**, 1 (1934).

where x represents the percentage of water and

$$a = 0.0059 \pm 0.0005$$

$$b = 0.423 \pm 0.006.$$

For $x=0$, the specific volume for dry (over P_2O_5) graphitic oxide is found to be 0.423 ± 0.006 . For $x=100$, the calculated specific volume for water is $(0.590 \pm 0.050) + (0.423 \pm 0.006) = 1.013 \pm 0.056$. The known specific volume of normal water at $25^\circ C$ is: 0.997.

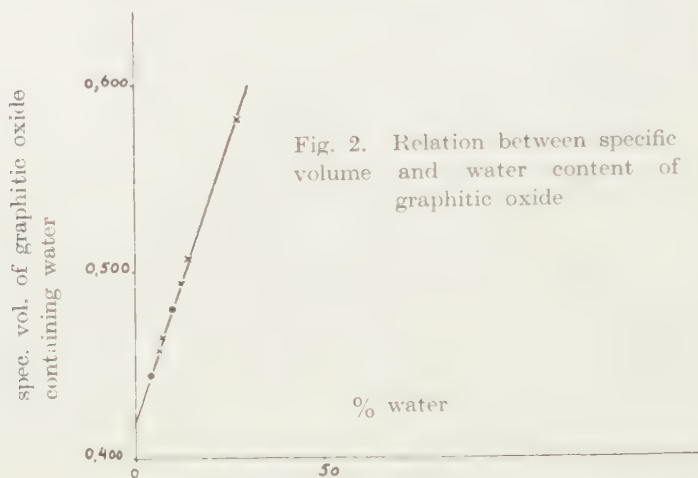


Fig. 2. Relation between specific volume and water content of graphitic oxide

× = values pertaining to the samples 2 A, -B, -C, -D and -E
 • = values pertaining to the samples 7 E and 7 H

The specific volume of three samples of graphitic oxide (each being oxidized twice) was determined after drying the samples over P_2O_5 in high vacuum at room temperature. Elementary analyses were carried out with well reproducible results. From these results the empirical formula was calculated to be: $C_6O_{3.4}H_{1.7}$ (see table 3).

TABLE 3

Results of elementary analysis and specific volume of dry graphitic oxide

Sample	% C	% H	% O	Specific volume	Formula
1	56.94	1.35	41.71	0.431	$C_6O_{3.3}H_{1.7}$
2	55.94	1.40	42.66	0.427	$C_6O_{3.4}H_{1.8}$
3	56.37	1.36	42.28	0.427	$C_6O_{3.4}H_{1.7}$

The agreement between these experimentally determined values of the specific volume and the calculated value (i.e. 0.423, see above) is quite satisfactory.

The empirical formula for graphitic oxide, containing water, should then be: $C_6O_{3.4}H_{1.7} \cdot n H_2O$. This was confirmed by the elementary analyses of the samples 2 C and 2 D.

The results are given below (see table 4).

TABLE 4

Sample	% C	% H	% O	Formula
2 C	49.6	2.5	47.9	$C_6O_{3.4}H_{1.7}H_{1.9}O_{0.9}$
2 D	47.8	2.7	49.5	$C_6O_{3.4}H_{1.7}H_{2.3}O_{1.2}$

The water content of the samples 2 C and 2 D calculated from these elementary analyses is 11.8 % and 14.4 % respectively. These values are in good agreement with the values calculated from the increase in weight in the isotherm determination, viz. 12.1 % and 14.2 % water respectively (see table 2).

d. *Comparison between twice- and seven-times-oxidized samples*

An elementary analysis of two samples, oxidized seven times (see table 1), gave the following results (see table 5).

TABLE 5

Sample	% C	% H	% O	Formula
7 E	54.3	1.7	44.0	$C_6O_{3.4}H_{1.7}H_{0.6}O_{0.2}$
7 H	51.2	2.2	46.6	$C_6O_{3.4}H_{1.7}H_{1.4}O_{0.7}$

The water contents, calculated from the results of the elementary analysis are 4.2 % and 9.8 % resp., the specific volumes were found to be 0.445 and 0.480 resp. These figures of corresponding water content and specific volume are located on the straight line obtained for the twice oxidized samples, which was shown in fig. 2. It seems justifiable therefore to conclude that the same graphitic oxide is obtained whether graphite is oxidized twice or seven times.

e. *A direct estimation of the water content*

Eventually, we determined the water content of the graphitic oxide samples by a direct method, the Karl Fischer technique. By this method the same values for the water content were found as those obtained by drying over P_2O_5 at room temperature in high vacuum (see table 6).

TABLE 6

Sample	% H_2O (K. Fischer technique)	% H_2O (drying over P_2O_5)
1	20.11	20.15
2	17.14	17.18

The titrations with the K. Fischer reagent were made according to the method described by JOHANSSON ⁷⁾. 25 ml of a sulphur dioxide-pyridine solution (SO_2 dissolved in a mixture of equal parts of dry pyridine and

⁷⁾ A. JOHANSSON; Svensk. Papperstidn. **50**, 124 (1947).

dry methanol) is brought into a titration flask: then, the graphitic oxide, containing water, is added. The water is titrated with iodine (dissolved in dry methanol). Well reproducible results were obtained even at low water contents. To rule out a reaction between the graphitic oxide itself and the reagent under titration conditions, we carried out the following experiments.

A part of two samples of graphitic oxide were titrated with the K. Fischer reagent and were found to contain 1.80 % and 2.69 % water resp. We now added a calculated amount of water to another part of the same samples, thus bringing up their water contents to 58.5 % and 61.3 % resp. By titration with the K. Fischer reagent we found 58.4 % and 61.2 % water resp.

CONCLUSIONS

Our experiments indicate that it is possible to prepare a graphitic oxide having a constant chemical composition, the empirical formula being $C_6O_{3.4}H_{1.7}$ or $C_7O_4H_2$.

To obtain this graphitic oxide:

- 1) the graphite must be thoroughly oxidized;

A twofold oxidation performed in the way described suffices.

- 2) during the preparation all steps have to be carried out at temperatures not exceeding 60–70° C.

The experiments described in this article do not yet allow to say anything conclusive about the structure of graphitic oxide. It seems reasonable, however, to express the hydroperoxide character of graphitic oxide—which appears i.a. from its sometimes explosive decomposition and its behaviour towards reducing agents as $SnCl_2$, $TiCl_3$ and acidified KJ solutions—in the structural formula $C_7(OOH)_2$ (Graphitic oxide had then better be called graphitic hydroperoxide).

Recently, ROSALIND E. FRANKLIN⁸⁾ gave the chemical composition of graphitic oxide as C_4O_2H i.e. $C_8O_4H_2$. Her formula differs by only one C-atom from the one we derived from our experiments. As Miss FRANKLIN gives no details about the way in which she prepared the graphitic oxide, we are unable to comment on this discrepancy.

Graphitic oxide is assumed to have a partly ionic structure. According to Miss Franklin, the cations are formed by the simple graphite layers, and the anions by multiple layers composed of $(O_xH_y)_n$, the structure of the latter resembling that of water which has lost part of its hydrogen. In dry graphitic oxide x should then be equal to or of the order of $2y$, while in hydrated graphitic oxide $2y > x > y/2$.

From the nature of the cationic exchange, as first found by THIELE⁹⁾, and later confirmed by many investigators, one has to conclude, however,

⁸⁾ E. R. FRANKLIN, J. chim. phys. **50**, C 26 (1953).

⁹⁾ H. THIELE, Kolloid Z. **80**, 1 (1937).

that the cations of graphitic oxide are H^+ ions. This is not contradictory to our conception of graphitic oxide as a hydroperoxide, as it is well-known that many hydroperoxides have acidic properties.

We hope to return to the subject of this hydroperoxide character of graphitic oxide in a future publication.

One of the authors (A. v. D.) gratefully acknowledges the permission of the National Defence Research Council T.N.O. to publish the results of this investigation. He also wishes to express his thanks to the Director of the Lab. of Chem. Research of this Council, Mr J. v. ORMONDT, for his constant interest in this study.

The authors are greatly indebted to Miss M. TH. SCHUELER and Mr J. R. REINSMA for their able assistance in the experimental work.

January 1954

*Geleen, Staatsmijnen (Netherlands
State Mines) Central Laboratory*

*Delft, Laboratory for Chemical
Engineering of the
Technological University*

*Delft, Chemical Laboratory of the
Nat. Def. Res. Council T.N.O.*

CONTRIBUTIONS TO THE PROBLEM OF THE ASSOCIATION
BETWEEN PROTEINS AND LIPIDS. VII *)¹⁾

The coacervation of gelatin + cetyl trimethylammonium bromide + KCNS

BY

H. G. BUNGENBERG DE JONG AND W. W. H. WEIJZEN

(Communicated at the meeting of December 19, 1953)

1. *Introduction and materials*

In the preceding communications of this series, we have studied exclusively coacervation of the type: linear protein + anionic soap + salt (carboxyl and sulfate soaps).

PANKHURST²⁾ has described examples of soap-rich associations of gelatin and soap, in which cationic soaps (e.g. of cetylamine) are used.

We do not doubt, that the nature of these associations is in principle the same as of those, studied previously in this series, namely associations in which the sandwich micelles of soap ions are covered on both sides by a protein monolayer.

The immediate inducement to the present investigation was the failure of PANKHURST to obtain (in the presence of M NaCl) analogous soap-rich associations, when using the cationic soap cetyl trimethylammonium bromide.

Under the most favourable conditions (pH 12.5), the binding of the soap to the protein was only 1.3 millimoles/g gelatin, a ratio which is practically equivalent to the total of the anionic side chains of the protein (1.24 millimoles/g gelatin). Lowering the pH decreased the number of soap ions; on the acid side of the I.E.P. of the gelatin, no association was brought about at all (from fig. 1 of the communication of K. G. A. PANKHURST it is read off that about 0.3 millimoles soap are bound to 1 g gelatin at pH 8; at pH 5 this ratio is 0.15 millimoles soap/g gelatin).

PANKHURST attributed the absence of the association between the protein and the cationic soap, to the large cross-sectional area of the head-group (the quaternary ammonium group), as a result of which the cetyl trimethylammonium cations would be unable to penetrate between

*) The term lipid is used here in a wide sense, including fatty acids and other long chain electrolytes.

¹⁾ Part I has appeared in these Proceedings, **45**, 601 (1942), Part II (A, B and C), III and IV in these Proceedings, Series **B55**, 317, 329, 338, 347, 360 (1952), Part V in these Proceedings, Series **B56**, 203 (1953) and Part VI (A and B) in these Proceedings, Series **B57**, 1, 13 (1954).

²⁾ PANKHURST, K. G. A., Discussions of the Faraday Society, **6**, 52 (1949).

the protein side chains and to approach sufficiently close to the keto-imide groups.

In our opinion, the failure must be ascribed to the use of an unsuitable salt (NaCl). In Part II of this series, a hypothesis has been given concerning the nature of the protein-soap association, namely, sandwich micelles of soap ions covered on both sides by a protein monolayer. The rôle played by the salt in this type of associations consists of the transformation of spherical soap micelles into precursors of large sandwich micelles.

From this hypothesis it follows, that the coacervation of gelatin + alkyl trimethylammonium soap + salt must be possible, provided that the salt used is able to cause the formation of sandwich micelles in the soap solution. The latter is seen from the formation of viscous elastic systems ³⁾ or (at higher salt concentration) from the coacervation of the soap solution⁴⁾.

Salts, like for example KBr, KCl, NaCl and Na₂SO₄, added to a 1 % solution of cetyl trimethylammonium bromide at 40°, do not produce these changes. This explains, from our point of view, the reason why in the coacervation gelatin + cetyl trimethylammonium soap, a soap-rich association cannot be realised by using the above-mentioned salts.

It appeared that KCNS, in relatively low concentrations, is able to cause the formation of elastic-viscous systems and coacervation, whereby CNS ions are bound to the cetyl trimethylammonium cations ⁵⁾.

Accordingly, it can be expected that the desired coacervation: gelatin + cetyl trimethylammonium bromide + salts is realisable with the use of KCNS and that relatively small concentrations are required.

Throughout the experiments isoelectric gelatine prepared from Gelatin F 00 of the Lijm en Gelatinefabriek Delft, at Delft, Holland (I.E.P. 5.0) and the commercial preparation of cetyl trimethylammonium bromide "Cetavlon" also employed in the above-mentioned investigation (on the binding of CNS⁻ ions) was used. Cetavlon contains 80.2 % trimethyl (long-chain alkyl) ammonium bromides calculated as cetyl trimethylammonium bromide. The experiments have been performed at 40°, using mainly the coacervate-volume method, described many times in preceding communications.

2. *The coacervation of mixtures of iso-electric gelatin and Cetavlon with KCNS*

First, the binding of CNS⁻ to the soap at 40° (using the same method as in the investigation mentioned in note 5) was determined anew, but now only for the comparable coacervate volume $V = C \times 40\%$ and for

³⁾ High temperatures or the presence of contaminations of organic compounds, may increase the damping to such an extent, that elastic phenomena are not observed at salt concentrations lower than needed for coacervation.

⁴⁾ H. J. VAN DER BERG, Thesis Leiden (1953). (Streaming Birefringence of Elastic-Viscous Oleate Systems).

⁵⁾ H. G. BUNGENBERG DE JONG and A. RECOURT, these Proceedings, Series B56, 303, 315, 342 (1953).

the limit dynamic-elastic/static-elastic systems. It was found that the KCNS concentrations needed to reach the first mentioned criterion are: 25.2 millimoles/l at 0.5 % Cetavlon, 32.8 millimoles/l at 1 % Cetavlon and 40.7 millimoles/l at 1.5 % Cetavlon. From the slope of the straight line through these points (upper straight line in fig. 1), follows a degree of occupation of 70 % and an equilibrium concentration of 17.4 millimoles/l KCNS (the part cut off from the abscis axis). The difference between these results and those obtained in earlier experiments (see note 5), lies within the experimental error.

The KCNS concentrations needed to reach the limit dynamic-elastic/static-elastic systems are 14.0 millimoles/l at 0.5 % Cetavlon, 18.5 millimoles/l at 1 % Cetavlon and 22.9 millimoles/l at 1.5 % Cetavlon. These values are used in drawing the middle straight line in fig. 1. Here a degree of occupation of 40 % and an equilibrium concentration of 9.6 millimoles/l KCNS is calculated. The difference between these results and those of the earlier investigation does not exceed the experimental error.

The third straight line in fig. 1, representing the limit non-elastic dynamic-elastic, is drawn from data of the earlier determinations (lower straight line).

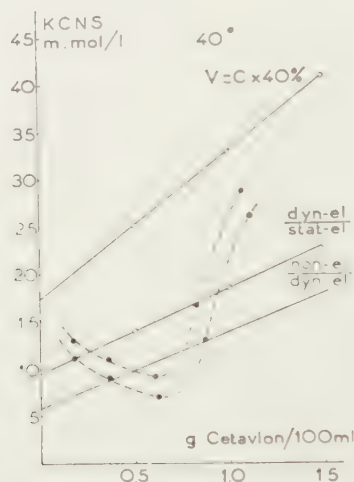


Fig. 1. Explanation see text.

The two dotted curves in fig. 1 represent the results of an preliminary experiment on the occurrence of coacervation in the system gelatin + Cetavlon + KCNS. In performing this experiment, five mixtures were prepared from a 2 % Cetavlon solution and a 1 % solution of iso-electric gelatin. The ratios Cetavlon/gelatin in these mixtures were 6 : 1, 2 : 1, 1 : 1, 1 : 2 and 2 : 9 respectively. Taking into account the water content of the gelatin (15 %) and the purity of the Cetavlon (80.2 %), these ratios expressed in millimoles cetyl trimethylammonium bromide/g gelatin become 15.5, 5.2, 2.6, 1.3 and 0.6 respectively. To a known quantity of

each of these mixtures, KCNS 0.1 n was added in successive quantities of 0.25 ml. After each addition the mixture was examined for coacervation. The KCNS and the Cetavlon concentrations were then calculated (from the volume of the KCNS added and corrected for the increase in the volume of the mixture) for two successive additions of KCNS, the first of which did not yet cause coacervation, the next did cause coacervation. These concentrations were plotted as ordinates and abscissae respectively in fig. 1; the lower dotted curve thus refers to the mixtures not yet coacervated, the upper dotted curve to the mixtures with coacervation.

The coacervation limit of the gelatin-Cetavlon mixtures must lie in between the two dotted curves. The relative position of these curves with respect to the upper straight line (representing the coacervation of Cetavlon systems without gelatin) shows clearly, that in the mixtures of gelatin and Cetavlon, coacervation occurs at a lower KCNS concentration than in the analogous systems, which contain the same concentration of Cetavlon, without gelatin. The dotted curves show a minimum (at about 8 millimoles/l KCNS) which is situated lower than the limit between dynamic and static elasticity, even lower than the limit non-elastic/dynamic-elastic systems.

In the discussion of the above-mentioned communication (see note 5), the conclusion was reached that at the limit dynamic-elastic/static-elastic systems small sandwich micelles and at the limit non-elastic/dynamic-elastic systems, precursors of sandwich micelles, easily deformable by shear, are present.

In the figure it is seen that the dotted curves cut the middle and the lower straight line. This supports the hypothesis that gelatin, when present in a sufficient amount as to give a favourable ratio gelatin/soap, unites with small sandwich micelles and even with the precursors of the sandwich micelles⁶). It can be argued, from the following observations, that these coacervates differ from those obtained with KCNS from a Cetavlon solution without gelatin, namely:

1. at increase of the KCNS concentration in a Cetavlon solution, the coacervate starts with a volume of 100 %, which decreases with increasing KCNS concentrations. On the contrary, in the mixtures of Cetavlon and gelatin, increase of the KCNS concentration induces coacervation the volume of which increases from 0 % up to a maximum.

2. The coacervate obtained from a Cetavlon solution is lighter than the equilibrium liquid and floats. The coacervate, separated from not too extreme mixtures of Cetavlon and gelatin is heavier than the equilibrium liquid and collects as a layer at the bottom of the sedimentation tube.

⁶) In a recent investigation on elastic systems with Cetavlon, it was found from measurements of the streaming birefringence that sandwich micelles are present: H. G. BUNGENBERG DE JONG, H. J. VAN DEN BERG and W. W. H. WEIJZEN; to be published shortly in these Proceedings.

3. *The optimal mixing ratio for the coacervation of iso-electric gelatin + Cetavlon + KCNS*

Of course, we are very interested in the optimal mixing ratio of Cetavlon and gelatin. As the experiments of section 2 are too inaccurate, a more accurate method used also in the foregoing parts of this series, has been employed.

A soap and a gelatin solution of known concentration and both containing the same concentration of the salt are mixed in various proportions. The coacervate volumes obtained, are plotted as a function of the mixing ratio soap/gelatin. The mixing ratio, corresponding with the maximum of the curve is read off. This mixing ratio yields the composition of the characteristic association, which has been substantiated in Part III of this series by analysis ⁷⁾.

In applying the method to the systems: gelatin + Cetavlon + KCNS we have to reckon with the relatively strong affinity of the CNS^- ions for the cetyl trimethylammonium cations. It is not advisable to use for example 1 % solutions of Cetavlon and gelatin both containing the same KCNS concentration. At different mixing proportions the absolute Cetavlon concentration will differ and hence, the degree of occupation of the soap micelles with CNS will also be different. To keep the initial degree of occupation of the soap micelles constant in the mixing series, the Cetavlon and the gelatin solution must have different KCNS concentrations. A degree of occupation of 40 % was chosen. This degree of occupation corresponds in fig. 1 with all points of the middle straight line.

For a 1 % Cetavlon system, this line gives an ordinate value of approximately 18 millimoles/l KCNS. The line cuts the ordinate axis at approximately 10 millimoles/l. This means that a Cetavlon solution of 1 % and containing 18 millimoles/l KCNS can be diluted in any proportion with a solution containing 10 millimoles/l KCNS without causing a change in the degree of occupation of the soap micelles with salt ions.

The formula for preparing the mixtures is now:

$$a \text{ ml Cetavlon } 1 \% + (10-a) \text{ ml iso-electric gelatin } 1 \% + 10 \text{ ml KCNS } 0.1 \text{ n.}$$

(containing 18.3 mmol/l KCNS)	(containing 10 mmol/l KCNS)
----------------------------------	--------------------------------

These mixtures now correspond with a mixing series of 0.5 % Cetavlon (C_1) and 0.5 % gelatin (G_1), in which the degree of occupation of the soap is 40 %. (A possible adsorption of the CNS ions to the gelatin is neglected.)

The mixtures were made in sedimentation tubes and the coacervate volumes read off after standing overnight in a thermostate of 40°. It appeared that a small fraction of the coacervate had not yet sedimented

⁷⁾ It was found that the solubility of the coacervate is minimal, when the mixing ratio soap/gelatin in the coacervate is the same as in the equilibrium liquid. The water content of the coacervate is now maximal as is the coacervate volume.

and was visible in the form of very fine droplets. For this reason the coacervate volume was read off anew 24 hr later. After this time, the mixtures containing 70 and 80 % Cetavlon still contained droplets, not yet sedimented.

The coacervate volumes were plotted against the mixing proportions of the two solutions, and expressed as % Cetavlon solution (fig. 2). The

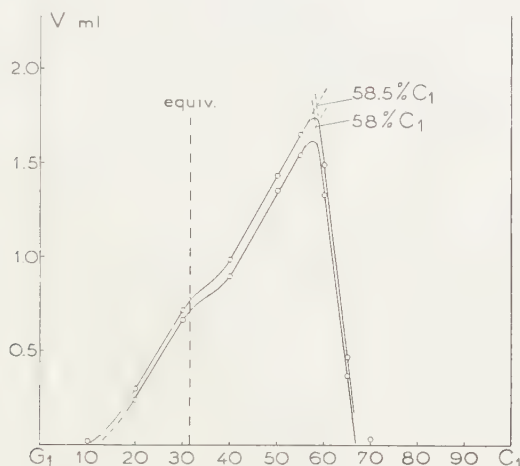


Fig. 2. Mixing diagram representing the coacervation of isoelectric gelatin and Cetavlon in the presence of 10 millimoles/l free KCNS.

points of the upper part of the ascending branch of the curve and also the points on the right branch lie on straight lines. The intersection point of these two straight lines was taken as the optimal mixing proportion. The curve of the first reading gave an optimum at 58 %; the reading of 24 hr later (after which the coacervate layer had cleared up) gave 58.5 %. In a second similar mixing series, we found after 36 hr 58 %.

In two other mixing series (based on the same principle, i.e. a initial degree of occupation of the soap of 40 %), the colloid concentrations are different from the foregoing, namely, 0.75 % gelatin with 1.5 % Cetavlon and 0.6 % gelatin with 1.2 % Cetavlon, respectively. The mixing proportions of optimal coacervation (calculated as 1 % solutions) determined after 36 hr are 60 and 59.5 % respectively. From the mean of the four values after 36 hr (59 %), taking into account a correction for the water content of the gelatin (15 %) and the degree of purity of the Cetavlon (80.2 %), a binding of 3.7 millimoles pure soap/g dry gelatin was calculated.

In fig. 2 a vertical dotted line is drawn which represents the equivalent mixing proportion, i.e. the cationic soap is present in an equivalent amount to the ionized $-\text{COOH}$ groups of the gelatin. This mixing proportion (31.4 %) was calculated by using the figure 1.19 millimoles/g gelatin⁸), which indicates the total anionic side chains of the protein.

⁸) BOWES and KENTEN, *Biochemical Journal*, **43**, 358 (1948), who give for the

In the above experiments at pH values rather near to the iso-electric point of the gelatin (5.0), the association corresponding with the maximum of the curve contains about three times as much soap cations (3.7/1.19) as corresponds with the anionic groups of the gelatin. It is striking how much the situation is changed by an appropriate choice of the anion (CNS^-), in comparison with the results of PANKHURST (section 1 of the present communication; in the presence of M NaCl, about 0.15 millimoles cetyl trimethylammonium cations/g gelatin at pH 5).

Attention is drawn to the slight S-shaped bend in the ascending branch of the coacervate volume curve (fig. 1). This bend, situated near the equivalent mixing proportion, will be discussed later.

4. *The influence of the pH*

The ratio 3.7, found in section 3, is rather low with respect to the typical association of long-chain ions and gelatin. This might be due to an unfavourable pH.

For this reason, mixing series were made at a number of pH values, using acetate and phosphate buffers.

The general formula in preparing these mixtures is:

$$\begin{array}{cc} \text{a ml Cetavlon 1 \%} + (10 - \text{a}) \text{ ml iso-electric gelatin 1 \%} \\ \text{(containing 18.3 mmol/l KCNS)} & \text{(containing 10 mmol/l KCNS)} \end{array}$$

+ 5 ml KCNS 0.020 n + 5 ml buffer.

This formula is in principle the same as the formula given in section 3, but as the buffer had to be added to the mixture too, the 10 ml KCNS 0.01 n of the former formula is replaced by 5 ml KCNS 0.020 n. The buffers had not the usual composition, for there had to be reckoned with a possible influence of the buffer salts on the coacervation⁹).

For this reason the six acetate buffers used (pH values of 4.1, 4.7, 4.85, 5.0, 5.3 and 5.7), contained the same final concentration of Na-acetate (40 millimoles l). The pH was varied by choosing different concentrations of acetic acid. In a phosphate buffer, both the components are salts. As it is likely that salts which monovalent anions (e.g. KH_2PO_4) exert less influence than salts in which one of the ions is divalent (e.g. Na_2HPO_4), the concentration of the secondary phosphate was kept con-

sum of the aspartic acid + glutamic acid 1.24 millimoles/g collagen. In gelatin there are hardly any amide groups left. TRISTRAM (Adv. Prot. Chem., 5, 83, 1949) gives 0.053 millimoles/g gelatin. W. A. LOEVEN (Thesis, Leiden 1953) reports for Eastman Kodak gelatin (I.E.P. 4.84) an amide content of 0.047 millimoles/g gelatin. For the free COOH groups in the side chains of the gelatin is calculated $1.24 - 0.05 = 1.19$ millimoles/g gelatin (0.05 is the mean of the above values of TRISTRAM and LOEVEN).

⁹) From preliminary experiments, it is known, that neutral salts when present in a sufficient concentration suppress the coacervation.

stant (40 mmol/l). The variation of the pH was brought about by different concentration of the primary phosphate. The phosphate buffers used were: pH 5.6, 5.8, 6.4 and 6.8.

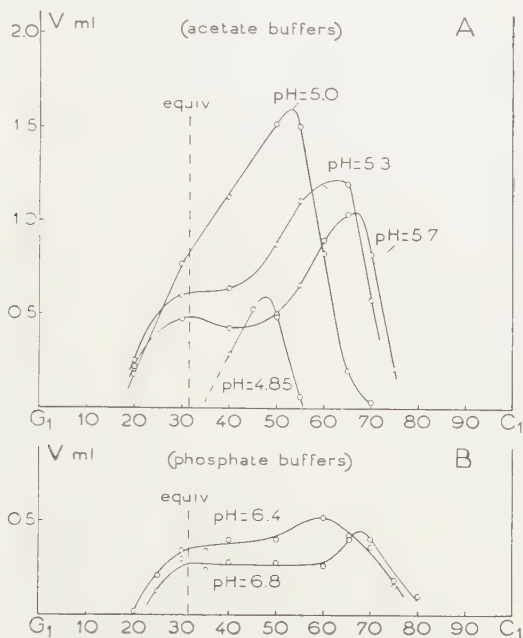


Fig. 3. Influence of the pH on the coacervation in mixtures of $\frac{1}{2}\%$ Cetavlon and $\frac{1}{2}\%$ gelatin in the presence of 10 millimoles/l free KCNS.

In the series with the acetate buffers as well as in the series with the phosphate buffers, the viscosity¹⁰⁾ of the coacervate increases with increasing pH, and the rate in which the coacervate layer collects at the bottom of the sedimentation tubes decreases¹¹⁾.

¹⁰⁾ This is seen from the time necessary for the coacervate layer to clear up. The coacervates are during the first hours after sedimentation turbid as a consequence of the fact that small droplets of the equilibrium liquid are entrapped in the coacervate. These droplets move slowly upward and reaching the interface equilibrium liquid/coacervate, escape into the equilibrium liquid, and the coacervate layer clears up.

In the mixing series with acetate buffers at pH 4.85, the coacervates were clear after standing one night and one day; at pH 5.0 and 5.3 they were still turbid after 36 hr but cleared up after 1 night and two days; at pH 5.7 the coacervates still contained vacuoles.

¹¹⁾ At increase of the pH, the tendency of the coacervate to stick to the wall of the sedimentation tube and to form cuffs of clear coacervate, becomes more and more pronounced. It might be that this increasing tendency is effected by the lowering of the difference of the specific density of the equilibrium liquid and the coacervate (with increase of the ratio soap/gelatin at higher pH values). The layers of the coacervate on the wall of the tube move downwards but very slowly. At increasing pH, the viscosity increases and the difference in density becomes less; hence, this process takes much more time.

Fortunately, the simple state of affairs found already in section 2 with respect to the estimation of the optimal mixing proportion, is not altered¹²⁾. In the following survey the graphically determined mixing ratios of optimal coacervation at various intervals for the mixing series with acetate buffers are recorded (n = night, d = day). In the last column of the survey, the binding of the soap is given, which is derived from the optimal mixing ratios. The coacervate volume curves corresponding to the last reading are given in fig. 3A. The survey also contains the results obtained with the phosphate buffers. It is seen (fig. 3B) that the maxima of the coacervate volume curves are here rather flattened, in such a way that the mixing ratios corresponding to the maxima cannot but roughly be estimated. For this reason only one reading (after one night + one day) has been taken. At pH 6.8, the coacervate sticks very much to the wall of the glass tube and there is no point in investigating this mixing series at higher pH values.

Buffers	pH	Optimal mixing proportion in %C after:					Cetyl trimethylamm. cations/g gelatin
		1n	1n+1d	1n+2d	1n+3d	1n+4d	
Acetate	4.1	no coacervation					—
	4.7	no coacervation					—
	4.85	—	± 47	—	—	—	± 2.3
	5.0	54	53.5	53.5	—	53.5	3.0
	5.3	62.5	63	63	—	63	4.4
	5.7	67	67	—	67	—	5.3
Phosphate	5.6	no coacervation					—
	5.8	no coacervation					—
	6.4	—	59	—	—	—	3.7
	6.8	—	68	—	—	—	5.5

The results of the above experiments show that increase of the pH:

a. increases the binding of the cetyl trimethylammonium cation to the gelatin, and

b. the bend in the ascending branch of the coacervate volume curve, at the equivalent mixing proportion, becomes more pronounced and gives rise to a secondary maximum (fig. 5A).

Apart from the pH influence, salt influences play a rôle. This is seen in fig. 4, in which two curves are obtained, one from the experiments with acetate buffers, the other from the experiments with phosphate buffers and which are separated by at least one pH unit.

The points a and b are further discussed in the following section. The influence of salts, is studied in one of the next communications of this series.

¹²⁾ The mixing ratio, corresponding to the maximum of the coacervate volume curve does not change, though the curve as a whole, shifts slightly upwards with time.

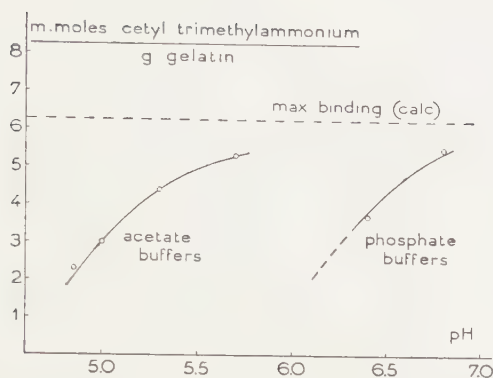


Fig. 4. Diagram representing the binding of soap to the gelatin as a function of the pH, determined with acetate and phosphate buffers. For the ordinate value of the horizontal dotted line: see Discussion, section 5.

5. Discussion and Summary

For the associations between long chain anions and linear proteins, rich in long chain anions, a simple scheme has been given in Part II of this

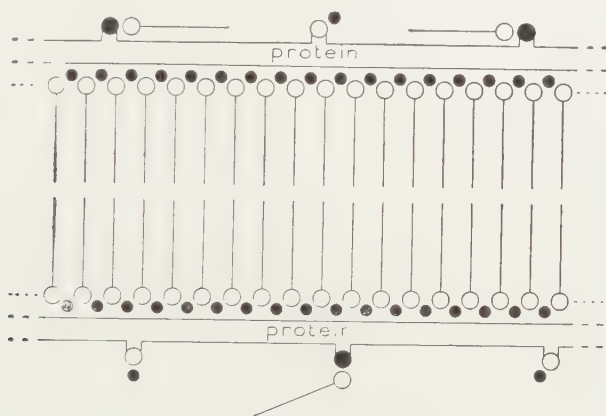


Fig. 5. Scheme for the oleate rich association. Explanation, see text.

series. In Part VI, it has been extended to a more detailed scheme, represented in fig. 5 which accounts for

1. the equivalent binding of the soap anions (white circles with tails) to the emerging positive groups of the protein monolayer (black circles), and
2. cations of the added salt (black dots), being an essential component of the sandwich micelle (black dots uniting the white circles of the parallel long chain anions).

The binding of the linear protein to the sandwich micelle is supposed to be an interaction of the dipoles of the keto-imide groups of the protein with the charge pattern on the surface of the micelle. It seems, therefore, logical that the same scheme will hold for associations with long chain

cations, in which case all the black circles now represent negatively charged groups or anions, and all the white circles positively charged groups or cations.

That long-chain cation—gelatin associations, which are rich in long chain cations, exist, has already been reported by PANKHURST (e.g. experiments with cetylamine; see note 2) though he could not realise them with quaternary ammonium soaps. Our scheme (fig. 5) does not forbid the existence of these; it only supposes that the anions of the added salts will have a sufficient affinity for the charged positive heads of the soap to form sandwich micelles. This induced us to investigate KCNS which gave the desired effect (see for details the sections 1 and 2, and note 6).

The curves in the figs. 2, 3A and 3B show more or less pronounced bends or even a secondary maximum (pH 5.7 in fig. 3A), situated approximately at the equivalent mixing proportion. This of course points to the existence of a binding of cetyl trimethylammonium cations to the emerging negative groups of the protein monolayer, as pictured in the scheme.

It has been argued (Part VI of this series) that such secondary maxima in the coacervate volume curve may arise from favourable tricomplex relations. One of the conditions is that the pH at which the experiments are carried out is not too far from the iso-electric point of the protein. This indeed is applicable here. A second condition, not mentioned in Part VI, is, that the other kind of emerging ionized groups of the protein monolayer, are sufficiently screened off. In the case of Cetavlon the basic groups of the monolayer are screened off by the CNS⁻ ions (and when buffers are used, by other anions also). At the relatively small salt concentrations used, we may suppose that this screening off is not maximal as a result of which the tricomplex relations will not be very effective, if not assisted by the separation of a coacervate rich in associations of the type given in fig. 5.

Accordingly, when the coacervation of the latter type is weak, (in fig. 3A at pH 4.85) or does not occur at all (in fig. 3B at pH 5.2 and 5.8) there is no longer any trace of coacervation with a maximum corresponding to the equivalent mixing proportion.

The experimental results (fig. 3) show further that the binding of the soap cations is favoured by increase of the pH.

In this respect, the cetyl trimethylammonium-gelatin association does not differ from the analogous long-chain cation and long-chain anion associations studied by PANKHURST (e.g. with cetyl ammonium cations and with dodecylsulphate anions). We can accept here in principle the explanation given by PANKHURST (change in the keto-imide groups which favours the ion-dipole interactions)¹³).

The highest value for the binding of cetyl trimethylammonium cations

¹³) K. G. A. PANKHURST, in *Surface Chemistry* 109, (Butterworths Scientific Publications, London, 1949).

recorded in the survey are 5.3 and 5.5 millimoles/g dry gelatin. These values seem small compared with those obtained from analogous soap-rich gelatin associations where values were recorded of 10 or more. PANKHURST reported for cetylammonium cations values between 8 and 10 millimoles/g dry gelatin (see note 2).

The cross sectional area of the positive head of the cetylammonium cation is not larger than the cross sectional area of the carbonchain (20 \AA^2). The cross sectional area of the cetyl trimethylammonium cation is much larger (31 \AA^2)¹⁴.

The same area of the sandwich micelle in fig. 5, when composed of dense packed cetyl trimethylammonium cations will thus contain only $20/31$ of the number of cetylammonium cations. We may now calculate from the above-mentioned data of PANKHURST the maximal values of the binding of cetyl trimethylammonium cations taking into account that 1.19 millimoles/g gelatin, bound to the emerging negative heads of the protein, must not be reduced by the figure $20/31$.

It is then found that the value of the binding must lie in between 5.6 and 6.9 millimoles/g dry gelatin.

The highest values in fig. 4 (5.3 and 5.5) are therefore less small, than appeared at first sight. They lie not far below the dotted horizontal line, drawn at an ordinate value of 6.25 (the mean of the above calculated limits).

The curves in fig. 4 suggest that the binding has not yet reached its maximal value, but the physical properties of the coacervate made it impossible to investigate the further course of these curves.

Summarizing the results, we may state that the realisation of the soap-rich association of a quaternary ammonium soap (cetyl trimethylammonium bromide) and gelatin in using KCNS as added salt, gives a strong support to our conception of the nature of the soap-rich associations (sandwich micelle covered on both sides with a protein monolayer). The failure of the analogous attempts by PANKHURST resided in using an unsuitable salt (NaCl), the anion of which does not transform the spherical micelles into precursors of sandwich micelles.

*Department of Medical Chemistry
University of Leyden*

¹⁴) In the publication mentioned in note 2, PANKHURST gives 49 \AA^2 . This area was obtained by measuring the projection of scale atom models. In the general discussion, J. H. SCHULMAN remarked, that from studies on monolayers, a value of 31 \AA^2 is obtained. The latter value is used in the text. We cannot understand in which way PANKHURST arrived at a value of 49 \AA^2 , as we used the same method in measuring the area and obtained a value which comes close to the one reported by SCHULMAN.

CONTRIBUTIONS TO THE PROBLEM OF THE ASSOCIATION
BETWEEN PROTEINS AND LIPIDS. VIII *)¹⁾

*Influence of the n.primary alcohols on the coacervation of cetyl trimethyl-
ammonium bromide + gelatin + KCNS*

BY

H. G. BUNGENBERG DE JONG AND A. RECOURT

(Communicated at the meeting of January 30, 1954)

1. *Introduction*

In the preceding part of this series, the coacervation of cetyl trimethylammonium bromide + gelatin + KCNS has been studied¹⁾. The conclusion was reached, that the characteristic soap-rich association, present in the coacervate, is in principle of the same nature as in the analogous coacervates of anionic soaps + gelatin + salt (oleate and sec. alkylsulphate).

The characteristic association is considered to consist of a sandwich micelle covered on both sides with a protein monolayer (compare the schemes given in the parts VI and VII).

In the present investigation, the influence of *n*.primary alcohols is studied with the purpose, whether a further analogy can be established, between long-chain cation - gelatin associations and long-chain anion - gelatin associations.

The influence of alcohols has been studied already on the coacervation of gelatin + oleate + K-tetraborate (see Part I and Part III) and on the coacervation of gelatin + sec. alkylsulphates + KCNS (see Part II). The influence of the alcohols on the coacervation appeared to resemble much the effect of alcohols on the coacervation of oleate + K-tetraborate and sec. alkylsulphate + KCNS respectively. This is easily explained as already, in the soap coacervates without gelatin, sandwich micelles are present.

It turned out, however, that the transition in the homologous series of *n*.primary alcohols is shifted in the direction of the higher terms, compared to the position of the transition for the coacervation of anionic soaps with the salts used.

*) The term lipids is used here in a wide sense, including fatty acids and other long-chain electrolytes.

¹⁾ Part I has appeared in these Proceedings, **45**, 301 (1942); Parts II (A, B and C), III and IV in these Proceedings, Series **B55**, 317 329, 338, 347, 360 (1952); Part V in these Proceedings, Series **B56**, 203 (1953); Part VI (A and B) and Part VII in these Proceedings, Series **B57**, 1, 13, 192 (1954).

In Part II, it has been explained that such a shift must result from a decrease of the total number of ion-dipole interactions between the protein monolayer and the negative charges, constituting the surface of the sandwich micelle. As it is known now that the surface of the sandwich micelle is a pattern of positive and negative charges (compare the Parts VI and VII), the interaction between sandwich micelle and protein can better be described as the interaction between a charge pattern on the surface of the micelle and the dipoles of the protein. We may expect that the shift in the homologous series of the *n*.primary alcohols will occur as well in gelatin – cationic soap associations as in gelatin – anionic soap associations (compare the schemes in fig. 1). In both cases the interaction

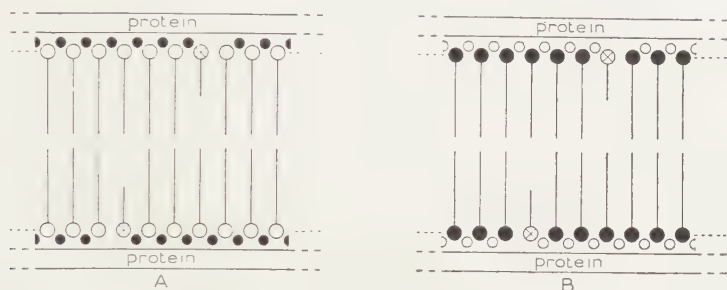


Fig. 1. Schemes to explain the influence of alcohol molecules taken up in the long-chain ion — linear protein association, rich in long-chain ions. In A: the long-chain ion is an anion; in B: the long-chain ion is a cation. Black: cations or positively charged groups; Open circles: anions or negatively charged groups; Open circles with cross: the polar heads of the alcohol molecules

between the charge pattern of the sandwich micelle and the protein monolayer is absent at those places, where an alcohol molecule is taken up in the sandwich micelle.

The influence of the alcohols on the coacervation of cetyl trimethylammonium bromide with KCNS has already been studied in a former communication²⁾, the results of which are given in fig. 2. It is seen that the lower terms (methanol to *n*.butanol, indicated in the graph by the numbers 1 to 4) exert a salt-demanding influence, i.e. more KCNS is needed for coacervation in the presence of these alcohols than in the blank. The higher terms (*n*.pentanol to *n*.decanol, indicated by the numbers 5 to 10) exert a salt-sparing influence (less KCNS is needed for coacervation in the presence of these alcohols than in the blank). The transition between the salt-sparing and the salt-demanding influence lies between *n*.butanol and *n*.pentanol. From the foregoing, it may be expected that the transition, for the coacervation of cetyl trimethylammonium bromide + gelatin + KCNS will be found higher up in the homologous series of the *n*.primary alcohols.

²⁾ H. G. BUNGENBERG DE JONG and A. RECOURT, these Proceedings, Series B56, 451, 461 (1953).

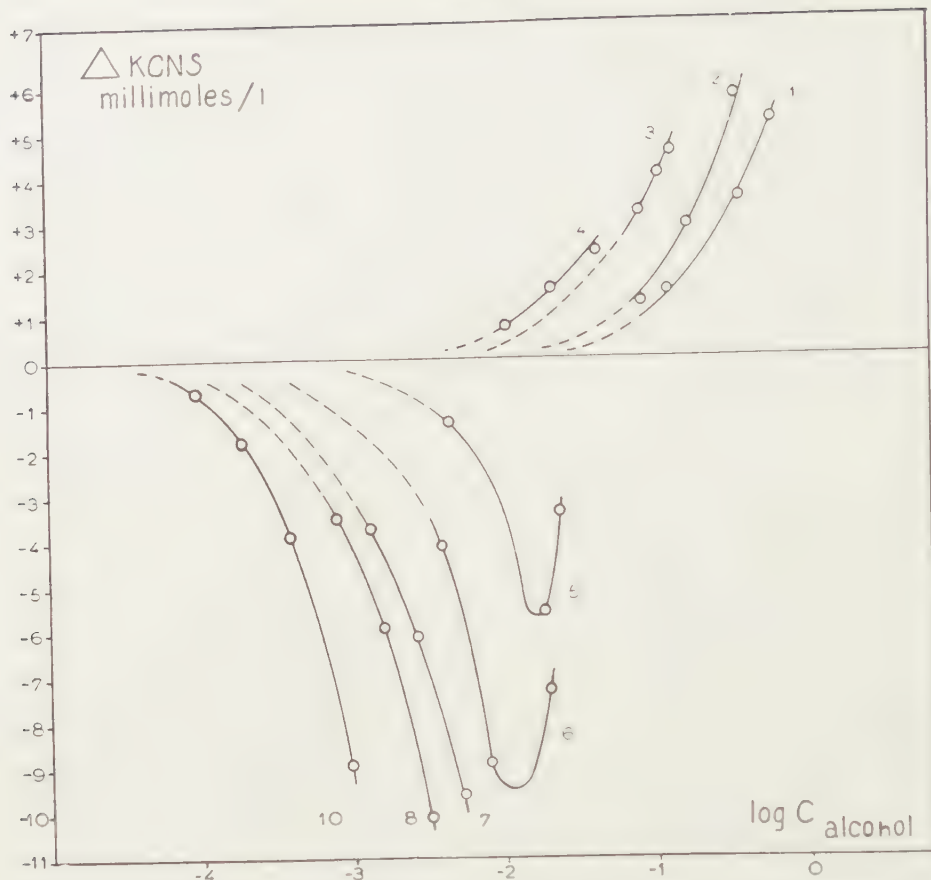


Fig. 2. Influence of the terms of the homologous series of the *n*-primary alcohols on the coacervation of Cetavlon with KCNS at 40°. Ordinates: Shifts of the KCNS concentration at 50 % coacervate volume in the presence of alcohols (referred to the blank). A + sign indicates a salt demanding action; a - sign indicates a salt sparing action. Abscissae: logarithms of the alcohol concentrations in moles/l

2. *Materials, working temperature. Transition in the homologous series, for the coacervation of Cetavlon with KCNS at 64°*

In the following investigation, the same gelatin preparation and cetyl trimethylammonium bromide, called Cetavlon, was used (Part VII). The influence of alcohols on the coacervation of Cetavlon (fig. 2) has been investigated at 40°; the same temperature was chosen initially for the present experiments. It appeared, however, that at 40°, the influence of the alcohols on the coacervation of Cetavlon + gelatin + KCNS could be investigated only with alcohols of maximally six C-atoms. The higher terms caused dense flocculations which, however, did not take place at higher temperature. Accordingly, 64° was chosen as the working temperature. This implies that comparison of the results at 64° with those of fig. 2 is not allowed as this figure refers to a working temperature of 40°. It is clear that first, in order to make a comparison possible, the experiments of fig. 2 have to be repeated at 64° to establish the localisation of the transition.

This was done with the same methods as applied at 40°.

The KCNS concentration needed to obtain a coacervate volume of 50 % (from a 1 % solution of Cetavlon) was investigated as a function of the concentration of the alcohols *n*.butanol, *n*.pentanol, *n*.hexanol.

The differences with the KCNS concentration of the blank have been plotted in fig. 3 against the logarithms of the alcohol concentration. This

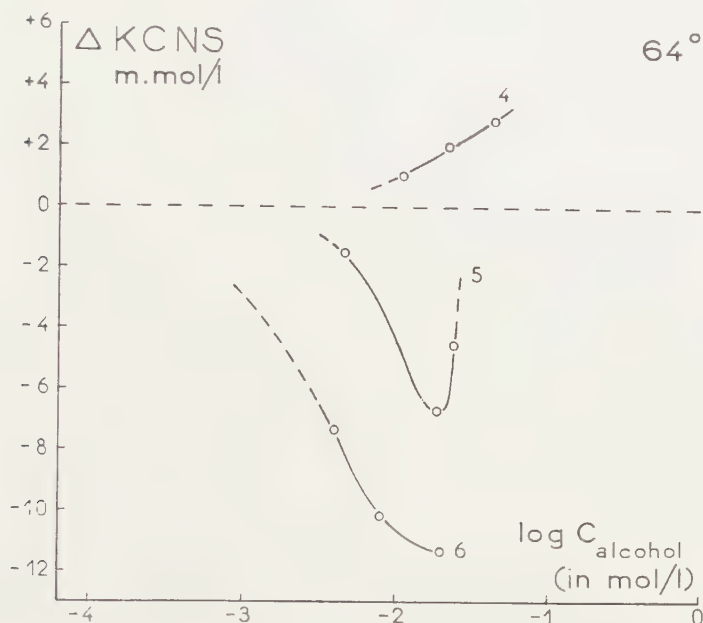


Fig. 3. Influence of some alcohols on the coacervation of Cetavlon with KCNS at 64°. Ordinates and abscissae as in fig. 2

figure shows, that the transition between salt-demanding and salt-sparing influence is situated at the same place at 64° as at 40° (compare fig. 2), i.e. between *n*.butanol and *n*.pentanol.

3. Methods to determine the salt-demanding or salt-sparing influences of alcohols on the coacervation Cetavlon + gelatin + KCNS

The influence of alcohols on the coacervation of isoelectric gelatin + Cetavlon + KCNS has been studied at two mixing ratios, namely, at 40 % and at 62.5 % Cetavlon. The series of mixtures were made with the aid of stock solutions of double strength (8 g Cetavlon + 12 g gelatin in 2000 ml water and 12.5 g Cetavlon + 7.5 g gelatin in 2000 ml water). The stock solutions were divided into smaller portions, which were stored in the refrigerator (2° C) until use.

For the investigation of the effect of the lower terms of the homologous series of alcohols (up to *n*.pentanol), the formula in preparing the mixtures was: 10 ml stock solution + *x* ml alcohol solution + *y* ml KCNS solution + (10-*x*-*y*)ml H₂O.

From each alcohol, four series were made, each series containing different amounts of alcohol (constant within one series) and variable amounts of KCNS.

For the investigation of the higher alcohols, three secondary stock solutions were made by dissolving different amounts of alcohol into portions of the stock solution.

The formula for preparing the mixtures in these series was: 10 ml stock solution containing alcohol + y ml KCNS solution = (10 + y) ml water.

Here too, four series for each alcohol were prepared, one of which is the blank. The mixtures are made in sedimentation tubes. After thoroughly mixing the contents, the tubes are left overnight in the thermostat at 64°. Afterwards the coacervate volumes are read off, and plotted in a graph as a function of the KCNS concentration.

The first ten terms of the homologous series of alcohols were investigated at a mixing proportion of 40% Cetavlon.

In the ten graphs obtained, a horizontal line has been drawn at a coacervate volume of about 50% of the maximal coacervate volume of the blank curve, i.e. at 0.4 ml coacervate.

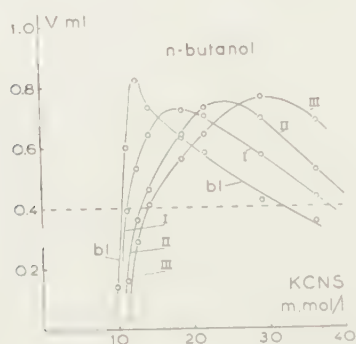


Fig. 4

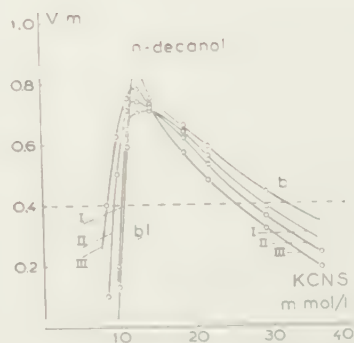


Fig. 5

Figs. 4 and 5. Examples of graphics used in studying the salt-demanding or salt-sparing influence of alcohols. The mixing ratio is here 40% Cetavlon. V = the coacervate volume in ml; bl = blank curve. I, II, III are curves obtained at three increasing alcohol concentrations. At both the intersections of the blank curve with the level, *n*.butanol exerts a salt-demanding influence (fig. 4) and *n*.decanol exerts a salt-sparing influence (fig. 5)

As examples are given in the figs. 4 and 5 the graphs for the influence of *n*.butanol and *n*.decanol respectively. The curves indicated by I, II and III refer to increasing alcohol concentrations: in fig. 4: I = 9.5, II = 32.8 and III = 54.0 millimoles/l; in fig. 5: I = 0.13, II = 0.25 and III = 0.38 millimoles/l.

It is seen that the curves have two intersections with the level (dotted line) at 0.4 ml. The salt-demanding or salt-sparing effect of an alcohol can

be studied from the direction and magnitude of the shift of each of the two intersections of the blank curve, at increase of the alcohol concentration.

It appears for example from fig. 4, that both the intersections are shifted to the right by *n*.butanol, in other words, *n*.butanol exerts a salt-demanding influence. The reverse is the case for *n*.decanol, which exerts a salt-sparing influence.

At the mixing proportion of 62.5 % Cetavlon, only four alcohols were studied: *n*.pentanol, *n*.hexanol, *n*.heptanol and *n*.octanol.

Two of the graphs obtained with these alcohols, are given in the figures 6 (for *n*.hexanol) and 7 (for *n*.octanol).



Fig. 6

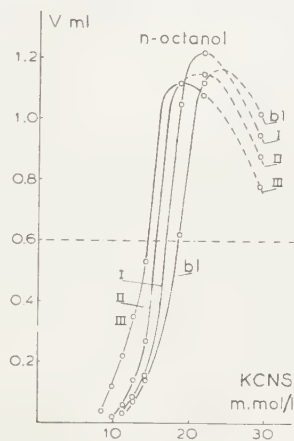


Fig. 7

Fig. 6 and 7. Examples of graphs used in studying the salt-demanding or salt-sparing influence of alcohols. The mixing proportion is here 62.5 %. The same symbols are used as in the figs. 4 and 5. The right intersection of the blank curve with the level at 0.6 ml cannot be reached here as a result of certain complications which occur in those experiments, represented in the figure by dotted curves. At the left intersection, *n*.hexanol (fig. 6) exerts a salt-demanding influence and *n*.octanol (fig. 7) exerts a salt-sparing influence

The curves denoted by I, II and III refer to increasing concentrations of the alcohol (in fig. 6: I=3.65, II=7.3 and III=14.9 millimoles/l; in fig. 7: I=0.36, II=0.72 and III=1.59 millimoles/l).

It seems likely that the curves have the same character as the curves obtained with the 40 % Cetavlon. Certain complications occur, however, which are discussed below, and as a result of which the dotted parts of the curves are not reliable. As the presumable maximum of the blank curve lies at about 1.2 ml, the level was drawn accordingly higher here (at 0.6 ml).

It is clear that, for the determination of the salt-sparing or the salt-demanding effect, the shift of the left intersection can be used only. It is obvious from the figures 5 and 6, that at the alcohol concentrations used, *n*.hexanol exerts a salt-demanding influence and *n*.octanol a salt-sparing influence.

4. Experimental results

a. Displacement of the left intersection of the blank curve as a function of the alcohol concentration

First, the results at the mixing proportion of 40 % Cetavlon are discussed. The graphs obtained with methanol, ethanol, *n*.propanol, *n*.pentanol and *n*.hexanol show, that just as in fig. 4 for *n*.butanol, the left intersection is displaced to the right at increase of the alcohol concentration. These shifts have been plotted in fig. 8 against the logarithms

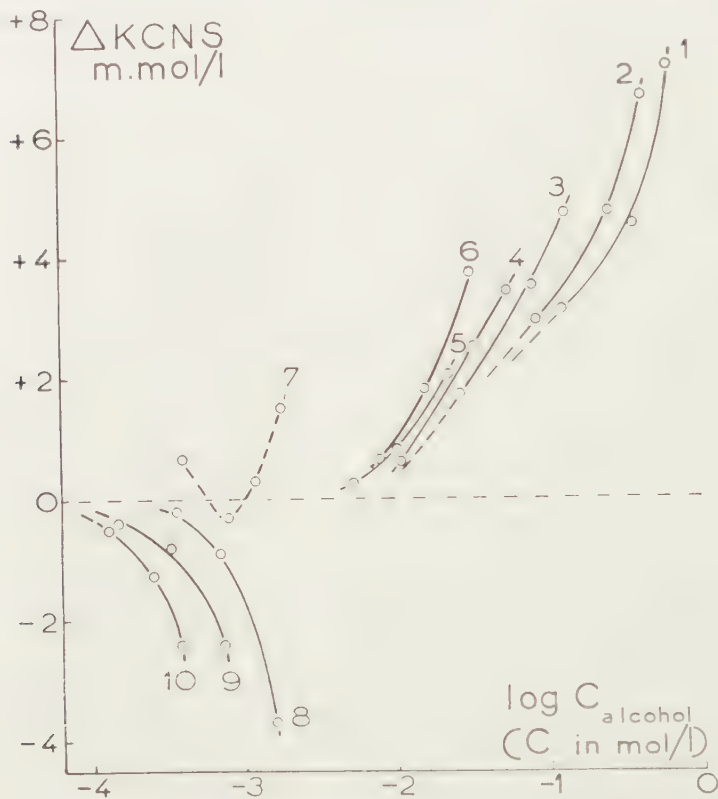


Fig. 8. Influence of the *n*.primary alcohols on the coacervation Cetavlon + gelatin + KCNS at a mixing proportion of 40 % Cetavlon, derived from the shift of the left intersection of the blank curve in graphs of which the figs. 4 and 5 give two examples. Δ = shift expressed in millimoles/l KCNS. For the dotted curve, see text. The transition between salt-demanding and (initially) salt-sparing influence occurs between *n*.hexanol and *n*.heptanol

of the alcohol concentration. The same has been done with the graphs for *n*.octanol and *n*.nonanol which have in common with fig. 5 for *n*.decanol, that they shift the intersection in the reverse direction. The results with *n*.heptanol were somewhat irregular (dotted curve in fig. 8). It seems probable, that by some unknown cause, the whole curve has been shifted in the positive direction. When we accept this, then *n*.heptanol must be

considered as a term lying close to the transition in the homologous series, which, however still exerts a slight salt-sparing influence at the lower concentrations.

We thus come to the result, that the transition from salt-demanding to salt-sparing must lie between *n*.hexanol and *n*.heptanol.

The results obtained at a mixing proportion of 62.5 % are given in fig. 9. Though we have used only four alcohols here, the localisation of the

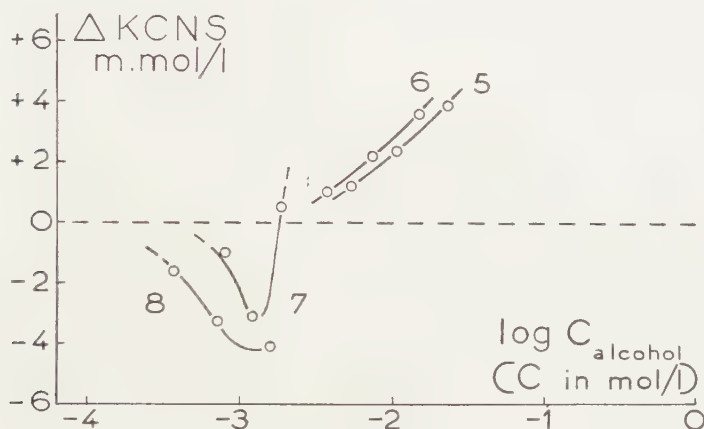


Fig. 9. Same as in fig. 8 but for the mixing proportion of 62.5 % Cetavlon. (Examples of the graphs used are the figs. 6 and 7). The transition in the homologous series of *n*.primary alcohols lies at the same place as in fig. 8, namely, between *n*.hexanol and *n*.heptanol

transition can be pointed out without doubt. The transition appears to lie (just as in fig. 8), between *n*.heptanol and *n*.hexanol.

The results obtained in fig. 8 and fig. 9 may be summarized as follows:

$$10 - 9 - 8 - 7 \mid 6 - 5 - 4 - 3 - 2 - 1$$

The alcohols are denoted by their number of C-atoms. The vertical line indicates the transition from salt-demanding (to the right of the vertical line) to salt-sparing influence (to the left of the line).

For the coacervation of Cetavlon + KCNS, the transition in the homologous series of the *n*.primary alcohols lies between *n*.butanol and *n*.pentanol (figs. 2 and 3). Accordingly, the binding of the gelatin to the soap results in a shift of the transition over two terms in the homologous series in the direction of the higher terms.

b. Displacement of the right intersection of the blank curve as a function of the alcohol concentration

In the graphs obtained with the experiment at 40 % Cetavlon (e.g. the figs. 4 and 5), the displacement of the intersection of the descending branch of the blank curve and the level can also be used in studying the influence of alcohols. This intersection is situated at a higher KCNS concentration. As the slope of the descending branch is much smaller than the slope of the ascending branch, greater

errors are made in reading off, the KCNS concentration corresponding to the right intersection.

In some cases (methanol, ethanol, *n*.propanol and *n*.butanol) curve II has been extrapolated to gain one more intersection. It will, therefore, not wonder, that the bundle of curves in fig. 10 has a less regular character than the bundle in fig. 8.

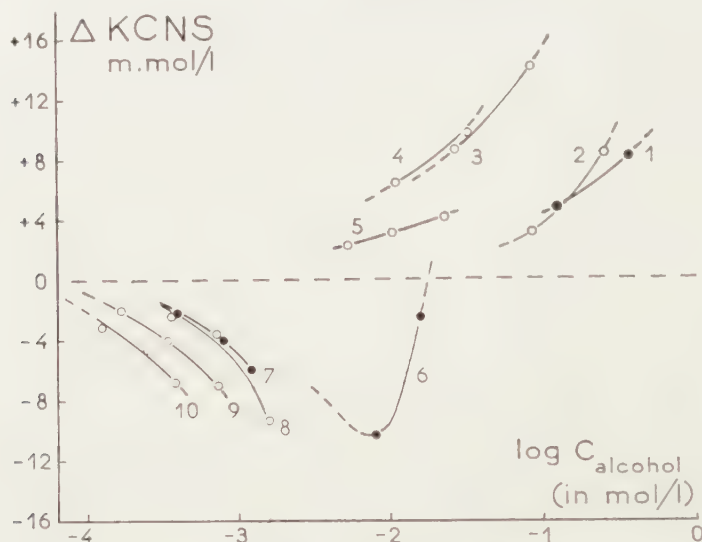


Fig. 10. Influence of the *n*.primary alcohols on the coacervation Cetavlon + gelatin + KCNS at a mixing proportion of 40 % Cetavlon, derived from the shifts of the right intersection of the blank curve of which the figs. 4 and 5 are two examples. The same symbols are used as in fig. 8. The transition in the homologous series of the *n*.primary alcohols lies here between *n*.pentanol and *n*.hexanol. For the irregular aspect of the curve bundle: see text.

Nevertheless, we are able to conclude, that the transition in this case must be situated between *n*.pentanol and *n*.hexanol:

$$10 - 9 - 8 - 7 - 6 \mid 5 - 4 - 3 - 2 - 1$$

Accordingly, at the right intersection, the shift of the transition in the homologous series of the *n*.primary alcohols in the direction of the higher terms amounts to one term only.

We now turn to the experiments at 62.5 % Cetavlon.

Here, serious complications were met which made it impossible to draw a certain conclusion from the descending branches (dotted in figs. 6 and 7) of the curves. At 21.7 millimoles/l KCNS, everything is still normal, i.e. one coacervate layer only at the bottom of the sedimentation tubes. At 29.2 millimoles KCNS, apart from the coacervate layer at the bottom of the tube, a second layer at the top of the tube made its appearance. In the graphs of the figs. 6 and 7, the volume of the coacervate layer at the bottom of the sedimentation tube has been used only. At 36.4 millimoles KCNS, the coacervate layer at the bottom of the sedimentation tube has disappeared and is replaced by one coacervate layer at the top of the tube.

It is not quite clear what happens here at increase of the KCNS concentration. One might suppose for instance, that the normal gelatin-Cetavlon association is partially decomposed at 29.2 millimoles KCNS and ceases to exist at 36.4 millimoles KCNS. The floating coacervate layer would then represent a coacervate consisting of Cetavlon and KCNS only.

When it is tried to get an impression of the relative position of the dotted curves and use the same expressions (salt-demanding or salt-sparing influence), we may come to the conclusion that *n*.octanol and *n*.hexanol exert a salt-sparing influence (figs. 7 and 6). In the analogous graph, *n*.pentanol shows a salt-demanding influence. We thus arrive to a localisation of the transition in the homologous series of the alcohols between *n*.pentanol and *n*.hexanol. The same was found above in the experiments with a mixing proportion of 40 % Cetavlon (fig. 9). This may mean that the complications, manifest at 62.5 % Cetavlon, are present too at 40 % Cetavlon but lead not yet to the formation of a second floating coacervate layer.

Accordingly, it seems safe to conclude that the results in fig. 10 are possibly not representative of the characteristic coacervation Cetavlon + gelatin + KCNS.

5. Discussion

In the discussion, the results obtained in section 4, sub b, will at first be neglected and we will consider those obtained in section 4, sub a, as representative of the coacervation Cetavlon + gelatin + KCNS.

These results (compare the figs. 8 and 9) and those for Cetavlon + KCNS (compare the figs. 2 and 3) are given in symbols in the next survey, together with analogous results of former parts of this series (oleate + gelatin + K-tetraborate: see Parts I and III; T-pol (sec.alkylsulphate) + gelatin + KCNS: see Part II).

Systems (salt containing)	Salt-sparing influence	Salt-demanding influence
Cetavlon	10-9-8-7-6-5	4-3-2-1
Cetavlon + gelatin	10-9-8-7	6-5-4-3-2-1
Oleate (pH 9.2)	8-7-6-5	4-3-2-1
Oleate + gelatin (pH 9.2)		8-7-6-5-4-3-2-1
T-pol	9-8-7-6-5-4-3-2-1	
T-pol + gelatin	9-8-7-6	5-4-3-2-1

The question put forward in the introduction whether an analogy can be established between long-chain cation - gelatin associations and long-chain anion - gelatin associations with regard to the influence of alcohols on these associations, can now be answered in the affirmative: the binding of the gelatin to the Cetavlon shifts the transition in the homologous series of the *n*.primary alcohols in the direction of higher terms. We refer to section 1 and fig. 1, for an explanation of this shift ³⁾.

The shift in the case Cetavlon + gelatin + KCNS is but small (two terms), compared to the shift in the other two cases of the survey (gelatin + oleate: at least 4 terms; gelatin + T-pol: 5 terms).

³⁾ *Note added in proof.* — As a result of recent investigations (see next part of this series, Part IX), it is now realized that two types of gelatin-long chain ion associations exist, in which the details of the interaction between the protein monolayer and the charge pattern of the sandwich micelle are different. The association with oleate belongs to one type, the other two cases of the survey to the second type. Nevertheless, the explanation of the shift given in section 1 and fig. 1, remains in principle the same: the gap in the charge pattern, formed by the alcohol molecule taken up in the sandwich micelle, decreases the total interaction between the charge pattern and the protein monolayer.

This may be due to the fact, that the present investigation has been performed at pH 5. From the preceding part of this series, we know that at this pH, the Cetavlon content of the gelatin - Cetavlon association has not yet reached its maximal value.

In Part VII (note 9), attention was drawn to the fact that at sufficient salt-concentrations (e.g. with NaCl and with other salts), the coacervation Cetavlon + gelatin + KCNS is suppressed. It is quite conceivable that even with KCNS the same occurs at sufficiently high concentration. The complications met with in section 4, sub b, concerning the formation of a second coacervate layer, point in this direction.

It would then become understandable that the shift to the left in the homologous series of the *n*.primary alcohols is less at these higher KCNS concentrations (shift over one term only) than the shift at the lower KCNS concentrations found in section 4, sub a (over two terms).

6. Summary

1. The influence of the *n*.primary alcohols on the coacervation cetyl trimethylammonium bromide + KCNS and on the coacervation cetyl trimethylammonium bromide + isoelectric gelatin (I.E.P. 5.0) + KCNS has been studied at the same temperature.

2. The results can be represented symbolically as follows:

Cetavlon + KCNS	10 - 9 - 8 - 7 - 6 - 5 4 - 3 - 2 - 1
Cetavlon + gelatin + KCNS	10 - 9 - 8 - 7 6 - 5 - 4 - 3 - 2 - 1

in which the alcohols are denoted by their number of C - atoms and the vertical line gives the position of the transition from salt-demanding influence (to the right of the line) to salt-sparing influence (to the left of the line). The binding of the gelatin to the cationic soap thus shifts the transition in the direction of the higher terms in the homologous series of the *n*.primary alcohols.

3. The direction of the shift in the homologous series of the *n*.primary alcohols is the same as in the earlier investigated examples in which the coacervation of anionic soaps (oleate, sec.alkylsulphates) + salts and of anionic soaps + gelatin + salts have been compared.

4. It has been argued from the schemes for the soap-rich - gelatin association (developed in Part II and extended in the Parts VI and VII), that the shift of the transition must be in the direction of the higher terms in the homologous series of the *n*.primary alcohols, and that this will hold both for long-chain anion - gelatin associations and for long-chain cation - gelatin associations.

5. Compared to the earlier investigated examples, the shift is but small here (over two terms). This may be due to the fact that the experiments were performed at pH 5, at which pH the long-chain cation - content of the cetyl trimethylammonium - gelatin association has not yet reached its maximum value.

*Department of Medical Chemistry
University of Leyden*

INFLUENCE OF ORGANIC COMPOUNDS ON SOAP AND PHOSPHATIDE COACERVATES. XX ¹⁾

THE ACTION OF ETHERS AND SULFIDES ON AN OLEATE COACERVATE

BY

H. L. BOOIJ, H. KWESTROO-VAN DEN BOS*) AND J. H. BLEKKINGH*)²⁾

(Communicated by Prof. H. G. BUNGENBERG DE JONG at the meeting of Jan. 30, 1954)

1. Introduction

Preceding investigations on the influence of organic compounds on soap coacervates led to the division of these substances into two groups:

- 1) salt-demanding substances (the concentration of salt needed to give a certain coacervate volume—50 % is usually chosen—shifts to higher values);
- 2) salt-sparing substances (a shift in the reverse direction is observed).

In the first case we see practically always a swelling of the coacervate (increase of water content) when the concentration of salt is kept constant. In the second case a shrinking of the coacervate volume takes place. The background of these actions may, however, be different.

It has been suggested that the action of any added substance depends primarily upon its distribution in the soap/water system. Four possible places might be mentioned (fig. 1):

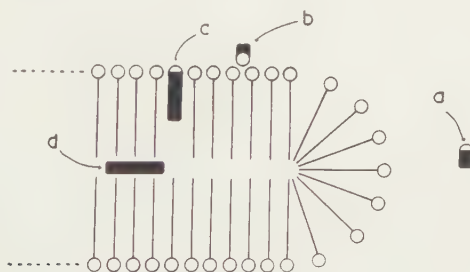


Fig. 1. Possibilities as regards the distribution of substances in the soap/water system.

*) Aided by grants from the "Netherlands Organization for Pure Research (Z.W.O.)".

¹⁾ Publication no. XIX of this series will be found in Proc. Kon. Ned. Akad. v. Wetensch. Amst., **B 56**, 451 (1953).

²⁾ Publication no. 25 of the Team for Fundamental Biochemical Research (under the direction of H. G. BUNGENBERG DE JONG, T. H. VAN DEN HONERT, E. HAVINGA and H. L. BOOIJ).

- a) in the medium (practically no influence on coacervation),
- b) on the surface of the micelle (here we think especially of ions of the opposite sign, organic as well as inorganic),
- c) parallel to the soap molecules in the micelle (the substances are then anchored to the medium—water—by virtue of their polar groups),
- d) in between the CH_3 -planes of the micelle (organic substances with a weakly hydrophilic group only).

In the second case a strong salt-sparing action results as the negative groups of the soap-ions are discharged (see e.g. the action of the H^+ -ions; BUNGENBERG DE JONG *et al.* 1938 *a*). In the third case, however, the result depends on the polar group of the added substance. Alcohols have a salt-sparing action (BOOIJ *et al.* 1950 *a*), while on the other hand long chain anions have a salt-demanding action on oleate coacervates (BOOIJ *et al.* 1949). It has been suggested that the salt-demanding activity of long paraffins is caused by an uptake of these molecules between the CH_3 -planes within the micelle (BOOIJ *et al.* 1950 *b*). This supposition has been strengthened by a study of the influence of a substance preferably taken up at *c* (fig. 1) on the action of other substances, presumably distributed between *c* and *d* (BOOIJ *et al.* 1951). We were interested to see whether homologous series of ethers and sulfides show the same phenomena as paraffins, alkyl derivatives of benzene and halogen derivatives of paraffins (BOOIJ *et al.* 1950 *b*, *c* and *e*).

2. The influence of ethers on an oleate coacervate

a) Aliphatic ethers

The method described by BOOIJ *et al.* (1950 *b*) has been slightly altered. An oleate solution of the following composition was prepared:

20 g Na-oleate
120 ml KOH 2*n*
980 ml H_2O

As some ethers (especially the higher ones) do not dissolve readily into this solution, the substance to be investigated was weighed in an erlenmeyer flask and dissolved in exactly 1 ml *n*-propanol. Then 25 ml of the oleate solution was introduced in the flask. The various oleate solutions containing different amounts of the ethers (and a blank containing oleate and propanol only) were coacervated with the aid of KCl according to the following scheme:

x ml KCl 3.8 *n*
(6.5-*x*) ml H_2O
3 ml oleate solution

The mixtures were shaken vigorously in stoppered tubes and left overnight in a thermostat (25° C). The following day the volumes of the coacervate

layers were measured (in per cent. of the total volume). The concentration of KCl needed for a coacervate volume of 50 % was determined graphically and the shift with respect to the blank computed. In the following graphs this shift (+ for salt-demanding activity and - for salt-sparing activity) is plotted along the ordinate.

Fig. 2 shows the action of a number of aliphatic ethers. There is a strong resemblance with the action of normal paraffins (BOOIJ *et al.* 1950 *b*) but the first term of the homologous series which turns from a salt-sparing to a salt-demanding action is somewhat longer for the ether series (heptane

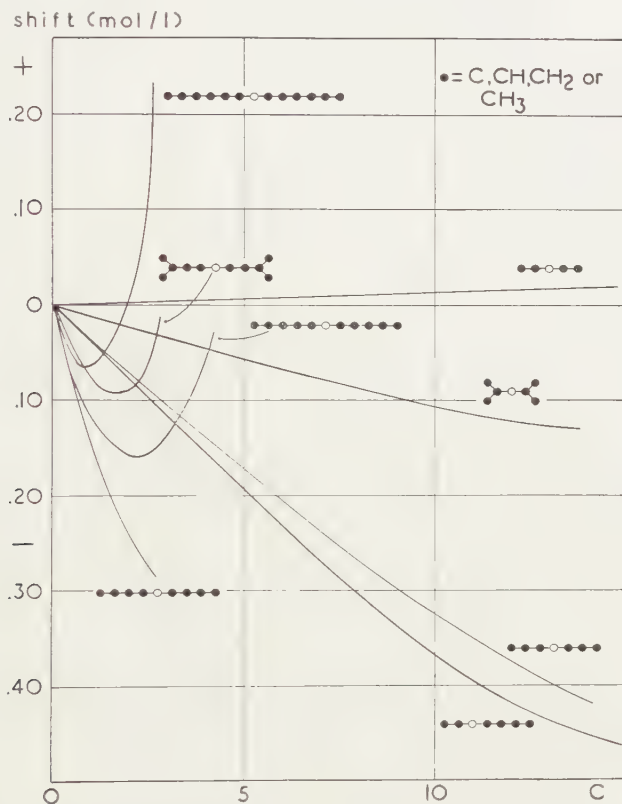


Fig. 2. Activity of aliphatic ethers on an oleate coacervate. Abscissa = concentration of the added substances in millimoles/l.

versus di-*n*-amylether). This tallies with the hypothesis that a hydrophilic group tends to hold the molecule in position *c* (fig. 1). Thus in the case of the ethers the apolar part of the molecule must be pretty large to overcome the opposing factor due to the slightly hydrophilic group.

From fig. 2 it appears that diisopropylether has a much lower activity than di-*n*-propylether. This effect of branched chains has been observed already by BUNGENBERG DE JONG *et al.* (1938 *b*). The distribution of isomers between medium and micelle lies more to the side of the medium in the case of isomers with branched chains. Diisoamylether has—in low

concentrations—a smaller activity than di-*n*-amyl- and di-*n*-hexylether, but it takes an intermediate position at higher concentrations. This too seems to have a general background (see BOOIJ *et al.* 1951) as the partition equilibrium within the micelle is shifted somewhat to the place between the CH₃-planes in the case of branched substances. So di*iso*amylether has a lower salt-sparing, but a higher salt-demanding action than the straight chain isomer. Finally we observe that ethyl-*n*-butylether has a slightly stronger action than di-*n*-propylether. Here we have the general phenomenon that the salt sparing action is stronger when the hydrophilic group is placed at the end instead of at the middle of the molecule.

We did some experiments with ethers where the balance between hydrophilic and lipophilic groups lies to the side of the hydrophilic groups (methylal, acetal, methoxymethylal, dioxan and diethylene glycol). These substances showed a small salt-demanding action, except the last, which did not influence the oleate coacervate at all. This reminds us of the action of the small alcohols (methanol and ethanol).

b) Aromatic ethers

When comparing some aromatic ethers with aliphatic ones, some interesting phenomena come to the fore (fig. 3). First of all, there seems to be no tendency for a salt-demanding action. This is in accordance with the view that the benzene nucleus itself is a slightly hydrophilic group (BOOIJ *et al.* 1950 *c*). In the second place we may try to give the "value" of the benzene nucleus in aliphatic carbon atoms (the aliphatic equivalent).

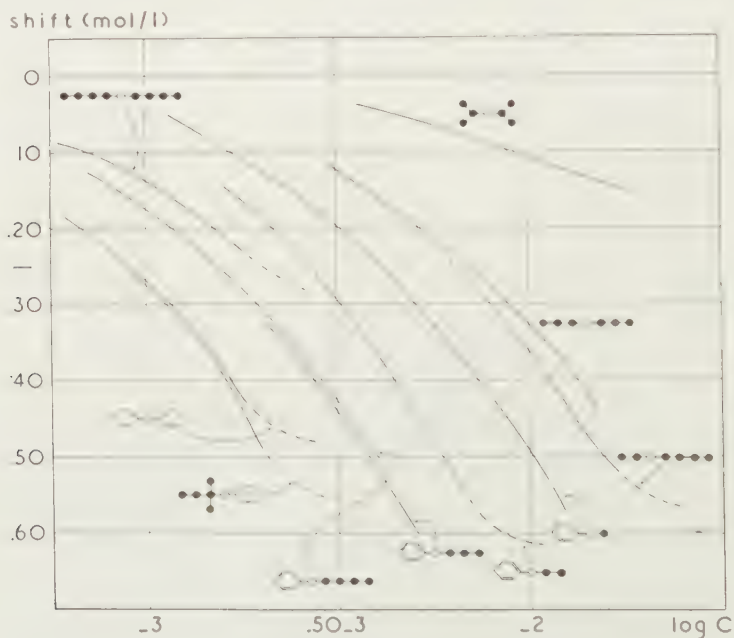


Fig. 3. Action of some aromatic ethers as compared with aliphatic ones. Abscissa = log. concentration of the added substance in moles/l.

As anisole has a stronger activity than ethyl-*n*-butylether, we may say that the benzene nucleus is equivalent to at least five aliphatic carbon atoms. Compare also *p*-methoxy-*tert*.amylbenzene and diphenylether. This value is somewhat higher than those found by BUNGENBERG DE JONG *et al.* (1938 *b*) for alcohols and by BOOIJ *et al.* (1950 *d*) for esters. This leads to the assumption that the aliphatic equivalent of the benzene nucleus depends on the molecular structure. Finally we see that lengthening of the carbon chain leads to an increased activity in the series anisole, phenylethylether, phenylpropylether (though this increase does not follow TRAUBE's rule). Though a real salt-demanding action does not show, it seems to be hidden in phenylbutylether which substance has no stronger activity than phenylpropylether.

We will now turn to some benzylethers (fig. 4). There the remarkable fact is observed that the benzene nucleus seems to have much less "value"

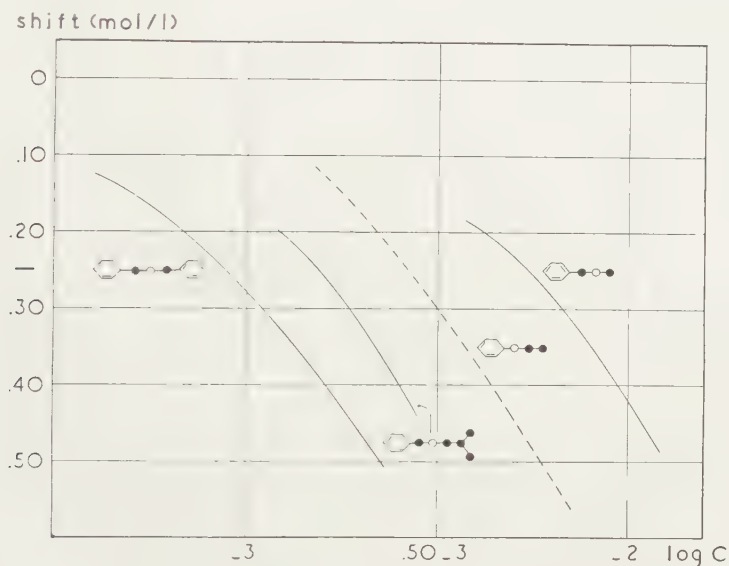


Fig. 4. Action of some benzylethers on an oleate coacervate. Abscissa, compare fig. 3.

than in the phenylethers. We see that benzylmethylether (8 carbon atoms) is less active than anisole (7 carbon atoms); benzylisobutylether (11 carbon atoms) has approximately the same activity as phenylpropylether (9 carbon atoms) and dibenzylether is about as active as diphenylether. This means that in this case (the benzene nucleus is separated from the ether-oxygen by a methylene group) the aliphatic equivalent of the benzene nucleus is only 3-4 carbon atoms. The difference between phenyl- and benzylethers suggests that in the phenyl-ethers a change in the benzene nucleus influences the distribution of the substance between the medium (fig. 1, *a*) and the micelle (fig. 1, *c*) in such a way that a phenyl-ether prefers *c* more above *a* than a benzyl-ether with the same number

of carbon atoms. The benzene nucleus has become more hydrophobic; presumably a redistribution of electrons takes place under the "deactivating" (electron attracting) influence of the ether-oxygen.

These interactions between the benzene nucleus and its side chains play a large, though in many cases incomprehensible, rôle. This has been found in the isomeric cresylmethylethers and the dimethoxybenzenes (fig. 5). It is not clear why we find the following series for the respective activities:

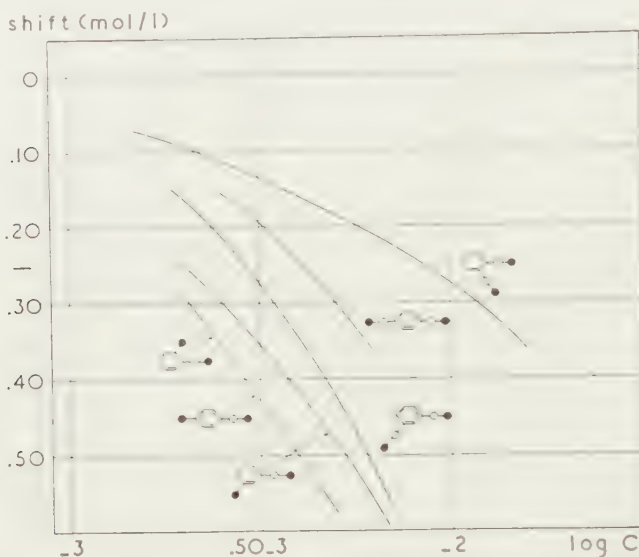
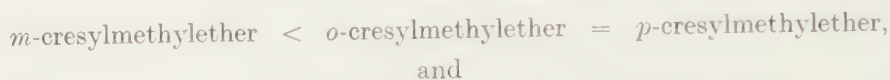


Fig. 5. Comparison of isomeric cresylmethylethers and dimethoxybenzenes. Abscissa, compare fig. 3.

It must be remarked that the cresylmethylethers (especially *p* and *o*) have a stronger activity than the isomeric phenylethylether (fig. 3).

In figure 6 we find that *o*- and *p*-cresylethylether differ somewhat, in contrast to the cresylmethylethers. The latter is stronger than the isomeric phenylpropylether (fig. 3), the former has the same activity.

The experiments with naphthylethers did not lead to interesting observations (fig. 7). The four substances measured do not show much difference. This we expected, because the apolar parts of these molecules are so big that they will be taken up in the micelles practically completely at place *c* (fig. 1). So the distribution medium/micelle does play only a secondary rôle (as for instance in heptanol and higher alcohols: see BOOLJ *et al.* 1950 *a*). As the lengths of the molecules do not differ very much, there will be not much difference in activity.

It is interesting to note that the substances I and II differ in activity,

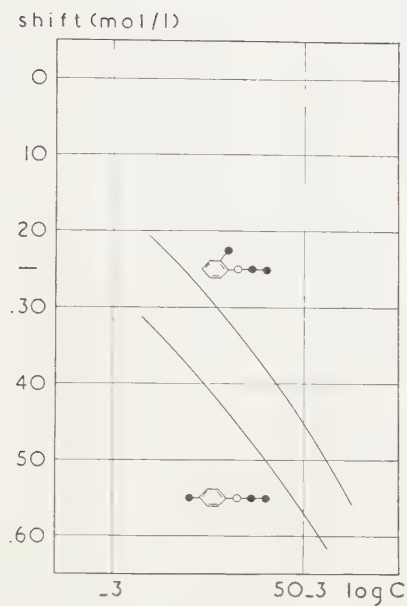


Fig. 6. Activity of two isomeric cresylethylethers. Abscissa, compare fig. 3.

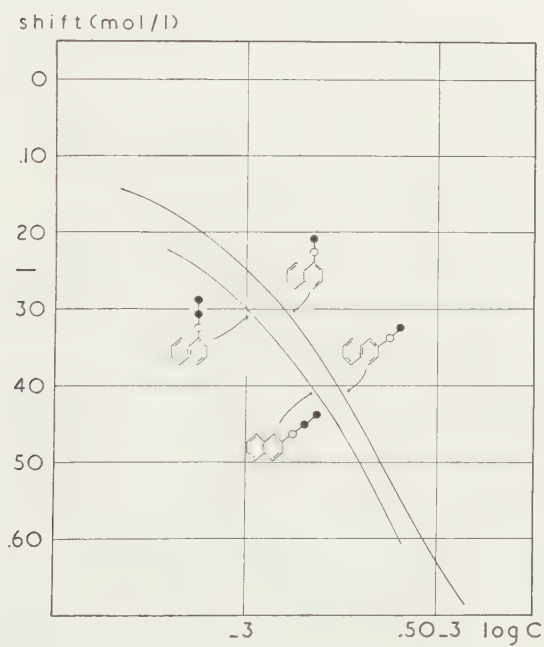
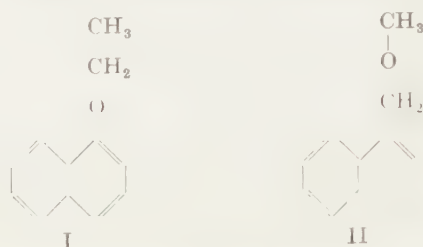


Fig. 7. Influence of some naphthylethers on an oleate coacervate. Abscissa, compare fig. 3.

I having a stronger activity than II (KRUYT and VELDSTRA, 1951). This reminds us of the difference between the phenyl- and benzylethers.



The introduction of halogen atoms into aromatic ethers has the expected effect. For *p*-anisoles we find the series (increasing activity):



The chloro-derivative has approximately the same activity as the methyl-derivative (compare fig. 5). The isomeric iodoanisoles show an increase in activity according to the series (fig. 8):



This is the expected series for the introduction of a hydrophobic group (BOOIJ, 1952).

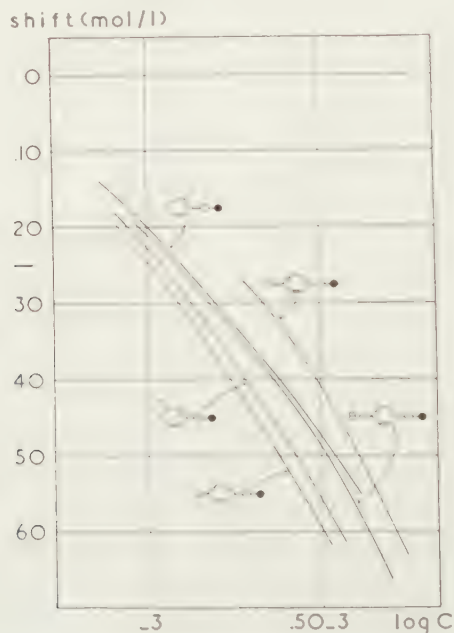


Fig. 8. A comparison of halogen derivatives of anisole. Abscissa, compare fig. 3.

Finally we have compared diphenylether with *o*-methoxydiphenylether and two isomeric methyl-diphenyl-ethers (fig. 9). From the influence of the first pair of substances we see that the methoxy-group has a distinct hydrophilic character (see also fig. 5, which leads to the same conclusion).

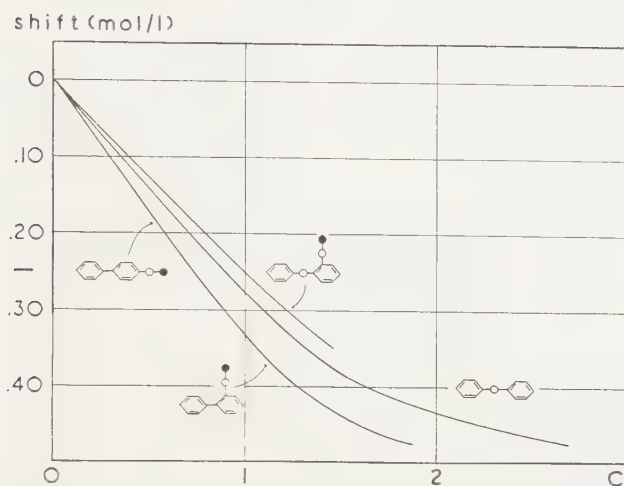


Fig. 9. The influence of some miscellaneous methoxy derivatives. Abscissa, compare fig. 2.

3. The influence of sulfides on an oleate coacervate

a) Aliphatic sulfides

Using the method described in the preceding section, we compared a series of aliphatic sulfides (fig. 10). Generally speaking, the picture resembles that of the ethers and of the paraffins very much. There are

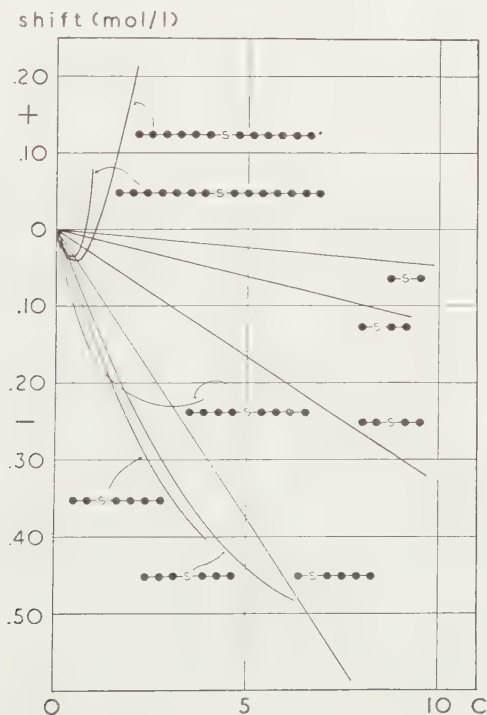


Fig. 10. Action of a series of aliphatic sulfides. Abscissa, compare fig. 2.

however, typical differences between the ethers and the sulfides, which may be readily explained. When we compare e.g. di-*n*-propylether and di-*n*-propylsulfide, we see that the last substance has a stronger salt sparing activity than the first. This must be a result of the difference in the hydrophilic groups, influencing the distribution medium micelle (fig. 1, *a* and *c*). The sulfides are more hydrophobic than the ethers.

The same property effects the distribution within the micelle (fig. 1, *c* and *d*). The -S- group being a less strong hydrophilic "anchor" of the molecule than the -O- group, the sulfides will (when going up in the homologous series) lose their salt-sparing activity sooner than the ethers. This is clearly shown by comparison of di-*n*-hexylether and di-*n*-hexylsulfide (fig. 2 and fig. 10). The difference between di-*n*-propylether, di-*n*-propylsulfide and "di-*n*-propylmethane" (*n*-heptane) is shown in fig. 11. At first sight this is a rather complex picture, but it becomes clear when we realise that distribution between three places (fig. 1, *a*, *c* and *d*) is involved. Starting from the sulfide in fig. 11—which prefers place *c*—we

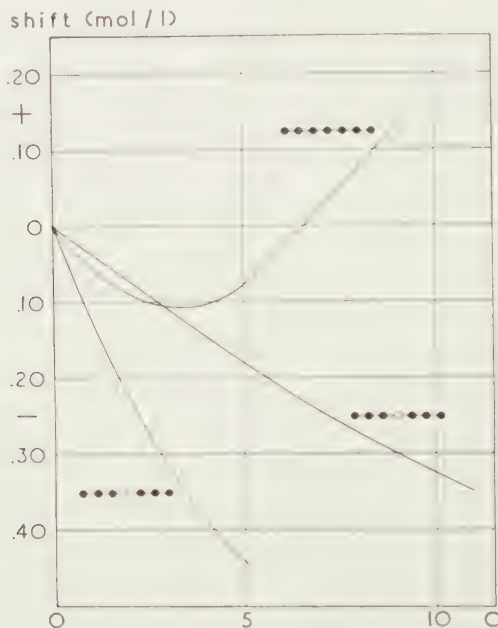


Fig. 11. A comparison of a paraffin, a sulfide and an ether of approximately the same length. Abscissa, compare fig. 2.

get a tendency to go to *a* of the ether (diminished salt-sparing activity) and a preference for *d* of the paraffin (salt-demanding activity comes to the fore, especially at high concentrations).

b) Aromatic sulfides

As the number of aromatic sulfides available to us was very small, our experiments do not give much information about the activity of this class

of substances (fig. 12). The most remarkable fact is that *p*-cresylmethylsulfide has a stronger action than *p*-cresylethylsulfide. This reminds us of the alkylbenzenes (Booiw *et al.* 1950 *c*) and indicates that the aromatic sulfides show much more tendency than the ethers to go into the space

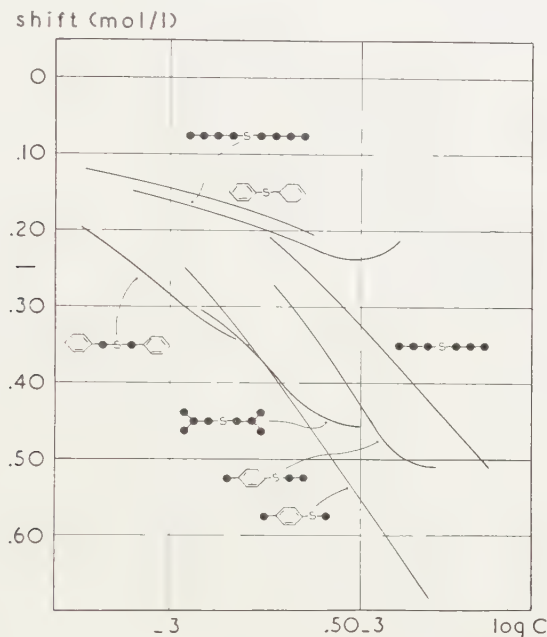


Fig. 12. Influence of a number of aromatic sulfides on an oleate coacervate. Abscissa, compare fig. 3.

between the CH_3 -planes of the oleate micelles (fig. 1, *d*). The unusual course of the curves for diphenylsulfide and dibenzylsulfide points in the same direction (compare di-*n*-butylsulfide!). It goes without saying that in this case we cannot give the aliphatic equivalent of the benzene rings.

Summary

1) The action of ethers, sulfides and paraffins on an oleate coacervate shows much resemblance.

2) The transition from a salt-sparing to a salt-demanding activity takes place at different terms of the homologous series. This is explained by a decrease in hydrophilic character in the series ether—sulfide—paraffin, which will presumably affect the distribution equilibrium of the substances within the oleate micelle (fig. 1).

3) The salt-sparing "value" of the benzene ring may be given as the number of aliphatic carbon atoms to which it is equivalent. This aliphatic equivalent is approximately five for phenylethers and three to four for benzylethers. This suggests that in the case of phenylethers the benzene ring has grown more hydrophobic, presumably by the deactivating

(electron attracting) effect of the ether-oxygen. This difference may have a bearing on such cases where an unexpected difference between the pharmacological activity of phenyl and benzyl derivatives is found.

*Department of Medical Chemistry
University of Leyden*

REFERENCES

- BOOIJ, H. L., *Rec. trav. chim. Pays-Bas* **71**, 101 (1952).
 ——— and H. G. BUNGENBERG DE JONG, *Biochim. Biophys. Acta* **3**, 242 (1949).
 ——— and E. S. VAN CALCAR, *Proc. Kon. Ned. Akad. Wetensch. Amst.* **53**, 1169 (1950 *d*).
 ———, J. C. LYCKLAMA and C. J. VOGELSANG, *Proc. Kon. Ned. Akad. Wetensch. Amst.* **53**, 407 (1950 *b*).
 ———, ——— and ———, *Proc. Kon. Ned. Akad. Wetensch. Amst.* **53**, 1413 (1950 *e*).
 ——— and P. J. VAN MULLEM, *Proc. Kon. Ned. Akad. Wetensch. Amst.* **54**, 273 (1951).
 ———, C. J. VOGELSANG and J. C. LYCKLAMA, *Proc. Kon. Ned. Akad. Wetensch. Amst.* **53**, 59 (1950 *a*).
 ———, ——— and ———, *Proc. Kon. Ned. Akad. Wetensch. Amst.* **53**, 882 (1950 *c*).
 BUNGENBERG DE JONG, H. G., H. L. BOOIJ and G. G. P. SAUBERT, *Protoplasma* **29**, 536 (1938 *a*).
 ———, G. G. P. SAUBERT and H. L. BOOIJ, *Protoplasma* **30**, 1 (1938 *b*).
 KRUYT, W. and H. VELDESTRA, *Landbouwk. Tijdschr.* **63**, 398 (1951).

MIOGYPSINA IN NORTHERN ITALY. I

BY

C. W. DROOGER

(Communicated by Prof. G. H. R. VON KOENIGSWALD at the meeting of Jan. 30, 1954)

Abstract: A revision is given of the species of *Miogypsina* that were previously described from the "Colli di Torino". Eighteen newly collected assemblages are described. *Miogypsina irregularis* (MICHELOTTI) is re-defined and the systematic position of *Miogypsina negrii* (FERRERO) clarified on the basis of the new material. Furthermore, the new species *Miogypsina socini* is established.

The assemblages with known stratigraphic relations are shown to have developed in accordance with the principle of nepionic acceleration. Development of the local *Miogypsina*-stock gave rise to *Miogypsina burdigalensis* and *M. negrii* of the subgenus *Miolepidocyclina*.

The vertical distribution of the *Miogypsina* species in the series Aquitaniano-Langhiano-Elveziano of Turin appears to be suitable for stratigraphic correlation in northern Italy. Comparison with the succession of *Miogypsina* species in the region of Bordeaux admits of the conclusion that the existing stratigraphic correlation of the Oligo-Miocene stages involved, has to be revised.

Introduction

The hilly country south of Turin has become one of the classical regions for the study of the Miogypsinidae. Reports on these Foraminifera started in 1841 and up till the early years of the twentieth century several more papers appeared on this subject. From the "Colli di Torino" the following taxonomic units of the Miogypsinidae were described:

in 1841 by MICHELOTTI *Nummulites irregularis* and *Nummulina globulina*;

in 1893 by DERVIEUX *Flabelliporus orbicularis* and *F. dilatata*;

in 1904 by PREVER *Miogypsina Dervieuxi*, *M. taurinensis* and *M. irregularis* var. *a* and var. *b*;

in 1909 by FERRERO *Lepidocyclina negrii*.

Moreover, in 1893 the genera *Miogypsina* SACCO and *Flabelliporus* DERVIEUX were established on the basis of specimens from this region, and both genera were described with essentially the same species (*M. irregularis*) as type. Since *Miogypsina* was published some days earlier than *Flabelliporus*, the latter name must be suppressed as a synonym of *Miogypsina*.

The enumerated species and varieties were mainly founded on external characteristics of the individuals, whereas but few details became known concerning the internal features. In later years, especially *M. irregularis* has often been referred to in the literature, though most features of its

original material were still unknown. For reasons of nomenclature a re-study of the *Miogypsinidae* of the hills of Turin had become highly necessary. A liberal grant from the Netherlands Organization for Pure Research (Z.W.O.) afforded the opportunity of making a journey to Italy in 1952, while the University of Utrecht enabled me to finish this investigation during 1953.

It appeared that owing to various causes hardly anything of the original collections of the Turinese species could be retraced. For this search the geological institutes of Turin and Rome were visited. Some specimens, which might with doubt belong to MICHELOTTI's original material of *Nummulites irregularis*, were found in the Istituto di Geologia of Rome. At any rate, this material would be insufficient for a detailed specific analysis. Further, a number of sections of FERRERO's *Lepidocyclina nigrii* were found in the collections of the Istituto di Geologia of Turin. These sections were sufficient for an unquestionable recognition of this species in the material collected at its type locality. No original material of DERVIEUX's and PREVER's species could be re-found.

Because of these disappointing results most conclusions of this re-investigation have to be based on the new material that could be collected in the field.

Locality details

Several samples, rich in *Miogypsina* specimens, were taken in the hills of Turin during the stay in northern Italy. The sampling was greatly facilitated by the ample support of Prof. E. FERUGLIO and Prof. C. SOCIN (Turin). All localities were visited in the company of Prof. SOCIN.

Samples from the following localities (see pl. 1, fig. A-E) contained a sufficient number of individuals for specific determination of the assemblage:

1. Villa Giuseppina (= Villa Sacco of earlier authors). Aquitaniano (fig. B).

2-9. Along the main road from Superga to Baldissero in the southeastern flank of the Gæssino-anticline (fig. A). Sample 2 (Aquitaniano) was taken between Bric del Duca and Bric Palouch; localities 3 and 4 (Lower Elveziano) are situated, with a stratigraphic interval of about 25 meters, between Bric del Pilonetta and Tetti Vigna, at the place where a side road branches off to Rivodora; 5-9 (Elveziano) are from a short section along the road, east of Croce Berton (stratigraphic distances from bottom to top 5, 3, 3 and $3\frac{1}{2}$ m respectively). The stratigraphic interval between 4 and 5 is estimated at about 200 meters.

10. Along the road close to the Fontana dei Francesi. Elveziano (fig. C).

11. East of the Rio Dora, about half way between the villages Rivodora and Tetti Lupo. Aquitaniano (fig. D).

12-18. Along the course of the Rio Torello between the altitudes of Cascina Fratelli and Tetti Rossi (fig. E). No exact stratigraphic observations could be made during the short stay. The stratigraphic intervals

PLATE I

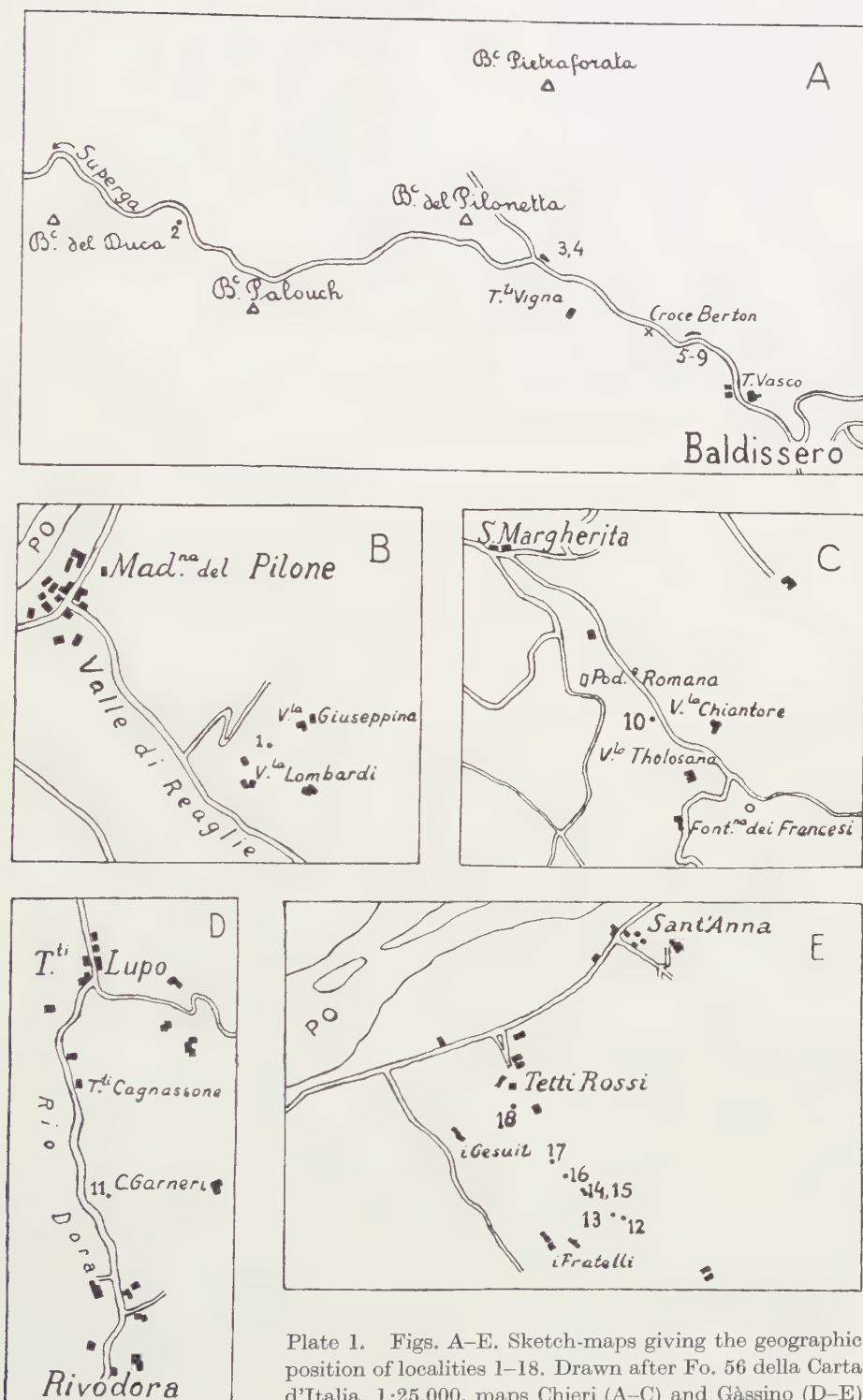


Plate 1. Figs. A-E. Sketch-maps giving the geographic position of localities 1-18. Drawn after Fo. 56 della Carta d'Italia, 1:25,000, maps Chieri (A-C) and Gassino (D-E)

are roughly estimated to be from bottom to top: (12) 15 m (13) 50 m (14) 5 m (15) 25 m (16) 25 m (17) 170 m (18). Sample 17 was taken some 15 meters below a complex of grey limestones with a thickness of several meters. Localities 12 and 13 are probably of Langhiano age, the higher ones of Elveziano age.

The age of the strata at the various localities was concluded from the geological map of the region by BEETS (lit. 2), except that of localities 1 and 10, which were taken from a much older map by SACCO. The Italian names Aquitaniano, Langhiano and Elveziano have been employed since it is considered unlikely that these lithologic units fully correspond in time with the deposits of the Aquitanian, Burdigalian and Helvetian in the region of Bordeaux, where the stages Aquitanian and Burdigalian were defined (see chapter on stratigraphic conclusions).

The relative age of the samples 2-9 and 12-18 are clear within each of the sections since they were derived from strata dipping regularly south-east, respectively northwest. No tectonic complications were noted in these sections, though it must be remarked that the exposures are not continuous. Evidently, BEETS neither observed nor anticipated such anomalies in the sections involved. Stratigraphic relations between localities 2 and 11 are not clear from BEETS's map; they are probably of about equal age. The exact stratigraphic positions of samples 1 and 10 in connection with the others are uncertain; and as for older maps, the conclusion may be drawn that the beds, exposed at locality 1, are probably oldest of all.

Description of species and assemblages

Most features of the *Miogypsina* assemblages, that can be numerically expressed, are listed in table 1¹). Further details are given below.

Miogypsina (*Miogypsinoides*) *complanata* SCHLUMBERGER

(table 1)

Miogypsina complanata SCHLUMBERGER, 1900, Bull. Soc. géol. France, 3d ser., vol. 28, p. 330, pl. 2, f. 13-16, pl. 3, f. 18-21; DROOGER, 1951, Proc. Kon. Ned.

¹) In this table N = number of individuals; X = number of chambers of the main (protoconchal) nepionic spiral (excluding I and II), given by means of the observed range (R), the mean (M) and the standard error of the mean (σ_M). Similar observations are listed for the other nepionic spirals of some assemblages; the derivation of the numbers of spiral chambers of each individual are shown in text fig. 1. By means of their range, mean and standard error of the mean are given the values of $200 \alpha/\beta$, γ and the diameter of I; the average diameter of the deuteroconch is shown in M_{II}/M_I . For most assemblages the numbers of individuals with but one principal auxiliary chamber are given in a separate column under 1, those with two such chambers under 2. Furthermore, a column is added giving for each sample the number of individuals with the position of the protoconch peripheral, in between the periphery and a point at one quarter of the test's diameter from the periphery (intermediate), and in between the latter point and central (subcentral) respectively. For further explanation of the symbols and the employed methods one is referred to lit. 8, pp. 4-12.

Ak. Wetensch., ser. B, vol. 54, p. 360, f. 7; DROOGER, 1952, Study of American Miogypsinidae, Acad. thesis Utrecht, p. 47.

The assemblages from localities 1 (Villa Giuseppina) and 2 (Bric del Duca) clearly belong to this species. At both localities the species is accompanied by numerous individuals of the genera *Lepidocyclina* and *Heterostegina*.

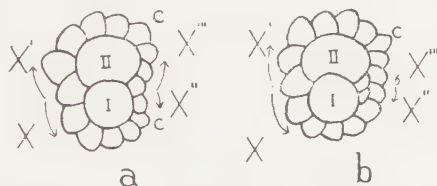


Fig. 1. Schematic figures showing the derivation of the number of chambers for each of the nepionic spirals. Each closing chamber is counted as a full chamber for each of the two encountering spirals, unless one of these spirals continues on top of the other. I = protoconch, II = deuterocoenoch, c = closing chamber. The numbers of chambers in the respective nepionic spirals are:

for a: X	(II' _p) = 6	for b: X	(II' _p) = 10
X'	(II' _d) = 6	X'	(II' _d) = 7
X''	(II'' _p) = 3	X''	(II'' _p) = 2
X'''	(II'' _d) = 4	X'''	(II'' _d) = 1.

The specimens from Villa Giuseppina²⁾ are rather ill-preserved. In most of them numerous sand grains are firmly cemented to the outer wall, usually far more on one side than on the other. The frontal margin is nearly always damaged. The peripherally situated initial portion and its spiral are usually distinct from the exterior. The larger pustules are thickenings of the horizontal walls of the separate chambers. In large individuals some irregular cavities were observed in the outer walls at places where these lateral walls are broken.

In fact at Villa Giuseppina three different samples were taken at intervals of about 60 cm. Differences between their values of M_x (from bottom to top 18.9 ± 0.77 , 20.2 ± 0.59 and 20.6 ± 0.67 respectively, based on 10 individuals for each sample) are too small to be of any statistical significance. For table 1 these data have been combined.

In these three samples many small individuals were found, consisting of a distinct *Rotalia*-stage with 9–14 chambers in the final coil, and a variable, but small, number of equatorial chambers of arcuate shape. The spiral part of these specimens possesses one or more umbonal bosses at the ventral side. The wall is covered with numerous coarse pustules,

²⁾ There is some confusion in the literature about the Miogypsinidae from Villa Giuseppina (V. Sacco auct.). SCHLUMBERGER's suggestion (1900) that this is a locality where *M. irregularis* has been found, must be erroneous, as was noted already by SACCO (lit. 16). The only *Miogypsinidae* specimens in the collection PREVER (Turin), I found, came from V. Giuseppina and they were correctly labeled as *M. complanata*. Some other specimens from the same locality were determined earlier by DROOGER (lit. 7, p. 361).

especially dorsally. These small specimens somewhat resemble *Miogypsina bermudezi* DROOGER from the Cuban Oligocene (lit. 7), but they are different in that they have much thicker outer walls (70–180 μ) and by the possession of the pustulous surface ornamentation. By the latter feature they resemble *Rotalia mexicana* NUTTALL better than do the young individuals of *M. bermudezi*. Since in these samples also large individuals of *M. complanata* occur in considerable numbers, and since immature individuals of *Heterostegina* are equally common in addition to adult ones, it is considered likely that we are dealing here with juvenile specimens of *M. complanata*, rather than with a morphologically intermediate population between typical populations of *M. complanata* and *M. bermudezi*. The relative abundance of these immature individuals may be due to some unfavourable environmental circumstance that influenced the average duration of individual life.

In the specimens from sample 2 the initial spiral is much shorter and less distinctly trochoid than in those of the assemblages from Villa Giuseppina. The latter feature could be observed best in transverse sections. In none of the sectioned individuals were observed other nepionic chambers than those of the primary spiral. In some specimens the outer wall of the embryonic chambers is thickened at the place of the possible second principal auxiliary chamber, but cavities of such a chamber were observed in none of them.

In transverse sections of some of the larger individuals, which probably are all microspheric, cavities in the lateral walls were noted near the frontal margin. They occur either as vertical rows of small cavities above the walls between the median chambers (as in the type of *Miogypsina primitiva* TAN SIN HOK), or as tiers of low, flattened chambers, situated above the median chambers. Moreover, the outer walls often show distinct lamellar structures, as were observed for the first time in *Miogypsina dehaarti* VAN DER VLERK. In megalospheric specimens of sample 2 these features occur but rarely, for which reason the assemblage is considered still to belong to the subgenus *Miogypsinoidea* and not to *Miogypsina* s.str..

***Miogypsina* (*Miogypsina*) *gunteri* COLE**

(pl. 2, fig. 25–27; table 1)

Miogypsina gunteri COLE, 1938, Florida State Dept. Conserv., Geol. Bull. no. 16, p. 42, pl. 6, f. 10–12, 14, pl. 8, f. 1–9; DROOGER, 1952, Study of American Miogypsiniidae, Acad. thesis Utrecht, pp. 21, 51, pl. 2, f. 11–15.

The specimens from sample 11 (Rio Dora), which are considered to belong here, are rounded in outline with the apical portion occasionally protruding; they are unequally biconvex to planoconvex. Microspheric individuals, which are generally more irregular in shape, may attain a size of 4 mm.

In three out of twenty sectioned specimens a second principal auxiliary

chamber was observed, in one case with a short protoconchal spiral originating from this chamber. In at least two individuals, there is also a short deuteroconchal spiral from the first principal auxiliary chamber. Trochoidity of the main nepionic spiral could not be observed, neither in horizontal, nor in transverse sections. The equatorial chambers are about ogival in shape.

The transverse sections that were made, all show numerous well-developed lateral chambers, imbricately arranged.

Miogypsina (Miogypsina) socini n.sp.
(pl. 2, fig. 20–24; textfig. 2a, b; table 1)

Diagnosis: This species is established for populations of *Miogypsina*, in which the individuals possess distinctly developed lateral chambers and a peripheral position of the embryonic-nepionic stage (which may be slightly removed from the periphery only in a minority of the individuals of the population). The value of M_X is greater than 7, that of $M_{200\alpha/\beta}$ smaller than 45, while at least 50 per cent of the total number of sectioned specimens possess a second principal auxiliary chamber.

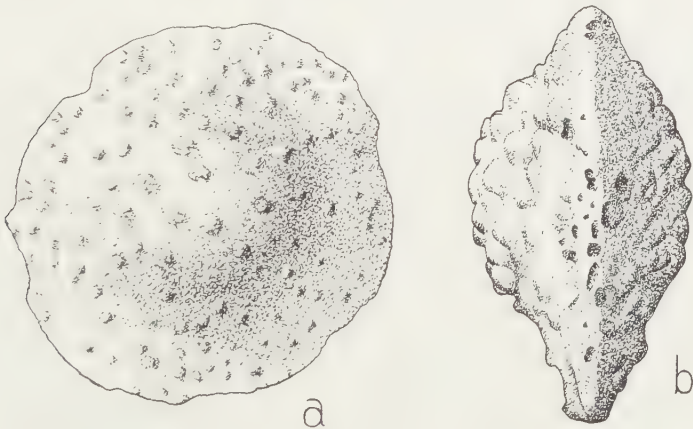


Fig. 2. *Miogypsina socini* n. sp.. Holotype; a, side view; b, peripheral view. X 30
Langhiano, loc. 13, Rio Torello

Description of the type sample: The numerous individuals of sample 13 (Langhiano of Rio Torello) show the following characteristics:

Test about rounded in outline; usually strongly and often unequally biconvex, occasionally planoconvex; greatest thickness situated eccentrically between the centre and the periphery, commonly closest to the centre. In many individuals the test consists of a strongly inflated sub-central portion and a rather thin, flange-like marginal part. These individuals strongly resemble representatives of some species of *Lepidocyclina*. The early portion of the test, though usually not protruding, is often discernible from the pustulation of the surface combined with the position of the thickest part of the test. The pustules are rather uniformly

scattered on the surface with the larger ones on and near the subcentral knob.

The quality of the sections is moderate, since most individuals have the chamber-cavities filled with calcareous material, which often greatly effaces the borders of the walls of the chambers. This drawback is too small for it to influence the conclusions that are drawn.

In most specimens protoconchal and deuterococonchal nepionic spirals are all well-developed. The embryonic-nepionic apparatus is situated directly at the periphery; in some specimens it is slightly removed from the border by a collar-like structure, which is formed by the bending of closely-set lateral layers. Only in two out of 20 sectioned individuals some equatorial chambers (one row or less) are intercalated between the nepionic chambers and the periphery. In 8 out of 20 specimens the presence of a second principal auxiliary chamber could not be ascertained, which absence may sometimes be due to the moderate state of preservation of the individuals. The equatorial chambers are arcuate, mainly ogival and occasionally rhombic in shape.

In transverse sections the lateral chambers cover one another imbricately; they are often arranged in irregular layers, occasionally in tiers. Up to eight lateral chambers were observed in vertical succession at the most convex side of the test on top of the median layer.

The bad sections, made of some microspheric specimens (diameter up to 7 mm) show that the early chambers are situated at the periphery, as far as could be ascertained from the arrangement of the equatorial chambers.

Remarks: About identical observations were made for the assemblage of locality 12, Rio Torello (see table 1), which also belongs to the Langhiano (= probably Aquitanian of general stratigraphy).

These assemblages from Rio Torello are morphologically near the border-line between the two groups of species of the subgenus *Miogypsina* that possess one and two principal auxiliary chambers respectively in the majority of the individuals of their populations. However, the coexistence of a relatively long, primary spiral and the presence of a second principal auxiliary chamber in more than half the total number of sectioned individuals of these Italian assemblages, necessitate the establishing of a new species. Evidently, the boundary that was previously drawn between *Miogypsina tani* DROOGER and *M. irregularis* (MICHELOTTI) (lit. 8, pp. 52, 54) is too complicated. The earlier given diagnosis of these species are:

for *M. tani*: "Populations with values of M_X below 9. ...these populations generally contain specimens, in which a second principal auxiliary chamber and sometimes short spirals from the latter are present, which feature should not occur in more than 50 % of the individuals, however. Moreover, these small spirals should be covered in more than 50 % of the observations by the later chambers of the main spiral".

for *M. irregularis*: "Populations with the mean values of $200\alpha/\beta$ between 0 and 45. The value 0 — absence of the second principal auxiliary chamber — should occur

in no more than half the number of observations per sample. In the specimens with two principal auxiliary chambers the smaller spiral may not be covered by the chambers of the main spiral in more than 50 % of these individuals”.

Though all observed American occurrences (lit. 8) and also several others I determined, do fit these definitions, it seems practical at the moment to drop the limitations that are caused by the condition that the smaller spirals should (or should not) be covered by the longer ones. This does not affect the earlier determinations, but it facilitates the determination of the exceptional assemblages from northern Italy, for which an easier taxonomic solution has become possible.

The assemblages from Rio Torello involved possess an extremely high M_X for *M. irregularis*, to which species they would belong when the determination would be based on the modified diagnosis, given above. However, they are morphologically very different from all other known assemblages of this species. In order to avoid this wide range of variation of *M. irregularis*, the best thing is to establish the new species, *Miogypsina socini*. The theoretical limits of *M. socini* are set by the definition that it should comprise the populations of *Miogypsina* s.str. with more than 50 per cent of the individuals in possession of a second principal auxiliary chamber, with $M_{200\alpha/\beta}$ between 0 and 45, and yet having M_X greater than 7. The populations with the same features, but with M_X smaller than 7 belong to *M. irregularis*. *M. tani* and *M. gunteri* which have similar M_X values as *M. socini*, are different in having in each sample less than 50 per cent of the individuals in possession of two principal auxiliary chambers. So we have got two different, complementary, morphological species between *M. gunteri* and *M. irregularis*: *M. tani* and *M. socini*.

The described assemblages of *M. socini* do not consist purely of specimens with a strictly peripheral position of the embryonic-nepionic stage. As divergencies are very small, and few in number, however, the assemblages are considered to be sufficiently distinct for them to be placed in the subgenus *Miogypsina* s.str.. Hence, one of the samples from Rio Torello could be taken as type sample for the new species, the more so since no other assemblages were available.

The species is named in honour of Prof. COSTANTINO SOCIN (Turin), whose valuable support in the field greatly contributed to the results of this investigation.

The holotype (no. S 366) and the type sample have been deposited in the collection of the Mineralogisch-Geologisch Instituut, State University of Utrecht.

Miogypsina ex. interc. *socini-burdigalensis* (table 1)

The individuals of samples 3, 14 and 15 resemble those of *M. socini* of samples 12 and 13 in outward appearance and in most internal features as well. Microspheric specimens (diameter mostly 3–7 mm) are flattened and

rather broad with an irregular and undulated frontal border. Especially in sample 3 they are quite common.

In horizontal sections of macrospheric specimens the position of the early chambers appears to be highly variable, from strictly peripheral to subcentral. In most individuals (except in sample 3) the early chambers occupy some intermediate position between these extremes. In horizontal sections of microspheric individuals (about 15 observations) the early chambers are seen to be situated directly at the periphery; in some of the specimens from sample 14 the early stage may have shifted slightly towards the centre of the test, but this could not be ascertained with certainty.

Because of the variable position of the early stage in megalospheric individuals of these assemblages, they are intermediate between those of *Miogypsina* (*Miogypsina*) *sacini* and *Miogypsina* (*Miolepidocyclina*) *burdigalensis*. As to the position of the early stages in the microspheric generation, the assemblages would belong to the subgenus *Miogypsina* s.str. or *Miogypsinita*.

***Miogypsina* (*Miolepidocyclina*) *burdigalensis* (GÜMBEL)**
(pl. 2, fig. 13–19; table 1)

Orbitoides burdigalensis GÜMBEL, 1868, Abh. k. Ak. Wiss., vol. 10, p. 719.

Miogypsina burdigalensis (GÜMBEL), SCHLUMBERGER, 1900, Bull. Soc. géol. France, 3d ser., vol. 28, p. 330, pl. 2, f. 11, 12, pl. 3, f. 22, 25; BRÖNNIMANN, 1940, Schweiz. Pal. Abh., vol. 63, p. 81, pl. 7, f. 1–6, pl. 8, f. 20–22, pl. 9, f. 4–7, 9; DROOGER, 1952, Study of American Miogypsinidae, Acad. thesis, Utrecht, p. 48, pl. 1, f. 30–34.

The assemblages from localities 4 and 16 are considered to belong to this species. In both samples the individuals are rounded in outline, unequally biconvex to planoconvex in shape, with an eccentric inflated portion and sometimes possessing a distinct marginal flange. Microspheric specimens (diameter up to 5.5 mm) are relatively more flattened and irregular in shape.

Sample 16 (Rio Torello) yielded but very few *Miogypsina* specimens. Distinct horizontal sections were obtained of but three megalospheric individuals. Their initial chambers are situated near the centre of the median layer. The value of $M_{200.5}$ corresponds well with those of *M. burdigalensis* of southwestern France (still unpublished data). The mean values for the numbers of chambers of the four nepionic spirals deviate from the corresponding mean values of the French assemblages of this species, but this may be due to the small size of the sample. In fact these values for the larger assemblage from locality 4 agree much better to the French data. The latter Italian sample differs from the typical assemblages of *M. burdigalensis* by the occurrence of one individual with a peripheral position of the early chambers, and another in which the initial stage occupies some intermediate position between the centre and the periphery of the test. In both Italian samples the equatorial chambers are equidimensional-arcuate in shape; occasionally they are ogival towards the periphery.

In the sectioned microspheric individuals (two in sample 16, one in sample 4) the early stages are situated closer to the centre than to the periphery of the test.

Miogypsina (Miolepidocyclina) negrii (FERRERO)
(pl. 2, fig. 6-12; table 1)

Lepidocyclina negrii FERRERO, 1909, Bull. Soc. Geol. Ital., Roma, vol. 28, p. 135, pl. 3, f. 1-13.

This species was recognized in the sample from locality 17 (Rio Torello). The individuals of this sample are rounded in outline, unequally biconvex, occasionally planoconvex, with the greatest thickness situated near the centre of the test. One side is sometimes so strongly inflated that the thickness of the test equals its diameter. A marginal flange is more or less distinct in most individuals. The pustules are regularly distributed on the surface around the centre of the test. Microspheric specimens are relatively flattened and irregularly rounded in shape (diameter up to 5.5. mm).

Eight sections of FERRERO's original collection that were still in the Istituto di Geologia di Turin, could be studied. Four of them are transverse sections of microspheric (two) and macrospheric individuals, which show or suggest that the early chambers are situated near the centre of the median layer, as seen in the sections. The other four are horizontal sections of macrospheric specimens, which again show the early chambers situated nearly centrally. Two of them allow of a rather correct establishing of the arrangement of the nepionic chambers (see pl. 2, fig. 6, 7).

In all sectioned individuals, macro- and microspheric, the early stages are situated close to the centre of the median layer. The equatorial chambers are mainly of equidimensional-arcuate shape; often they are ogival and occasionally rhombic near the periphery.

Remarks: Though one of FERRERO's specimens is slightly beyond the range of variation of the assemblage from locality 17, the latter is probably sufficiently close to FERRERO's original material—which had also been derived from the Rio Torello—to be considered as the basis of a better evaluation of *M. negrii*.

Miogypsina negrii evidently belongs to the subgenus *Miolepidocyclina*, in which it differs from the type species, *M. burdigalensis*, by the higher average development of the nepionic spirals that originate from the second principal auxiliary chamber.

A theoretical boundary has to be defined between *M. burdigalensis* and *M. negrii*. The $M_{200\alpha/\beta}$ values are evidently most suitable for this purpose. So this boundary is set at the level of 45 of the $M_{200\alpha/\beta}$ scale, analogous to the subdivision of *Miogypsina* s.str.. *M. burdigalensis* then comprises all populations with $M_{200\alpha/\beta}$ values smaller than 45, *M. negrii* those with such values greater than 45. If in future other populations with still better symmetry of the nepionic apparatus are found, the upper limit of *M. negrii* has to be taken at the level 75 of the $M_{200\alpha/\beta}$ scale.

Miogypsina (Miogypsina) irregularis (MICHELOTTI)

(pl. 2, fig. 1-5; table 1)

Nummulites irregularis MICHELOTTI, 1841, Mem. Soc. Ital. Sci. Modena, vol. 22, p. 44, pl. 3, f. 5.

Miogypsina irregularis (MICHELOTTI), SCHLUMBERGER, 1900, Bull. Soc. géol. France, 3d ser., vol. 28, p. 328, pl. 2, f. 1-7, 9, 10, pl. 3, f. 17; BRÖNNIMANN, 1940, Schweiz. Pal., Abh., vol. 63, p. 88, pl. 8, f. 1-11, pl. 10, f. 6-11, pl. 11, f. 1, 4; DROOGER, 1952, Study of American Miogypsinidae, Acad. thesis Utrecht, p. 54, pl. 2, f. 25-29.

As this is one of the most frequently recorded *Miogypsina* species in the literature, a re-description, based on the original material, was highly necessary. MICHELOTTI and the later Italian authors gave no exact data about the nepionic apparatus. The first one to do so was SCHLUMBERGER in 1900, who based his description of the species on material from southwestern France and northern Italy. From his figures it appears that he had at his disposal *Miogypsina* specimens with two principal auxiliary chambers and with a very asymmetric appearance of the protoconchal nepionic spirals, while the embryonic-nepionic apparatus was situated directly at the periphery. This concept was followed later by BRÖNNIMANN and others. In accordance with these ideas, limits were given to this species (lit. 8, p. 54; slightly modified above), which were not based on MICHELOTTI's material, however. According to this diagnosis *M. irregularis* should be applied to populations with M_X smaller than 7, with $M_{200\alpha/\beta}$ smaller than 45 and in which a second principal auxiliary chamber occurs in more than half the number of sectioned individuals.

The search for MICHELOTTI's original material in the collections in Rome gave the following disappointing results. Several *Miogypsinæ* from the "Colli di Torino" were present, but only with some of them there were labels on which had been written "Coll. Mich.". These were certainly not the original labels of MICHELOTTI, since they were also marked with "*Tinoporus irregularis Michelotti*", a name this author never used in his papers. So it is uncertain whether they represent MICHELOTTI's original specimens. The more so as nothing was found of his second species of 1841, *Nummulina globulina*. Anyhow, there were too few specimens for a reliable species analysis. Most of them are very large (up to 1 cm) microspheric individuals; the few smaller ones do not resemble those from the Aquitaniano or from the Langhiano and Lower Elveziano, but they are closest in external features to the specimens from localities 5-9. One gets the same impression from MICHELOTTI's figures. Evidently MICHELOTTI, as well as some of the later Italian authors, placed all *Miogypsinæ* from the neighbourhood of Turin in *M. irregularis* (or in some other species, based on external features, which species cannot be evaluated. Probably they are mainly variants of *M. irregularis*). Although no satisfactory conclusions may be drawn from this, it is recommendable to maintain the name *M. irregularis* for practical reasons. The locality details given in the past,

are too vague to be of any use. Therefore it is considered best to select a new type sample, which is in accordance with the generally accepted idea of the species and which is probably not in contradiction with MICHELOTTI's original material. For this I take sample 5 from the Elveziano near Croce Berton.

The specimens of sample 5 are more or less circular in outline, occasionally with a distinctly protruding apical portion. The thickness of the test is variable from relatively much flattened to very thick and unequally biconvex; all intermediates between these two extreme external types were found. Very thick individuals lack a peripheral flange. Microspheric specimens, which are of irregular and broadly rounded shape may attain the size of 6 mm. The embryonic-nepionic apparatus is always situated directly at the periphery. The equatorial chambers are ogival and rhombic in shape.

These external and internal features are about the same for the assemblages 6-9, 10 and 18. In sample 18 (Rio Torello) one individual with a long spiral and negative γ value may have been reworked from older strata. The assemblages from localities 6, 10 and 18 also belong to *M. irregularis*, whereas those from localities 7-9 get the determination *M. ex. interc. irregularis-intermedia*, because of the slightly higher $M_{200\alpha/\beta}$.

In samples 5-9 the Miogypsinae are accompanied by numerous individuals of *Operculina complanata* (DEFRANCE), which are the only other larger Foraminifera encountered in these samples. This species was not observed in the other *Miogypsina*-bearing samples, with the exception of that from locality 14 (Rio Torello), where it accompanies *M. ex interc. socini-burdigalensis*.

(to be continued)

MIOGYPSINA IN NORTHERN ITALY. II

BY

C. W. DROOGER

(Communicated by Prof. G. H. R. VON KOENIGSWALD at the meeting of Jan. 30, 1954)

Remarks on the earlier described species of Turin

As to the species, described between 1841 and 1909, which were mentioned in the introduction, little can be said to clarify their systematic position. Except the eight thin-sections of *Lipidocyclina negrii* FERRERO, which species could be satisfactorily analyzed, no original material of these species was found again. It may have got lost, probably on account of the war.

In addition to *Nummulites irregularis*, which has been dealt with in detail above, MICHELOTTI described in 1841 a second species: *Nummulina globulina*. Regarding his figure of the latter species it is quite probable that this is a rounded and inflated variant of *M. irregularis*, as was assumed by most later authors. Such variants occur in great numbers in our samples of *M. irregularis*.

Both species of DERVIEUX (*Flabelliporus orbicularis* and *F. dilatata*) were stated by their author to be identical with MICHELOTTI's species. As such they would have to be placed in the synonymy of *M. irregularis*.

In 1912 PREVER suppressed his earlier described *Miogypsina taurinensis* as a synonym of *M. irregularis*. This is quite likely, since the species was only based on the crenulations of the frontal margin, which feature may be found in several, if not in all, other species. A similar attitude has to be taken towards his two variants of *M. irregularis* (var. *a* and var. *b*) which were only based on the shape of the test.

In his later paper (1912) PREVER only retained his *Miogypsina Dervieui*, of which he gives a more extensive report than in 1904. From PREVER's figures it is clear that we are dealing mainly with microspheric individuals. They are said to be typical by their large size and the broad and somewhat undulated test, while it may be concluded from the figures that they probably possess a peripheral position of the initial stage. Similar individuals were frequently observed in nearly all new samples from the Langhiano and Elveziano. So again the systematic position cannot be established, as PREVER's localities are too vaguely stated and since his material seems to have got lost.

In summarizing we had better consider the various specific names as nomina dubia, with the exception of *M. irregularis* and *M. negrii*.

Phylogenetic conclusions

One of the results of the investigation is that in several instances differences between the *Miogypsina* assemblages appear to be clearly in accordance with the principle of nepionic acceleration.

Accepting the assumed stratigraphic relations between samples 1 and 2, it would follow that this principle holds true for the assemblages with representatives of the subgenus *Miogypsinoides* ($d/\sigma_d=15$ for the difference between the M_X values of both samples). Though the separate M_X values of the three samples from Villa Giuseppina give the impression of nepionic retardation, the differences are not statistically significant; they may be entirely due to random effects in the sectioned parts of the populations involved.

The small difference in age between localities 2 and 11, concluded from BEETS's geological map, agrees with the statistically insignificant difference between the M_X values. The stratigraphic level of locality 11 may be higher, because of the presence of distinctly developed lateral chambers in its *Miogypsina* specimens, whereas the assemblage from locality 2 is still classified in the subgenus *Miogypsinoides*.

The changes in the successive *Miogypsina* assemblages from the localities of the Rio Torello section in the order of from 12 to 17 also correspond with the principle of nepionic acceleration (see table 1). Assuming a lower stratigraphic position of sample 11 (Rio Dora)—which again follows from BEETS's map—, the difference of the M_X values between the assemblages 11 and 12 or 13 is significant ($P=0.003$ and slightly less), and points to acceleration. From 12 and 13 to 14 and 15, M_X shows a slight increase, which is statistically insignificant. The M_X values show distinct decrease again of from 15 to 16 and 17, though the difference cannot be evaluated for 16, because of the low number of observations in this sample. A similar increase in mean values of the numbers of chambers in the other nepionic spirals is observed in the succession 11, 12–13, 14–15 and 17. These differences are not always statistically significant. For the $M_{200\alpha/\beta}$ values such significance appears only between the assemblages 15 and 17, though for this feature an unmistakable increase may be observed of from 11 to 15 as well. Another distinct change in this succession of *Miogypsina* assemblages is found in the position of the embryonic-nepionic apparatus. In assemblages 11–13 this stage is nearly always peripheral; occasionally it is slightly removed from the periphery when a collar-like structure is commonly intercalated. In assemblages 14 and 15 a wide variance is shown, the early chambers being variously situated between strictly peripheral and nearly central. The latter position is obtained, to the exclusion of others, in the individuals of assemblages 16 and 17. The early stage in the microspheric individuals appears to be distinctly removed from the periphery in the assemblages 16 and 17 only.

The data from the Rio Torello section allow of the conclusion that the

changes in M_X , $M_{200\alpha/\beta}$ and the position of the early chambers in the megalospheric generation did not occur with constant and fully correlated rates throughout the section. So the change of from 11 to 12-13 is visible from M_X and $M_{200\alpha/\beta}$; the change of from 12-13 to 14-15 only affected $M_{200\alpha/\beta}$ and the position of the embryonic-nepionic apparatus, whereas M_X remained about constant. From 14-15 to 16 (and the corresponding

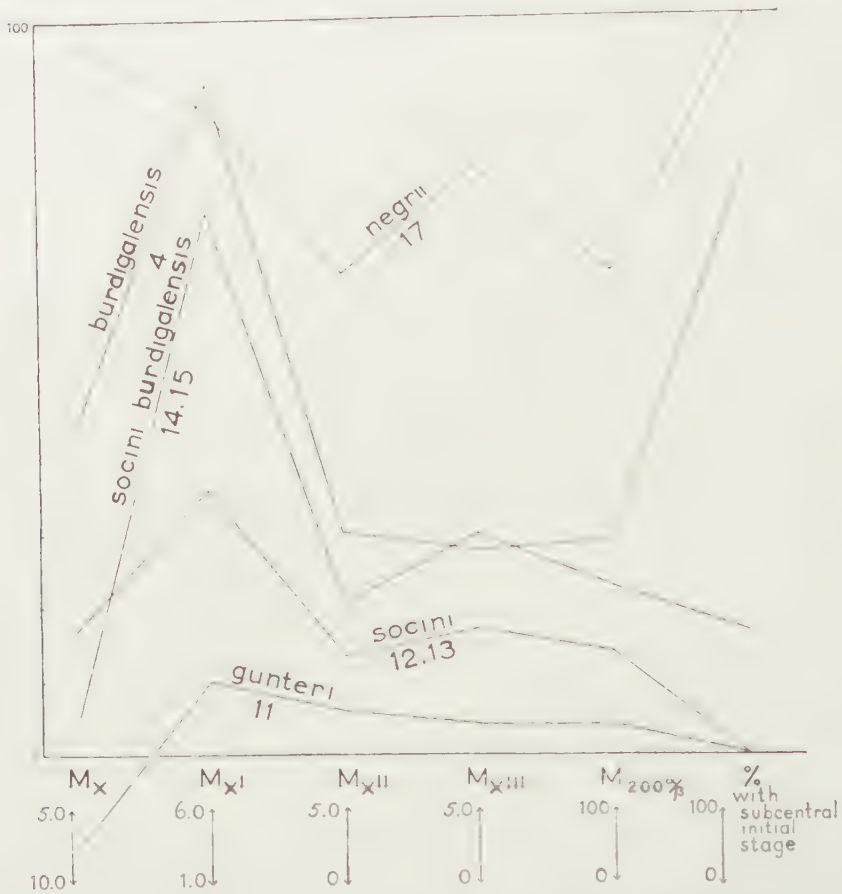


Fig. 3. Diagram showing the relative rates of development of six characteristics of the nepionic stage in the series *Miogypsina gunteri*–*M. negrii* (samples 11–17; instead of 16, the values of sample 4 have been taken). Some of the differences between successive samples are without significance, since for each sample (or couple of samples) only the mean values have been plotted, so that the influence of their standard errors is not accounted for

assemblage from locality 4) the increase in $M_{200\alpha/\beta}$ appears to be very slight in comparison with that in M_X and the change of position of the initial chambers. Finally of from 16 (and 4) to 17 the development mainly (if not only) affected M_X and $M_{200\alpha/\beta}$.

It is considered to be very unlikely that the assemblage from locality 18 of Rio Torello, developed from that of locality 17. Not only is the

former assemblage of much lower morphological development with respect to the values of M_X and $M_{200\alpha/\beta}$. Such development would involve also a complete reversal of the previous change in average position of the initial apparatus from subcentral to peripheral, for which reversed direction no proof is forthcoming in the material from northern Italy. Evidently, the populations of *M. irregularis* in this region represent the later invasion of another *Miogypsina*-stock.

Regarding the assemblages of the Superga-Baldissero section distinct nepionic acceleration (in M_X and $M_{200\alpha/\beta}$) and change of the average position of the early chambers are shown in the succession of the assemblages 2, 3 and 4. Samples 3 and 4 correspond with 14–15 and 16 of the Rio Torello section respectively. The assemblages 5–9, higher in this section, represent the later *Miogypsina* stock. In these assemblages slight fluctuations—which may be entirely due to the random selection of the sectioned individuals—occur in the succession of the calculated means (M_X , $M_{200\alpha/\beta}$) and the differences between the means of any two successive samples are nowhere statistically significant. However, the difference between the M_X values of assemblages 5 and 9 is distinctly so, even when ample allowance is made for the errors of measuring. The difference between the $M_{200\alpha/\beta}$ values of these two samples is less distinct ($P=0.016$). The changes again favour nepionic acceleration.

The other observed features of the *Miogypsina* assemblages appear to be of lesser taxonomic importance. Within the subgenus *Miogypsina* s.str. the populations of *M. gunteri* and *M. socini* have a negative M_v , whereas M_v is positive in the populations of *M. irregularis*. Further discrimination on the basis of this feature is impossible. The values of M_I are of no use. It is apparent from table 1, that differences between the values of M_I are unmistakable in several instances. Yet, there is no regular change in this feature in the course of time, the fluctuations of the M_I values being completely haphazard. For instance, the difference between the values for samples 1 and 9, oldest and youngest respectively, is not statistically significant even. The values of M_{II}/M_I show a general, but irregularly fluctuating increase, from the older assemblages to the younger ones. As to the shape of the equatorial chambers it is worth mentioning that in the assemblages of *M. burdigalensis* and *M. negrii* this is mostly about equidimensional-arcuate, which is different from the most common shape in *Miogypsina* s.str., but which compares nicely with the observations on *M. burdigalensis* from southwestern France. From table 1 it may be seen that the maximal dimensions of the equatorial chambers, as well as the diameter and thickness of the test, and the diameter of the pustules are characteristics without taxonomic value. This might be expected as such features depend for the greater part on environmental factors. The *Lepidocyclus*-like shape of many individuals of the lineage *M. socini*–*M. burdigalensis*–*M. negrii* may be regarded as a feature of local importance only; in fact the flange is lacking in the individuals of *M. burdigalensis* from the region of Bordeaux.

In northern Italy *Miogypsina* s.str. (*M. gunteri*) probably developed directly from *Miogypsinoides* without intercalation of populations that have the morphological characteristics of *M. basraensis* BRÖNNIMANN. *M. gunteri* evidently developed in a somewhat aberrant direction, giving rise to the sequence *M. socini*–*M. burdigalensis*–*M. negrii*.

Apparently *M. burdigalensis*, which is known as a rootless species elsewhere (France, Marocco), had its origin in northern Italy, from where it spread into western direction. So it has become unlikely that this species is related to morphologically similar American species (*M. panamensis* (CUSHMAN) and *M. ecuadorensis* TAN SIN HOK), which was considered most likely some years ago (DROOGER, lit. 8, p. 67).

In the assemblages intermediate between *M. socini* and *M. burdigalensis* (3, 14, 15) the position of the initial spiral in the microspheric individuals could not clearly be shown to have shifted from the periphery towards the centre of the median layer. So it follows that in the course of evolution the shift of the initial apparatus in the microspheric generation lagged behind that in the corresponding megalospheric individuals. Attention has to be drawn to the very wide variance in position of the early chambers in the macrospheric specimens of these intermediate assemblages. This variance is distinctly different from the observed narrower range of variation in the position of the early chambers in the American assemblages of the subgenus *Miogypsinita*, as well as in the assemblages that are intermediate between the respective *Miogypsinita* species and their ancestral species in the subgenus *Miogypsina* s.str. In the succession of Italian populations the *Miogypsinita* level of development (which is found in the American species *M. brönnimanni* and *M. mexicana*) was evidently very short between the *Miogypsina* s.str. level and that of *Miolepidocyclina*. In fact it only covers the widely variable populations between *M. socini* and *M. burdigalensis*.

Finally it must be concluded that the rate of nepionic acceleration was more rapid in the *Miolepidocyclina* lineage than in the *Miogypsina* s.str. stock, which furnished the populations of the uppermost *Miogypsina* bearing strata of the hills of Turin.

Stratigraphic conclusions

Regarding the location of the samples on BEETS's geological map (textfig. 4), it becomes apparent that the various species of *Miogypsina* bear a rather constant relation to the succession of stratigraphic units. *M. complanata*, accompanied by *Lepidocyclina*, was found only in the Aquitaniano. Also *M. gunteri* may be restricted to this stage, probably to its uppermost beds. The sandy intercalations of the Langhiano near Tetti Rossi yielded *M. socini*. Otherwise the Langhiano in this region is in marly-calcareous facies without larger Foraminifera, as for instance in the section Superga-Baldissero. *M. ex. interc. socini-burdigalensis* was determined from the beds of the basal Elveziano of both flanks of the

Gàssino anticline. It is followed higher up in the section by *M. burdigalensis*. *M. negrii*, which is still younger, was not found in the southern section, where the beds, equivalent to those with *M. negrii* from Rio Torello, are probably all marls. The youngest species *M. irregularis* (and probably *M. intermedia*) was found again in both sections.

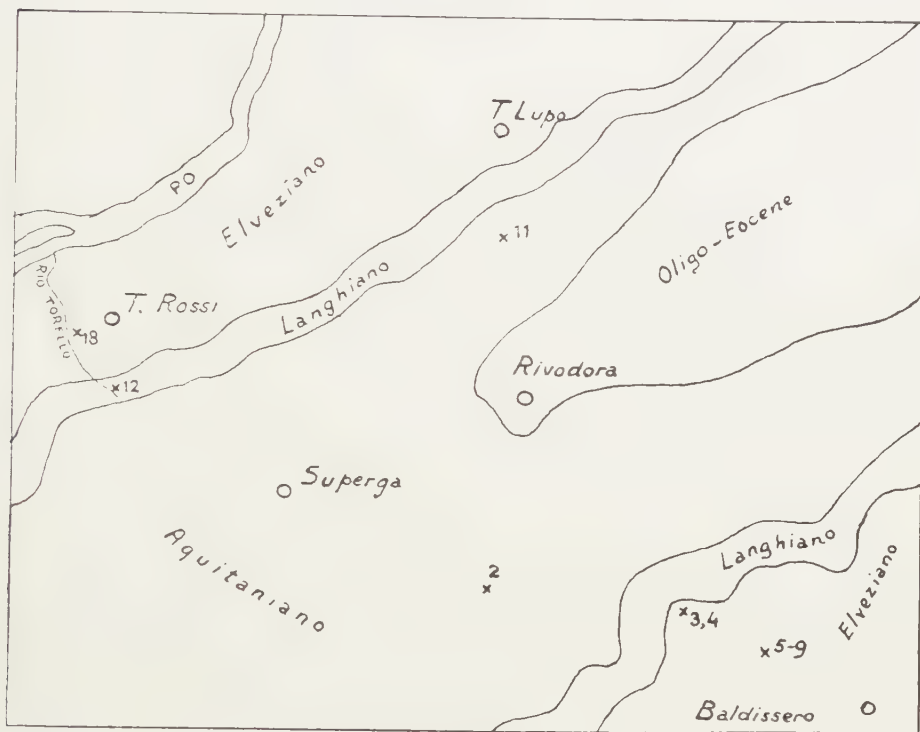


Fig. 4. Location of the samples (except 1 and 10) on the geological map of the Gàssino anticline. Scale 1: 50,500. Drawn after C. BEETS, 1941

The comparison of these data with the sequence of *Miogypsina* species in the region of Bordeaux (still unpublished report) meets with some difficulties. First of all, it appears that comparison by means of stratigraphic intervals between succeeding species is worthless. These intervals are many times wider in the hills of Turin than in the Bordelais. This points to a much more rapid sedimentation near Turin. Furthermore, *M. socini* and *M. negrii* occur only in Italy, whereas *M. tani* was found only in France.

Stratigraphic correlation of both regions by means of the species of the Miogypsinidae is still considered to be possible and reliable, since both successions of species are consistent in general outline. *M. tani* and *M. socini* represent equivalent stages of development, following that of *M. gunteri*. Because of the different directions of development it might be possible that changes did not occur with equal rates in both regions, so that morphologically identical populations would not necessarily be

contemporaneous. Fortunately some exchange of species must have taken place since it is very likely that *M. burdigalensis*, which is an exotic species in the area of Bordeaux, was derived from the Italian stock. So this is a check for the synchronism of the *Mioqypsina* sequences in both regions (see textfig. 5).

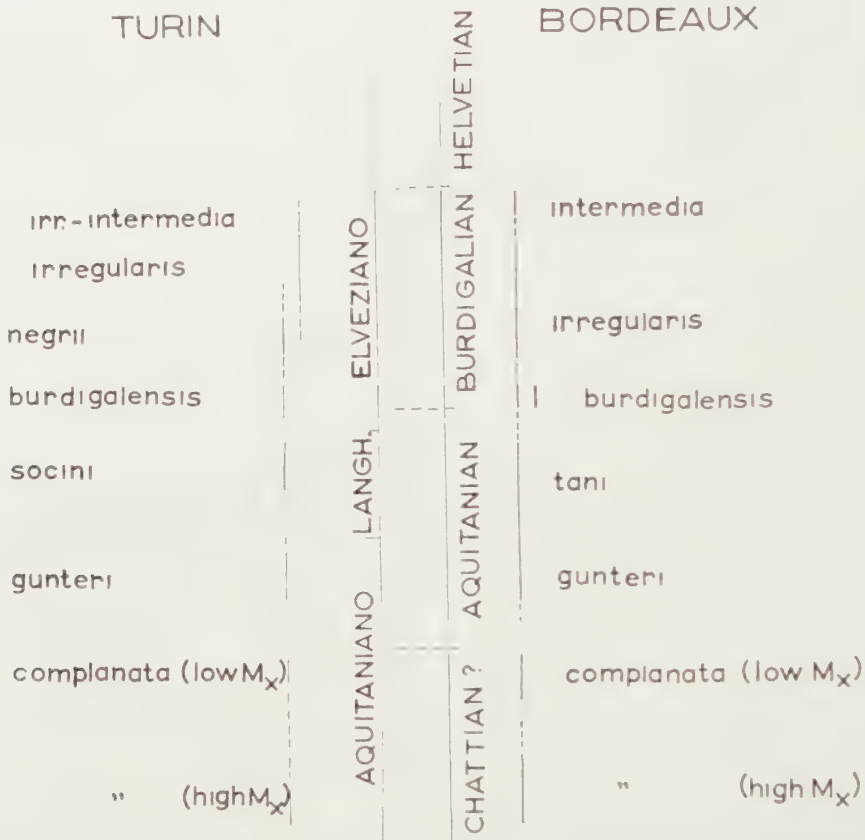


Fig. 5. Diagram showing the correlation of the *Mioqypsina*-bearing beds of the regions of Turin and Bordeaux (Bordelais). Neither the distances between the species nor their ranges are proportional to the corresponding thicknesses of the strata. Moreover, the column of Turin has been greatly reduced as compared to that of Bordeaux as to their absolute total heights. The columns have been arranged in respect to one another in such a way that species of equivalent morphological development of the nepionic stage are at the same horizontal level at most places.

As a result it must be concluded that *M. burdigalensis* could not appear in the basal Burdigalian of Bordeaux, long before it existed in Italy, where it was found well above the base of the Elveziano. So we have to shift the lower limit of the Burdigalian some way up into the Lower Elveziano of northern Italy. *M. irregularis*, that characterizes the Lower-Middle Burdigalian of the Bordelais, arrived from elsewhere in the Italian area after the disappearance of *M. burdigalensis* and probably also *M.*

TABLE 1

Locality	N	$\Pi'_p(X)$		$\Pi'_d(X')$		$\Pi''_p(X'')$		$\Pi''_d(X''')$		$200\alpha/\beta$		Number of		Number of (macrosph.) individuals with position protoconch			γ°		Diameter I (μ)		M_{II}/M_I	Maximal dimensions eq. chambers (μ)	Diameter test (mm)	Thickness test (mm)	Diameter pustules (μ)	Det.
												1	2													
		R	$M + \sigma_M$	R	$M + \sigma_M$	R	$M + \sigma_M$	R	$M + \sigma_M$	R	$M + \sigma_M$			princ. aux. ch.	peri- pheral	inter- mediate	sub- central	R	$M + \sigma_M$	R						
		9	30	7-4	5.7 ± 0.14			1-5	2.4 ± 0.17			15-81	47 ± 2.9	—	30	30	—	—	0-75	24 ± 3.2						
8	6	6-5	5.5 ± 0.22			1-3	2.5 ± 0.34			26-59	48 ± 5.1	—	6	6	—	—	15-45	27 ± 4.6	145-225	176 ± 16.7	1.29	110×160	1.3-2.0	0.5-1.2	45-135	irr.-int.
7	20	8-5	6.1 ± 0.21			1-4	2.3 ± 0.19			14-67	42 ± 3.6	—	20	20	—	—	0-70	33 ± 4.6	110-190	155 ± 4.2	1.33	160×205	1.0-2.8	0.3-1.4	35-110	irr.-int.
6	20	9-5	6.6 ± 0.24			1-4	2.2 ± 0.19			18-67	38 ± 2.6	—	20	20	—	—	5-70	35 ± 4.4	135-225	171 ± 5.8	1.24	150×200	1.0-3.5	0.5-1.3	45-90	irr.
5	30	9-4	6.5 ± 0.19			1-3	1.7 ± 0.12			16-74	38 ± 2.4	—	30	30	—	—	5-60	24 ± 3.3	115-190	149 ± 3.8	1.33	160×225	1.2-2.3	0.4-1.0	25-65	irr.
10	10	8-5	6.7 ± 0.30			1-3	2.2 ± 0.20			19-59	37 ± 4.2	—	10	10	—	—	0-35	13 ± 3.6	135-225	185 ± 9.1	1.10	135×160	1.0-2.5	0.5-1.0	50-150	irr.
18	5	8-5	6.6 ± 0.51	1-3	2.0 ± 0.32	0-4	1.8 ± 0.66	0-3	1.4 ± 0.51	0-50	26 ± 8.1	1	4	5	—	—	-90-+45	- 3 \pm 23.5	150-180	161 ± 5.8	1.28	100×120	1.6-2.3	0.4-1.0	35-130	irr.
17	15	7-4	5.1 ± 0.26	4-7	5.4 ± 0.21	2-4	3.3 ± 0.16	2-5	4.0 ± 0.22	44-89	66 ± 3.4	—	15	—	—	15			170-240	189 ± 4.5	1.17	135×135	1.5-3.0	0.7-1.6	60-240	negrui
16	3	7-6	6.3	7-10	7.7	1-2	1.7	2	2	20-40	29	—	3	—	—	3			130-250	192	1.21	120×135	1.8-3.3	0.9-1.7	50-200	burd.
4	10	11-5	7.8 ± 0.57	2-7	5.7 ± 0.52	0-3	1.5 ± 0.39	0-4	1.4 ± 0.40	0-52	29 ± 5.6	2	8	1	1	8			145-215	170 ± 7.3	1.17	145×145	1.4-2.7	0.4-1.4	25-210	burd.
15	14	13-7	10.1 ± 0.50	2-6	4.4 ± 0.36	0-2	1.1 ± 0.21	0-3	1.3 ± 0.27	0-46	25 ± 4.2	3	11	3	9	2	-125-+10	-47 \pm 9.6	135-190	170 ± 5.1	1.12	120×150	1.8-2.9	0.6-1.5	35-180	soc.-burd.
14	17	11-8	9.6 ± 0.29	3-7	4.9 ± 0.35	0-2	1.0 ± 0.15	0-5	1.7 ± 0.33	0-46	21 ± 3.2	3	14	6	8	3	-90-+40	-27 \pm 8.4	145-240	176 ± 6.7	1.06	130×160	1.2-4.2	0.8-2.0	25-160	soc.-burd.
3	25	12-7	9.1 ± 0.21	2-6	4.3 ± 0.29	0-2	0.7 ± 0.12	0-3	1.0 ± 0.21	0-37	16 ± 2.7	10	15	14	7	4	-90-+45	-28 \pm 8.5	125-250	179 ± 5.6	1.07	120×165	1.0-3.5	0.5-2.7	35-270	soc.-burd.
13	20	12-6	9.1 ± 0.34	1-4	2.5 ± 0.18	0-1	0.6 ± 0.12	0-4	0.9 ± 0.22	0-33	14 ± 2.7	8	12	18	2	—	-110-+10	-51 \pm 8.0	120-180	150 ± 4.0	1.12	135×185	1.2-2.5	0.3-1.5	30-180	socini
12	17	12-7	9.2 ± 0.35	1-5	3.1 ± 0.28	0-2	0.7 ± 0.15	0-2	0.8 ± 0.21	0-44	14 ± 3.3	7	10	15	2	—	-100-0	-51 \pm 8.0	120-190	153 ± 4.8	1.02	135×170	1.0-2.7	0.7-1.3	25-135	socini
11	20	14-7	10.6 ± 0.32			0-3	0.3 ± 0.07			0-69	4 ± 3.7	17	3	20	—	—	-160-+15	-92 \pm 9.8	115-190	149 ± 4.1	0.97	135×180	1.0-2.5	0.4-1.5	45-360	gunteri
2	20	19-9	11.2 ± 0.38									20	—	20	—	—	-160-+60	-81	115-250	181 ± 8.5	1.05	225×270	1.4-3.0	0.4-1.3	35-315	compl.
1	30	24-16	19.9 ± 0.40									30	—	30	—	—	-150-+170	- 1	100-240	148 ± 5.9	1.00	225×270	1.0-2.8	0.5-1.1	?-200	compl.

negrii. This does not necessarily mean that *M. burdigalensis* in France is younger than it is in Italy, which assumption would bring the lower Burdigalian limit still higher in the Elveziano of Italy. It is more likely that *M. irregularis* near Bordeaux was contemporaneous with *M. burdigalensis* and *M. negrii* near Turin.

In both regions *Miogypsina* s.str. reaches about the same level of morphological development: *M. intermedia*. Near Bordeaux this species marks the topmost Burdigalian beds. So the best thing would be to place the Burdigalian-Helvetian boundary in the Italian region directly on top of the uppermost *Miogypsina* bearing beds, so far found. If we place the lower Burdigalian limit in the Turin area directly below the appearance of *M. burdigalensis*, the beds of the Langhiano with *M. socini* would be of Aquitanian age ¹). This is certainly in accordance with the similar level of development of *M. tani* in the Aquitanian of the Bordelais. *M. gunteri* is certainly Aquitanian in France but the stratigraphic placement of *M. complanata* is less certain in this region. As yet, it is thought to be mainly of Chattian age, though it may range into the basal Aquitanian. Anyhow it is considered likely that the lower Aquitanian limit in northern Italy is taken too low, if an about contemporaneous development of the Miogypsinidae in both regions is assumed.

Summarizing, the following conclusions may be given, when the species of *Miogypsina* are taken as the basis for stratigraphic correlation, which basis is considered to be at least as good as the earlier employed methods.

1. It is unlikely that the lithologic units Aquitaniano, Langhiano and Elveziano are synchronous with the Aquitanian, Burdigalian and Helvetian of the Bordelais.

2. A large part of the Aquitaniano is of Chattian age.

3. The upper part of the Aquitaniano, the Langhiano and possibly the lowermost beds of the Elveziano are of Aquitanian age.

4. The lower part of the Elveziano, possibly with the exception of its lowermost strata, is of Burdigalian age, the Helvetian beginning after the disappearance of the Miogypsinidae.

REFERENCES

1. AMICIS, G. A. DE, Osservazioni critiche sopra talune Tinoporinae fossili. Soc. Tosc. Sc. Nat., Tipogr. T. Nistri e C., Pisa (1894).
2. BEETS, C., De geologie van het westelijk deel van het heuvelland van Monferrato tusschen Turijn en Murisengo. Leidsche Geol. Meded., **12**, afl. 1 (also acad. thesis Leiden, 1941).
3. BRÖNNIMANN, P., Über die tertiären Orbitoididen und die Miogypsiniden von Nordwest-Marokko. Schweiz. Pal. Abh., **63** (1940).

¹) The stratigraphic gap between the typical Aquitanian and Burdigalian in the Bordelais is certainly not wide enough to cover a considerable stretch of the sequence of strata of Turin. This gap is too small to have much influence on the above conclusions.

4. DERVIEUX, E., Osservazioni sopra le "Tinoporinae" e descrizione del nuovo genere *Flabelliporus*. Atti R. Acc. Sc. Torino, **29** (1893).
5. ———, Osservazioni alle osservazioni sopra il nuovo genere di Foraminiferi *Miogypsina* Sacco o *Flabelliporus* Dervieux. Riv. Ital. Paleont., **6**, fasc. 3, 147-148 (1900).
6. DOUVILLÉ, ROBERT, and P. L. PREVER, Succession des faunes à *Lépidocyclines* dans le bassin du Piémont. Bull. Soc. géol. France, ser. **4**, **5**, 861-862 (1905).
7. DROOGER, C. W., Notes on some representatives of *Miogypsinella*. Proc. Kon. Ned. Ak. Wetensch., ser. **B**, **54**, 357-365 (1951).
8. ———, Study of American *Miogypsinidae*. Acad. thesis Utrecht (1952).
9. FERRERO, L., Osservazioni sul Miocene medio nei dintorni di S. Mauro Torinese. Boll. Soc. Geol. Ital., Roma, **28**, 131-144 (1909).
10. MICHELOTTI, G., Saggio storico dei Rizopodi caratteristici dei terreni sopracretacei. Mem. Soc. Ital. Sc. Modena, **22** (1841).
11. ———, Description des fossiles des terrains miocènes de l'Italie septentrionale. Natuurk. Verh. Holl. Maatsch. Wetensch. Haarlem, 2e verz., 3e deel (1847).
12. PREVER, P. L., Osservazioni sulla sottofamiglia delle Orbitoidinae. Riv. Ital. Paleont., **10**, fasc. 4, 112-127 (1904).
13. ———, Aperçu géologique sur la colline de Turin. Mém. Soc. géol. France, **4** (1907).
14. ———, La fauna a Nummuliti e ad Orbitoidi dei terreni terziarii dell'Alte Valle dell'Aniene. Mem. Deser. Carta Geol. d'Ital., **5**, 1-257 (1912).
15. SACCO, F., Catalogo Paleontologico del Bacino Terziario del Piemonte. Boll. Soc. Geol. Ital., Roma, **8**, fasc. 3 (1889).
16. ———, Sur quelques Tinoporinae du Miocène de Turin. Bull. Soc. Belge Géol., **7**, procès-verb., 204-207 (1893).
17. ———, Sur les couches à Orbitoides du Piémont. Bull. Soc. géol. France, ser. **4**, **1**, 188 (1901).
18. ———, Sur la valeur stratigraphique des *Lépidocyclina* et des *Miogypsina*. Bull. Soc. géol. France, ser. **4**, **5**, 880-892 (1905).
19. SCHLUMBERGER, C., Note sur le genre *Miogypsina*. Bull. Soc. géol. France, ser. **3**, **28**, 327-333 (1900).

-
- Plate 2. Drawings of the embryonic-nepionic stage in median sections of:
 Figs. 1-5. *Miogypsina irregularis* (MICHELOTTI). Elveziano, loc. 5, Croce Berton.
 Figs. 6, 7. *Miogypsina negrii* (FERRERO). After two specimens of the original collection of *Lépidocyclina negrii* FERRERO from Rio Torello.
 Figs. 8-12. *Miogypsina negrii* (FERRERO). Elveziano, loc. 17, Rio Torello.
 Figs. 13, 14. *Miogypsina burdigalensis* (GÜMBEL). Elveziano, loc. 16, Rio Torello.
 Figs. 15-19. *Miogypsina burdigalensis* (GÜMBEL). Elveziano, loc. 4, between Bric del Pilonetta and Tetti Vigna.
 Figs. 20-24. *Miogypsina socini* n. sp.. Langhiano, loc. 13, Rio Torello.
 Figs. 25-27. *Miogypsina gunteri* COLE. Aquitaniano, loc. 11, Rio Dora.

Enlargement approximately X 30. The apical-frontal line is directed vertically, except in figs 6-19. The drawings are accurate only as to arrangement and relative size of the chambers; stolons and thicknesses of the walls have been neglected.

PLATE II



1



2



3



4



5



6



7



8



9



10



11



12



13



14



15



16



17



18



19



20



21



22



23



24



25



26



27

ON THE BENDING OF CANTILEVER, RECTANGULAR PLATES. I

BY

W. T. KOITER AND J. B. ALBLAS

(Communicated by Prof. C. B. BIEZENO at the meeting of January 30, 1954)

1. *Introduction*

Several approximate solutions of the cantilever plate problem have been obtained in recent years, (a review of many papers is contained in ref. 1), but the accuracy of these approximations is often doubtful. It was therefore considered worthwhile to attempt a more rigorous solution.

The stress distribution in a cantilever plate (fig. 1) with a uniform

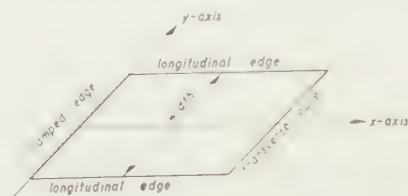


Fig. 1. Nomenclature

distribution of loads over its width may be obtained from the corresponding (simple) primary stress distribution in a plate of infinite width by superposition of the (complicated) secondary stress distribution in the rectangular plate, loaded only by bending moments along its longitudinal edges, these loading bending moments being equal in magnitude and opposite in sign to the bending moments which exist along these lines in the plate of infinite width. If the plate is loaded by a uniformly distributed moment over its transverse free edge, the secondary loading case consists of uniformly distributed bending moments along the longitudinal edges, equal to ν times the primary bending moments along the free transverse edge. In this case the solution may also be obtained by superposition of the stress distribution in the plate, considered as a beam and therefore with uniform anticlastic curvature, and the stress distribution in this plate if the clamped edge is loaded by an equilibrium system of bending moments and shear forces (the other edges being free) such that the anticlastic curvature due to the beam solution is compensated at the clamped edge.

If the load distribution over the width of the plate is non-uniform a similar approach may be used. The stress distribution in a plate of infinite width may be obtained, e.g. by Fourier transforms (ref. 2), and the resulting bending moments and shear forces along the longitudinal edges of the plate of finite width may be compensated by superposition of the stress distribution in the plate, loaded by the opposite of these bending

moments and shear forces along its longitudinal edges. We may return to this more general problem in a later paper.

An important simplification of the problem is achieved if the length of the plate is assumed to be infinite. This assumption of a semi-infinite strip introduces only very small errors if the length of the plate is large compared with its width; even for a *square* plate the inaccuracies in the bending and torsional moments are estimated to be less than 4 percent of the maximum moment occurring in the plate (cf. para. 4.5). Therefore this approximation is entirely justified if the width of the plate does not exceed its length.

Even with the simplification of the semi-infinite strip considerable difficulties were encountered in our attempt to obtain an accurate solution (cf. para. 4.1). These difficulties are undoubtedly due to singularities in the corners of the strip where the clamped edge intersects the free edges. A separate investigation of these singularities was therefore made for the simpler problem of an infinite right-angled wedge plate, one edge of which is rigidly clamped and the other edge free but loaded by a distribution of bending moments. The exact solution of this problem (para. 3) proved very helpful in the ultimate solution of our main problem (para. 4).

2. The basic equations

A point of the middle surface of the semi-infinite strip of width $2b$ is described by its coordinates $\bar{x} > 0$, $|\bar{y}| < b$ and its deflection is denoted by \bar{w} . We introduce non-dimensional coordinates and deflection, defined by

$$x = \bar{x}/b, \quad y = \bar{y}/b, \quad w = \bar{w}/h,$$

where h is the plate thickness, and non-dimensional stress resultants, defined by

$$m_x, m_{xy}, m_y = \frac{12(1-\nu^2)b^2}{E h^4} \bar{m}_x, \bar{m}_{xy}, \bar{m}_y,$$

$$q_x, q_y = \frac{12(1-\nu^2)b^3}{E h^4} \bar{q}_x, \bar{q}_y,$$

where \bar{m}_x , \bar{m}_y are the bending moments, \bar{m}_{xy} is the torsional moment, \bar{q}_x , \bar{q}_y are the shear forces per unit length, E is YOUNG'S modulus and ν is POISSON'S ratio. The deflection w satisfies the biharmonic equation

$$(1) \quad \Delta \Delta w = 0$$

and the (non-dimensional) stress resultants are expressed by (fig. 2)

$$(2) \quad \left\{ \begin{array}{l} m_x = \frac{\partial^2 w}{\partial x^2} + \nu \frac{\partial^2 w}{\partial y^2}, \\ m_y = \frac{\partial^2 w}{\partial y^2} + \nu \frac{\partial^2 w}{\partial x^2}, \\ m_{yx} = m_{xy} = (1-\nu) \frac{\partial^2 w}{\partial x \partial y}, \\ q_x = -\frac{\partial m_x}{\partial x} - \frac{\partial m_{yx}}{\partial y} = -\frac{\partial^3 w}{\partial x^3} - \frac{\partial^3 w}{\partial x \partial y^2}, \\ q_y = -\frac{\partial m_{xy}}{\partial x} - \frac{\partial m_y}{\partial y} = -\frac{\partial^3 w}{\partial x^2 \partial y} - \frac{\partial^3 w}{\partial y^3}. \end{array} \right.$$

The *reduced* shear forces are given by

$$(3) \quad \begin{cases} q_{xr} = q_x - \frac{\partial m_{xy}}{\partial y} = -\frac{\partial^3 w}{\partial x^3} - (2-\nu) \frac{\partial^3 w}{\partial x \partial y^2}, \\ q_{yr} = q_y - \frac{\partial m_{yx}}{\partial x} = -\frac{\partial^3 w}{\partial y^3} - (2-\nu) \frac{\partial^3 w}{\partial x^2 \partial y}. \end{cases}$$

We first consider the strip with a uniform loading over its width. Considered as a part of a plate of infinite width with the same uniform

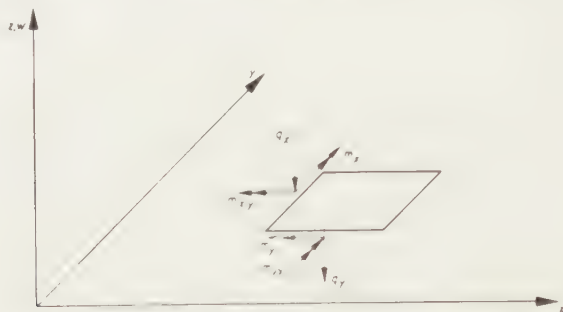


Fig. 2. Definition of stress resultants

loading the primary bending moments $m_{yp} = \nu m_{xp}$ are independent of y and the primary torsional moment m_{xyp} vanishes. In order to obtain the solution for the strip of finite width we have to superimpose the secondary solution of the plate equation (1) with the boundary conditions along $x=0$

$$(4) \quad w = 0, \quad \frac{\partial w}{\partial x} = 0$$

and along the edges $|y|=1$

$$(5) \quad \begin{cases} m_y = \frac{\partial^2 w}{\partial y^2} + \nu \frac{\partial^2 w}{\partial x^2} = -m_{yp} = -\nu m_{xp} \\ q_{yr} = -\frac{\partial^3 w}{\partial y^3} - (2-\nu) \frac{\partial^3 w}{\partial x^2 \partial y} = 0. \end{cases}$$

If the primary bending moments are independent of x as well (pure bending of the plate of infinite width) the solution may also be obtained from the beam solution $m_x = \text{const.}$, $m_y = 0$ by superposition of the solution of the plate equation (1) with the boundary conditions along $x=0$

$$(6) \quad w = \frac{1}{2} \frac{\nu y^2}{1-\nu^2} m_{xp}, \quad \frac{\partial w}{\partial x} = 0,$$

and along the edges $|y|=1$

$$(7) \quad \begin{cases} m_y = \frac{\partial^2 w}{\partial y^2} + \nu \frac{\partial^2 w}{\partial x^2} = 0, \\ q_{yr} = -\frac{\partial^3 w}{\partial y^3} - (2-\nu) \frac{\partial^3 w}{\partial x^2 \partial y} = 0. \end{cases}$$

The prescribed parabolic deflection along $x=0$ compensates the local anticlastic curvature due to the beam solution.

In the rectangular wedge plate the x -axis is chosen along the free edge

and the y -axis along the clamped edge. Any suitable length is chosen as the unit b for the nondimensional coordinates. The secondary deflection has to satisfy the plate equation (1) for $x > 0$ and $y > 0$ and the boundary conditions along $x = 0$

$$(8) \quad w = 0, \quad \frac{\partial w}{\partial x} = 0,$$

and along $y = 0$

$$(9) \quad \begin{cases} m_y = \frac{\partial^2 w}{\partial y^2} + \nu \frac{\partial^2 w}{\partial x^2} = m_{y0}(x) = -\nu m_{xp}(x), \\ q_{yr} = -\frac{\partial^3 w}{\partial y^3} - (2 - \nu) \frac{\partial^3 w}{\partial x^2 \partial y} = 0, \end{cases}$$

where $m_{y0} = -m_{yp}$ is the loading moment.

3. The rectangular wedge plate

3.1 Formal solution

The plate equation (1) with the boundary conditions (8) and (9) can be solved formally by means of Fourier transforms.¹⁾ Introducing the Fourier sine transform for the deflection

$$(10) \quad W(\lambda, y) = \int_0^\infty w(x, y) \sin \lambda x \, dx,$$

using the boundary condition $w = 0$ at $x = 0$ and assuming that w and its derivatives vanish at infinity, the biharmonic equation (1) is transformed into the ordinary differential equation (cf. ref. 6, p. 27)

$$(11) \quad \frac{d^4 W}{dy^4} - 2\lambda^2 \frac{d^2 W}{dy^2} + \lambda^4 W = -\lambda p(y),$$

where

$$(12) \quad p(y) = \left(\frac{\partial^2 w}{\partial x^2} \right)_{x=0}.$$

The boundary conditions (9) at $y = 0$ are transformed into

$$(13) \quad \frac{d^2 W}{dy^2} - \nu \lambda^2 W = M_y(\lambda),$$

$$(14) \quad \frac{d^3 W}{dy^3} - (2 - \nu) \lambda^2 \frac{dW}{dy} = 0,$$

where

$$(15) \quad M_y(\lambda) = \int_0^\infty m_{y0}(x) \sin \lambda x \, dx$$

¹⁾ A simpler and more direct solution has been obtained by means of the Mellin transform by one of the authors, and independently by WOJNOSKY-KRIEGER for a similar problem (ref. 4,5), but the solution by means of Fourier transforms is preferred here because a similar method of solution will be applied to the strip problem.

is the Fourier sine transform of the loading bending moment along the x -axis. It should be observed that the auxiliary function $p(y)$ is as yet unknown.

Introducing the Fourier cosine transform

$$(16) \quad \overline{W}(\lambda, \mu) = \int_0^{\infty} W(\lambda, y) \cos \mu y \, dy$$

the ordinary differential equation (11) is transformed into

$$(17) \quad (\lambda^2 + \mu^2)^2 \overline{W} = -\lambda \bar{p}(\mu) - (\mu^2 + \nu \lambda^2) q(\lambda),$$

where

$$(18) \quad \bar{p}(\mu) = \int_0^{\infty} p(y) \cos \mu y \, dy,$$

$$(19) \quad q(\lambda) = \left(\frac{dW}{dy} \right)_{y=0},$$

and the boundary condition (14) has been used to eliminate $(d^3 W / dy^3)_{y=0}$. It may be noted that $q(\lambda)$ is a second auxiliary unknown function.

Formally applying the Fourier cosine inversion formula

$$(20) \quad W(\lambda, y) = \frac{2}{\pi} \int_0^{\infty} \overline{W}(\lambda, \mu) \cos \mu y \, d\mu,$$

we obtain

$$(21) \quad \begin{cases} W(\lambda, y) = -\frac{2}{\pi} \int_0^{\infty} \frac{\lambda}{(\lambda^2 + \mu^2)^2} \bar{p}(\mu) \cos \mu y \, d\mu + \\ \quad - \frac{1}{2} q(\lambda) e^{-\lambda y} \left[\frac{1+\nu}{\lambda} - (1-\nu) y \right], \end{cases}$$

where the well-known formulae

$$(22) \quad \int_0^{\infty} \frac{1}{(\lambda^2 + \mu^2)} \cos \mu y \, d\mu = \frac{\pi}{2\lambda} e^{-\lambda y}$$

$$(23) \quad \int_0^{\infty} \frac{1}{(\lambda^2 + \mu^2)^2} \cos \mu y \, d\mu = \frac{\pi}{4\lambda^3} e^{-\lambda y} \left(\frac{1}{\lambda} + y \right)$$

have been used. Applying the Fourier sine inversion formula

$$(24) \quad w(x, y) = \frac{2}{\pi} \int_0^{\infty} W(\lambda, y) \sin \lambda x \, d\lambda,$$

where $W(\lambda, y)$ is given by (21), and interchanging the order of integration, we obtain

$$(25) \quad \begin{cases} w(x, y) = -\frac{1}{\pi} x \int_0^{\infty} \frac{\bar{p}(\mu)}{\mu} e^{-\mu x} \cos \mu y \, d\mu + \\ \quad - \frac{1}{\pi} \int_0^{\infty} q(\lambda) e^{-\lambda y} \left[\frac{1+\nu}{\lambda} - (1-\nu) y \right] \sin \lambda x \, d\lambda, \end{cases}$$

where the well-known formula

$$(26) \quad \int_0^{\infty} \frac{\lambda}{(\lambda^2 + \mu^2)^2} \sin \lambda x \, d\lambda = \frac{\pi}{4\mu} x e^{-\mu x}$$

has been used.

On the assumption that the integrals in (25) converge, differentiations with respect to x and y may be performed under the integral sign for $x > 0$ and $y > 0$, and it is easily verified that our solution satisfies the biharmonic equation and the boundary conditions $w=0$ along $x=0$ and $q_{,y}=0$ along $y=0$. The unknown functions $\bar{p}(\mu)$ and $q(\lambda)$ are now determined by the requirement that the other two boundary conditions must also be satisfied. From (25) the derivative $\partial w / \partial x$ is obtained

$$\begin{aligned} \frac{\partial w}{\partial x} = & -\frac{1}{\pi} \int_0^{\infty} \frac{\bar{p}(\mu)}{\mu} e^{-\mu x} \cos \mu y \, d\mu + \frac{1}{\pi} x \int_0^{\infty} \bar{p}(\mu) e^{-\mu x} \cos \mu y \, d\mu + \\ & -\frac{1}{\pi} \int_0^{\infty} q(\lambda) e^{-\lambda y} [1 + \nu - (1 - \nu) \lambda y] \cos \lambda x \, d\lambda; \end{aligned}$$

writing the third integral as a Fourier cosine integral with respect to y (using the formulae (22) and (23)), the slope at $x=0$ is found to be

$$(27) \quad \left(\frac{\partial w}{\partial x} \right)_{x=0} = -\frac{1}{\pi} \int_0^{\infty} \left\{ \frac{\bar{p}(\mu)}{\mu} + \frac{4}{\pi} \int_0^{\infty} q(\lambda) \frac{\nu \lambda^2 + \mu^2}{(\lambda^2 + \mu^2)^2} \lambda d\lambda \right\} \cos \mu y \, d\mu,$$

The second boundary condition (8) now requires

$$(28) \quad \frac{\bar{p}(\mu)}{\mu} = -\frac{4}{\pi} \int_0^{\infty} q(\lambda) \frac{\nu \lambda^2 + \mu^2}{(\lambda^2 + \mu^2)^2} \lambda d\lambda.$$

The only remaining condition for the edge moment m_y along $y=0$ is applied to its Fourier transform (13). Substitution of (21) in (13) yields the equation

$$(29) \quad \frac{2}{\pi} \int_0^{\infty} \frac{\nu \lambda^2 + \mu^2}{(\lambda^2 + \mu^2)^2} \bar{p}(\mu) \, d\mu - \frac{1}{2} (3 + \nu) (1 - \nu) q(\lambda) = \frac{M_y(\lambda)}{\lambda}.$$

One of the unknown functions $\bar{p}(\mu)$ or $q(\lambda)$ may be eliminated from the simultaneous integral equations (28) and (29) but it is more convenient to solve the simultaneous equations directly by means of the Mellin transformation (ref. 7, p. 304).²⁾ Introducing the Mellin transforms

$$(30) \quad P(s) = \int_0^{\infty} \frac{\bar{p}(\mu)}{\mu} \mu^{s-1} \, d\mu,$$

$$(31) \quad Q(s) = \int_0^{\infty} q(\lambda) \lambda^{s-1} \, d\lambda,$$

$$(32) \quad \bar{M}(s) = \int_0^{\infty} \frac{M_y(\lambda)}{\lambda} \lambda^{s-1} \, d\lambda,$$

²⁾ The fact that we need Mellin transforms in the solution of our integral

we multiply (28) by μ^{s-1} and (29) by λ^{s-1} and integrate over the range $(0, \infty)$ and obtain

$$(33) \quad P(s) = -\frac{4}{\pi} \int_0^\infty \mu^{s-1} d\mu \int_0^\infty q(\lambda) \frac{\nu\lambda^2 + \mu^2}{(\lambda^2 + \mu^2)^2} \lambda d\lambda,$$

$$(34) \quad \frac{2}{\pi} \int_0^\infty \lambda^{s-1} d\lambda \int_0^\infty \frac{\nu\lambda^2 + \mu^2}{(\lambda^2 + \mu^2)^2} \bar{p}(\mu) d\mu - \frac{1}{2} (3 + \nu) (1 - \nu) Q(s) = \overline{M}(s).$$

Changing the order of integration and using the well-known formulae (ref. 6, p. 527)

$$K_1(s) = \int_0^\infty \frac{x^{s-1}}{x^2 + 1} dx = \frac{\pi}{2 \sin(\pi s/2)},$$

$$K_2(s) = \int_0^\infty \frac{x^{s-1}}{(x^2 + 1)^2} dx = \frac{\pi(1 - \frac{1}{2}s)}{2 \sin(\pi s/2)},$$

valid if $0 < \operatorname{Re}(s) < 2$, we obtain from equation (33)

$$(35) \quad \left\{ \begin{aligned} P(s) &= -\frac{4}{\pi} \int_0^\infty q(\lambda) \lambda^{s-1} d\lambda \int_0^\infty \mu^{s-1} \lambda^{2-s} \frac{\nu\lambda^2 + \mu^2}{(\lambda^2 + \mu^2)^2} d\mu = \\ &= -\frac{4}{\pi} \int_0^\infty q(\lambda) \lambda^{s-1} d\lambda \int_0^\infty \left(\frac{\mu}{\lambda}\right)^{s-1} \frac{\nu + (\mu/\lambda)^2}{[1 + (\mu/\lambda)^2]^2} d\left(\frac{\mu}{\lambda}\right) = \\ &= -\frac{4}{\pi} Q(s) [K_1(s) - (1 - \nu) K_2(s)], \end{aligned} \right.$$

and in a similar way from eq. (34)

$$(36) \quad \frac{2}{\pi} P(s) [\nu K_1(s) + (1 - \nu) K_2(s)] - \frac{1}{2} (3 + \nu) (1 - \nu) Q(s) = \overline{M}(s).$$

The solution of these linear algebraic equations for $P(s)$ and $Q(s)$ is

$$(37) \quad P(s) = \frac{\overline{M}(s)}{N(s)} \left[\frac{1}{2} (1 - \nu) s + \nu \right] \sin \frac{\pi}{2} s$$

$$(38) \quad Q(s) = -\frac{\overline{M}(s)}{N(s)} \frac{1}{2} \sin^2 \frac{\pi}{2} s,$$

where the denominator $N(s)$ is given by

$$(39) \quad \left\{ \begin{aligned} N(s) &= \frac{1}{4} (3 + \nu) (1 - \nu) \sin^2 \frac{\pi}{2} s - \frac{1}{4} [(1 - \nu)s + 2\nu] [(1 - \nu)s - 2] \\ &= \frac{1}{8} \{ (3 + \nu) (1 - \nu) \cos \pi(s - 1) - 2(1 - \nu)^2 (s - 1)^2 + 5 + 2\nu + \nu^2 \}. \end{aligned} \right.$$

Our auxiliary unknown functions $\bar{p}(\mu)$ and $q(\lambda)$ are now obtained by the Mellin inversion formula (ref. 7, p. 7)

equations confirms the view that a *direct* application of the Mellin transformation to biharmonic problems is more appropriate for a wedge-shaped region than Fourier transforms (cf. footnote 1).

$$(40) \quad \left\{ \begin{aligned} \frac{\bar{p}(\mu)}{\mu} &= \frac{1}{2\pi i} \int_{c-i\infty}^{c+i\infty} P(s) \mu^{-s} ds = \\ &= \frac{1}{2\pi i} \int_{c-i\infty}^{c+i\infty} \frac{\bar{M}(s)}{N(s)} \left[\frac{1}{2} (1-\nu) s + \nu \right] \sin \frac{\pi}{2} s \cdot \mu^{-s} ds, \end{aligned} \right.$$

$$(41) \quad \left\{ \begin{aligned} q(\lambda) &= \frac{1}{2\pi i} \int_{c-i\infty}^{c+i\infty} Q(s) \lambda^{-s} ds = \\ &= \frac{1}{2\pi i} \int_{c-i\infty}^{c+i\infty} -\frac{\bar{M}(s)}{N(s)} \frac{1}{2} \sin^2 \frac{\pi}{2} s \cdot \lambda^{-s} ds, \end{aligned} \right.$$

where c is a real number ($0 < c < 2$).

The loading bending moment $m_{y0} = -vm_{xp}$ enters our solution in the expression

$$\bar{M}(s) = \int_0^\infty \lambda^{s-2} M_y(\lambda) d\lambda = \int_0^\infty \lambda^{s-2} d\lambda \int_0^\infty m_{y0}(x) \sin \lambda x dx.$$

Changing the order of integration and using the well-known relation (ref. 8, p. 260)

$$(42) \quad \int_0^\infty \lambda^{s-2} \sin \lambda x dx = \Gamma(s-1) \sin \frac{\pi}{2} (s-1) \cdot x^{1-s},$$

valid for $0 < \text{Re}(s) < 2$, we obtain

$$(43) \quad \bar{M}(s) = \Gamma(s-1) \sin \frac{\pi}{2} (s-1) \cdot \phi(s),$$

where

$$(44) \quad \phi(s) = \int_0^\infty x^{1-s} m_{y0}(x) dx.$$

Our formal solution has now been expressed in a rather awkward form, viz. as a sum of repeated infinite integrals, obtained by substitution of (40) and (41) in (25). However, if we change the order of integration we can evaluate the inner integrals with respect to μ and λ and our result is simplified to a single complex integral, which may be evaluated by means of the theory of residues. The inner integrals with respect to μ and λ are of the type (ref. 8, p. 260)

$$(45) \quad \int_0^\infty \mu^{-s} e^{-\mu x} \cos \mu y d\mu = r^{s-1} \Gamma(1-s) \cos \left(\frac{\pi}{2} - \theta \right) (1-s), \quad \text{Re}(s) < 1,$$

$$(46) \quad \int_0^\infty \lambda^{-s} e^{-\lambda y} \sin \lambda x d\lambda = r^{s-1} \Gamma(1-s) \sin \theta s, \quad \text{Re}(s) < 2,$$

where

$$(47) \quad r = \sqrt{x^2 + y^2}, \quad \theta = \text{tg}^{-1} \frac{y}{x}.$$

After a somewhat tedious reduction, using the well-known properties of the gamma function

$$\Gamma(z+1) = z\Gamma(z), \quad \Gamma(z)\Gamma(1-z) = \frac{\pi}{\sin \pi z},$$

the formal solution for the deflection is finally obtained in the form

$$(48) \quad \left\{ w = \frac{1}{2\pi i} \int_{c-i\infty}^{c+i\infty} \frac{\phi(s)}{8N(s)} r^s \frac{1}{s-1} \left\{ [(1-\nu)s+2\nu] \cos \frac{\pi}{2} s [\cos s\theta - \cos(2-s)\theta] + \right. \right. \\ \left. \left. + [(1-\nu)s+1+\nu] \sin \frac{\pi}{2} s \left[\frac{s-2}{s} \sin s\theta + \sin(2-s)\theta \right] \right\} ds, \right.$$

where $N(s)$ and $\phi(s)$ are given by (39) and (44).

(to be continued)

REFERENCES

1. WILLIAMS, M. L., A review of certain analysis methods for swept-wing structures. Journ. Aeron. Sci., **19**, 615 (1952).
2. JARAMILLO, T. J., Deflections and moments due to a concentrated load on a cantilever plate of infinite length. Journ. of Appl. Mech., **17**, 67 (1950).
3. WILLIAMS, M. L., Surface stress singularities resulting from various boundary conditions in angular corners of plates under bending. Proc. First U.S. Nat. Congr. Appl. Mech. 325 (1951).
4. WOINOWSKY-KRIEGER, S., Ueber die Anwendung der Mellin-Transformation zur Lösung einer Aufgabe der Plattenbiegung. Ing. Arch., **20**, 391 (1952).
5. KOITER, W. T., Einige ergänzende Bemerkungen zum Aufsatz des Herrn WOINOWSKY-KRIEGER. Ing. Arch., **21**, 381 (1953).
6. SNEDDON, I. N., Fourier transforms. (Mc Graw-Hill, New York, 1951).
7. TITCHMARSH, E. C., Introduction to the theory of Fourier integrals. (Oxford University Press, Oxford, 1937).
8. WHITTAKER, E. T., and G. N. WATSON, A course of modern analysis. (4th ed., Cambridge University Press, Cambridge, 1927).

ON THE BENDING OF CANTILEVER RECTANGULAR PLATES. II*)

BY

W. T. KOITER AND J. B. ALBLAS

(Communicated by Prof. C. B. BIEZENO at the meeting of January 30, 1954)

3.2. Verification of formal solution

The expression (48) is easily recognized as a Mellin integral; it agrees completely with the solution obtained by a direct application of the Mellin transformation to our problem in polar coordinates.

In order to verify our formal solution we impose suitable restrictions on our loading bending moment $m_{y0}(x)$.

We require that the integral

$$(49) \quad \int_0^{\infty} x^{1-c} m_{y0}(x) dx$$

is absolutely convergent for all values of c in an arbitrarily narrow range $c_1 < c < c_2$, where $c_1 > 0$ and $c_2 < 2$. On this assumption the integrand of (48) is regular in the strip $c_1 < \operatorname{Re}(s) < c_2$ because $N(s)$ has no zeros in the strip $0 < \operatorname{Re}(s) < 2$, whereas for large values of $|s|$ in this strip the integrand approaches to zero exponentially for $\theta < \pi/2$. Therefore the integral (48) is convergent for $0 \leq \theta < \pi/2$. Moreover in this region its derivatives of any order with respect to r and θ may be obtained by differentiation under the integral. The biharmonic equation in polar coordinates reads

$$(50) \quad \left(\frac{\partial^2}{\partial r^2} + \frac{1}{r} \frac{\partial}{\partial r} + \frac{1}{r^2} \frac{\partial^2}{\partial \theta^2} \right)^2 w = 0$$

and it is easily verified that (48) satisfies this equation. It is also easily seen that our solution satisfies the boundary conditions (8) along the clamped edge $x=0$ or $\theta=0$.

The stress resultants are also described most conveniently in polar coordinates (fig. 3). The bending moment m_y along the free edge is obtained from the tangential bending moment m_t for $\theta = \pi/2$. Substituting (48) in the formula for the non-dimensional tangential bending moment (ref. 9, p. 259)

$$(51) \quad m_t = \frac{1}{r} \frac{\partial w}{\partial r} + \frac{1}{r^2} \frac{\partial^2 w}{\partial \theta^2} + \nu \frac{\partial^2 w}{\partial r^2},$$

and taking the limit for $\theta \rightarrow \pi/2$, we obtain the bending moment along the free edge

$$(52) \quad (m_y)_{y=0} = (m_t)_{\theta=\pi/2} = \frac{1}{2\pi i} \int_{c-i\infty}^{c+i\infty} \phi(s) r^{s-2} ds.$$

*) See the first communication in these Proceedings, B57, 250—258 (1954).

Observing that $\phi(s)$ is expressed in the loading bending moment m_{y0} by means of the Mellin integral (44) and remembering our assumption on the absolute convergence of (49), it is easily seen that (52) represents the

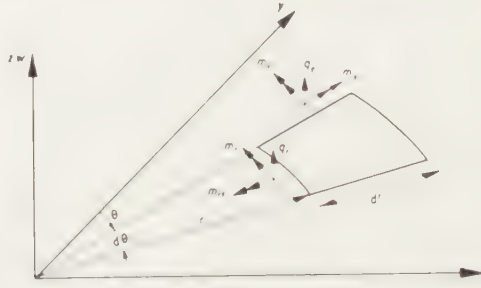


Fig. 3. Non-dimensional stress resultants in polar coördinates

inverse Mellin transform of $\phi(s)$ (ref. 10, p. 88), i.e. the prescribed loading bending moment m_{y0} .

The reduced shear force q_{yr} along the free edge is also obtained from the tangential reduced shear force (ref. 9, p. 259)

$$(53) \quad q_{tr} = \frac{1}{r^3} \frac{\partial^3 w}{\partial \theta^3} + 2(1-\nu) \frac{1}{r^3} \frac{\partial w}{\partial \theta} - (1-2\nu) \frac{1}{r^2} \frac{\partial^2 w}{\partial r \partial \theta} + (2-\nu) \frac{1}{r} \frac{\partial^3 w}{\partial r^2 \partial \theta}.$$

Substituting (48) and taking the limit for $\theta \rightarrow \pi/2$, a rather laborious but straightforward calculation shows that the reduced shear force indeed vanishes along the free edge. Our formal solution is therefore completely verified.

3.3. The stress resultants

The bending moment and the reduced shear force along the clamped edge are calculated from our solution in polar coordinates

$$(m_x)_{x=0} = (m_t)_{\theta=0}, \quad (q_{xr})_{x=0} = -(q_{tr})_{\theta=0}.$$

Substituting (48) into (51) and (53) and putting $\theta = 0$ and therefore $r = y$, we obtain

$$(54) \quad (m_x)_{x=0} = -\frac{1}{4\pi i} \int_{c-i\infty}^{c+i\infty} \frac{\phi(s)}{N(s)} y^{s-2} [(1-\nu)s + 2\nu] \cos \frac{\pi}{2} s ds,$$

$$(55) \quad (q_{xr})_{x=0} = \frac{1}{4\pi i} \int_{c-i\infty}^{c+i\infty} \frac{\phi(s)}{N(s)} y^{s-3} (s-2) [(1-\nu)s + (1+\nu)] \sin \frac{\pi}{2} s ds.$$

The torsional moment along the free edge is given by

$$(m_{yx})_{y=0} = -(m_{tr})_{\theta=\pi/2}.$$

Introducing (48) into the formula (ref. 9, p. 259)

$$m_{tr} = (1-\nu) \left(\frac{1}{r} \frac{\partial^2 w}{\partial r \partial \theta} - \frac{1}{r^2} \frac{\partial w}{\partial \theta} \right),$$

taking the limit $\theta \rightarrow \pi/2$ and therefore $r=x$, we obtain

$$(56) \quad (m_{yx})_{y=0} = \frac{1-\nu}{8\pi i} \int_{c-i\infty}^{c+i\infty} \frac{\phi(s)}{N(s)} x^{s-2} \sin \pi s \, ds.$$

In order to evaluate the stress resultants (54), (55) and (56) we must now assume some distribution of our (secondary) loading bending moment m_{y0} . We take $m_{y0} = -\nu$ for $0 < x < 1$ and zero for $x > 1$. This assumption corresponds with a *primary* bending moment distribution in the plate of infinite width $m_{xp} = 1$, $m_{yp} = \nu$ for $0 < x < 1$ and bending moments zero for $x > 1$ (see para. 2), i.e. loading by an external bending moment of intensity 1 per unit width of the plate along the line $x=1$. The Mellin transform of m_{y0} is

$$(57) \quad \phi(s) = \int_0^\infty x^{1-s} m_{y0} \, dx = \int_0^1 -\nu x^{1-s} \, dx = \frac{\nu}{s-2}.$$

Upon introduction of (57) into (54), (55) and (56) the stress resultants may be evaluated by means of the calculus of residues. The poles of the integrands in (55) and (56) are the zeros of $N(s)$, whereas the integrand of (54) has the additional pole $s=2$. The equation $N(s)=0$ is written

$$(58) \quad \cos \pi(s-1) = 2 \frac{1-\nu}{3+\nu} (s-1)^2 - \frac{5+2\nu+\nu^2}{(3+\nu)(1-\nu)}.$$

The zeros of $N(s)$ are distributed symmetrically with respect to the real axis and also with respect to the line $\text{Re}(s)=1$. Taking $\nu=\frac{1}{4}$ we have calculated the two real zeros

$$(59) \quad s = 1 \pm 2.3870$$

and the first seven sets of complex zeros

$$(60) \quad \left\{ \begin{array}{l} s = 1 \pm 1.0799 \pm 0.3951 \, i, \\ s = 1 \pm 3.8231 \pm 0.7276 \, i, \\ s = 1 \pm 5.8673 \pm 1.0672 \, i, \\ s = 1 \pm 7.8897 \pm 1.2734 \, i, \\ s = 1 \pm 9.9043 \pm 1.4253 \, i, \\ s = 1 \pm 11.9146 \pm 1.5466 \, i, \\ s = 1 \pm 13.9231 \pm 1.6476 \, i, \end{array} \right.$$

For $k > 7$ the zeros of the k th set are approximated by the asymptotic formula

$$(61) \quad s = 1 \pm \left[2k - \frac{2}{k\pi^2} \ln 4k \right] \sqrt{\frac{1-\nu}{3+\nu}} \pm \frac{2i}{\pi} \ln 4k \sqrt{\frac{1-\nu}{3+\nu}}$$

The accuracy of this asymptotic formula may be assessed from its application to $k=7$, giving the approximation $s = 1 \pm 13.925 \pm 1.655 \, i$, in good agreement with the correct values.

In order to apply the theorem of residues the line-integrals (54), (55)

and (56) are replaced by contour integrals, the contour consisting of the line $\text{Re}(s)=c$ and part of the circle $|s|=R$, where $R \rightarrow \infty$. For $y < 1$ in (54) and (55), $x < 1$ in (56), the part of the circle in the half-plane $\text{Re}(s) > c$ is used and for $y > 1$ in (54) and (55) and $x > 1$ in (56), the part of the circle in the half-plane $\text{Re}(s) < c$. In this way the integral over the part of the circle under consideration tends to zero for $R \rightarrow \infty$ and our line-integral may be replaced by $-2\pi i$ times the sum of the residues in the poles in the halfplane $\text{Re}(s) > c$ for $y < 1$ or $x < 1$, and by $+2\pi i$ times the sum of the residues in the poles in the half-plane $\text{Re}(s) < c$ for $y > 1$ or $x > 1$.

The resulting formulae for the root bending moment are

$$(62) \quad (m_x)_{x=0} = -1 + \frac{\nu}{2} \sum_n^{\text{Re}(s_n) > 2} \frac{[(1-\nu)s_n + 2\nu] \cos(\pi/2)s_n}{(s_n - 2) N'(s_n)} y^{s_n - 2} \text{ for } y < 1,$$

$$(63) \quad (m_x)_{x=0} = -\frac{\nu}{2} \sum_n^{\text{Re}(s_n) < 0} \frac{[(1-\nu)s_n + 2\nu] \cos(\pi/2)s_n}{(s_n - 2) N'(s_n)} y^{s_n - 2} \text{ for } y > 1,$$

where

$$(64) \quad N'(s_n) = -\left[\frac{\pi}{8} (3 + \nu) (1 - \nu) \sin \pi (s_n - 1) + \frac{1}{2} (1 - \nu)^2 (s_n - 1) \right]$$

is the derivative of (39) with respect to s at the pole s_n . The corresponding formulae for the reduced shear force along the clamped edge are

$$(65) \quad (q_{xr})_{x=0} = \frac{\nu}{2} \sum_n^{\text{Re}(s_n) > 2} \frac{[(1-\nu)s_n + 1 + \nu] \sin(\pi/2)s_n}{N'(s_n)} y^{s_n - 3} \text{ for } y < 1,$$

$$(66) \quad (q_{xr})_{x=0} = -\frac{\nu}{2} \sum_n^{\text{Re}(s_n) < 0} \frac{[(1-\nu)s_n + 1 + \nu] \sin(\pi/2)s_n}{N'(s_n)} y^{s_n - 3} \text{ for } y > 1.$$

Similar formulae are obtained for the torsional moment along the free edge

$$(67) \quad (m_{yx})_{y=0} = -\frac{1}{4} \nu (1 - \nu) \sum_n^{\text{Re}(s_n) > 2} \frac{\sin \pi s_n}{(s_n - 2) N'(s_n)} x^{s_n - 2} \text{ for } x < 1,$$

$$(68) \quad (m_{yx})_{y=0} = \frac{1}{4} \nu (1 - \nu) \sum_n^{\text{Re}(s_n) < 0} \frac{\sin \pi s_n}{(s_n - 2) N'(s_n)} x^{s_n - 2} \text{ for } x > 1.$$

Except in the neighbourhood of $y = 1$ and $x = 1$ respectively, the series (62)–(68) converge rapidly. Even in $y = 1$ the series (62), (63), (65) and (66) appear to be convergent but the series (67) and (68) for the torsional moment along the free edge are divergent in $x = 1$. This corresponds with the logarithmic singularity of the integral (56) at $x = 1$, which is due to the discontinuity in the loading bending moment m_{y0} at this point.

In order to evaluate the torsional moment along the free edge in the

neighbourhood of $x=1$, we rewrite eq. (56) in the form

$$(69) \quad \left\{ \begin{aligned} (m_{yx})_{y=0} &= \frac{-2\nu}{3+\nu} \frac{1}{2\pi i} \int_{c-i\infty}^{c+i\infty} \frac{\operatorname{tg} \pi s}{s-2} x^{s-2} ds + \\ &+ \frac{\nu}{4(3+\nu)} \frac{1}{2\pi i} \int_{c-i\infty}^{c+i\infty} \frac{\operatorname{tg} \pi s}{(s-2)N(s)} [5 + 2\nu + \nu^2 - 2(1-\nu)^2(s-1)^2] x^{s-2} ds. \end{aligned} \right.$$

It should be observed that in this form poles at $s=\frac{1}{2}$ and $s=\frac{3}{2}$ have been introduced in the strip $0 < \operatorname{Re}(s) < 2$. Therefore both integrals must be evaluated along the same line $\operatorname{Re}(s)=c$, where $c \neq \frac{1}{2}, \frac{3}{2}$.

We choose $c=1$.

The first integral in (69) can be obtained in closed form by means of the calculus of residues and summing of the resulting series:

$$(70) \quad \left\{ \begin{aligned} \frac{1}{2\pi i} \int_{1-i\infty}^{1+i\infty} \frac{\operatorname{tg} \pi s}{s-2} x^{s-2} ds &= \frac{2}{\pi} \sum_{k=1}^{\infty} \frac{1}{2k+1} x^{-(2k+1)/(2)} = \\ &= \frac{1}{\pi} \left[-\frac{2}{\sqrt{x}} + \ln \frac{\sqrt{x}+1}{\sqrt{x}-1} \right] \text{ for } x > 1, \end{aligned} \right.$$

$$(71) \quad \left\{ \begin{aligned} \frac{1}{2\pi i} \int_{1-i\infty}^{1+i\infty} \frac{\operatorname{tg} \pi s}{s-2} x^{s-2} ds &= \frac{2}{\pi} \sum_{k=1}^{\infty} \frac{1}{2k-3} x^{(2k-3)/(2)} = \\ &= \frac{1}{\pi} \left[-\frac{2}{\sqrt{x}} + \ln \frac{1+\sqrt{x}}{1-\sqrt{x}} \right] \text{ for } x < 1. \end{aligned} \right.$$

The second integral in (69) is expanded with respect to $\ln x$; in the neighbourhood of $x=1$ this expansion is rapidly convergent.

$$\begin{aligned} &\frac{1}{2\pi i} \int_{1-i\infty}^{1+i\infty} \frac{\operatorname{tg} \pi s}{(s-2)N(s)} [5 + 2\nu + \nu^2 - 2(1-\nu)^2(s-1)^2] x^{s-2} ds = \\ &= \frac{1}{2\pi i} \int_{1-i\infty}^{1+i\infty} \frac{\operatorname{tg} \pi s}{(s-2)N(s)} [5 + 2\nu + \nu^2 - 2(1-\nu)^2(s-1)^2] [1 + (s-2) \ln x + \\ &\quad + \frac{1}{2}(s-2)^2 (\ln x)^2 + \dots] ds. \end{aligned}$$

Putting $s=1+it$ and writing

$$(72) \quad \frac{5+2\nu+\nu^2+2(1-\nu)^2 t^2}{N(1+it)} = F(t) = F(-t),$$

we obtain for our integral

$$\frac{i}{2\pi} \int_{-\infty}^{\infty} \frac{\operatorname{tgh} \pi t}{-1+it} F(t) [1 + (-1+it) \ln x + \frac{1}{2}(-1+it)^2 (\ln x)^2 + \dots] dt.$$

Using the symmetry of $F(t)$ and the antimetry of $\operatorname{tgh} \pi t$, this result is reduced to

$$(73) \quad \frac{1}{\pi} \int_0^{\infty} \frac{\operatorname{tgh} \pi t}{t^2+1} F(t) t dt - \frac{(\ln x)^2}{2\pi} \int_0^{\infty} \operatorname{tgh} \pi t \cdot F(t) t dt + \dots,$$

where the first order term in $\ln x$ vanishes. The integrals in (73) have been evaluated by numerical integration.

3.4. Numerical results

The bending moment $(m_x)_{x=0}$ along the clamped edge is shown in figs. 4 and 5. In the first figure two linear scales are used and in fig. 5 a loga-

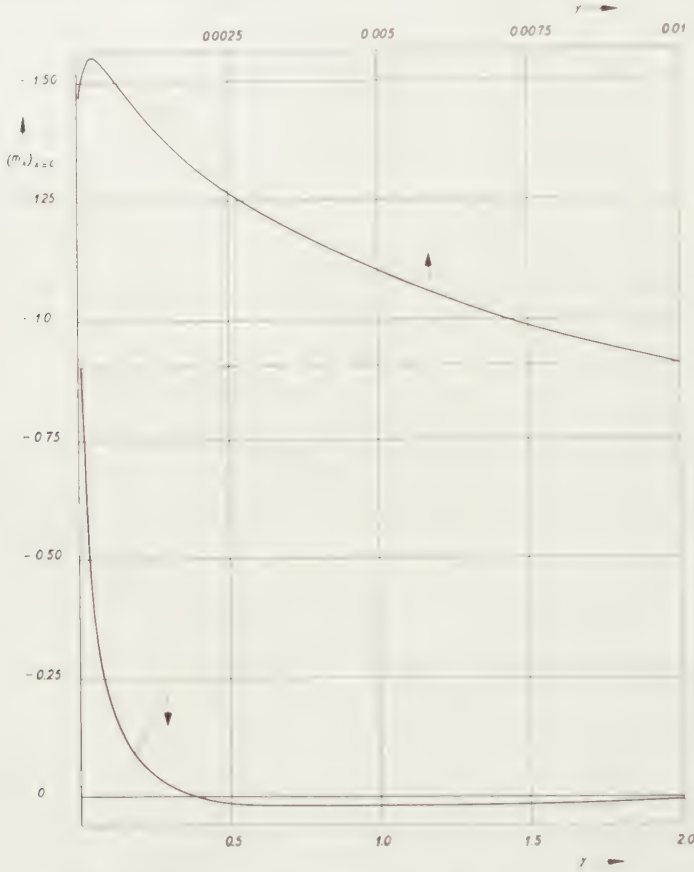


Fig. 4. The bending moment along the clamped edge

rithmic scale is used for the y -coordinate in order to give a clear picture of the oscillating behaviour of the bending moment near the corner $x=0$, $y=0$. These oscillations are confined to a very small region near the corner, the first extreme value of magnitude -1.555 occurring at $y = 2.24 \cdot 10^{-4}$. It should be noted that this minimum value is considerably smaller than the limiting value -1 at the corner.

It may be noted that the limiting value $(m_x)_{x=0} = -1$ at $y=0$ can be obtained directly from the first boundary condition along the free edge at the corner

$$\left(\frac{\partial^2 w}{\partial y^2}\right)_{x=0, y=0} + \nu \left(\frac{\partial^2 w}{\partial x^2}\right)_{x=0, y=0} = -\nu.$$

Observing that $\partial^2 w / \partial y^2 = 0$ along $x=0$, it follows that

$$\left(\frac{\partial^2 w}{\partial x^2}\right)_{x=0, y=0} = (m_x)_{x=0, y=0} = -1,$$

if the assumption is made that the bending and torsional moments are continuous at the corner.

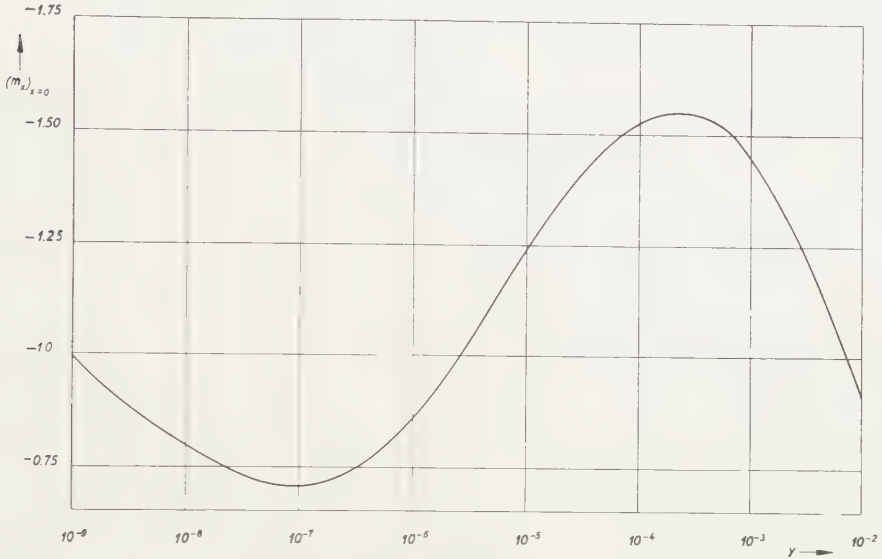


Fig. 5. The bending moment along the clamped edge

The behaviour of the bending moment near the corner is described with adequate accuracy by the first two terms of the series (62)

$$(74) \quad (m_x)_{x=0} = -1 - 1,1099 \cdot y^{0,0799} \cos [0,3951 \ln y + 3,5191].$$

The second term in (74) shows an infinite number of oscillations with decreasing wavelength and amplitude when $y=0$ is approached. The ratio between two successive zeros (or between two successive extreme values) is given by

$$(75) \quad \frac{y_{k+1}}{y_k} = e^{-\frac{\pi}{0,3951}} \cong 0,000350$$

and the ratio between the absolute values of two successive extremes is

$$(76) \quad e^{-\pi \frac{0,0799}{0,3951}} \cong 0,530.$$

The reduced shear force $(q_{xr})_{x=0}$ along the clamped edge is shown in figs. 6 ($0,02 < y < 2,0$) and 7 ($0,005 < y < 0,05$). Its behaviour near the corner is adequately described by the first two terms in the series (65).

$$(77) \quad (q_{xr})_{x=0} = -0,6958 y^{-0,9201} \cos [0,3951 \ln y + 3,1247];$$

this formula shows that the reduced shear force is also an oscillating function with the same decreasing wave length, characterized by (75), but

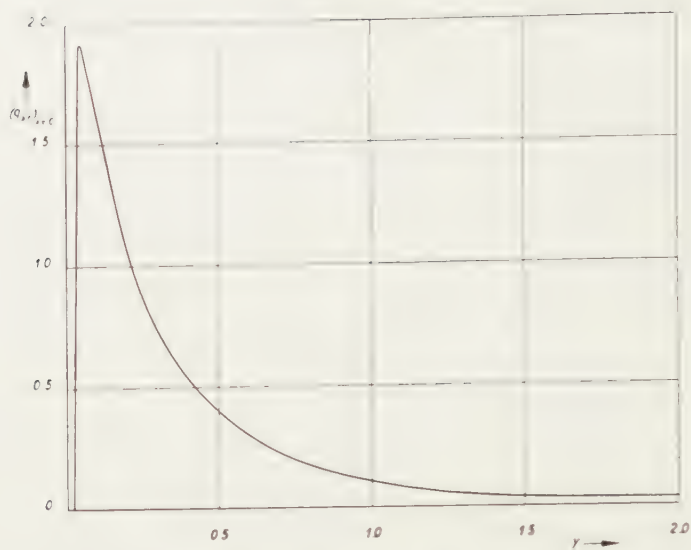


Fig. 6. The reduced shear force along the clamped edge

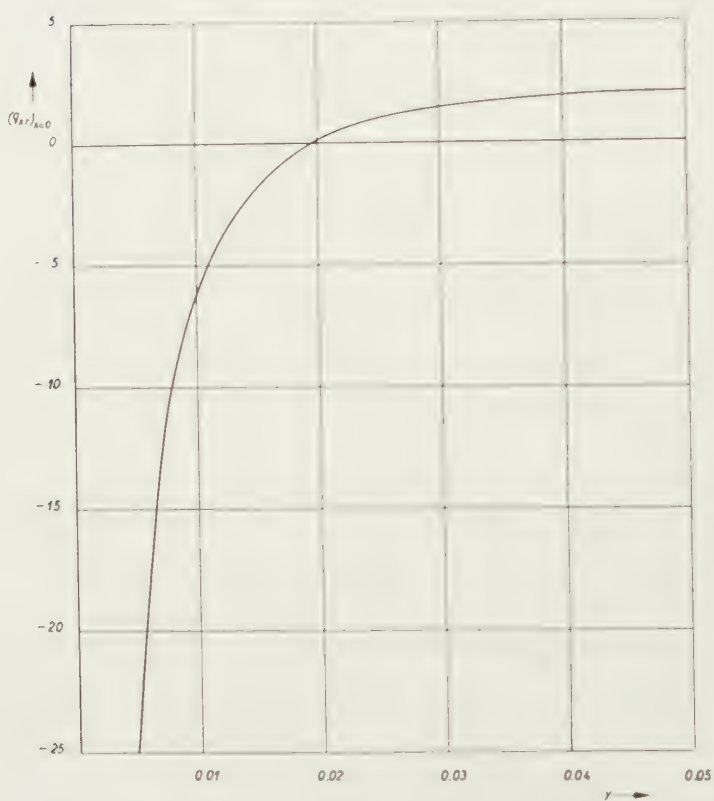


Fig. 7. The reduced shear force along the clamped edge

with a sharply increasing amplitude which is unbounded when $y=0$ is approached. The ratio between the absolute values of two consecutive extremes is

$$(78) \quad e^{\pi \frac{0.9201}{0.3951}} \cong 2080.$$

The bending moment $(m_x)_{x=0}$ and the reduced shear force $(q_{xr})_{x=0}$ must be in equilibrium with the applied load $m_{x0} = -\nu$ along the free edge for $0 < x < 1$; the torsional moment m_{xy} vanishes at the corner (cf. (67)) so that no concentrated force occurs at this corner. The conditions of overall equilibrium therefore require

$$\begin{aligned} \int_0^\infty (m_x)_{x=0} dy &= 0, \\ \int_0^\infty (q_{xr})_{x=0} dy &= 0, \\ \int_0^\infty (q_{xr})_{x=0} y dy &= - \int_0^\infty m_{y0} dx = \nu. \end{aligned}$$

These relations are most easily verified by means of a Mellin transformation applied to (54) and (55).

Introducing the Mellin transforms

$$\begin{aligned} \int_0^\infty (m_x)_{x=0} y^{\sigma-1} dy &= F(\sigma) \\ \int_0^\infty (q_{xr})_{x=0} y^{\sigma-1} dy &= G(\sigma) \end{aligned}$$

and applying the Mellin inversion formulae

$$\begin{aligned} (m_x)_{x=0} &= \frac{1}{2\pi i} \int_{c-i\infty}^{c+i\infty} F(\sigma) y^{-\sigma} d\sigma \\ (q_{xr})_{x=0} &= \frac{1}{2\pi i} \int_{c-i\infty}^{c+i\infty} G(\sigma) y^{-\sigma} d\sigma \end{aligned}$$

we obtain by comparison with (54) and (55)

$$\begin{aligned} \int_0^\infty (m_x)_{x=0} dy &= F(1) = -\frac{1}{2} \left\{ \frac{\phi(s)}{N(s)} [(1-\nu)s + 2\nu] \cos \frac{\pi}{2} s \right\}_{s=1} = 0, \\ \int_0^\infty (q_{xr})_{x=0} dy &= G(1) = \frac{1}{2} \left\{ \frac{\phi(s)}{N(s)} (s-2) [(1-\nu)s + (1+\nu)] \sin \frac{\pi}{2} s \right\}_{s=2} = 0, \\ \int_0^\infty (q_{xr})_{x=0} y dy &= G(2) = \frac{1}{2} \left\{ \frac{\phi(s)}{N(s)} (s-2) [(1-\nu)s + (1+\nu)] \sin \frac{\pi}{2} s \right\}_{s=1} = \nu, \end{aligned}$$

thereby verifying the conditions of overall equilibrium.

The torsional moment along the free edge is shown in figs. 8 (with linear scales) and 9 (with a logarithmic scale for x). It approaches zero for $x \rightarrow 0$

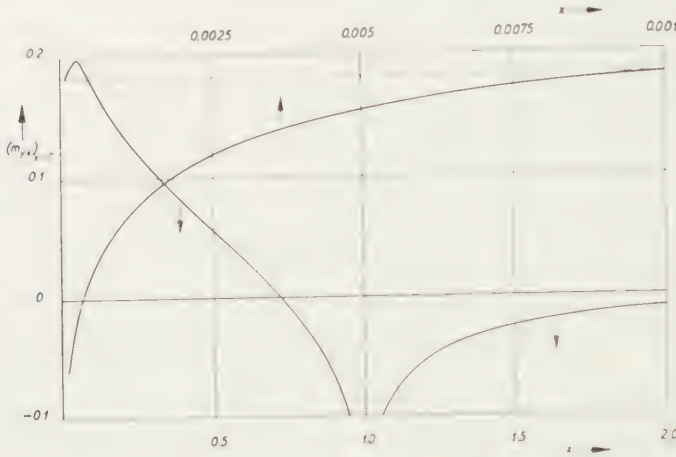


Fig. 8. The torsional moment along the free edge

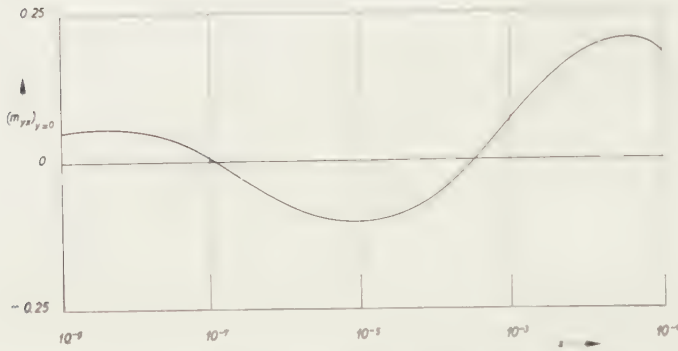


Fig. 9. The torsional moment along the free edge

like the root bending moment, with an infinite number of oscillations with decreasing wave length, described by (75), and decreasing amplitude given by (76).

3.5. Discussion of the singularity in the corner

The foregoing results show that the stress distribution has an essential singularity in the corner of the plate. Moreover this singularity is strongly dependent on the value of Poisson's ratio ν . For $\nu = 1/4$, the value assumed in this paper, the zeros of $N(s)$ with the smallest positive real part are complex (cf. (59), (60)), whereas for very small values of ν ($0 < \nu < 0.0353$) the zero of $N(s)$ with smallest positive real part is purely real. Because the zero with the smallest positive real part governs the behaviour in the neighbourhood of the corner, this behaviour is essentially different for $\nu < 0.0353$ and $\nu > 0.0353$. In the former case no oscillations occur in the principal terms of the series (62), (65), (67).

The question naturally arises whether these singularities are due to the approximate character of plate theory. The approximations involved are certainly too crude in the region near the corner because the shear forces are unbounded. In other words, the plate thickness h cannot be considered very small in the neighbourhood of the corner. It might therefore be surmised that a more accurate plate theory, i.e. REISSNER's theory, which takes into account shear deformations, would lead to more intelligible results. However, the singularity is not removed or even reduced if REISSNER's theory is applied; this conclusion is taken from WILLIAMS' investigation on the singularities in angular corners (ref. 3). This unexpected result is explained if it is realized that near the corner the plate thickness is *large* compared with the coordinates along the middle surface. The stress distribution near the corner therefore approaches to the stress distribution in plane strain and it is well known that a rectangular corner in plane strain similar singularities can occur (ref. 11, 12). The explanation of our singularities must therefore not be sought in the approximate character of plate theory *but in the intersection of a free and a rigidly clamped boundary*.

(to be continued)

REFERENCES *)

9. TIMOSHENKO, S. P., Theory of plates and shells. (McGraw-Hill, New York, 1940).
10. COURANT, R. und D. HILBERT, Methoden der mathematischen Physik, Bd 1 (2 Aufl., Springer, Berlin, 1931).
11. KNEIN, M., Zur Theorie des Druckversuchs. Der Spannungszustand bei ebener Formänderung und vollkommen verhinderter Querdehnung. Abh. Aerodyn. Inst. Techn. Hochschule Aachen, Heft 7, 43 (1927).
12. WILLIAMS, M. L., Stress singularities resulting from various boundary conditions in angular corners of plates in extension. J. Appl. Mech., **19**, 526 (1952).

*) For ref. 1-8 cf. these Proceedings, **B57**, 258 (1954).

THE CHEMISTRY OF ACETYLENIC ETHERS

PART VI¹⁾REACTIONS OF ETHOXYACETYLENE WITH AMINES
IN THE PRESENCE OF WATER

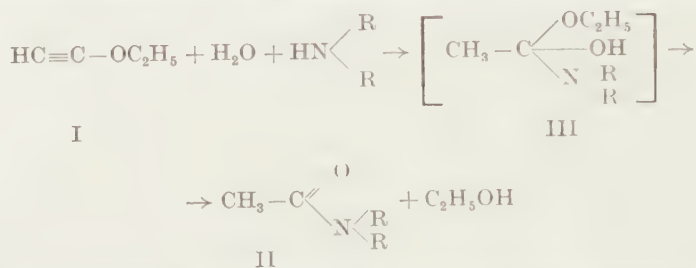
BY

J. F. ARENS AND TH. R. RIX

(Communicated by Prof. H. J. BACKER at the meeting of January 30, 1954)

Summary:

The simultaneous addition of water and an amine to ethoxyacetylene I results in the formation of an N-substituted acetamide II and of alcohol.



Weakly basic amines like aniline and diphenylamine behave differently and act as catalysts for the formation of ethylacetate by hydration of ethoxyacetylene.

This addition of water can be catalysed too by small quantities of diethylamine and N-acetylpiperidine.

The addition of ammonia and of amines to acetylenic compounds has been studied by several investigators²⁾.

In most instances the reaction needs a catalyst or proceeds only at high temperatures. Only with the highly reactive α -acetylenic ketones does addition proceed spontaneously at room temperature³⁾.

¹⁾ Part V these Proceedings B56, 372 (1953).

²⁾ For reviews see:

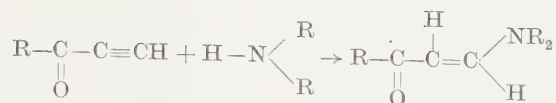
W. REPPE, *Neue Entwicklungen auf dem Gebiete des Acetylens und Kohlenoxyds*, p. 19-22 (Springer Verlag, 1949).

J. A. NIEUWLAND, R. R. VOGT, *The Chemistry of Acetylene*, p. 136 and 156-159 (Reinhold Publ. Corp., 1945).

A. W. JOHNSON, *The Chemistry of Acetylenic Compounds*, Vol. I and II (Edward Arnold Co., 1946 and 1950).

³⁾ E. R. H. JONES, c.s., *J. Chem. Soc.* 1946, 45; 1949, 1423, 1430.

J. CHAUVELIER, *Ann. Chim.* [12], 3, 393 (1948).

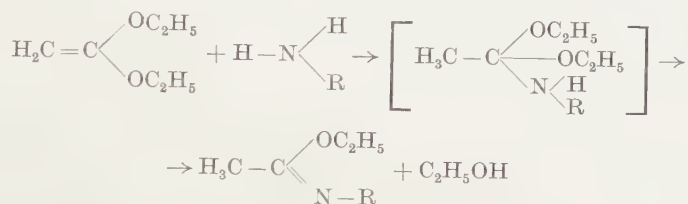


Although ethoxyacetylene I contains a rather reactive triple bond — it is easily hydrated at room temperature with acidified water, yielding ethylacetate — the addition of pure amines is generally slow ⁴).

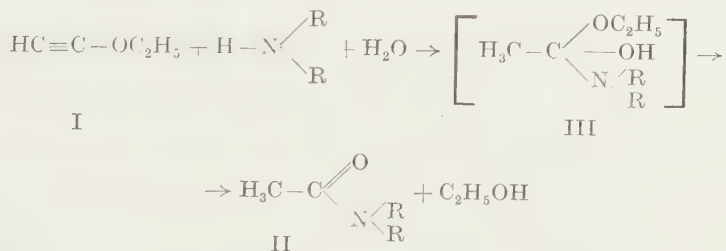
We observed, however, that in the presence of at least one molecular equivalent of water, a rather smooth reaction occurs, resulting in the formation of an N-substituted acetamide II and of alcohol.

As far as we know the simultaneous addition of a secondary amine and of water to an acetylenic bond has not been described before. REPPE studied the addition of tertiary amines and water to acetylene ²).

It is interesting at this point to recall the investigations of MC. ELVAIN and his associates into the reaction of amines with the diethylacetal of ketene ⁵). Here the formation of an iminoether and of alcohol was observed. The reaction was believed to proceed via an unstable derivative of orthoacetic acid.



Ethoxyacetylene can be considered as the yno-ether of ketene ⁶) and in analogy with MC. ELVAIN's formulation we are inclined also to assume a derivative of orthoacetic acid as an intermediate (III).



The reaction of ethoxyacetylene with aqueous solutions of ammonia, methylamine, benzylamine, dimethylamine and piperidine proceeds in analogy with that of diethylamine.

Diphenylamine and also aniline behave differently from the aliphatic secondary amines. These compounds are only very weakly basic and react

⁴) Our investigations into these reactions are in progress now.

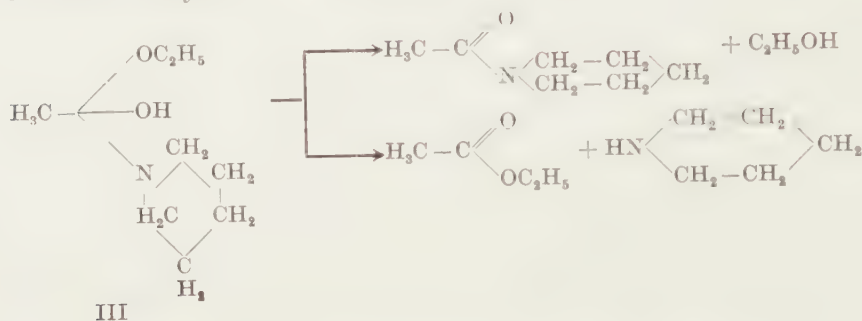
⁵) H. M. BARNES, D. KUNDIGER and S. M. MC. ELVAIN, J. Am. Chem. Soc. **62**, 1281-1287 (1940).

⁶) TH. L. JACOBS, R. CRAMER and F. F. WEISS, J. Am. Chem. Soc. **62**, 1849 (1940).

very slowly with ethoxyacetylene and water. Ethylacetate is the main product of the reaction. The amines remain mostly unchanged.

Apparently the weak bases catalyse the addition of water. It has appeared that a small amount of the amine is sufficient. This addition of water, however, proceeds very slowly, in contrast to the acid catalysed hydration which proceeds very quickly. The hydration of ethoxyacetylene can also be catalysed by small amounts of diethylamine and of N-acetyl-piperidine, also here the reaction rate is slow.

In the case of the reaction between ethoxycarbonylene, piperidine and water we obtained together with N-acetylpiperidine, considerable amounts of ethylacetate. Obviously the intermediate product III decomposes in two different ways:



We cordially thank Mr LIEM ENG KIM for technical assistance.

EXPERIMENTAL PART

(all distillations at 700 mm unless otherwise stated)

1. Preparation of ethoxyacetylene

In a previous publication⁷⁾ we mentioned the preparation of ethoxyacetylene from *cis*-ethyl- β -chlorovinyl-ether and potassiumhydroxyde. It is more convenient, however, to use the crude mixture of the *cis* and *trans* compounds, prepared from dichloroacetal.

The overall yield based on the *cis*-ether is the same.

2. *Reaction of ethoxyacetylene with ammonia (2 n)*

Ethoxyacetylene (7 g, 0,1 mole) and 50 ml ammonia (2 n, 0,1 mole) were shaken for 150 hours. The mixture was distilled over a 30 cm Vigreux column. After a forerunning of alcohol and ethylacetate (3 g) and a fraction mainly consisting of water, a residue was obtained. This was distilled without a column and yielded acetamide (bp 200–215°, mp 78–81° (after recrystallisation from chloroform). (According to literature bp 222°, mp 81°). The yield was 3 g (51 %).

3. Reaction of ethoxyacetylene with methylamine and water

Ethoxyacetylene (7 g 0,1 mole), a 33 % solution of methylamine in water (9,3 g, 0,1 mole) and 20 ml water were shaken.

⁷⁾ D. A. VAN DORP, J. F. ARENS and O. STEPHENSON, *Rec.* **70**, 289 (1951).

After 50 hrs a homogeneous solution was obtained and the odour of ethoxyacetylene had disappeared. The mixture was extracted with ether. Distillation of the extract yielded 3 g N-methylacetamide, bp 195–202° (according to the literature bp 206°, mp 26°).

Distillation of the watery phase yielded another 3,5 g of N-methylacetamide, bp 195–202°.

Total yield 6,5 g (89 %). The liquid solidified on cooling in ice-water.

4. *Reaction of ethoxyacetylene with benzylamine and water*

Ethoxyacetylene (7 g, 0,1 mole), benzylamine (10,7 g, 0,1 mole) and 20 ml water were shaken. After 75 hours the mixture was homogeneous; it was extracted with 50 ml ether. After evaporation of the ether the residue weighed 15 grams and solidified partly when standing. It was distilled. After a forerunning of some alcohol and benzylamine, N-benzylacetamide was obtained 11,4 g (77 %), mp 60–61°. No depression of mp with an authentic sample of N-benzylacetamide (mp 59,5–61°).

5. *Reaction of ethoxyacetylene with aniline and water*

Ethoxyacetylene (7 g, 0,1 mole), aniline (9,3 g, 0,1 mole) and 20 ml water were shaken for 210 hrs.

The mixture was extracted 3 times with ether and the extract distilled. After a forerunning of ether 5 g bp 70–71° were obtained (ethylacetate and some alcohol). Aniline distilled at 170–190°. The odour of N-phenylacetiminoether was observed. The residue weighed 1,75 g. It solidified partly when standing in the ice-box for several days. After purification the mp was 112–114° (no depression with authentic sample of acetanilide).

6. *Reaction of ethoxyacetylene with diethylamine (or dimethylamine) and water*

A mixture of ethoxyacetylene (7 g, 0,1 mole), diethylamine (7,3 g, 0,1 mole) and 15 ml water was stirred. Heat was evolved and the mixture was cooled from time to time in ice-water.

After 2½ hrs a homogeneous solution was obtained and the characteristic odour of ethoxyacetylene had disappeared. After standing overnight the solution was once extracted with an equal volume of ether and the extract distilled.

We obtained 2½ g N-diethylacetamide bp 175–182°.

Upon distillation of the watery phase a small amount of alcohol and diethylamine was obtained together with another 3 g N-diethylacetamide. Total yield of this substance 5,5 g (48 %) n_D^{25} 1,4300.

In an analogous manner the reaction between ethoxyacetylene, dimethylamine and water was performed, yielding N-dimethylacetamide bp 161–171°, n_D^{25} 1,4327.

7. *Reaction of ethoxyacetylene with water and a trace of diethylamine*

A mixture of ethoxyacetylene (3,5 g, 0,05 mole), 7,5 ml water and two

drops of diethylamine was shaken for 212 hrs. The mixture was extracted with ether, the extract dried with sodiumsulphate and distilled. We obtained 0,9 g (20 %) ethylacetate bp 68–73°; the forerunning contained unchanged ethoxyacetylene.

8. *Reaction of ethoxyacetylene with piperidine and water*

A mixture of ethoxyacetylene (7 g, 0,1 mole), piperidine (8,5 g, 0,1 mole) and 15 ml water was stirred for 3 hrs with cooling.

A homogeneous solution was then obtained. After standing overnight the liquid was distilled. We obtained the following fractions:

- a. bp 69–71°, 5 g ethylacetate and alcohol.
- b. bp 71–98°, 20 g mainly consisting of water and alcohol and of some piperidine.
- c. bp 200–220°, 4,5 g N-acetylpiperidine (35 % yield).

9. *Reaction of ethoxyacetylene with water and a small amount of diphenylamine*

A mixture of ethoxyacetylene (3,5 g, 0,05 mole), diphenylamine (50 mg) and 17,5 ml water was shaken for 212 hrs at room temperature.

Then the mixture was extracted with ether, the extract dried with sodiumsulfate and distilled. We obtained 2,1 g (48 %) ethylacetate bp 73–75°.

*Laboratory for Organic Chemistry,
University of Indonesia,
Bandung, Java*

June 1953

THE CHEMISTRY OF ACETYLENIC ETHERS

PART VII

THE REACTIONS OF ETHOXYACETYLENE WITH AMINES IN THE ABSCENCE OF WATER

BY

J. F. ARENS AND TH. R. RIX

(Communicated by Prof. H. J. BACKER at the meeting of January 30, 1954)

Summary:

In the absence of water, ethoxyacetylene reacts with primary amines to yield N-substituted amidines IV or iminoethers III and with secondary amines to yield a mixture of 1-ethoxy-1-dialkylamino-ethene V and 1,1-bis-dialkylamino-ethene VI.

These reactions are much slower than the additions in the presence of water, which yield, as has been reported earlier, N-substituted acetamides.

In previous papers of this series¹⁾ we did report on the reaction of ethoxy-acetylene with primary c.q. secondary amines *and water*. N-alkylated (c.q. N-dialkylated) acetamides are formed in rather smooth reactions.

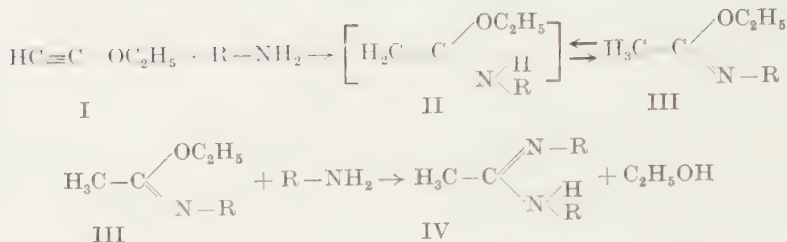
We now investigated the reactions of ethoxyacetylene with n-propylamine, aniline, p-toluidine and benzylamine, and also with diethylamine in the *absence* of water. In these cases a rather slow reaction occurs and prolonged refluxing is necessary.

The reaction of ethoxyacetylene with n-propylamine leads to a mixture of N-n-propyl-acetimino-ethylether (III $R = n.C_3H_7$) and N, N'-bis-n-propyl-acetamidine (IV, $R = n.C_3H_7$). The reaction can be somewhat accelerated by the addition of a trace of water. The other primary amines give analogous results.

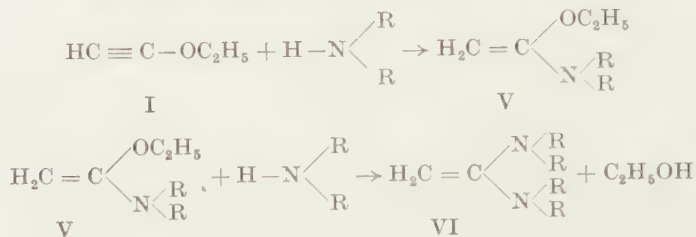
We mention the fact that from ethoxyacetylene and aniline even in the presence of water, N-phenyl-acetimino-ethylether (III $R = C_6H_5$) is formed together with a small amount of the N, N'-diphenyl-acetamidine (IV $R = C_6H_5$).

The following equations picture the observed reactions.

¹⁾ Part VI, these Proceedings **B57**, 270—274 (1954).



Iminoether formation from *secondary* amines by a tautomeric shift of the intermediate V is impossible. The substance V as such can be isolated. Furthermore it can react with a second molecule of the amine to yield VI.



Substances of the structures V and VI ($\text{R}=\text{C}_2\text{H}_5$) have been prepared by Mc. ELVAIN²⁾ from the diethylacetal of ketene and diethylamine. Our substances seem to be identical with those of Mc. ELVAIN, although we did not obtain VI in analytically pure condition.

Our thanks are due to Mr YO KIM TEK for assistance in the laboratory.

EXPERIMENTAL PART

All distillations at 700 mm. unless otherwise stated

1. Addition of *n*.propylamine to ethoxyacetylene

A mixture of freshly distilled *n*.propylamine (14.5 g, 0.25 mole) and of ethoxyacetylene (8.5 g, 0.12 mole) was heated in an oil bath of 90°.

The mixture stood overnight at room temperature and was then again refluxed. The boiling point of the mixture increased as the reaction proceeded. After 5½ hrs. of additional heating the reaction seemed to be complete.

The mixture was fractionally distilled using a 20 cm column packed with glass helices. We obtained the following fractions.

1. bp 43–45° 3.5 g unchanged *n*.propylamine
2. bp 45–74° 2 g
3. bp 74–75° 2 g (mainly ethanol).

The distillation was continued in vacuum.

4. bp 45–46° (27 mm) 4.5 g $n_D^{24.5}$ 1.4144.
5. bp 46–100° (27 mm) 1.5 g
6. bp 100–101° (27 mm) 4.8 g n_D^{24} 1.4645

²⁾ H. M. BARNAS, D. KUNDIGER, S. M. McELVAIN, J. Am. Chem. Soc. **62**, 1281 (1940).

Fraction 4 constitutes N-n.propyl-acetimino-ethylether (III, $R = n.C_3H_7$).
Analysis (KJELDAHL) Found: 10.2 and 10.3 % N.

Calculated for $C_7H_{15}ON$: 10.8 % N.

Fraction 6 constitutes N,N'-bis-n.propyl-acetamidine (IV, $R = n.C_3H_7$).
Analysis (KJELDAHL) Found: 19.5 and 19.6 % N.

Calculated for $C_8H_{18}N_2$: 19.7 % N.

In another experiment we divided the mixture of ethoxyacetylene and n.propylamine prior to refluxing in two equal parts. One part was heated as such and to the other part we added two drops of water. This second mixture needed about half the refluxing time of the first to complete the reaction.

2. *Addition of aniline to ethoxyacetylene*

A solution of ethoxyacetylene (10.3 g, 0.15 mole), and aniline (13.7 g, 0.15 mole) in 30 ml. of abs. ethanol was boiled for 28 hours under reflux.

The mixture was distilled. After a forerunning of ethanol the following fractions were collected:

- a. 108°–203°, 2.1 g of aniline and N-phenyl-acetimino-ethylether.
- b. 203°–208°, 15.8 g of N-phenylacetimino-ethylether (66 %)

$$n_D^{25} = 1.5197.$$

- c. residue 3 g of N,N'-diphenyl-acetamidine, solidified after standing, mp 129°–131° after two recrystallisations from ethanol.

No depression after mixing with an authentic sample (mp 129°–131°).

3. *Synthesis of N-phenyl-acetimino-ethylether and of N,N'-diphenylacetamidine from ethylorthoacetate and aniline*

A mixture of ethylorthoacetate (8.1 g, 0.05 mole) and of aniline (4.7 g, 0.05 mole) was heated. The ethanol was slowly distilled off over a 20 cm Vigreux-column.

We collected 3.8 g of ethanol (calculated 4.6 g). The residue was distilled without a column.

The fraction boiling 206°–207°, consisting of N-phenyl-acetimino-ethylether, weighed 4.6 g (58 %) and had n_D^{25} 1.5173.

The residue (1.5 g of N,N'-diphenyl-acetamidine (28 %)) solidified on standing and after two recryst. from ethanol had mp 129°–131°. (mp. according to literature 131°–132°).

4. *The addition of benzylamine to ethoxyacetylene*

A mixture of ethoxyacetylene (7 g, 0.1 mole), benzylamine (10.7 g, 0.1 mole) and 30 ml. of abs. ethanol was refluxed for 7 hrs, and then distilled. After removal of a forerunning of ethanol the distillation was performed in vacuum. The fraction with bp 90°–105° (6.5 mm) weighed 10.5 g (60 %) and consisted mainly of N-benzyl-acetimino-ethylether.

After redestillation at ordinary pressure the bp was 215° – 218° (n_D^{28} 1.5072).

From the residue of the distillations no N,N'-diphenylacetamidine could be isolated.

5. *Synthesis of N-benzyl-acetimino-ethylether from ethylorthoacetate and benzylamine*

The reaction was carried out with ethylorthoacetate (8.1 g, 0.05 mole) and benzylamine (5.4 g, 0.05 mole) as described under 4. The yield was 4 g (44 %) of N-benzylacetimino-ethylether with bp 216° – 218° and n_D^{28} 1.5149.

Analysis (KJELDAHL): calculated for $C_{11}H_{15}ON$ N: 7.90 %.

Found: 7.64 and 7.52 %.

6. *The addition of p-toluidine to ethoxyacetylene*

A solution of ethoxyacetylene (6.3 g, 0.09 mole) and of p-toluidine (9.3 g, 0.09 mole) in 30 ml. of abs. ethanol was refluxed for 25 hours. After a forerunning of ethanol the following fractions were collected:

- a. 200° – 220° , 1.5 g.
- b. 220° – 226° , 9 g, N-p-tolyl-acetimino-ethylether (57 %); n_D^{27} 1.5149, (according to litt. bp₇₆₀ 232°).
- c. 226° – 238° , 1.5 g.
- d. residue 3 g; solidified on standing. Mp 118° – 120° (after recrystallisation from ethanol). No depression of mp. after mixing with an authentic sample of N,N'-bis-(p-tolyl)acetamidine. (mp 119° – 120°). (according to lit. mp 121° – 121.5°).

7. *Synthesis of N-p-tolyl-acetimino-ethylether and of N,N'-bis-(p-tolyl)-acetamidine from ethylorthoacetate and p-toluidine*

The reaction was carried out with ethyl-orthoacetate (6.5 g, 0.4 mole) and p-toluidine (4.3 g, 0.4 mole).

We isolated 3.8 g N-p-tolyl-acetimino-ethylether with bp 125° – 127° (27 mm) n_D^{26} = 1.5165, and 2.8 g N,N'-bis(p-tolyl)acetamidine mp 114° – 117° . Mp after recrystallisation from alcohol 119° – 120° .

8. *Addition of diethylamine to ethoxyacetylene*

a. Equimolecular quantities

A mixture of freshly distilled diethylamine (11.8 g, 0.16 mole) and of ethoxyacetylene (11 g, 0.16 mole) was refluxed during 20 hrs. The reflux condenser was provided with a calcium chloride tube to exclude moisture. After standing at room temperature for 5 days, the brown liquid was distilled, at first at ordinary pressure. A 20 cm column packed with helices was used.

- a 1. bp 40° – 60° 0.8 g, strong odour of diethylamine.
- a 2. bp 60° – 70° 1.2 g with diethylamine odour, containing alcohol.

- a 3. in vacuum bp 75–81° (46 mm) 4.6 g n_D^{26} 1.4327.
 a 4. bp 81–87° (46 mm) 4.5 g n_D^{26} 1.4344.
 a 5. bp 87–93° (50 mm) 2.4 g n_D^{26} 1.4390.
 a 6. residue, brown oil, 5.3 g.

Fractions 3–6 consist of a mixture of the substances V and VI ($R = C_2H_5$).

Purification was performed together with corresponding fractions of the following experiment.

- b. 2 moles of diethylamine per mole of ethoxyacetylene

A mixture of freshly distilled diethylamine (17.3 g, 0.24 mole) and of ethoxyacetylene (8.3 g, 0.12 mole) was refluxed during 20 hrs., and then fractionally distilled using a 20 cm column packed with helices.

- b 1. bp 48–54° 6.75 g, mixture of diethylamine and ethoxyacetylene.
 b 2. 54–65° 2.25 g, strong amine odour.
 b 3. 65–70° 1.4 g alcohol with some diethylamine.
 b 4. in vacuum bp 75–80° (40 mm) 0.5 g.
 b 5. bp 80–89° (40 mm) 5 g n_D^{28} 1.4390.
 b 6. residue, brown oil, 1 g.

The fractions a 3, 4, 5 and b 4, 5 were mixed and redistilled in vacuum using a column of about 1 m length, packed with helices.

- c 1. bp 72–73° (32 mm) $n_D^{26.5}$ 1.4370.
 c 2. bp 73–77° (32 mm) n_D^{27} 1.4331 } small fractions.
 c 3. bp 77–80° (32 mm) n_D^{27} 1.4335 }
 c 4. bp 80–82° (32 mm) $n_D^{26.5}$ 1.4424.

Fraction c 1 analysed approximately correct for V.

Found: 10.2 % N (KJELDAHL).
 Calc. for $C_8H_{18}ON$: 9.8 % N.

Fraction c 4 is very impure VI.

Found: 13.9 % N (KJELDAHL).
 Calc. for $C_{10}H_{22}N_2$: 16.5 % N.

The residues a 6 and b 6 were combined and distilled without a column.

- d 1. bp 87–90° (30 mm) 1.5 g n_D^{25} 1.4500.
 d 2. bp 90–100° (30 mm) 1.25 g n_D^{25} 1.4516.

The fractions c 4, d 1 and d 2 were mixed and redistilled in a 1 m column packed with helices.

- e 1. bp 82–84° (28 mm) $n_D^{25.5}$ 1.4435.
 e 2. bp 84–87° (28 mm) $n_D^{25.5}$ 1.4459.
 e 3. bp 87° (28 mm) $n_D^{25.5}$ 1.4480.

Fraction e 3 was still impure VI; Found: 15.3 % N; Calc.: 16.5 % N.

The sample was too small to allow further purification.

Mc. ELVAIN ³⁾ reported the following constants for VI:
bp 89-93 (40 mm), n_D^{20} 1.4520, d_4^{20} 0.8226. No analysis was reported.

From the reported refractive index and spec. gravity a value of 55.8 can be calculated for the molecular refraction (Lorentz-Lorenz formula). The expected value for a substance of the formula VI is 55.8 (calculated with the aid of the values of Eisenlohr ⁴⁾).

The low refractive index and the low nitrogen content of our sample indicate that it is still contaminated, probably with N-diethylacetamide (bp 93-100 (40 mm) n_D^{20} 1.4310, calc. 12.2 % N).

*Laboratory for Organic Chemistry.
University of Indonesia.
Bandung, Java.*

³⁾ See: N. BAUER, K. FAJANS in A. WEISSBERGER, *Technique of organic chemistry* Vol. 1, p. 673 (1st Ed., Interscience Publishers Inc., New York, 1945).

THE CHEMISTRY OF ACETYLENIC ETHERS

PART VIII

THE FORMATION OF SOME HETEROCYCLIC COMPOUNDS FROM
ETHOXYACETYLENE

BY

J. F. ARENS AND TH. R. RIX

(Communicated by Prof. H. J. BACKER at the meeting of January 30, 1954)

Summary:

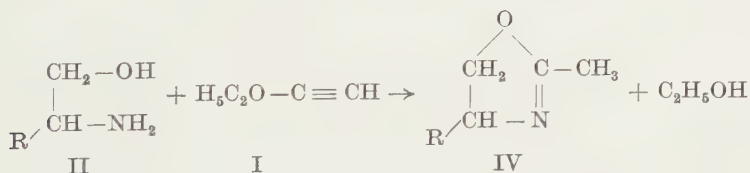
Ethoxyacetylene I adds mono-ethanolamine II ($R=H$) c.q. ethylene-diamine III to yield 2-methyl-oxazoline IV ($R=H$) c.q. 2-methyl-imidazoline V. With other 2-hydroxy-amines or 1,2-diamines similar results are obtained.

The addition of mercapto-ethylamine results in the formation of 2-methyl-thiazoline.

The results of the reactions of ethoxyacetylene with primary amines ¹⁾ in alcohol or without solvent, where the formation of imino-ethers and amidines was observed, suggested the possibility of preparing oxazolines c.q. imidazolines from the ether. These heterocyclic bases can be considered as cyclic imino-ethers c.q. amidines.

Indeed it has proven possible to perform the expected syntheses.

Ethoxyacetylene reacts easily with ethanolamine. After 30 minutes refluxing the reaction is complete and 2-methyl-oxazoline (IV $R=H$) can be isolated by distillation of the reaction mixture.



The compound exhibits the same properties as the substance prepared from 1-bromo-2-amino-ethane and aceticanhydride by GABRIEL ²⁾.

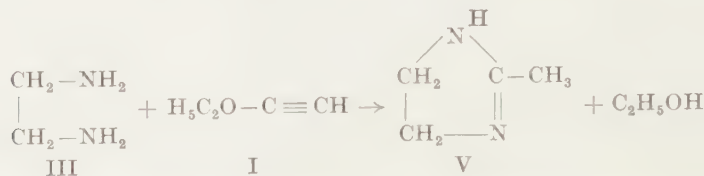
In a similar manner the reaction with dl-alaninol (2-amino-propanol-1, II $R=\text{CH}_3$) leads to 2,4-dimethyl-oxazoline (IV $R=\text{CH}_3$).

From ethylene-diamine on the other hand the crystalline lysidine

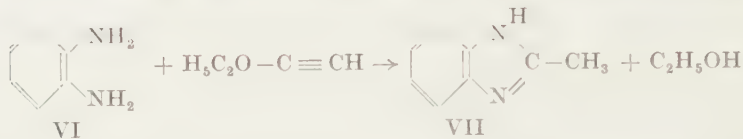
¹⁾ These Proceedings **B57**, 275—280 (1954).

²⁾ GABRIEL, c.s., Ber. **22**, 2221 (1889), **23**, 2502 (1890) and **30**, 2495 (1897).

(2-methyl-imidazoline V) can be prepared, identical in all respects with the compound obtained by LADENBURG ³⁾ by heating the hydrochloride of ethylenediamine with sodium acetate.



Likewise ortho-phenylene diamine VI yields 2-methyl-benzimidazole VII.



Ethoxyacetylene also adds mercapto-ethylamine. The reaction product is 2-methyl-thiazoline identical in properties with the substance prepared by PINKUS ⁵⁾ from thioacetamide and ethylenebromide.

Our thanks are due to Mr YO KIM TEK and Miss PARWATI for assistance in the laboratory.

EXPERIMENTAL PART

All distillations were performed at 700 mm unless otherwise stated.

1. Reaction of ethoxyacetylene with ethanolamine (formation of 2-methyl-oxazoline)

A mixture of freshly distilled ethanolamine (5.7 g, 0.093 mole) and ethoxy-acetylene (6.5 g, 0.093 mole) was refluxed in an oil bath of 100° C. After ½ hr. the refluxing had ceased due to increased boiling point of the mixture. The odour of ethoxyacetylene had disappeared.

The reaction mixture was fractionally distilled using a 20 cm column packed with glass helices. After a fore-running containing alcohol we obtained 3½ g of 2-methyl-oxazoline bp 100–107° (mostly 106–107°), literature ²⁾ bp 760 109.5–110.5. Odour resembling that of pyridine.

With a cold alcoholic solution of picric acid a picrate of mp 158–161° (litt. 157–159°) is formed. On standing with the mother liquor, this substance redissolved again forming the picrate of beta acetoxy-ethylamine. This is in accordance with the observations of GABRIEL ²⁾.

2. Reaction of ethoxyacetylene with dl-alaninol (formation of 2,4-dimethyl-oxazoline)

A mixture of ethoxyacetylene (6 g, 0.087 mole) and dl-alaninol ⁴⁾

³⁾ LADENBURG, Ber. 27, 2952 (1894) and 28, ref. 199 (1895).

⁴⁾ KARRER, PORTMAN, SUTER, Helv. Chem. Acta 31, 1617 (1948).

(6.25 g, 0.083 mole) was refluxed. After 4 hrs. the bp did not increase further. The mixture stood overnight and was then distilled using a 20 cm column packed with helices.

1. bp 55–74° 0.25 g.
2. bp 74–87° 2.25 g, mainly ethanol. (n_D^{25} 1.3709).

Distillation was continued in vacuum. A cold trap was placed between the pump and the distillation apparatus.

3. bp 30° (35 mm) 3.75 g of 2,4-dimethyloxazoline, n_D^{25} 1.4220.

The substance has an odour resembling that of alpha picoline.

The last part of this fraction was collected separately and showed n_D^{25} 1.4246.

4. residue 1.25 g.

The cold trap contained 2 g of a liquid with n_D^{25} 1.4064, consisting for the greater part of 2,4-dimethyloxazoline, as was proven by the isolation from it of the picrate of this substance (mp 130–135°).

Fraction 3 yielded a picrate of mp 130–135° which could not be recrystallised without decomposition.

3. *Reaction of ethoxyacetylene with ethylenediamine* (formation of lysidine)

Freshly distilled ethylenediamine (7 g, 0.12 mole) was mixed with ethoxyacetylene (5.75 g, 0.082 mole). Heat was evolved and a reaction took place. To complete this, the mixture was heated in an oil bath of 100° during $\frac{1}{2}$ hr. On cooling 2-methyl-imidazoline crystallised out.

By evaporation of the mother liquor in vacuum a second crop of crystals could be obtained. Total yield 3.5 g, mp 98–101°. The picrate, prepared with an alcoholic solution of picric acid had mp 197–201 (uncorr), after recrystallisation from water mp 200–203 (uncorr.)

LADENBURG ³) reported for the mp of 2-methyl-imidazoline (lysidine): 105°.

The mp of the picrate was not reported.

4. *Reaction of ethoxyacetylene with o-phenylenediamine* (formation of 2-methyl-benzimidazole)

A mixture of ethoxyacetylene (3 g, 0.043 mole) and o-phenylenediamine (4.6 g, 0.052 mole) was heated under reflux until a homogeneous solution was obtained (8 hrs). After cooling and addition of low boiling petroleum ether unchanged ortho-phenylenediamine crystallised out (2 $\frac{1}{2}$ g). This was removed by filtration. The mother liquor was evaporated. The residue solidified partly on standing. The solid was filtered out and recrystallised from water. Yield 1 g mp 173–176°. No depression of the mp after mixing with an authentic sample of 2-methyl-benzimidazole (mp 173–175°).

5. *Reaction of ethoxyacetylene with mercapto-ethylamine* (formation of 2-methyl-thiazoline)

A mixture of ethoxyacetylene (6 g, 0.087 mole) and mercapto-ethylamine

(6.6 g, 0.1 mole) was refluxed during 2 hrs. and distilled, using a 20 cm column packed with helices.

- a. bp 75–76° 1.5 g (ethanol).
- b. in vacuum (30 mm) bp 50–53° 3.75 g, odour like pyridine.
- c. residue 3.75 g, thick brown oil.
- d. the cold trap between the vacuum pump and the distillation apparatus contained 2 g of a clear liquid (mainly ethanol).

Fraction b was redistilled and showed the following constants: bp 50° (28 mm), $n_D^{24.5}$ 1.5128, picrate mp 168–171°. The literature ⁵⁾ reports the following data: bp 769 144.5–145°, mp of picrate 169–170°, odour like pyridine.

*Laboratory for Organic Chemistry,
University of Indonesia,
Bandung, Java*

⁵⁾ PINKUS, Ber. **26**, 1083 (1893). See also GABRIEL Ber. **24**, 1117 (1891).

CONTRIBUTIONS TO THE PROBLEM OF THE ASSOCIATION
BETWEEN PROTEINS AND LIPIDS. IX_A *) ¹⁾

- a. *Influence of salts on the coacervation of gelatin + cetyl trimethylammonium bromide + KCNS*
- b. *The existence of two types of gelatin—long chain ion associations rich in long chain ions.*

BY

H. G. BUNGENBERG DE JONG AND W. W. H. WEIJZEN

(Communicated at the meeting of March 20, 1954)

1. *Introduction*

In Part VII, section 4, the influence of the pH on the coacervation of gelatin + cetyl trimethylammonium bromide + KCNS has been studied. In these experiments, the pH was kept constant by means of acetate and phosphate buffers. The results showed clearly that salt influences must play an important role. In fig. 1, two curves are obtained, one from the

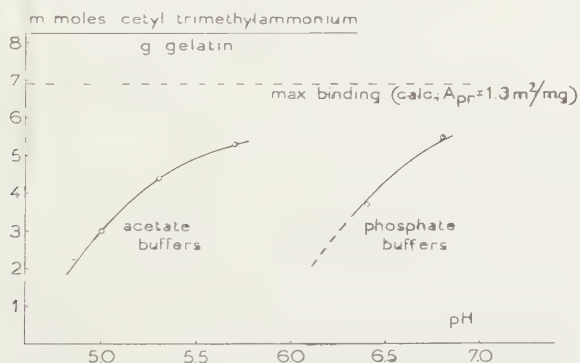


Fig. 1. Diagram representing the binding of cetyl trimethylammonium ions to the gelatin as a function of the pH from experiments with acetate and phosphate buffers

experiments with acetate buffers, the other from experiments with phosphate buffers. In the present communication, the salt influences are studied systematically. The conclusion will be reached that in this par-

*) The term lipids is used here in a wide sense, including fatty acids and other long chain electrolytes.

¹⁾ Part I appeared in these Proceedings, **45**, 601 (1942); the Parts II (A, B and C), III and IV in these Proceedings, Series B, **55**, 317, 329, 338, 347, 360 (1952), Part V, *ibid.*, **56**, 203 (1953), and the Parts VI (A and B), VII and VIII, *ibid.*, **57**, 1, 13, 192, 204 (1954).

At 25 millimoles/l NaCl the maximum is shifted considerably to the right and is estimated at $70 \pm 1\%$ Cetavlon, which corresponds to a binding of 6.0 ± 0.3 millimoles cetyl trimethylammonium cations/g dry gelatin²⁾.

Thus NaCl in relatively small concentration, promotes the formation of cetyl trimethylammonium rich — gelatin associations.

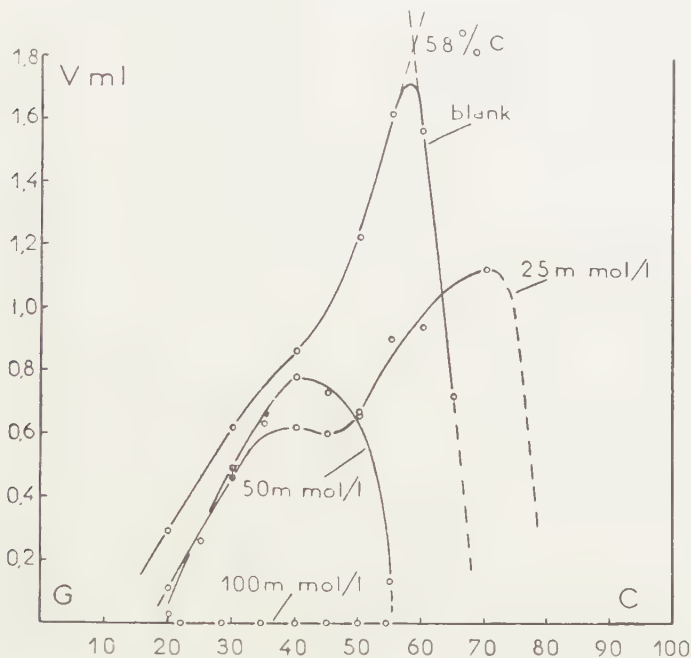


Fig. 2. Influence of NaCl on the coacervate volume curve in the mixing diagram

Remarkable is that at 50 millimoles/l NaCl the maximum of the curve has been shifted back to the left—even to the left of the maximum of the blank curve—and lies at about 42 % Cetavlon.

This corresponds to a binding of 1.9 millimoles cetyl trimethylammonium cations/g dry gelatin.

Thus NaCl at higher concentrations counteracts the formation of the cetyl trimethylammonium cation rich — gelatin associations. With 100 millimoles/l NaCl, at not a single mixing proportion occurs coacervation

²⁾ Unfortunately, not enough experimental data were available to locate the precise course of the coacervate volume curve in the range of the mixing proportions higher than 60 % Cetavlon. The most probable course has been guessed as indicated by the dotted part of this curve in fig. 1. We have been guided here by the course of the curves in fig. 3, Part VII, which deal with the influence of the pH. The shift of the curve which occurs in fig. 3 between pH 5.0 and 5.7, has in all controllable points the same character as in fig. 2. It appears that at 70 % Cetavlon the experimental point must lie close to the maximum of the curve. It is, however, safe to assume a possible error of 1 mixing percentage, which account for the error in the binding of 0.3.

This suppression of the coacervation can of course be considered as the result of a still further decomposition of the cetyl trimethylammonium cation—rich gelatin association.

From the above experiments, it is seen, that NaCl in small concentrations promotes the formation of cetyl trimethylammonium cation-rich gelatin associations. In higher concentrations, it counteracts the above formation.

The above results will be discussed later.

4. Importance of the valency of cation and anion in the influence of salts on the coacervation of gelatin + cetyl trimethylammonium bromide + KCNS

The suppression of the coacervation by NaCl, at a sufficient concentration, is not outstanding as other salts possess this property too. It reminds strongly of the suppressing influence of salts on the complex coacervation of macromolecular colloids.

In the latter case the valency of cation and anion of the suppressing salt is very important. We decided, therefore, to investigate the role of the above valencies on the coacervation of gelatin + cetyl trimethylammonium bromide + K⁺NS.

In this section we do not follow the cumbersome method of section 3, (investigation of the influence on the course of the coacervate volume curves in the mixing diagram) but choose a simpler method. The experiments are performed at one mixing proportion only (50 % Cetavlon) and the influence of a number of salts in various concentrations was tested on this particular mixture.

The general formula of the mixtures was:

5 ml Cetavlon 1 % + 5 ml gelatin 1 % + 5 ml KCNS 0.02 N + 5 ml salt
(containing 18.3 mmol/l KCNS) (containing 10 mmol/l KCNS)
solution.

The salts used were KCl , CaCl_2 , $\text{Co}(\text{NH}_3)_6\text{Cl}_3$ and K_2SO_4 ³).

Written in symbols, in which the valency of the cation and the anion are each denoted by a number, the salts are of the type:

1-1, 2-1, 3-1 and 1-2.

The results are given in figure 3, in which the salt concentrations have been given in milli equivalents/l.

First, our attention is drawn to the sequence of those parts of the curves which proceed definitely downwards to a coacervate volume zero. The salt concentration needed to suppress the coacervation becomes smaller in the sequence

$$\text{KCl} - \frac{\text{CaCl}_2}{2} - \frac{\text{Co}(\text{NH}_3)_6\text{Cl}_3}{3}$$

³⁾ As Cetavlon yields a precipitate with small concentrations of $\text{K}_3\text{Fe}(\text{CN})_6$ and $\text{K}_4\text{Fe}(\text{CN})_6$, these types of salt could not be investigated.

But a salt does not only become more active in its suppressing action when the valency of the cation is increased (at a constant valency of the anion), but the reverse is applicable too. It is seen that the salt concentration needed to suppress the coacervation becomes smaller too in the sequence:

$$\text{KCl} - \frac{\text{K}_2\text{SO}_4}{2}$$

The above is quite characteristic for the suppression of complex relations (Coulomb interactions) in complex colloid systems, for which is applicable

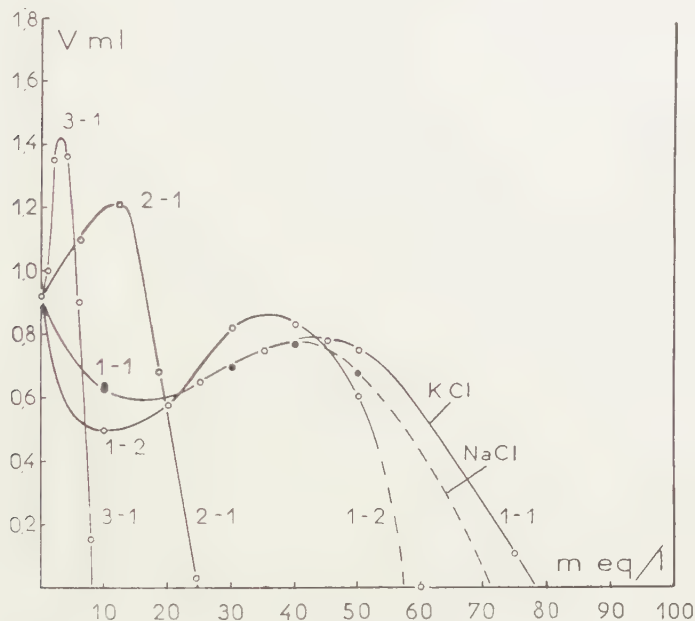


Fig. 3. Influence of salts on the coacervate volume at constant mixing ratio of 50 % Cetavlon. 3 - 1 = luteocobaltic chloride, 2 - 1 = calcium chloride, 1 - 1 = KCl and NaCl and 2 - 1 = potassium sulphate.

the so-called "double valency rule"⁴⁾. This rule states that the suppressing activity increases as the valency of the cation or the valency of the anion increases. This rule may be written in symbols as follows:

$$4-1 > 3-1 > 2-1 > 1-1 \quad \text{valency rule of cations}$$

$$1-4 > 1-3 > 1-2 > 1-1 \quad \text{valency rule of anions}$$

In the influence of salts on complex colloid systems, another sequence of the salts may be met with, at salt concentrations which are smaller than those needed for suppression. In this sequence the same salt types as

⁴⁾ H. G. BUNGENBERG DE JONG, in H. R. KRUYT, Colloid Science II, Chapter X, § 2f. (Elsevier Publishing Company, Amsterdam, 1949).

above are arranged in the so-called "*continuous valency rule*", which is written in symbols:

$$4-1\dots 3-1\dots 2-1\dots 1-1\dots 1-2\dots 1-3\dots 1-4$$

relative positivation relative negativation

This rule is met with in properties of complex systems which depend on the algebraic sum of the positive and negative charges of the complex components⁵). Instances are: electrophoretic velocity of coacervate drops, volume of the complex coacervate, water content of the complex coacervate, solubility of the complex coacervate, etc.

The property considered can then be influenced by salts in small concentrations as a result of the simultaneous screening off of the negatively charged complex component by the cation and the screening off of the positively charged complex component by the anion of the salt.

The screening effect of an ion depends on its valency. Therefore, the salt will alter the property considered in the sequence of the above continuous valency rule.

In general this sequence is found with relatively low salt concentrations as in higher concentrations the salt will exert its suppressing effect (according to the double valency rule).

In fig. 3, we meet this continuous valency series in the sequence in which the coacervate volume curves start to proceed from the blank point. The most steep upwards proceeds the curve of luteocobaltic chloride (type 3—1), less steep the curve for calcium chloride (type 2—1). The curves for the salt types 1—1, i.e. KCl and 1—2, i.e. K₂SO₄ both proceed downwards, the latter more strongly than the former.

It is seen now, that a relative positivation leads to a larger coacervate volume and a relative negativation to a smaller coacervate volume.

Without further data it is, however, not possible to draw any conclusions from the change of the coacervate volume.

The change of a coacervate volume depends on two factors:

- a. the change of the water content of the coacervate, and
- b. the change of the solubility of the coacervate.

Increase of intensity of complex relations diminishes the water content of the coacervate and decreases in turn the solubility.

The former leads to a smaller, the latter to a larger coacervate volume. It will depend on the circumstances which of the two factors has the greatest effect on the coacervate volume.

Hence, the fact that a relative positivation (by a 3—1 salt in small concentrations) leads to an increase of the coacervate volume does not permit to conclude that relative positivation leads to an increase in the intensity of the complex relations. As will be seen later on, the reverse comes true.

⁵) See note 4.

For the present we can only conclude that complex relations play an important role in the cetyl trimethylammonium—gelatin associations. It remains also unknown, which components are directly involved in the existing complex relations.

Before any further experiments will be carried out concerning this question, in the next section the connection between the results presented in figs. 2 and 3 will be considered.

From fig. 3 are known the approximate salt concentrations at which the curves show:

- a. a minimum,
- b. an minimum, and
- c. where the coacervation is totally suppressed.

These data are recorded in the survey below.

Salt and valency type	Approximate concentration in meq/l		
	maximum	minimum	total suppression
$\text{Co}(\text{NH}_3)_6\text{Cl}_3$. . . 3-1	3	—	9
CaCl_2 2-1	12	—	25
KCl 1-1	43	17	78
NaCl 1-1	41	17	68-73
K_2SO_4 1-2	35	11	55-60

5. *Influence of the concentration of salts (of various valency types) on the composition of the cetyl trimethylammonium—gelatin associations*

From now on, the expression millimoles cetyl trimethylammonium cation bound to 1 g dry gelatin will be indicated by the following symbol: CTA/G.

The influence of NaCl on the CTA/G-value has already been derived in section 3 from the position of the maxima of the coacervate volume curves in the mixing diagram (fig. 2). The three values of CTA/G are: blank = 3.6; curve for 25 meq./l = 6 and the curve for 50 meq/l NaCl = 1.9. These values have been plotted in fig. 4 against the salt concentration. Further data in drawing this curve through these three experimental points can be derived from the peculiarities of the NaCl curve in fig. 3.

This figure refers to a mixing proportion of 50 % Cetavlon, i.e. a ratio of 2.6 millimoles cetyl trimethylammonium cation/g dry gelatin in the total system. From the relative positions of the curves in fig. 2 it is seen, that at a definite NaCl concentration between 25 and 50 meq/l, a coacervate volume curve must exist, which has its maximum just at the mixing proportion of 50 % Cetavlon, which corresponds to a CTA/G value of 2.6.

It can easily be argued that the maximum of the NaCl curve in fig. 3 must be situated at the above mentioned "definite NaCl concentration". In this way a fourth experimental point is obtained for the NaCl curve in fig. 4, namely for the CTA/G value of 2.6 at approximately 41 meq/l NaCl (see also the survey).

From the minimum of the NaCl curve in fig. 3 another—though less

certain—information is gained which can be used in constructing fig. 4. It seems reasonable to assume that at the NaCl concentration corresponding to the minimum of the NaCl curve in fig. 3, the maximum of the coacervate volume curve in fig. 2 has been displaced maximally to the right. At this concentration—17 meq/l (see the survey)—the NaCl curve in fig. 4 must have its maximum.

In this way, the NaCl curve has been drawn tentatively, using four known points and with the aid of the information that its maximum must be situated near 17 meq/l NaCl.

About the other salt, much less information is available, as the analogous experiments have not been carried out.

As the similarity of the K_2SO_4 curve and the NaCl curve is very striking (in fig. 3) it will be clear that the K_2SO_4 curve in fig. 4 must have the same

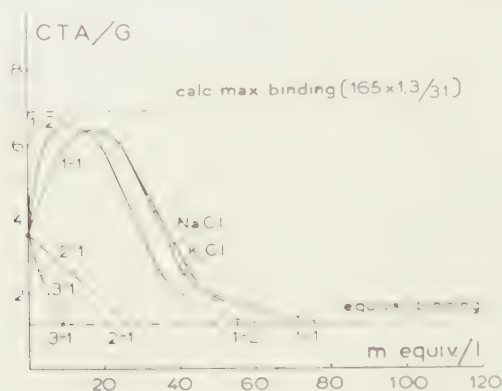


Fig. 4. Influence of salts on the ratio CTA/G

character as the NaCl (or KCl) curve in the same figure. The K_2SO_4 curve has been drawn tentatively, using the information of fig. 3: CTA/G = 2.6 at 35 meq/l (the position of the maximum in fig. 3) and a maximum at about 11 meq/l K_2SO_4 (the position of the minimum in fig. 3).

About the two remaining salts, still less information is available from fig. 3. We only know that the $CaCl_2$ in fig. 4 must go through CTA/G = 2.6 at 12 meq/l (the position of the maximum of the $CaCl_2$ curve in fig. 3), similarly that the curve for luteocobaltic chloride in fig. 4 must go through a CTA/G value of 2.6 at 3 meq/l (the position of the maximum of the luteocobaltic chloride curve in fig. 3).

Though the precise course of the curves in fig. 4 is somewhat uncertain, the magnitude of the errors cannot be such as to endanger the relative positions of the four curves.

Fig. 4 thus gives the influence of increasing concentrations of salts of the types 3—1, 2—1, 1—1 and 1—2, on the composition of the characteristic cetyl trimethylammonium cation—gelatin association. It is seen that K_2SO_4 shares with NaCl the property to increase the CTA/G ratio in small concentrations, and to decrease this ratio at higher concentrations.

Quite different is the influence of CaCl_2 and $\text{Co}(\text{NH}_3)_6\text{Cl}_3$, which only decrease the CTA/G ratio.

In fig. 4, the two characteristic valency rules for complex systems are met once more, namely, in the range of the smaller concentrations the continuous valency rule:

$$\begin{array}{ccc} \text{(decrease of} & & \text{(increase of} \\ \text{CTA/G)} & & \text{CTA/G)} \\ 3-1\dots 2-1\dots 1-1\dots 1-2 & & \end{array}$$

and at higher salt concentrations the double valency rule for the succession of the definitely downward directed branches of the CTA/G curves:

$$3-1 > 2-1 > 1-1 \text{ and } 1-2 > 1-1$$

At the latter concentrations, all salts decrease the CTA/G value.

The long chain-rich gelatin association breaks down which leads to suppression of the coacervation. It seems that the suppression is completed when the CTA/G value has been diminished to about the value which refers to an equivalent binding of the cetyl trimethylammonium cations to the COO^- groups of the gelatin. This equivalent binding is indicated by the dotted line, drawn at an ordinate value of $\text{CTA/G} = 1.2$. On this level are plotted the salt concentrations (given in the survey, section 4) for complete suppression (squares or bars; the latter are used when the salt concentration is not accurately known).

The curves drawn in fig. 4 have been connected with these experimental points (dotted parts of the curves) which can be done without much doubt as to their courses being improbable.

This supports the above supposition, i.e. that the coacervation is suppressed when the CTA/G ratio has been diminished to about the value for the equivalent binding of the cetyl trimethylammonium cations to the gelatin.

It was already pointed out in Part VII, section 5, that at the CTA/G ratio, which corresponds to an equivalent binding, the tricomplex relations are too weak for coacervation.

Summarizing the results in this section, it is concluded that complex relations (Coulomb interactions) play an important role in regulating the composition of the cetyl trimethylammonium gelatin associations.

A discussion concerning the question which complex relations play such an important role, seems at this place not yet opportune, and will be postponed to section 7, after having investigated whether an analogous salt influence is already at work in the system consisting of cetyl trimethylammonium bromide + KCNS, i.e. in systems without gelatin.

6. *Influence of $\text{Co}(\text{NH}_3)_6\text{Cl}_3$, CaCl_2 , KCl and K_2SO_4 on the formation of elastic systems and on the coacervation of cetyl trimethylammonium bromide + KCNS. Fixation of CNS^- ions to the soap*

These experiments have been performed at the same temperature as in

the preceding experiments. First, a series of experiments concerning the influence of the above mentioned salts on the coacervation of Cetavlon with KCNS were carried out. The Cetavlon concentration was $\frac{1}{2}$ % and the KCNS concentration was kept constant at 22.7 millimoles/l, which yields a coacervate volume of 34 %.

The results of the experiments are given in fig. 5.

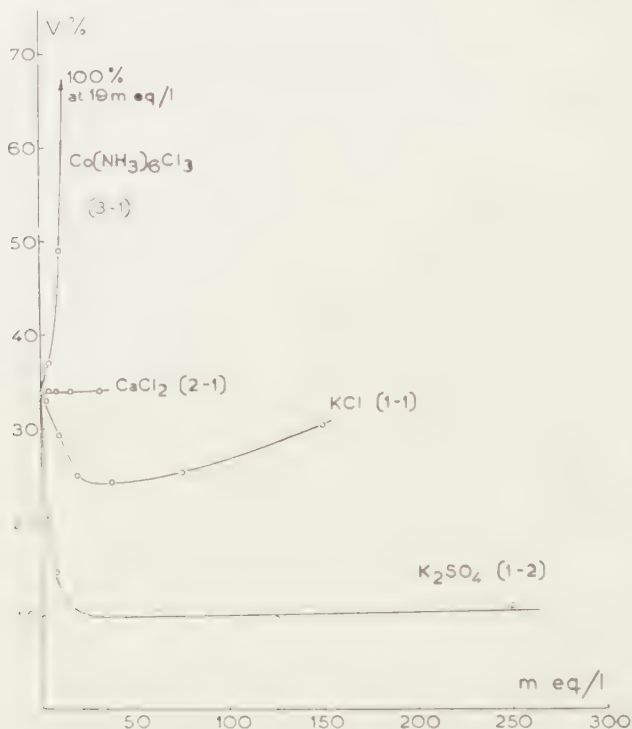


Fig. 5. Influence of salts on the coacervation of cetyl trimethylammonium bromide at a constant KCNS concentration

It is seen that the coacervate volume:

- increases strongly by luteocobaltic chloride,
- remains constant (in the investigated range of concentrations) with CaCl_2 ,
- decreases with KCl (followed by an increase at higher concentrations), and
- decreases much stronger with K_2SO_4 at first, but then remains approximately constant in the investigated range of concentrations.

As the coacervation with KCNS starts with a coacervate volume of 100 %, which decreases strongly (to about a coacervate volume of 9 %) on further increase of the KCNS concentration, it can be concluded that luteocobaltic chloride counteracts the coacervation with KCNS (a higher KCNS concentration is needed to obtain the same coacervate volume as the blank). CaCl_2 exerts practically no influence, and both KCl and K_2SO_4 intensify the coacervation, the latter much stronger.

From former experiments it is known that for obtaining coacervation, a certain percentage of the cetyl trimethylammonium cations must have bound CNS^- ions. The salt influences in fig. 5, therefore suggest that, e.g. $\text{Co}(\text{NH}_3)_6\text{Cl}_3$ counteracts the fixation of the CNS^- ions to the soap ions and K_2SO_4 promotes this fixation. To check this point, a method was used, already described in an earlier communication in detail ⁶). It consists in determining the KCNS concentration needed to obtain a comparable coacervate volume at a number of different soap concentrations. In this way the influence of 30 meq/l luteocobaltic chloride and 20 meq/l potassium sulphate was determined, using four different Cetavlon concentrations ⁷).

The results are collected in Table I and plotted in fig. 6.

TABLE I

KCNS concentrations needed to obtain a comparable coacervate volume ($C \times 40\%$) for 0.5, 1, 1.5 and 2 % Cetavlon, and the influence of 10 millimoles/l potassium sulphate and luteocobaltic chloride respectively

Cetavlon %	blank	K_2SO_4	Cetavlon %	blank	$\text{Co}(\text{NH}_3)_6\text{Cl}_3$
0.5	24.3	21.6	0.5	24.2	25.4
1.0	30.8	29.3	1.0	30.9	32.2
1.5	36.6	35.8	1.5	38.6	40.4
2.0	44.8	44.3	2.0	45.3	46.2

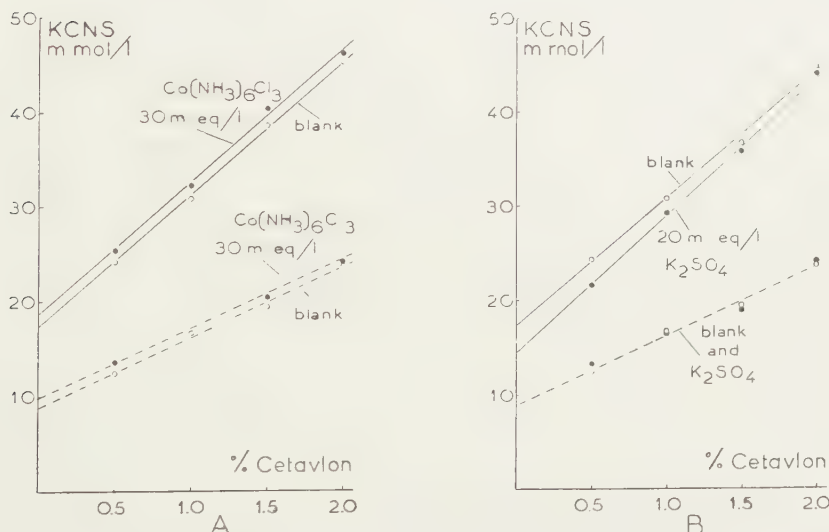


Fig. 6. Influence of luteocobaltic chloride (A) and potassium sulphate (B) on the binding of CNS^- to cetyl trimethylammonium ions. Upper line: limit of the coacervation; lower dotted line: limit dynamic-elastic/static-elastic systems

It is seen that the blank line is shifted upwards by $\text{Co}(\text{NH}_3)_6\text{Cl}_3$, which

⁶) H. G. BUNGENBERG DE JONG and A. RECOURT, these Proceedings, Series B, 56, 303, 315 (1953).

⁷) These experiments have been performed by A. DE BAKKER, to whom we express our sincere thanks for his valuable help.

means that the fixation of the CNS^- ions becomes more difficult. The effect of K_2SO_4 is just the reverse. The equilibrium concentration of the CNS^- ions (the concentration of CNS^- ions, indicated by the intersection of the straight line with the ordinate axis) is increased in the case of luteocobaltic chloride with approximately 1.3 meq/l, and decreased in the case of K_2SO_4 by approximately 3 meq/l.

Next, the influence of both salts on the transition of dynamic elastic to static elastic systems was investigated (this transition is indicated in the graphs by the dotted lines). It was found that with K_2SO_4 no influence could be detected which exceeds the experimental error (about 0.5 millimol/l). Luteocobaltic chloride induces a shift in the direction of higher KCNS concentrations and amounts to 0.9 millimoles/l.

As it is shown that potassium sulphate does promote the fixation of CNS^- ions to the cetyl trimethylammonium cations and that luteocobaltic chloride counteracts this fixation, we may conclude from fig. 5 that the adsorption of CNS^- ions is influenced by salts according to the continuous valency rule:



decreasing adsorption of CNS^-

increasing adsorption of CNS^-

in which the salt of the type 2-1 (CaCl_2) is indifferent.

(to be continued)

CHEMISTRY

CONTRIBUTIONS TO THE PROBLEM OF THE ASSOCIATION BETWEEN PROTEINS AND LIPIDS. IX_B

- a. *Influence of salts on the coacervation of gelatin + cetyl trimethylammonium bromide + KCNS*
- b. *The existence of two types of gelatin — long chain ion associations rich in long chain ions.*

BY

H. G. BUNGENBERG DE JONG AND W. W. H. WEIJZEN

(Communicated at the meeting of March 20, 1954)

7. Discussion

- a. *The results in the sections 3 to 5 are in contradiction to the scheme for long chain — gelatin associations given in Part VI*

The scheme in fig. 7 is reproduced from Part VI.

The long chain ions of the sandwich micelle are bound together by oppositely charged salt ions. These salt ions are necessary to obtain coacervation of the type gelatin + soap + salt.

The positively or negatively charged groups of the gelatin monolayers, which cover the sandwich micelle on both sides, are turned towards the surrounding medium. The binding of these monolayers to the sandwich micelle is supposed to be due to ion-dipole interactions between the pattern of charges on the surface of the micelle and the peptide groups in the gelatin. The polypeptide chains accordingly have their side chains in the plane of the monolayer, or tilted out to some extent towards the surrounding medium.

In Part VII of this series it was provisionally assumed that the scheme of fig. 7 applies also for the long chain ion — rich associations in the coacervation of gelatin + cetyl trimethylammonium bromide + KCNS. In this case the black circles represent negatively charged groups or anions, and the white circles represent positively charged groups or cations. In Part VII it was observed that this coacervation is influenced markedly by salts.

A closer study of this was postponed till later.

In the present investigation, the influence of salts has been investigated systematically and the results in section 4 (occurrence of the continuous valency rule and the double valency rule) showed clearly that complex relations must play an important part in these associations.

In the scheme of fig. 7, no complex relations are present between the

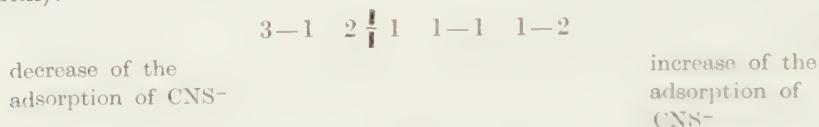
sandwich micelle and the gelatin monolayers. The possible point of action for the salt influences is restricted to the relation between the cetyl trimethylammonium cations and the CNS^- ions.

When this is correct, one should meet the continuous and the double valency rules too for the influence of salts on the formation of viscous-elastic systems and on the coacervation of cetyl trimethylammonium bromide + KCNS — i.e. in systems without gelatin. The experiments in section 6 have been performed for this reason.

The influence exerted by small salt concentrations is discussed first. It appears from section 5 (fig. 4) that the coacervation gelatin + cetyl trimethylammonium bromide + KCNS is influenced by salts according to the continuous valency rule:



This sequence is also met with in section 6 for the influence of salts on the coacervation of cetyl trimethylammonium bromide + KCNS (without gelatin):



The transition from decrease to increase (indicated by a vertical line in both series), lies approximately at the same place.

The close correspondence of the two continuous valency rules seems to support strongly the assumption that the point of action is localized in the interaction between the cetyl trimethylammonium cations and the CNS^- ions.

It can be argued indeed that increase of the adsorption of CNS^- to the long chain cations leads to an increase of the ratio CTA/G in our experiments ⁸⁾, and that decrease of the adsorption will lead to a decrease of the ratio ⁹⁾.

⁸⁾ These experiments are carried out at conditions ($\text{pH} = \text{I.E.P.} = 5.0$ and 10 millimoles/l "free" KCNS) at which in the blank experiments the ratio CTA/G has not yet reached its maximal value, and thus can be varied into both directions.

⁹⁾ In the experiments with cetyl trimethylammonium bromide + KCNS a concentration of 10 millimoles/l "free" KCNS was present. In the experiments without gelatin, this corresponds to a degree of occupation of the soap micelles with CNS^- ions of 40 %. In the associations formed with gelatin, this degree of occupation will have been increased to a certain extent. When now a salt is present, which in the absence of gelatin increases or decreases the adsorption of CNS^- ions, the association formed with gelatin will contain sandwich micelles between the two covering protein monolayers, which are more or less closely packed, as a consequence of the change of the degree of occupation with CNS^- ions.

A more closely packed sandwich micelle means that the ration CTA/G will be

When, however, the question is put forward, whether the increase or the decrease of the binding of the CNS^- ions to the soap will suffice to explain the large effects shown in fig. 4, serious doubts arise.

The effect of 20 meq/l K_2SO_4 and of 30 meq/l luteocobaltic chloride on the binding of CNS ions at the coacervation limit appears to be relatively small, whereas these concentrations have a great effect on the CTA/G value (fig. 4) (compare for instance that with 9 meq/l $\text{Co}(\text{NH}_3)_6\text{Cl}_3$ the coacervation is already suppressed).

But strictly speaking, the influence of salts on the binding of CNS^- ions at the limit dynamic-elastic/static-elastic systems should be compared with fig. 4. Here the effects appear to be still smaller (dotted lines in fig. 6, where for instance the effect of 20 meq/l potassium sulphate and the experimental error are of the same order of magnitude).

At higher salt concentration, no trace of a double valency rule is met with (fig. 5). Hence the double valency rule in the figs. 3 and 4 cannot be explained. Summarizing, it is concluded that the scheme of fig. 7 does not apply for the gelatin-cetyl trimethylammonium associations.

b. A modified scheme which accounts for the influence of salts and the pH

A second complex relation can be introduced by altering the scheme. The binding of the gelatin monolayer to the surface of the sandwich micelle (in the manner given in fig. 8) has no longer the nature of an ion-dipole interaction (as in fig. 1) but is due to Coulomb interactions. Salts, if present in a sufficient concentration, will break these binding by screening off the COO^- groups of the gelatin from the positively charged groups on the surface of the micelle.

As a result the enclosed sandwich micelle is set free, but cannot remain unaltered at the given concentration of free KCNS. It crumbles down to much smaller sandwich micelles or to precursors of sandwich micelles characteristic for that KCNS concentration. The scheme in fig. 8 thus removes at once the difficulty inherent to the scheme of fig. 7. It explains readily:

- a. that salts can suppress the coacervation of gelatin + cetyl trimethylammonium bromide + KCNS,
- b. that for this suppression the double valency rule is met with (fig. 4), and
- c. that the value of CTA/G decreases when this suppression becomes manifest at increase of the salt concentration (fig. 4, the downward course of the curves).

The scheme of fig. 8 is also able to account for the occurrence of the continuous valency rule in fig. 4 and for the influence of the pH (fig. 1).

higher than in the blank, a less closely packed sandwich micelle means that the ratio CTA/G is less than in the blank.

By analogous reasoning, it is found that a salt which decreases the adsorption of CNS^- ions will lead to a lower value of CTA/G.

It must be realized that the experiments were carried out at pH values close to the isoelectric point of the gelatin. At this stage the gelatin is supplied with negatively charged groups with at the same time an equivalent amount of positively charged groups. In fig. 8 it has been assumed

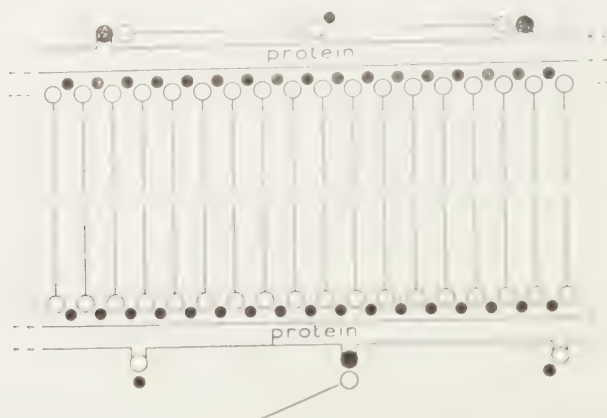


Fig. 7. Scheme of the oleate rich — gelatin associations. Explanation see text. Black dots are positively charged groups or ions, the white circles are negatively charged groups or ions

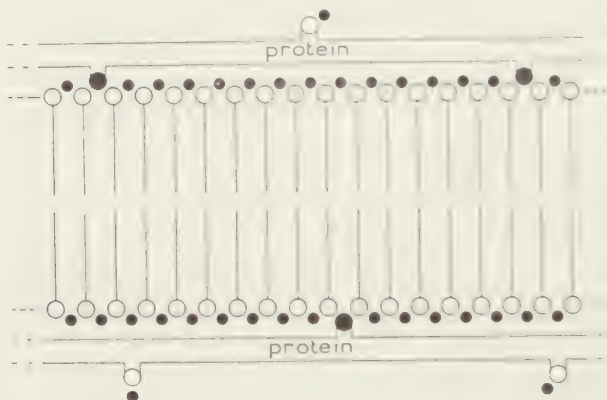


Fig. 8. Scheme for the cetyl trimethylammonium rich — gelatin associations. Explanation see text. Black dots: negatively charged groups or ions, the white circles: positively charged groups or ions.

that the positive groups do not take part in the binding of the gelatin monolayer to the sandwich micelle. Accordingly they have been designed in the scheme to be situated on the external surface of the protein monolayer. However the position of the positive groups may be, it will be reasonable to assume that the positive groups will tend to counteract the binding of the monolayer to the sandwich micelle.

When the prevailing conditions (e.g. a given concentration of free KCNS of 10 millimoles/l) are not such, that a closely packed sandwich micelle is already present enclosed between the monolayers, a negatvation will

lead to a tighter packing, which results in an increase of the CTA/G value. A positivation of the gelatin will act in the reverse direction.

This explains the influence of the pH in fig. 1. It is seen that increase of the pH (a negativation of the gelatin) increases the CTA/G value ¹⁰).

In the preceding section it was seen, that the continuous valency rule can be explained in principle by the influence of salts on the fixation of the CNS ions to the cetyl trimethylammonium cations. The effect, however, is very small and serious doubt arose whether the large effects as shown in fig. 4 can be explained in this way.

It is now interesting that the above reasoning about the influence of a negativation or a positivation of the gelatin also leads to an explanation of the occurrence of the continuous valency rule in figs. 3 and 4.

At constant pH, a negativation or a positivation of the gelatin can be brought about by salts in small concentrations and depending on the valency of the salt.

When a salt of the type 1—2 is considered, the polyvalent anions screen off strongly the positive groups of the gelatin.

This means that the counteraction of these groups on the formation of the association is much decreased. On the other hand, the negative groups of the gelatin are screened off but weakly.

Thus it may be explained that in fig. 4 the ratio CTA/G is increased considerably at small concentrations of K_2SO_4 before at higher concentrations the general suppressing effect becomes the dominating factor. It may seem astonishing that KCl and NaCl — both salts of the type 1—1 — have the same action too.

It only means, however, that the monovalent anion screens off the positive groups of the gelatin more than the monovalent cation screens off the negative groups. In previous work, (measurements of the electrophoretic velocity of gelatin at pH values close to the I.E.P. of the gelatin) it has been found that KCl exerts a negativation of the gelatin ¹¹). The smaller slope of the NaCl and the KCl curve upwards compared to the slope of the K_2SO_4 curve is due to the fact that the monovalent Cl^- ions

¹⁰) The final concentration of Na-acetate in the experiments with acetate buffers was constant (10 millimoles/l). At this concentration the suppressing action is not yet felt.

The final concentration of Na_2HPO_4 in the experiments with phosphate buffers was kept constant too at 10 millimoles/l. But in this case, to obtain pH values much lower than the pK_2 of phosphoric acid, relative high concentrations of KH_2PO_4 had to be used. As a result, the total salt concentration in the experiments with phosphate buffers was such that a relatively strong suppressing effect can be expected. It then follows that at the same pH, the ratio CTA/G which is obtained with these buffers will be much lower than the value obtained with acetate buffers at the same pH. This explains why in fig. 1 the curve obtained with phosphate buffers lies to the right of the one obtained with acetate buffers, and why at pH 5.6 and 5.8 no coacervation can be obtained with these phosphate buffers.

¹¹) L. TEUNISSEN-VAN ZIJP. Thesis, Leiden (1938).

screen off the counteracting positive charges of the gelatin less than the divalent sulphate ion.

We now return to the curves for CaCl_2 (type 2—1) and $\text{Co}(\text{NH}_3)_6\text{Cl}_3$. The polyvalent cations screen off strongly the negative charges of the gelatin. As the latter are directly involved in the binding of the protein to the sandwich micelle, this binding is strongly weakened.

The monovalent anions on the other hand screen off the positive groups of the gelatin much less.

Thus the counteraction of the negatively charged groups is not much decreased. It will therefore not wonder that in fig. 4 the ratio (TA/G is promptly lowered by these salts. As the valency of the cations are different, the curve for the 3—1 salt proceeds steeper than the curve for the salt of the 2—1 type. The continuous valency rule as shown in fig. 4 can, therefore, be explained as the results of the primary action on the two kinds of charges of the gelatin. It is believed that the large effects as shown in fig. 4 are mainly due to the above mechanism, and not to the one considered in the preceding section (influence of salts on the fixation of CNS^- ions to the long chain cations), which yields much too small effects.

Apart from the characteristic associations rich in long chain ions (figs 7 and 8), there also exist characteristic associations which are poor in long chain ions and do not contain micelles (Compare the Parts VI and VII). In principle, there is no difference in the structure of the associations poor in long chain ions, whether they are made up with oleate (an equivalent amount of oleate ions is bound to the basic groups of the gelatin molecule) or with cetyl trimethylammonium ions (the COO^- groups of the gelatin molecule have bound an equivalent amount of cetyl trimethylammonium cations).

In the oleate rich association, the oleate ions bound to the basic groups are found on the outside of the association (fig. 7).

In the associations rich in cetyl trimethylammonium cations, the long chain ions which are bound to the COO^- groups of the gelatin take part in the central sandwich micelle (fig. 8).

c. Connection between the two schemes for long chain ion — gelatin associations

The two schemes of the figs. 7 and 8, for long chain ion — gelatin associations, rich in long chain ions, have in common the central sandwich micelle and the two protein monolayers on both sides of the sandwich micelle.

In a recent communication, ELLIS and PANKHURST reported that it is possible to spread collagen from formic acid solution on $(\text{NH}_4)_2\text{SO}_4$ solutions ¹²⁾.

The surface pressure-area diagrams show two characteristic areas: $1.8\text{m}^2/\text{mg}$ collagen and $1.3\text{m}^2/\text{mg}$ collagen. It was concluded that $1.8\text{m}^2/\text{mg}$ corresponds to close packing of the polypeptide chains with their side

¹²⁾ S. C. ELLIS and K. G. A. PANKHURST, Transactions of the Faraday Society, 50, 82 (1954).

chains parallel to the water surface, and that $1.3 \text{ m}^2/\text{mg}$ corresponds to close packed polypeptide chains with their side chains perpendicular to the water surface.

It will be clear that these results are of direct importance to our problem. They suggest that two kinds of long chain ion — gelatin associations are possible in principle. In the fig. 9, the gelatin molecules are represented by rectangular bars. In this figure, the details as given in the figs. 7 and 8 are left out.

In fig. 9A the side chains lie flat on the surface of the sandwich micelle. Accordingly the keto-imide groups are close enough to the surface of the sandwich micelle that ion-dipole interactions can become effective to bind the protein monolayer to the sandwich micelle.

Fig. 9A thus quite corresponds to the situation as given in the scheme of fig. 7 for the oleate rich — gelatin associations.

In fig. 9B, however, the keto-imide groups stand so much further off

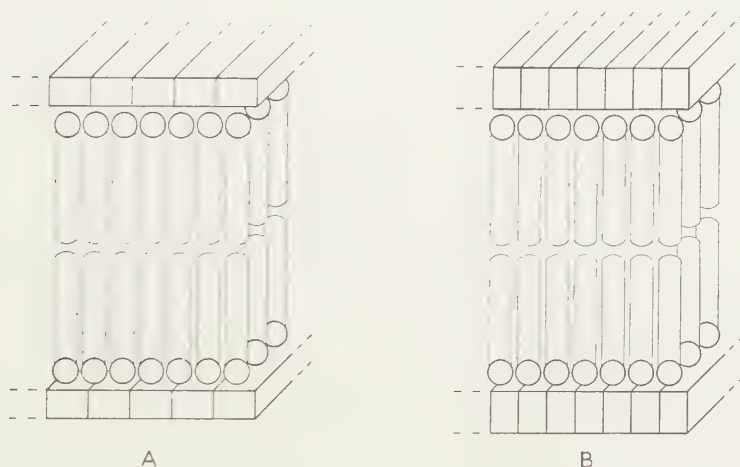


Fig. 9. Scheme for the two kinds of associations of gelatin + long chain ions.

from the surface of the sandwich micelle, that the contribution of the ion-dipole interactions to the binding of the protein monolayer to the sandwich micelle will have no importance. The ionized groups in the side chains of the gelatin will now be in favourable position to bind the protein monolayer to the sandwich micelle by means of Coulomb interactions.

There is of course a difference with the monolayers spread on the water/air interface. In this case, all side chains carrying ionized groups (and hydrophilic groups) are turned as much as possible to that side of the monolayer which is adjacent to the water.

In the long chain ion — gelatin associations, the chains carrying ionized groups of the opposite charge will be turned as much as possible to that side of the monolayer which is adjacent to the sandwich micelle. The side chains carrying ionized groups of the same signs as the long chain

ions, will—as they cannot be bound by Coulomb interactions to the sandwich micelle—be turned towards the surface of the monolayer adjacent to the surrounding watery medium.

Fig. 9B thus quite corresponds to the characteristics of the scheme of fig. 8, given for cetyl trimethylammonium — gelatin associations.

d. The maximal binding capacity with regard to the two variants of the packing of the polypeptide chains in the protein monolayer. Comparison with the experimental results

In the following, the maximal binding capacity will be expressed as usual in millimoles long chain ions per gram dry protein. The amount of long chain ions, bound to the protein, consists in general of two parts, namely, the part bound in the sandwich micelle and the part bound to the oppositely charged groups of the protein on the outside of the protein monolayer. This latter quantity (in millimoles/g dry gelatin) will be designed in the following by B.

The amount of soap, bound in the sandwich micelle between the covering protein monolayers is calculated from the data on the spreading as follows. The area taken up by 1 g protein as a close-packed protein monolayer is divided by the area taken up by one molecule of the amphipatic electrolyte, taken up in a close-packed monolayer. This quotient gives the number of amphipatic ions which in close packing can be placed perpendicular on the surface of a close-packed protein monolayer of 1 g protein. This number can be expressed in millimoles by dividing the number by the number of Avogadro and multiplying by 10^3 .

For the total binding capacity the following expression is obtained:

$$\frac{\text{millimoles long chain electrolyte}}{\text{g dry protein}} = 165.0 \times \frac{A_{\text{pr}}}{A_{\text{ich}}} + B$$

in which:

A_{pr} = surface of the close-packed monolayer of the linear protein expressed in m^2/mg

A_{ich} = area taken up by one molecule of the long chain electrolyte in a close-packed monolayer, expressed in \AA^2

B = millimoles long chain ions bound to the oppositely charged groups of the protein monolayer which are directed towards the surrounding medium.

This calculation will now be applied to the gelatin-oleate associations and the associations consisting of gelatin + cetyl trimethylammonium cations.

Strictly speaking, the data on the spreading areas of the gelatin preparations in our experiments should be used. However, these are not available. Good grades of gelatin, however, can be considered as but

slightly modified collagen. In the following calculations, the above mentioned values on the spreading areas of collagen, given by ELLIS and PANKHURST will be used. In this way, an error will be introduced, but this will not be very great.

In addition to this, another error is introduced, as the data of PANKHURST refer to a close packing at the interface air/water, both for the protein and for the long chain compound. It is not sure, whether the areas for close packing will be the same for the interface monolayer/sandwich micelle. But here too, the mentioned data are the only ones, available.

In the calculations are used the values given by PANKHURST for A_{pr} , namely, 1.3 and 1.8 m²/mg protein. In this way, two values for the binding capacity are obtained, to be compared with the obtained experimental value.

For A_{lch} is used in the calculations in the case of oleate 20.5 A² ¹³⁾ and in the case of cetyl trimethylammonium bromide the value reported by SCHULMAN, 31 A² ¹⁴⁾. The values of B are taken from previous parts of this series.

The calculated values for the binding capacity are given in the columns 4 and 5 of Table II, while the experimental data are recorded in column 3.

TABLE II

associations of gelatin +	A_{lch} A ²	max. binding observed mmol/g gelatin	calculated max. binding for:	
			$A_{pr} = 1.3 \text{ m}^2/\text{mg}$	$A_{pr} = 1.8 \text{ m}^2/\text{mg}$
oleate	20.5	<u>15.2</u>	<u>10.5</u>	14.5 + 1.2 = <u>15.7</u>
cetyl trimethylammonium	31	<u>6.2</u>	<u>6.9</u>	9.6 + 1.2 = <u>10.8</u>

The value for the observed maximal binding in the case of the associations of gelatin + oleate is the mean of three values obtained with different gelatin preparations and using different methods ¹⁵⁾. It is certain that all three values refer to experiments where the maximal value is reached (no increase of the binding at increase of the pH or saltconcentration). A fourth—relatively low—value has not been used, because it

¹³⁾ N. K. ADAM, in the Physics and Chemistry of Surfaces, page 40, (3 Ed., Oxford University Press, 1941).

¹⁴⁾ Discussions of the Faraday Society, 6, 59 (1949); J. H. SCHULMAN in the general discussion of the communication by K. G. A. PANKHURST.

¹⁵⁾ H. G. BUNGENBERG DE JONG, C. R. VAN SOMEREN and F. KLEIN, these Proceedings, Series B, 57, 1,13 (1954).

The ratios obtained with one gelatin preparation (I.E.P. 5.0) were 15.8 ± 0.7 millimoles/g (found by the coacervate volume method) and 15.0 ± 0.2 millimoles/g (found by analysis of the coacervates). With pigskin gelatin (I.E.P. 9.2) a value of 14.9 ± 0.6 millimoles/g was found by the coacervate volume method.

was suspected that the gelatin preparation used cannot be considered as "a but slightly altered collagen preparation"¹⁶).

Taking into account what is said above concerning the possible errors introduced in the calculation, we may say that a satisfactory agreement is reached, in the case of oleate, between the observed maximal binding capacity and the calculated values in column 5. It may be concluded that the oleate — gelatin associations correspond to the schemes given in the figs. 7 and 9A, i.e. the variant of close packing of the polypeptide chains in which the side chains ly parallel to the surface of the sandwich micelle.

In the case of the associations of gelatin + cetyl trimethylammonium, a "satisfactory agreement" seems to be present between the observed values for the maximal binding capacity in column 3 and the calculated values in column 4.

Before drawing a conclusion, however, it must be taken into account, that the value for the observed maximal binding in the case of Cetavlon (6.2 ± 0.3) is not truly a value lying on a constant level (salt concentration or the pH). The value given corresponds to the maximum of het NaCl curve in fig. 4. The ascending branch is presumably on its way to reach such a level, but before reaching it, the suppressing action of higher NaCl concentration sets in already.

At increase of the pH (fig. 1), the binding increases too, but the maximal level was not reached in the experiments because of technical difficulties at higher pH values.

From the course of the curves in fig. 1 it seems unlikely that the level to which they tend will lie higher as the level (dotted line), which indicates the calculated maximal binding using $A_{pr} = 1.3 \text{ m}^2/\text{mg}$.

It seems, therefore, reasonable to assume that the cetyl trimethylammonium associations correspond to the schemes of the figs. 8 and 9B, i.e. the variant of close-packed polypeptide chains with the side chains of the monolayer perpendicular to the sandwich micelle. This conclusion is in agreement with the discussion in sub-section c.

e. Reinterpretation of the maximal binding capacities given in the literature

PANKHURST¹⁷) has given a number of values for the maximal binding capacity for other gelatin — long chain ion associations. As the values obtained with primary alkyl sulphates are nearly of the same order as the number of amino-acid residues in the gelatin molecule, it was supposed that the long chain ions are bound to the keto-imide groups by ion-dipole interactions.

¹⁶) H. G. BUNGENBERG DE JONG and C. MALLEE, these Proceedings, Series B, 56, 203 (1953).

The ratio found was 12.7; doubt arose as the isoelectric point of the gelatin preparations used was unusually low (I.E.P. 4.5 — Eastman Kodak Gelatin (Purified Calfskin)).

¹⁷) K. G. A. PANKHURST in Discussions of the Faraday Society, 6, 52, (1949).

For certain long chain ions, however, lower binding values were obtained (e.g. secondary alkyl sulphate and alkyl naphthalene sulphonate) and even a binding value of zero for flavianate, alkyl trimethylammonium and alkyl pyridinium. These observations lead to the idea that, when the cross-section of either the polar heads or the carbon chain structures become larger, the "penetrability" into the backbone of the protein diminishes, i.e. more and more keto-imide groups are no longer accessible for engaging ion-dipole interactions with the long chain ion.

Our own experiments made the above interpretation very unprobable. For the oleate — gelatin associations a maximal binding capacity of 15 mmols/g gelatin is found. This would mean a penetrability of 150 % which seems very strange. According to PANKHURST, the cetyl trimethylammonium cation has a penetrability zero. In our experiments, this association was realized, by using a suitable salt, i.e. KCNS, the anion of which is able to transform the spherical micelles into sandwich micelles (Part VII).

From the point of view, which is developed in the successive parts of the series, i.e. the associations consist of sandwich micelles covered on both sides by a protein monolayer, it is obvious that the maximal binding capacities will be different in each case.

Table III shows that the binding capacities obtained by PANKHURST (column 3) can be explained in the same way as our own values in the preceding sub-section.

TABLE III

Association of gelatin with	A_{Ich} in \AA^2	Maximal binding capacity observed mmol/g gelatin	Calculated maximal binding mmol/g gelatin	
			$A_{\text{pr}} = 1.3 \text{ m}^2/\text{mg}$	$A_{\text{pr}} = 1.8 \text{ m}^2/\text{mg}^*)$
prim. alkyl sul- phate . . .	20.5	$\underline{10.0} \pm 0.5$	$\underline{10.5}$	$14.5 + 1.2 = \underline{15.7}$
cetyl amine . .	20.5	$\underline{9.0} \pm 1.0^{**})$	$\underline{10.5}$	$14.5 + 1.2 = \underline{15.7}$
7-alkyl naphtha- lene-3-sulpho- nate	35	$\underline{6.2}$	$\underline{6.1}$	$8.5 + 1.2 = \underline{9.7}$
sec.alkyl sulphate	41	$\underline{4.6}$	$\underline{5.2}$	$7.2 + 1.2 = \underline{8.4}$

*) The same values for B (1.2 millimoles/g) as in Table II have been used for the calculation. Whether the gelatin which is used has not precisely the same value, has no influence on the conclusions drawn from a comparison of the values in the columns 3, 4 and 5.

**) PANKHURST gives in his communication, Table I, a value of 100 % penetrability for primary alkyl amine, which means that the maximal binding is the same as in the case of primary alkyl sulphate (10 ± 0.5). In the text of the above communication (see note 17), we found the following statement: "A few experiments with cetylamine showed that at pH 5.5 and 11, between 8 and 10 millimoles/g were adsorbed. A more accurate estimation of the ratio was not possible with this compound owing to its low solubility".

In the column 3, therefore, we have given the maximal binding capacity of 9.0 ± 1.0 .

In column 2, the values for A_{leb} on the first, second and fourth row are those obtained from actual spreading experiments¹⁸⁾; the value on the third row is given by PANKHURST¹⁹⁾.

It appears from Table III that there exists a satisfactory agreement between the observed values and the calculated values in column 4. Hence all associations consist of close-packed sandwich micelles covered on both sides with a gelatin monolayer in which the side chains of the close-packed polypeptide chains are perpendicular to the surface of the micelle.

There has to be assumed, just as in the case of the gelatin — cetyl trimethylammonium associations, a binding of the protein monolayer by Coulomb interactions to the surface of the enclosed sandwich micelle. The only difference is that the intensity of the complex relations is much stronger here (as they have been realized with molar NaCl).

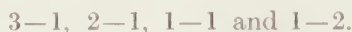
It seems reasonable to ascribe the much smaller intensity of the complex binding in the case of cetyl trimethylammonium ions as complex partner, to the tetrahedral structure of the polar head of the soap, as a result of which the negatively charged groups cannot approach near enough to the positively charged centre of the $-\text{N}^+(\text{CH}_3)_3$ group to yield a strongly NaCl resistant salt bond.

Summary

1. The influence of salts on the coacervation of gelatin + cetyl trimethylammonium bromide + KCNS has been investigated at pH 5 and at a concentration of 10 millimoles/l "free" KCNS. The salts used are:



which correspond to the following valency symbols:



2. The binding ratio CTA/G (millimoles cetyl trimethylammonium/g gelatin), for which the blank value is 3.6, is influenced by salts in small concentrations according to the "continuous valency rule",



in which the vertical line denotes the transition from decreasing to increasing influence. The maximal value of CTA/G reached with salts, to the right of the vertical line was 6.2 ± 0.3 .

3. All salts suppress at sufficient concentration the coacervation. This suppression is accompanied by a decrease of the CTA/G ratio. This sup-

¹⁸⁾ J. H. SCHULMAN (see note 14) gives for alkyl sulphates 20 A^2 . For uniformity with Table II, the value of 20.5 A^2 given by ADAMS (note 13) is used; for cetyl amine the same value has been used in the calculations. For secondary alkyl sulphates, 41 A^2 is used.

¹⁹⁾ See note 17.

pression is complete when CTA/G has decreased to about 1. The suppressing action of the salts follows the "double valency rule":

$$\begin{array}{ll} 3-1 > 2-1 > 1-1 & \text{valency sequence of the anions} \\ 1-2 > 1-1 & \text{valency sequence of the cations.} \end{array}$$

4. In the hitherto developed scheme for long chain ion — gelatin associations, the Coulomb interactions do not play an important role in the binding of the protein monolayer to the enclosed sandwich micelle. The point of action for salts is here only the interaction between the charged polar heads of the long chain ions and the oppositely charged ions from the salt which brings about the coacervation of gelatin + long chain electrolyte + salts.

5. Accordingly, it has been investigated whether the continuous valency rule and the double valency rule are present in the influence of salts on the formation of viscous-elastic systems and on the coacervation of cetyl trimethylammonium bromide + KCNS. It appeared that the continuous valency rule is present:

$$\begin{array}{ll} \text{decrease of the} & \text{increase of the} \\ \text{adsorption of CNS}^- & \text{adsorption of CNS}^- \\ 3-1 & 2-\frac{1}{2} \quad 1 \quad 1-1 \quad 1-2 \end{array}$$

but the effects are much too small to explain the large effects on the ratio CTA/G as mentioned sub 2.

The double valency rule is absent.

It is concluded that the scheme developed for the gelatin — oleate associations does not hold for the associations of cetyl trimethylammonium cations + gelatin + CNS.

6. A modified scheme has been given which accounts for the salt influences. In this scheme, the protein monolayer is bound to the surface of the sandwich micelle by Coulomb interactions. It is suggested that the polypeptide chains in the monolayer stand perpendicular to the surface of the sandwich micelle.

7. The validity of the two schemes developed for long chain — gelatin associations can in principle be controlled by comparing the observed maximum binding capacity with the binding capacities calculated from spreading data. The latter is expressed by:

$$\frac{\text{millimoles long chain electrolyte}}{\text{gram protein}} = 165.0 \times \frac{A_{pr}}{A_{lch}} + B,$$

in which A_{pr} = the surface of a close-packed monolayer of the linear protein expressed in m^2/mg , A_{lch} = the area taken in by a close-packed molecule of the long chain electrolyte in \AA^2 and B = millimoles long chain electrolyte/g protein, which is bound to the oppositely charged groups of the protein monolayer which are directed towards the surrounding medium.

8. For the calculation were used recent data on the spreading of collagen (ELLIS and PANKHURST) viz., $A_{pr} = 1.3 \text{ m}^2/\text{mg}$ for close-packed polypeptide chains with side chains perpendicular to the water surface and $A_{pr} = 1.8 \text{ m}^2/\text{mg}$ for close packed polypeptide chains with side chains parallel to the water surface. In using these data for collagen in the calculation concerning gelatin, an error is introduced so that it cannot be expected that the experimental binding capacities correspond precisely to one of the two calculated values. It appears, however, that the experimental binding capacities come close to one of the calculated values and are very different from the other calculated values.

9. It then appears that the oleate-gelatin associations correspond to the scheme hitherto developed (side chains in the plans of the monolayer covering the sandwich micelle). In the case of the associations of cetyl trimethylammonium cations + gelatin, a close correspondence is found with the modified scheme (side chains perpendicular to the surface of the sandwich micelle). From the binding capacities for primary alkyl sulphates, cetylamine, 7-alkylnaphtalene-3-sulphonate, and secondary alkyl sulphate, reported by PANKHURST, it can be concluded that they all belong to the latter type of associations.

10. It is concluded that two types of long chain ion — linear protein associations exist. They have in common the centrally situated sandwich micelle, which is covered on both sides with a protein monolayer. They differ by the mode of packing of the polypeptide chains in the monolayer and accordingly in the forces involved in the binding of the monolayer to the sandwich micelle. The maximal binding capacities can be calculated in principle from spreading data at the interface water/air.

*Department of Medical Chemistry
University of Leyden.*

THE HYDROLYSIS AND AMINOLYSIS OF ETHYL THIO- ACETATE. I. KINETIC ANALYSIS OF THE ALKALINE HYDROLYSIS

BY

J. TH. G. OVERBEEK AND V. V. KONINGSBERGER

(*Van 't Hoff Laboratory, University of Utrecht*)

(Communicated at the meeting of April 24, 1954)

1. *Introduction*

In a preceding paper [1] concerning the rôle of nucleic acids in the biosynthesis of the peptide bond an acylating interaction of enzyme systems involving coenzyme A (CoA) or similar—SH compounds has been assumed. Recently analogous actions of acyl CoA [2–6] and acyl glutathione [6] derivatives were made probable, but the data on the kinetics of some simpler reactions of the same type, such as the hydrolysis and the aminolysis of thiolesters are still contradictory [7–12].

Preliminary results of our investigations on the reaction kinetics of the hydrolysis and the aminolysis of ethyl thioacetate (E.T.A.) have been communicated previously [12]; we now present our completed data on the alkaline hydrolysis.

2. *Experimental part*

As it was described in an earlier paper [12] all our measurements of reaction velocities have been carried out at a temperature of 37° C., the reacting compounds being dissolved in 0.2 m boric acid—0.05 m borate buffers. Furthermore, the experiments were performed in nitrogen atmosphere in order to exclude oxygen [12]. Before the experiments E.T.A. was freshly distilled from K_2CO_3 also under exclusion of oxygen. The amount of E.T.A. in samples of the reaction mixture was determined according to the method of LIPMANN and TUTTLE [13], which had been rigorously standardized in order to obtain reproducible results.

The sample was mixed with a 2 m hydroxylamine solution at pH 6 and was kept 30 minutes at 37° C, the formation of acetyl hydrozamic acid being completed after 5–15 minutes. The colour, due to the ferric acetyl hydroxamate faded slowly, which made it necessary to measure extinctions at well determined times (30 minutes) after the addition of a 1.66 % $FeCl_3$ solution in 1 N HCl. These measurements were carried out at an average wavelength of 530 m μ by means of an "Engel" colorimeter.

From the extinctions measured the percentages of E.T.A. left after increasing times of incubation were calculated. First order rate constants

were determined by plotting the logarithm of the concentration of E.T.A. left against the time of incubation; second order rate constants were calculated from curves in which the reciprocal value of the concentration of E.T.A. left was plotted against the time of incubation.

The pH of the reaction mixture was determined by means of a "Philips pH-meter G.M. 4491" preferably with the liquid and the glass- and calomel electrodes at a temperature of 37° C. The apparatus was adjusted with the aid of a temperature-independent "Electrofact" standard buffer solution (pH 7) before every experiment. Some pH data obtained at a lower temperature (29° C) were corrected to 37° C by means of an empirical correction.

From the obtained pH data the OH-ion activities were calculated with K_{water} at 37° C = $2,4 \times 10^{-14}$. These OH-ion activities were approximately converted into OH-ion concentrations with the use of the ionic activity

functions $\frac{\gamma_{\text{H}}\gamma_{\text{OH}}}{a_{\text{H}_2\text{O}}}$ [14] of water in NaCl-solutions according to:

$$(1) \quad [\text{OH}] = \frac{2,4 \times 10^{-14}}{\text{antilog}(-\text{pH})} \frac{1}{\sqrt{\gamma_{\text{H}}\gamma_{\text{OH}}/a_{\text{H}_2\text{O}}}}.$$

Concentrations are indicated by symbols between square brackets.

3. Hydrolysis

The results of our measurements dealing with the alkaline hydrolysis of E.T.A. are summarized in table 1.

TABLE 1

Hydrolysis at 37° C of 0.0025 m and 0.00125 (exp. 44, 45) m E.T.A. solutions at various pH. In exp. 1, 4, 19 and 46 borate buffers were used. In exp. 43, 44 and 45 the high pH was obtained by using solutions of NaOH. In these experiments [OH] was calculated from the composition of the mixtures. The pH was calculated from: $\text{pH} = \text{p}K_{\text{water}} + \log f \pm [\text{OH}]$. In exp. 43 and 44 the concentrations of E.T.A. and OH-ions were equal.

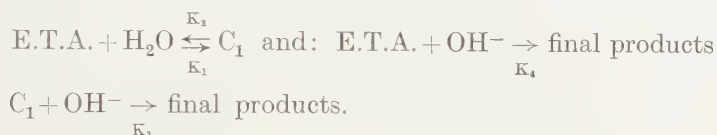
Exp. No.	pH	$[\text{OH}] \times 10^9$ (mol. ml. ⁻¹)	$K_{\text{H}\cdot\text{obs}} \times 10^6$ (sec. ⁻¹)	$\{K_{\text{H}\cdot\text{obs}}/[\text{OH}]\} \times 10^{-2}$ (ml. mol. ⁻¹ sec. ⁻¹)
1	8,34	6,6	8,3	12,5
4	8,68	14,9	16,5	11,1
46	9,01	32,0	30,6	9,6
19	9,56	114	61,6	5,4
44	10,71	1250	—	1,9
43	11,01	2500	—	1,7
45	11,92	24.000	3610	1,5

At all pH's investigated the rate of alkaline hydrolysis of E.T.A. was first order with respect to the concentration of E.T.A. Up to a pH of about 8,7 the rate is also proportional to the concentration of OH-ions. Above this pH the second order rate constant begins to decrease rapidly. However, at very high pH, when the rate constant has diminished to about

10 % of its original value, the rate of hydrolysis again is almost exactly first order with respect to the concentrations of both E.T.A. and OH⁻ ions.

This phenomenon could only be explained by the assumption that the alkaline hydrolysis of E.T.A. occurs by two different pathways. One of these, prevailing at a relatively low pH-range, involves a stepwise mechanism as was assumed before [12]; the other one, involving a rate of hydrolysis which is first order with respect to the OH⁻ ion concentration over the whole pH-range, determines the velocity of hydrolysis for the greater part at high pH.

The first step of the stepwise mechanism is either a monomolecular activation of E.T.A., or, more probably a reaction between E.T.A. and water. A reaction scheme of the following type is assumed:



A reaction kinetic analysis of this scheme gives the following equation for the disappearance of E.T.A. with the time of incubation ¹⁾.

$$(2) \quad \left\{ \begin{array}{l} V_{\text{H}} = \text{velocity of hydrolysis} = \\ = - \frac{d[\text{E.T.A.}]}{dt} = \text{K}_1' \frac{\text{K}_3}{\text{K}_2} [\text{E.T.A.}] [\text{OH}] \frac{1}{1 + (\text{K}_3/\text{K}_2) [\text{OH}]} + \\ + \text{K}_4 [\text{E.T.A.}] [\text{OH}] \end{array} \right.$$

with $\text{K}_1' = \text{K}_1[\text{H}_2\text{O}]$.

When the observed hydrolysis constant is defined as:

$$\text{K}_{\text{H}\cdot\text{obs}} = \frac{V_{\text{H}}}{[\text{E.T.A.}]}$$

it follows from (2) that $\text{K}_{\text{H}\cdot\text{obs}}$ should be a pseudo first order rate constant if the reaction velocity measurements are carried out in buffered solutions or in the presence of an excess of OH⁻ ions for:

$$(3) \quad \text{K}_{\text{H}\cdot\text{obs}} = [\text{OH}] \left\{ \text{K}_1' \frac{\text{K}_3}{\text{K}_2} \cdot \frac{1}{1 + (\text{K}_3/\text{K}_2) [\text{OH}]} + \text{K}_4 \right\} = \text{constant.}$$

For very low concentrations of OH⁻ ions equation (3) may be written as:

$$\lim_{[\text{OH}] \rightarrow 0} \text{K}_{\text{H}\cdot\text{obs}} = [\text{OH}] \left\{ \text{K}_1' \frac{\text{K}_3}{\text{K}_2} + \text{K}_4 \right\}$$

or:

$$(4) \quad \lim \frac{\text{K}_{\text{H}\cdot\text{obs}}}{[\text{OH}]} = \text{K}_1' \frac{\text{K}_3}{\text{K}_2} + \text{K}_4.$$

¹⁾ For the derivation of this equation: See appendix.

For very high OH-ion concentrations, however, eq. (3) can be given as:

$$\lim_{[\text{OH}] \rightarrow \infty} K_{\text{H-obs}} = K_1 + K_4 [\text{OH}]$$

or:

$$(5) \quad \lim \frac{K_{\text{H-obs}}}{[\text{OH}]} = K_1' \frac{1}{[\text{OH}]} + K_4$$

K_1' and K_4 are determined by plotting $\frac{K_{\text{H-obs}}}{[\text{OH}]}$ against $\frac{1}{[\text{OH}]}$ (eq. 5) and extrapolating to $\frac{1}{[\text{OH}]} = 0$.

By plotting $\frac{K_{\text{H-obs}}}{[\text{OH}]}$ against $[\text{OH}]$ (eq. 4) and extrapolating to $[\text{OH}] = 0$ $K_1' \frac{K_3}{K_2} + K_4$ can be determined; as K_1' and K_4 are already known $\frac{K_3}{K_2}$ can be calculated.

Fig. 1A and B and table 2 are illustrations of the procedure outlined above.

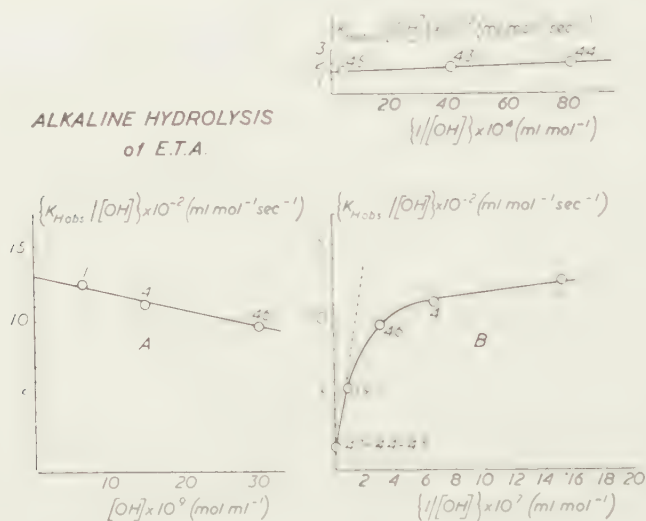


Fig. 1. Alkaline hydrolysis at 37° C of E.T.A.:

A: $\frac{K_{\text{H-obs}}}{[\text{OH}]}$ plotted against $[\text{OH}]$ at low $[\text{OH}]$

B: $\frac{K_{\text{H-obs}}}{[\text{OH}]}$ plotted against $\frac{1}{[\text{OH}]}$ with two different scales of $\frac{1}{[\text{OH}]}$.

TABLE 2

Alkaline hydrolysis of E.T.A.: rate constants determined according to the equations (4) and (5)

$K_1' = 6 \times 10^{-5} \text{ sec.}^{-1}$
$K_4 = 1,5 \times 10^2 \text{ ml. mol.}^{-1} \text{ sec.}^{-1}$
$K_4 + K_1' (K_3/K_2) = 13 \times 10^2 \text{ ml. mol.}^{-1} \text{ sec.}^{-1}$
$K_3/K_2 = 1,9 \times 10^7 \text{ ml. mol.}^{-1}$

These figures will be discussed in the following paper of this series.

The authors wish to thank the students E. M. DUYVIS, P. W. WIERSEMA, W. P. J. D. VAN DER DRIFT, P. W. HENDRIKSE and A. H. WAGENAAR for their help in carrying out the measurements.

4. Appendix

Derivation of equation (2) for the velocity of hydrolysis of E.T.A.:

According to the proposed reaction scheme the reaction velocity can be written as:

$$(2a) \quad -\frac{d[\text{E.T.A.}]}{dt} = K_1[\text{E.T.A.}][\text{H}_2\text{O}] + K_4[\text{E.T.A.}][\text{OH}] - K_2[\text{C}_1].$$

Assuming the existence of a stationary state with respect to C_1 we may write:

$$\frac{d[\text{C}_1]}{dt} = 0 = K_1[\text{E.T.A.}][\text{H}_2\text{O}] - K_2[\text{C}_1] - K_3[\text{C}_1][\text{OH}]$$

or:

$$(2b) \quad [\text{C}_1] = \frac{K_1[\text{E.T.A.}][\text{H}_2\text{O}]}{K_2 + K_3[\text{OH}]}.$$

After substitution of $[\text{C}_1]$ eq. 2a is written as:

$$\begin{aligned} -\frac{d[\text{E.T.A.}]}{dt} &= K_1[\text{E.T.A.}][\text{H}_2\text{O}] + K_4[\text{E.T.A.}][\text{OH}] - K_2 \frac{K_1[\text{E.T.A.}][\text{H}_2\text{O}]}{K_2 + K_3[\text{OH}]} \\ &= K_1[\text{E.T.A.}][\text{H}_2\text{O}] \frac{K_3[\text{OH}]}{K_2 + K_3[\text{OH}]} + K_4[\text{E.T.A.}][\text{OH}]. \end{aligned}$$

By substituting $K_1' = K_1[\text{H}_2\text{O}]$ and rearranging we obtain:

$$(2) \quad \left\{ V_H = -\frac{d[\text{E.T.A.}]}{dt} = K_1' \frac{K_3}{K_2} [\text{E.T.A.}][\text{OH}] \frac{1}{1 + (K_3/K_2)[\text{OH}]} + K_4[\text{E.T.A.}][\text{OH}]. \right.$$

5. Summary

1. Reaction velocities of the alkaline hydrolysis of ethyl thioacetate (E.T.A.) have been measured at 37° C.

2. The rate of the alkaline hydrolysis of E.T.A. proved to be first order in E.T.A. and to increase less than proportionally with the concentration of OH⁻ions.

3. The data obtained are explained by assuming two different pathways for the hydrolysis; one involves an attack of the E.T.A. molecules by OH⁻ions, the other one involves a similar attack but on hydrated E.T.A. molecules.

BIBLIOGRAPHY

1. KONINGSBERGER, V. V., J. TH. G. OVERBEEK, *Proc. Kon. Ned. Akad. v. Wetensch. Series B56*, 248 (1953).
2. CHANTRENNE, H., F. LIPMANN, *J. Biol. Chem.* **187**, 757 (1950).
3. KORKES, S., A. DEL CAMPILLO, I. C. GUNSALUS, S. OCHOA, *J. Biol. Chem.* **193**, 721 (1951).
4. BURTON, R. M., E. R. STADTMAN, *J. Biol. Chem.* **202**, 873 (1953).
5. STADTMAN, E. R., *J. Biol. Chem.* **203**, 501 (1953).
6. RACKER, E., I. KRIMSKY, *Nature* **169**, 1043 (1952).
7. SCHAEFGEN, J. R., *J. Am. Chem. Soc.* **70**, 1308 (1948).
8. RYLANDER, P. N., D. S. TARBELL, *J. Am. Chem. Soc.* **72**, 3021 (1950).
9. HAWKINS, P. J., D. S. TARBELL, *J. Am. Chem. Soc.* **75**, 2982 (1953).
10. SCHWYZER, R., *Helv. Chim. Acta* **36**, 414 (1953).
11. NODA, L. H., S. A. KUBY, H. A. LARDY, *J. Am. Chem. Soc.* **75**, 913 (1953).
12. KONINGSBERGER, V. V., J. TH. G. OVERBEEK, *Proc. Kon. Ned. Akad. v. Wetensch. Series B57*, 81 (1954).
13. LIPMANN, F., C. TUTTLE, *J. Biol. Chem.* **159**, 21 (1945).
14. HARNED, S. H., B. B. OWEN, *The physical Chemistry of electrolytic Solutions*—Appendix. (New York, 1943).

THE THERMAL RESISTANCES OF CUBIC METALS AT
INTERMEDIATE TEMPERATURES

BY

P. VAN DER LEEDEN

(Bosscha Laboratory for Physics, University of Indonesia, Bandung)

(Communicated at the meeting of February 27, 1954)

Summary

It is shown that all data concerning the thermal resistances w of cubic metals at intermediate temperatures ($\Theta/10 < T < \Theta$) may be described by a unique function $w_T/w_\Theta = F(T/\Theta)$.

1. *Introduction*

The theory of DEBYE [1] for the specific heat may be considered as giving the specific heat of "isotropic" materials as a function of T/Θ . As several approximations are made, which certainly are fulfilled roughly only, one might expect that under certain conditions c_v for several materials will much more closely be represented by a unique function of T/Θ than this function will agree with the DEBYE function. It was shown by v. D. LEEDEN [2], that for cubic metals (after subtracting the specific heat due to the electrons) this statement is certainly in agreement with experimental evidence.

In the theory of electrical resistivity the situation is somewhat different. At high temperatures ($T \gg \Theta$) R/T will according to BLOCH [3] approximate a constant. The deviations from this prediction may well be due to the inharmonicity of the vibrations, related with thermal expansion. At low temperatures $R \sim (T/\Theta)^5$ is predicted by him. Again this prediction is restricted. For all cubic metals an exponent 4.5 is in far more close agreement with experimental evidence. The sign of these deviations does not support PEIERLS' criticism [4]. A rigorous $(T/\Theta)^5$ -law might, however, not have been expected, knowing that systematic deviations from the DEBYE spectrum make themselves felt even below $T/\Theta = .05$ [2]. At intermediate temperatures the theoretical predictions have a less rigorous basis. GRÜNEISEN [5] making a rather bold assumption, was, however, able to predict the $R/T - T/\Theta$ -curve. It was found to be in close agreement with experimental evidence, if Θ was given a suitable value. The Θ -values found here are somewhat higher than those deduced from specific heat. Contrary to the opinion held by several authors, this does *not* form a contradiction with theory, as Θ_{el} will have a value between

Θ_{long} and Θ_{th} , if $\Theta_{\text{long}} = \frac{h v_{\text{long}}}{k \lambda_{\text{min}}}$ and Θ_{th} — the DEBYE characteristic temperature, where v_{long} stands for "the" velocity of propagation of longitudinal waves. Again BLOCH's and GRÜNEISEN's predictions may be considered as giving the $R/T = T/\Theta$ curves. One may, however, restrict oneself to the conclusion, that there will exist a unique function in the whole temperature region, more closely followed by all cubic metals than this function agrees with their predictions. Again this correspondence-statement comes nearer the truth.

In the case of thermal resistivity exist the following theoretical predictions [6]. For $T \gg \Theta$, w should be independent of temperature. For $T \ll \Theta$, w should be proportional with $(T/\Theta)^2$. It was shown by V. D. LEEDEN [2], that the latter statement is not contradicted by the existing experimental evidence. The former statement is fulfilled rather well. For the intermediate region no theoretical predictions have been made. In this paper we shall try to answer the question, whether there exists a unique curve in the intermediate region for all cubic metals.

2. The reduction procedure

At not too low temperatures the thermal resistance is practically independent of T , but has rather different values for different metals. The decrease does not "start" at the same temperature for all metals, but at lower T -values the heavier the atoms and the softer the material. Thus if a unique relation exists, both the w - and the T -scales must be "reduced". In other words one might put

$$(2.1) \quad \frac{w_T}{w_\Theta} = F\left(\frac{T}{\Theta}\right),$$

where Θ is a characteristic temperature and w_T and w_Θ the thermal resistance at the temperatures T and Θ resp. Here F then might be a unique function, i.e. F might be independent of the cubic metal considered. We intentionally will *not* take w_∞ as reference value for the following reason: w_∞ is a pure theoretical abstraction, neglecting such experimental phenomena as thermal expansion and melting; this causes unnecessary uncertainties in carrying through a "correspondence test".

The values of Θ are at best defined relatively by (2.1) only. In view of the close theoretical relations between w , R and c_v it seemed indicated to try the further step of putting Θ in (2.1) equal to either the Θ_{th} or to the Θ_{el} -value found with the help of GRÜNEISEN's formula [5]. The latter values as f.i. given by DE HAAS and VOOGD [7] are systematically somewhat higher. This would not enter into our considerations, if $\Theta_{\text{el}}/\Theta_{\text{th}}$ were constant. This is, however, only a first approximation. Moreover there is some doubt as to the best Θ -values to be chosen in each case, as the "best- Θ -values" depend on temperature region considered and relative weight given to higher and lower temperatures. The author believes in principle that all Θ -values ought to be calculated by one and the same

procedure for the same T/Θ (not T) range. This program was carried out by him, using the $R/T - T/\Theta$ -curves for $\Theta/10 < T < \Theta$. Although this certainly leads to Θ -values differing somewhat from those given by other authors; the differences are not very important here. For the sake of objectivity he will use the values of Θ_{th} and Θ_{el} as given by DE HAAS and VOOGD [7].

3. *Some remarks concerning the reliability of experimental data*

Just as with the data concerning the electrical resistivity, some care is needed in selecting reliable data for the purpose under consideration. First of all the purity of the material used may easily impair the results to such an extent as to make them useless. In fact the correction to an ideally pure material may easily become comparable with w itself, especially at the lowest temperatures. Such extrapolations may be carried out using a formula [8, 9, 10]:

$$(3.1) \quad w_{\text{id}} = w - \zeta/LT,$$

with $L = \pi^2 e^2 / 3k^2$. It was, however, shown by v. D. LEEDEN [2] and it also follows from earlier data by GRÜNEISEN and GOENS [9], that this extrapolation gives too high a value for w_{id} . In fact the correction may be too low by 20 %. Next the precision of the determinations of thermal resistances is much more liable to serious systematic errors than the electrical ones.

The first criterion has been applied rigorously. All data, where $\zeta/5LT$ might give too large an uncertainty in w_{id} , were not taken into account, the reason sometimes being that ζ was too high, in other cases that ζ was too poorly known.

The second argument, being far less objective, was only applied to some very early determinations and in cases of sufficient evidence.

4. *Sources of information*

We found data fulfilling the requirements mentioned for Ag, Al, Au, Cu, Pb and Pt. It may be, that some existing data have not come to our notice as our sources of information are limited here. The data for Al and Cu seem somewhat less sure than those for the other metals. The values of $w_{0^\circ\text{C}}$ were taken from the Int. Crit. Tables after critical selection.

Al. For Al we used the data given by GRÜNEISEN and GOENS [9] (Al1). Using their determination of R/R_0 at 21°K , we estimated the z -value. Excepting a preliminary Θ -value, we found $z = .72 \cdot 10^{-3}$ and $\zeta = .74 \cdot 10^{-10}$. The reduction to w_{id} was done by subtracting ζ/LT , without any numerical coefficient. This gave $w/w_0 = -.756$ at $T = 83.2$. At lower temperatures the uncertainties were too high.

Ag. For Ag we used the data of v. D. LEEDEN [2] (Ag1) extending continuously from 14 – 100°K . The residual resistance was extremely small and well known.

Au. For gold there exist data given by MEISSNER [11], by GRÜNEISEN and GOENS [9] and by V. D. LEEDEN [2]. The data of the two former authors are in fair agreement at 80° K. The same statement holds for the data of the two latter authors at 20.4° K. At this temperature MEISSNER's data seem systematically somewhat high. This might be expected from his data concerning his measuring technic. Below 20° K there exist only data by V. D. LEEDEN [2]. The correction to w_{id} is somewhat impaired by the insufficient purity of his purest sample (Au1). GRÜNEISEN and GOENS' purest sample was very pure indeed.

Cu. The data given by MEISSNER [11] have not been used, ζ being rather too large and inaccurately known. GRÜNEISEN and GOENS' measurements [9] at 21° K were only used to estimate z ($z=3.10^{-4}$). A value of $w/w_\Theta=.70$ at 83.2° K was found from their purest sample applying a correction according to (3.1) without a numerical coefficient. At lower temperatures sufficiently reliable information is lacking.

Pb. For this metal there exist several series of determinations. As Θ for lead is relatively small, only the determinations below $T=\sim 100^\circ$ K are of interest. Continuous series in this region are due to DE HAAS and BREMMER [12], to V. D. LEEDEN [2] and to DE HAAS and RADEMAKERS [13]. At the lower temperatures we preferred the results given in the latter two papers.

Pt. At the higher temperatures we used MEISSNER's [11] data, at the lower those given by V. D. LEEDEN [2] for his sample Pt1.

5. Results

The values of $(w_T/w_\Theta)_{\text{id}}$ were calculated. The value of w_Θ did not differ significantly whether Θ_{el} or Θ_{th} was used. For the sake of objectivity we abstained from selecting Θ -values in any way. Although some doubt exists as to whether the Θ_{el} and Θ_{th} -values given by DE HAAS and VOOGD [7] in their study on the electrical analogon are the best possible for the present purpose (cf. § 1), we used their values, for the reasons mentioned, throughout this paper. It was found, that the points in a $w/w_\Theta-T/\Theta_{\text{el}}$ -graph fitted somewhat more closely to a common curve than when using a $w/w_\Theta-T/\Theta_{\text{th}}$ -graph. The former graph is shown in fig. 1. The difference does not seem significant. From our analysis of the $R/T-T/\Theta$ -curves, applying GRÜNEISEN's formula [5] and restricting ourselves consequently to the interval $\Theta/10 < T < \Theta$, we derived the impression, that $\Theta_{\text{el}}/\Theta_{\text{th}}$ was more nearly constant than assumed by DE HAAS and VOOGD [7]. This difference might be due to the greater weight attached to them to the "lower" points, especially for $T < \Theta/10$. In fact they used a double logarithmic graph, which leads to giving more weight to the lower temperature region.

From the above we concluded that:

The reduction of the thermal resistance of cubic face centred metals for temperatures between $\Theta/10$ and Θ to a unique curve is about equally well possible as for R/T and c_θ .

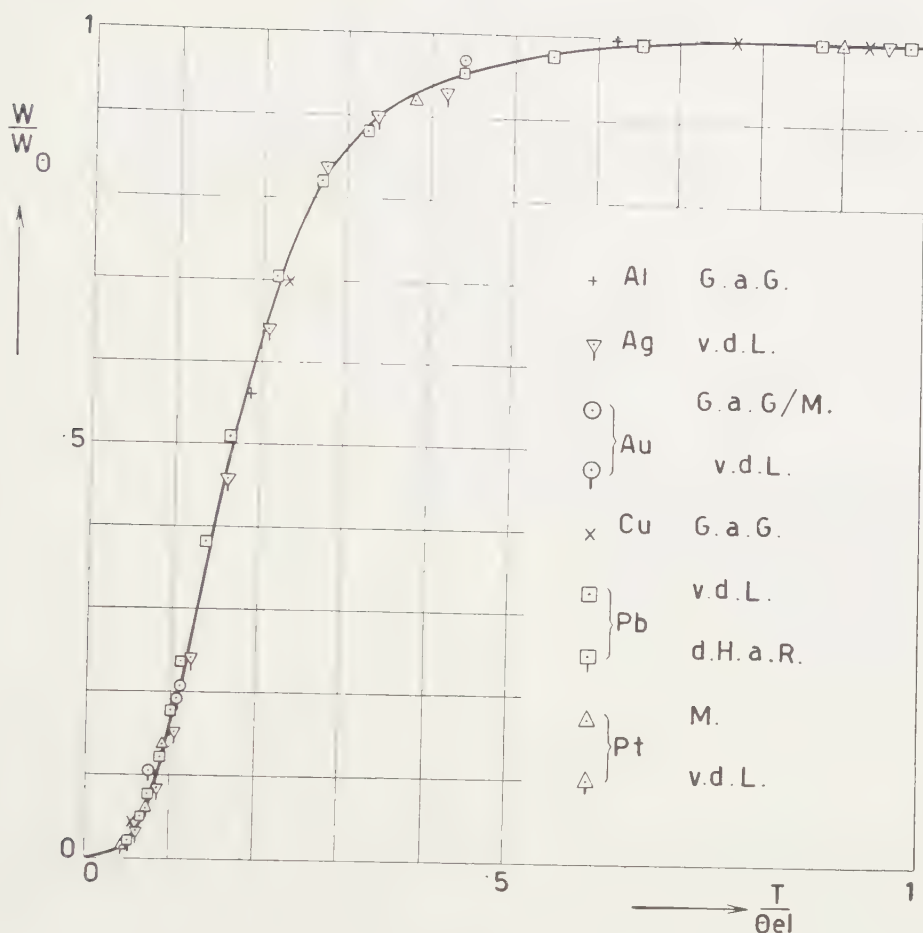


Fig. 1

REFERENCES

1. DEBYE, P., *Ann. d. Phys.* **39**, 789 (1912).
2. LEEDEN, P. v. d., Thesis for the doctorate, Leiden (1940).
3. BLOCH, F., *Zs. f. Phys.* **52**, 555 (1928); **59**, 208 (1930).
4. PEIERLS, R., *Ann. d. Phys.* **4**, 121 (1930); **5**, 244 (1930); **12**, 154 (1932); *Zs. f. Phys.* **81**, 697 (1933).
5. GRÜNEISEN, E., *Ann. d. Phys.* **16**, 530 (1933); *Leipz. Vortz.* 1930 pg 46.
6. PEIERLS, R., *Ann. d. Phys.* **4**, 121 (1930); **5**, 244 (1930).
7. HAAS, W. J. DE and J. VOOGD, *Rapp. No. 10. Congrès Int. d'Electr. (Paris, 1932), Comm., K.O. Lab., Leiden Suppl. 73b.*
8. NORDHEIM, L., *Ann. d. Phys.* **9**, 641 (1931).
9. GRÜNEISEN, E. and E. GOENS, *Zs. f. Phys.* **44**, 615 (1927).
10. ———, *Zs. f. Phys.* **46**, 151 (1927).
11. MEISNER, W., *Ann. d. Phys.* **47**, 1001 (1915); *Zs. f. Phys.* **2**, 373 (1920).
12. HAAS, W. J. DE and H. BREMMER, *Comm. K.O. Lab., Leiden*, 214d; *Proc. Kon. Akad. v. Wet., Amst.*, **34**, 325 (1931); *Physica, s'Grav.*, **3**, 672 (1936); *Comm. K.O. Lab. Leiden*, 243a.
13. ——— and A. RADEMAKERS, *Physica, s'Grav.*, **7**, 992 (1940).

PETROLOGY

THE MINERAL ASSEMBLAGE OF SOME RESIDUAL MONAZITE- AND XENOTIME-RICH CASSITERITE DEPOSITS OF BANKA (INDONESIA)

BY

J. W. A. BODENHAUSEN

(Communicated by Prof. H. A. BROUWER at the meeting of February 27, 1954)

CHOICE OF MATERIAL

Some residual deposits of cassiterite on granite bed-rock in the Muntok district of Northwest Banka are characterized by the occurrence of large quantities of monazite and xenotime. Granite bodies extend over a large part of the region under consideration. In his synopsis of various aspects of the mineralization on the Indonesian Tin Islands, WESTERVELD (1941) distinguished these granite masses as, respectively, the Menumbing granite (after its highest summit, Mt. Menumbing, 445 m) and the Plangas granite. The intrusive rocks are surrounded by a monotonous series of metamorphosed shales and sandstones of Permian or Triassic age. Outside the thermometamorphic aureoles around the granite bodies, this series only shows signs of slight regional metamorphism.

In connection with KIEFT's (1952) investigations on the heavy transparent minerals in granite samples collected in the Djebus district in North Banka, the present author has studied concentrates of monazite- and xenotime-rich residual tin ore from two open pit mines in the Menumbing area, viz. mines Nos. 2 and 4 of the Muntok section indicated in Fig. 1. Mine No. 4 furnished the most abundant material. In addition, a magnetic fraction of the ore concentrate from mine No. 4 and the heavy mineral residues of two samples of strongly weathered granite from the vicinity of mine No. 2 were subjected to examination¹⁾.

The magnetic fraction had been obtained in a local plant by electromagnetic separation of carefully washed material. The ore concentrate of mine No. 2 and the heavy mineral residues of the strongly weathered granite samples from its surroundings were obtained by washing at the locality itself, after the mine had been closed on account of the large quantity of monazite in the ore.

MINERALOGICAL COMPOSITION OF SAMPLES

The mineralogy of the samples referred to above has been examined

¹⁾ One of these granite samples already macroscopically showed intensive tourmalinization, while the other, despite its normal appearance, equally proved to contain a considerable amount of tourmaline on further examination.



Fig. 1. Distribution of residual cassiterite deposits (black) in the Muntok district, NW. Banka (after J. WESTERVELD, 1941).

quantitatively by counting separate mineral grains, of which the relative abundance is expressed in percentages of total numbers by the figures given in the table on the following page ¹).

In the commercial ore concentrate of mine No. 4, approximately 450 separate grains were identified and counted, while in the case of each of the other samples counting extended over somewhat more than 200 grains.

Characteristic features exhibited by the different minerals and the methods used to identify them lead to the following remarks.

Cassiterite could always be identified by means of the reaction with metallic zinc and hydrochloric acid, which two reagents cause tinstone to be envelopped by a thin film of metallic tin through reduction, whereas no other mineral species is visibly affected in this way. The mineral

¹) It should be borne in mind that these figures only represent relative abundances of counted fragments and not volume or weight percentages. The volume and weight percentages of cassiterite are certainly somewhat higher than the percentages of the numbers of grains of this mineral, because the cassiterite normally shows a larger grain size than the other mineral species.

Distribution of mineral species in percentages of numbers of grains identified in individual samples (x means sporadic)

	Mine No. 4		Mine No. 2		
	Ore concentrate	Magnetic fraction	Ore concentrate	Less tourmalinized granite; heavy mineral residues	More
Cassiterite.	36	x	60	13	3
Ilmenite	31	83	11	30	5
Monazite	19	2	22	2	3
Xenotime.	5	10	1	x	x
Tourmaline	4	5	2	52	89
Zircon	3	x	3	3	x
Anatase.	1	—	x	x	—
Quartz	1	x	x		
Brookite	x	—	1	—	—
Corundum	x	—	—	—	—
Rutile	x	—	x	—	—
Ankerite	x	—	x	—	—

mostly occurs as fragments of occasionally twinned crystals (Figs. 2a and b). The colour ranges from different shades of brown to red, very pale orange, yellow, and almost colourless. Sometimes, the grains are almost entirely opaque. Most grains are more or less pleochroic. Irregular distribution of colour may occur, while zoning has also been observed.

Ilmenite, very abundant in the opaque fraction of various samples, has been identified in polished sections, mounted in sealing-wax, with the aid of the ore microscope. No indications of opaque substances other than ilmenite have been found.

The identification of ilmenite received further support from X-ray examination. In addition, some crystals of ilmenite were measured with the goniometer. The crystals are usually tabular and exhibit the forms 0001, $10\bar{1}1$, and $02\bar{2}1$. All individuals examined with reflected light appeared to be free of hematite ex-solution lamellae.

Monazite occurs as crystal fragments and tabular crystals (Figs. 5a, b, and c) of a characteristic bright yellow, sometimes yellowish brown, colour. It could be distinguished from xenotime by its refractive indices (using for this purpose pure methylene iodide and methylene iodide saturated with sulphur); furthermore by means of its optic character, monazite being biaxial and positive with a small optic axial angle, and xenotime uniaxial positive. The monazite in our samples shows a faint pleochroism in yellow.

Measurements with the goniometer revealed the development of the forms 010, 100, 120, 110, 011, 021, 101, $\bar{1}01$, and $\bar{1}11$.

Xenotime could be identified by means of the chemical reaction on phosphate, by its uniaxial and positive optic character, by its refractive indices ($n_w=1.72$), and by measuring the angles of some crystal faces.

The xenotime grains in our samples are greyish white to yellowish, sometimes greenish, in colour. In transmitted light they also show various colour shades. There are apparently two main varieties, linked by transitions. In thicker grains, the most frequent variety shows a pleochroism from a pale greenish brown (n_e) to a pale brownish red (n_w) of almost equal intensities, or with n_w slightly darker than n_e . The other main variety, which sometimes forms cores in the former, is pleochroic from pale green (n_e) to very pale brown (n_w), with the absorption scheme $n_e > n_w$.

Well developed xenotime crystals are rare (Figs. 6a, b, c, and d). Most grains are crystal fragments with a prismatic habit. Under the binocular microscope they can, therefore, be easily distinguished from the zircon of our samples, which latter mineral normally shows little fracturing.

Two well developed crystals were measured with the goniometer, and showed the following forms (elements of GOLDSCHMIDT):

I: 110, 011, and subordinately 010.

II: 010 and 011.

Intergrowths of xenotime and tourmaline appeared to be rather common.

Bastnäsite, a fluo-carbonate of Ce, etc., has the same optic character and similar refractive indices as xenotime. In a few cases, our mineral could be distinguished from bastnäsite by applying the phosphate reaction to a number of grains, and by the goniometric measurements of the two crystals already referred to (xenotime belongs to the tetragonal, bastnäsite to the hexagonal crystal system). Both methods did not however exclude the possible admixture of a small quantity of bastnäsite among mineral grains classified as xenotime in the first instance. Therefore, in order to acquire a still greater certainty, recourse was had to the method of FOSTER (1949) for the distinction of these minerals. A hundred grains with the appearance and refringence of xenotime were ignited at red heat for about one minute. Upon microscopic examination, the grains were all found to be optically unaffected, which proves the absence of any noticeable quantity of bastnäsite.

Tourmaline usually occurs as vertically striated, black crystal fragments with a prismatic habit. Microscopically, it shows a characteristic pleochroism in bluish colours.

Zircon mostly exhibits a well developed idiomorphism and prismatic habit (Fig. 7), rounded grains being rare. The mineral occurs in brownish yellow, violet, pale yellow, greyish, and rarely in colourless and pink varieties. The rounded grains always show a pink or violet colour. Zonal structure is often well developed. The refractive indices are much higher than those of xenotime.

Two crystals were measured with the goniometer, one belonging to the most frequent type of our samples, and the other to a rare type. In the first case, the forms 100, 110, and 111 were identified, in the second case the forms 100, 110, and 311.

Anatase commonly occurs as well-preserved idiomorphic crystals of a characteristic habit (Figs. 3a and b), bounded in most cases only by 011 (orientation BREZINA, unit VEGARD), and showing a horizontal striation on these pyramidal faces. Only few crystals with a basal plane were observed, whilst tabular crystals appeared to be rare.

The mineral occurs in several varieties showing different colours, and may be pleochroic in blue of different shades, in violet or in yellow, with the absorption scheme $n_e < n_o$. The optic character is negative and uniaxial, or biaxial with a very small optic angle. In addition, the mineral shows a strong dispersion and extremely high refractive indices.

In a minor degree, anatase appeared to form an accessory constituent of rutile pseudomorphs after ilmenite (see under rutile).

Quartz occurs both in angular and in rounded grains. The optical investigation of one hundred quartz-like grains proved the absence of any noticeable quantity of topaz.

Brookite could easily be identified by means of its characteristic interference figure with crossed axial plane dispersion. It may also be recognized by the absence of total extinction between crossed nicols.

The mineral mostly builds tabular, slightly elongated crystals and crystal fragments (Figs. 4a, b, and c). Usually, some parts of the crystals are black and opaque, while others are translucent with a yellowish to greenish brown colour. There is a very weak pleochroism in yellowish and brownish shades. Observed forms (orientation and unit HAIDINGER) are 010, 140, 120, 012, 011, 111, and 131.

Rutile, identified with the aid of its X-ray powder diffraction pattern, builds brownish pseudomorphs after ilmenite, with a silk lustre and the common tabular habit of the latter mineral. Apart from the rutile lines, the powder diagram also showed the strongest lines of ilmenite and anatase. Evidently, we are dealing here with original ilmenite crystals, replaced by rutile as well as by anatase through loss of iron oxide.

Ankerite has been observed as a few spherical aggregates of radial crystal fibres with a white colour, which in one instance have been observed as an overgrowth on cassiterite. The powder diagram appeared to correspond very well with those of ankerite and dolomite, whereas it differs distinctly from those of members of the magnesite-siderite series. Since the refractive indices correspond with those of a Mg-poor member of the former series, we are dealing with a carbonate of a composition approaching that of ankerite.

Corundum is extremely rare. Only two grains of this species were recognized in a very large quantity of ore from mine No. 4. Both grains were pleochroic in blue. The mineral is uniaxial and negative with a weak birefringence, and refractive indices of approximately 1.76.

DISCUSSION OF RESULTS

Grouping the various identified mineral species according to their

origin, ilmenite, monazite, xenotime, the bulk of the zircon, and part of the quartz may be considered as original constituents of the granite, whereas cassiterite, tourmaline, anatase, brookite, and another part of the quartz have probably been formed by pneumatolytic-hydrothermal processes. As to corundum, this mineral may have been formed by the assimilation of country rock by the granite, but it may also have been derived from its contact zone. The possibility of the latter suggestion receives support from the occurrence of some rounded crystals of zircon, which in the author's opinion have been derived from the eroded country rock.

The very fine-grained rutile pseudomorphs after ilmenite are to be considered as of late secondary origin, while the spherical ankerite aggregates have certainly grown after the residual concentration of the cassiterite.

The relatively small diversity of minerals found in the samples may be explained by the almost exclusively granitic composition of the country rock of the cassiterite-bearing heavy mineral deposits which yielded the investigated concentrates.

As to the absence of topaz in our samples, the conclusion seems warranted that this phenomenon is due to the irregular distribution of this mineral. In the Djebus granites, for instance, KIEFT (1952) found topaz in only four out of eight granite samples.

Considering the quantitative relations between the various mineral species, the most striking feature is the presence of relatively large quantities of monazite and xenotime in the ore concentrates. The low percentages of these minerals in the granite samples from mine No. 2, on the other hand, have apparently been caused by the intensive tourmalinization of both specimens, in which the content of tourmaline is many times that of the ore concentrates. The abundance of tourmaline in the two granites suggests that their content of cassiterite is also of pneumatolytic origin.

The large amounts of monazite and xenotime in the ore concentrates are clearly illustrative of the high content of rare earths of the tin granites in question, a fact already apparent from VAN TONGEREN's (1938) spectrographic analyses of East Indian rocks, and stressed by other investigators (WESTERVELD, 1941, pp. 193-195; KIEFT, 1952).

The large concentration of xenotime in the magnetic fraction as compared with its original content in the commercial ore concentrate of mine No. 4 illustrates the magnetic properties of this mineral, a fact already recognized by VAN DER LINGEN and WALKER (1925a and b) in their papers on xenotime in certain Cape Province granites.

Another remarkable feature is the absence of any noticeable quantity of magnetite, and the occurrence of ilmenite as the main, and apparently unique, opaque mineral. According to NEWHOUSE (1935, p. 9) and RAMDOHR (1940, p. 30), magnetite generally seems to be the main opaque

oxide in granites and allied rocks, although ilmenite and ilmenite-hematite intergrowths are likewise mentioned as being of common occurrence along with magnetite. RAMDOHR states, however, that in exceptional cases ilmenite may be the predominant opaque mineral. Since this alternative seems to apply to the Menumbing granite mass near Muntok, it might be asked whether a predominance of ilmenite among the opaque constituents of a tin granite is a regular or an incidental feature of this type of rock, which in the opinion of WESTERVELD (1936, p. 1208) more or less represents an ultimate state of magmatic differentiation, characterized, among others, by a very low content of iron oxides. In our case, the absence of ilmenite-hematite intergrowths and of magnetite in all samples seems to be indicative of a low Fe: Ti ratio in the residual liquid out of which the ilmenite individuals may be conceived to have crystallized without an excess of dissolved ferric oxide.

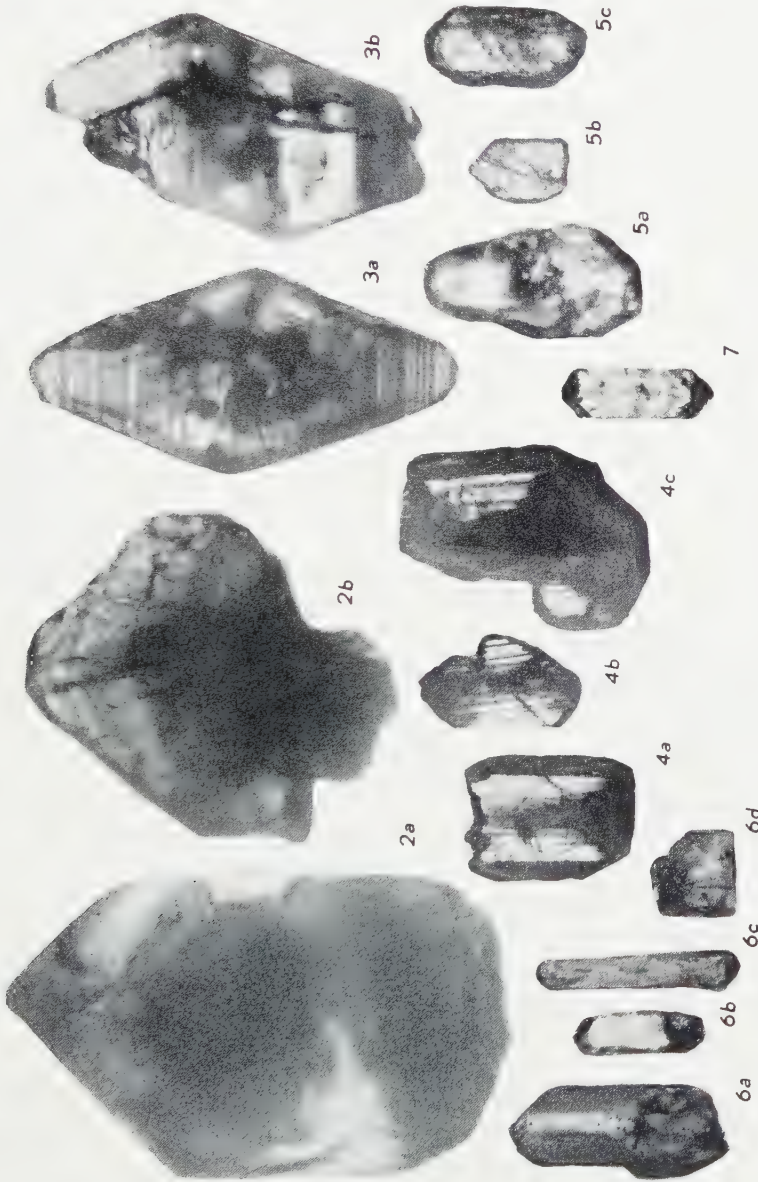
Acknowledgements. The author wishes to express his gratitude to Dr W. P. DE ROEVER for his valuable advices concerning methods of mineral identification. Prof. Dr C. H. MACGILLAVRY kindly provided X-ray photographs of several of the minerals studied. The manuscript has been critically read by Prof. Dr J. WESTERVELD, who offered some constructive suggestions.

*Amsterdam, Geological
Institute of the University*

REFERENCES

- FOSTER, W. R., *Petrographic distinction of xenotime and bastnäsite*, Am. Min., **34**, 830-834 (1949).
- KIEFT, C., *Accessory transparent minerals in tin granites of North Banka, Indonesia*, Proc. Kon. Ned. Akad. van Wetensch., **55**, 140-149 (1952).
- LINGEN, J. VAN DER and A. R. R. WALKER, *Xenotime: An accessory constituent of certain Cape Province granites*, Trans. Geol. Soc. of South Africa, **28**, 73-77 (1925a).
- and ———, *On a heavy mineral concentrate from the Kuils River district C.P. and the occurrence of xenotime therein*, Trans. Geol. Soc. of South Africa, **28**, 69-72 (1925b).
- NEWHOUSE, W. H., *Opaque oxides and sulphides in common igneous rocks*, Bull. Geol. Soc. of America, **47**, 1-52 (1936).
- RAMDOHR, P., *Die Erzminerale in gewöhnlichen magmatischen Gesteinen*, Abh. Preusz. Akad. der Wiss., Math.-naturw. Kl., Nr. 2, 43 p. (1940).
- TONGEREN, W. VAN, *On the occurrence of the rarer elements in the Netherlands East Indies*, Dissertation, Utrecht, 181 p. (1938).
- WESTERVELD, J., *The granites of the Malayan tin-belt compared with tin-granites from other regions*, Proc. Kon. Akad. van Wetensch., **39**, 1199-1208 (1936).
- , *Mineralisatie op de Tineilanden*, Jaarboek der Mijnbouwkundige studenten te Delft 1938-1941, 187-233 (1941).

J. W. A. BODENHAUSEN: *The mineral assemblage of some residual monazite- and xenotime-rich cassiterite deposits of Banka (Indonesia)*



Figs. 2a, b. *Cassiterite*, ore concentrate, mine No. 4 ($\times 120$)
 Figs. 3a, b. *Anatase*, ore concentrate, mine No. 4 ($\times 120$)
 Figs. 4a, b, c. *Brookite*, ore concentrate, mine No. 4 ($\times 40$)
 Figs. 5a, b, c. *Monazite*, ore concentrate, mine No. 4 ($\times 40$)
 Figs. 6a, b, c, d. *Xenotime*, magnetic fraction, mine No. 4 ($\times 40$)
 Fig. 7. *Zircon*, ore concentrate, mine No. 4 ($\times 40$)

GEOLOGY

PREDOMINANCE OF INTERMEDIATE AND MORE ACID ROCKS AMONG THE CRETACEOUS VOLCANIC PRODUCTS IN THE SOUTHERN PART OF THE CORDILLERA BLANCA, PERU

BY

C. G. EGELER

(Communicated by Prof. H. A. BROUWER at the meeting of February 27, 1954)

In 1952 the author, in company with T. DE BOOY, carried out a geological exploration in the southern part of the Cordillera Blanca in NW Peru ¹⁾. The present paper is the first of a number of preliminary notes on various results of this exploration ²⁾. It is based on field observations of both participants as well as on microscopical determinations by the author.

The main scope of this paper is to point out that, in the southern Cordillera Blanca region, the cretaceous volcanism was predominantly of intermediate to more acid nature, instead of being exclusively basic, as generally accepted for the Peruvian Andes.

One of the most characteristic features of the Mesozoic in the region of the South American Cordilleras, is the intensive volcanic activity, which in many places has prevailed during that era. The following general data on the occurrence of the volcanic products may be derived from STEINMANN's renowned publication on the geology of Peru (Lit. 3). In Chili and the Argentine the volcanic activity started during the Triassic with the production of predominantly acid rocks, whereas the later volcanic products, of jurassic and cretaceous age, are said to be of exclusively basic character. The main rock types produced during this basic phase, were diabase, diabase-porphyrite, augite-porphyrite, labradorite-porphyrite and melaphyre. The basic series is mostly indicated as the "Porphyrite formation", though the name "Andean diabase-melaphyre formation" was proposed by STEINMANN as being more appropriate on account of the exclusively basic nature of the rocks in question. In the Peruvian Andes, contrary to the regions just mentioned, the mesozoic eruptive activity apparently started at a much later date. Here, with a

¹⁾ The participants of the Cordillera Blanca expedition gratefully acknowledge grants from the Netherlands Organization for Pure Research (ZWO), the Royal Netherlands Geographical Society (KNAG), the Royal Netherlands Geological and Mining Society (KNGMG), the Molengraaff Fund, the Prins Bernhard Fund, the Royal Netherlands Alpine Club (KNAV), as well as from various Dutch industrial and business concerns.

²⁾ For a brief report on the expedition and its main results, refer to Lit. 1.

single exception³), the eruptions were said to have begun only in the Cretaceous, the first definite traces being found in the Neocomian, in the higher beds of the coal-sandstones (slate-sandstone formation). By this time the basic material was said to be widely distributed in the western Cordilleras, developed as flows, sills and tuffs, intercalated between the sedimentary strata. Higher in the Neocomian, basic tuffs were also said to be represented, while volcanics of basic character have further been described from the Upper Cretaceous.

Rocks varying in composition from intermediate to acid were hitherto only known from the Tertiary of the Cordillera Blanca, the members of the group being indicated by STEINMANN as rhyoandesites. Elsewhere in Peru, acid volcanic rocks are also represented in the Rimac formation, for which, according to GERTH (Lit. 2), a tertiary age seems most probable. In the Quaternary, intermediate varieties (andesites) seem to have predominated almost to the exclusion of all other rock types (Lit. 3).

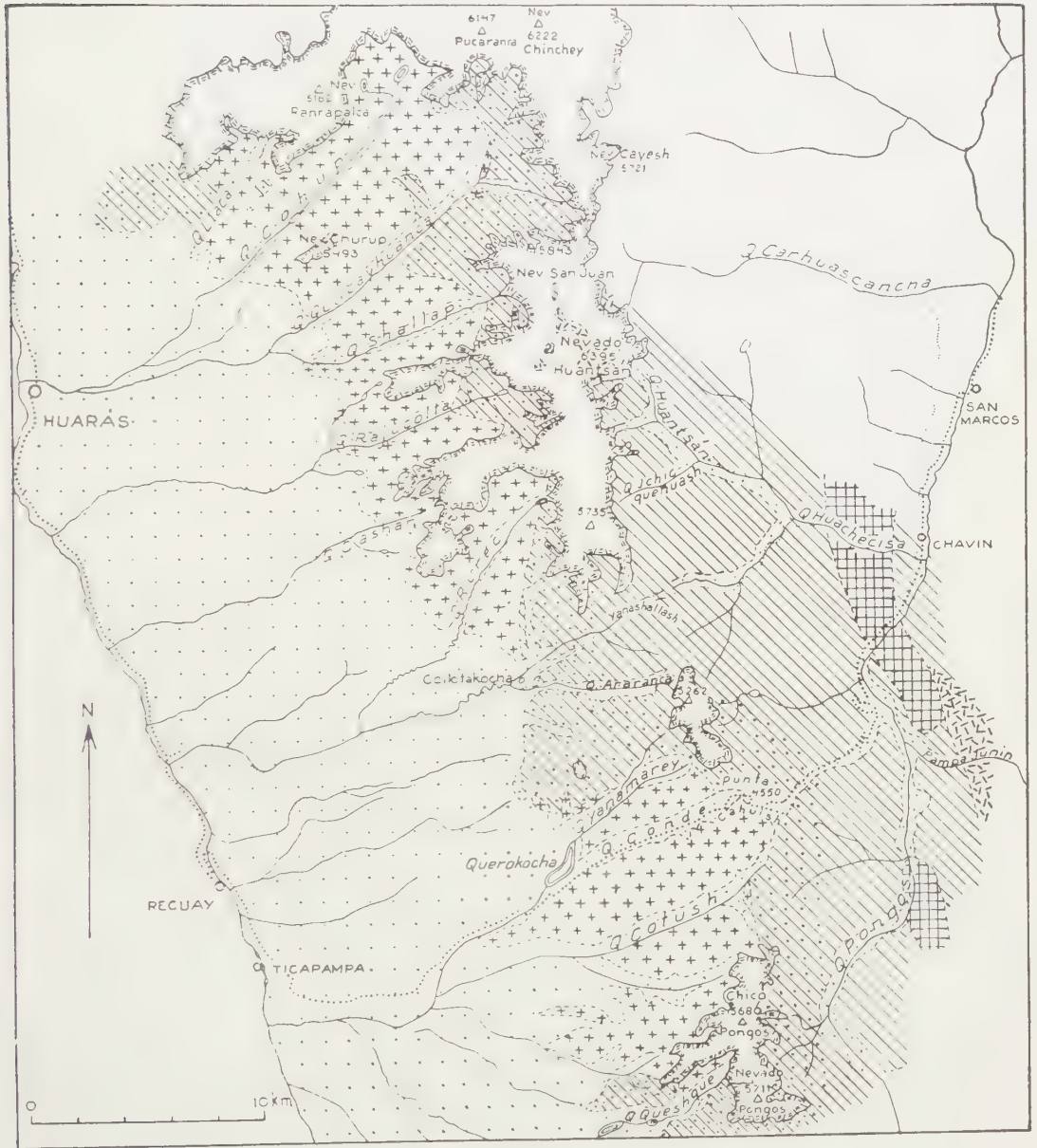
Our 1952 exploration in the southern part of the Cordillera Blanca found volcanic and subvolcanic rocks of cretaceous age to be of widespread occurrence. However, instead of being exclusively basic, these volcanics proved to be for the greater part of intermediate to more acid character. Andesitic varieties are especially abundant, but they are almost universally associated with dacites and occasionally also with rhyolites, and therefore cannot be considered as the most acid representatives of the Andean diabase-melaphyre formation. More basic rocks are also found, though more subordinately, the chief types represented being diabase, diabase-porphyrite and basalt.

In view of the widespread occurrence in Peru of intermediate and acid volcanic rocks of post-cretaceous age, and in view of the discrepancy of our findings with those of others, it will be clear that the age-relations of the rocks under consideration deserve special attention. Therefore the mode of occurrence of the cretaceous volcanics in the Cordillera Blanca region, will be discussed in some detail, beginning with their general geological setting.

The Cretaceous within the southern part of the Cordillera Blanca is chiefly represented by the monotonous series of originally argillaceous and arenaceous sediments of mainly terrestrial origin, which in the Peruvian Cordilleras is considered to be of lower neocomian age, i.e. on account of its occurrence between marine deposits of the Tithonian and massive limestones of the Barremian (see e.g. STEINMANN, Lit. 3 and GERTH, Lit. 2). In several places within the investigated region, this slate-sandstone formation is found to contain conglomeratic intercalations, while coal-layers are of local occurrence along the eastern slopes of the range. Most of the intermediate and more acid volcanic rocks

³) The exception is found in Morro de Arica and neighbouring regions, where, according to STEINMANN, basic eruptions already occurred during the Jurassic.

Fig. 1. Geological sketch map of part of the southern Cordillera Blanca



Ice cover



Plutonic rocks: mainly granodiorites and tonalites. Tertiary



Limestones, sandstones and marls



Slates and sandstones, with local coal-layers, conglomerates and predominantly intermediate and more acid volcanic and subvolcanic rocks: "slate-sandstone formation"



Ditto, thermally metamorphic; mainly hornfelses and quartzites



Alluvia



Volcanic rocks: mainly dacitic and andesitic lavas, tuffs, or agglomerates. Cretaceous (and possibly younger)

Neocomian

mentioned above, were found in association with these lower neocomian sediments. On the eastern side of the Cordillera the slate-sandstone formation is locally covered by massive limestones, presumably representing the base of the Barremian. Then follows a series mainly consisting of sandstones and marls, while the sequence is completed by richly fossiliferous limestones.

In the Cordillera Blanca the main (Incaic) phase of the Andean folding, which, according to STEINMANN, took place in the older Tertiary, was followed by large-scale plutonic intrusion. The plutonic masses have attained their largest visible extension in the northern and central parts of the range, but fairly large masses, mainly of granodioritic and tonalitic composition, are also found further south. In the investigated region they are almost entirely restricted to the western side of the range, where they are intrusive in the folded lower neocomian rocks, with a thermal aureol approximately 2 km in width. Locally the large plutonic bodies are accompanied by smaller irregular masses and cross-cutting dikes of porphyritic rocks within the sedimentary series, which differ from the volcanic rocks mentioned above, as they have suffered no thermal metamorphism. Their restricted occurrence in the vicinity of the larger masses, suggests a direct relationship to the latter, as also indicated by the considerable resemblance in composition. Nevertheless, these tertiary porphyritic rocks—STEINMANN's so-called intrusive rhyoandesites—may also resemble the subvolcanic rocks of the Cretaceous and in certain cases they may even be difficult to distinguish.

The volcanic rocks of the Cretaceous, which in the region investigated are of much more widespread occurrence than the porphyritic rocks of the Tertiary, are mostly developed as sills, though effusive types are also represented.

Sills were only found in the lower neocomian slate-sandstone formation and not in the upper neocomian deposits. In some parts of the range considerable numbers of these concordant bodies are assembled in restricted areas, e.g. in the higher eastern slope directly below the Yanashallash Pass (see fig. 2), and on the northern side of Quebrada Ichicqueñuash. In the Yanashallash locality, andesitic and dacitic rocks form sills of varying thickness (up to 16 m), which are conspicuous even at a distance, on account of their diverging colour and erosional shape with respect to the enclosing sediments. In this instance the intrusive character could be definitely established: small fragments of the country rock are enclosed in the marginal zones on both sides of the igneous bodies, while chilled margins are found, the groundmass in the central parts of the sills often being of relatively coarse grain. The uniform thickness of these igneous bodies, often over distances of many hundreds of metres, is a very characteristic feature. In the Ichicqueñuash locality, the sills of dacite and andesite are found to be locally associated with cross-cutting dikes of diabase. The igneous rocks at the Yanashallash Pass have almost escaped



Fig. 2. Dacitic and andesitic sills in the slate-sandstone formation on the east side of the Yanashallash Pass

the thermal influence of the plutonic intrusions, whereas those in the Q. Ichicqueñuash are considerably more metamorphosed.

In other localities along the western slopes of the Cordillera, the thermal metamorphism of comparable igneous bodies is still much stronger, and has sometimes attained such an intensity that in the field the igneous rocks are even difficult to distinguish from the adjacent sediments. Especially the original sandstone layers, now converted to quartzites, may from a distance show a considerable resemblance to the metamorphic sills, both in colour and in shape of erosion. While the sandstones are changed to quartzites and the, initially more argillaceous sediments to hornfelses (rich in such minerals as biotite and andalusite, occasionally together with garnet, cordierite or sillimanite), the igneous rocks may also have acquired a truly hornfelsic habit. Newly formed biotite is very abundant; in rare cases some garnet is found, whereas more basic rock types are rich in amphibole of metamorphic origin. In general the metamorphism has caused the breaking down of the igneous structure; almost without exception the groundmass is completely recrystallized and in general the only initial structural feature of the rocks preserved, is represented by blastoporphyritic crystals of feldspar and occasionally quartz, often in course of granulation. Notwithstanding this far advanced degree of transformation, the mineral composition indicates that in the majority of cases andesitic and dacitic varieties are dealt with, though more basic rock types are also represented in various localities. Good examples of these metamorphic bodies, considered as sills, are found e.g. N of Laguna Collotakocha.

A shallow intrusive origin of, at any rate a number of the sills, is suggested by the occurrence of pebbles of porphyritic rocks of similar type as those forming the igneous bodies, in metamorphosed conglomerates exposed in their vicinity, e.g. in Quebrada Rajucolta.

It is clear that in the neighbourhood of the granodioritic intrusions, where the thermal metamorphism is strongest, it is in many cases not easy to distinguish between sills and lava flows, as such criteria as chilled margins are lost. Moreover, the situation may be further complicated by the folding, which sometimes has caused distortion of the igneous bodies. However, some of the intensely changed volcanic rockbodies found in the slate-sandstone formation on the western side of the range, are considered to be of effusive origin, as for instance the irregular mass exposed on the southern side of Quebrada Araranca. This fairly large mass is mainly composed of almost white, metamorphic rhyolitic to dacitic rocks of a conspicuous type rarely encountered in the region. It occurs amid thermally metamorphosed, lower neocomian sediments, which in the vicinity contain conglomerates with fragments of the same type of white lava. The acid lavas are characterized by large phenocrysts of quartz, which under the microscope often appear remarkably well preserved, in contrast to the original feldspar phenocrysts, which are considerably changed to micaceous material. The quartzo-feldspathic groundmass is completely recrystallized and contains large amounts of sericitic mica, besides varying amounts of newly formed biotite of patchy distribution. In several of the investigated samples some garnet occurs, while other products of the thermal metamorphism may be andalusite, cordierite, a pale green spinellid, and occasionally tourmaline.

Lavas were also found outside the zone of strong thermal metamorphism, viz. on the eastern side of the range, in the volcanic complex of the Nevado Huantsán. Here they are associated with agglomeratic and tuffaceous rocks of dacitic, andesitic and basaltic composition, which in most cases appear to be only slightly affected by thermal metamorphism. Besides occurring in the Huantsán complex, agglomerates and tuffs were only found in the volcanic complex of Pampa Junin, in the E of the region investigated, here being represented by acid varieties ⁴⁾. Our observations warrant no direct conclusions as to the relation of these volcanic complexes to the sedimentary series.

In view of the foregoing, our main indications as to the age of the intermediate and acid volcanic products in the southern part of the Cordillera Blanca, appear to be: (1) the occurrence in the lower neocomian slate-sandstone formation, of sills of dacite and andesite, (2) the presence of pebbles of volcanic rocks of similar type in intercalated conglomerates, and (3) the occurrence in said formation, of acid volcanics considered to be of effusive origin.

⁴⁾ These volcanic complexes are separately indicated on the sketch map.

While the sills in the slate-sandstone formation prove that intrusive volcanism was active either during or after the deposition of the lower neocomian sediments, and the pebbles of igneous rocks of similar type in the conglomerates, show that the corresponding eruptions started either before or during this deposition, volcanic activity during the Lower Neocomian is proved by the effusive rock types. In combination with these indications, the widespread distribution of sills in the slate-sandstone formation, as contrasted with their apparent absence within the investigated region, in the younger deposits of the Neocomian, strongly suggests a lower neocomian age for at least the majority of the igneous rocks under consideration. On all account, the ubiquitous thermal metamorphism of the volcanic and subvolcanic rocks in the neighbourhood of the plutonic intrusions, forms conclusive evidence that they are of pre-granodiorite age, a conclusion which also holds good for the effusive rocks of the Huantsán complex.

The predominance of intermediate and more acid instead of basic rock types among the cretaceous volcanic products in the southern part of the Cordillera Blanca, is of interest in view of Stille's general conception of an initial magmatism of preponderantly basic character, as contrasted with acid plutonism in connection with the succeeding folding (Lit. 4, p. 11). In the present case, the chemical composition of the pre-orogenic volcanics shows no conspicuous difference from that of the granodioritic and tonalitic intrusions, emplaced after the main phase of the Andean folding, nor from that of the subsequent volcanism. Seen in this light, the intermediate to more acid nature of the cretaceous volcanism in the investigated region, appears to be of more than local importance. It may influence current views on the relationship between magmatism and tectonic evolution in folded mountain chains of the Andean type.

Amsterdam, Geological Institute of the University

REFERENCES

1. EGELER, C. G. and T. DE BOOY, De geologisch-alpinistische exploratie in de Cordillera Blanca, Peru (with English summary). Tijdschr. Kon. Ned. Aardr. Gen. 2nd ser., 71, no. 1, 47-61 (1954).
2. GERTH, H., Geologie Südamerikas. Geologie der Erde I (Berlin, 1941).
3. STEINMANN, G., Geologie von Perú (Heidelberg, 1929).
4. STILLE, H., Zur Frage der Herkunft der Magmen. Abh. Preusz. Akad. d. Wiss. 1939, Math.-naturw. Kl., Nr. 19, 1-31 (1940).

THE STATUS OF *HASSELLTIDES PRIMIGENIUS* WEYENBERGH, 1869

BY

C. O. VAN REGTEREN ALTENA

(Communicated by Prof. H. BOSCHMA at the meeting of February 27, 1954)

Hasseltides primigenius is a fossil from the lithographic stone of Solnhofen, Bavaria, and consequently of Jurassic age. It was cited for the first time by WINKLER in 1865 as "Arachnide? sp. de Solenhofen". WEYENBERGH (1869b) originally took it for an arachnid of the family Agelenidae, probably related to the genus *Argyroseta*. Dr A. W. M. VAN HASSELT, however, suggested to WEYENBERGH that it rather might be an opilionid or a phalangid. He drew attention to the resemblance the fossil showed to the opilionid genera *Acantholophus*, *Nemastoma*, *Zacheus*, etc., and WEYENBERGH (1873) concluded that it might be related to the opilionid genus *Acantholophus*. To MEUNIER (1897), however, who misspelled the name "*Hasseltites*", it seemed probable that the fossil would prove to be no arthropod at all. He was the first to call attention to the "long cilia" occurring at the end of the legs. Recently PETRUNKEVITCH (1953), on the other hand, backed the opinion of VAN HASSELT and WEYENBERGH as to the opilionid nature of the fossil, but he would rather class it with the suborder Laniatores than with the Palpatores, to which *Acantholophus* belongs.

As to the nomenclature of the species PETRUNKEVITCH's statements are not quite correct. WEYENBERGH published the name *Hasseltia primigenia* (as a nomen nudum) in the "Tijdschrift voor Entomologie", and *Hasseltides primigenius* (with description and figure) in the "Archives du Musée Teyler", both in 1869. PETRUNKEVITCH interchanged the references, and erroneously put the author's name between brackets. Besides, there seems to be no reason for his contention that the name *Hasseltia* was changed into *Hasseltides* because the former was preoccupied, for, as far as I could ascertain, the name *Hasseltia* had not been used before as a generic name in zoology. WINKLER (1876; 1896) twice referred to the species under the name *Hasseltia primigenia*. These critical remarks on minor details should not give the impression that I do not admire the revisional work on fossil Arachnoidea lately done by Prof. PETRUNKEVITCH.

I became interested in *Hasseltides* when Prof. PETRUNKEVITCH visited me in August 1949 in order to examine the fossil arachnoids in Teyler's Museum, among which is the type and unique specimen of *Hasseltides primigenius*. It then occurred to me that it might be a poorly preserved

specimen of the crinoid *Saccocoma*, an opinion I communicated to Prof. PETRUNKEVITCH afterwards, when sending him the specimen on loan for a closer examination. When it appeared that he had nevertheless come to the conclusion that the specimen represented the only mesozoic opilionid hitherto discovered, I resolved to study the fossil more closely. This study convinced me that *Hasseltides primigenius* Weyenbergh is a synonym of *Saccocoma bajeri* (König, 1825), and consequently no harvestman at all, but a sea-lily.

For comparison I could dispose of a series of *Saccocoma* in the Teyler Museum. Specimens belonging to that genus were listed by WINKLER (1864, 1878) as *Saccocoma pectinata*, *S. filiformis*, *S. sp.*, and *Ophiurella sp.* On reexamination these specimens proved to belong to *Saccocoma bajeri* (König, 1825)¹⁾ (= *Comatula pectinata* Goldfuss, 1829), the mysterious *Saccocoma schwertschlageri* Walther, 1904, and *Saccocoma sp.*²⁾ Among the last mentioned there may be some badly preserved *S. tenella* (Goldfuss, 1829).

The morphology of *Saccocoma* was described in detail by JAECKEL (1892). *Saccocoma* is an unstalked crinoid in which all skeletal elements are very thin. The theca consists of five large radialia and probably some rudiment of the basalia. Each of the radialia bears an arm which forks on the second brachial. Each arm-branch gives off alternating ramuli from about its 15th brachial onward. The proximal brachials bear paired wing-like expansions.

Generally the specimens of *Saccocoma* are embedded with the axis of the theca perpendicular to the bedding plane, thus showing more or less clearly the radial arrangement of the arms. Only rarely the theca lies on its side; this is the case in a specimen figured by GOLDFUSS (1831, fig. 2c), in another figured by JAECKEL (1892, textfigure 8), and in the specimen no. 5724 in the Teyler Museum.

Hasseltides primigenius appears to be a *Saccocoma bajeri* embedded with the theca lying on its side and with only six of the ten arm-branches preserved. Three radialia can be recognized, and with a lens some remains of their reticulate surface structure can be seen. The basal part of the arms is too badly preserved for examination, but details of the arm-branches agree strikingly with those of unquestioned specimens of *Saccocoma bajeri* in the same state of preservation. The separate brachials cannot be seen, but their wing-like expansions show like pairs of spines. In five of the six preserved arm-branches the ramuli are more or less distinctly

¹⁾ It was shown by BATHER (1924) that this is the valid name for the species.

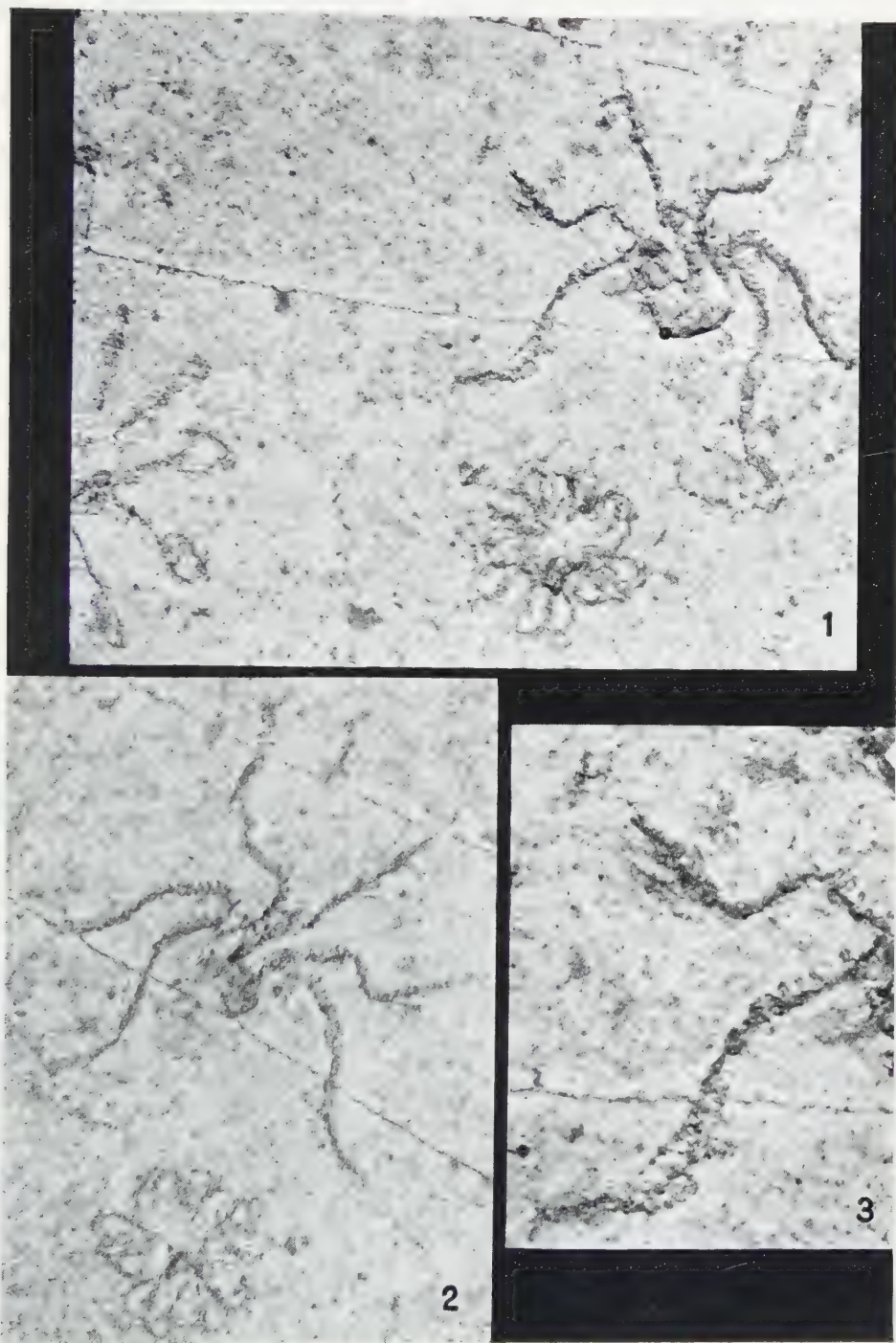
²⁾ I refer the numbers 5702–5705, 5707–5709, 5711, 5715, 5716, 5721, 5724, 5738 to *S. bajeri*; 5720 (with doubt), 5726, 5727, 5728, 5729/5730 to *S. schwertschlageri*, and 5699/5700, 5701, 5710, 5712/5713, 5714, 5717, 5718/5719, 5722, 5723, 5725, 5735, 5736/5737, 14173 to *S. sp.*, while no. 14174/14175 is a large slab containing a great number of young *Saccocoma*, of which some can be recognized as *S. bajeri*, and at least one belongs to *S. schwertschlageri*.

visible. In short, though the specimen is incomplete and some details are indistinct because of bad preservation, there is no feature which cannot be readily explained when the fossil is considered a specimen of *Saccocoma bajeri*.

Professor PETRUNKEVITCH was so kind as to explain to me his arguments for considering the fossil an opilionid in a letter dated June 2, 1953. He writes: "I thought that the segmentation of the six preserved appendages of the specimen of *Hasseltides primigenius* are of Arthropod type and that in three of them one can recognize the femur, tibia and tarsus. Although their armature is distinctly rectangular at first sight, on closer examination one sees several curved and fairly pointed, thorn-like protuberances. The majority of Gonyleptidae have, of course, spine-like or thorn-like protuberances, but in some, such as *Microconomma*, *Progyndes*, they are fairly blunt and short. Again, *Saccocoma* has typical 5-radial symmetry with each arm forming two branches close to base and as in all Crinoidea subdivided into short segments or vertebrae. If *Hasseltides* is a *Saccocoma* it lacks as many appendages as it does if it is an Opilionid, but their origin from the body should be much more radially symmetric than they are in the specimen in question. The latter, by its appearance, undoubtedly resembles a Gonyleptid. The chelicerae of Gonyleptids are in Recent species held bent downward, appear short and would be easily concealed from view in fossilization."

When we compare these arguments with the evidence adduced above for the opinion that the fossil is a crinoid, they appear to be much less convincing, and, besides, Prof. PETRUNKEVITCH leaves some details of the fossil unexplained. So in my opinion the arthropoid type of segmentation of the appendages is not manifest. Even in those arm-branches in which Prof. PETRUNKEVITCH believes to recognize femur, tibia, and tarsus, the angles between these supposed segments are not sharp, and it seems unlikely to me that opilionid legs would assume a gently curved shape as seen in some of the others. On the other hand the angles in some of the appendages do not plead against the crinoid nature of the fossil, as JAECKEL (1892, p. 678) states that he frequently saw specimens of *Saccocoma* in which the arm-branches were folded angularly. It may be true that the armature of the arm-branches reminds one of that of the legs of certain opilionids, but it seems that the very evident paired arrangement of the "spines" is more naturally explained by assuming that they are the edges of the wing-like expansions of the brachials of *Saccocoma*. Finally, when considering the fossil an opilionid, there seems to be no plausible explanation for the lines delimiting three of the five radials which are clearly visible in *Hasseltides*, and for the tiny side branches of the distal part of five of the six preserved appendages.

The photographs reproduced on plates I and II may serve to illustrate my views. Slab no. 15431 bears one more specimen of *Saccocoma*, slab no. 15432, its partial counterpart, besides this second specimen a third



Figures 1-3. *Saccocoma bajori* (König), type specimen of *Hasseltides primigenius* Weyenbergh, Teyler Museum, Haarlem. Fig. 1. Cat. no. 15432, showing two more specimens of *Saccocoma* in the same slab. Fig. 2. Cat. no. 15431, partial counterpart of no. 15432. Fig. 3. Detail of Cat. no. 15432, showing the armature of two arm-branches. Figures 1, 2, \times nearly 1.7; figure 3, \times nearly 3.2

Photographs W. F. Tegelaar



Figures 1-3. *Saccocoma bayeri* (König), Teyler Museum, Haarlem. Fig. 1. Cat. no. 5703, a specimen with well preserved arm-branches. Fig. 2. Cat. no. 5705, a poorly preserved specimen. Fig. 3. Detail of Cat. no. 5705, showing the armature of two arm-branches. Figures 1, 3, \times nearly 3.2; figure 2, \times nearly 1.7.

Photographs W. F. Tegelaar.

one. This is in perfect agreement with the frequent occurrence of greater or smaller numbers of specimens of *Saccocoma* in the same slab of Bavarian lithographic stone.

In general trying to identify badly preserved fossils on the base of certain similarities to recent animals seems less advisable than comparing them in the first place with better preserved specimens from the same deposits. By using the former method WEYENBERGH was repeatedly put on the wrong track. By applying the latter, however, I think to have solved the problem of the status of *Hasseltides primigenius*, and I have been able to identify a number of WEYENBERGH's insect types in the collection of the Teyler Museum with earlier described species, often belonging to other orders of insects than those with which WEYENBERGH originally classed them. I hope to publish upon these in the near future.

After the aforesaid had been written I received a letter dated February 3, 1954, from Prof. PETRUNKEVITCH, to whom I had sent some of the photographs reproduced on the plates accompanying this paper. In this letter Prof. PETRUNKEVITCH writes: "Considering everything I believe that you are right in removing *Hasseltides* from the Arachnida and synonymizing it with *Saccocoma*".

REFERENCES

- BATHER, F. A., *Saccocoma cretacea* n. sp.: a Senonian Crinoid. *Proc. Geol. Ass.* **55**, 111 (1924).
- GOLDFUSS, A., *Petrefacta Germaniae* **1**, 204, 205 (1829).
- , *Op. cit.*, pl. 62 (1831).
- JAECKEL, S., Ueber Plicatocriniden, Hyocrinus and *Saccocoma*. *Zeitschr. D. Geol. Ges.* **44**, 659 seq. (1892).
- KÖNIG, E., *Icones fossilium sectiles*, Cent. **1**, 2, fig. 27 (1825) [non vidi!].
- MEUNIER, F., Sur les prétendues empreintes d'Arachnides du Corallien de la Bavière. *Ann. Soc. Scientif. Bruxelles* **21**, part 2, 38 (1897).
- PETRUNKEVITCH, A., Palaeozoic and Mesozoic Arachnida of Europe. *Mem. Geol. Soc. America* **53**, 47 (1953).
- WALTHER, J., Die Fauna der Solnhofen Plattenkalke. *Denkschr. Med.-Naturw. Ges. Jena* **11**, 166 (1904).
- WEYENBERGH, H., *Prodromus en algemeene beschouwing der fossiele insekten van Beijeren*. *Tijdschr. Entom.* **11**, 237 (1869a).
- , Sur les insectes fossiles du calcaire lithographique de la Bavière, qui se trouvent au Musée Teyler. *Arch. Mus. Teyler* **2**, 253 (1869b).
- , Notes sur quelques insectes du calcaire jurassique de la Bavière. *Op. cit.* **3**, 234 (1873).
- WINKLER, T. C., Musée Teyler, Catalogue systématique de la collection paléontologique, 190, 191 (1864).
- , *Idem*, 421 no. 6547, 6548 (1865).
- , *Idem*, suppl. **2**, 83 (1876).
- , *Idem*, suppl. **3**, 139 (1878).
- , *Idem*, suppl. **5**, 299 (1896).

INFLUENCE OF ORGANIC COMPOUNDS ON SOAP AND PHOSPHATIDE COACERVATES. XXI ¹⁾

THE ACTION OF ALCOHOLS AND KETONES ON AN OLEATE COACERVATE

BY

H. L. BOOIJ, J. H. BLEKKINGH *) AND H. KWESTROO-VAN DEN BOS *) ²⁾

(Communicated by Prof. H. G. BUNGENBERG DE JONG at the meeting of Febr. 27, 1954)

1. Introduction

A study on the influence of alcohols on oleate coacervates has shown that very short alcohols (methanol, ethanol and propanol) have a salt-demanding effect (more KCl is needed to get the same degree of coacervation as the blank). The longer alcohols all show a salt-sparing effect with a maximal activity at a chain length of 14 carbon atoms (BooiJ *et al.* 1950). We have now studied a number of aromatic alcohols. In our preceding study on the influence of ethers we had found a marked difference between the phenylethers (aliphatic equivalent of the benzene nucleus approximately 5 carbon atoms) and the benzylethers (aliphatic equivalent 3-4). We have tried to find the aliphatic equivalent of the benzene nucleus in aromatic alcohols. In the second place we were interested in the effect of the introduction of side chains on the activity of the alcohols. Finally a number of ketones have been studied, especially as regards the aliphatic equivalent of the benzene nucleus.

2. The influence of aromatic alcohols on an oleate coacervate

The method described by us (1954) has been used throughout this study. An oleate solution containing the alcohol to be investigated (the substance was dissolved in a small amount of propanol, which was then added to the oleate solution) was coacervated by means of a concentrated KCl-solution (3.8 mol/l) and the volumes of the resulting coacervate were compared with those of the blank oleate.

*) Aided by grants from the "Netherlands Organization for Pure Research (Z.W.O.)".

¹⁾ Publication no. XX of this series will be found in Proc. Kon. Ned. Akad. Wetensch. Amst. B57, 215-226 (1954).

²⁾ Publication no. 27 of the Team for Fundamental Biochemical Research (under the direction of H. G. BUNGENBERG DE JONG, T. H. VAN DEN HONERT, E. HAVINGA and H. L. BOOIJ).

We compared (fig. 1) the straight aromatic alcohols with the aliphatic ones (see BOOIJ *et al.* 1950a). It is clear that in this case the benzene nucleus has only a relatively small aliphatic equivalent (3 carbon atoms).

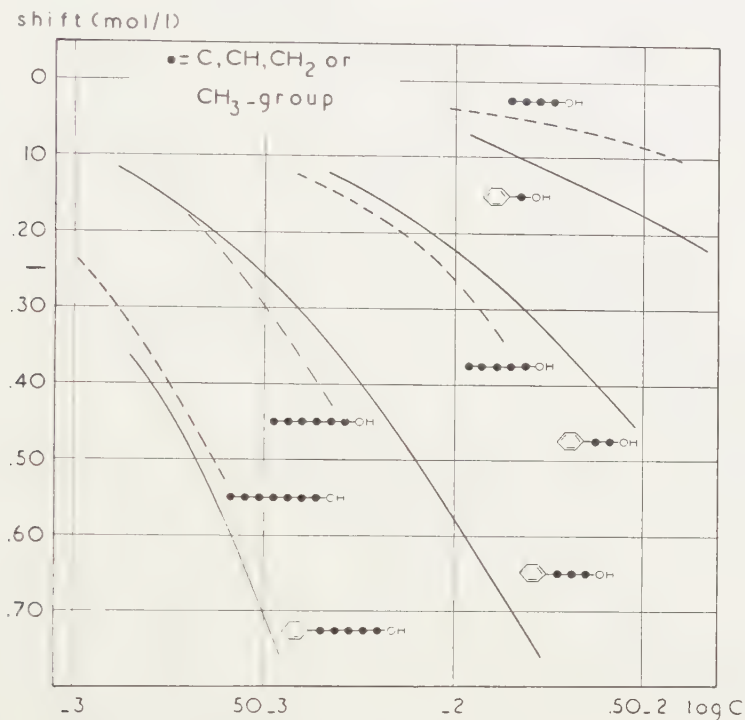


Fig. 1. A comparison of the activity of aromatic and aliphatic alcohols on an oleate coacervate. Ordinate = shift of the KCl-concentration — in respect to the blank — needed for a coacervate volume of 50 % (+ = salt-demanding activity and — = salt-sparing activity). Abscissa = logarithm of the concentration of the added substance (moles/l)

The introduction of aliphatic side chains into aromatic alcohols does not lead to unexpected results (see fig. 2 for derivatives of benzylalcohol, fig. 3 for derivatives of phenylethylalcohol and fig. 4 for derivatives of phenylpropylalcohol). A well-known rule comes to the fore: a substance with a branched chain has always less activity than the straight chain isomer (compare e.g. phenylmethylcarbinol and phenylethylalcohol). We may compute an "activity quotient" for some isomers investigated: (See following page).

The influence of branching on the activity is clearly demonstrated. A straight chain isomer is approximately $1\frac{1}{2}$ times as active as an isomer with one methyl side chain and 2–3 times as active as an isomer with two methyl side chains.

In our preceding publication the hypothesis has been framed that the high aliphatic equivalent of the benzene nucleus must be ascribed to a redistribution of electrons within the molecule. One might suggest that

substance	"activity quotient"
I <chem>CC(C)COc1ccccc1</chem>	$\frac{\text{activity I}}{\text{activity II}} = 1.66^1)$
II <chem>COc1ccccc1</chem>	
III <chem>CCCCOc1ccccc1</chem>	$\frac{\text{activity III}}{\text{activity IV}} = 1.59$
IV <chem>CC(C)COc1ccccc1</chem>	
V <chem>CC(C)(O)c1ccccc1</chem>	$\frac{\text{activity III}}{\text{activity V}} = 3.09$
VI <chem>CCCCCCOc1ccccc1</chem>	$\frac{\text{activity VI}}{\text{activity VII}} = 2.24$
VII <chem>CC(C)COc1ccccc1</chem>	

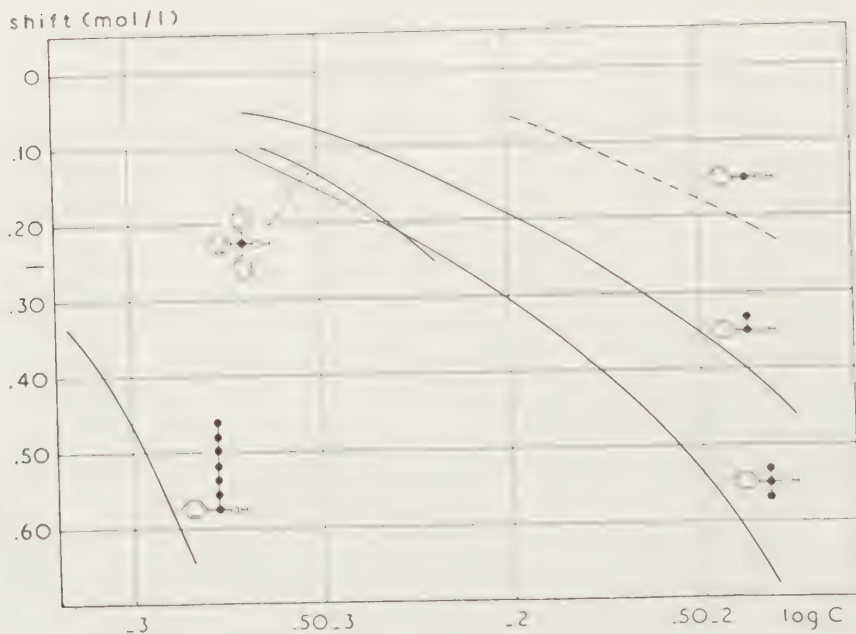


Fig. 2. Action of some derivatives of benzylalcohol on an oleate coacervate

¹⁾ Activity measured at a KCl-shift of -0.40 mol/l.

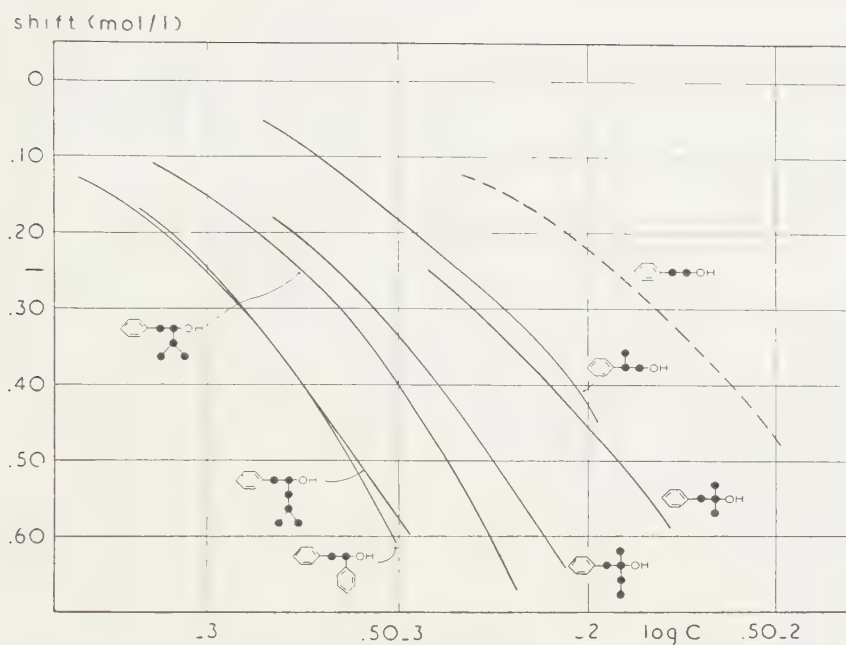


Fig. 3. Influence of some derivatives of phenylethylalcohol

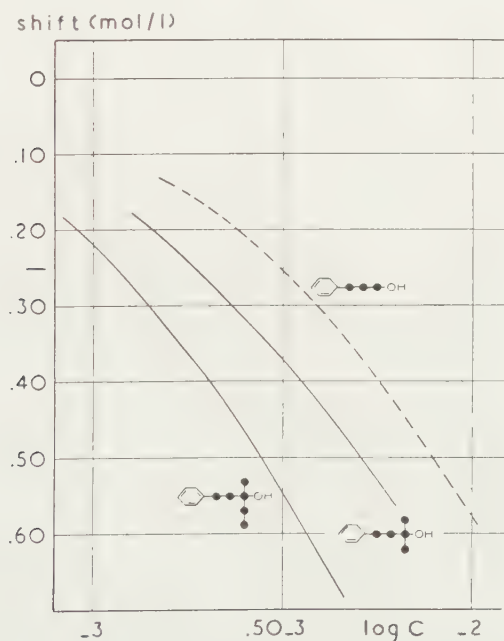


Fig. 4. Activity of derivatives of phenylpropylalcohol

an electron attracting influence of the ether-oxygen results in a stronger hydrophobic character of the benzene nucleus.

In this respect it is interesting to note that there is a distinct difference in activity between cinnamylalcohol and phenylpropylalcohol (fig. 5).

As cinnamylalcohol contains a double bond one would have expected that it would be less active than the saturated alcohol (see BOOIJ, 1949). The unsaturated alcohol is, however, somewhat more active than the saturated one. It might be possible that in this case too an electron-attracting influence

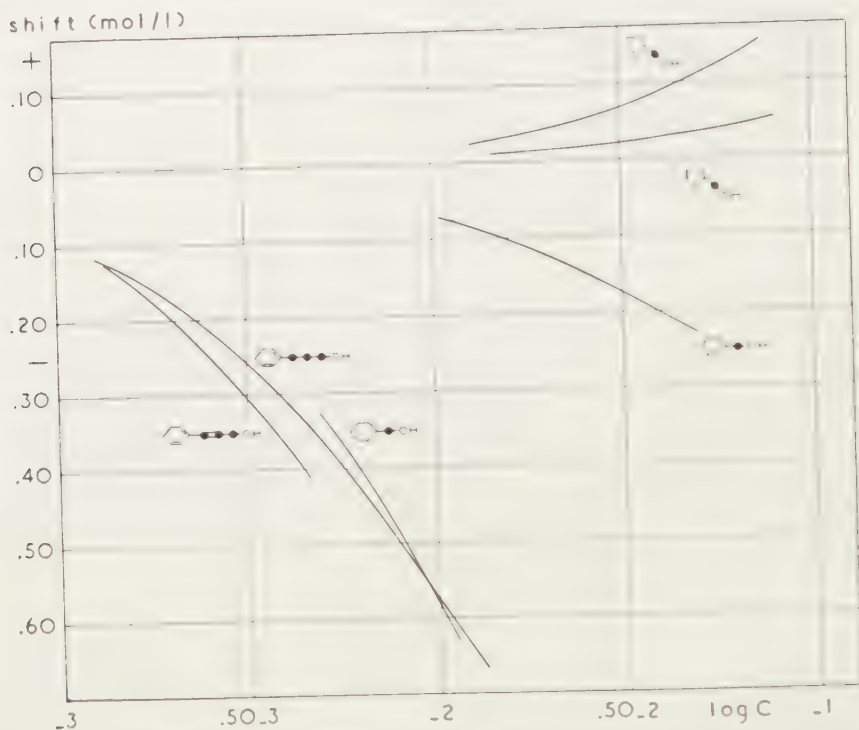


Fig. 5. Examples of the influence of hydrogenation of double bonds on activity

of the OH-group would be "conducted" through the conjugated system of the double bond plus the benzene nucleus. Then the benzene nucleus would grow more hydrophobic and the molecule more active.

Experiments with benzylalcohol and *cyclohexylcarbinol*, and with *furfurylalcohol* and *tetrahydrofurfurylalcohol* demonstrated the difference between aromatic and hydro-aromatic substances (fig. 5). In both cases the hydro-aromatic substance shows a stronger action than the aromatic one (though in the first case we deal with a salt-sparing and in the second case with a salt-demanding activity). In the case of benzylalcohol and *cyclohexylcarbinol* we have tried to analyse the background of the profound difference in activity. There are two possibilities:

a) the substances show the same distribution between the oleate micelles and the medium, but the salt-sparing activity pro molecule is much higher for the hydroaromatic substance,

b) the substances show completely different distribution equilibria between micelle and medium, but their molecular activity is approximately equal (compare fig. 1 of our preceding article — 1954). The large difference

between their solubilities in water speaks in favour of the latter suggestion.

We tried to get some insight in this question by performing experiments with soap solutions of different concentrations (see BOOIJ *et al.* 1949). We compare the concentrations of the added substances needed to give a certain shift of the KCl-concentration (at 50 % coacervate volume)¹). In case *a* the equilibrium concentration will be the same for benzylalcohol and *cyclohexylcarbinol*, but the slope of the lines will be completely different. In the other case (*b*) the slope of the lines will be the same, but the equilibrium concentrations differ very much. It is clear from fig. 6

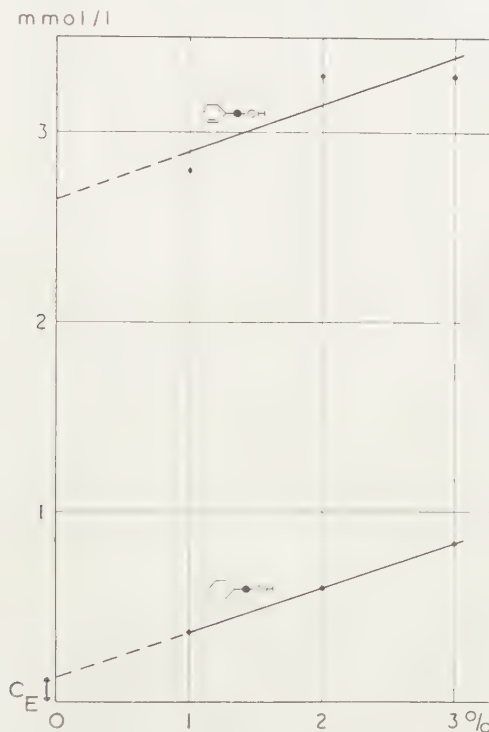


Fig. 6. The difference between benzylalcohol and *cyclohexylcarbinol* as regards their activity on an oleate coacervate must be ascribed to a difference in equilibrium-concentration. Ordinate = concentration (mmol/l) of the added substances required to give a certain KCl-shift. Abscissa = concentration of the oleate solution used

that here we deal with case *b*. The marked difference between benzylalcohol and *cyclohexylcarbinol* must be ascribed primarily to differences in their distribution equilibrium medium/micelle. As far as we can judge from the slope of the lines in figure 6, their activity within the micelle is more or less equal. Compare also the experiments on the activity of benzene and *cyclohexane*, which gave a comparable result (BOOIJ *et al.*, 1950b).

¹) Our sincere thanks are due to Mrs E. S. DE BOCK-VAN CALCAR who kindly performed these experiments for us. No propanol was used in this study; the substances have been dissolved directly into the oleate solution.

3. The influence of ketones on an oleate coacervate

The investigation of a number of aliphatic ketones as regards their influence on the oleate coacervate did not give unexpected results. ROSENTHAL (1939) measured the activity of some ketones soluble in water and found a salt-demanding effect of acetone and methylethylketone and a salt-sparing effect of methyl *n* propylketone, methyl *n* butylketone and methylisobutylketone. We found a salt-demanding influence of diethylketone, methylisopropylketone and methyl-*n*-propylketone¹⁾. In figs. 7

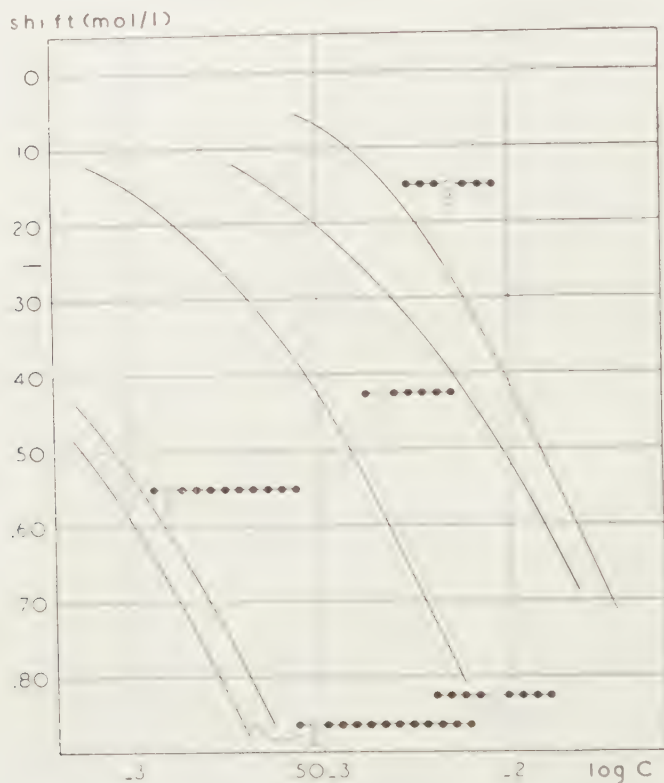


Fig. 7. Influence of some aliphatic ketones on an oleate coacervate

and 8 our results with salt-sparing substances have been put together. The longer the chain, the stronger the activity. The increase in activity is less that would follow from TRAUBE's rule. This we expected as the longer ketones will be taken up into the oleate micelles practically completely. We see that an isomer with the polar group in the centre of the molecule has less activity than the isomer with an eccentric ketone-group (compare di-*n*-propylketone and methyl-*n*-amylketone). Branching of the

¹⁾ This difference is caused by the fact that we used propanol to dissolve the substances throughout our study.

chain(s) results in a decreased activity (compare diisopropylketone and di-*n*-propylketone).

The investigation of aromatic ketones has led to some interesting data. As we have only two suitable aliphatic ketones for comparison (fig. 9),

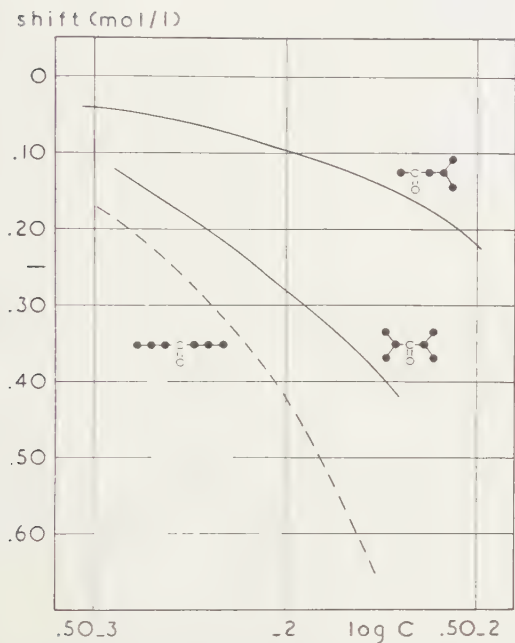


Fig. 8. The effect of branching in the carbon chain on the activity of the ketone

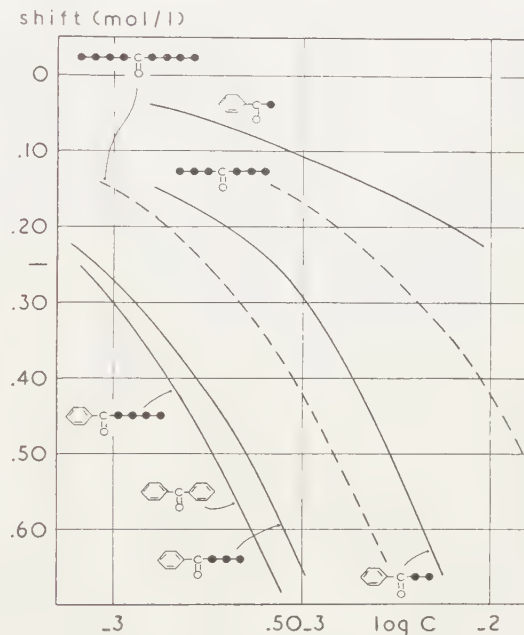
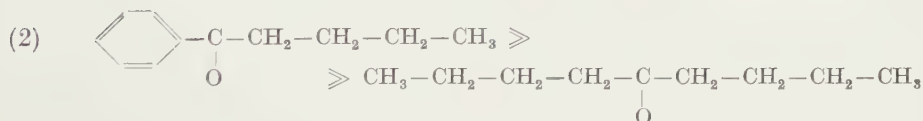
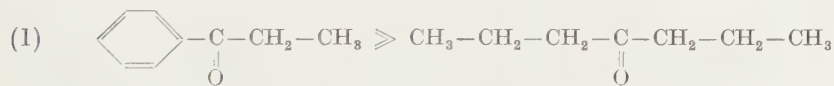


Fig. 9. Activity of some aromatic ketones as compared with aliphatic ones

it will not be easy to give the aliphatic equivalent of the benzene nucleus exactly. We can read from fig. 9 the following sequences of activity:



From these facts we may deduce that the aliphatic equivalent of the benzene nucleus must be in the neighbourhood of five carbon atoms. This is the same value which we found in the case of phenylethers (Boon *et al.* 1954).

Here too the introduction of methylene groups between the phenyl group and the polar group results in a strong decrease of the aliphatic

equivalent of the benzene nucleus. In figure 10 the marked difference in activity between some isomeric ketones comes clearly to the fore.

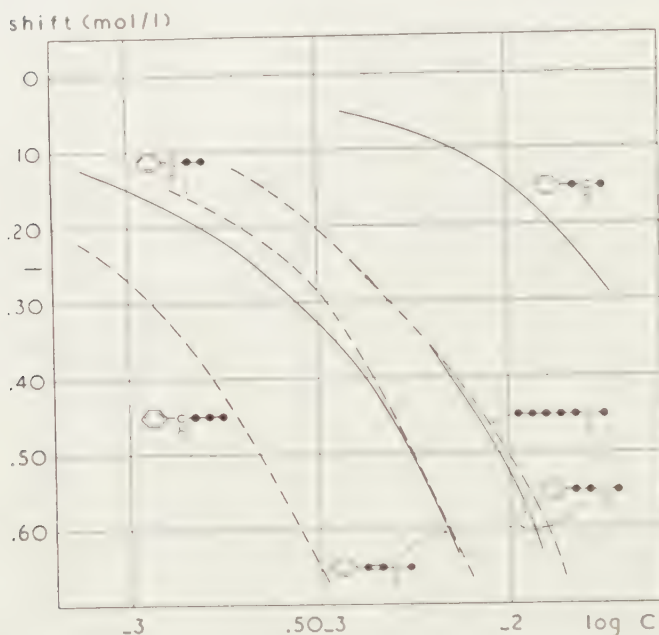
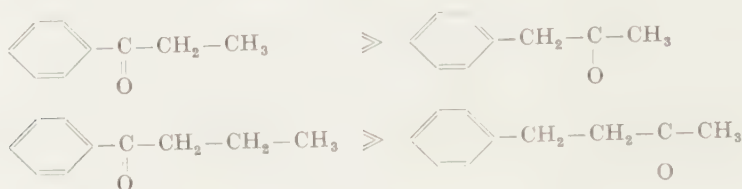
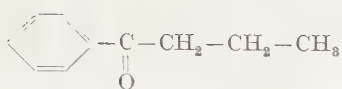
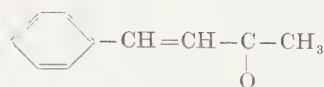
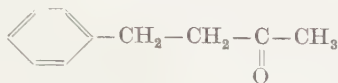


Fig. 10. The introduction of a CH_2 -group between the carbonyl group and the benzene nucleus has a pronounced influence on the activity

In these cases the aliphatic equivalent of the benzene nucleus is only three carbon atoms, which follows from a comparison of methyl-*n*-amylketone and benzylacetone. This is the same value which we found for the aromatic alcohols. These data give new arguments for the hypothesis framed in our preceding publication (Boorj *et al.* 1954). The benzene nucleus has an aliphatic equivalent of about three carbon atoms, when there is no interaction with side chains. The introduction of an electron attracting group (ether-oxygen, carbonyl-) presumably causes a redistribution of electrons and the benzene nucleus grows more hydrophobic. Hence the marked difference between phenyl- and benzylderivatives.

The introduction of a double bond into benzylacetone has a remarkable effect (compare cinnamylalcohol and phenylpropanol). The sequence of activity and the computed aliphatic equivalents of the benzene nucleus are given below:

aliph. equiv. = ± 5 aliph. equiv. = ± 4 aliph. equiv. = ± 3

In the case of benzalacetone too we may suppose that the double bond "conducts" the electron attracting effect of the carbonyl group to some extent, thus causing an intermediate aliphatic equivalent.

Finally we measured the influence of some miscellaneous ketones (fig. 11). A comparison with figs. 7 and 9 shows that the naphthalene

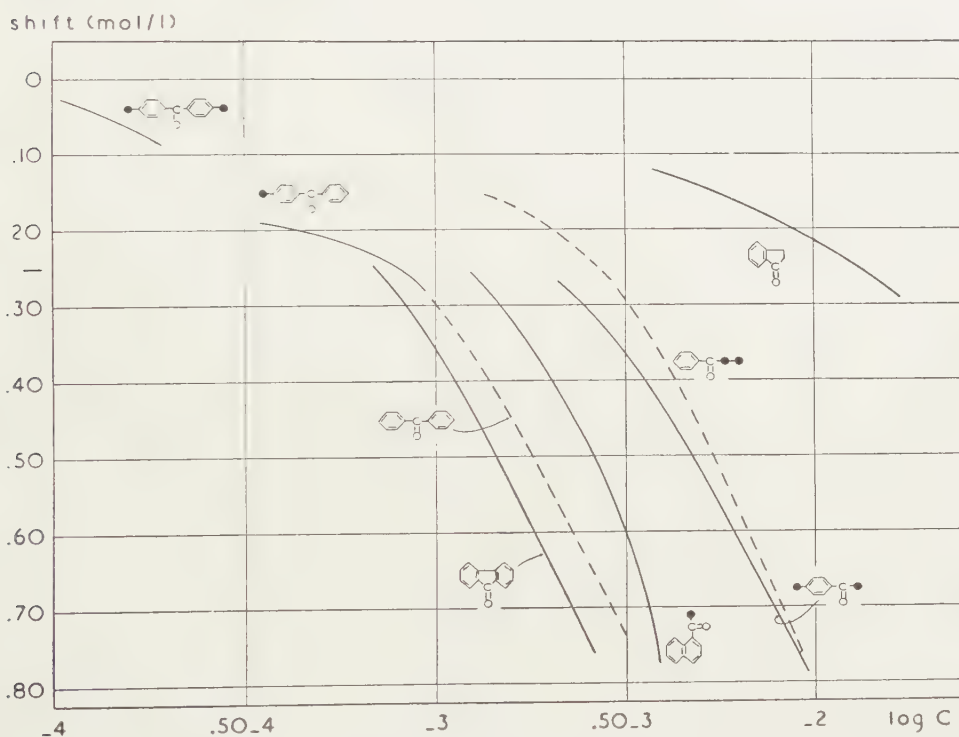


Fig. 11. Action of some miscellaneous ketones on an oleate coacervate

nucleus in aceto-(1)-naphthone has an aliphatic equivalent of about 7 carbon atoms.

Summary

1. The activity of aromatic alcohols and ketones on an oleate coacervate has been compared to that of aliphatic ones.

2. The aliphatic equivalent of the benzene nucleus depends on the molecular structure. In aromatic alcohols it has a value of 3 carbon

atoms. In ketones with the phenyl group next to the carbonyl group the value is 5 carbon atoms. Introduction of methylene groups between the benzene nucleus and the carbonyl group decreases the value to 3 carbon atoms.

3. Introduction of a conjugated double bond between the polar group and the benzene nucleus results in an increase of the latter's aliphatic equivalent.

4. The experiments provide new arguments for the hypothesis that the normal aliphatic equivalent of the benzene nucleus is 3 carbon atoms and that by interaction with side chains (redistribution of electrons) the benzene nucleus may get a more hydrophobic character (aliphatic equivalent = 5).

5. The large difference in activity of benzylalcohol and *cyclohexylcarbinol* is caused by the fact that the latter substance is much more hydrophobic than the former. Thus their distribution equilibria medium/oleate micelle have different values. Their activities within the oleate micelles are presumably more or less equal.

*Department of Medical Chemistry,
University of Leiden*

LITERATURE

- BOOIJ, H. L., in *Kruyt's Colloid Science II*, Chapter XIV (Elsevier, Amsterdam, 1949).
 ——— and H. G. BUNGENBERG DE JONG, *Biochem. et Biophys. Acta* **3**, 242 (1949).
 ———, H. KWESTROO-VAN DEN BOS and J. H. BLEKKINGH, *Proc. Kon. Ned. Akad. Wetensch. Amst.* **B57**, 215—226 (1954).
 ———, C. J. VOGELSANG and J. C. LYCKLAMA, *Proc. Kon. Ned. Akad. Wetensch. Amst.* **B53**, 59 (1950a).
 ———, ——— and ———, *Proc. Kon. Ned. Akad. Wetensch. Amst.* **B53**, 882 (1950b).
 ROSENTHAL, S., Thesis (Leiden, 1939).

SOME RECENT OSTRACODA OF MANILA (PHILIPPINES)

BY

A. J. KEY

(Communicated by Prof. G. H. R. VON KOENIGSWALD at the meeting of March 20, '54)

INTRODUCTION

LIENENKLAUS (1900, Zeitschr. d. geol. Gess., v. 52, p. 544), while making mention of the occurrence of *Cytheropteron caudatum* LIENENKLAUS 1894 (which species belongs to *Payenborchella* (*Payenborchella*) KINGMA) in the Middle Oligocene deposits of Pietzpuhl (Germany), remarked that according to SCHACKO this species lives in the Philippines. TRIEBEL (1949, p. 193) doubted whether this Oligo-Miocene species should be still living.

The author was in the fortunate position to check Schacko's statement, since Prof. G. H. R. VON KOENIGSWALD recently collected a sample from the Bay of Manila. This sample was taken from a heap of sand from the harbour of Manila, or just outside it. The sediment is largely composed of dark volcanic material and it contains numerous Foraminifera and Ostracoda, many Molluscs, abundant ambulacral ossicles of Ophiuroidea, some Sponge spicules and anchors of Holothurians and some Bryozoans, otoliths and fish teeth. The Foraminifera, among which *Elphidium crispum* (LINN.) and small *Streblus beccarii* (LINN.) dominate, indicate shallow water, probably somewhat brackish. Among the Ostracoda *Clithrocytheridea spinulosa* (BRADY) and *Cytheromorpha cancellata* (BRADY) are most abundant.

Three species of *Payenborchella* (*Neomonoceratina*) KINGMA have been found: *Payenborchella* (N.) *koenigswaldi* n. sp. (most common), *Payenborchella* (N.) *mediterranea* RUGGIERI and *Payenborchella* (N.) *entomon* (BRADY) (rarest). But the more or less expected *Payenborchella* (*Payenborchella*) *caudata* (LIENENKLAUS) has not been found.

Payenborchella (N.) *mediterranea* RUGGIERI is a cosmopolitic, mainly tropical species; it is known today from the Gulf of Paria (Venezuela), Port Saïd (Egypt), Bay of Djakarta (Java) and now of Manila, all localities in warm, shallow water. *Payenborchella* (N.) *entomon* (BRADY) was reported by Brady from Nouméa, New Caledonia (5-11 m) and Vanua Levu, Fiji Isl. (7 m). This species too seems to be a tropical, shallow-water dweller.

Another interesting fact is the presence of *Atjehella semiplicata* KINGMA. This species was only known from the Lower Pliocene of Acheh (N. Sumatra) and the Upper Pliocene of Middle and East Java. In Acheh *Atjehella*

semiplicata has been found together with *Payenborchella* (N.) *columbiformis* KINGMA, in Java together with *Payenborchella* (N.) *microreticulata* KINGMA, so that it is probable that both genera are confined to about the same environments.

The material has been stored in the collection of the Geological Institute of the State University of Utrecht, with the numbers S. 1375—1408.

The writer is gratefully indebted to Prof. G. H. R. VON KOENIGSWALD for collecting the sample.

SYSTEMATIC DESCRIPTION

Cytherelloidea cavernosa (BRADY); Pl. 1, fig. 1.

Cytherella cavernosa BRADY, 1868, Les Fonds d. 1. Mer, v. 1, p. 65, pl. 8, f. 13, 14; 1880, Challenger Rep., v. 1, p. 177, pl. 36, f. 5.

Cytherelloidea cavernosa, HORNIBROOK, 1952, N. Zeal. Geol. Surv. Pal. Bull. 18, p. 14, 17.

Paracypris zealandica (BRADY); Pl. 1, fig. 6.

Phlyctenophora zealandica BRADY, 1880, Challenger Rep., p. 33, pl. 3, f. 1.

Paracypris zealandica, FYAN, 1916, Kon. Akad. Wet. Amsterdam, v. 23, p. 1175, f. 17; VAN DEN BOLD (in GERMERAAD) 1946, p. 77; KINGMA, 1946, Contr. knowl. Young-Caen. Ostr. Mal. reg., p. 67, pl. 6, f. 18; VAN DEN BOLD, 1950, Ann. Mag. Nat. Hist., s. 12, v. 3, p. 901.

Bairdia spp.

Remarks: Only a few valves were found, probably belonging to several species. With this difficult genus the number of valves is too small to give a specific determination.

Clithrocytheridea spinulosa (BRADY); Pl. 1, fig. 2.

Cytheridea spinulosa BRADY, 1868, Ann. Mag. Nat. Hist., s. 4, v. 2, p. 182, pl. 13, f. 1-6; 1880, Challenger Rep., v. 1, p. 112, pl. 33, f. 6; 1890, Trans. Roy. Soc. Edinburgh, v. 35, p. 505.

Cytheridea (*Haplocytheridea*) *spinulosa*, VAN DEN BOLD (in GERMERAAD), 1946, p. 78.

PLATE 1

Fig. 1. *Cytherelloidea cavernosa* (BRADY); external view of the right valve. 80 ×

Fig. 2. *Clithrocytheridea spinulosa* (BRADY); 2a: external view of the left valve of a female; 2b: dorsal view of the same valve; 2c: hinge of the same valve. 85 ×

Fig. 3. *Leptocythere demissa* (BRADY); 3a: external view of the left valve; 3b: internal view of the same valve. 85 ×

Fig. 4. *Leptocythere inconspicua* (BRADY); external view of the right valve. 85 ×

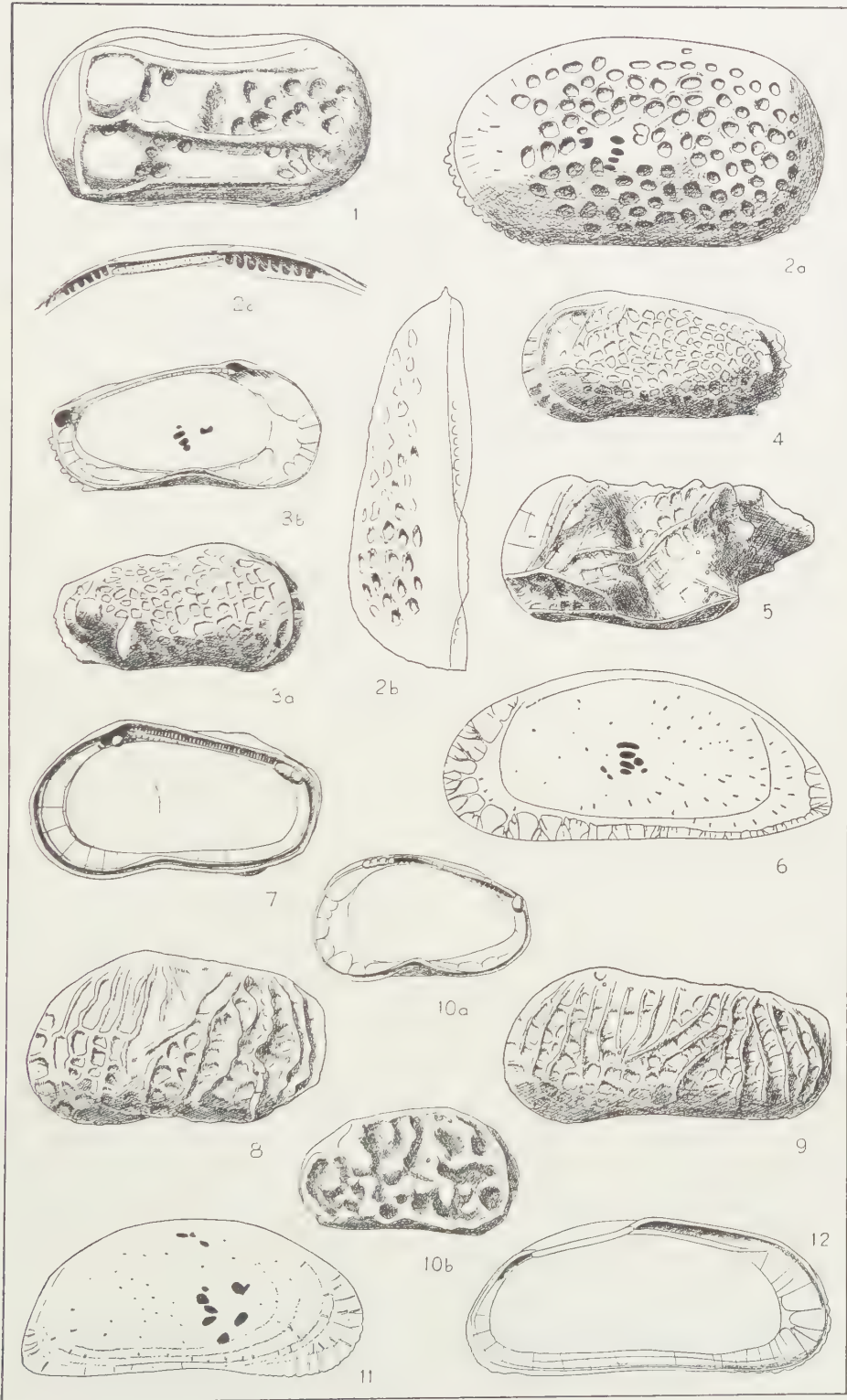
Fig. 5. *Paracytheridea longicaudata* (BRADY); external view of the left valve. 85 ×

Fig. 6. *Paracypris zealandica* (BRADY); external view of the left valve. 60 ×

Fig. 7-9. *Cytheromorpha cancellata* (BRADY); 7: internal view of the right valve of a female; 8: external view of the left valve of a female; 9: external view of the left valve of a male. 85 ×

Fig. 10. *Leptocythere* sp.; 10a: internal view of the right valve; 10b: external view of the right valve. 85 ×

Fig. 11-12. *Cytherideis sulcata* (BRADY); 11: external view of the right valve of a female; 12: internal view of the left valve of a male. 85 ×



Paracytheridea longicaudata (BRADY); Pl. 1, fig. 5.

Cytheropteron longicaudatum BRADY, 1890, Trans. Roy. Soc. Edinburgh, v. 35, p. 511, pl. 3, f. 18-19.

Leptocythere demissa (BRADY); Pl. 1, fig. 3.

Cythere demissa BRADY, 1868, Ann. Mag. Nat. Hist., s. 4, v. 2, p. 180, pl. 12, f. 1-2; 1880, Challenger Rep., v. 1, p. 66, pl. 12, f. 1; 1890, Trans. Roy. Soc. Edinburgh, v. 35, p. 497.

Leptocythere demissa, HORNIBROOK, 1952, p. 13, 17, 21.

Leptocythere inconspicua (BRADY); Pl. 1, fig. 4.

Cythere inconspicua BRADY, 1880, Challenger Rep., v. 1, p. 70, pl. 13, f. 1; VAN DEN BOLD (in GERMERAAD), 1946, p. 78.

Leptocythere sp.; Pl. 1, fig. 10.

Remarks: Our specimens are for the greater part immature; a specific determination is not attempted.

Cytherideis sulcata (BRADY); Pl. 1, fig. 11-12.

Xestoleberis sulcata BRADY, 1886, Jour. Linn. Soc. London, Zool., v. 19, p. 314, pl. 40, f. 28-30.

Cytheromorpha cancellata (BRADY); Pl. 1, fig. 7-9.

Cythere cancellata BRADY, 1868, Les Fonds d. 1. Mer, v. 1, p. 62, pl. 7, f. 9-11; 1880, Challenger Rep., v. 1, p. 73, pl. 14, f. 9.

Atjehella semiplicata KINGMA; Pl. 2, fig. 9-10.

Atjehella semiplicata KINGMA, 1948, Contr. knowl. Y. — Caen. Ostr. Mal. reg., p. 76, pl. 8, f. 1.

Hemicythere packardii (BRADY); Pl. 2, fig. 1-2.

Cythere packardii BRADY, 1880, Challenger Rep., v. 1, p. 88, pl. 19, f. 2; 1890, Trans. Roy. Soc. Edinburgh, v. 35, p. 501, pl. 2, f. 19.

Hemicythere packardii, VAN DEN BOLD, 1950, Ann. Mag. Nat. Hist., s. 12, v. 3, p. 901.

PLATE 2

Fig. 1-2. *Hemicythere packardii* (BRADY); 1: external view of the right valve; 2: internal view of the right valve. 85 ×

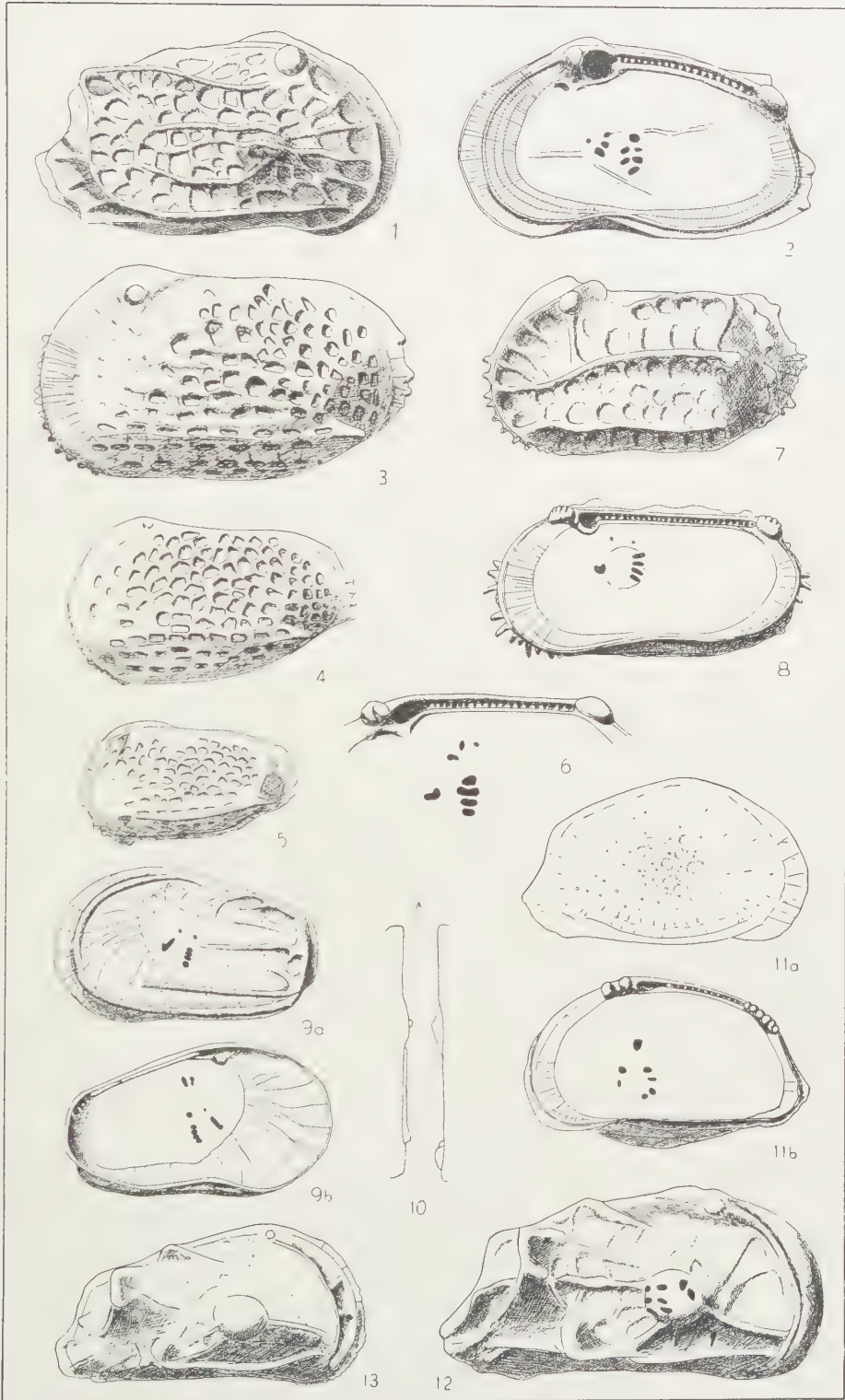
Fig. 3-6. *Trachyleberis goujoni* (BRADY); 3: external view of the left valve of a female; 4: external view of a left valve of the last instar but one; 5: external view of the left valve of the last instar but two; 6: hinge and muscle scar of the right valve of an adult specimen. 80 ×

Fig. 7-8. *Cythereis hamata* (G. W. MÜLLER); 7: external view of the left valve of the female; 8: internal view of the right valve of the male. 85 ×

Fig. 9-10. *Atjehella semiplicata* (KINGMA); 9a: external view of the left valve; 9b: internal view of the same valve; 10: dorsal view of the hinges of the right and left valve. 85 ×

Fig. 11. *Quadracythere?* sp.; 11a: external view of the right valve; 11b: internal view of the same valve. 60 ×

Fig. 12-13. *Caudites javana* (KINGMA); 12: external view of the right valve of an adult specimen; 13: external view of the right valve of the last instar but one. 85 ×



Cythereis hamata G. W. MÜLLER; Pl. 2, fig. 7-8.

Cythereis hamata G. W. MÜLLER, 1894, Fauna & Flora Golfes v. Neapel, monogr. 21, p. 373, pl. 29, f. 19, pl. 31, f. 14-16; KINGMA, 1948, Contr. knowl. Y. -Caen. Ostr. Mal. reg., p. 80, pl. 9, f. 5.

Trachyleberis hamata, VAN DEN BOLD, 1950, Ann. Mag. Nat. Hist., s. 12, v. 3, p. 901.

Trachyleberis cribriformis (BRADY).

Cythere cribriformis BRADY, 1865, Trans. Zool. Soc. London, v. 5, p. 379, pl. 61, f. 6; 1880, Challenger Rep., v. 1, p. 98, pl. 19, f. 3; TRIEBEL, 1941, Senckenbergiana, v. 23, pl. 3, f. 21.

Cythereis cribriformis KINGMA, 1948, Contr. knowl. Y. -Caen. Ostr. Mal. reg., p. 78, pl. 9, f. 3.

Trachyleberis cribriformis, VAN DEN BOLD, 1950, Ann. Mag. Nat. Hist., s. 12, v. 3, p. 901.

Trachyleberis goujoni (BRADY); Pl. 2, fig. 3-6.

Cythere goujoni BRADY, 1868, Les Fonds d. 1. Mer, v. 1, p. 78, pl. 10, f. 9-10; 1880, Challenger Rep., v. 1, p. 96, pl. 25, f. 7; 1886, Journ. Linn. Soc. London, Zool., v. 19, p. 308; 1890, Trans. Roy. Soc. Edinburgh, v. 35, p. 502.

Trachyleberis scutigera (BRADY); Pl. 3, fig. 2.

Cythere scutigera BRADY, 1868, Les Fonds d. 1. Mer, v. 1, p. 70, pl. 8, f. 15-16; 1880, Challenger Rep., v. 1, p. 109, pl. 22, f. 5.

Cythereis scutigera KINGMA, 1948, Contr. knowl. Y. -Caen. Ostr. Mal. reg., p. 83, pl. 9, f. 6.

Trachyleberis scutigera, VAN DEN BOLD, 1950, Ann. Mag. Nat. Hist., s. 12, v. 3, p. 901.

PLATE 3

Fig. 1. "*Cythere*" *caudata* BRADY; 1a: external view of the right valve; 1b: internal view of the same valve. 80 ×

Fig. 2. *Trachyleberis scutigera* (BRADY); external view of the right valve. 55 ×

Fig. 3. *Loxocythere kingi* HORNIBROOK; external view of the right valve. 85 ×

Fig. 4. *Loxococoncha lilljeborchi* BRADY; external view of the left valve of the female. 85 ×

Fig. 5. *Cytherura cryptifera* BRADY; external view of the left valve. 85 ×

Fig. 6. *Cytherura* sp.; external view of the right valve. 85 ×

Fig. 7. *Hemicytherura scutellata* (BRADY); external view of the left valve. 80 ×

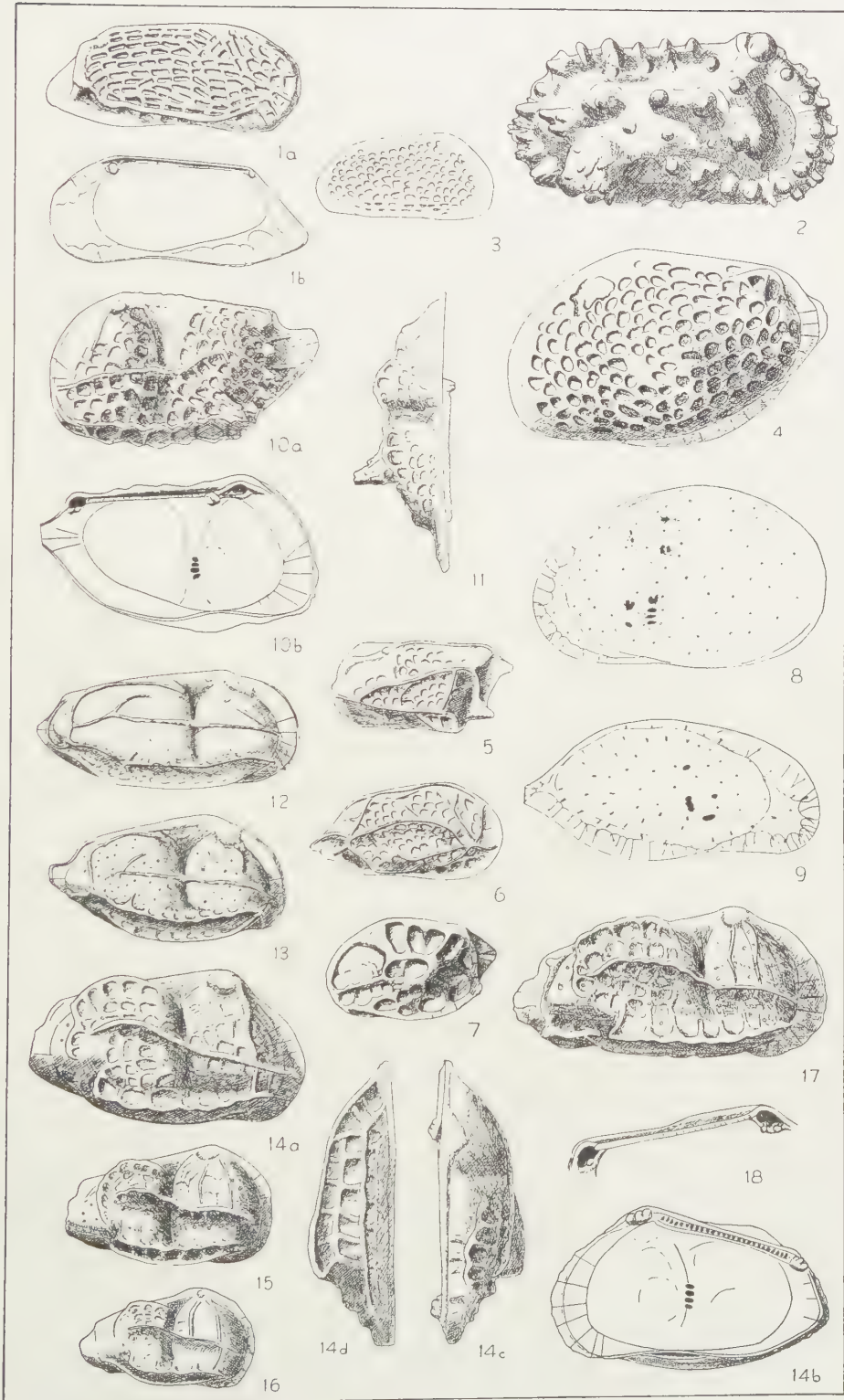
Fig. 8. *Xestoleberis variegata* BRADY; external view of the left valve of the female. 75 ×

Fig. 9. *Paradoxostoma* sp.; external view of the right valve. 75 ×

Fig. 10-11. *Payenborchella* (*Neomonoceratina*) *entomon* (BRADY); 10a: external view of the left valve; 10b: internal view of the same valve, 11: dorsal view of the left valve. 80 ×

Fig. 12-13. *Payenborchella* (*Neomonoceratina*) *mediterranea* RUGGIERI; 12: external view of the right valve of the male; 13: external view of the right valve of the female. 85 ×

Fig. 14-18. *Payenborchella* (*Neomonoceratina*) *koenigswaldi* n. sp.; 14a: external view of the right valve of the female (holotype); 14b: internal view of the same valve; 14c: dorsal view of the same valve; 14d: ventral view of the same valve; 15: external view of the right valve of the last instar but one; 16: external view of the right valve of the last instar but two; 17: external view of the right valve of the male; 18: hinge of the left valve. 75 ×



Caudites javana KINGMA; Pl. 2, fig. 12-13.

Caudites medialis CORYELL & FIELDS var. *javana* KINGMA, 1948, Contr. knowl. Y.-Caen. Ostr. Mal. reg., p. 85, pl. 10, f. 5.

Caudites javana, KEY, 1953, Proc. Kon. Akad. Wet. Amsterdam, s. B, v. 56, p. 159, pl. 1, f. 8-9.

Loxocythere kingi HORNIBROOK; Pl. 3, fig. 3.

Loxocythere kingi HORNIBROOK, 1952, N. Zeal. Geol. Surv. Pal. Bull. 18, p. 31, pl. 2, f. 32, 36, 37.

Quadracythere ? sp.; Pl. 2, fig. 11.

Remarks: Our two right valves differ from typical *Quadracythere* HORNIBROOK, in having two anterior terminal teeth instead of one.

Loxoconcha australis BRADY.

Loxoconcha australis BRADY, 1880, Challenger Rep., v. 1, p. 119, pl. 28, f. 5, pl. 29, f. 3; 1890, Trans. Roy. Soc. Edinburgh, v. 35, p. 507; HORNIBROOK, 1952, N. Zeal. Geol. Surv. Pal. Bull. 18, p. 15, 23, 24.

Loxoconcha gibbera BRADY.

Loxoconcha gibbera BRADY, 1886, Jour. Linn. Soc. London, v. 19, p. 312, pl. 40, f. 25-27; 1890, Trans. Roy. Soc. Edinburgh, v. 35, p. 508.

Loxoconcha alata BRADY, 1880, Challenger Rep., v. 1, p. 122, pl. 27, f. 6.

Loxoconcha lilljeborchi BRADY; Pl. 3, fig. 4.

Loxoconcha lilljeborchi BRADY, 1868, Ann. Mag. Nat. Hist., s. 4, v. 2, p. 183, pl. 13, f. 11-15.

Cytherura cryptifera BRADY; Pl. 3, fig. 5.

Cytherura cryptifera BRADY, 1880, Challenger Rep., v. 1, p. 134, pl. 32, f. 4.

Cytherura sp.; Pl. 3, fig. 6.

Remarks: Only a few valves were found. No specific name could be found for them. Their number is too small to justify establishing a new species.

Hemicytherura scutellata (BRADY); Pl. 3, fig. 7.

Cytherura scutellata BRADY, 1890, Trans. Roy. Soc. Edinburgh, v. 35, p. 509, pl. 3, f. 30-31.

Cytherura sp., VAN DEN BOLD (in GERMERAAD) 1946, Geol. Centr. Seran, p. 78.

Remarks: The specimens described by KINGMA (1948, p. 97, pl. 11, fig. 18) as *Cytherura* cf. *scutellata* (BRADY) belong to *Hemicytherura videns* (G. W. MÜLLER).

Cytheropteron sp.

Remarks: Only one valve was found, which could not be specifically named.

Payenborchella (*Neomonoceratina*) *entomon* (BRADY); Pl. 3, fig. 10-11.

Cytherura entomon BRADY, 1890, Trans. Roy. Soc. Edinburgh, v. 35, p. 509, pl. 3, f. 26-27.

Remarks: BRADY reported this species from Nouméa, New Caledonia (5–11 m) and Sava-Sava bay, Vanua Levu, Fiji Isl. (7 m). Unfortunately BRADY's original material could not be traced. The description and figures given by BRADY are clear enough, however, to identify our specimens with this remarkable species.

Payenborchella (Neomonoceratina) koenigswaldi n. sp.; Pl. 3, fig. 14–18.

Holotype: Right valve of a female (coll. no. S. 1402).

Type-locality: Bay of Manila, Luzon, Philippines.

Type-stratum: Recent.

Diagnosis: A species belonging to the genus *Payenborchella (Neomonoceratina)* with the following characteristics: Surface coarsely reticulate. The middle longitudinal ridge ends posteriorly in a short, very broad spine. Caudal process very short and broad. In most individuals two vertical ridges connect the eye-tubercle with the anterior part of the upper longitudinal ridge. The tooth beneath the anterior end of the bar of the hinge of the left valve is absent, as the corresponding socket in the right valve.

Description: Dorsal margin straight anteriorly, convex posteriorly. Anterior margin broadly rounded in the lower part, somewhat flattened or concave in the upper part. The slight convexity of the ventral margin is affected by the lower longitudinal ridge. The posterior margin is formed by a short, very broad subdorsal process. A deep, slightly curved, vertical sulcus runs between the dorsal margin and the middle longitudinal ridge.

The surface of the valve is covered by a coarse reticulation. The lower longitudinal ridge runs parallel to the free edge and forms the ventral margin of the valve. It starts in the antero-ventral corner of the valve, runs over the ventral surface and continues on the posterior lateral surface, sometimes ending into a knoblike elevation. The middle longitudinal ridge is shorter but higher. It starts in the antero-ventral corner of the valve, runs along two thirds of the valve's length, where it ends into a short broadly based spine. Dorsal and ventral surface of this fairly high ridge show 8 to 10 broad, shallow depressions sculptured out. The upper longitudinal ridge is long, nearly straight between the anterior margin and the vertical sulcus, and curved behind this sulcus. It ends posteriorly against another ridge that is the prolongation of a strongly curved ridge. The eye-tubercle is connected by two vertical ridges with the anterior part of the upper longitudinal ridge. The anterior one of these two is always distinct and it continues beneath the upper longitudinal ridge, forming a connection between the upper and middle longitudinal ridge. The posterior vertical ridge is only distinct in younger individuals and the adult males, but hardly perceptible in the adult females.

Sexual dimorphism is well-developed. The females are relatively shorter and higher than the males.

The anterior marginal area is moderately broad; the posterior marginal

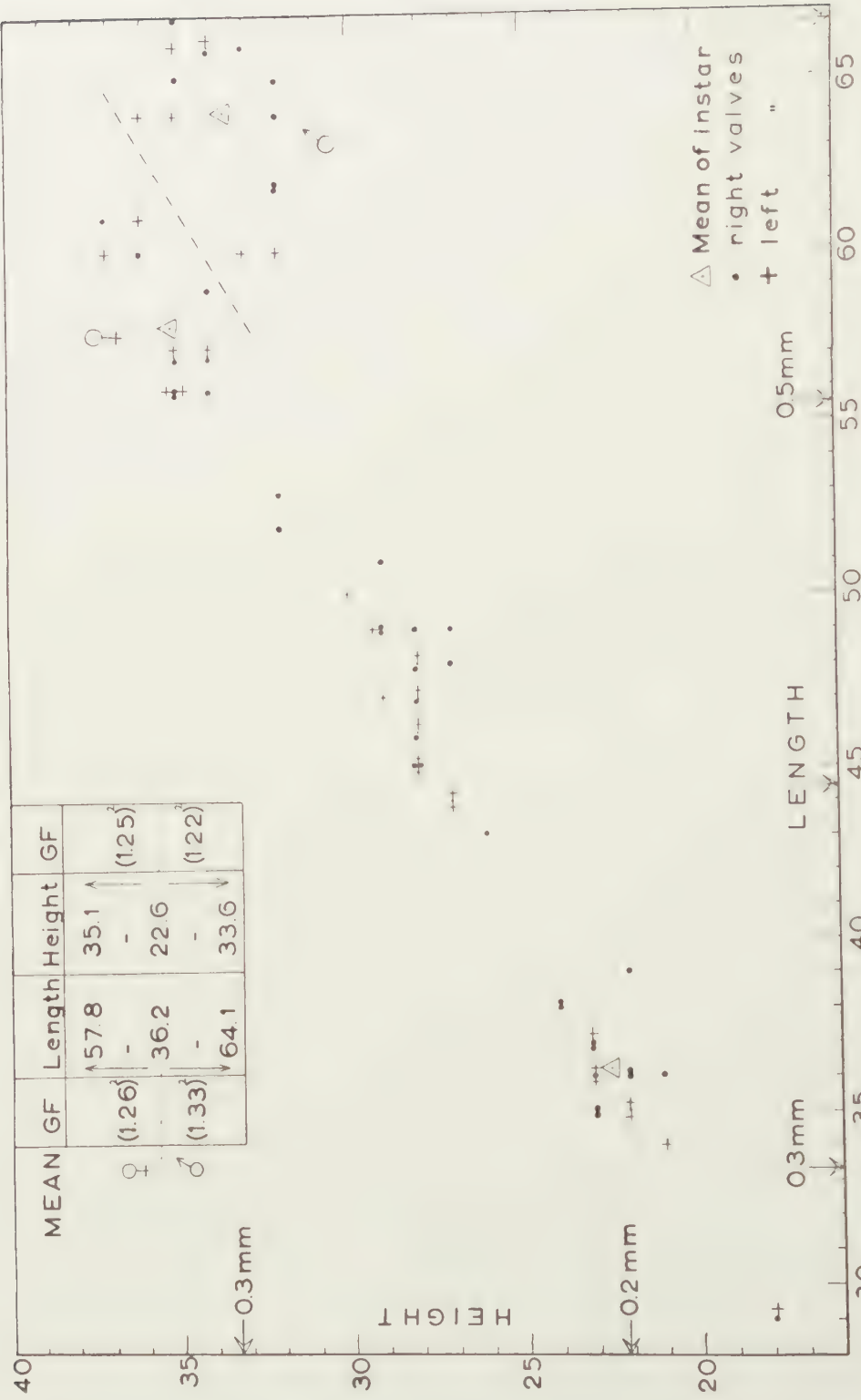


Fig. 1. Scatter-diagram of the length and height of *Pagurarchella (Neomonacerrina) mediterranea* Ruggieri of Manila.

area is rather narrow. Seven or eight widely spaced, straight radial pore canals perforate the anterior duplicature. Three of them are present in the caudal process, and there are at least five along the ventro-posterior margin. The anterior margin is fringed by a broad thin flange. In the dorsal part of the anterior margin the flange is sometimes reduced to two or three short spines.

Of the muscle-scar pattern only the vertical row of four scars is visible. This row is situated on the ridge, that corresponds with the sulcus on the outer side.

The hinge of the right valve consists of a cusped anterior and posterior tooth, and a long, straight crenulated groove in-between. The hinge of the left valve is the complement. One small cusp is situated below the posterior end of the posterior socket of the left valve; two such cusps are situated ventrally of the anterior socket of the left valve. There is neither the tooth beneath the anterior end of the bar of the left valve, nor is there a corresponding socket in the right valve.

Dimensions: Holotype: L: 0.51, H: 0.21, $\frac{1}{2}$ W: 0.16.

For the dimensions of the other valves, see fig. 1.

Remarks: *Payenborchella* (*Neomonoceratina*) *koenigswaldi* somewhat resembles *Payenborchella* (*N.*) *iniqua* (BRADY) in ornamentation, but it differs from this species in the more triangular outline (especially the females), in the short broad caudal process, the ornamentation of the antero-dorsal quadrant with its two vertical ridges, and the ornamentation of the postero-dorsal quadrant with its long strongly curved ridge.

Payenborchella (*N.*) *koenigswaldi* shows a remarkable variation on the hinge pattern of the genus, i.e. the absence of the anterior tooth in the left valve with the corresponding socket in the right valve.

The length and height of some 70 detached valves were measured and the values are plotted in fig. 1. Three successive instars could be traced in our material. The males are represented by two instars; only the last but one instar could not be separated from the corresponding instar of the females.

Payenborchella (*Neomonoceratina*) *mediterranea* RUGGIERI; Pl. 3, fig. 12-13.

Payenborchella (*Neomonoceratina*) *mediterranea* RUGGIERI, 1953, Atti Soc. It. Sc. Nat., v. 92, p. 4, textfig. 1-5.

Remarks: This species is known from Port Saïd (Egypt), the Gulf of Paria (Venezuela), and the Bay of Djakarta (Java).

Of some 50 detached valves the length and height were measured and the values plotted in a scatter-diagram (fig. 2). Three successive instars are present in our material. The last but one instar of the females and males are already separable.

Xestoleberis variegata BRADY; Pl. 3, fig. 8.

Xestoleberis variegata BRADY, 1880, Challenger Rep., v. 1, p. 129, pl. 31, f. 8; 1886,

Jour. Linn. Soc. London, Zool., v. 19, p. 314; 1890, Trans. Roy. Soc. Edinburgh, v. 35, p. 508; VAN DEN BOLD, 1950, Ann. Mag. Nat. Hist., s. 12, v. 3, p. 901.

Paradoxostoma sp.; Pl. 3, fig. 9.

Remarks: Only two valves were found, which could not be specifically determined.

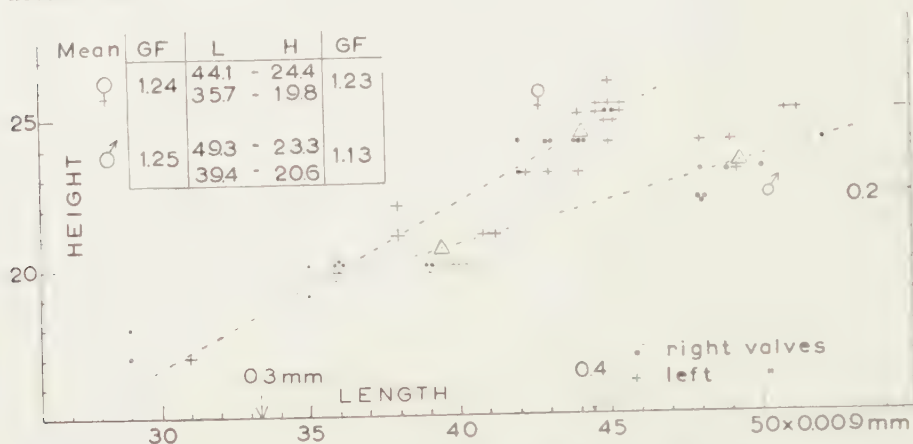


Fig. 2. Scatter-diagram of the length and height of *Payenborchella* (*Neomonoceratina*) *koenigswaldi* n. sp. of Manila

Cythere ? *caudata* BRADY; Pl. 3, fig. 1.

Cythere caudata BRADY, 1890, Trans. Roy. Soc. Edinburgh, v. 35, p. 499, pl. 2, f. 10-11.

Remarks: Three right valves were found. The genus to which these specimens belong is unknown to the writer.

REFERENCES

- BOLD, W. A. VAN DEN, List of Ostracoda in J. H. GERMERAAD: "Geology of Central Seran." Thesis Univ. Utrecht (1946).
- , Hemikrithe, a new genus of Ostracoda from the Indo-pacific. Ann. Mag. Nat. Hist. s. 12, 3 (1950).
- BRADY, G. S., Description of Ostracoda in BERCHON, DE FOLIN et PERIER: "Les Fonds de la Mer, etc.", 1 (1868).
- , a). Marine Ostracoda from the Mauritius.
b). Marine Ostracoda from Tenedos.
Ann. Mag. Nat. Hist. s. 4, 2 (1868).
- , Ostracoda. Report of the scientific results of the voyage of H.M.S. Challenger (1880).
- , Notes on Ostracoda collected by Mr A. HALY in Ceylon. Journ. Linn. Soc. London, Zool., 19 (1886).
- , On Ostracoda collected in the South sea Islands. Trans. Roy. Soc. Edinburgh, 35, 2 (1890).
- FYAN, E. C., Eenige jongpliocene Ostracoden van Timor. Versl. Gew. Verg. Kon. Akad. Wet. Amsterdam, afd. Wis- en Natuurk., 23 (1916).
- HORNIBROOK, N. DE B., Tertiary and recent marine Ostracoda of New Zealand. N. Zeal. Geol. Surv. Pal. Bull. 18 (1952).

- KEY, A. J., Preliminary note on the recent Ostracoda of the Snellius expedition. Proc. Kon. Ned. Akad. Wet. Amsterdam, s. B, **56**, 2 (1953).
- KINGMA, J. TH., Contributions to the knowledge of the Young-Caenozoic Ostracoda from the Malayan region. Thesis Univ. Utrecht (1948).
- MÜLLER, G. W., Die Ostracoden des Golfes von Neapel, etc. Fauna und Flora des Golfes von Neapel, Monogr. **21** (1894).
- RUGGIERI, G., Ostracodi del genere Payenborchella viventi nel Mediterraneo. Atti d. Soc. It. Sc. Nat., **92** (1953).
- TRIEBEL, E., Zur Morphologie und Oekologie der fossilen Ostracoden. Senckenbergiana, **23** (1941).
- , Zur Kenntnis der Ostracoden-Gattung Payenborchella. Senckenbergiana, **30** (1949).

CRYSTAL STRUCTURE OF d(-)-ISOLEUCINE HYDROCHLORIDE
MONOHYDRATE. II.

THE [001] PROJECTION AND FINAL STRUCTURE

BY

J. TROMMEL

(Communicated by Prof. J. M. BIJVOET at the meeting of February 27, 1954)

The [100] projection has been described in part I. After one refinement with a least squares method of the [100] projection of figure 1 [1] the reliability factor R had decreased very little. So a $(F_o - F_c)$ synthesis [2] was made, which revealed that the methyl group must be displaced. With this new model least squares methods rapidly diminished the R down to 0.18.

Since the [001] FOURIER projection obtained by the method of isomorphous substitution was very imperfectly resolved, approximate x coordinates were adopted from a vector convergence map [3] and from spatial considerations. Refinement was carried out by repeated FOURIER syntheses and least squares methods. The final [100] and [001] FOURIER projections are shown in the figures 2a and 2b.

$(F_o - F_c)$ syntheses indicated an asymmetric temperature factor for the chlorine ion and greater temperature factors for the carbon atoms C_4 , C_5 and C_6 than for the other atoms (for the numbering of the atoms see figure 3). For the chlorine a temperature factor $\exp. - (B + \beta \cos^2 \varphi) (\sin \theta / \lambda)^2$ [4] was applied where φ denotes the angle between the direction of maximum vibration and the normal of the reflecting net-plane, with $B = 2.80 \text{ \AA}^2$ and $\beta = 1.00 \text{ \AA}^2$, and for the other atoms $\exp. - B (\sin \theta / \lambda)^2$ with $B = 6.00 \text{ \AA}^2$ for C_5 and C_6 , $B = 4.40 \text{ \AA}^2$ for C_4 and for the other atoms $B = 2.80 \text{ \AA}^2$. With this correction R has the value 0.147 for all $0kl$ reflexions and 0.143 for all $h k 0$ reflexions.

No conclusive evidence for the location of the 16 hydrogen atoms could be found from $(F_o - F_c)$ syntheses. The positions of 13 hydrogens have been calculated from the model with the assumption that the $C-NH_3$ group is a tetrahedron with the three hydrogens directed to the chlorine ion and to two water molecules. The positions of the hydrogens belonging to the two methyl-groups were taken from spatial considerations, assuming that the hydrogen atoms of these two methyl-groups were at the greatest distance from each other, free rotation being excluded by steric hindrance. The assumed positions of these 13 hydrogens are indicated by crosses in the figures 2a and 2b. Structure factors have been calculated for these

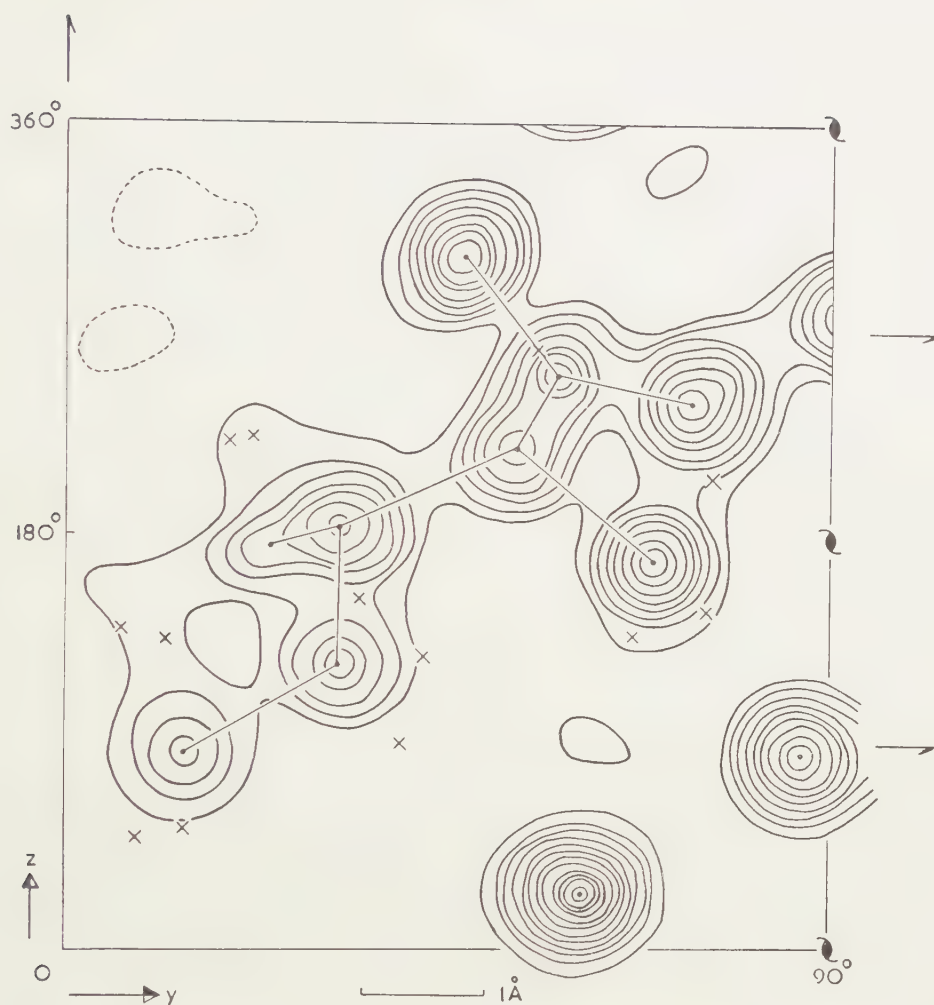


Figure 2a

TABLE I
Atomic parameters

	<i>x</i>	<i>y</i>	<i>z</i>
C ₁	0.708	0.158	0.692
C ₂	0.487	0.148	0.600
C ₃	0.503	0.090	0.522
C ₄	0.628	0.090	0.328
C ₅	0.694	0.038	0.231
C ₆	0.276	0.065	0.489
O ₁	0.758	0.129	0.839
O ₂	0.799	0.203	0.660
N	0.417	0.190	0.467
Cl	0.153	0.168	0.072
H ₂ O	0.756	0.243	0.226

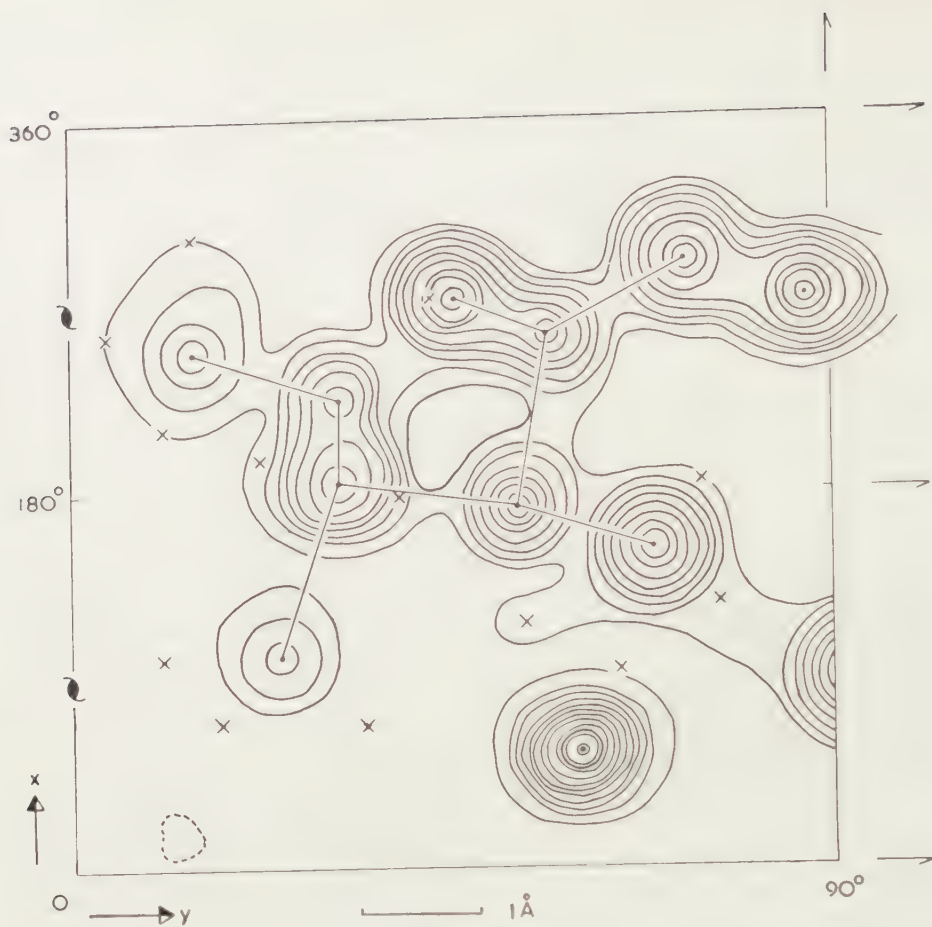


Figure 2b

Figure 2a and 2b. [100] resp. [001] FOURIER projection of d-isoleucine-HCl.1 H₂O. Contours are drawn at intervals of 1 electron per Å², for the chlorine of 2 electrons per Å²; the zero level is dotted, the first full contour is drawn at two electrons per Å²

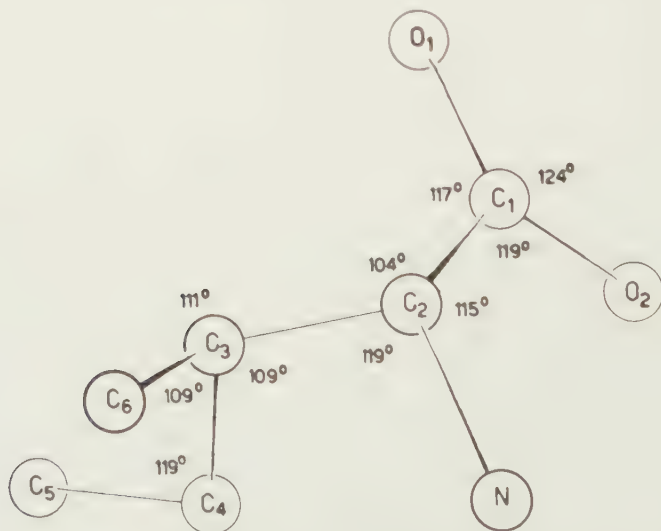


Figure 3. The shape of the isoleucine molecule

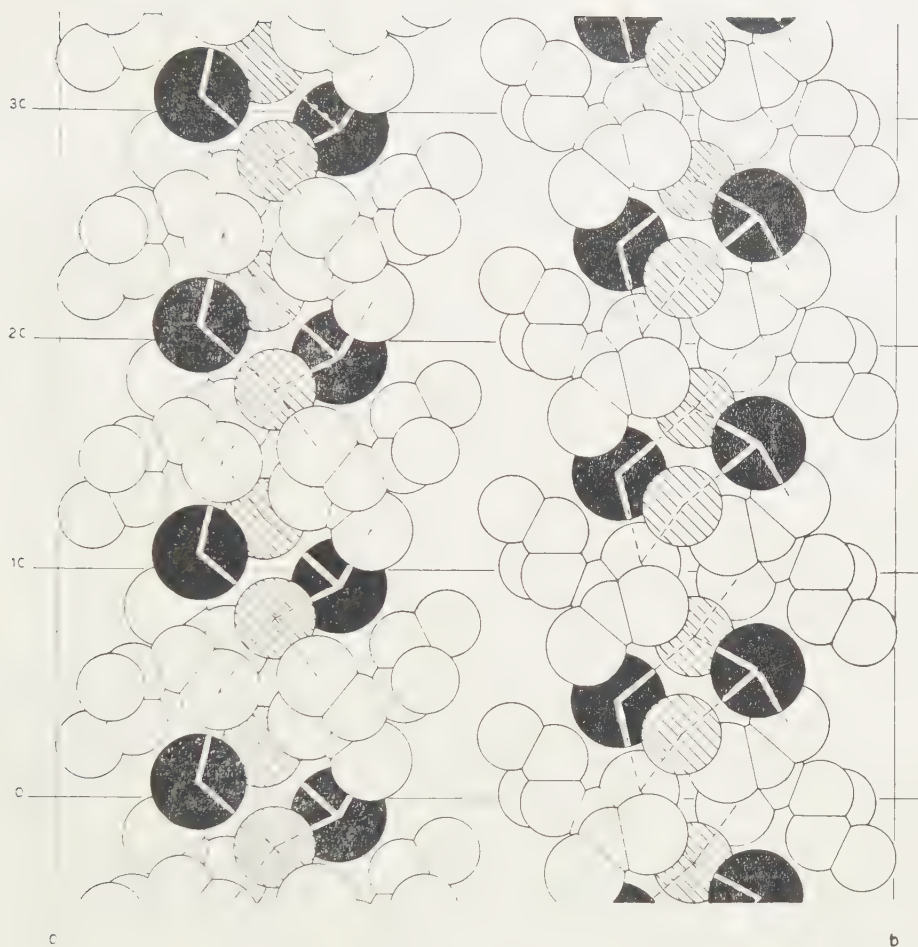


Figure 4a

hydrogens, but the agreement between observed and calculated F-values was improved only for a few reflexions with low value of $\sin \theta$. For most of the reflexions the contributions of the hydrogens was found to cancel out.

The final atomic parameters are enlisted in table I, all atoms being in the general four-fold position 4(a) of the spacegroup $P2_12_12_1$. The shape of the molecule of isoleucine is drawn in figure 3. The intermolecular and intramolecular distances, given in table II, are in accordance with the values determined in other similar compounds. The molecule is not flat; in the crystal the carbon atoms C_1 , C_2 , C_3 and C_6 approximately are in a plane and so do the carbon atoms C_2 , C_3 , C_4 and C_5 . The angle $C_3-C_4-C_5$ is much greater than the tetrahedral angle of 109° ; this deviation may be real and caused by steric hindrance between C_5 and C_6 , the distance C_5-C_6 being but 3.18 \AA . The other deviations from the value of 109° , especially about C_2 , are probably to be described to inaccuracies in the structure determination. Within the limits of error the HOOC-CH-NH_2 group is flat. The same

value is found for the distances C_1-O_1 and C_1-O_2 . Since the inaccuracy in the interatomic distances is estimated to be of the order of 0.05 Å, no

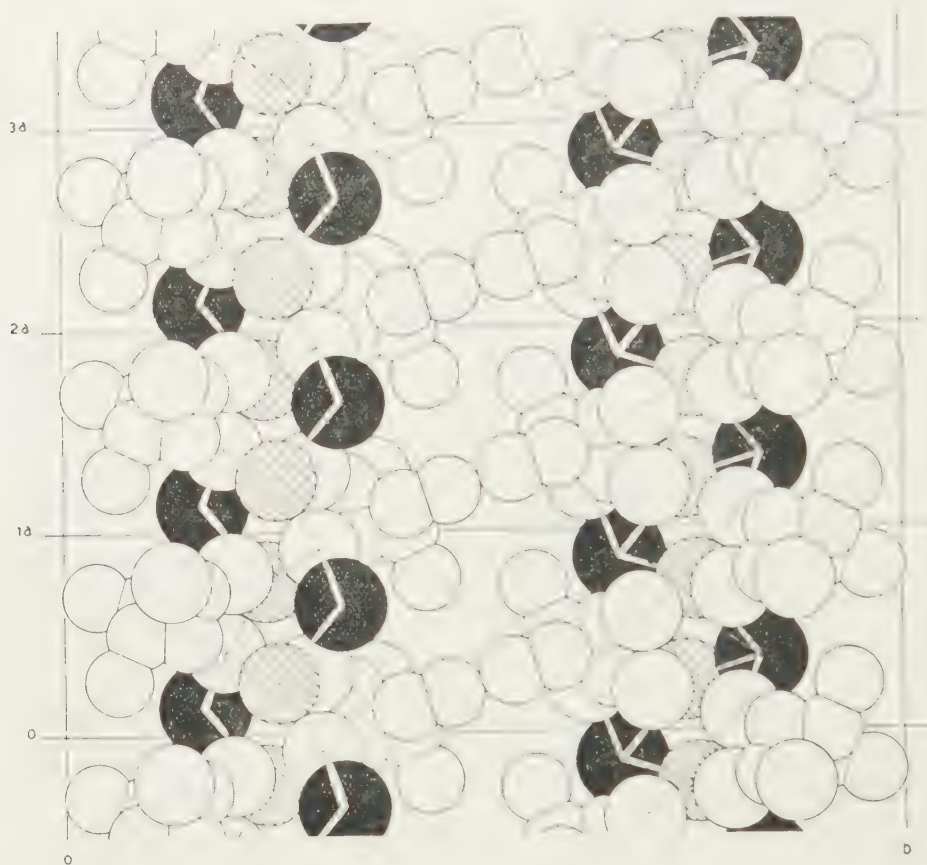


Figure 4b

Figure 4a and 4b. The structure of d-isoleucine-HCl.H₂O projected along the a- resp. c-axis. The chlorine ions are black, the water molecules are shaded. The dashed lines indicate the hydrogen bonds

TABLE II
Interatomic distances in Å

Intramolecular:	Intermolecular:
$C_1-O_1 = 1.27$	$Cl-N = 3.18$
$C_1-O_2 = 1.27$	$Cl-O_1 = 3.05$
$C_2-N = 1.43$	$Cl-H_2O = 3.07 \text{ and } 3.24$
$C_1-C_2 = 1.51$	$N-H_2O = 2.85 \text{ and } 2.96$
$C_2-C_3 = 1.55$	$N-O_2' = 2.90$
$C_3-C_4 = 1.53$	$C_5-C_5' = 3.95$
$C_4-C_5 = 1.52$	$C_5-C_5' = 3.96$
$C_3-C_6 = 1.54$	$C_5-C_6' = 4.03$

conclusions can be drawn from these distances about the structure of the carboxyl-group. From the intermolecular distances hydrogen bridges are

possible between O_1 and Cl and between O'_2 and N; the angle $C_2-N-O'_2$, however, amounts to 160° , so it is probable that this distance corresponds only to a short approach without a hydrogen bridge, and that consequently the O_1 atom is the hydroxyl-group.

The amino-group and the methyl-group are in *cis*-position with respect to each other. So D-isoleucine is D- α (d)-amino- β (d)-methyl-valeric acid and thus D-allo-isoleucine [5] is D- α (d)-amino- β (l)-methyl-valeric acid.

The packing of the molecules is seen in the figures 4a and 4b. In the a and c direction the molecules are held together by a network of hydrogen bonds *via* the chlorine ions and the water molecules. Thus the structure can be seen as built up by layers parallel to the ac plane, held together in the b direction by VAN DER WAALS forces between the methyl-groups. This is in accordance with the very easy cleavage along (010).

Full details will be published elsewhere.

*Laboratorium voor Kristalchemie
der Rijksuniversiteit, Utrecht*

REFERENCES

1. These Proceedings, Series B56, 272 (1953).
2. W. COCHRAN, Acta Cryst. 4, 408 (1951).
3. C. A. BEEVERS and J. H. ROBERTSON, Acta Cryst. 3, 164 (1950).
4. L. HELMHOLTZ, J. Chem. Phys. 4, 316 (1936).
5. J. P. GREENSTEIN, L. LEVINTOW, C. G. BAKER and J. WHITE, J. Biol. Chem. 188, 647 (1951).

GEOLOGY

THE STRATIGRAPHY AND MAIN STRUCTURAL FEATURES OF AFGHANISTAN. I

BY

SULTAN ACHMAD POPOL

(Director of the Geol. Dept. of the Royal Govt. of Afghanistan)

AND

S. W. TROMP

(Geological Consultant, United Nations Techn. Ass. Adm.)

with 1 Locality chart

(Communicated by Prof. I. M. VAN DER VLERK at the meeting of April 24, 1954)

I. INTRODUCTION

In 1950 the United Nations Technical Assistance Administration in New York received a request from the Royal Government of Afghanistan for assistance in the geological study of Afghanistan, in particular, a study of its possible oil resources. The second author was selected by the United Nations for this survey, which was to cover most of Afghanistan.

After studying references in the Netherlands, the second author arrived in October 1950 in Kabul, via Peshawar and the Khaiber Pass. During the following three months, both authors visited various areas designated on the locality map, either by jeep or on horseback, during which trips a great many detailed stratigraphic sections were measured, and many samples were collected both for micropaleontological and petrographic studies (see locality chart).

Traveling was not always easy in this beautiful, extremely mountainous country which is separated into a northern and a southern part by the over 3000 m high Hindu Kush range. The roads are difficult and one passes through narrow gorges and along steep ravines ¹⁾.

For political reasons, the oil problems of Afghanistan and the distribution of other economic deposits cannot be discussed in this article. Only the general stratigraphy of Afghanistan and some interesting structural relations will be reviewed.

In October 1952 the second author spent another three months in Afghanistan, this time as head of a hydrological expedition for the United Nations. The drilling equipment was transported through Quetta (in Baluchistan, W. Pakistan) and Kandahar to Kabul. Due to many delays during the transportation of the equipment, the second author had an

¹⁾ S. W. TROMP, It was only due to the excellent guidance of Dr SULTAN POPOL and his great knowledge of the country that a large number of detailed stratigraphical and structural data could be collected in such a short period.

opportunity to study briefly the general stratigraphy of West Baluchistan, and to compare this area with S.E. Afghanistan. A trip from Kabul over the Shiber Pass to Pul-I-Khumri (see loc. map) enabled the second author to revisit some of the previously studied sections and to rectify some of the observations made in 1950. In the near future an article will be published by the second author in the Journal "Geologie en Mijnbouw" ¹⁾ (Netherlands), giving the stratigraphy of W. Baluchistan and a comparison with S.E. Afghanistan.

The present article is based on both study periods in Afghanistan. As can be seen from the bibliography attached, which gives a rather complete review of the published sources on Afghanistan, many geologists and mining engineers have visited this country, mainly, however, for very short periods or only to study a small area in detail. As a result, no over-all stratigraphic study of the country had been made.

Without mentioning specific names we should like to refer specially to the excellent work done by a great number of prominent geologists of the Geological Survey of India, the published reports of which are listed in the attached bibliography.

The fusulines collected by the authors in the Permo-carboniferous sections of the Hindu Kush range near the Shiber Pass were described by Prof. CARL O. DUNBAR of Yale University, who will publish the results of his determinations in the near future. A brief summary is given in Annex no. 1.

Macro-fossils were studied by the paleontologists of the Iraq Petroleum Co. in London, Dr R. G. S. HUDSON, Mr G. F. ELLIOT and Mr A. H. SMOUT, through the kind intermediation of Dr R. F. S. HENSON (head of the geological research dept of I.P.C.), who also studied some of the large foraminifera in the rock samples. The authors wish to express their gratitude to all these research workers for their valuable contributions.

The authors wish to avail themselves of this opportunity to thank most sincerely H. E. NAIM KHAN, the former Minister of Mines, for his confidence in their work; the many government officials who facilitated their work during the journey should also be remembered for their kindness and hospitality.

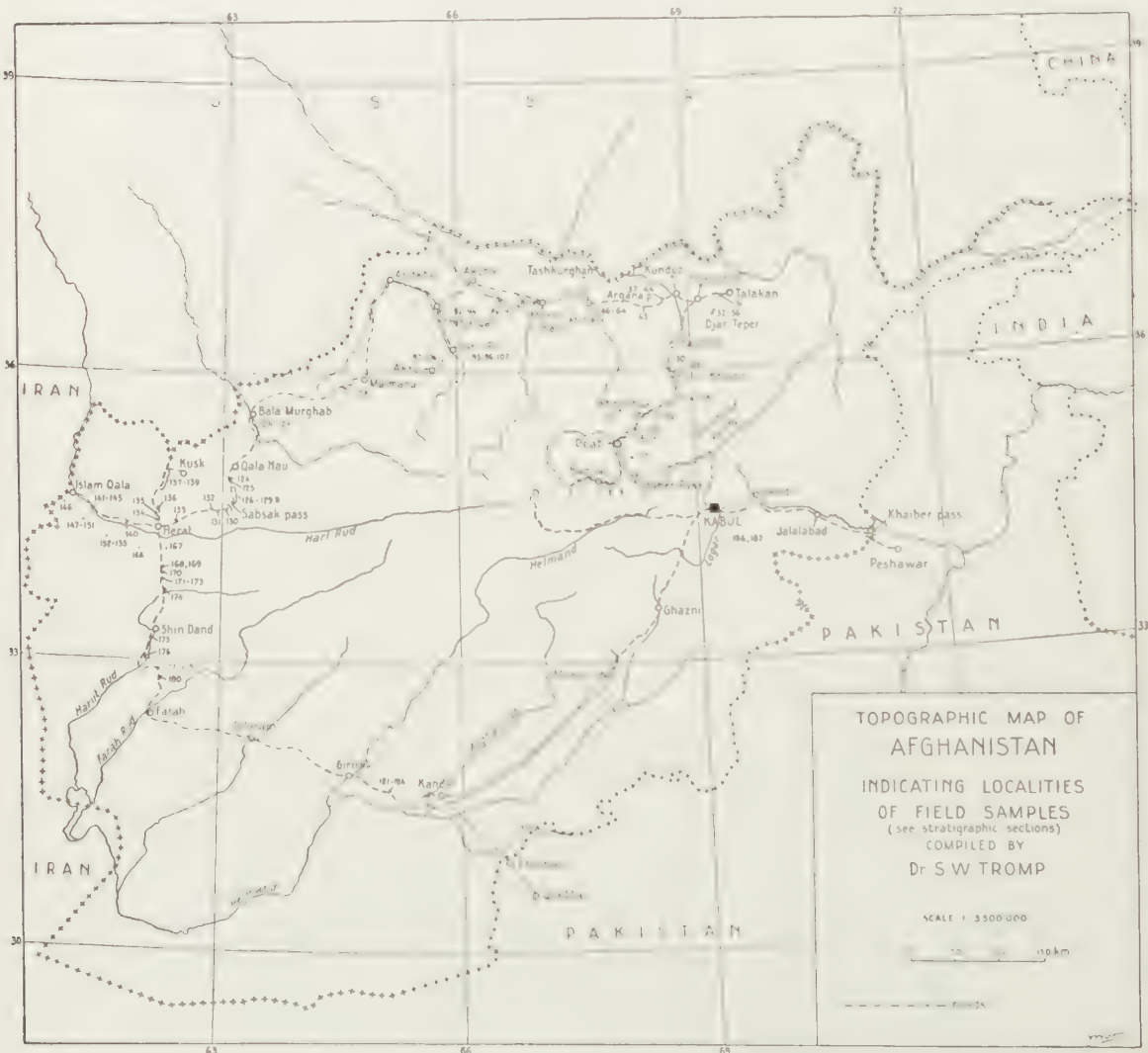
II. GENERAL STRATIGRAPHY OF AFGHANISTAN

The present summary represents a preliminary compilation of all stratigraphic data on hand. The stratigraphic classification is based on actual field observations and on laboratory studies, both micro-paleontological and macro-fossil. A brief description will be given of the different periods, beginning with the oldest known Paleozoic beds. Only the most important standard sections will be discussed more in detail.

¹⁾ No. 5, 130—134 (May 1954).

I. *Metamorphic schists:*

In different parts of Afghanistan extensive areas occur covered by metamorphic schists (marbles, phyllites, micaschists, hornstein, etc.), which often have been given a Pre-Cambrian age. A careful study of this section seems to indicate, however, that all schists may not be older than Devonian. The Devonian and younger beds have been metamorphosed by the enormous igneous intrusions during the Lower Jurassic (Doab series), the Oligocene (Sabsak series) and perhaps during the Upper Paleozoic. Particularly coming from Herat to Kabul (where the gradual transition of ordinary sediments into completely metamorphic schists can be seen) one is inclined to place all schists in the Upper Paleozoic or younger periods.



II. *Devonian*:

Along the West foot of Kotal-I-Hajigak, in the Kalu area (about 90 Kms W.N.W. of Kabul), an Upper Devonian section is exposed (according to Hayden) composed of three units (from top to bottom).

- 1) Slates, schists and black fossiliferous limestones
Fossils: *Spirifer Verneuilli*, *Strophalosia*, *Rhynchonellas*,
Corals (*Zaphrentis*, *Syringopora*) and a Trilobite.
- 2) Hematite bed.
- 3) Thick greenish coarse conglomerate.

A similar section is exposed on the East side of the Ghorband valley N.W. of Charikar (N. of Kabul), where the hematite beds are capping the high ridges in the region.

III. *Carboniferous*:

A) LOWER CARBONIFEROUS:

At Ak-Ribat (140 Kms W.N.W. of Kabul) a dark limestone section occurs which (acc. to F. R. Cowper Reed) contains a Lower Carboniferous fauna (Lower Carboniferous Brachiopods, Crinoids and Fusulines). The section covers the so-called Helmand metamorphic series.

B) UPPER CARBONIFEROUS:

In the Khwajagar ravine (25 Kms S.E. of Ak-Ribat) an Upper Carboniferous section was found by Hayden and others which consists of the following beds (from top to bottom):

- 1) Thin bedded coral limestone.
- 2) Black compact limestone with Brachiopods (*Productus punctatus* M., *Reticularia lineata* M., *Dielasma*, *Uncinulus*, *Spirifers*) and shaly thin bedded limestone rich in Fusulinidae (*Fusulina elongata* Shumard, *F. Uralica* Krotow, *Schwagerina Princeps* E.)
- 3) Alternation of thin bedded quartzites and slates.
- 4) Massive unfossiliferous limestone.

This section is covered by a Permian Fusulinidae limestone (see below).

At Khurd Kabul (25 Kms S.E. of Kabul) an Upper Carboniferous limestone occurs which is overlying a schist series. The section is composed of the following units (from top to bottom):

- 1) Grey limestone (perhaps Permian or younger).
- 2) Dark limestone full of Calcitic cross sections of *Spirifers*.
- 3) Dark limestone full of *Productidae*.

In North western Afghanistan 6 Kms south of Zindajan (40 Kms W. of Herat, south of the river Hari Rud) an almost 1200 Metres thick black limestone section was found by the authors rich in brachiopods (*Spirifers*, *Productidae*, etc.); in places also Crinoids and Corals were found. The section probably represents both Lower and Upper Carboniferous.

IV. *Permian*:

In the Khwajagar ravine (see above), S.E. of Ak-Ribat, the Upper

Carboniferous limestones are covered by a Permian limestone section which consists of two parts (from top to bottom):

- 1) Thick mass of light grey limestone rich in *Sumatrina Annae* Voltz (probably representing UPPER PERMIAN).
- 2) Dark limestones full of *Neoschwagerina Craticulifera* Schw., *N. primigena* Hayden (and other species), other Foraminifera such as *Spiroloculina*, *Textulariidae* (*Bigennerina*), *Valvulinidae*, etc. (probably representing LOWER PERMIAN).

75 Kms W. of the Shiber Pass, near the granite contact, a black limestone section occurs full of *Fusulinidae*, which represents the Upper Permian (see Annex no. 3).

The Carboniferous, Permian and Lower Triassic limestone seem to form a continuous section without any erosional hiatus. As they cover different metamorphic schists it seems probable that an unconformity exists between the Carboniferous and Devonian. The post-Devonian transgression probably covered gradually an irregular Devonian topography.

MESOZOIC

V. *Triassic*:

The Triassic in Afghanistan seems to be represented by two facies: the Northern LIMESTONE- or SAROBI FACIES (discovered by Hayden and others) and the ARGILLACEOUS- or DOAB FACIES (discovered by Rosset in recent years) in the Central Hindu Kush.

A) SAROBI FACIES:

Lower Triassic: It occurs between Khurd Kabul and Butak (S.E. of Kabul) as light grey limestones, with few fossils (*Meekoceras*, *Ophiceras* and *Pseudomonotis*).

Upper Triassic: It was found west of Sarobi (E. of Kabul) as light grey limestone containing *Megalodon* and *Dicerocardium* species.

B) DOAB FACIES:

The Triassic of the Central Hindu Kush is a stratigraphically complicated series because of two unconformities: one at the top of the Lower Triassic limestones and one at the base of the Lower Jurassic volcanic series (Upper Doab series). It is mainly due to the excellent work of Mr L. F. ROSSET (French school teacher at Kabul, who spent several summers at Doab collecting fossils) that the rich *Ceratites* and *Daonella* fauna of Doab was discovered, which was described by Furon and Boureau in Bibl. no. 35.

VI. *Jurassic*:

Between the Triassic shales and limestones of Doab and the superimposed volcanic series a clear erosional hiatus exists which can be observed at different places between Doab and Ishpushta. 4 Km. S. of Doab a post-Triassic lava flow separated the basal conglomerates and shales of the Middle Triassic (L. Doab) series.

A) LOWER JURASSIC (UPPER DOAB SERIES):

The age of the Upper Doab series is based on two facts:

- 1) It is unconformably overlying a thick post-Carboniferous limestone section (probably L. Triassic in age, see above) and a Middle Triassic shale section.
- 2) It is covered by the Saighan series, which for reasons given below, should be Middle or Upper Jurassic in age.

The succession of the various volcanic extrusions and intrusions is based on both field observations and petrographic laboratory studies. About 22 Km South of Doab and 60 Km north of Ishpushta very large granite batholites occur, which are probably of L. Jurassic (Upper Doab) age.

The Late-DOAB age of these granite intrusions is indicated by the following field observations:

- 1) Great similarity between the border facies of the granite massives near Doab and the quartz porphyry dikes in this region.
- 2) Lack of granite pebbles in the basal Doab conglomerate, which contains only limestone pebbles, although both granites and limestones are outcropping at present near those conglomerates.
- 3) Presence of a large granite massive (near quartz porphyry dikes) in the middle of the Doab porphyritic and basalt masses.
- 4) Occurrence of large thin bedded basalt enclaves, with irregular shape, floating in the middle of the granite mass (abt. 60 Kms North of Doab).
- 5) Presence of granitic dikes in a basalt mass 65 Kms North of Doab.

THE PRE-CRETACEOUS AGE OF THE GRANITE INTRUSIONS in the Doab region is indicated by the presence of granite pebbles in conglomerates of the Lower-Cretaceous Red Grit series (abt. 70 Metres above the base of this series).

Apart from large granite intrusions, gabbroidic rocks also occur in large masses in the Central Hindu Kush, e.g. between Bamian and Doab.

Although no direct evidence is available indicating a Doab age of the gabbroidic intrusions in the Doab region, there is sufficient indirect evidence, such as the intrusion of serpentine in Permo-Carboniferous limestones, occurrence of gabbroidic rocks near the granite massives and finally the presence of extensive basaltic extrusions in the beginning of the Doab period.

B) UPPER AND MIDDLE JURASSIC (SAIGHAN SERIES):

This section is beautifully exposed near the Ishpushta coal mines and has been studied in detail particularly by West (Bibl. nos 104 and 105), formerly Director of the Geol. Survey of India. The present authors restudied this section which is composed of three units (from top to bottom):

- 1) *Upper Saighan series*: More than 100 Metres of greenish grey shales

with loosely cemented conglomerate intercalations (containing quartz and black lydite pebbles). Coal seams seem to be absent in contrast with the Middle Saighan series.

2) *Middle Saighan series*:

160 Metres: Bluish green and greenish shales with reddish brown sandstone and conglomerate intercalations (about 20 M. shale against 4 Metres sandstone). Pebbles composed of only quartz and black lydite. Several coal seams, main seam at base of this unit. Shales near coal seams rich in plant fragments. Particularly abundant are: "*Cladophlebis denticulata* Brogniart" and "*Kukia exilis* (Philips) Raciborski", both, according to T. M. HARRIS, typical of Middle and Upper Jurassic of Europe and Asia.

About 40 M: Slightly calcareous conglomeratic sandstones with 2 M thick greenish shale intercalations.

About 60 M: Greenish shale without sandstone intercalations.

3) *Lower Saighan series*:

About 200 M: slightly calcareous light grey gritty sandstones with conglomeratic and shaly intercalations, near base few white and reddish tuff intercalations.

About 20 M: Reddish brown tuff clay.

Base always composed of a reddish zone, which seems to have been an erosional surface at the end of the Lower Jurassic. This is indicated by the following observations:

- (1) Near Ishpushta a clear angular unconformity can be seen between the Saighan and Upper Doab series.
- (2) 7 Kms North of Ishpushta overlap conditions prevail, different horizons of the Saighan series being in contact with the underlying Doab series.
- (3) 22 Kms North of Ishpushta the green Saighan series is filling up irregular basins which were formed during an erosional period at the end of the Doab period.

SEWART, SITHOLEY and JACOB (Bibl. nos 87, 88, 89, 104) who made detailed studies of the Saighan flora, agree that this series is definitely Jurassic in age, but no further specification is given. FURON, BOUREAU and ROSSET (Bibl. no. 35) believe in Lower Jurassic age of the Saighan series, without giving any concrete evidence, except that similar coalbearing beds seem to occur in Liassic (Lower Jurassic) beds of the Elbourz in Iran.

The data given above (particularly the presence of unconformities and the age determinations of HARRIS) suggest a late Jurassic age for the Saighan series. Also the gradual transition of the Saighan series into Lower Cretaceous Red Grit series (although a small hiatus seems to exist, see later) indicates that the Saighan series must represent the highest Jurassic unit.

LEMMON (Bibl. no. 65) described the coalbearing section of Masjd-

I-Chobi (108 Kms N.E. of Herat) as composed of 160 Metres of light grey and dark grey shales with 1-20 cm thick coal seams and one thick (1 M) coal seam about 52 Metres below the top of this section. This unit is covered by a 300 M thick series composed of an alternation of limestone, marl, shale and sandstone with a 5 M conglomerate at the base, composed of quartz pebbles. About 100 Metres below the top Orbitolina limestones were found.

The coalbearing section is underlain by a thick (at least 200 M) red sandstone and claystone series. According to Lemmon, this coalbearing section would represent the Saighan series, the underlying red sandstone probably Triassic.

It seems more likely, however, that this coalbearing unit represents a Lower Cretaceous or basal Cenomanian section for the following reasons:

- (1) In Tashkurghan and Pista Mazar Cretaceous sections (see later) thin coal seams have also been found.
- (2) The Cretaceous section of the Murghab valley (15 Kms S. of Bala Murghab) is the same as the one described above (see later), the deepest red sandstones are definitely the Red Grit series (see below), which is present all over this area.
- (3) The triassic both in Iran and Afghanistan is only known in a facies different from the one mentioned above.

TRANSITION JURASSIC - CRETACEOUS:

At the Ishpushta coalmine the transition seems to be gradual without any hiatus, only a sudden change in colour occurs from greenish into dark red. Even the same type of pebbles are found directly above and below the contact. Still, a careful study along this contact over a longer distance shows that a small hiatus exists. This is indicated by the following facts:

- 1) Although near the contact the differences are small, the Red Grit series as a whole is completely different (both in lithology and colour) from the Saighan series, suggesting sudden changes in conditions of sedimentation due to tectonic movements.
- 2) The sudden appearance of granite, porphyry and limestone pebbles, 70 metres above the base of the Red Grit series, which are missing in all the conglomerates of the Saighan series, indicate sudden movements and increased erosion at the beginning of the Red Grit period.
- 3) The sudden change in colour suggests a similar process, the dark red colours probably due to ferruginous minerals of the Doab series (volcanic).
- 4) 7 Kms North of Ishpushta the Red Grits are directly covering the coalbearing M. Saighan series.

Further north the Red Grits are covering still deeper beds.

VII. *Cretaceous*:

In contrast with the older formations with rather regular facies conditions, the Cretaceous is characterized by rapidly changing facies both in

N.S. and E.W. directions. Still, there is a great similarity in the general sections as far as North Afghanistan is concerned. In West and S.W.-Afghanistan a completely different facies is developed, which is considerably less argillaceous than the sections in North Afghanistan.

A) LOWER CRETACEOUS (so-called "RED GRIT SERIES") thickness 80-320 M. Greenish clay beds, in places rich in gypsum beds, alternate with reddish sandstones. Sandstone usually dominates. Except near Ishpushta, few conglomeratic intercalations seem to occur in this section: near the top, beds with plant fragments and thin coal seams have been found.

B) CENOMANIAN (so-called "GREEN BEDS"):

1) *North and North-west Afghanistan*: Thickness 160-250 M.

Alternation of grey (in the sun green or dark green in colour) clays and marls, particularly in the lower part of the section alternating with grey calcareous sandstones.

Several thin greenish glauconitic (oölitic) limestone intercalations occur, rich in *Exogyra* and *Ostrea* fragments. Some of the argillaceous sections are very rich in *Exogyras* and *Grypheas*.

In the Tashkurghan area and the Koh-I-Elburz the marls are replaced for a considerable part by limestones.

In the Koh-I-Elburz (near Mazar-I-Sharif) and the Aksu region (35 Kms S.W. of Sar-I-Pul) non-calcareous sandstones occur at the top of the argillaceous section, which changes abruptly into the Turonian limestone series (see below).

In the Ishpushta region shales are missing and only a thick section of reddish and grey sandstones is developed, near the top a few green shales and gypsum intercalations directly overlain by the Turonian massive limestone.

2) *West and South-west Afghanistan*:

Top:

120 Meters: Alternation of yellow-brown sandy limestones, greenish marly limestones, black limestones and brownish and grey calcareous sandstones.

Base:

More than 50 M.: Grey calcareous sandstones and gritty or pebbly sandstones. This section is usually considerably changed as a result of contact metamorphosis by the Oligocene Sabsak intrusions (see below).

C) TURONIAN (so-called "MASSIVE LIMESTONE SERIES") Thickness 200-400 M.

The Turonian limestones are unconformably covering the Cenomanian beds, although in most places the contact makes the impression of being a gradual transition. This statement is based on the following observations:

1) In the Darra-I-Suf area N.W. of Ishpushta an angular unconformity

exists between the Cenomanian (developed in the Red Grit facies of Ishpushta, see above) and the Turonian limestones. As a result, the Red Grit series varies considerably in thickness and the limestones sometimes cover directly the Saighan series and deeper beds (in the Saighan valley).

- 2) The beds underlying the massive limestone in N. Afghanistan vary from one locality to the other, apart from this, the presence of non-calcareous sandstones suddenly covered by pure, non-sandy massive limestones suggests a hiatus in deposition.

North Afghanistan facies:

The Turonian massive limestone series in North Afghanistan usually varies in facies on both flanks of the structure, usually one flank being developed as thick bedded massive grey limestone with few silex beds near the top and the other flank composed of white thin bedded porous chalky limestones. The limestones are as a rule non-fossiliferous, except a few Gastropods and Oysters. In a few places also small Exogyras and Grypheas were found.

S.W. of Sar-I-Pul the basal section is composed of creamish coloured argillaceous limestones or marly limestones full of *Inoceramus*. Near Aksu the whole Turonian section is changed into *Inoceramus* limestones.

West and S.W. Afghanistan facies:

In the neighbourhood of Milkoh (between Farah and Shin Dand) a thick limestone section is covering the sandy Cenomanian series (see plate 2 A). This section is composed of a lower part consisting of dark grey or black limestone with many cross sections of large Rudists and Gastropods. In places the limestone is completely made up of *Orbitolinas* and *Cuneolinas*. This lower section which cannot be distinguished lithologically from the dark carboniferous limestones, is covered by light grey Rudist limestones. Both limestone sections are rich in chert, probably secondary deposits as a result of magmatic activity in this region. Micro-faunal studies revealed that the dark grey lower section belongs to the Cenomanian, whereas the upper light grey section represents the Turonian massive limestone.

D) SENONIAN:

Senonian and Lower Eocene beds seem to be absent in Afghanistan except in the sections north of the massive Turonian limestone at Tashkurghan and below the Argana pass (20 Km. W. of Kunduz, in the north-eastern plain). Both micro- and macro-fossil studies confirmed our assumption in the field that the marly sections above the massive Turonian limestone represent a Senonian section, near Tashkurghan gradually changing into L. Eocene gypsiferous marls. This so-called "TASHKURGHAN SERIES" is composed of a 270 M. thick grey (in the sun green) marl section near the base composed of white

weathering greenish marls. About 80 Metres above the base a thin section of black oil shales occurs.

In the Ishpushta region, in the Central Hindu Kush, the Turonian massive limestones are covered by brownish grey (green in sun) marls, with sandstone and limestone intercalations, which also may represent a Senonian or L. Eocene section.

CENOZOIC

VIII. *Eocene*:

A) LOWER EOCENE: As indicated above, L. Eocene could be established with certainty only in the Tashkurgan section. In most parts of Afghanistan this section seems to be missing, probably as a result of regional uplift during the beginning of the Middle Eocene.

B) MIDDLE EOCENE: Middle Eocene deposits also seem to be extremely rare in Afghanistan. The authors could establish only the following localities:

1) *Tashkurgan Section*: a grey marl section with a basal Middle Eocene Oyster fauna is overlying the above mentioned L. Eocene and Senonian marls. A thin white sandstone is lying at the base of the M. Eocene. Although no unconformity could be observed in the field, the thin development of the L. Eocene as compared with E. Persia would suggest disconformable relationships.

2) *Section at Shiboglu pass*: (80 Km. W. of Kunduz)

In this area isolated limestone outcrops were found in the surrounding plain containing an (Upper) Middle Eocene Oyster fauna.

3) *Section between Qala Darband and Daban-I-Kushak*: (N.W. Afghanistan)

In the Murghab valley, 15 Kms S. of Bala Murghab, a probably Upper Eocene limestone section occurs, the basal part of which (below the clay beds) may represent Middle Eocene limestones. They are covering the Cenomanian beds in perfectly parallel order, although a large hiatus exists.

(C) UPPER EOCENE:

The only known section which may represent Upper Eocene beds was found by the authors in the Murghab valley, about 15 Kms S. of Bala Murghab. It consists of 3 units:

An Upper Unit: Composed of more than 100 M. of greenish marls, near the top whitish weathering, near the base containing grey fossiliferous limestone intercalations.

A Middle Unit: Composed of 125 M. of grey limestones, in the upper part thin bedded, in the lower part thick bedded and massive.

A Lower Unit: Composed of 30 M. of green clays with reddish limestone and claystone intercalations. This Unit seems to be absent further south.

The top beds of the middle unit contain very small Nummulites and

Operculinas which suggest an Upper Eocene age. The limestones are also rich in Echinoid fragments and worm tubes. It is possible that the thin bedded Echinoid limestones which cover the massive Turonian limestone of the structures near Shibarghan (further N.E.) belong to the same Upper Eocene unit.

IX. *Oligocene* :

The Turonian limestone and older beds near Herat and further south are intruded and covered by enormous extrusions, the age of which is difficult to establish accurately. They are most likely Oligocene in age for the following reasons:

- 1) Presence of M. and U. Eocene beds in the Bala Murghab-Qala Nau area, which seem to be covered by the Sabsak tuff series.
- 2) Between the Sabsak Pass and a place 10 Kms S. of Qala Nau Senonian greenish marls are developed which are covered by a few metres thick red conglomerate composed of limestone and sandstone pebbles. This conglomerate in its turn is covered by 60 M. reddish tuffstones, with few clay intercalations near the base. This indicates a post Cretaceous volcanic activity.
- 3) 35 Kms N. of Herat near Chos Robat a 150 M. thick volcanic section occurs composed of "Lahar" (i.e. volcanic mudstreams) beds with few thin reddish tuff and porphyry-lava flows. The Lahar is almost completely composed of quartz porphyry pebbles. The tuff beds are similar to those observed in the Sabsak region.
- 4) In the Elburz in N.E. Iran tremendous (probably submarine) extrusions have taken place in the Uppermost Eocene or Oligocene, known as the "GREEN BED SERIES", an over 3000 M. thick greenish tuff series covering Middle-Eocene Nummulitic limestones; also in Iran the tuffs are intercalated with basic lava flows.
- 5) Between Herat and Shin Dand, apart from extrusions, extensive intrusions in Carboniferous and U. Cretaceous limestones occur, the oldest intrusions being composed of porphyrites, followed by basalt and brownish quartz Keratophyres, in their turn covered by reddish tuffs and lahars (with porphyry pebbles).

It seems logical to assume that this whole volcanic sequence, which is widely exposed in W. Afghanistan (in the whole region between Herat-Farah-Dilaram as far as Kandahar) and which we have called "Sabsak series", belongs to the same post-Cretaceous and probably post-Eocene volcanic period.

East of Herat, near Obeh, large granitic intrusions occur which have penetrated the Lower Cretaceous Red Grit series. North of the Sabsak Pass the Red Grit series is penetrated by porphyrites and granitic veins. East of Ghazni (S.E. Afghanistan) serpentines have intruded Turonian limestones.

All these observations suggest that these granites and serpentines belong to the same post-Cretaceous volcanic period as the "Sabsak series"

and that apart from surface extrusions the Oligocene was characterized by large scale granitic and gabbroidic intrusions, which represented the abyssal facies of the Oligocene effusive series.

The fact that in India and Pakistan the Deccan trap resembles in some ways the Sabsak volcanic period and that several observations indicate a top Cretaceous-Oligocene age, could suggest the possibility that extrusions actually started in Afghanistan in the Eocene and continued into the Oligocene.

X. *Miocene*:

Miocene beds have not been found with certainty, except the thick saliferous section near Namakab, south of Talakan; but also here the accurate age awaits further confirmation.

Although the base of this, probably few hundred metres thick, section is not known, it is most likely, in view of the general geology of the area, that the Miocene beds cover directly the Turonian limestones.

The section is not well known because of a diapyric penetration of the following beds:

- Top 1) grey or greenish marls (more than 50 metres).
 2) limestones (5-10 M)
 3) gypsum (5-10 M)
 4) thick rocksalt section (original thickness unknown but at present more than 400 metres)
 5) It is very likely that the rocksalt is again underlain by gypsum, limestone and marl.

XI. *Pliocene*:

This often over 600 Metres thick section is known as HERAT SERIES (because of the thick development near Tirpul, West of Herat), BAKHTIARI SERIES (in Iran) or SIWALIK SERIES (in India).

The section varies considerably in lithologic composition. North of Tash-Kurghan, for example, it is composed of red clays with thick red sandstone and conglomerate intercalations, the conglomerates being composed of pebbles of limestone, porphyry, quartz etc.

North of Herat a basal section (about 80 M) of very sandy marls with calcareous sandstone intercalations is covered by a few metres thick boulder bed, covered in turn by more than 600 metres of grey calcareous sandstones with pebbly intercalations composed of granite, schist, red grit sandstone and porphyritic pebbles. It is covered by more than 100 metres of greenish and reddish sandy marls alternating with calcareous sandstones.

100 Kms west of Herat the greatest part of the Herat series is composed of greenish marls with calcareous sandstone intercalations. This over 700 metres thick section is covered by light reddish sandy marls with a few calcareous pebbly intercalations. Many of the red marls still show greenish spots which indicate that probably all the argillaceous beds of

the Herat series were originally greenish but were weathered into reddish, lateritic deposits.

The Herat series usually covers conformably the Cretaceous limestone beds and is steeply folded with these beds in perfectly parallel order, indicating that the main folding period seems to have taken place at the end of the Pliocene.

XII. *Pleistocene* :

The Pliocene of North Afghanistan is unconformably covered by a more than 100 M thick series, usually composed of brownish grey loess marls, with a few metres thick coarse, loosely cemented conglomerate at the base. In West and S.W. Afghanistan the Diluvial series is composed of brownish or grey sandstones and conglomerates with a few shaly intercalations.

This Pleistocene series, known as TURKOMAN SERIES, is filling up many of the intra mountainous basins in Central Afghanistan (e.g. the Kabul plateau, the valley around Bamian, etc.) as a result of the strong uplift and erosion at the end of the Pliocene period.

The Pleistocene is not folded any more, which suggests that folding movements ceased at the end of the Pliocene. However, vertical movements of Afghanistan may have continued up to recent times which is indicated by the many thick terrace deposits, often occurring at different topographic levels. Also the many small earthquakes in Afghanistan (recorded by the UNESCO seismic team at Quetta) may be partly due to these recent uplifts.

It is very likely that large parts of Afghanistan were covered by glaciers during the Pleistocene period. This is indicated by enormous (a few metres large) erratic blocks in the plains, which could not have been transported by ordinary rivers in the region.

Some of the rocks must have come from very great distances because they are not outcropping near the places where they occur.

XIII. *Alluvium* :

The Diluvial deposits are unconformably covered by recent river deposits, either sandstones, boulders or shales.

(to be continued)

GEOLOGY

THE STRATIGRAPHY AND MAIN STRUCTURAL FEATURES OF AFGHANISTAN. II

BY

SULTAN ACHMAD POPOL

(Director of the Geol. Dept. of the Royal Govt. of Afghanistan)

AND

S. W. TROMP

(Geological Consultant, United Nations Techn. Ass. Adm.)

with 1 Locality chart

(Communicated by Prof. I. M. VAN DER VLERK at the meeting of April 24, 1954)

III. MAIN VOLCANIC PERIODS OF AFGHANISTAN

The previous stratigraphic summary indicates that two main periods of enormous volcanic activity can be distinguished in Afghanistan:

- 1) LOWER JURASSIC DOAB INTRUSIONS AND EXTRUSIONS (particularly developed in the Central Hindu Kush)
- 2) (probably) OLIGOCENE SABSAC VOLCANIC SERIES (particularly developed in W., S.W. and S. Afghanistan).

A large number of field samples of these igneous rocks was collected. 58 thin sections were prepared and were studied in detail both by S. ALTHUIS and the second author.

Field observations combined with these petrographic studies indicate the following succession of volcanic intrusions and extrusions:

DOAB VOLCANIC SERIES (L. Jurassic) SABSAC VOLCANIC SERIES (Oligocene?)

- | | |
|--|--|
| 1. First volcanic activity:
Gabbroidic intrusions at great
depth and basalts on the surface. | 1. First volcanic activity:
Quartz-keratophyre extrusions |
| 2. Renewed basalt flows | 2. Basalt and quartz-keratophyre
lava flows |
| 3. Greenish quartz-diorite porphyrite
(dense masses) | 3. Rhyolites and Rhyodacites |
| 4. Intrusions of granite and
granodiorite | 4. Rhyolite tuffs and tuff-breccias
and lahar flows. |
| 5. Greenish quartz-diorite-porphyr-
ite and reddish andesite extrusions | |
| 6. Greenish and reddish porphyrite
tuffs followed by white rhyolites
and rhyolite tuffs (last Jurassic
volcanic activity) | |

The data above indicate that the Doab volcanic period was characterized by large scale (almost batholithic) extrusions at shallow depth in the earth crust, whereas during the Sabsak volcanic period more surface volcanism dominated, characterized by "Quellkuppen" of lava flows, thick tuff deposits and "lahars" (mud-streams).

Particularly the thick lahar series north of Herat, on the road to Kusk, is an interesting unit, indicating conditions similar to recent volcanic regions in tropical countries.

The Sabsak volcanic series also differs from the Doab series in the more alkaline nature of some of the Sabsak rocks (e.g. the quartz keratophyres).

The Lower Jurassic Doab volcanic period seems to have been restricted to the central parts of the Afghan orogen, whereas the Oligocene eruptions occurred in N.W., W. and S.W. Afghanistan, i.e. in the W. and S.W. plunging areas of the Hindu Kush Ranges.

The Sabsak series created kilometers wide contact metamorphic zones, changing Cretaceous and older sediments into metamorphic rocks, resembling a pre-Cambrian metamorphic series.

The dark Carboniferous and Cretaceous limestones are often completely saturated with igneous material of the Sabsak intrusions, causing a greenish colour which in the field often make it difficult to distinguish these limestones from ordinary porphyrites. Most rocks in these volcanic areas are covered with black crusts of manganese oxides. As our surveys were mainly carried out to establish potential oil areas in Afghanistan, it is evident that not sufficient time could be spent in these volcanic regions despite their extremely interesting contact metamorphic and other petrological phenomena.

The tremendous extrusions of the Sabsak series created also the many "volcanic structures" of W. and S.W. Afghanistan, characterized by steeply dipping monoclines of Turonian and older limestones, which we shall discuss in the following chapter.

IV. MAIN STRUCTURAL FEATURES OF AFGHANISTAN

The geological history of Afghanistan has been an extremely complex one. Periods of regional subsidence alternated with regional uplifts followed by erosion and renewed sedimentation during the following subsidence.

Disconformities and age of folding

The many disconformities (only a few angular unconformities occur) indicate that in the older periods large vertical movements with little or no folding phenomena were the main characteristic features in Afghanistan. The first strong folding took place at the end of the Pliocene, which seems to represent the main period of folding in Afghanistan. This relatively young folding is mainly indicated by the following observations:

1. In most structures of North Afghanistan the Turonian limestones are conformably covered by a thickly developed Pliocene Herat series.

Both formations are steeply folded in a perfectly concordant manner.

2. North-west of the village of Tala (15 Kms N.E. of Ishpushta in the Surkhab valley) a coarse boulder bed occurs above the Red Grit series, containing boulders and pebbles of Turonian limestone. This non-consolidated boulder bed, which resembles the boulder beds of the Pliocene and younger series, is covered by Turonian limestone in an overthrust contact. The limestone in its turn is covered by the Red Grit series. The presence of Turonian limestone boulders in the boulder bed indicates a post-Cretaceous age of the tectonic movements, the similarity to Plio-Pleistocene gravel deposits suggests late Pliocene overthrust movements.

Volcanism

Two of the periods of uplift were characterized (apart from overthrusts) by tremendous igneous activity during the Lower Jurassic (Doab series) and during the Oligocene (Sabsak series).

Whereas the period of Lower Jurassic volcanic activity seems to have been restricted to the Central parts of Afghanistan, the Oligocene volcanism seems to have occurred mainly in N.W., W. and S.W. Afghanistan.

If one considers the dimensions of these different intrusions (e.g. granite massive South of Doab: 24 Kms; 60 Kms North of Doab: more than 5 Kms) and the extensive areas covered by the porphyric and porphyritic intrusions and extrusions (Sabsak series occurs almost all the way from Herat to Kandahar, a distance of 680 Kms; Doab series at least 120 Kms), one realizes the tremendous forces which were active during these two periods of tectonic movements. It can also be easily understood that such enormous igneous masses must have created kilometres wide metamorphosed zones which often resemble ordinary metamorphic schists. It is due to these same intrusions that the chromium, magnetite and many other ore deposits in Afghanistan were formed.

Remnants of real volcanoes are scarce, but an interesting fossil volcano occurs e.g. 60 Kms north of Ishpushta where the hard basaltic volcanic channel is still preserved as a high cone surrounded by a thick tuff series.

In the Shin Dand region a typical "Quell Kuppen" area occurs, the viscid lava flowing from central points in all directions, without tuff explosions, creating a number of lava domes.

Different types of tectonic structures

The different parts of Afghanistan are characterized by different structures:

A) CENTRAL AFGHANISTAN

1. *Fault tectonics:*

In the area covered with Doab series only, considerable faulting can be observed with vertical throws up to 50 M. and more. Little thrusting seems to occur. The age of these faults, considering the irregular topography on which the Saighan series was deposited, may be in part Lower-Jurassic.

2. *Thrust faulting and recumbent folds:*

In the areas where the Saighan series and Cretaceous beds are covering the Doab series, the Doab volcanic series seems to have acted as a large resistance creating a number of overthrusts ("Ecaille" or Imbricated structures) or recumbent folds. As a result, Turonian limestones may occur above and below the Lower Cretaceous Red Grit series. Particularly near Tala (see above) these relations can be clearly seen.

Not only the rigidity of the large masses of porphyrite and basalt are responsible for these structures, but also the irregular topography of the Doab series on which the Saighan series was deposited. As a result of these overthrusts the Ishpushta coal has been completely pulverised.

In the Saighan valley the Permo-Carboniferous fusulina limestones and underlying Helmand Schists also are included in these overthrusts.

B) NORTH AFGHANISTAN:

Three types of structures occur:

1. *Diapiric saltdomes:*

In the Talakan area the, probably Miocene, Saliferous section has broken through the covering Marl section, forming enormous Salt-domes with a diameter of 900 Metres to one Km. and a height of at least 200 Metres; at Namakab the surface is estimated by Ree at 750,000 sq. yds.

As in the Namakab region the Herat series are completely conformable with the steep dipping marls flanking the salt-dome, it is most likely that the salt-domes are created as a result of Upper Pliocene movements, the salt rising isostatically along predetermined anticlinal faults.

2. *Anticlinal folds:*

In the plains of North Afghanistan, south of the Oxus river (Shibarghan, Kunduz and Maimana sedimentary basins), a number of usually asymmetric structures occur with one flank dipping often 70–80° and the other 30°. The structures are probably not real anticlines as a result of tangential compression, but anticlinal folds due to tilted blockmovements of consolidated Pre-Cretaceous beds ¹⁾.

3. *Overthrusts:*

In the valley of the Tashkurghan river, and S.W. of Sar-I-Pul (in the Qara Khawal area) large overthrusts occur of Turonian

¹⁾ The mechanism of such folds was extensively discussed by Tromp in his publ.: "On the Mechanism of Geological Undulation Phenomena" (Sijthoff's Publ. Co., Leiden, 1937).

"Blockfolding phenomena in the Middle East" (Geologie en Mijnbouw, Holland, pp. 273–276 (Sept. 9, 1949)).

limestones (with part of the underlying argillaceous section) on other Turonian limestones.

In this Northern region of Afghanistan three directions seem to prevail: In the Eastern part, the Northwest-Southeast direction; in the Central part, the East-West direction; in the Western part, the Northeast-Southwest direction, which seems to be a continuation of the Northeast-Southwest direction of the structures in the Termez basin in Russia. This Termez basin seems to consist of two parts of which the Eastern part is downthrown with respect to the Western part.

C) NORTH-WESTERN AFGHANISTAN:

1. *Boxfold structures:*

In the Qala-Nau basin a remarkable type of structure occurs which can be described as "Boxfolds". For example, the Western nose of Band-I-Turkestan is a big twenty Kms wide fold of Upper Eocene limestones with a 30° dipping North flank, and an 80° dipping South flank, abruptly turning to Zero in the flat crestral area without the slightest break in the flanks.

Even more remarkable are the Luk-I-Sarkh structures with an almost vertical (or even overturned) North flank which changes within 20 Metres into an almost horizontal crestral area without the slightest faulting near the bend.

2. *Buried ridges:*

In the Hari Rud basin west of Herat a number of tilted Permo-Carboniferous or Devonian limestone blocks occur, which are usually intruded by the Oligocene volcanic Sabsak series. Further west towards the Iranian border the blocks are buried under tilted Pliocene Herat beds.

A great part of the tilting seems to have taken place in Pre-Pliocene periods and, considering the phenomena in Western Afghanistan, it seems quite likely that the tilting was for a considerable part due to volcanic intrusion and not purely tectonic.

D) WESTERN AFGHANISTAN:

This whole area is characterized by steeply dipping monoclines of Turonian (in part Carboniferous) limestones which are intruded and contact metamorphic changed by huge porphyritic and basaltic masses. The irregular steep dips of these limestone domes suggest that they are not tectonic but volcanic thrust domes.

About 55 Kms East of Shin Dand an overthrust of Turonian Rudist limestones on an anticlinal fold was observed, but this seems to be the only exception in the general picture of steep, intruded, limestone cones which seem to prevail as far as Kandahar.

E) SOUTH-CENTRAL AFGHANISTAN:

Between Kandahar and Ghazni the effusive rocks seem to have disappeared. A relatively quiet Turonian limestone section with underlying

Cenomanian beds (developed in the less argillaceous facies, see page 378) seems to cover large parts of the area. North-east of Ghazni (near Danesheer) large serpentine intrusions penetrate the probably Cretaceous limestone series. North of Ghazni also granitic intrusions occur. The intrusions continue Northwards and seem to be connected with the large chromium bearing serpentine massive of the Logar Valley. About 60 Kms North of Ghazni greenish coloured schists occur which make the impression of being Mesozoic rocks strongly contact metamorphically changed by huge batholithic masses at great depth. The marbles of Maidan, about 40 Kms S.W. of Kabul, which occur in close contact with porphyric granites also indicate similar contact phenomena. If the latter intrusions are the same as those intruding the Cretaceous limestones near Danesheer, one is inclined to assume that perhaps all the schists of the Kabul region may be Mesozoic or young Paleozoic rocks (not older than Devonian) metamorphosed by regional intrusions during the post-Cretaceous (probably Oligocene) and Doab periods.

Oegstgeest, December 1953.

Annex no. 1

*Fusulines and the age of the Bamian limestone near Shibar Pass
in the Hindu Kush Range, Afghanistan*

In the samples collected 1 KM E. of the junction of the main road from Shibar Pass to Doab and the road to Bamian Prof. CARL O. DUNBAR discovered the following micro-fauna:

- Schwagerina furoni Thompson
- „ cfr. S. pseudochihsiaensis Chen
- „ Sp. A.
- „ hindukushensis Dunbar n. sp.
- Parafusulina sp. A.
- Polydiexodina afghanensis Thompson
- „ trompi Dunbar n. sp.
- Misellina pamirensis ? (Doutkevitch and Khabakoo)
- Verbeekina heimi Thompson and Foster
- Cancellina primigenia (Hayden)
- Neoschwagerina haydeni (Doutkevitch and Khabakov)
- Afghanella Schencki Thompson

This assemblage according to Dunbar clearly indicates correlation with the Lower part of the widespread Maokou limestone of South China which lies in the Upper part of the Permian system, but well below its summit. The horizon should fall within the upper half of the Guadalupian Series of the American section.

BIBLIOGRAPHY

1. Afghan Oil Concessions, *Oil News*, p. 55 (Jan. 28, 1937).
2. Afghanistan — Iran Concessions of American interests are about to see first development, characterized as a long shot and a long pull. *The Oil Weekly*, 88, No. II, 102-115 (1938); (same, Feb. 21, 1938).
3. Afghanistan prospect for mining for future. *Petroleum World*, p. 80 (July 1938).
4. BARGER, E., Exploration of ancient sites in Northern Afghanistan. *Geographical Journal*, 93, No. 5 (1939).
5. BARTHOUX, J., Le Siwalik et les roches volcaniques récentes en Afghanistan. *Acad. Sc. Paris, C.R.*, 196, No. 13, 944-947, No. 27 (1933).
6. ———, Lapis-Lazuli et rubis balais des cipolins Afghans. *Acad. Sc. Paris, C.R.*, 196, No. 15, 1131-1134 (April 10, 1933).
7. ———, Notes Minéralogiques sur L'Afghanistan. *Soc. Française Miner. B.*, 56, No. 6-7-8, 324-334 (1933).
8. ———, Notes géologiques sur L'Afghanistan. *Soc. Sav. Paris*, 66e Cong., Toulouse, 1933, *Soc. Sci., C.R.*, 126-133 (1933).
9. BILALOV, N. I., The oil of Karnap-Chulsk Steppes (Western Uzbekistan) (Translation from Russian) (1935).
10. BRÜCKL, K., Über die Geologie von Badakhshan und Kataghan (Afghanistan) *Neues Jb.*, 74, part B, H. 3, 360-401 (1935).
11. ———, Die Minerallagerstätten von Ostafghanistan; Versuch einer Gliederung nach genetischen Gesichtspunkten. *Neues Jb.*, 72, part A, H. I, 1-97 (1936).
12. BURACHEK, A. P., Geomorphology of South Tadzhik depression (Tadzhik-Pamir complex expedition, 1934, Trans. No. 4) (Translation from Russian.)
13. ———, Tertiary continental deposits of South-Western Tadzhikistan (Tadzhik-Pamir complex expedition 1934, Trans. No. 4) (Translation from Russian).
14. BURRARD, S. G. and H. H. HAYDEN, The geography and geology of the Himalaya mountains and Tibet (1907/1908).
15. CIZANCOURT, H. DE, Mme H. DE CIZANCOURT and H. VAUTRIN, Remarques sur la Structure de l'Hindou-Kouch. *Soc. Géol. France*, 5, t. 7, fascicule 7, 377-400 (April 1938).
16. CIZANCOURT, MARIA DE and L. R. COX, Contribution à l'étude des faunes tertiaires de l'Afghanistan. *Soc. Géol. France, Mém.*, 17, f. 1, 1-44 (1938).
17. CIZANCOURT, H. DE, Location of oil fields in tectonic belts. *The science of petroleum*, 1, 244-246 (London, 1938).
18. ———, Remarques sur le genre *Orbitocyclina* Vaughan. *Soc. Géol. France*, 5, t. 8, f. 7-8, 645-652 (1939).
19. CLAPP, F. G., Geology of Afghanistan. *Geol. Soc. Am.*, 50, No. 12, Pt. 2, 1904 (1939).
20. ———, Explorations in Iran and Afghanistan. *Oil Weekly*, 92, No. 12, 71-72 (27 Feb. 1939).
21. ———, Geology of Eastern Iran. *Bulletin of the Geol. Soc. of Am.*, 51 No. 1, 1-102 (Jan. 1, 1940).
22. ———, Geologic work and experiences in the Middle-East. (Iran and Afghanistan) *Tulsa Geol. Soc. digest*, 36-38 (1940).
23. COX, L. G., Contributions on the Paleontology of Afghanistan; Oligocene Mollusca. *Ann. & Mag. Nat. Hist. S. II*, 5, No. 28, 362-371 (April 1940).
24. Die Erdölmöglichkeiten Afghanistans. *Erdöl und Kohle*, No. 3, No. 5, 48 (May 1940).

25. Die Erschliessung der Edöllagerstätten des Nahen Ostens. Oel und Kohle, **15**, No. 8, 153-156 (22 Feb. 1939).
26. Die Wichtigsten Lagerstätten der Erde, Heft 7: Die Bodenschätze des Indisch-Malaischen Raumes (Reichsamt f. Bodenforschung, p. 8, Afghanistan, 1942).
27. DRATH, A., Report on oil seepage of Terpul region (Report to Afghan Gouvernement) (2 Sept. 1940).
28. DRUMMOND, C., On the mines and mineral resources of northern Afghanistan Journ. Ass. Soc. Bengal, **10**, 74 (1841).
29. FURON, R., Notes préliminaires sur la géologie de l'est de l'Afghanistan (l'Hindou-Koush, région nord et sud). Bulletin Géol. France, p. 1 (1924).
30. ———, L'Hindou-Koush et le Kaboulistan (Thesis, Paris, 1927).
31. ———, Sur les relations géologiques et géographiques de l'Hindou-Koush et du Pamir. Acad. Sci. Paris, C.R., **198**, No. 10, 963-964 (March 1934).
32. ———, Sur la géologie de l'Hindou-Koush et du Pamir. Soc. Géol. France, **5**, t. 4, f. 1-3, 69-78 (1934).
33. ———, Sur l'existence d'un axe Ouralien déterminant la structure du plateau Iranian, Acad. Sci. Paris, C. R., **203**, No. 10, 516-517 (1936).
34. ———, La géologie du plateau Iranian (Perse, Afghanistan, Beloutshistan). Revue générale science Paris, **48**, No. 2, 36-43 (Jan. 1937). (same article: Mémoires du Museum Nat. d'Histoire Naturelle, Paris 1941, **7**, f. 2, 177-414 (same article: Geol-Zentralblatt Abt. A., **70**, I pt. 30, Sept. 15, 1942)).
35. ———, E. BOUREAU and L. F. ROSSET, Contribution à l'étude des flores jurassiques d'Asie. Mém. du Musée Nat. d'Hist. Nat., **30**, f. 2, (Paris, 1950).
36. Gisements Pétrolifères en Afghanistan. Courriers des Petroles, **3**, No. 77, 1-2, (Paris, March 25, 1922).
37. GOTA, T. T. and N. A. SCHLUMBERGER, Oil fields of Middle Asia, Oil Economics, **2**, (1934) (Russian translation).
38. ———, Oil Industry of Middle Asia according to the latest geological data. Oil Economics, **9** (1935) (Russian translation).
39. GRIESBACH, C. L., Report on the geology of the section between the Bolan Pass in Baluchistan and Girishk in southern Afghanistan. Memoires of the geological survey of India, **18**, pt. 1 (1881).
40. ———, Afghan field notes. Mem. Geol. Surv. of India, **18**, 57 (1885).
41. ———, Afghan and Persian field notes. Mem. Geol. Surv. of India, **19**, 48 (1886).
42. ———, Field notes from Afghanistan: No. 3, Turkistan. Memoires of the geological survey of India, **19**, 235-267, (1886).
43. ———, Field notes from Afghanistan: No. 4, from Turkistan to India. Mem. Geol. Surv. of India, **20**, 17 (1887).
44. ———, Field notes No. 5 to accompany a geological sketch-map of Afghanistan and North-Eastern Khorassan. Mem. Geol. Surv. of India, **20**, 93 (1887).
45. ———, Geology of the Safed Koh. Mem. Geol. Surv. of India, **25**, 59 (1892).
46. GUNDACH, K., Die östliche Forsetzung des Kaukasus. Geologische Rundschau (Dec. 15 1935) with extensive bibliography.
47. HAY, C., Fossil shells discovered in the neighbourhood of Bajgah, Afghanistan. Journ. Ass. Soc. Bengal, **9**, 1126 (1840).
48. HAYDEN, H. H., On the geology of Tirah and the Bazar valley. Mem. Geol. Surv. of India, **28**, 96 (1900).
49. ———, The geology of Spiti. Mem. Geol. Surv. of India, **36**, pt. 1 (1904).
50. ———, Fusulinidae from Afghanistan. Mem. Geol. Surv. of India, **38**, 230 (1909).

51. ———, Notes on some monuments in Afghanistan. Mem. Ass. Soc. Bengal, 2, No. 10, 341 (1910).
52. ———, The geology of Northern Afghanistan. Mem. Geol. Surv. India, 29, 1911, 1-97 (1911).
53. HARRISON, J. V., The geology of some salt-plugs in Laristan. Geol. Soc. London, Quarterly Journal, 86, 463-475 (1930).
54. HERBORDT, O., Über nutzbare Lagerstätten in Afghanistan. Zeitschr. f. prakt. Geol. p. 193 (1925).
55. ———, Über die Aussichten Afghanistans als Bergbauland. Int. Bergwirtschaft, Jahrg. H. 11/12, 269 (1926).
56. Inland Exploration Co. acquires all Afghanistan for oil search. Petroleum Times, 38, No. 967, 78-79 (July 17, 1937); 121-122 (July 24, 1937).
57. JERMAIN, G. D. and R. E., Middle Asia oil deposits a compilation (1935).
58. KALITZKI, K. P., On the conditions of oil deposits in Ferghana region (Neftyanoi Geologo-Razved Institute trans. ser. a, 73 (1936) (Translation from Russian).
59. KLUNNIKOV, S. I., Continental tertiary beds of the southern Pamir. Tadzhik-Pamir complex expedition, 3 (1934).
60. KÖHLER, R. and J. H. HELLMERS, Bodenphysikalische und Mineralogische Beschreibung eines Loessvorkommens aus dem Tal des Wardak in Afghanistan. Zeitschr. prakt. Geol., 46, H. 11, 207-211 (1938).
61. KOSYGIN, A., Oilfield of Turkmania (Mining-Geology-Oil Gov. Publ. Moscow 1933) (Russian translation).
62. KRAFFT, A. VON, Geologische Ergebnisse einer Reise durch das Chanat Bokhara. Denkschr. Kars. akad. Wissensch., Wien, 70, 49.
63. KULAYEV, P. M., New data concerning the oil field at Neftedag, Turkmania, U.S.S.R. Oil Economics, 12 (1935) (Translation from Russian).
64. LEMMON, D. M., Farinjal lead mine, Kabul province, Afghanistan (Report to the Afghan Government, July 1950).
65. ———, The Masjid-I-Chobi coal mine, Karrukh, Herat (Report to the Afghan Government, July 1950).
66. LEUCHS, K., Handbuch der regionalen Geologie, 5, pt. 7, Zentral Asien.
67. LINDTROP, N. L., The results of Gusher tests at Neftabad and Khandag. Oil Economics, 2 (1934). (Translation from Russian).
68. ———, Dzhar-Kurghan Oilbearing region of South Province. Oil Economics No. 10 (1935).
69. MAILLEUX, E., Note sur des fossiles Dévonien de l'Afghanistan. Musée Royal Hist. Nat. Belgique, 16, No. 41 (1940).
70. MC MAHON, C. A. and W. H. HUDDLESTON, Fossils from the Hindu Khoosh. Geol. Mag. new ser., dec. IV, 9, pt. 3, 49 (1902).
71. MERZBACHER, G., Afghanistan. Geogr. Zeitschr., 31, H. 5, 289-293 (1925). Geol. Zentralbl. No. 10, 32 (1925).
72. OGNIOW, V. N., From Aladag to Sundzo, Transactions of the United Geol. and prospecting service of the U.S.S.R., 247.
73. Oil possibilities of Afghanistan; Note from Afghan Minister London. Oil News, 17, No. 647, 451-452 (April 1925).
74. Afghan Oil Concession, The Petroleum Times, p. 43 (Jan. 9, 1937).
75. ORYEV, G. K., New data on the geology and oil of central Karakums. Oil Economics, 4 (1935) (Russian translation).
76. PETRUSHEVSKY, B. A., Paleogeography and tectonics of Afghanistan and Tadzhikistan. Acad. Sci. U.S.S.R. Int. Geol. Sci. Transactions No. 8, Geol. Ser., 3, 69 (1941).
77. PILGRIM, G. E., The geology of parts of the Persian provinces of Fars, Kerman and Laristan. Mem. Geol. Surv. of India (1924).

78. PORFIRYEV, B., Natural Gases of Turkmenistan, Natural Gases of U.S.S.R. (1935) (Russian translation).
79. PRASHAD, B., Some fresh water and land fossil Molluscs, (Miocene?) from near Chorband, Afghanistan. Mem. Geol. Surv. of India, 72, pt. 1, 125-129 (April 1937).
80. REE, E. R. and T. C. SETH, Report from the salt sources of Afghanistan with particular reference to future exploitation (Report to the Government of Afghanistan, 1940).
81. REEVES, F., Report submitted to the Afghan Government by the Inland Exploration Co. (30 Aug. 1938).
82. RIEBEN, H., Contribution à la Géologie de l'Azerbeïjan Persan. Bulletin de la Soc. Neufchatelloise des sci. Nat., 59, 19-144 (1934).
83. RIVIÈRE, A., Contribution à l'étude Géologique de l'Elburz, (Perse). Revue de Géogr. Phys. et de Géol. Dynam., 7, f. 1 & 2 (1934).
84. SCHENK, W., Travel reports submitted to the Inland Exploration Co. (1938).
85. SCHLUMBERGER, R. A., Report on oil possibilities of North Afghanistan (Submitted to the Afghan Government on Aug. 5, 1948).
86. SCHROEDER, J. W., Essai sur la structure de l'Iran. Eclogae Geol. Helvetiae, 37, No. 1, 37-81 (1944).
87. SEWARD, A. C., Mesozoic plants from Afghanistan and Afghan-Turkistan. Mem. Geol. Surv. of India, 4, No. 4, 1-57 (1912).
88. SITHOLEY, R. V., Jurassic plants from Afghan-Turkestan, Indian Science Congress, (Calcutta, 1938).
89. ———, Jurassic plants from Afghan-Turkestan, Mem. Geol. Surv. of India, 29, No. 1 (1940).
90. STAHL, A. F., Zur Geologie von Persien. Petermanns Mitt. Ergänzungs Heft, 122, 72 (1897).
91. ———, Persien. Handbuch der Region. Geol., 5, pt. 6, 46 (1911).
92. ———, Sind Erdöllager in Belutschistan und Afghanistan vorhanden? (Petroleum Zeitschrift, 23, No. 31, 1348 (Berlin, Nov. 1, 1927) Same in Zeitschrift der Int. Bohrtechn. Verbandes, 13, 204 (1928)).
93. SUSS, E., Beiträge zur Stratigraphie Central-Asiens. Denkschr. Kais. Akad. Wiss. (Wien), 59, 431 (1894).
94. THOMPSON, M. L., Upper Permian Fusulinid Foraminifera from Afghanistan. Geol. Soc. Am., 52, No. 12, pt. 2, 1984 (1941).
95. ———, Permian Fusulinids from Afghanistan. Journal of Paleontology, 20, No. 2, 140-157 (1946).
96. TIETZE, E., Bemerkungen über die Tektonik des Alburs Gebirges in Persien. Jahrb. k.k. Reich, 27, 375-430 (1887).
97. TRINKLER, E., Aus dem westlichen Teil des Afghanischen Hindukusch. Petermanns Mitt., 117-118 (1925).
98. ———, Die geologisch-morphologische Entwicklungsgeschichte des Süd-Westlichen Zentral Asiens. Petermanns Mitt., 50-52 (1926).
99. ———, Afghanistan. Eine landeskundliche Studie auf Grund des vorhandenen Materials und eigener Beobachtung. Petermanns Mitt., 196, (1928).
100. The Middle East, pp. 17-26, (Europa Publishing Ltd., 39 Bedford Sq. London, 1948).
101. TUAYEV, N. P., On undulated deposits of Paleocene-Danian limestone in south oilbearing province of Middle Asia. Oil Economics, 8, 23-27 (1936). (Russian Translation).
102. UKLONSKY, A. S., Chemical Composition of some surface waters of Afghanistan. Vernadsky Jubilee Vol., Acad. Sci. U.S.S.R., I, 301-314, 1936) (Russian Translation).

103. VYALOV, O. S., Note on the Miocene of Afghanistan. Problems Soviet Geology 6, No. 1, 43-44 (1936) (Russian translation.)
104. WEST, W. D., Progress report on the work of the Government of India's Coal Survey Party in Afghanistan during 1940 (Report to the Afghan Government).
105. ———, Final report on the work of the Government of India's Coal Survey Party in Afghanistan (Report to the Afghan Government) (1940-1942).
106. Will Afghanistan Oil enter World Markets? World Petroleum, pp. 6-8 (Jan, 1935).

CORRELATION BETWEEN GEOMAGNETIC FIELD AND TECTONIC MOVEMENTS?

BY

F. A. VENING MEINESZ

(Communicated at the meeting of May 29, 1954)

The hypothesis of BULLARD [1] and ELSASSER [2] about currents in the outer core of the earth of a dynamic as well as an electric character which can explain the geomagnetic field, has found a strong support by the discovery of a correlation by VESTINE [3] and MUNK and REVELLE [6] of, on one side, the irregularities in the movements of the areas of geomagnetic change and of the non-dipole part of the geomagnetic field and, on the other side, the irregularities in the earth's rotation found by the astronomers of which BROUWER [5] recently gave an important analysis. The explanation of this correlation is evident; changes of currents in the core must be expected to have an angular momentum which together with that of the inner core must be neutralized by an angular momentum of the mantle and crust. Though BULLARD objected that the viscous friction between outer core and mantle can not be powerful enough for the conservation of the angular momentum to be extended to the mantle, we may expect this to be carried out by electromagnetic couples which can be proved to be strong enough.

Since long the writer has advocated the existence of slow currents in the mantle with velocities of the order of a few cm/year which can explain the large tectonic forces working in the crust and bringing about the folding and overthrusting in the folded mountain ranges and the coming into being of the deep ocean trenches. He attributed them to thermal convection caused by the earth's cooling. It now appears likely that also forces are operating on the inner boundary of the mantle—caused by the currents in the core—which must bring about movements. These movements can not only affect the mantle as a rigid whole; they must gradually also assume the character of currents and so this likewise points to flow in the mantle.

The writer does not wish here to go deep into the problems raised by these concepts but he wants to draw attention to some remarkable correlations between the distribution of the geomagnetic secular changes and the tectonic deformations of the earth's crust. The figures 1 and 2 show VESTINE's maps [4] of the geomagnetic secular changes of the vertical intensity for the periods 1912.5 and 1942.5. In the first place we can derive from them a general westward drift which is now well established;

it has already been discovered at a much earlier date, e.g. by BAUER [7] in 1895. VESTINE [3] from all the data now available finds a westward velocity of $0^{\circ}.30$ per year and by another method BULLARD [8] obtained $0^{\circ}.18$ per year. Now it has since long been remarked that the folded mountain ranges on the earth's surface have a tendency to occur in the north-south direction which is in good agreement with this westward drift and the same is true for the fact that the high latitudes are tectonically not very active.

But the maps of fig. 1 and 2 appear to show also some curious more detailed correlations with tectonic movements of the present period. One of the best known and most spectacular cases of such movements is the relative shift on both sides of the San Andreas fault and other parallel shear-zones in California where all the data concur in proving a movement to the northwest of the Pacific side with regard to the continental side. Comparing the maps of figures 1 and 2 we see clear evidence in that part of the Pacific of a movement in the same sense.



Fig. 1. Geomagnetic secular change in gamma/yr, vert. intensity, 1912.5

Another noteworthy case is presented by the SSE movement shown by the contours of the geomagnetic maps near Japan, China and Indonesia which seem to correspond to the direction of the tectonic compression in those areas as it follows from the writer's investigations of the gravimetric field and other geophysical and geological evidence in Indonesia and the other areas [9].

There is not much known about relative tectonic movements in other areas and so it is difficult to state whether there are more instances of correlation. We may perhaps mention the SW movement in the eastern half of the Caribbean which can probably be brought in harmony with the crustal deformation in that area as it seems to follow from the gravimetric field and other geophysical data but these data are less complete and less clear than in Indonesia.

A direct relation of these tectonic deformations and connected phenomena to the changes of the geomagnetic field is not likely as the velocity of the movements is of an entirely different order; the latter are of an

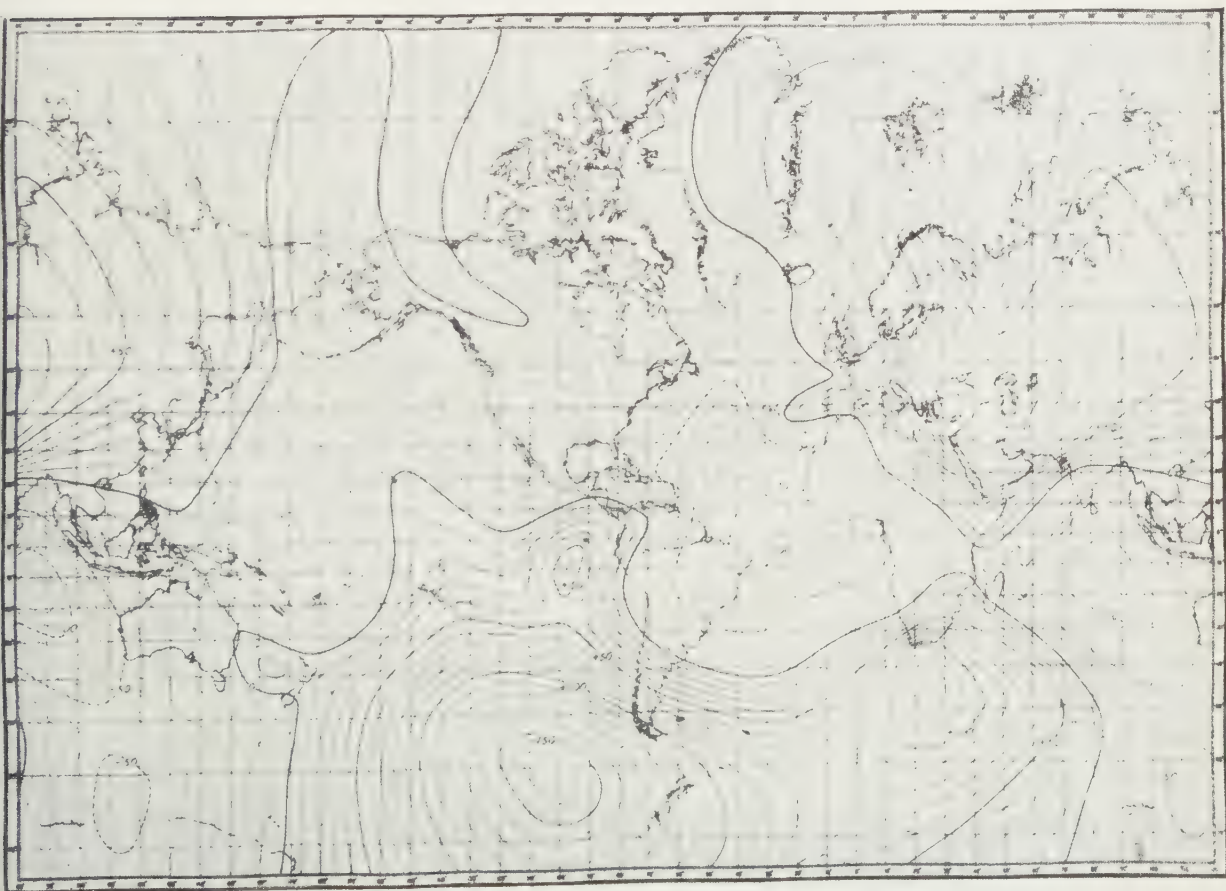


Fig. 2. Geomagnetic secular change in gammas/year, vert. intensity, 1942,5

order of 10^7 cm/year, the former do not amount to more than a few cm/year. We may, however, consider a relation of the kind as mentioned above for the irregularities of the earth's rotation. It is true that the sign of the earth-rotation movement is opposite to the correlated movement of the geomagnetic field while for the above mentioned tectonic movements it is the same but it is easy to show that this ought to be expected. The coupling forces between the core and the mantle which bring about the conservation of the angular momentum for the core and the mantle combined, must have a different effect on the mantle if they are relatively short-lived—as it is the case for those connected with the irregularities in the secular geomagnetic terms—than if they operate over long periods. In the first case they practically can only bring about a moving of the mantle as a rigid whole (combined with a negligible elastic deformation), in the second they must also cause a viscous flow in the mantle and this must normally have about opposite velocity at the surface of the mantle to that at its lower boundary where it is caused by the currents in the core. We must expect such a viscous flow in the mantle to be extremely slow.

In connection with these considerations and also with the conservation of the angular momentum we can understand that the irregularities of the earth's rotation are contrary to the westward drift of the short-lived geomagnetic secular change areas and that they are relatively large, i.e. of the order of several hundreds of meters per year at the equator. According to what we mentioned, however, the effect on the crust of currents in the core of long duration, must be transmitted by slow currents in the mantle and must, therefore, be much smaller and more or less of the same direction as the geomagnetic effect of these core-currents. So it may well be explained that such tectonic currents have a velocity of only a few cm/year.

The evidence here given for such tectonic effects of core-currents may be admitted not to be strong and not to be sufficient to come to any conclusions but the assumption seems a possibility worth considering. We may add that probably the mantle currents bringing them about must also be affected by thermic conditions caused by the cooling of the upper layers of the mantle; they must more or less also have the character of convection-currents.

The supposition involves the assumption of core-currents lasting during long periods. This appears already quite acceptable for the currents responsible for the westward drift. It does not seem impossible that it is also true for other parts of the core's current-system.

REFERENCES

1. BULLARD, Sir EDW. C., The magnetic field within the earth, *Proc. Roy. Soc.A*, 197, 433–453 (1949).
2. ELSASSER, W. M., The Earth's Interior and Geomagnetism, *Rev. o. Mod. Physics*, 22, No. 1, 1–35 (1950).

3. VESTINE, E. H., On Variations of the Geomagnetic Field, Fluid Motions, and the Rate of the Earth's Rotation, *Journ. o. Geophys. Res.*, **58**, No. 2, 127-145 (1953).
4. ——— and collaborators, Publications 578 and 580 of the Carnegie Inst. o. Washington (1947).
5. BROUWER, D., A New Discussion of the Changes in the Earth's Rate of Rotation, *Proc. Nat. Acad. Sci.*, **38**, 1-12 (1952).
6. MUNK, W. and R. REVELLE, On the geophysical interpretations of irregularities in the rotation of the earth, *M.N.R.A.S., Geophys. Suppl.*, **6**, No. 6, 331-347 (1952).
7. BAUER, L. A., *Amer. Journ. o. Sci.*, **50**, 109, 189, 314 (1895).
8. BULLARD, Sir EDW. C., The westward drift of the earth's magnetic field, *Phil. Trans. Roy. Soc. A*, **859**, 243, 67-92 (1950).
9. VENING MEINESZ, F. A., Indonesian Archipelago: a geophysical study, *Bull. G.S.A.*, **65**, 143-164 (1954).

ORGANIC CHEMISTRY

ULTRAVIOLET SPECTROFOTOMETRIC RESEARCH OF THE PROTEINS OF THE EYE LENS

BY

W. F. BON

(From the Anatomical-Embryological Institute, University of Amsterdam
Director: Prof. M. W. WOERDEMAN, M.D., D.Sc.)

(Summary of a contribution published in Series C, 57, No. 3 of these Proceedings)

The amino acid composition of proteins is determined by de-esterification i.e. hydrolysis and chemical identification by qualitative and quantitative analysis of the resulting complex of components. This analysis is one of the most difficult in organic chemistry.

In general to control the correctness of an organic analysis the most convincing evidence is to synthesize the chemical substance out of the components which are present according to the analytical results. This conclusive method is impossible in protein research, the synthesis of proteins having not yet succeeded. So the analysis of proteins is still lacking absolute certainty.

Ultraviolet spectrophotometry gives the possibility to prove the exactness of the analytical results. The hydrolysed mixture of amino acids and the protein itself have at least one quality in common, namely their absorption in the ultraviolet, *the absorption-curves of mixture and protein being similar within certain limits.*

The method is very simple to accomplish, the first thing to do is to make a solution of the amino acids in the same proportion as is given by the analytical data and to compare the ultraviolet spectrogram of this solution with that of the protein itself (in the same total concentration).

The analytical results can be checked also by means of a graphical addition of the spectrograms of each amino acid in the relative quantity in which the components are present in the protein. Differences observed in the diagrams of mixture and protein can be investigated by analysing these diagrams and also by comparing the diagram of the mixture with the diagram of the completely hydrolysed protein.

As an example of this method we give in Proceedings, series C the results of our investigation about the chemical composition of alpha- and beta-crystallin, the main soluble proteins of the eyelens of the vertebrates.

There are some differences of which the most striking is that the peaks in the spectrograms of the mixtures seem to be shifted towards the short side of the ultraviolet. This could be a logical consequence of

the fact that the inner energy of the mixture is greater than that of the corresponding protein, in which energy is freed by the chemical binding of the amino acids to peptid chains. So it seems possible that this method can give some insight in the finer structure details of the protein molecule.

We checked the phenomenon also by comparing the spectrograms of *ovalbumin* (albumen ovi siccum, a technical product according to the "Nederlandsche Pharmacopee Ed. V) and of its amino acids mixture, according to the investigations of CHIBNALL (1946). We observed similarity between these two curves, with a small shifting towards the short side of the spectrum of the amino acids curve. Details and figures are given in Proceedings Vol. LVII nr. 3 Series C.

STATISTICAL PROBLEMS CONNECTED WITH THE SOLUTION OF
A SIMPLE NON-LINEAR PARTIAL DIFFERENTIAL EQUATION.
— CONTINUATION. I

BY

J. M. BURGERS

(Mededeling No. 78 uit het Laboratorium voor Aero- en Hydrodynamica der Technische
Hogeschool te Delft)

(Communicated at the meeting of June 26, 1954)

1. *Introduction.* — This paper is a continuation of two others which have appeared in the January/February and the March/April issues, respectively, of these Proceedings ¹⁾, in particular of the second one. Its object is to generalise certain results of its predecessor and to obtain a basis for the evaluation of formulae developed in a paper of 1950 ²⁾, referring to the correlation function $\overline{v_1 v_2}$ connected with solutions of the partial differential equation:

$$(1) \quad \frac{\partial v}{\partial t} + v \frac{\partial v}{\partial y} = \nu \frac{\partial^2 v}{\partial y^2}.$$

It may be useful to recapitulate briefly the reasons which have led to this investigation. Equation (1) is the simplest analogue of the hydrodynamic equations, in so far as it contains a non-linear term with a space derivative of the first order, and a linear term with a second order space derivative multiplied by a factor which can be taken very small. Its properties with regard to dimensions consequently are the same as those of the hydrodynamic equations. The solutions of (1) exhibit the property that regions make their appearance with very high values of $|\partial v / \partial y|$ ("steep fronts"), which can be considered as analogous to the regions of high dissipation appearing in the solutions of the hydrodynamic equations (regions of very high vorticity or shock waves). It has been thought, therefore, that solutions of (1) might present certain features which would be typical of turbulence, in particular of compressible turbulence, as the analogy of steep fronts with shock waves seems to be a more direct one than the analogy with regions of high vorticity.

The first point which had to be considered in this connection was that equation (1) has a uniquely determined solution whenever the initial

¹⁾ These Proceedings B 57, 45–72 and 159–169 (1954). Equation (30) of the last mentioned paper should be read: $\partial \psi / \partial x = J_0 (\partial^2 \psi / \partial s^2)$.

²⁾ Correlation Problems in a One-dimensional Model of Turbulence, these Proceedings 53, 247–260, 393–406, 718–742 (1950).

values of v , $v_0(y)$, have been given for all y (from $-\infty$ to $+\infty$). It follows that statistical properties can enter into the problem only when a family of initial functions $v_0(y)$ is introduced, or, in other words, when $v_0(y)$ is considered as a random function. It has been assumed that the statistical properties of this random function are invariant with respect to a translation along the y -axis, and that at every point positive and negative values of v are equally probable.³⁾ It is then possible to introduce a correlation function:

$$(2) \quad \overline{v_1 v_2} = \overline{v(y) v(y + \zeta)},$$

and it is found that this function satisfies the equation:⁴⁾

$$(3) \quad \frac{\partial}{\partial t} (\overline{v_1 v_2}) = \frac{\partial}{\partial \zeta} (\overline{v_1^2 v_2}) + 2v \frac{\partial^2}{\partial \zeta^2} (\overline{v_1 v_2}).$$

The latter equation is the simplest analogue of VON KARMAN's equation for the propagation of correlation in homogeneous isotropic hydrodynamic turbulence. The integral:

$$(4) \quad J = \int_0^\infty \overline{v_1 v_2} d\zeta$$

is independent of the time; it is the analogue of LOITSIANSKI's invariant for hydrodynamic turbulence. This led to the idea that solutions of eq. (1) could give a simplified model of "homogeneous turbulence" and that the central function to be considered should be $\overline{v_1 v_2}$.⁵⁾

No direct solution of VON KARMAN's equation for the propagation of correlation is known: actually it is a single equation relating two different functions $\overline{v_1 v_2}$ and $\overline{v_1^2 v_2}$. The extensive discussions of this equation occurring in the literature all have been derived with the aid of auxiliary hypotheses. In the case of the correlation function connected with equation (1), however, use can be made of the circumstance that the solution of (1) can be written down for any given initial condition. Hence it must be possible to obtain statistical properties referring to a family of solutions in a direct way, without introducing additional suppositions.

³⁾ Equation (1) is invariant with respect to a simultaneous change of sign of both v and y (or rather: dy). This is compatible with equal probability of positive and negative values of v at a given point. When considering correlations, the simultaneous change of signs of v and of spatial distances must be observed.

⁴⁾ Compare equation (12) of the paper mentioned in footnote 2). The variable η of that equation has been replaced by ζ in the present text, since η is used for other purposes.

⁵⁾ In the first one of the two papers mentioned in footnote 1) a different problem was considered, referring to the propagation along the y -axis of impulses introduced at $y = 0$, at a series of successive instants. In that case there is no homogeneity in space, but the system is statistically stationary with respect to the time. It is then possible to study time correlation functions. The type of solutions considered in the present paper and in its immediate predecessor, the same as in the paper mentioned in footnote 2), is slightly easier to handle and affords the desired analogy with turbulence homogeneous in space.

The attempt made in the paper of 1950 was directed at the construction of expressions for $\overline{v_1 v_2}$ and $\overline{v_1^2 v_2}$ in terms of statistical quantities referring to the distribution of the steep fronts and of their amplitudes. At that time no further result could be obtained, since there was not available an explicit expression for the solution of (1) corresponding to a given initial condition, although it was made evident that a solution could be obtained by a step-by-step process. With the aid of the methods developed in the papers quoted in footnote 1) a further step can be carried out: it has become possible to obtain asymptotic expressions for the statistical quantities just mentioned, in the form of certain integrals, so that the calculation is reduced to a problem of quadratures. It has been found, moreover, that the only statistical property of the random function $v_0(y)$ which enters into these expressions, is the integral of its correlation function, which integral is equal to the constant value J , mentioned in formula (4).

Hence it is possible, in principle, to find $\overline{v_1 v_2}$ and $\overline{v_1^2 v_2}$ for all values of ζ and of t . This will make it possible to investigate the behaviour of these functions and to test certain of the suppositions enunciated with respect to the hydrodynamic problem. It is found that a particular similarity hypothesis applied in the hydrodynamic problem is an automatic outcome of the asymptotic relations developed here. ⁶⁾

It must be stated, nevertheless, that there are a number of gaps in the execution of the program. In the first place, the expressions derived are asymptotic in two respects: (a) they refer to very large values of the time elapsed since the initial state; (b) they refer to such small (although finite) values of ν , that ν does not appear explicitly in the results. Hence special corrections will be necessary in case it would be desired to investigate properties depending on the magnitude of ν .

In the second place it must be observed that the integrals upon which the evaluation depends, contain certain functions to be derived from solutions of an ordinary diffusion equation with a *moving absorbing boundary* in the field (a parabolic absorbing boundary in the representation used in the present paper). Convenient and sufficiently exact expressions for these functions are not yet known, although upper and lower bounds can be given, while a series development can be constructed, valid in a certain domain. More complete expressions will be needed before all the integrals can be evaluated. Even in that case the labour involved seems to be considerable. — Finally there are some details in the deductions which may need refinement.

⁶⁾ In principle it also should be possible to check a partial differential equation for $\overline{v_1 v_2}$, proposed in a paper presented at the VIIIth Intern. Congress of Theor. and Applied Mechanics (Istanbul, 1952). But much labour would be involved, and it is possible that the asymptotic nature of the results deduced here will not allow a complete check. This problem is not further considered in the present paper.

The arrangement of the present paper is as follows: Section 2 briefly summarizes certain results obtained in the immediately preceding paper. In section 3 the asymptotic form of a frequency function is considered, necessary for the attack of the statistical problem: it is found that this frequency function asymptotically satisfies the ordinary diffusion equation. In section 4 the introduction of the absorbing barrier into the diffusion problem is discussed; while section 5 defines some functions to be used in calculating probabilities. In section 6 statistical formulae are developed referring to the spacing between successive steep fronts, and the connection is established with expressions given in the paper of 1950, quoted in footnote 2). Since the integrals become rather involved, no attempt has been made at their reduction; it is possible, perhaps, that future research may reveal some relations by means of which they can be simplified. In section 7 the change with time of certain integrals is considered, partly in view of obtaining a further connection with formulae of the paper of 1950, partly in order to derive an integral equation for one of the functions, which makes it possible to construct a series development for this function. Sections 8 and 9 bring approximations for the two functions occurring in the integrals, and in section 10 a rough evaluation of some integrals is given.

2. *Summary of results referring to the solution of eq. (1).* — As has been shown in the immediately preceding paper, the solution of (1) for a given value of t , assuming the initial course of v to be known for all values of y , can be found with the aid of a geometrical construction. For this purpose a parabola

$$(5) \quad s_p(\eta) = (\eta - y)^2/2(t - t_0)$$

is made to glide over a certain curve (called the “summation curve”)

$$(6) \quad s(\eta) = \int_0^{\eta} a(\xi) d\xi,$$

where $a(\xi) = -v_0(\xi)$. The value of a at the point of contact of the parabola with the summation curve, taken with the negative sign, gives the value of $v(y, t)$ at the point y determined by the axis of the contacting parabola.

For certain values of y a double contact is obtained; such a double contact marks a sudden jump (steep front) in the value of $v(y, t)$. These cases of double contact form the chief interest of the investigation, which is directed at finding their probability and the mean distance between the two contact points on the parabola.

When y increases from $-\infty$ to $+\infty$ a series of parabolas making double contact is obtained. In between these parabolas there remain short arcs of the summation curve, like $\eta' \dots \eta''$ in fig. 1, along which the parabola glides with a single contact. If it is assumed that these short arcs can be approximated by a formula of the type:

$$(7) \quad s = \text{constant} - \frac{1}{2}\alpha(\eta - \eta_0)^2,$$

the corresponding course of $v(y, t)$ becomes linear and is given by:

$$(8) \quad v(t, y) = \frac{y - \eta_0}{t - t_0 + 1/\alpha}.$$

The total change of $v(y, t)$ along such an arc will be: $\alpha(\eta'' - \eta')$. On the other hand the sudden jump in the value of v , corresponding to a parabola with two contact points at a horizontal distance l , is given by $l/(t - t_0)$. Since the mean values of these two quantities must be the same, it follows that the ratio $(\eta'' - \eta')/l$ will be of the order $1/\alpha(t - t_0)$ and consequently will decrease indefinitely when $t - t_0$ becomes larger and larger. We are particularly interested in the behaviour of the solution for large values of

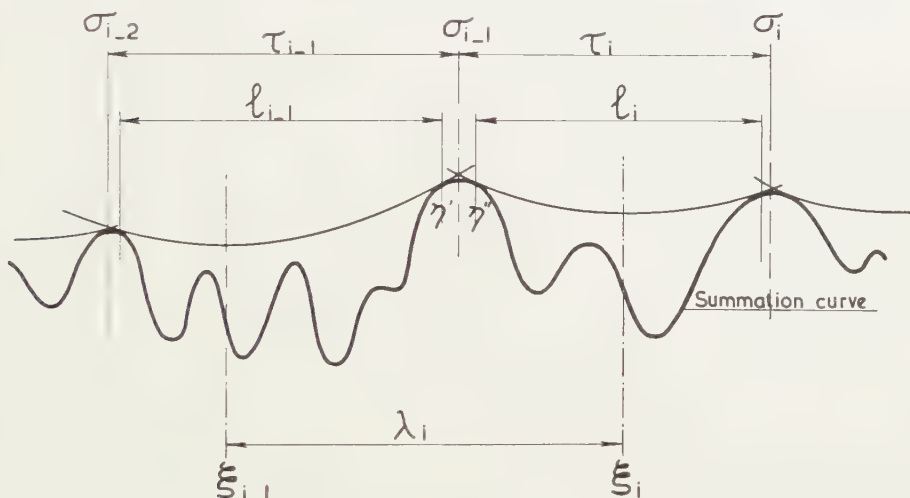


Fig. 1

$t - t_0$ and it has been found already before that in this case the distances l will become of order $(t - t_0)^{2/3}$. In the asymptotic treatment one therefore can neglect the difference between the distance l_i measured between two contact points, and the corresponding distance τ measured between the tops of the arcs.⁷⁾

The proper formulation of a statistical problem requires a specification of the family of initial functions $v_0(y)$ or $a(\xi)$, or of the family of summation curves derived from them. Since the kind of specification needed will depend on the statistical problem, it is necessary to work in two directions: one must define the statistical problem and one must find which statistical properties of the functions $a(\xi)$ are relevant to its solution.

The circumstance that arbitrary functions are admitted, instead of

⁷⁾ The distances τ_i indicated in fig. 1 correspond to the quantities denoted by the same letter in the paper of 1950 (footnote 2). To make the comparison exact it would be necessary to assume $\alpha = 1/t_0$ for all i . — Fig. 1 of the text can be compared with fig. 4 of the paper of 1950, or with fig. 2 of the second paper mentioned in footnote 1).

expressions like (17) and (18) used in the previous paper, or curves defined by means of separate points⁸⁾, leads to greater generality and efficacy of treatment. Certain difficulties are inherent to this procedure, but it is expected that these must have no influence on the asymptotic behaviour and it will be attempted to by-pass them with the aid of an artifice.

As has been done in previous papers in analysing the statistical problem connected with the distances l , it is convenient to imagine all parabolas, together with the corresponding parts of the summation curve, to be shifted in such a way that they always start from the origin.⁹⁾ — For convenience the letter s is used to indicate the ordinate of a summation curve at an arbitrary point, while S will be reserved for the ordinate of a point of contact with the parabola. To simplify notation $t-t_0$ is replaced by t .

3. *The asymptotic form of the frequency function for $s(\eta)$.* — Each summation curve will be considered as the trajectory of a point, moving with unit velocity in the direction of the horizontal η -axis, and endowed with a variable velocity a in the vertical direction. The variable η in this picture plays the part of a time, which, however, has no connection with the time t occurring in equation (1) or in $v(y, t)$: all considerations concerning $a(\xi)$ refer to the initial state of the system.¹⁰⁾

In order to investigate the distribution of the possible values of s for a given η , it is convenient to write $s(\eta)$ temporarily as the limit of a sum:

$$s = \lim_{\varepsilon \rightarrow 0} \varepsilon \sum_{i=1}^{i=\eta/\varepsilon} a_i, \text{ where } i = \xi/\varepsilon.$$

The quantities a_i , being random variables of the indices i , will be subjected to the following conditions:

- (a) all statistical properties of the a_i , whether single or occurring in combination, shall be invariant with respect to a translation along the ξ -axis (condition of homogeneity);
- (b) positive and negative values of any a_i shall be equally probable;^{a)}
- (c) two quantities a_i and a_j shall be independent of each other, when $\varepsilon|i-j| = |\xi_i - \xi_j|$ exceeds a certain limit ϑ : when $\varepsilon|i-j|$ is smaller than this limit, there will exist a certain correlation which prevents a non-analytic behaviour of the function $a(\xi)$;
- (d) a correlation may also exist between a group of more than two quantities $a_i, a_j, a_k, \dots, a_q$, provided the differences between successive values

⁸⁾ See these Proceedings B 57, p. 58 seqq.

⁹⁾ In doing so the short arcs between such points as η' , η'' in fig. 1 will be neglected. In eq. (20) a minimum length δ will be defined, which will determine the limit of accuracy to be observed in measuring distances along the horizontal axis; distances like $\eta'' - \eta'$ will be small compared with δ and thus will become "unobservable".

¹⁰⁾ The letter x , introduced in eq. (22) of the second paper of footnote 1), will not be used here.

of the indices (these being arranged in order of magnitude) are smaller than ϑ/ε .

The correlation function or "covariance" required by (c) will be written:

$$(9) \quad \overline{a(\xi) a(\xi + \zeta)} = R(\zeta),$$

where the mean value is defined with respect to the family of functions $a(\xi)$, for fixed ξ and ζ . In consequence of (a) the function $R(\zeta)$ will be independent of ξ . [It follows that $R(\zeta)$ might also be calculated as the mean value for a single function of the ensemble, taken over a large domain of values of ξ .] — We have $R(\zeta)=0$ when $|\zeta|>\vartheta$.

In consequence of (b) the mean value of s , and similarly the mean value of any odd power of s , will be zero for all η .

Since the square of s is determined by the formula:

$$s^2 = \varepsilon^2 \sum_i \sum_j a_i a_j,$$

it follows that the mean value is given by:

$$\overline{s^2} = \int_0^\eta d\xi_i \int_0^\eta d\xi_j R(\xi_i - \xi_j) = 2 \int_0^\eta d\xi \int_0^\xi d\zeta R(\zeta) = 2 \int_0^\eta d\zeta (\eta - \zeta) R(\zeta).$$

As soon as $\eta > \vartheta$ this can be written:

$$(10) \quad \overline{s^2} = 2J\eta - 2J',$$

where

$$(11) \quad J = \int_0^\vartheta R(\zeta) d\zeta \quad ; \quad J' = \int_0^\vartheta \zeta R(\zeta) d\zeta.$$

To find the mean value of s^4 we consider:

$$\overline{s^4} = \varepsilon^4 \sum_i \sum_j \sum_k \sum_l a_i a_j a_k a_l.$$

In order that the mean value of the product of four factors may be different from zero, it is necessary, either that all three differences between the properly arranged successive indices remain smaller than ϑ/ε ; or that the differences within two complementary pairs of indices remain below this limit. Since the latter case can present itself in three ways it is convenient to write the general term of the sum in the form:

$$(12) \quad R_4^* + \overline{a_i a_j \cdot a_k a_l} + \overline{a_i a_k \cdot a_j a_l} + \overline{a_i a_l \cdot a_j a_k},$$

where

$$(12a) \quad R_4^* = \overline{a_i a_j a_k a_l} - (\overline{a_i a_j \cdot a_k a_l} + \overline{a_i a_k \cdot a_j a_l} + \overline{a_i a_l \cdot a_j a_k}).$$

It will be evident that R_4^* can be different from zero only when all three differences between successive indices are below ϑ/ε . Hence, when η is sufficiently large, one can write:

$$(13) \quad \int d\xi_i \int d\xi_j \int d\xi_k \int d\xi_l R_4^* = K\eta - K',$$

where K and K' are independent of η .

The products $\overline{a_i a_j} \cdot \overline{a_k a_l}$, etc. on the other hand will be different from zero in a much wider domain. The integral

$$\int d\xi_i \int d\xi_j \int d\xi_k \int d\xi_l \overline{a_i a_j} \cdot \overline{a_k a_l}$$

can be decomposed into the product of two independent integrals:

$$\int d\xi_i \int d\xi_j \overline{a_i a_j} \quad \text{and} \quad \int d\xi_k \int d\xi_l \overline{a_k a_l},$$

each of which takes the value $2J\eta - 2J'$, when η is large. The value of the quadruple integral consequently will be of the order $\eta^2(2J)^2$. Since the three products of this type occurring in (12) play a symmetrical part (all four integration variables describe the same domain), it follows that for large values of η :

$$(14) \quad \overline{s^4} = 3\eta^2(2J)^2 - 24\eta JJ' + K\eta + 12J'^2 - K',$$

where the first term is of order η^2 , while the other terms are of lower order.

Finally consider an arbitrary even power of s :

$$s^{2n} = i^{2n} \sum_i \dots \sum_q a_i a_l a_k a_l \dots a_r a_q.$$

In order to obtain a non zero mean value for a product $a_i a_j a_k a_l \dots a_p a_q$ it is necessary, either that all differences of successive indices (arranged in order of magnitude) are smaller than ϑ/ε ; or that the multiple product can be decomposed into partial products, each containing an even number of factors for which the differences of successive indices are smaller than ϑ/ε . The following notation is introduced:

$$(15) \quad \left\{ \begin{array}{l} R_{2n}^* = \overline{a_i a_j a_k a_l \dots a_p a_q} - \overline{a_i a_j} \cdot \overline{a_k a_l \dots a_p a_q} - \overline{a_i a_k} \cdot \overline{a_j a_l \dots a_p a_q} - \\ - \text{analogous terms (in all } 2n-1 \text{ terms to be subtracted).} \end{array} \right.$$

When this is integrated with respect to all variables from 0 to η , the $2n-1$ terms of analogous type all will give the same result. Hence in view of such an integration the following equivalence holds:

$$\overline{a_i a_j a_k a_l \dots a_p a_q} (=) R_{2n}^* + (2n-1) \overline{a_i a_j} \cdot \overline{a_k a_l \dots a_p a_q}.$$

In carrying out the integration, the factor $\overline{a_i a_j} = R(\xi_i - \xi_j)$ can be integrated independently of the factor $\overline{a_k a_l \dots a_p a_q}$. Treating the latter factor in a similar manner, the equivalence

$$\overline{a_k a_l \dots a_p a_q} (=) R_{2n-2}^* + (2n-3) \overline{a_k a_l} \cdot \overline{a_m \dots a_p a_q}$$

is obtained. Finally one arrives at:

$$\overline{a_i a_j a_k a_l \dots a_p a_q} (=) R_{2n}^* + (2n-1) R \{ R_{2n-2}^* + (2n-3) R \{ R_{2n-4}^* + \dots$$

Again each factor can be integrated independently of the other factors, and each factor, when integrated, will give a result which becomes a linear function of η , when η is large enough. It follows that the most

important contribution to the result will be given by the integration of $(2n-1) R (2n-3) R \dots R$ (n factors R in all), which leads to:

$$(16) \quad \overline{s^{2n}} = (2n-1) (2n-3) \dots 3 \eta^n (2J)^n + \text{terms of a lower order of magnitude.}$$

In this way asymptotic expressions are obtained for the "moments" of $s(\eta)$ for large values of η . The moments suffice to determine the frequency function of s , provided certain conditions of convergence are satisfied, which is the case here. Since the asymptotic values of the moments are identical in structure with the moments corresponding to the "normal" distribution, as represented by the function of Gauss, it follows that the asymptotic form of the frequency function will be given by:

$$(17) \quad \psi(\eta, s) ds = \frac{1}{2\sqrt{\pi J \eta}} \exp\left(\frac{-s^2}{4J\eta}\right) ds.$$

It can be concluded that the frequency function asymptotically satisfies the ordinary diffusion equation:

$$(18) \quad \frac{\partial \psi}{\partial \eta} = J \frac{\partial^2 \psi}{\partial s^2}.$$

Formula (17) corresponds to unit discharge at the origin.

In this way it has become evident that in the asymptotic case a single feature characterising the family of random functions $a(\xi)$ is of importance, *viz.* the integral J of the covariance R . This furnishes a proof of a guess expressed at the end of the previous paper. All other particularities, *e.g.* mean quadratic amplitude, mean duration of the correlation, discontinuities, the frequency function for the values of a_i at a given point, etc. are of no interest. It will be assumed that the integral J has a given value.¹¹⁾

¹¹⁾ The circumstance that the asymptotic statistical problem is dependent only on the value of the integral J for the family of initial functions, makes it possible to leave out of sight questions concerning the proper definition of this family and concerning "measures" that might be assigned to various possible types of functions. Such questions of measure would have to be considered when it is desired to calculate the value of J from specific data describing the family of functions; for the present purpose, however, one can assume that these calculations have already been made, and it is not necessary to pay attention to their details.

On the other hand, if it should be desired to calculate more exact values of the moments $\overline{s^{2n}}$, further data will be needed. For instance, when one wishes to find $\overline{s^2}$ for all values of η , the precise course of $R(\xi)$ must be known; in order to obtain more accurate data concerning $\overline{s^4}$, one must know R_4^* ; etc. If very small values of η are of importance, one finds:

$$\overline{s^{2n}} = \eta^{2n} \overline{(a_i^{2n})},$$

and in that case all depends on the moments of the frequency function for a_i at a given point.

It will thus be seen that an infinity of distribution laws is possible, depending on a detailed specification of the family of random function $a(\xi)$. It is not a priori certain whether always a differential equation can be found, which is satisfied by such more complicated distribution laws. As has been mentioned already in the previous paper, a particular case has been discussed very fully by S. GOLDSTEIN, *Quart. Journ. Mech. and Applied Mathem.* **4**, 129-156 (1951).

4. *The absorbing barrier.* — Formula (17) expresses the probability that a summation curve or trajectory, starting from the origin, shall pass between the ordinates s and $s+ds$ at the abscissa η . The next problem is to find the probability that such a curve will make contact with a parabola

$$(19) \quad s_p = \alpha\eta + \eta^2/2t,$$

both at the origin and at a point with a prescribed abscissa l , without reaching anywhere above the parabola.¹²⁾

In selecting curves which satisfy this condition, all curves crossing the parabola must be rejected. In the language of the diffusion problem this can be obtained by considering the parabola as an *absorbing barrier*, so that every particle which crosses it is automatically eliminated.

In the asymptotic formulation of the diffusion problem an absorbing barrier is a line along which the density function ψ must be equal to zero. This causes some difficulty, since the starting point of the diffusion is situated on the parabola itself, while also the second contact point is on the parabola. An exact treatment of what is happening at these points would require that the parabola is not considered as a line along which the density function must be exactly zero; and in devising a more appropriate condition it would at the same time be necessary to pay attention to the circumstance that the trajectories must be tangent to the parabola. In its turn this would introduce the need of data concerning the diffusion at small distances. It is to be expected, however, that these particularities will drop out in the asymptotic form of the results. If this is true, it must be possible to obtain equivalent results by making use of an artifice. With this purpose in view the following rules are introduced:

(a) The absorbing barrier is placed at a small constant distance Δ above the parabola; and "contacting the parabola" will be interpreted as "penetrating for a limited time into the zone between the parabola and the barrier". It is necessary to pay attention to the "*duration of the contact*", that is, the length in the η -direction of the segment of the curve situated in the zone between parabola and barrier. The following mean value will be taken for this duration:

$$(20) \quad \delta = \Delta^2/n_1J.$$

Here n_1 is a number of order unity, to be adjusted later on in such a way that a possible inaccuracy of the artifice may be corrected. The distance δ should be small in comparison with the mean value of the distance l ; at the same time it must be large both in comparison with ϑ and with the distances $\eta'' - \eta'$ mentioned in connection with fig. 1.¹³⁾

¹²⁾ The letter α will no longer be used in the sense in which it was introduced in eq. (7).

¹³⁾ It will be found that dimensionally Δ and Δ_1 are proportional to $J^{2/3} t^{1/3}$, while δ is proportional to $J^{1/3} t^{2/3}$ (see section 8). In both cases it can be assumed that the factor of proportionality is small compared with unity. The presence of a positive power of t always suffices to make δ large in comparison with ϑ and with $\eta'' - \eta'$.

(b) The starting point for the diffusion will not be taken exactly at the origin, but in a point at the distance Δ_1 below the barrier (coordinates: $0, \Delta - \Delta_1$). The ratio $n_2 = \Delta_1 / \Delta$ will be another adjustable parameter to be used for eliminating inaccuracies. In the same train of thought the point of observation where the density function ψ must be found in order to calculate the probability of making contact with the parabola, will be taken at the distance Δ_1 below the absorbing barrier.

(to be continued)

STATISTICAL PROBLEMS CONNECTED WITH THE SOLUTION OF A SIMPLE NON-LINEAR PARTIAL DIFFERENTIAL EQUATION. — CONTINUATION. II

BY

J. M. BURGERS

(Mededeling No. 78 uit het Laboratorium voor Aero- en Hydrodynamica der Technische Hogeschool te Delft)

(Communicated at the meeting of June 26, 1954)

5. Functions to be used in calculating probabilities

(I) A function $E(\alpha)$ will be introduced, defined as follows:

(21) $E(\alpha)$ = probability that curves starting from the point 0, $\Delta - \Delta_1$, will arrive at $+\infty$ without having been absorbed by the barrier situated along $s_b = \alpha\eta + \eta^2/2t + \Delta$.

The function $E(\alpha)$ thus refers to all curves which either make contact with the parabola (19) at some abscissa η —in the sense defined above—, or lie completely below that parabola. The function is normalised in an absolute way, in so far as $E(+\infty) = 1$; $E(-\infty) = 0$.

Differentiation of $E(\alpha)$ with respect to α gives:

(22) $(dE/d\alpha)d\alpha$ = probability that curves, starting from the point 0, $\Delta - \Delta_1$, will have at least one summit within the domain between the parabolas $(\alpha + d\alpha)\eta + \eta^2/2t + \Delta$ and $\alpha\eta + \eta^2/2t + \Delta$, without ever crossing the first mentioned parabola.

It follows that these curves will make contact—in the sense defined before—with the parabola $(\alpha + d\alpha)\eta + \eta^2/2t$ or will lie below this parabola, while at the same time they must reach above the parabola $\alpha\eta + \eta^2/2t$.

The group of curves to which refers $(dE/d\alpha)d\alpha$ can be subdivided by asking for the curves which have their *first* summit between two prescribed abscissae l and $l + dl$. These summits will be situated within a domain of area $ld\alpha dl$. When their number density is written $Y^*(l, \alpha)$, one obtains:

$$dE/d\alpha = \int_0^\infty dl \cdot l \cdot Y^*(l, \alpha).$$

It is necessary to associate a mean horizontal extension with every summit; the same value δ will be used for this purpose as has been defined in

(20).¹⁴⁾ Since the density function used in connection with the diffusion equation refers to the number of trajectories crossing a vertical line with a given abscissa, the value Y of this function corresponding to the quantity Y^* introduced in the preceding equation will be given by the relation: $Y = Y^* \delta$. Hence:

$$(23) \quad dE/d\alpha = \frac{1}{\delta} \int_0^\infty dl \cdot l \cdot Y(l, \alpha),$$

and it follows that:

$$(23a) \quad E(\alpha) = \frac{1}{\delta} \int_{-\infty}^\alpha d\alpha' \int_0^\infty dl \cdot l \cdot Y(l, \alpha').$$

The curves to which refer $Y^*(l, \alpha)$ and $Y(l, \alpha)$, have their first summit at the abscissa l with ordinate

$$(24) \quad S = \alpha l + l^2/2t.$$

In equation (23a) we can use S' as a variable instead of α' ; this gives:

$$(25) \quad E(\alpha) = \frac{1}{\delta} \int_0^\infty dl \int_{-\infty}^S dS' Y(l, S').$$

(II) *Expression for $Y(l, S)$.* — Consider a source with unit discharge at the point 0, $\Delta - \Delta_1$, and determine the value $\Psi(l, S)$ of the density function at the point with coordinates $l, S + \Delta - \Delta_1$, in the presence of the absorbing barrier $s_p = \alpha\eta + \eta^2/2t + \Delta$. The value $\Psi(l, S)$ differs in two respects from the function $Y(l, S)$:

(a) $\Psi(l, S)$ is a measure for the number of curves starting from the origin and making contact with the parabola (19) at the point A with coordinates l, S ; they may, however, also have made another contact with that parabola somewhere between 0 and A . On the other hand $Y(l, S)$ refers to curves having their *first* summit—and consequently their first contact—at the point A . However, the number of cases where another contact is made between 0 and A is very small and can be neglected (compare footnote 19).

(b) The calculation of Ψ as a density function for the diffusion from $\eta=0$ to $\eta=l$ does not make any reference to what happens with the diffusing particles beyond l . The function $Y(l, S)$ on the other hand refers to curves which remain below the contacting parabola also beyond l . In order to eliminate the cases which might reach above this parabola beyond l , it is necessary to multiply $\Psi(l, S)$ with $E(\alpha + l/t)$, when $\alpha + l/t$ is the inclination of the parabola at A . This treatment may not do full justice to what is happening at A , but it is in order to correct for a possible inaccuracy that the parameters n_1 and n_2 have been introduced.

In this way the following formula is obtained:

$$(26) \quad Y(l, S) = \Psi(l, S) E(\alpha + l/t).$$

¹⁴⁾ It should be kept in mind that the contacting parabola is always very flat when t is large. The more important values of α are found to be of order $J^{1/3} t^{-1/3}$.

Equations (23) and (25) can now be written:¹⁵⁾

$$(27) \quad \frac{dE}{d\alpha} = \frac{1}{\delta} \int_0^{\infty} dl \cdot l \cdot \Psi(l, S) E(\alpha + l/t);$$

$$(28) \quad E(\alpha) = \frac{1}{\delta} \int_0^{\infty} dl \int_{-\infty}^S dS' \Psi(l, S') E(\alpha' + l/t),$$

where $S' = \alpha'l + l^2/2t$ and $\alpha' + l/t = l/2t + S'/l$.

(III) *Probability that a curve will make contact with a given parabola both at 0 and A, without ever crossing the parabola.* — Thus far attention has been paid only to the behaviour of a curve starting from the origin towards the right. No attention has been paid to the condition that the curve must make contact with the parabola at the origin, and that it must remain below the parabola also in the domain from the origin to the left. The introduction of these conditions will lead to a reduction of the discharge at the origin, since unit discharge had been taken as the measure for "all possible curves".

Now in the diffusion problem there is symmetry, for any given parabola, between diffusion with positive horizontal unit velocity in the direction from 0 to A, and diffusion with negative horizontal velocity in the direction from A to 0. One consequence of this symmetry is the relation

$$(29) \quad \Psi(l, S) = \Psi(l, -S),$$

which will be proved along other lines below (compare section 8). Another consequence is that the point 0 can be treated on the same footing as A and that consequently a factor $E(-\alpha)$ must be introduced, which will cut out the curves that would reach above the parabola to the left of the origin. Here $-\alpha$ is the inclination of the parabola (19), measured from 0 in the negative direction. Further, since the discharge considered in the diffusion problem is a density referring to the number of particles or of trajectories intersecting a certain ordinate per unit of length, the corresponding number of summits per unit area is to be obtained by dividing once more through δ .

It follows that the probability of finding curves, which contact a given parabola both at the origin 0 and at the point A with abscissa l and ordinate S , is given by:

$$(30) \quad p(l, S) \cdot dl dS = \frac{1}{\delta^2} E(\alpha_I) \Psi(l, S) E(\alpha_{II}) \cdot dl dS,$$

where $\alpha_I = -\alpha = l/2t - S/l$; $\alpha_{II} = \alpha + l/t = l/2t + S/l$.

¹⁵⁾ It will be found in section 8 that the function $\Psi(l, S)$ can be written $\Phi(l) \cdot \exp(-S^2/4Jl)$, where $\Phi(l)$ is proportional to $l^{-3/2}$ for very small values of l . This raises the question whether the integrals with respect to dl will be convergent in the neighbourhood of $l = 0$. It has been checked that this is the case with equations (27), (28) (provided α is finite); (32), (38), (44), (49), (50).

The only exception will be mentioned in footnote 19).

The expression $E(\alpha_I)\Psi(l, S)E(\alpha_{II})$ does not change when S is replaced by $-S$.

The probability of finding curves which make contact with a parabola both at the origin and at a point with abscissa l , when *all* values of S are admitted, is given by:

$$(31) \quad P(l) \cdot dl = \frac{1}{\delta^2} \int_{-\infty}^{+\infty} dS E(\alpha_I) \Psi(l, S) E(\alpha_{II}) \cdot dl.$$

When the calculations are correct we now must have:

$$(32) \quad (\bar{l})^{-1} = \frac{1}{\delta^2} \int_0^{\infty} dl \int_{-\infty}^{+\infty} dS E(\alpha_I) \Psi(l, S) E(\alpha_{II}),$$

where \bar{l} represents the mean value of l for all possible double contacts; ¹⁶⁾ and also:

$$(33) \quad 1 = \frac{1}{\delta^2} \int_0^{\infty} dl \int_{-\infty}^{+\infty} dS \cdot l \cdot E(\alpha_I) \Psi(l, S) E(\alpha_{II}).$$

The numbers n_1 and n_2 must be adjusted so that (27) and (33) will be satisfied. We shall come to this point in section 9 (II), where it will be found that $n_1 n_2^2 = 1$. It will appear in section 9 (III) that this is the only combination of n_1 and n_2 which occurs in the integrals, so that no further condition is needed, and it will appear in section 10 (I) that it is satisfactory.

A consequence of the relations obtained above is:

$$(34) \quad \bar{l}^n = \frac{l}{\delta^2} \int_0^{\infty} dl \int_{-\infty}^{+\infty} dS \cdot l^n \cdot E(\alpha_I) \Psi(l, S) E(\alpha_{II}).$$

The quantity \bar{l}^n corresponds to $\overline{\tau_i^n}$ of the paper mentioned in footnote 2); and in a notation of that paper [*l.c.* p. 258, form. (31)] we have:

$$\bar{l}^2 = (1 - \omega) \cdot (\bar{l})^2; \quad \bar{l}^3 = (1 + \omega^*) \cdot (\bar{l})^3.$$

It is further found that the quantity ζ_i defined in form. (26) of that paper (*l.c.* p. 255) is equal to $S_i t / l_i$ in the present notation. It follows that the quantity $\tilde{\omega}$ will be given by: $\overline{\tau_i \zeta_i^2} = \tilde{\omega} \cdot (\bar{l})^3 = \overline{S^2 t^2 / l} = \text{integral (34) with } l^n \text{ replaced by } S^2 t^2 / l$.

6. Formulae referring to the spacing between successive steep fronts ("shock fronts", or "N-waves")

(I) In equation (32) the factor $E(\alpha_{II})$ can be replaced by the integral given in (28). In order to obtain a more symmetrical expression l_0, S_0 will

¹⁶⁾ In the paper mentioned in footnote 2) this mean value was denoted by l without a bar. — For the argumentation involved in eqs. (32), (33) compare the first paper mentioned in footnote 1), p. 61, eqs. (42)–(44).

be written for l, S ; l_1, S_1 for l', S' ; and the notation S_1^* will be used for the quantity:

$$S_1^* = \alpha(l_0 + l_1) + (l_0 + l_1)^2/2t - S_0 = l_1\{S_0/l_0 + (l_0 + l_1)/2t\},$$

the meaning of which is indicated in fig. 2 (when comparing this with fig. 1, take $i=1$). The following result is obtained:

$$(35) \quad 1 = \frac{l}{\delta^3} \int_0^\infty dl_0 \int_{-\infty}^{+\infty} dS_0 \int_0^\infty dl_1 \int_{-\infty}^{S_1^*} dS_1 E(\alpha_I) \Psi(l_0, S_0) \Psi(l_1, S_1) E(\alpha_{II}),$$

where now $\alpha_I = -\alpha = l_0/2t - S_0/l_0$; $\alpha_{II} = l_1/2t + S_1/l_1$.

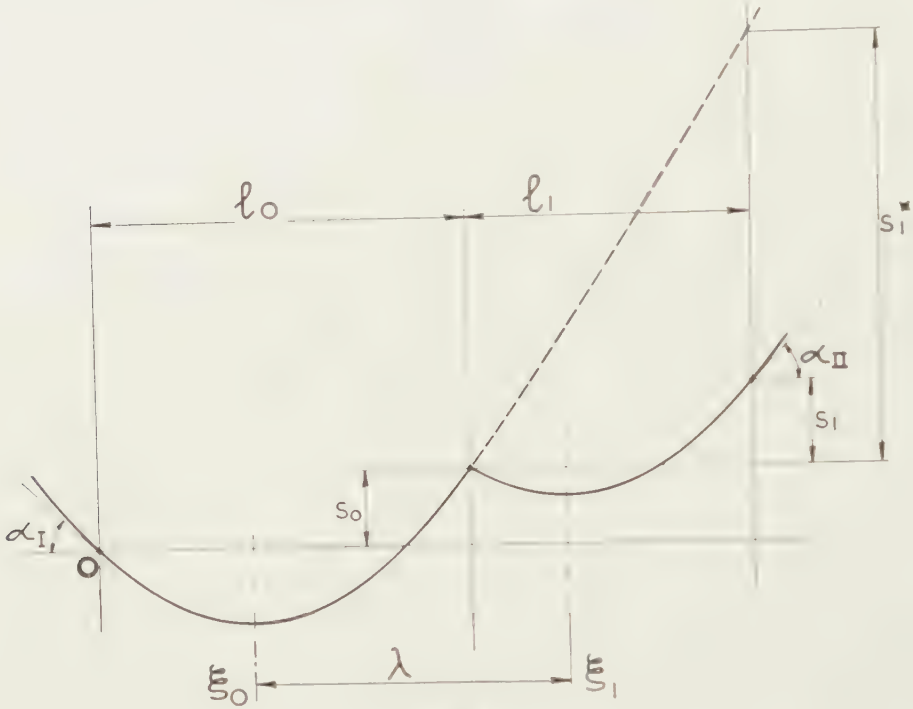


Fig. 2

The positions of the axes of the two parabolas in fig. 2, determining the location of the steep fronts, are determined by the expressions:

$$(36) \quad \xi_0 = l_0/2 - S_0 t/l_0; \quad \xi_1 = l_0 + l_1/2 - S_1 t/l_1.$$

By subtraction we obtain the distance λ between two successive steep fronts:¹⁷⁾

$$(37) \quad \lambda = \xi_1 - \xi_0 = (l_0 + l_1)/2 + (S_0/l_0 - S_1/l_1)t.$$

¹⁷⁾ When t increases the parabolas become flatter and the positions of the axes change. Equation (37) then gives:

$$d\lambda/dt = (S_0/l_0 - S_1/l_1) = \{\lambda - \frac{1}{2}(l_0 + l_1)\}/t.$$

This formula is identical with one given in the paper of footnote 2), *l.c.* p. 256, sub (VI).

The condition $S_1 \leq S_2^*$ occurring in the last integral of (35) is equivalent to the condition $\lambda \geq 0$.

The following transformation of variables is introduced:

$$S_0 = l_0(2m + \lambda - l_1)/2t; \quad S_1 = l_1(2m - \lambda + l_0)/2t.$$

The Jacobian of the transformation from the variables l_0, l_1, S_0, S_1 to the variables l_0, l_1, λ, m has the value $l_0 l_1 / t^2$ and it follows that the integral (35) can be written:

$$(38) \quad 1 = \frac{l}{\delta^3 t^2} \int_0^\infty dl_0 \int_0^\infty dl_1 \int_0^\infty d\lambda \int_{-\infty}^{+\infty} dm \, l_0 l_1 E_I \Psi_0 \Psi_1 E_{II}.$$

A function $f_1(\lambda)$ is defined by means of:

$$(39) \quad f_1(\lambda) = \frac{l}{\delta^3 t^2} \int_0^\infty dl_0 \int_0^\infty dl_1 \int_{-\infty}^{+\infty} dm \, l_0 l_1 E_I \Psi_0 \Psi_1 E_{II}.$$

Equation (38) then gives:

$$(38a) \quad \int_0^\infty f_1(\lambda) d\lambda = 1.$$

From the symmetry of the integral (35) with respect to the indices 0 and 1 it can be deduced that:

$$(40) \quad \int_0^\infty f_1(\lambda) \lambda d\lambda = \bar{l}.$$

This leads to the conclusion that $f_1(\lambda)$ can serve as frequency function for λ

(II) By repeating the same procedure a number of times the following integral is obtained:

$$(41) \quad 1 = \frac{l}{\delta^{k+2}} \int_0^\infty dl_0 \int_{-\infty}^{+\infty} dS_0 \int_0^\infty dl_1 \int_{-\infty}^{S_1^*} dS_1 \dots \int_0^\infty dl_k \int_{-\infty}^{S_k^*} dS_k \mathbf{X}_k,$$

where:

$$\begin{aligned} \mathbf{X}_k &= E(\alpha_I) \Psi(l_0, S_0) \Psi(l_1, S_1) \dots \Psi(l_k, S_k) E(\alpha_{II}), \\ \alpha_I &= l_0/2t - S_0/l_0; \quad \alpha_{II} = l_k/2t + S_k/l_k, \\ S_i^* &= l_i \{ S_{i-1}/l_{i-1} + (l_{i-1} + l_i)/2t \}. \end{aligned}$$

The multiple integral refers to a chain of $k+1$ parabolas. The positions of the axes of the first and the last parabolas are determined by:

$$(42) \quad \xi_0 = l_0/2 - S_0 t/l_0; \quad \xi_k = l_0 + l_1 + \dots + l_{k-1} + l_k/2 - S_k t/l_k,$$

respectively. The distances between successive steep fronts are given by

$$(43) \quad \lambda_i = (l_{i-1} + l_i)/2 + (S_{i-1}/l_{i-1} - S_i/l_i)t.$$

The following notation is introduced:

$$\begin{aligned} L &= l_0 + l_1 + \dots + l_k; \\ A &= \lambda_1 + \lambda_2 + \dots + \lambda_k = \xi_k - \xi_0; \\ S_0 t/l_0 &= m + \frac{1}{2}A - \frac{1}{2}L + \frac{1}{2}l_0, \end{aligned}$$

which gives

$$\begin{aligned} S_k/l_k &= m + \frac{1}{2}A = (\lambda_1 + \dots + \lambda_k) - \frac{1}{2}L = (l_0 + \dots + l_k) - \frac{1}{2}l_k; \\ S_k/l_k &= m - \frac{1}{2}A + \frac{1}{2}L - \frac{1}{2}l_k; \quad \xi_k + \xi_0 = L - 2m; \\ \alpha_I &= (L - A)/2t - m/t; \quad \alpha_{II} = (L - A)/2t + m/t. \end{aligned}$$

The Jacobian for the transformation from $l_0, l_1, \dots, l_k, S_0, S_1, \dots, S_k$ to the set of variables $A, \lambda_1, \dots, \lambda_{k-1}, l_0, l_1, \dots, l_k$ has the value $(\pm)l_0 l_1 \dots l_k/t^{k+1}$. Formula (41) now takes the form:

$$(44) \quad 1 = \frac{l}{\delta^{k+2} t^{k+1}} \int_0^A dA \int_0^A d\lambda_1 \int_0^{A-\lambda_1} d\lambda_2 \dots \int_0^{A-\lambda_{k-1}} d\lambda_k \int_{-\infty}^{\infty} dm \int_0^{\infty} dl_0 \dots \int_0^{\infty} dl_k \mathbf{Z}_k,$$

where $\mathbf{Z}_k = l_0 l_1 \dots l_k \mathbf{X}_k$.

In analogy with (39) one can introduce:

$$(45) \quad f_k(A) = \frac{l}{\delta^{k+2} t^{k+1}} \int_0^A d\lambda_1 \dots \int_0^{\infty} dl_k \mathbf{Z}_k;$$

the following relations are then satisfied:

$$(44a) \quad \int_0^{\infty} f_k(A) dA = 1;$$

$$(46) \quad \int_0^{\infty} f_k(A) A dA = k\bar{l}.$$

The functions $f_1(\lambda)$ and $f_k(A)$ are identical with the functions introduced in the paper mentioned in footnote 2), *l.c.* p. 394, form. (36) and (38).

(III) With the aid of integrals as considered here it is now possible to write down expressions for the "restricted" mean values introduced in section 12 of that paper (*l.c.* pp. 395/396).

In particular the functions $\varphi_k, \chi_k, \Phi_k, X_k$ defined *l.c.* p. 400, eqs. (45)–(46), and p. 403, eqs. (51)–(52), take the following forms in the present notation (with ζ written in the place of η):

$$(47a) \quad \bar{l} \cdot \varphi_k(\zeta) = \frac{1}{\delta^{k+2} t^{k+1}} \int_0^{\zeta} dA \int_0^A d\lambda_1 \dots \int_0^{\infty} dl_k \cdot l_0 l_k \mathbf{Z}_k$$

$$(47b) \quad (\bar{l})^2 \cdot \chi_k(\zeta) = \text{idem} \cdot A l_0 l_k \mathbf{Z}_k$$

$$(47c) \quad (\bar{l})^3 \cdot \Phi_k(\zeta) = \text{idem} \cdot (L - \frac{1}{2}l_0 - \frac{1}{2}l_k) l_0 l_k \mathbf{Z}_k$$

$$(47d) \quad (\bar{l})^4 \cdot X_k(\zeta) = \text{idem} \cdot A (L - \frac{1}{2}l_0 - \frac{1}{2}l_k) l_0 l_k \mathbf{Z}_k.$$

It follows that the functions $\overline{v_1 v_2}$ and $\overline{v_1^2 v_2^2}$, to which refer form. (47)–(48) and (53)–(54) of that paper, can be expressed by means of similar integrals, since, *e.g.*:

$$(48) \quad \frac{\partial}{\partial \zeta} R(\zeta) = \frac{\partial}{\partial \zeta} \overline{v_1 v_2} = -\frac{1}{t^2} \{ \bar{l}^2/2\bar{l} - \zeta + \bar{l} \sum_1^{\infty} \varphi_k(\zeta) \}.$$

Hence, in principle, they can be evaluated once sufficiently exact expressions have been obtained for the functions E and Ψ , which must be

derived from particular solutions of the diffusion equation. The labour involved in carrying out the integrations of course will be very great.

A particular quantity in the paper of 1950 was f_0 (*l.c.* p. 394); in the present notation it is given by:

$$(49) \quad f_0 = \bar{l} \delta^{-3} t^{-2} \int_0^\infty dl_0 \int_0^\infty dl_1 \int_{-\infty}^{+\infty} dm \cdot l_0 l_1 E_I \Psi_0 \Psi_1 E_{II}.$$

In consequence of the circumstance that $\lambda=0$, the values of $S_0, S_1, \alpha_I, \alpha_{II}$ occurring in this integral are given by:

$$S_0 = l_0(2m - l_1)/2t; \quad S_1 = l_1(2m + l_0)/2t;$$

$$\alpha_I = (l_0 + l_1)/2t - m/t; \quad \alpha_{II} = (l_0 + l_1)/2t + m/t.$$

In this case the parabolas pictured in fig. 2 have become arcs of a single parabola.

Other important quantities are:

$$\overbrace{f_0 \tau_i + \tau_{i+1}}^* ; \quad \overbrace{f_0 (\tau_i + \tau_{i+1}) \tau_i \tau_{i+1}}^* ; \quad \overbrace{f_0 (\tau_i + \tau_{i+1})^2 \tau_i \tau_{i+1}}^*$$

[compare *l.c.* p. 406, form. (65), (66), (67), and p. 727, form. (95), (96)].¹⁸⁾

In the present notation they can be written:

$$(50) \quad \bar{l} \delta^{-3} t^{-2} \int_0^\infty dl_0 \int_0^\infty dl_1 \int_{-\infty}^{+\infty} dm \cdot Z_* E_I \Psi_0 \Psi_1 E_{II},$$

where:

$$Z_* = (l_0 + l_1) l_0 l_1; \quad (l_0 + l_1) l_0^2 l_1^2; \quad (l_0 + l_1)^2 l_0^2 l_1^2,$$

respectively. The values of $S_0, S_1, \alpha_I, \alpha_{II}$ to be used in (50) are the same as those mentioned in connection with (49).

7. *Considerations on the change with time of certain integrals.* — Differentiation of (32) with respect to t gives:

$$(51) \quad \frac{1}{l} \frac{dl}{dt} = -\frac{l}{\delta^2} \int_0^\infty dl \int_{-\infty}^{+\infty} dS \frac{\partial}{\partial t} \{ E(\alpha_I) \Psi(l, S) E(\alpha_{II}) \}.$$

Consider the part depending on $\partial E(\alpha_{II})/\partial t$. The variation of $E(\alpha_{II})$ is dependent on the circumstance that the parabola (19):

$$s_p = \alpha\eta + \eta^2/2t = \eta(\eta - l)/2t + S\eta/l$$

changes with time. In the calculation l and S are treated as independent of t ; hence one finds:

$$\partial s_p / \partial t = -\eta(\eta - l)/2t^2.$$

¹⁸⁾ The condition "restricted value for $\lambda_i \rightarrow 0$ " stated in the paper of 1950 should rather have been "restricted value for $\lambda_{i+1} \rightarrow 0$ ", as follows from the considerations *l.c.* p. 404, second paragraph of section 18.

In a similar way as was done in the derivations leading to (27) one now can write:

$$-\frac{\partial E(\alpha_{II})}{\partial t} = \frac{1}{\delta} \int_l^{\infty} d\eta \frac{\eta(\eta-l)}{2t^2} \Psi(\eta-l, S_1) E(\alpha + \eta/t),$$

where $S_1 = \alpha\eta + \eta^2/2t - S = (\eta-l)(S/l + \eta/2t)$.

A change of variables is made by writing:

$$l = l_0; \quad \eta = l_0 + l_1; \quad S = S_0 = l_0(2m - l_1)/2t,$$

which gives:

$$S_1 = l_1(2m + l_0)/2t; \quad (l_0 + l_1)/2 + (S_0/l_0 - S_1/l_1) = 0.$$

The Jacobian of the transformation has the value l_1/t and it follows that:

$$(52) \quad \begin{cases} -\frac{l}{\delta^2} \int_0^{\infty} dl \int_{-\infty}^{+\infty} dS E(\alpha_I) \Psi(l, S) \frac{\partial}{\partial t} E(\alpha_{II}) = \\ = \frac{l}{2\delta^2 t^3} \int_0^{\infty} dl_0 \int_0^{\infty} dl_1 \int_{-\infty}^{+\infty} dm (l_0 + l_1) l_0 l_1 E(\alpha_I) \Psi_0 \Psi_1 E(\alpha_{II}), \end{cases}$$

where:

$$S_0 = S = l_0(2m - l_1)/2t; \quad S_1 = l_1(2m + l_0)/2t;$$

$$\alpha_I = -\alpha = l/2t - S/l = (l_0 + l_1)/2t - m/t;$$

$$\alpha_{II} = \alpha + \eta/t = (l_0 + l_1)/2t + m/t.$$

In consequence of symmetry the term in (51) depending on $\partial E(\alpha_I)/\partial t$ will give the same result.

It remains to consider:

$$-\frac{l}{\delta^2} \int_0^{\infty} dl \int_{-\infty}^{+\infty} dS E(\alpha_I) E(\alpha_{II}) \frac{\partial \Psi(l, S)}{\partial t}.$$

Here $\Psi(l, S)$ increases in consequence of the circumstance that certain curves, which originally just crossed the parabola between 0 and A and thus had to be eliminated, must be admitted as soon as the parabola slightly rises as a result of the decrease of t (compare fig. 3). The rise of

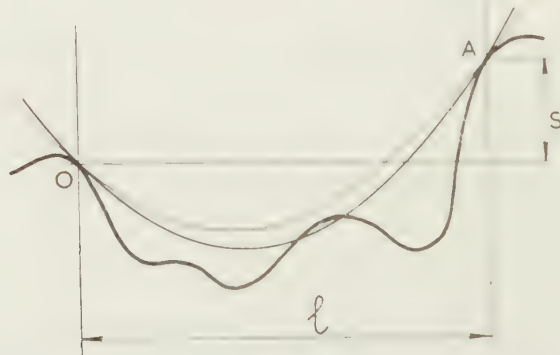


Fig. 3

the parabola at a point with abscissa η is again determined by:

$$\partial s_p / \partial t = -\eta(\eta - l) / 2t^2 = +\eta(l - \eta) / 2t^2.$$

The curves to be admitted must already have (or very nearly have) a contact with the parabola at the point η between the points 0 and A . Hence these curves can be characterised as making *three* contacts with the parabola. The number of cases in which this occurs must be found from a combination of two diffusion processes, first from 0 to the intermediate point of contact with abscissa η , then from this point to A ; and the number of summits per unit area is dependent on the expression:

$$\frac{1}{\delta} \Psi(\eta, s_p) \Psi(l - \eta, S - s_p).$$

Making use of this result one obtains:¹⁹⁾

$$(53) \quad \frac{\partial \Psi(l, S)}{\partial t} = \frac{1}{\delta} \int_0^l d\eta \frac{\eta(l - \eta)}{2t^2} \Psi(\eta, s_p) \Psi(l - \eta, S - s_p).$$

This will be introduced into the corresponding part of the integral (51). Again a change of variables will be made, as follows:

$$\eta = l_0; \quad l = l_0 + l_1; \quad S = m(l_0 + l_1)/t,$$

which gives:

$$s_p = S_0 = l_0(2m - l_1)/2t; \quad S - s_p = S_1 = l_1(2m + l_0)/2t.$$

The Jacobian has the value $(l_0 + l_1)/t$ and it follows that:

$$(54) \quad \begin{aligned} & \left(-\frac{l}{\delta^2} \int_0^\infty dl \int_{-\infty}^{+\infty} dS E(\alpha_I) E(\alpha_{II}) \frac{\partial}{\partial t} \Psi(l, S) = \right. \\ & \left. = -\frac{l}{2\delta^3 t^3} \int_0^\infty dl_0 \int_0^\infty dl_1 \int_{-\infty}^{+\infty} dm (l_0 + l_1) l_0 l_1 E(\alpha_I) \Psi_0 \Psi_1 E(\alpha_{II}), \right. \end{aligned}$$

where α_I and α_{II} are related to l_0, l_1, m in the same way as has been mentioned in connection with form. (52).

¹⁹⁾ The total number of cases presenting three points of contact will be given by:

$$(*) \quad \Psi_3 = \Delta / \delta \int_{\delta}^{l-\delta} d\eta \Psi(\eta, s_p) \Psi(l - \eta, S - s_p).$$

The limits of integration have been taken as δ and $l - \delta$, since a third contact at a distance smaller than δ either from 0 or from A must not be counted. Moreover, the integral would become divergent if the limits were taken as 0 and l . It must be observed that in this expression — similarly as in the case of the expression considered in the text — the E -factors connected with the contacts at 0 and A have not yet been inserted.

It will appear from form. (63) that the order of magnitude of Ψ is: Δ^2/J^2t . The order of magnitude of Ψ_3 comes out as: $(\Delta^2/J^2t) \cdot (\Delta/J^{2/3}t^{1/3})$. Hence with increasing t the number of cases with three points of contact can be neglected in comparison with the number of cases presenting two points of contact.

When the various terms are collected, the final result becomes:²⁰⁾

$$(55) \quad \frac{1}{l} \frac{dl}{dt} = \frac{l}{2\delta^3 t^3} \int_0^\infty dl_0 \int_0^\infty dl_1 \int_{-\infty}^{+\infty} dm (l_0 + l_1) l_0 l_1 E_I \Psi_0 \Psi_1 E_{II}.$$

Comparison with formula (50) gives:

$$(56) \quad \frac{1}{l} \frac{dl}{dt} = \frac{1}{2t} f_0 \overbrace{\tau_i + \tau_{i+1}}^* ,$$

which confirms eq. (65) of the paper of 1950 (*l.c.* p. 406).

At the same time we have obtained the integral equation (53) for the function $\Psi(l, S)$, which will find application in section 8 (V).

(to be continued)

²⁰⁾ The same method of calculation can be applied to the derivative with respect to t of eq. (33). It is then found that an extra factor l_0 appears in the part depending on $\partial E(\alpha_{II})/\partial t$; an extra factor l_1 in the part depending on $\partial E(\alpha_I)/\partial t$; and an extra factor $(l_0 + l_1)$ in the part depending on $\partial \Psi/\partial t$. It follows that the final result will be zero, as it must be, since the quantity on the left hand side of (33) is a constant.

STATISTICAL PROBLEMS CONNECTED WITH THE SOLUTION OF
A SIMPLE NON-LINEAR PARTIAL DIFFERENTIAL EQUATION.
— CONTINUATION. III

BY

J. M. BURGERS

(*Mededeling No. 78 uit het Laboratorium voor Aero- en Hydrodynamica der Technische Hogeschool te Delft*)

(Communicated at the meeting of June 26, 1954)

8. *Properties of the function $\Psi(l, S)$.* — As stated in section 5 (II) the function $\Psi(l, S)$ is defined as the density at the point $l, S + \Delta - \Delta_1$, for unit discharge at the point 0, $\Delta - \Delta_1$, calculated from the diffusion equation (18) with the boundary condition

$$\psi = 0 \text{ on } s = s_b = (\eta^2 - \eta l) / 2t + S\eta / l + \Delta,$$

which represents an “absorbing barrier”.

(I) *Similarity rules.* — It is possible to introduce non-dimensional variables with the aid of the transformation:

$$(57) \quad \left\{ \begin{array}{ll} \eta = \eta_* J^{1/3} t^{2/3} & s = s_* J^{2/3} t^{1/3} \\ l = l_* J^{1/3} t^{2/3} & S = S_* J^{2/3} t^{1/3} \\ \delta = \delta_* J^{1/3} t^{2/3} & \Delta = \Delta_* J^{2/3} t^{1/3} \end{array} \right.$$

It is then found that both t and J disappear from the equations. Hence all results can be intrinsically dependent only on the dimensionless variables:

$$l_*, S_*, \Delta_*.$$

For moderate or small values of Δ , which make Δ_* of the order $t^{-1/3}$ and δ_* of the order $t^{-2/3}$, it is found that these quantities occur only as factors, which drop out from the final results. It thus appears that the mean value \bar{l} of l will be given by an expression of the form:

$$(58) \quad \bar{l} = \bar{l}_* J^{1/3} t^{2/3},$$

where \bar{l}_* is the mean value of l_* . Hence \bar{l} increases proportionally with $t^{2/3}$.

This result proves that the “turbulence” exhibited by the model asymptotically satisfies a similarity rule, in which appear as parameters the time t and the integral J of the correlation function (the latter referring to the family of initial states, and at the same time representing a constant for the family of solutions).

(II) *Dependence of the function $\Psi(l, S)$ on S .* — The following substitutions are made:

$$(59) \quad \begin{cases} \eta = \eta_1; & s = s_1 + S\eta_1/l; \\ \psi = \psi_1 \exp \{ -(2Ss_1l + S^2\eta_1)/4Jl^2 \}. \end{cases}$$

It is then found that the new function ψ_1 satisfies the equation:

$$(60a) \quad \frac{\partial \psi_1}{\partial \eta_1} = J \frac{\partial^2 \psi_1}{\partial s_1^2},$$

with the boundary condition:

$$(60b) \quad \psi_1 = 0 \quad \text{on} \quad s_1 = s_{1b} = (\eta_1^2 - \eta_1 l)/2t + \Delta.$$

Hence ψ_1 is independent of S .

At the point A ($\eta_1 = l$, $s_1 = 0$) one obtains $\psi = \psi_1 \cdot \exp(-S^2/4Jl)$; consequently:

$$(61) \quad \Psi(l, S) = \Phi(l) \cdot \exp(-S^2/4Jl),$$

where $\Phi(l)$ is independent of S .

This result gives a confirmation of equation (29).

(III) *Approximations for $\Phi(l)$.* — Thus far no exact solution of the diffusion equation with an arbitrary parabolic boundary has been derived. An approximation can be obtained when the parabola is represented by means of a chain of straight segments. The calculations, however, become rather involved when more than two segments are used.

In the case where the symmetrical parabola ($S=0$) is replaced by an isosceles triangle formed by two straight segments of inclination b , the following result is obtained:

$$(62) \quad \Phi(l) = \frac{\Delta_1^2}{2\sqrt{\pi J^3 l^3}} B(\beta),$$

where

$$(62a) \quad B(\beta) = (1 + 2\beta^2) (1 - \text{Erf } \beta) - \frac{2}{\sqrt{\pi}} \beta \exp(-\beta^2);$$

$$(62b) \quad \beta = \frac{1}{2} b \sqrt{l/J}.$$

An upper and a lower bound for Φ are found by taking as limiting values for b :

$b_1 = l/4t$ (triangular boundary just inside the parabola: absorption too small); and

$b_2 = l/2t$ (triangular boundary just outside the parabola: absorption too large).

Since $B(\beta)$ becomes practically zero for $\beta \approx 3$, it is evident that Φ will be zero for $l > 8.3J^{1/3}t^{2/3}$ and probably already for smaller values of l .

With a slight change of notation we shall write $B(\beta) = \chi(l_*)$, where $l_* = l/J^{1/3}t^{2/3}$, so that:

$$(63) \quad \Phi = \frac{J_1^2}{2 \frac{1}{\pi} J^2 t} \frac{\chi(l_*)}{l_*^{3/2}}.$$

It can be assumed that the function $\chi(l_*)$ admits the following development for small values of l_* :

$$(64) \quad \chi(l_*) = 1 - a_1 l_*^{3/2} + a_2 l_*^3 - a_3 l_*^{9/2} + \dots$$

Making use of the approximate expression for $B(\beta)$ given in (62a) and having regard to the two limiting values for b , it is found that the coefficient a_1 in the series (64) must lie between the limits $\pi^{-1} = 0,564$ and $\frac{1}{2}\pi^{-1} = 0,282$.

(IV) *Absorbing boundary deviating only very slightly from a straight line.* — In this case a solution for the function Φ can be found with either one of the following two methods:

(a) The boundary is replaced by a chain of straight segments; for each segment an exact calculation is possible, based on the particular solution

$$\psi(\eta, s) = \frac{1}{2\sqrt{\pi J \eta}} \left[\exp \frac{-(s-s_1)^2}{4J\eta} - \exp \left\{ \frac{-(s+s_1)^2}{4J\eta} + \frac{\alpha s_1}{J} \right\} \right],$$

which gives $\psi = 0$ for $s = \alpha\eta$. In combining the results appertaining to the various segments the terms independent of the inclination and the terms of the first degree in the inclination are retained; terms of higher degree are rejected. The various correction terms can now be easily summed.

(b) The following transformation is applied:

$$\eta = \eta_1; \quad s = s_1 + s_b(\eta).$$

Equation (18) then takes the form:

$$\frac{\partial \psi}{\partial \eta_1} - J \frac{\partial^2 \psi}{\partial s_1^2} = \alpha(\eta_1) \frac{\partial \psi}{\partial s_1},$$

where $\alpha(\eta_1)$ has been written for $ds_b/d\eta$. The boundary condition becomes $\psi = 0$ for $s_1 = 0$. Since α is supposed to be very small, one can substitute the solution ψ_0 obtained for a straight boundary for ψ on the right hand side. The equation can then be used to find a correction, depending on $\alpha(\partial\psi_0/\partial s_1)$ as a system of known sources.

Both methods lead to the following result:

$$(65) \quad \Phi = \psi_0 - \int_0^l d\eta_1 \int_0^\infty ds_1 \alpha(\eta_1) \frac{\partial \psi_0}{\partial s_1} K(l - \eta_1; s, s_1),$$

where

$$K(\eta; s, s_1) = \frac{1}{2\sqrt{\pi J \eta}} \left\{ \exp \frac{-(s-s_1)^2}{4J\eta} - \exp \frac{-(s+s_1)^2}{4J\eta} \right\};$$

$$\psi_0 = \frac{s \cdot J_1}{2\sqrt{\pi J^3 \eta^3}} \exp \frac{-s^2}{4J\eta}.$$

In the final result s must be put equal to Δ_1 . This formula is valid for a boundary of arbitrary form, provided the inclination is everywhere small.

In the case of the parabolic boundary $s_b = (\eta^2 - \eta l)/2t$ the final result becomes:

$$(66) \quad \Phi = \frac{\Delta_1^2}{2\sqrt{\pi}l^{3/2}} \left(1 - \frac{\sqrt{\pi}}{4} l^{3/2} + \dots \right).$$

This is of the general form (63), and it is found that the correct value of the coefficient of the first term in (64) is: $a_1 = \sqrt{\pi}/4 = 0,443$.

(V) *Application of the integral equation* (53). — When the expression (63) is substituted into the integral equation (53), the following result is obtained, where the variables are the dimensionless variables introduced in (57), the asterisks having been dropped for convenience:

$$(67) \quad n_1 n_2^2 \int_0^l d\eta \frac{\chi(\eta)\chi(l-\eta)}{\sqrt{\eta(l-\eta)}} \exp \frac{-l\eta(l-\eta)}{16} = -\frac{8\sqrt{\pi}}{3} \frac{\chi'(l)}{\sqrt{l}},$$

with $\chi'(l) = d\chi/dl$. It will be found in section 9 (II) that $n_1 n_2^2$ must be equal to 1. With this value the equation gives:

$$\pi - \frac{8}{3} a_1 l^{3/2} + \left(\frac{5\pi}{8} a_2 + \frac{1}{6} a_1^2 - \frac{\pi}{128} \right) l^3 - \dots =$$

$$-\frac{8\sqrt{\pi}}{3} \left(\frac{3}{2} a_1 - 3a_2 l^{1/2} + \frac{9}{2} a_3 l^3 - \dots \right),$$

from which:

$$a_1 = \sqrt{\pi}/4 = 0,443;$$

$$a_2 = 1/12 = 0,083;$$

$$a_3 = 7\sqrt{\pi}/1536 = 0,0081.$$

The result for a_1 checks with the result deduced from the calculations referring to a boundary with very small slope.

The series can be used only for small values of l .

9. *Approximations for the function $E(\alpha)$* . — According to section 5 (I) the value of $E(\alpha)$ is defined as the amount not absorbed by the barrier $s = s_b = \alpha\eta + \eta^2/2t + \Delta$ for unit discharge at the point 0, $\Delta = \Delta_1$, calculated with the aid of eq. (18). The same similarity rules apply as in the case of the function $\Psi(l, S)$ and dimensionless variables will be used throughout the present section; for convenience the asterisk is omitted in writing.

(I) *Upper and lower bounds for $E(\alpha)$* . — An upper bound for $E(\alpha)$ can be found by replacing the parabola $s_b = \alpha\eta + \eta^2/2 + \Delta$ by a straight segment $s_b = \alpha_0\eta + \Delta$ of finite length, its endpoint $\eta = l_0$ being situated on the parabola, which requires $\alpha_0 = \alpha + l_0/2$. The absorption in this case is too small. With the notation $y = \frac{1}{2}\alpha l_0^{1/2} + \frac{1}{4}l_0^{3/2}$ the following result is found:

$$(68a) \quad E/\Delta_1 < \left\{ y(1 + \text{Erf } y) + \frac{1}{\sqrt{\pi}} \exp(-y^2) \right\} / l_0.$$

The upper bound obtained in this way can be improved by determining the value of l_0 for which the expression on the right hand side has its minimum value; this leads to numerical calculations, which give upper bounds for E corresponding to various values of α . Also $l_0=1$ gives a useful approximation. Some of the results obtained are:

for positive α :

$$E/\Delta_1 < 1,02\alpha + 2,9/\alpha^2; \text{ and}$$

$$E/\Delta_1 < \alpha + \frac{1}{2} + 2 \exp(-\alpha_1^2/\sqrt{\pi}\alpha_1^2), \text{ where } \alpha_1 = \alpha + \frac{1}{2};$$

for $\alpha=0$: $E/\Delta_1 < 0,848$;

for $\alpha < -5,2$: $E/\Delta_1 \cong 0$.

A lower bound (absorbion too large) is obtained by replacing the parabola by its tangent $s=\alpha\eta+\Delta$ until $\eta=l_0$, followed by another tangent touching the parabola in a point with abscissa $2l_0$ and extending to infinity. The following result is obtained:

$$(68b) \quad E/\Delta_1 > \frac{1}{2}\alpha(1 + \operatorname{Erf} \alpha\sqrt{l_0}/2) + \frac{1}{2}\alpha'(1 - \operatorname{Erf} \alpha'\sqrt{l_0}/2) \cdot \exp(2\alpha l_0^2 + 4l_0^3),$$

where $\alpha' = \alpha + 4l_0$.

The maximum value of the right hand member can be calculated, but it is more convenient to take $l_0=1$. One then obtains:

$$E/\Delta_1 > \alpha + \frac{2}{\sqrt{\pi}} \exp \frac{-\alpha^2}{4} \cdot \left\{ \frac{1}{\alpha^2} - \frac{6}{\alpha^4} - \frac{1}{(\alpha+4)^2} \right\}.$$

(II) *Application of equation (27).* — When written in dimensionless variables eq. (27) takes the form:

$$dE/d\alpha = (n_1/\Delta^2) \int_0^l dl \cdot l \cdot \Psi(l, S) E(\alpha + l).$$

In this equation a series development is substituted for $E(\alpha)$:

$$(69) \quad E(\alpha)/\Delta_1 = \alpha + b_1\alpha^{-2} + b_2\alpha^{-5} + \dots$$

One further has: $S = \alpha l + l^2/2$; hence according to (61) and (63):

$$\Psi(l, S) = \frac{\Delta_1^2}{2\sqrt{\pi}} l^{-3/2} \chi(l) \exp(-z^2),$$

where $z^2 = \alpha^2 l/4 + \alpha l^2/4 + l^3/16$. The integral equation arrived at in this way can be worked out, using z as integration variable, substituting the series (64) for $\chi(l)$ and developing according to inverse powers of α . One obtains:

$$\begin{aligned} & 1 - 2b_1\alpha^{-3} - 5b_2\alpha^{-6} - \dots = \\ & = n_1 n_2^2 \{ 1 + (b_1 - 1 - 8a_1/\sqrt{\pi})\alpha^{-3} + (b_2 - 7b_1 - 8a_1 b_1/\sqrt{\pi} + 15 + 128a_1/\sqrt{\pi} + \\ & \quad + 120 a_2)\alpha^{-6} \dots \}. \end{aligned}$$

This gives:

$$n_1 n_2^2 = 1, \text{ which result is independent of the values of}$$

$$a_1, a_2, \dots, b_1, b_2, \dots;$$

$$b_1 = \frac{1}{3} + 8a_1/3\sqrt{\pi} = 1;$$

$$b_2 = -8.$$

The series (69) evidently can be used only for large positive values of α ; in this domain it fits well between the upper and lower bounds found before. All expressions cease to be valid when α should become of the order $1/\Delta_1$; for $\alpha \rightarrow \infty$ one must have $E(\infty) = 1$.²¹⁾

(III) It has been found that the function $\Psi(l, S)$ carries the factor $\Delta_1^2 = n_2^2 \Delta^2$, while the function $E(\alpha)$ carries the factor $\Delta_1 = n_2 \Delta$. It follows that in an integral like (41) or (44) the integrand (\mathbf{X}_k or \mathbf{Z}_k) has the factor $(n_2 \Delta)^{2k+4}$. The factor δ^{-k-2} before the integral introduces the factor $n_1^{k+2} \Delta^{-2k-4}$. Hence Δ drops out and the only remaining factor is $(n_1 n_2^2)^{k+2}$, which, according to the result obtained above, is equal to unity. It can be checked that no other factor appears in the integrals. The relation $n_1 n_2^2 = 1$ consequently is the only condition to be satisfied by the numbers n_1, n_2 .

10. *Rough evaluation of certain integrals.*— In order to be able to calculate reliable numerical values for the various quantities considered in the preceding pages, it will be necessary to have at one's disposal more accurate data concerning the solution of the diffusion equation with the parabolic boundary. The preparation of such data will be very laborious. It has been thought useful, as an illustration of the nature of the results to be expected, to attempt a rough evaluation on the basis of the provisional data obtained in sections 8 and 9. The main uncertainties in these data refer to the values of the function $\chi(l)$ for large l (this uncertainty makes itself felt in the calculation of higher moments), and to the values of $E(\alpha)$ for α near zero. Some guidance in choosing probable values for χ and E in these domains can be obtained from a consideration of certain relations between integrals, which follow from eqs. (65)–(68) of the paper mentioned in footnote 2) (*l.c.* p. 406) in connection with the results of section 24 of that paper (*l.c.* pp. 726–727). However, it has not been thought worth while to make more than a rough adjustment and in one relation a discrepancy of about $7\frac{1}{2}\%$ has remained.

To shorten notation the following auxiliary functions will be introduced:

$$(70) \quad \left\{ \begin{aligned} Q_1 &= \frac{1}{\Delta_1^2} E\left(\frac{1}{2}l - m\right) E\left(\frac{1}{2}l + m\right) \exp(-m^2 l/4); \\ Q_2 &= \chi(l') \chi(l - l') \exp[-ll'(l - l')/16]; \\ B_* &= \int_{-\infty}^{+\infty} dm Q_1; \quad B_{**} = \int_{-\infty}^{+\infty} dm m^2 Q_1; \\ C_* &= \int_0^l dl' [l'(l - l')]^{-1/2} Q_2 = -\frac{8}{3} \frac{\pi}{l^{-1/2}} \frac{d\chi}{dl}; \\ C_{**} &= \int_0^l dl' [l'(l - l')]^{+1/2} Q_2. \end{aligned} \right.$$

²¹⁾ The approximation used in the first paper quoted in footnote 1), *l.c.* p. 66, form. (58), would correspond to:

$$E/\Delta_1 = \alpha \text{ for } \alpha > 0; \quad E/\Delta_1 = 0 \text{ for } \alpha < 0,$$

in the present notation. This is too crude for the values around $\alpha = 0$ and leads to a result for \bar{l} which now appears to be too large; compare section 10 (I).

Making use of the relation $n_1 n_2^2 = 1$ and writing $N = \bar{l}/2\sqrt{\pi}$, we then find: ²²⁾

$$(71a) \quad 1 = N \int_0^\infty dl \, l^{-1/2} \chi B_*$$

$$(71b) \quad \bar{l} = N \int dl \, l^{1/2} \chi B_*$$

$$(71c) \quad (1 + \omega) \cdot (\bar{l})^2 = \bar{l}^2 = N \int dl \, l^{3/2} \chi B_*$$

$$(71d) \quad (1 + \omega^*) \cdot (\bar{l})^3 = \bar{l}^3 = N \int dl \, l^{5/2} \chi B_*$$

$$(71e) \quad \tilde{\omega} \cdot (\bar{l})^3 = N \int dl \, l^{1/2} \chi B_{**}$$

$$(72a) \quad f_0 = -\frac{4}{3} N \int dl \, l^{-1/2} \frac{d\chi}{dl} B_*$$

$$(72b) \quad F_1 = f_0 \overline{(\tau_i + \tau_{i+1})}^* = -\frac{4}{3} N \int dl \, l^{1/2} \frac{d\chi}{dl} B_*$$

$$(72c) \quad F_2 = f_0 \overline{(\tau_i + \tau_{i+1}) \tau_i \tau_{i+1}}^* = \frac{N}{2\sqrt{\pi}} \int dl \, l C_{**} B_*$$

$$(72d) \quad F_3 = f_0 \overline{(\tau_i + \tau_{i+1})^2 \tau_i \tau_{i+1}}^* = \frac{N}{2\sqrt{\pi}} \int dl \, l^2 C_{**} B_*$$

The relations expected in consequence of the results of the paper of 1950 are:

$$(73) \quad \begin{cases} F_1 = 4/3; \\ F_2 = (2/3) (1 + \omega) \cdot (\bar{l})^2; \\ F_3 = (8/9) (1 + \omega^*) \cdot (\bar{l})^3 = (16/3) \tilde{\omega} \cdot (\bar{l})^3. \end{cases}$$

The first one of these relations requires:

$$(74) \quad \int dl \, l^{-1/2} \chi B_* = - \int dl \, l^{1/2} \frac{d\chi}{dl} B_* = 2 \int dl \, l^{1/2} \chi \frac{dB_*}{dl};$$

while the relation $1 + \omega^* = 6 \tilde{\omega}$ requires:

$$(75) \quad \int dl \, l^{5/2} \chi B_* = 6 \int dl \, l^{1/2} \chi B_{**}.$$

In working out the numerical integrations $\chi(l)$ has been calculated from formula (62a) for $B(\beta)$ with $\beta = 0,190 \, l^{3/2}$. This is not very accurate for small values of l , for which the proper coefficient would have been $\pi/16 = 0,1964$; it was thought, however, that with the latter coefficient $\chi(l)$ decreased to zero too rapidly for large l . The circumstance that apparently the value of $1 + \omega^*$ still comes out too low, seems to point out that the proper behaviour of the function for large l has not yet been attained.

²²⁾ To obtain the results (71a)–(71e) substitute $S = l m$ in formula (34), making $dS = l dm$.

The values adopted for the function $E(\alpha)$ are as follows:

$\alpha \leq -3,5 : E/\Delta_1 = 0$		$\alpha = +1,5 : E/\Delta_1 = 1,78$	
$\alpha = -3$	0,005	2	2,22
- 2,5	0,015	2,5	2,67
- 2	0,03	3	3,12
- 1,5	0,08	3,5	3,58
- 1	0,18	4	4,06
- 0,5	0,36	4,5	4,55
0	0,62	5	5,04
+ 0,5	0,96	5,5	5,53
1	1,36	6	6,03.

The following values have been obtained for B_* :

$l = 0 : B_* = 1,04$
1 2,08
2 3,66
3 5,72
4 8,16
5 10,82
6 13,68.

Intermediate values have been derived by means of graphical interpolation. — Values of B_{**} likewise have been calculated, while also some rough values for the function C_{**} have been obtained.

The results are as follows: ²³⁾

(I) *Value of \bar{l} .* — From (71a) we obtain: $N=1/3,86$; this gives

$$\bar{l} = 2N \sqrt{\pi} = 0,92.$$

At the same time (71b) gives:

$$\bar{l} = 3,57 N = 0,925.$$

The approximate equality of these two values is a check that the condition $n_1 n_2^2 = 1$ is satisfactory.

In dimensional variables we obtain:

$$\bar{l} = 0,92 J^{1/3} t^{2/3}.$$

This is markedly lower than the value estimated in the preceding communication, *l.c.* p. 167, eq. (28), which gave $\bar{m}L = \bar{l} = 1,8 (2J)^{1/3} t^{2/3}$. The difference will mainly be due to the unsatisfactory approximation previously used for the function $E(x)$, which made $B_*(0) = 0$, so that the smaller values of l received too little weight (compare footnote 21).

(II) There is further obtained:

$$(71c) \quad \dots \quad (1 + \omega) \cdot (\bar{l})^2 = 6,22/3,86 = 1,61; \quad 1 + \omega = 1,90$$

$$(71d) \quad \dots \quad (1 - \omega^*) \cdot (\bar{l})^3 = 13,96/3,86 = 3,62; \quad 1 - \omega^* = 4,64$$

$$(71e) \quad \dots \quad \bar{\omega} \cdot (\bar{l})^3 = 2,51/3,86 = 0,65; \quad \bar{\omega} = 0,835.$$

²³⁾ The decimals given in the results do not indicate an order of accuracy; they have been retained as they came out of the graphical integrations since they were convenient in making comparisons.

Since $6\tilde{\omega}=5,0$, there is a discrepancy of about $7\frac{1}{2}\%$ with the value found for $1+\omega^*$.

(III) Formula (72b) gives:

$$F_1 = (4/3) 3,88/3,86 \cong 4/3,$$

which is the required result.

Formula (72c) gives:

$$F_2 = 14,86/(2\sqrt{\pi} \cdot 3,86) = 1,09,$$

while $(2/3) (1+\omega) \cdot (\bar{l})^2 = 1,07$.

Formula (72d) gives:

$$F_3 = 47,6/(2\sqrt{\pi} \cdot 3,86) = 3,48,$$

while $(16/3) \tilde{\omega} \cdot (\bar{l})^3 = 3,47$.

These three checks come out fairly well. Apparently it is only the value of $1+\omega^*$, depending on the highest power of l in the integrand, which is in error.

Formula (72a) finally gives $f_0 \cong 0,86$.

THE DEHYDRATION OF ALUMINA HYDRATES. II

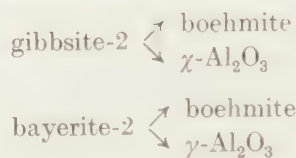
BY

J. H. DE BOER, J. M. H. FORTUIN AND J. J. STEGGERDA

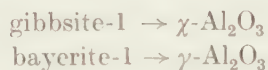
(Communicated at the meeting of June 26, 1954)

1. *Introduction*

In a previous paper ¹⁾ we have shown that the trihydrates of alumina, viz. gibbsite and bayerite, can exist in two forms differing in their behaviour during dehydration. On dehydration at about 250° C some specimens of gibbsite and bayerite give a mixture of boehmite and an anhydrous alumina. We shall indicate such specimens by the figure 2 behind the name:



Other samples of gibbsite and bayerite give only one of the forms of anhydrous alumina on dehydration, we shall indicate these samples with the figure 1:



In this paper we shall give recipes for the preparation of the trihydrates 1 and 2 and show how these samples can be converted into each other. The results of density measurements in water, helium and mercury are given in the last sections.

2. *Preparation of the trihydrates*

Gibbsite-1 is the product formed when a concentrated sodium-aluminate-solution (130 g $\text{Al}(\text{OH})_3$ and 180 g NaOH per liter) is exposed to the air at room temperature during a sufficiently long time, e.g. about three months. After that time the precipitate is filtered, washed with 4n HCl and with water, and dried at 120° C. X-ray analysis shows it to be gibbsite. It dehydrates to $\chi\text{-Al}_2\text{O}_3$ at 200–225° C. A differential thermal analysis confirms this one-step dehydration mechanism (see fig. 1).

Gibbsite-2 is the product of the usual "Bayer process", it precipitates when CO_2 is bubbled into a concentrated sodium aluminate solution at

¹⁾ J. H. DE BOER, J. M. H. FORTUIN and J. J. STEGGERDA, Proc. Kon. Ned. Ak. Wet. B57, 170 (1954).

80–90° C. The dehydration mechanism of this gibbsite-2 is discussed in detail in our previous communication ¹⁾.

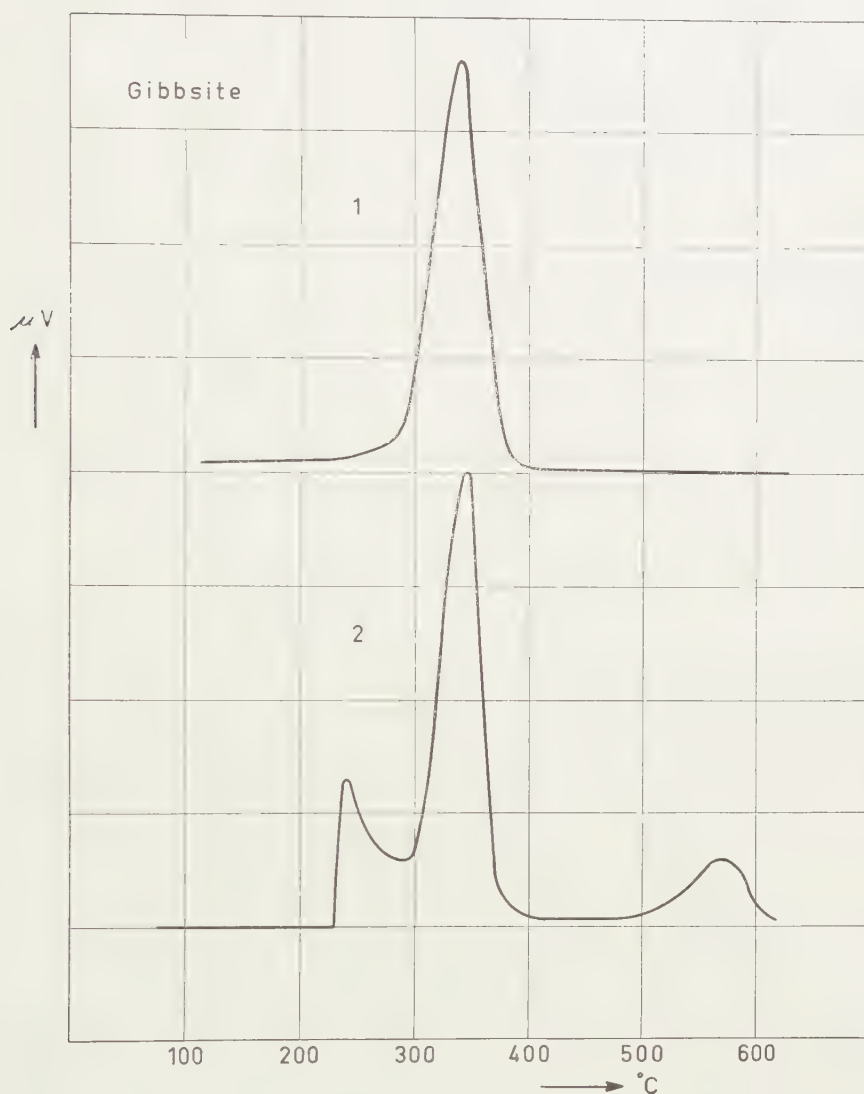


Fig. 1. Differential thermal analyses of (1) gibbsite-1; (2) gibbsite-2

Bayerite-1 can be prepared in the following ways:

- 1) By the action of water on amalgamated aluminium at room temperature ²⁾.
- 2) By precipitation with NH_3 of an Al-sulfate solution at room temperature ³⁾.

¹⁾ See note on foregoing page.

²⁾ H. SCHMÄH, Z. Naturforsch. 1, 323 (1946).

³⁾ H. KRANT, E. FLAKE, W. SCHMIDT and H. VOLMER, Ber. 75, 1357 (1942).

- 3) By passing CO_2 into a sodium aluminate solution (65 g $\text{Al}(\text{OH})_3$ and 90 g NaOH per liter) at room temperature. The precipitate must be filtered off after 4-5 hours, washed and dried at 120°C .

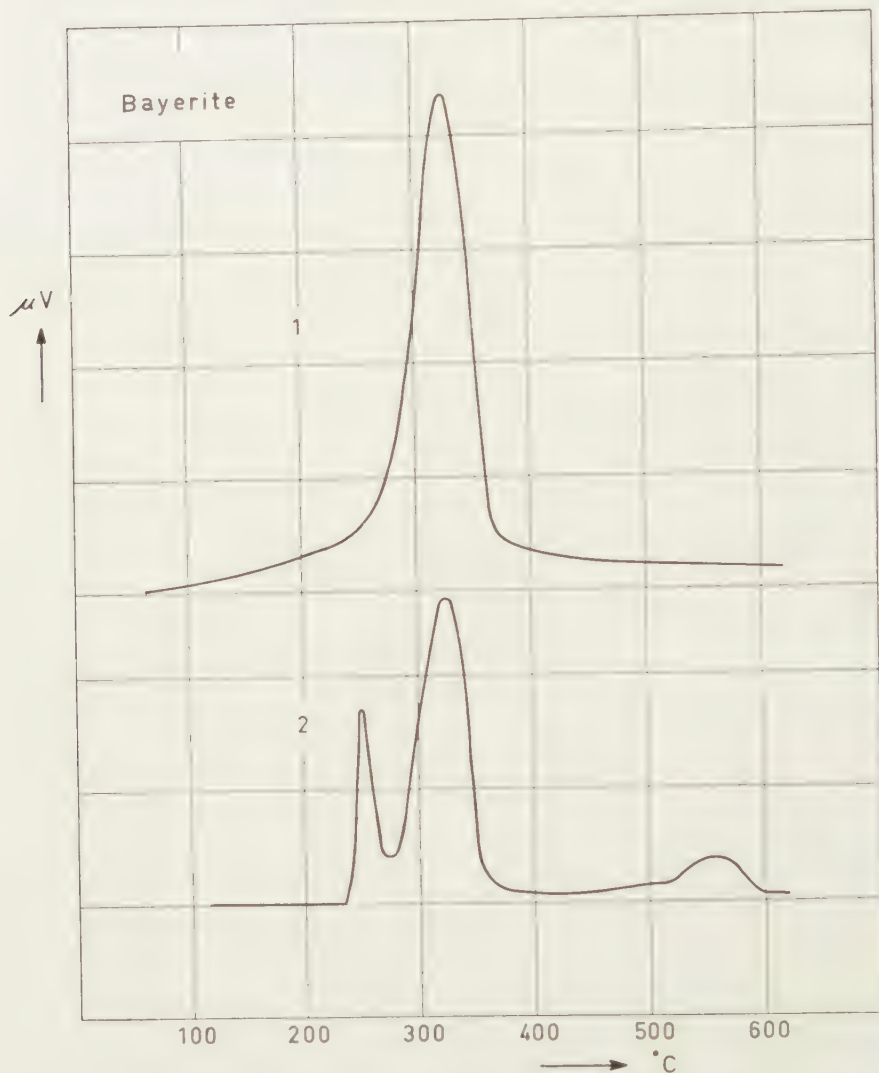


Fig. 2. Differential thermal analyses of (1) bayerite-1; (2) bayerite-2

Bayerite-2 is already described in our previous paper. It can be prepared by slow action of CO_2 (three weeks' exposure to the air) on an alkaline solution of *potassium* *) aluminate at room temperature. This method, however, is very sensitive to concentration and time variations, often the bayerite is partially converted into gibbsite.

The next recipe leads to bayerite-2 in a much faster and easier way:

*) In our previous communication we stated, erroneously, that sodium aluminate was used.

CO_2 is bubbled into a solution of 65 g $\text{Al}(\text{OH})_3$ and 90 g NaOH per liter at 50°C . The precipitate is filtered off after $3\frac{1}{2}$ –4 hours, washed with water and dried at 120°C .

The dehydration mechanism of the various samples can be controlled by X-ray and differential thermal analyses. Some results are given in figs 1 and 2. The X-ray patterns of $\chi\text{-Al}_2\text{O}_3$ (from gibbsite-1 heated at 300°C) and of $\gamma\text{-Al}_2\text{O}_3$ (from bayerite-1 heated at 300°C) are given in fig. 4.

3. *Influence of the size of the granules **)*

As a logical consequence of the hypothesis of intragranular hydrothermal conditions, the granule size may be expected to have an influence on the ratio in which boehmite and the anhydrous oxide are formed on dehydration. It was, indeed, found that this ratio decreases considerably when the size of the granules of gibbsite-2 and bayerite-2 is decreased by grinding. The differential thermal analysis of gibbsite-2, with a granule size of 150–175 μ and of the same sample ground to 5–10 μ in an agate mortar, are given in fig. 3. X-ray analyses fully confirm the results of the differential thermal analyses.

4. *The effect of sodium*

Owing to the method of preparation the alumina trihydrates may contain some traces of sodium. The effect of such small traces of sodium on the dehydration mechanism could be proved by the following experiments. If bayerite-2 is treated with 4n HCl , the relative amount of boehmite, formed on dehydration, decreases. When the HCl treatment is continued for several hours, we obtain a product (still bayerite) which on heating to 250°C gives only $\gamma\text{-Al}_2\text{O}_3$. It appears, therefore, that we have converted bayerite-2 into bayerite-1 by treatment with HCl .

When bayerite-1, prepared from bayerite-2 by an HCl -treatment, is treated with a saturated Na_2CO_3 solution for some hours, it is again transformed into bayerite-2. Neither the acid nor the soda treatment change the size of the granule or the X-ray pattern of the bayerite.

The samples of bayerite-1, prepared according to one of the methods described under section 2, do not show this 1 \longrightarrow 2 transformation when treated with soda. The granule size of these bayerites is far smaller than that of the bayerite-1, formed from an original bayerite-2.

From these experiments it seems as if a certain minimum size of the granules and the presence of a trace of sodium are the necessary conditions for the formation of boehmite on dehydration.

**) We shall use the expression "granule" throughout in this article, thus indicating the individual "particle" of the powder. Each granule may consist of an agglomeration of smaller "particles", glued together to form the granule; these smaller "particles" may be individual "crystallites". On grinding we may assume to break the granule up into smaller units, but we do, probably, not decrease the size of the crystallites, which in the case of alumina hydrates are very hard indeed.

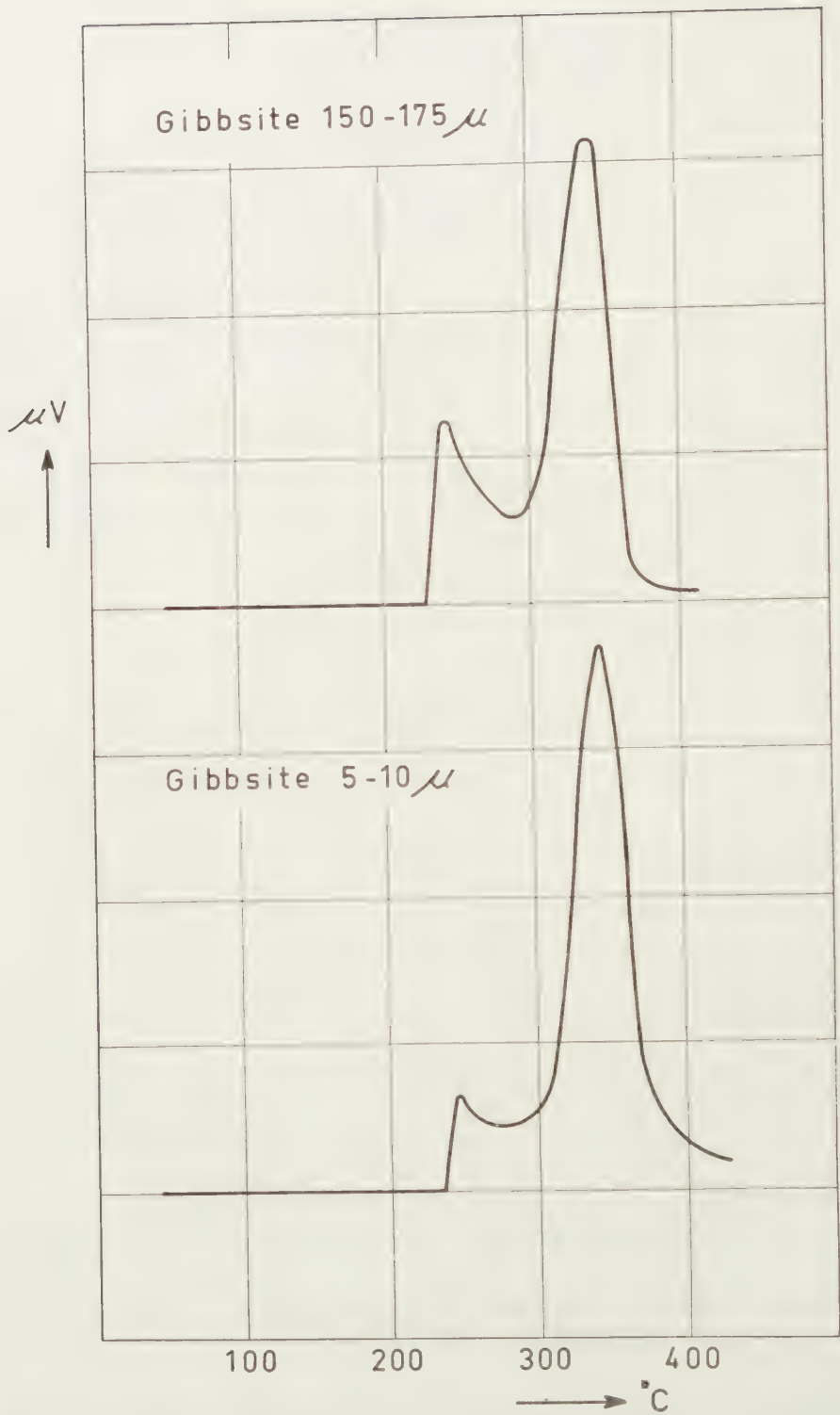


Fig. 3. Differential thermal analyses of (1) gibbsite with granule size 150-175 μ ;
(2) the same product to ground 5-10 μ

5. *The densities and specific volumina of gibbsite-2 and its dehydration products*

The densities of some samples, obtained by partial dehydration of gibbsite-2 were determined in water, helium and mercury. For a clear understanding of the results it is necessary to define the following expressions:

- a) The specific true volume is the volume of the solid substance, without intra- and intergranular space, per unit of mass (gram).
- b) The specific granule volume is the volume of the granules, including their intragranular spaces, per gram.
- c) The specific bulk volume is the volume of the powder per gram, included intra- and intergranular spaces.
- d) The true density, the granule density and the bulk density are the reciprocal values of the corresponding specific volumes.

We assumed that the densities measured in helium and in water would fairly approximate the true density of the sample. The density, measured in mercury at 1 atm. gives the granule density, provided the granule size be at least 125 μ .

The densities in water were measured in a pycnometer, after the sample had been degassed at 15 mm Hg and room temperature. To avoid serious rehydration the determination must be finished within one hour.

The densities in helium were measured on 20 g samples after degassing at 10^{-4} mm Hg and 100° C ***). Neither the time nor the temperature of degassing, provided the latter was at least 100° C lower than the dehydration temperature of the sample, exerted an influence on the results.

The densities in mercury were measured on samples with granule sizes between 125 and 175 μ . After degassing at room temperature, the mercury was admitted to the sample, paying careful attention that the mercury penetrated into all intergranular spaces.

The bulk densities were measured in the usual way in 2 cm³ tubes, after vibrating to attain the closest possible stacking of the granules.

The results of the density measurements are plotted as a function of the water content of the samples (calculated on anhydrous Al₂O₃) in figure 5.

The volumes per gram of anhydrous alumina V_0 can be calculated by the relation:

$$V_0 = \frac{1+a}{d},$$

where 100 a is the percentage of water, and d is the corresponding density of the sample.

The volumes in water, helium and mercury, and the bulk volume, all per gram anhydrous alumina, are plotted as a function of 100 a in figures 6 and 7.

***) We thank Mr P. ZWIETERING of the Central Laboratory of Staatsmijnen (Neth. State Mines) for his help in the helium density measurements.

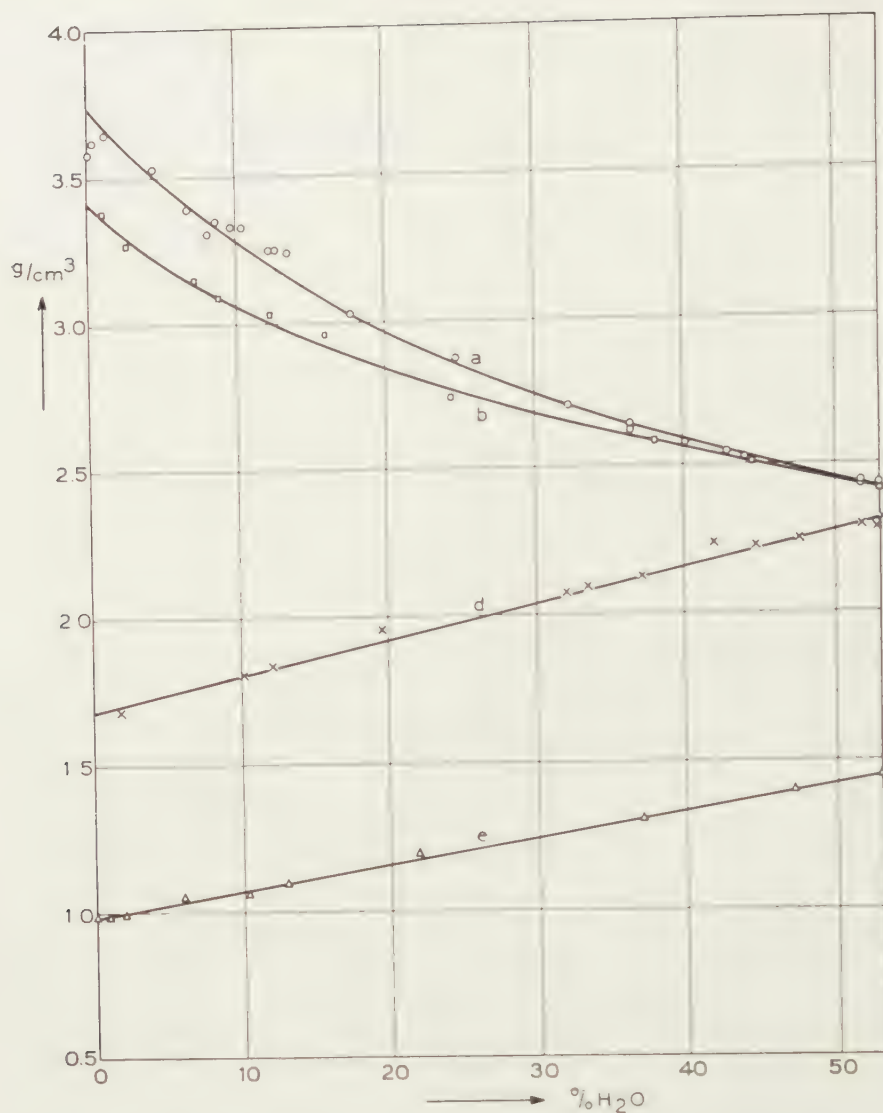
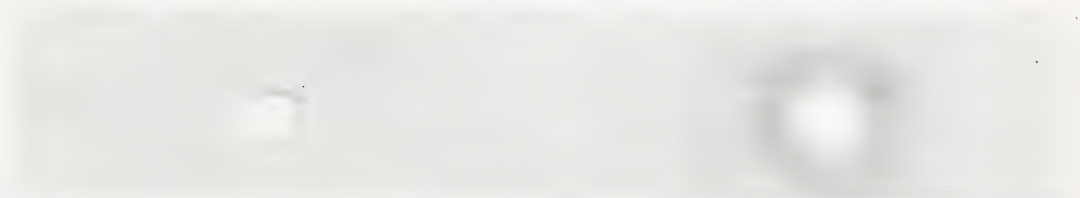


Fig. 5. Densities as a function of the water content, calculated on anhydrous Al_2O_3 . Density measurements: a) in water; b) in helium; d) in mercury; e) bulk densities

The curves *d* and *e* give the granule and the bulk volume respectively per gram anhydrous Al_2O_3 . Both volumes are nearly constant: the shrinking of the granules is not more than 10 % over the whole range of dehydration.

The volumes measured in water fit quite well the straight line drawn through three points corresponding with the volumes per gram anhydrous alumina, of:

- 1) pure gibbsite
- 2) pure boehmite, made by autoclaving gibbsite at 300° C, and
- 3) $\gamma\text{-Al}_2\text{O}_3$ (volume calculated from X-ray data).



(1)



(2)

Fig. 4. X-ray pattern of (1) γ - Al_2O_3 ; (2) χ - Al_2O_3

We can describe any sample obtained by partial dehydration of gibbsite as a mixture of (chemically bound) water with a specific volume of $0.68 \text{ cm}^3/\text{g}$ and Al_2O_3 with a specific volume of $0.27 \text{ cm}^3/\text{g}$.

The volumes measured in helium lay also on a straight line. It is a very remarkable fact, however, that these volumes are greater than the volumes measured in water.

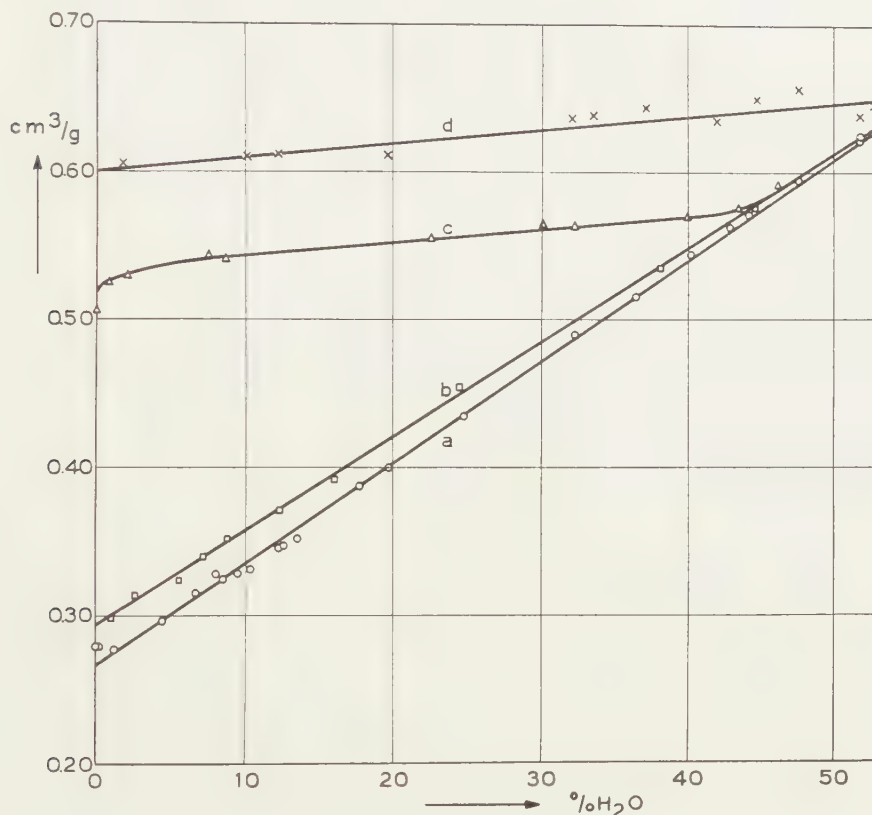


Fig. 6. Volumes per gram anhydrous Al_2O_3 as function of the water content, calculated on anhydrous Al_2O_3 , determined: a) in water; b) in helium; d) in mercury; c) in water, after filling the capillaries with water at 98 % R.H.

We have used also the following procedure for measuring the granule volumes. The intragranular spaces (the capillaries) were filled with water, by exposing the sample during one week at a relative humidity of 98 %. The density in water and the water content of the sample were determined and the volume per gram of anhydrous alumina calculated. These volumes are plotted as a function of the original water content of the sample (curves c in figures 6 and 7). The differences between these volumes and those determined with mercury make it clear that there are capillaries in which, at 1 atm., Hg cannot penetrate, and which can neither be filled by capillary condensation of water at 98 % R.H. The diameters of these

capillaries must therefore be 0.1 to $5\ \mu$. These small bursts in the granule structure will be formed by the high intragranular water pressure at the end of the first step of the dehydration or rather at the end of the conversion of gibbsite into boehmite. After the formation of these bursts the hydrothermal conditions cease to exist and no more bursts will be formed. The volume, which, at this moment, corresponds with the distance

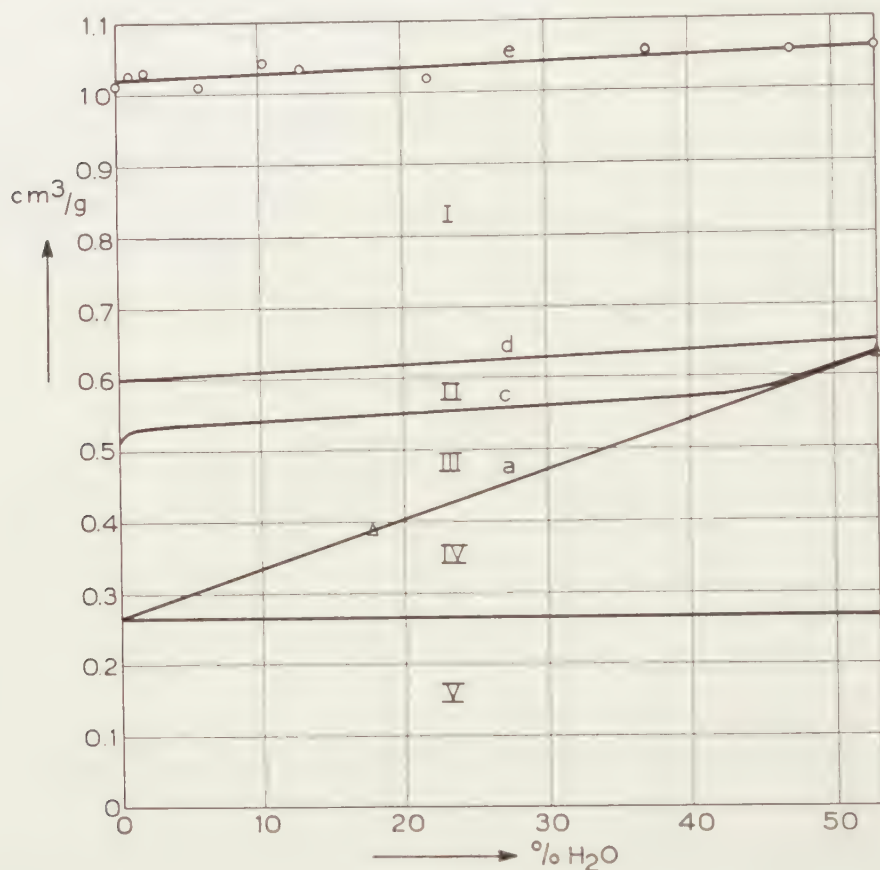


Fig. 7. Volumes per gram anhydrous Al_2O_3 as a function of the water content, calculated on anhydrous Al_2O_3

between the curves c and d , remains constant during the further progress of dehydration.

In figure 7, the distance I (between d and e) corresponds with the intergranular space, II with the volume of the bursts, III with the small intragranular spaces (capillaries), IV with the volume of the chemically bound water and V with the volume of the anhydrous alumina itself.

Acknowledgement

One of us, J. M. H. FORTUIN, gratefully acknowledges a grant from the Delfts Hogeschoolfonds enabling him to contribute to these investigations.

Summary

The influence of the granule size and of the presence of small impurities of sodium on the dehydration mechanism of gibbsite and bayerite are discussed. Density measurements in helium, water and mercury give new information about the dehydration of gibbsite.

*Delft, Laboratory of Chemical Engineering of the
Technological University and Geleen, Staatsmijnen
(Netherlands State Mines) Central Laboratory*

May 1954

ESTERS AND PHOSPHATIDIC ACIDS DERIVED FROM BATYL ALCOHOL (Preliminary communication)

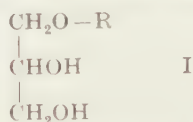
BY

P. E. VERKADE AND L. J. STEGERHOEK

(Laboratory of Organic Chemistry, Technical University, Delft, Netherlands)

(Communicated at the meeting of June 26, 1954)

Several years ago the presence of three glycerol α -*n*-alk(en)yl ethers I (R = univalent hydrocarbon radical) was demonstrated in the unsaponifiable matter left after hydrolysis of the liver oil of various *Elasmobranchii* (sharks, rays, etc.). In these compounds, which have been given the trivial



names of batyl alcohol, chimyl alcohol and selachyl alcohol, the radical R is octadecyl, hexadecyl and *cis*-octadec-9-enyl respectively.

It has subsequently been found that these "alcohols"—properly speaking the substances are glycols—are widely distributed in the animal kingdom; their presence has also been demonstrated, for example, in mammals and in the human body. There is no point in citing the relative literature here. This wide distribution naturally has given rise to investigations on the biological significance of the substances in question, which, however,—at least as far as we are aware—have not so far produced any appreciable results. The literature relating to this work may likewise be left unrecorded here.

On the basis of a simple grouping of the analytical data obtained with an oil investigated by them, *Tsujimoto* and *Toyama*¹⁾ made it clear immediately after their discovery of the compounds concerned that the latter are present in the liver oil of *Elasmobranchii* in the form of esters of higher fatty acids. Later investigations by *André* and *Bloch*²⁾, carried out specially for this purpose, have confirmed this fact. For the "alcohols" of a different origin the same undoubtedly holds good: in fact, here again these compounds were isolated from the unsaponifiable matter left after hydrolysis of lipids. Hitherto, however, no esters of these "alcohols" having higher fatty acids as component acids were known in pure condition.

¹⁾ M. TSUJIMOTO and Y. TOYAMA, Chem. Umschau Fette, Oele, Wachse, Harze 29, 28 (1922).

²⁾ E. ANDRÉ and A. BLOCH, Bull. soc. chim. France (5) 2, 789 (1935).

We have now prepared a number of monoacid and diacid esters of batyl alcohol of perfectly unambiguous constitution, *viz.* those having palmitic acid and stearic acid as component acids. This work had a double purpose. In the first place we wished to demonstrate that the methods for the synthesis of glycerides introduced by one of the present authors ³⁾, can also be successfully applied to the synthesis of esters of glycerol- α -*n*-alk(en)yl ethers. Secondly it appeared desirable to us to make such esters available for biochemical purposes. In fact, we are convinced that it is in general more obvious to inquire after the biological significance of such esters than after that of the "alcohols" on which the latter substances are based.

In addition, continuing the recent work in our laboratory on phosphatidic acids ⁴⁾, we have synthesized some phosphatidic acids derived from batyl alcohol, using a method which leads to products of perfectly unambiguous constitution. We are of the opinion that compounds of this nature also deserve attention from a biological point of view.

These investigations, to be briefly described below,—for a detailed account of the work we refer in advance to the thesis of one of the present authors (L.J.S.) and to papers to be published elsewhere—, concern only model experiments. Hence we have occupied ourselves only with batyl alcohol and indeed only with a racemic product synthesized by us, whereas the batyl alcohol occurring in nature is one of the optical antipodes ⁵⁾. Hence also we have used only palmitic acid and stearic acid as component acids.

Batyl alcohol I ($C_{18}H_{37}$ = octadecyl) was obtained by oxidation of allyl octadecyl ether with performic acid. The method worked out by us gives a yield of 87 % of pure product; this yield is considerably higher than that obtained upon application of the method described by *Kornblum* and *Holmes* ⁶⁾, the best hitherto available in the literature. Rather superfluously we carried out quantitative oxidation experiments with periodic acid in aqueous alcoholic medium; these showed that our batyl alcohol (m.p. 71.2–71.8°) consumed exactly one molecule of periodic acid per molecule of the substance, so that we had indeed to do with pure glycerol α -octadecyl ether; only this isomer contains two vicinal hydroxyl groups.

By the action of palmitoyl chloride or stearoyl chloride on batyl alcohol in the molecular ratio of 2 : 1 in a medium of chloroform and in the presence of an excess of dry pyridine, preferably at a temperature of about 40°, very good yields of *dipalmitoyl-batyl alcohol* (m.p. 53.7–54.3°) and

³⁾ For a survey of these methods, see P. E. VERKADE, *Chimie et Industrie* **69**, 239 (1953).

⁴⁾ See P. E. VERKADE and J. H. UHLENBROEK, *Proc. Kon. Nederl. Akad. Wetenschappen* **55**, 110 (1952) and several later papers in the *Rec. trav. chim.*

⁵⁾ W. H. DAVIES, I. M. HEILBRON and W. E. JONES, *J. Chem. Soc.* **1933**, 165; Y. TOYAMA and T. ISHIKAWA, *J. Chem. Soc. Japan* **59**, 1367 (1938).

⁶⁾ N. KORNBLUM and H. N. HOLMES, *J. Am. Chem. Soc.* **64**, 3045 (1942).

distearoyl-batyl alcohol (m.p. 61.3–62.0°) were obtained. These compounds undoubtedly possess the constitution II (A = acyl). Indeed, the possibility of migration of the octadecyl group from the α - into the β -position under the experimental conditions in question may be left out of account. The α - and also the β -monoalkyl ethers derived from glycerol are highly stable in alkaline and also in acid medium. We do not know of any (mutual) rearrangement of substances of these types.



In agreement with the above the two synthesized compounds of type II could be deacylated to batyl alcohol very readily and in very good yield on treatment with a solution of potassium hydroxide in absolute ethanol according to *Verkade and van der Lee*⁷⁾ or with a solution of sodium methoxide in absolute methanol according to *Zemplén c.s.*⁸⁾.

Apart from possible difficulties of an experimental nature—we are referring, for example, to difficulties encountered in purification by crystallization, owing to low melting point and/or high solubility of an ester—the method here described for the synthesis of *monoacid diesters* of batyl alcohol is universally applicable; esters of this type with an unsaturated fatty acid as component acid are also accessible in this way. The corresponding derivatives of chimyl alcohol, and also of selachyl alcohol, can be obtained in an analogous way.

Upon heating a solution of batyl alcohol and trityl chloride in the molecular ratio of 1:1 in an excess of dry pyridine for 3 hours at about 100°, monotrityl-batyl alcohol of m.p. 57.0–58.0° was obtained in a yield of about 90 %. Considering the well-known behaviour of trityl chloride towards polyhydroxy compounds with both primary and secondary hydroxyl groups⁹⁾, it was highly probable that this compound was α -*monotrityl-batyl alcohol* III (Tri = trityl). Evidence for this constitution was obtained by a synthesis of the same compound starting from the monotrityl-glycerol of m.p. 109–110°, which according to an investigation by *Verkade*¹⁰⁾ is positively the α -monotritylglycerol IV. This compound was treated with potassium in boiling benzene in a nitrogen atmosphere and the monopotassium derivative thus obtained was brought into reaction with octadecyl iodide in the same medium; the yield of this synthesis was about

7) P. E. VERKADE and J. VAN DER LEE, *Rec. trav. chim.* **57**, 417 (1938).

8) G. ZEMPLÉN and E. PACSU, *Ber.* **62**, 1613 (1929); G. ZEMPLÉN, A. KERECs and I. HADÁCSY, *ibid.* **69**, 1827 (1936).

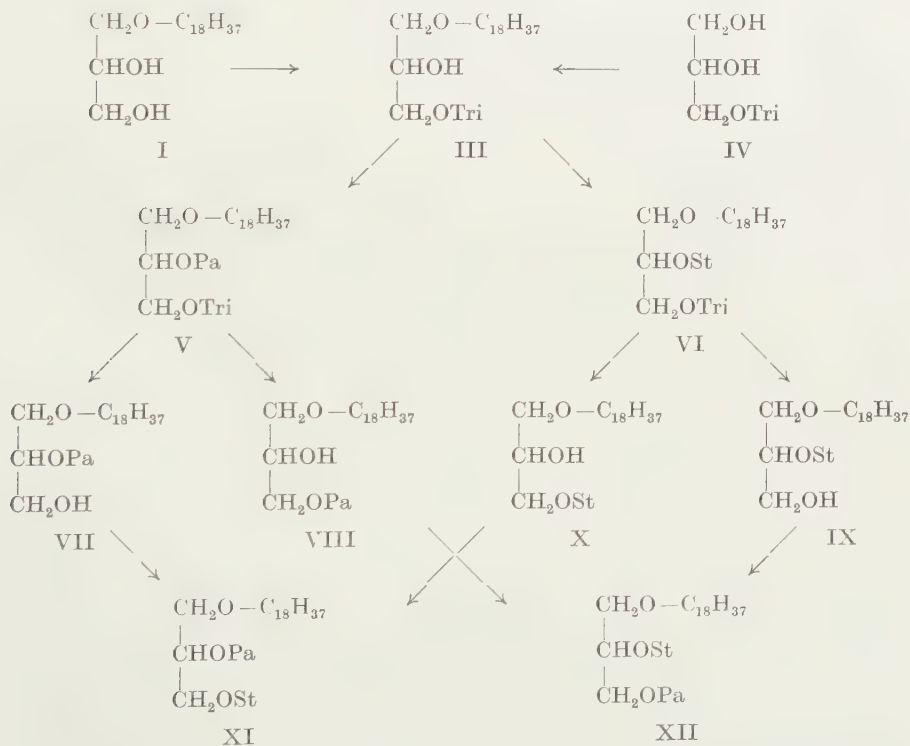
9) See, for example, P. E. VERKADE, J. VAN DER LEE and Miss W. MEERBURG, *Rec. trav. chim.* **56**, 613 (1937).

10) P. E. VERKADE, *Rec. trav. chim.* **57**, 824 (1938).

40 %. The identity of the two substances appeared incontestably upon determination of the mixed melting point.

By the action of palmitoyl chloride or stearoyl chloride on the compound III in the molecular ratio of 1:1 in a medium of chloroform and in presence of an excess of dry pyridine, preferably at a temperature of about 40°, very good yields of α -trityl- β -palmitoyl-batyl alcohol V (m.p. 45.8–46.2°) and α -trityl- β -stearoyl-batyl alcohol VI (m.p. 48.5–49.2°) were obtained. As was to be expected, upon catalytic deacylation of these substances in one of the manners indicated above α -monotrityl-batyl alcohol was formed back in both cases.

Upon detritylation of the compounds V or VI in ethereal or petroleum ethereal solution with gaseous hydrogen chloride according to *Verkade, van der Lee and Miss Meerburg*¹¹⁾ or upon shaking the solution of the compounds mentioned in absolute ethyl alcohol, or preferably in dioxan, at about 40° with hydrogen under slightly more than atmospheric pressure in the presence of a palladium/active carbon ("norit") catalyst according to *Verkade, Cohen and Vroege*¹²⁾, two different compounds were obtained: the two palmitoyl derivatives melted at 65.2–66.0° and 69.3–69.8° respectively, the two stearoyl derivatives at 70.8–71.4° and 72.3–72.6° respectively.



¹¹⁾ P. E. VERKADE, J. VAN DER LEE and Miss W. MEERBURG, *Rec. trav. chim.* **54**, 716 (1935).

¹²⁾ P. E. VERKADE, W. D. COHEN and A. K. VROEGE, *Rec. trav. chim.* **59**, 1123 (1940).

ively. All four compounds gave batyl alcohol upon catalytic deacylation in one of the manners indicated above. The two palmitoyl derivatives, upon being treated in the usual manner with palmitoyl chloride in the molecular ratio of 1 : 1, yielded the dipalmitoyl-batyl alcohol already discussed; starting from the two stearoyl derivatives and stearoyl chloride, the distearoyl-batyl alcohol already discussed was obtained. That these substances represent the two possible isomeric monopalmitoyl-batyl alcohols and monostearoyl-batyl alcohols, and not sets of polymorphic modifications, was already evident from the appearance of distinct melting point ranges upon determination of the mixed melting points.

With regard to the constitution of these isomers the two following facts are of special importance. On heating a solution of the higher melting isomer and trityl bromide in the molecular ratio of 1 : 1 in an excess of dry pyridine for 3 hours at about 100°, the α -trityl- β -acyl-batyl alcohol used as starting material for the preparation of the isomer in question (V and VI respectively) was formed back in a good yield. Under the same experimental conditions the lower melting isomer, however, reacted only slowly with trityl bromide, such with the formation of another trityl derivative, which therefore—it is to be borne in mind that the possibility of migration of the octadecyl group may be left out of consideration—must have the constitution XIII (A = palmitoyl or stearoyl); the latter compounds are therefore β -trityl- α -palmitoyl-batyl alcohol (m.p. 32.0–32.8°) and β -trityl- α -stearoyl-batyl alcohol (m.p. 37.5–38.0°). The higher melting isomers thus contain a free primary hydroxyl group, and are therefore β -monoacyl-batyl alcohols: β -monopalmitoyl-batyl alcohol VII and β -monostearoyl-batyl alcohol IX; the lower melting isomers are α -monoacyl-batyl alcohols: α -monopalmitoyl-batyl alcohol VIII and α -monostearoyl-batyl alcohol X.

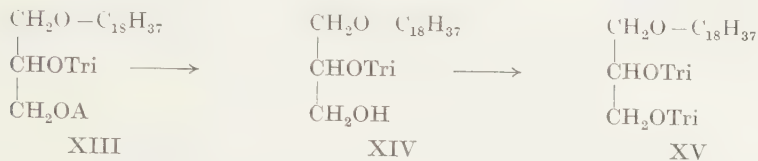
As far as we are aware, this is the first time that trityl bromide has been used for tritylation purposes of the nature in question. The use of this reagent imposed itself, because even the reaction between trityl chloride and the primary hydroxyl group of the compounds VII and IX proved to be very slow.

As was to be expected, the detritylation of α -trityl- β -acyl-batyl alcohols with a fatty acid as component acid—only such compounds have been investigated by us—shows the same characteristics as the detritylation of α -trityl- $\beta\gamma$ -diacylglycerols with such a component acid or with at least such a component acid in the β -position¹³). In the former case, too, detritylation in acid medium leads to migration of the acyl group from the β -position into the α -position which becomes available by the removal of the trityl group, whereas the detritylation with hydrogen in neutral medium proceeds without rearrangement. Verkade and van Lohuizen¹³), and later Martin¹⁴), have shown that with the monoglycerides in acid

¹³) P. E. VERKADE and O. E. VAN LOHUIZEN, Proc. Kon. Nederl. Akad. Wetenschappen 56, 324 (1953).

¹⁴) J. B. MARTIN, J. Am. Chem. Soc. 75, 5483 (1953).

medium mutual rearrangement of the two isomers occurs; in the equilibrium mixture the α -isomer greatly predominates. To our view it is not subject to doubt that with the diglycerides, with the monoacyl-batyl alcohols, etc. a similar equilibrium is established under analogous conditions. We have not yet investigated this problem, but it is on our program.



The β -trityl- α -acyl-batyl alcohols XIII (A = palmitoyl or stearoyl) were obtained in good yield by heating a solution of the corresponding α -monoacyl-batyl alcohol and trityl bromide in the molecular ratio of 1 : 3 in dry pyridine for at least 15 hours at about 100°. Deacylation of these compounds according to Zemplén⁸⁾ gave β -monotrityl-batyl alcohol XIV (m.p. 48.5–49.2°). Tritylation of this compound or the compound III with trityl bromide in the usual way yielded $\alpha\beta$ -ditrityl-batyl alcohol XV (m.p. 70.0–70.8°).

The compounds VIII and X are α -monoesters, the compounds VII and IX are β -monoesters of batyl alcohol. Again apart from possible difficulties of an experimental nature, the method described for the preparation of α -monoesters is applicable to all α -trityl- β -acyl-batyl alcohols containing an easily migrating acid as component acid; this category of acids includes the fatty acids, also the unsaturated fatty acids¹⁵⁾ (oleic acid, linoleic acid, linolenic acid, etc.). The corresponding derivatives of chimyl alcohol and selachyl alcohol can be obtained in the same way. The method described for the preparation of β -monoesters is applicable to all α -trityl- β -acyl-batyl alcohols which do not contain a component acid liable to be reduced under the conditions of the hydrogenolysis; unfortunately, β -monoesters with an unsaturated fatty acid as component acid therefore are not accessible by the method in question. The same applies with regard to β -monoesters of chimyl alcohol. The preparation of β -monoesters of selachyl alcohol by the method concerned is naturally quite out of the question.

Stearoylation of β -monopalmitoyl-batyl alcohol VII and palmitoylation of α -monostearoyl-batyl alcohol X in the usual way produced very good yields of α -stearoyl- β -palmitoyl-batyl alcohol XI (m.p. 52.3–52.8°). Starting from α -monopalmitoyl-batyl alcohol VIII or β -monostearoyl-batyl alcohol IX, α -palmitoyl- β -stearoyl-batyl alcohol XII (m.p. 51.2–52.0°) was obtained. A mixture of equal quantities of these two compounds, whose melting

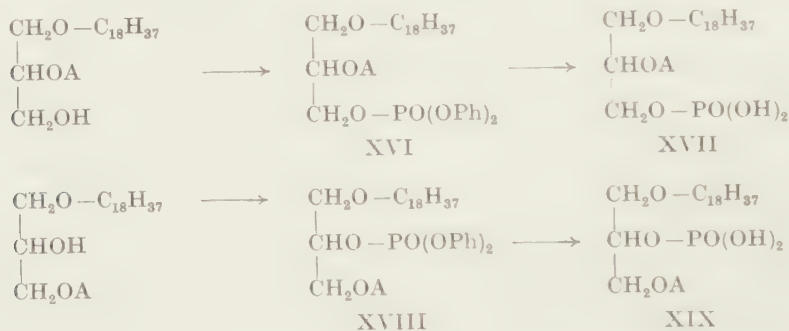
¹⁵⁾ See, for example, B. F. DAUBERT and E. S. LUTTON, J. Am. Chem. Soc. 69, 1449 (1947).

points differ but little, exhibited a clear melting point depression. Upon catalytic deacylation in one of the manners indicated, both compounds yielded batyl alcohol.

The compounds XI and XII are *diacid diesters* of batyl alcohol. Again apart from possible difficulties of an experimental nature, all such esters with two saturated or unsaturated fatty acids as component acids—we are again confining ourselves here to compounds of this kind—are now accessible. The same applies with regard to the corresponding derivatives of chimyl alcohol and selachyl alcohol.

We turned the availability of monoesters of batyl alcohol to account to prepare some *phosphatidic acids* derived from such compounds.

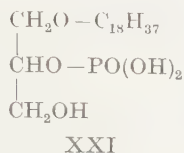
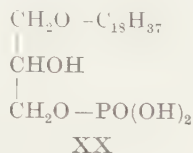
The compounds VII and IX reacted smoothly at about 40° and in the presence of an excess of a tertiary base, for example dry pyridine, with diphenyl phosphorochloridate: very good yields of *β*-palmitoyl-batyl alcohol *α*-phosphoric acid diphenyl ester (m.p. 46.0–46.5°) and *β*-stearoyl-batyl alcohol *α*-phosphoric acid diphenyl ester (m.p. 48.0–49.0°) XVI (A = palmitoyl and stearoyl respectively) were obtained. In the same way the compounds VIII and X produced very good yields of *α*-palmitoyl-batyl alcohol *β*-phosphoric acid diphenyl ester (m.p. 42.5–43.0°) and *α*-stearoyl-batyl alcohol *β*-phosphoric acid diphenyl ester (m.p. 45.5–46.0°) XVIII (A = palmitoyl and stearoyl respectively).



The hydrogenolysis of the phosphatidic acid diphenyl esters was effected by shaking a solution of the compound in dry dioxan at room temperature with hydrogen under slightly more than atmospheric pressure in the presence of a platinum/active carbon ("norit") catalyst according to Uhlenbroek and Verkade¹⁶). We obtained very good yields of the corresponding *α*-phosphatidic acids: *β*-palmitoyl-batyl alcohol *α*-phosphoric acid (m.p. 65.2–65.9°) and *β*-stearoyl-batyl alcohol *α*-phosphoric acid (m.p. 69.8–70.4°) XVII (A = palmitoyl and stearoyl respectively), and the corresponding *β*-phosphatidic acids: *α*-palmitoyl-batyl alcohol *β*-phosphoric acid (m.p. 57.7–58.1°) and *α*-stearoyl-batyl alcohol *β*-phosphoric acid (m.p. 62.0–62.5°) XIX (A = palmitoyl and stearoyl respectively).

¹⁶) J. H. UHLENBROEK and P. E. VERKADE, Rec. trav. chim. 72, 395 (1953).

These phosphatidic acids are structurally related to the acetal phosphatides (plasmals)¹⁷⁾, which occur in nature. It is also for this reason that in our opinion the former substances deserve attention from a biochemical point of view.



Klenk and Debuch¹⁸⁾ claim to have obtained a mixture of batyl alcohol phosphoric acid and chimyl alcohol phosphoric acid by hydrolysis of the hydrogenolysis product of a natural acetal phosphatide with methyl alcoholic hydrochloric acid. These investigators accept without proof that the substances obtained by them have the phosphoroyl group in the α -position. We are at present engaged in the synthesis of *batyl alcohol α -phosphoric acid* XX and *batyl alcohol β -phosphoric acid* XXI, starting from compounds of the types XVII and XIX respectively.

Many of the compounds discussed above show polymorphism. We cannot guarantee that the melting points given in this paper refer always to the most stable modification.

Delft, May 1954

¹⁷⁾ See H. C. BEYERMAN, Chem. Weekblad **44**, 589 (1948).

¹⁸⁾ R. KLENK and H. DEBUCH, Zeitschr. Physiol. Chem. **296**, 179 (1954).

REMARKS ON THE ORIGIN OF SATELLITES IN GENERAL AND ON THE METAMORPHOSIS OF THE SYSTEMS OF NEPTUNE AND THE EARTH IN PARTICULAR

BY

H. P. BERLAGE

(Communicated at the meeting of June 26, 1954)

Whenever we compare the qualities of recent views on the origin of satellites in our planetary system we find ourselves returning not only to the obvious thesis that the creation of secondary systems has occurred in fundamentally the same way as the creation of the primary one, but also to our conception of this origin. In particular insurmountable difficulties seem to arise against KUIPER's theory of the formation of satellites in the heavy envelopes of "protoplanets" by gravitational instability while these protoplanets were due to lose still 99 % or even more of their masses by evaporation, or else to be blown off by solar radiation [1b, c, d].

All satellites formed in the early protoplanet state must in this case have been lost. The present satellites, on the other hand, cannot have spiralled out significantly and must have been formed in the ultimate protoplanet state which shows exactly the characteristics of the state which was shown to produce secondaries spontaneously [2d].

In short, while the sun was once surrounded by a flat rotating disc composed of gas and dust in quasi steady motion, the planets also were once surrounded by flat rotating discs composed of gas and dust in quasi steady motion. In the latter case the nebular matter was almost certainly for the greater part dust, that is ice crystals, which probably existed in a continuous balance between volatilization by collision and spontaneous reformation [3], until circumstances allowed these particles to accumulate into meteorites. According to our theory the primary nebular disc was constrained to be transformed into a set of concentric rings with radii progressing in geometric series [2d, e, f]. Where portions of the rings eventually exceeded the appropriate critical density these portions became gravitationally stable.

The stable fragments of one ring revolving round about the sun in nearly the same approximately circular orbit united in the course of time into one planet, which during this operation became again surrounded by a rotating flat disc of meteoric dust. The secondary nebular discs again were transformed automatically into sets of concentric rings with radii progressing in geometric series. Three of these rings remained existent as such, the three rings of Saturn, which could not form singular massive satellites, because they circulate inside Roche's limit [4b].

Nor does the author agree with KUIPER's assumption that the Trojans are shedded satellites of Jupiter [1c], because these bodies so typically show the character of those remnants of the ring producing Jupiter and its system which stayed eventually near the two well-known equilateral stable positions.

When fragments of a ring unite, different cases may occur. When two bodies pursuing each other in one and the same orbit in one and the same plane of revolution unite, the resulting body will obtain the direct rotation about an axis perpendicular to the common plane of revolution [5]. The obvious frequency of this event explains the general tendency of planets to spin and satellites to circulate in the direct sense about axes which are perpendicular to the planes of revolution of these planets.

When, however, two bodies originally moving in appreciably different circular orbits in one and the same plane of revolution unite, the resulting body will evidently show the reverse sense of rotation. Hence, the outermost and innermost parts of a nebular ring will tend to communicate to a "protoplanet" the reverse sense of rotation. This tendency is clearly expressed by the retrograde motion of the outer satellites in some giant planets' secondary systems. In this case it is of course difficult to imagine that a complete nebular ring in retrograde motion could ever have been durable along the periphery of the directly rotating disc which generated the direct satellites.

The retrograde satellites are therefore "irregular" in so far as they were apparently captured in the outskirts of their primaries' nebular discs and brought "down" radially by the accumulation of particles from these discs, thereby acting as resisting media. Very probably therefore Jupiter's "partial" satellites VIII, IX, XI and XII, and Saturn's Phoebe have been circulating originally in much wider orbits. How much these orbits have been restricted is even liable to estimation, as we will see presently.

If this is the right interpretation we might have expected to meet in the borderzone between the direct and retrograde secondaries in Jupiter's and Saturn's system such satellites as VI, VII, X, and Japetus respectively, which are designated as "irregular" because they move in rather eccentric and oblique orbits. Perhaps Saturn's Hyperion is also one of these border satellites which has spiralled inward. The more pertinent question is raised by the rigorous structure of the central group of members of every family, the planetary family included, and not by the less strict behavior of some peripheral individuals.

A complication may arise when a ring is not a flat structure of the kind of the central nebular rings with the inclusion of the ring from which Saturn was born [2d], because when two fragments of a ring unite after having moved in orbits inclined on each other the resulting body gets a significant chance to spin about an axis coincident with its plane of revolution round the sun. Such a history has evidently been the fate of Uranus and its satellite system. It is all the same perfectly "regular", and

well explained, without requiring any perturbations by an extraneous objet moving through the solar system [1a].

A corollary to this feature of the system of Uranus is the great improbability that it encompasses retrograde members.

Now the theory of a nebular disc rotating about a central heavy mass in quasi steady motion proves that such discs are conformable with reference to the gravitational potential of the central body in points of the equatorial plane of the disc, provided the material composition is the same [2a, c] [6]. Hence, when this provision is assumed to be valid for the sake of simplicity, the discs will have extended to limits where the gravitational potentials are equivalent.

Let us discuss the planets and their satellite systems from this point of view, disregarding for the present moment the systems of the Earth and Neptune. Then it is the Martian system that is relatively most extended.

The particular problem of Mars and its satellites was posed repeatedly by JEANS [7] and JEFFREYS [8] and the author concedes that he also had been puzzled for a long time by the question how the small Mars managed to develop satellites at all [6]. However, there seems to be no objection against simply noticing the empirical fact and drawing the appropriate conclusions from it. The orbits of the two Martian satellites Phobos and Deimos are so strictly circular and so strictly co-incident with the planetary equator, while transformations by tidal action can only have remained relatively unimportant, that the Martian system must be considered as a normal and extremely "regular" creation. Our impression is that this system defies any other theory of its formation especially one specific feature: the period of revolution of the inner satellite is inferior to the planet's period of rotation. Moreover it confirms a remarkable theoretical conclusion previously obtained. The evolution of an even number of satellites is a more probable event than the evolution of an odd number of satellites, whereas two satellites constitute the least numerous mechanically possible creation [2f] when they are infinitely small. Mars operated, so to speak, along the lines of greatest efficiency.

TABLE 1

<i>Limit of satellite system in planet's radii</i>	<i>Semi-major axis of orbit of outermost satellite</i>
Mars. 7	Deimos. 7
Jupiter. 1120 (600)	VIII, IX, XI, XII 350
Saturn 420	Phoebe. 214
Uranus. 160	Oberon. 24

Table 1 contains the outer limit of each satellite system calculated on the basis of the Martian system and the semi-major axis of the orbit of the outermost known satellite, expressed in terms of the planet's equatorial radius. In Jupiter's case a dangerous limit pointed out by KUIPER [1c] is

smaller than the maximum extension calculated in the way indicated here and inserted in the Table in brackets.

We learn from Table 1 that the retrograde satellites of Jupiter and Saturn may indeed have been captured amply by the nebular discs spinning about these planets at the time, since the development of direct satellites at distances of no less than 600 and 420 planetary radii respectively might have been possible. It would thus seem probable that the retrograde satellites of Jupiter and Saturn were brought "down" to 0.58 and 0.51 of their initial distances respectively, by the resistance of the directly rotating media.

Now it is generally agreed upon that the system Earth-Moon is a singular case among satellite systems requiring special analysis of its origin and development. The ratio of the masses of Moon and Earth is exceptionally high and the fact that the Earth possesses only one satellite needs explanation, since the evolution of only one small secondary from a nebular disc initially surrounding a primary in quasi steady motion is no mechanically possible process [2f]. Moreover, the satellite orbit is highly inclined on the planetary equator.

When we disregard for a moment the minuscule Nereid, which is probably about 4000 times less massive than Triton [9], the same particulars apply to the system Neptune-Triton.

We discussed both satellite systems earlier [2f] and were able to point out that the heavy masses of the Moon and Triton have probably been the very condition for the possibility of their normal creation. Our conclusion was that the Moon must have originated at an initial distance of at least 14 times the Earth's radius. The minimum distance from Neptune where Triton could have come into existence was given to be 30 times Neptune's radius, when Triton's and Neptune's mean densities are assumed to be equal. This calculation has to be corrected. Triton's mass was erroneously stated to be the 300th part of Neptune's mass. It amounts to the 780th part of Neptune's mass [10], from which follows 78 times Neptune's radius for the minimum distance where Triton could originate.

From the genetic point of view it must be considered rather certain that the Moon's original orbit was very nearly circular and coincided very nearly with the Earth's equator. G. H. DARWIN's fundamental analysis of the development of the Earth-Moon system under the influence of tidal forces, allows us to retrace the dynamic structure of this system at the time of the Moon's condensation. The following primeval elements seem to fit in with all requirements [11].

Period of the Earth's rotation	7,5 hours
Period of the Moon's revolution	3 days
Inclination of the common orbital plane of the Moon and equatorial plane of the Earth on the ecliptic	15°
Moon's distance from the Earth in terrestrial radii	14
Eccentricity of Moon's orbit	.015

The Moon has receded since then to its actual distance of 60 times the Earth's radius. A body like our Moon very probably solidifies shortly after its formation. Now JEFFREYS pointed out that the distance with which the Moon's "fossil tide" corresponds is 22 times the Earth's radius [12]. Taking into account a partial redress of the Moon's "consolidated" deformation, let us assume that the distance where the Moon solidified is 20 times the Earth's radius. Theory proves that the change with time of the radius of a satellite orbit by tidal action is inversely proportional to the $5\frac{1}{2}$ th power of this radius [12]. When, say, 10^9 years is the time in which the Moon receded from a distance of 42 to a distance of 60 times the Earth's radius, it receded in $2,5 \times 10^6$ years from a distance of 14 to a distance of 20 times the Earth's radius. This result confirms that the solidification of the Moon was a short time process in any case.

Let us now turn our attention to Neptune's system. It is our conviction that KUIPER's discovery of Nereid and its direct sense of revolution peremptorily discloses that the retrograde Triton originated outside Nereid's orbit in the region where the example of the other giant planets' satellite systems leads us to expect retrograde satellites.

That the accent was shifted here from the directly circulating satellites to a preponderant retrograde mass is only a plausible consequence of the enormous width of the nebular ring from which Neptune was born. Hence it becomes almost certain that Triton approached Neptune from an initial distance of the order of 100 times the planet's radius to its actual distance of 13.3 times the planet's radius.

In the course of this evolution Triton must have crossed Nereid's orbit and come near to Nereid. The exceptionally high eccentricity of Nereid's orbit (0.76) [13] may well have been a consequence of this encounter. As a matter of fact when Triton passed Nereid it was Triton that was decelerated and Nereid that was accelerated. Nereid's actual shortest distance from Neptune amounts to 55 times the planet's radius. Probably Nereid revolved originally in the planet's equator in a nearly circular orbit having a radius roughly equal to, say, 60 times Neptune's radius. This is a reasonable value for the radius of the orbit of a small outer satellite revolving in the direct sense.

A first possibility to be considered is the one supposed by HIMPEL [14] that tidal forces may have hauled in the retrograde Triton towards its present small distance from Neptune.

However, if the original distance of Triton amounted to, say, 133 times Neptune's radius, that is 10 times its present distance, and when this distance was reduced to one half of the original value in, say, 3×10^9 years, the actual distance would be halved in 10^4 years. Such a change should have been easily perceptible in the course of the more than one century of observation which has elapsed since the discovery of Triton. Moreover no other giant planet is known to reveal significant tidal friction. The shrinkage of Triton's orbit must therefore have been a consequence of

Triton's accapuration of meteoric dust from the primeval disc rotating roundabout the planet in the direct sense.

This is also KUIPER's hypothesis [1c]. The perfect circularity of Triton's present orbit, although Triton is a retrograde satellite, could not be better explained than by this satellite's life-long motion through a resisting medium [15]. We may add that the plane of symmetry of this medium must have coincided with Neptune's equator, whereas the action of the spinning medium on a retrograde satellite is such that, while this body is spiralling inward the inclination of its orbit on the planet's equator increases.

In order to get sufficient quantitative information about this process, let us assume that Triton circulated during $t=10^9$ years within a globe of radius $R=10^{12}$ cm centered on Neptune and remaining all the time homogeneously filled with dust by internal equilibrium conditions. Let the velocity of Triton relative to the nebular matter through which it circulated in the retrograde sense be constant $=v=1$ km/sec, and the radius of Triton be constant $=r=1000$ km.

Consequently, while

$$dm = -\frac{3}{4} r^2 m v dt / R^3$$

is the part of the mass m which was accapared by Triton in the time dt

$$m = m_0 \exp \left(-\frac{3}{4} r^2 v t / R^3 \right)$$

is the mass of the remaining nebula after a lapse of time t , when the total mass of the original nebula was m_0 . When the assumed data are inserted in this formula we obtain

$$m = m_0 \times 10^{-11}.$$

The conclusion is that the original nebula was almost completely consumed by Triton. Now if Triton started its revolution about Neptune at a distance 9 times superior to its present distance from Neptune, it then possessed 3 times more angular momentum about the planet. Hence, $\frac{2}{3}$ of the primitive angular momentum of the satellite was destroyed by the directly revolving matter accumulated on it. Therefore Triton's mass grew by the $\frac{2}{5}$ part of its present mass in the course of its "accession". So this part of Triton's mass or roughly 1/2000 part of Neptune's mass must have been the mass of the primitive nebular disc revolving about the planet. If 4 main satellites had formed, each of them would have obtained a mass M = roughly 1/8000 Neptune's mass. Hence $\log M \sim -2.7$, when M is expressed in terrestrial units, and this is a value fitting excellently into the scheme of satellite masses [4b].

From the same data we calculate easily, although very roughly that $\sin i_0 \sim \frac{2}{5} \sin 20^\circ$, i_0 being the initial and 20° the actual inclination of Triton's orbit on Neptune's equator. Or $i_0 \sim 8^\circ$. Evidently this relatively low inclination must have aided Triton's capture by Neptune's flat nebular disc.

Triton's "crossing" evidently greatly impeded the generation of a numerous satellite system from the primitive nebular disc. Exhausting the available dust and gas Triton finally "landed", so to speak, in the zone where otherwise the most massive direct satellites would have formed and inside which only a very small fraction of the total matter ever existed in the disc's equilibrium state.

What happened to our Moon during its recession could no doubt also have happened to Triton during its travelling in the opposite direction. Besides being bombarded by numerous planetesimals it may have been bombarded by a couple of larger bodies, while Nereid, one of those heavier condensation products, escaped this fate. We are reminded here of a remarkable possibility imagined by LYTTLETON [16]. As a matter of fact Pluto crosses Neptune's system incidentally. If Triton and Pluto were originally twin satellites of Neptune moving both in the direct sense, but experiencing very near encounters, it may have occurred that Triton expelled Pluto from Neptune's system and reversed its own motion to retrograde. In the development described here, there is however no room for a process of this kind, which is after all a very improbable one.

The greater probability must, on the other hand, be attributed to an opposite event suggested by DAUVILLIER and CAMICHEL [17]. These authors regarded Pluto and Triton as twin primitive planets and investigated what might have occurred with these bodies. It is proposed here to interpret this hypothesis in the following way. Pluto and Triton may have started as two initially more or less independent outer and inner condensation products of the very wide ring from which Neptune was born. Both bodies came into touch with Neptune's nebular disc one day or other, Triton was captured and became a satellite, Pluto, however, although perturbed escaped this fate and continued its motion in an eccentric orbit about the sun as an independent planet. It should be borne in mind that the condensation by gravitational instability of a regular planet beyond Neptune remains a puzzling problem [2e].

The next question is, what further may have occurred in the Earth-Moon system. Several geologists, following G. H. DARWIN's suggestion have been advocates of the hypothesis that the Moon is a body which was launched from the Earth by tidal action, supported by resonance, and that the Pacific Ocean basin is the scar which was left at the surface of our globe after the process of separation. JEFFREYS showed the validity of the resonance theory to be very doubtful [18]. BULLEN, it is true, noticed [19] that the primitive Earth-Moon body may have yielded more easily to tidal forces, provided it was close to a characteristic instability pointed out by RAMSEY [20], but we are still short of a confirmation that the energy inherent in the instability would be sufficient to eject the Moon. VAN BEMMELEN recently put forward the similar theory that the Moon was jetpropelled from the Earth by deep-seated physico-chemical explosive forces, liberated by the tidal waves deforming the primitive Earth-Moon

body [21]. We fear, however, that it will be very difficult to explain how the ejected body, after having crossed Roche's limit and become gravitationally stable, was directed by its driving force in such a way that it did not continue to move in a very elongated orbit, neither a hyperbolic one along which it would be lost nor an elliptic one along which it would fall back on the Earth, but ended in a nearly circular orbit. A third possibility, discussed by DALY [22], that our Moon is an asteroid captured by the Earth after a tangential, slicing, collision with this planet is almost discarded by DALY himself on account of its incredibility.

Nevertheless it cannot be denied that some large scale geomorphological features are strongly suggestive of a cosmic disaster leading to the accumulation of a landmass in one hemisphere and the following break up of this primeval landmass into a number of continents.

This induced us to inquire whether the opposite phenomenon was not the more likely actual occurrence, that is the falling down of a second satellite on the Earth.

Let us assume that this hypothetical satellite II was a small one moving at a mean distance from the Earth of 35 terrestrial radii. The significance of this particular value will appear presently. In this case the Moon, revolving in a gradually widening orbit, while the effect of tidal action is proportional to the satellite's mass, must have overtaken the smaller companion at a certain time and perturbed its motion. The hypothesis is, that the perturbations of satellite II were so strong that it actually collided with our globe.

The hypothesis is supported by the circumstance that the original Earth's system in this case not only presented the more probable number of two satellites, but was quite similar to the satellite system of the only other terrestrial planet with satellites, that is Mars. The ratio of the radii of the orbits of both satellites is then equal in the two structures, namely $35 : 14 = 6.9 : 2.8 = 2.5$. Moreover, the values of the gravitational potential are equal in homologous points. It is noted that the ratio of the radii of the orbits of the two satellites, $\log r_{n+1} - \log r_n = 0.4$, seems high when compared with the average ratio of the radii of two successive satellites in the more numerous systems; however, it is rational to consider the evolution of satellite systems including four main members as the duplication of a system which includes only two members. In these cases, instead of two main rings four main rings were produced. Consequently in theory $\log r_{n+1} - \log r_n = 0.2$. As a matter of fact $\log r_{n+1} - \log r_n = 0.215$ and 0.173 in the systems of Jupiter and Uranus respectively [8]. A further duplication would yield $\log r_{n+1} - \log r_n = 0.1$ theoretically, whereas in Saturn's system we find $\log r_{n+1} - \log r_n = 0.110$ [4b]. Now indeed Saturn's regular system consists of 8 satellites. However, with regard to its actual rings and "unfinished" rings [4b] it encompasses 16 members potentially so that the impression prevails that a still further duplication has almost come into effect. It is therefore perhaps more reasonable to reconsider the

question from the other end and start from Saturn's system with roughly 16 possible members but 8 main members, descending to systems with roughly 8 possible members, but 4 main members, those of Jupiter and Uranus (and the planetary system itself) and eventually to systems with roughly 4 possible members, but 2 main members, those of the Earth and Mars.

A survey from this standpoint of the genesis of all known satellites and the serious dislocation of three of them is given in Table 2. The symmetry and logic revealed by this Table is no weak argument in favour of our speculations. It induces us to adopt the probability of the existence of one or more very small satellites of Uranus circulating in the direct sense outside Oberon.

One final remark should be made. When KOSTINKI's photographic magnitudes of the Martian satellites Phobos and Deimos are adopted, the diameters of these bodies are 10 km and 8 km respectively [23]. Their volumes are then in the ratio 2 : 1 and this ratio would hold perhaps also for their masses. Recent investigators would perhaps support a somewhat greater difference of the two masses, but this does not alter significantly the general shift of the heavier satellite masses from the centre to the periphery of the secondary systems which is so clearly noticeable in Table 2 when we pass from the Earth to Neptune, and which is a feature fitting so well into the general picture developed so far. It leaves us with the impression that we are gradually approaching a unified theory of the origin of satellites and should no longer be too rash with distinctions between "regular" and "irregular" satellites.

TABLE 2
Scheme of satellite systems supposed complete
(Semi-major axes of orbits of satellites in 10^{10} cm)

Direct										Retrograde	
Earth ← II(f)		Moon(s)				II(s)				Moon(f)	
		0,88				2,19				3,84	
Mars . . .		Ph				De					
		0,09				0,24					
Jupiter . .		V	I	II		III	IV	VI, VII, X	VIII, IX, XI, XII		
		1,8	4,2	6,7		10,7	18,8	~ 117	~ 235		
Saturn . .		Ring	Mi	En	Th	Di	Rh	* * Ti * *	* Ja *	Ph	
		1,9	2,4	3,0	3,8	5,3	12,2	35,6	129		
Uranus . .		Mi	Ar	Um		Ti	Ob	?			
		1,2	1,9	2,7		4,4	5,9				
Neptune .		*		* Tr(f)		*		Ne →	Tr(s)		
				3,6				16	~ 30		
(s) = start; (f) = finish; * = undeveloped; ? = probably existing.											

(s) = start; (f) = finish; * = undeveloped; ? = probably existing.

When we look at a falling satellite from the geological point of view it is interesting to note that the puzzling accumulation of radioactive substances in the Earth's crust could perhaps be reasonably explained

by the extra-terrestrial origin of these substances. Apart from this our first impression is that the sialic floating parts of the Earth's crust, the cluster of granitic continents could be the remnants of this satellite, while the total mass of sialic matter, if the extension of the continents and their thickness are estimated at one third of the Earth's surface and 30 km respectively, is $1/400$ of the terrestrial mass, or $1/5$ of the lunar mass.

However, a physico-chemical transformation of the Earth's initial crust into a granitic upper and a basaltic lower layer probably progressed with time, and the more promising hypothesis seems to be that the falling satellite plunged into the Earth's crust and by this operation created the Pacific Ocean basin. This basin would then have to be considered as a terrestrial analogon to the lunar maria, which almost certainly were produced by relatively large colliding objects. As a matter of fact the Pacific Ocean basin is very similar to one of these extensive circular pools of solidified lava in which apparently older lunar "circusses" were drawn and orogenesis was checked. Certain geomorphological features such as the apparent "creep" of the upper granite layer over the basaltic Pacific Ocean bottom, indicated by the deformations of the well-known andesite boundary [21], and some shearlines and linear arrangements of islands in the Pacific parallel to the ecliptic [24] are definitely in favour of this hypothesis.

When the Pacific Ocean and the Mare Imbrium are compared we find that the diameter of the latter is 1150 km, whereas the former covers a complete terrestrial hemisphere. Now the planetesimal that caused the Mare Imbrium is estimated by UREY [25] to have had a diameter of 230 km or one fifth of the diameter of the mare. If a similar dimensional proportion is valid in the case of the terrestrial catastrophe the collision of a satellite of a mass equal to the lunar mass is required. However, if the kinetic energy of the falling object is the relevant feature a mass of roughly $1/20$ of the lunar mass would seem adequate. Leaving final questions to the future, let us assume provisionally for the mass of satellite II a value of $1/10$ of the lunar mass, the order of magnitude of which seems to be right in any case.

A satellite of $1/10$ of the lunar mass will clearly as a rule be generated with a mean density ~ 2 [4a], showing that roughly half of its volume was water of density 1 and half was rock of density 3. Hence a part of satellite II equal to $3/40$ of the lunar mass was rock and a part equal to $1/40$ of the lunar mass was water. Therefore, having noted that the total quantity of water in the oceans is $1/50$ of the lunar mass, we are challenged to inquire whether perhaps a significant part of the superficial terrestrial waters, if not the total amount, emanated from the falling satellite. It is of course dubious whether a relatively small body condensed at temperatures corresponding with the earth's distance from the sun would be able to retain most of its original water content up to the moment of collision, and geochemistry is not in need of a hypothesis of this kind [26].

On the other hand the almost complete absence of water on Venus, a planet most similar to the Earth in structure, poses a problem [27] that might find a solution in the way indicated. Now when we try to picture what happened at the impact we find the melting of the satellite and a large part of the Earth's crust in such a short time that this probably went together with an explosion on a planetary scale. However, it certainly remains doubtful whether any substantial part of the mass directly involved in the disaster could thereby acquire velocities of escape and be lost to our globe. Volatilized matter was to form a heavy temporary atmosphere, which cooled down and rained out very rapidly.

We are perfectly aware of the fact that almost all actual fundamental characteristics of the Earth's crust, mountain chains, volcanic zones and zones of shallow and deep focus earthquakes are due to recent metamorphosis. We only wish to repeat that the hypothesis of a colliding satellite should be considered mainly as a means of understanding the remarkable first order spherical harmonic in the Earth's topography, which was derived by PREY and explained by VENING MEINESZ [28] not exactly satisfactorily as due to a single cell convection which may have turned the entire Earth inside out before and during the time of formation of the Earth's core. For we hesitate to assume that at the time when the Earth was still in that primitive, throughout fluid state, essential for the production of a core by physico-chemical differentiation, a one-sided deformation could have continued to exist as a permanent acquisition.

Finally, in order to get some quantitative information, let us disregard all minor complications and imagine the situation in which the Moon, after having approached the distance where the second satellite circulates, is slowly advancing on this satellite. The linear velocity of both satellites is the Keplerian velocity corresponding with 35 terrestrial radii, or 1.3 km/sec. The parabolic velocity with reference to the Moon is 2.4 km/sec. Hence, the angular momentum of the second satellite with reference to the Earth is reduced to zero, when the distance between the second satellite and the Moon is reduced to 3.4 times the Moon's radius if the second satellite is infinitely small, and to 2.3 times the Moon's radius if the mass of the second satellite is half the lunar mass. Hence this particular case may well have occurred with a second satellite of $1/10$ of the lunar mass, even without its crossing Roche's limit relative to the Moon. It is to be expected, of course, that in fact the motion of the second satellite was more or less perturbed every time the Moon came close to it, until the second satellite was pulled into a highly eccentric orbit relative to the Moon, resulting in its coming down and actually striking the Earth.

Kon. Ned. Meteorologisch Instituut, De Bilt, Netherlands

REFERENCES

1. KUIPER, G. P., (a) Proc. Nat. Acad. Sc. Washington 37, 1 (1951); (b) 37, 383 (1951); (c) 37, 717 (1951); (d) 39, 1153 (1953).

2. BERLAGE, H. P., (a) Proc. Kon. Ned. Akad. Wet. Amsterdam **35**, 553 (1932);
(b) **37**, 221 (1934); (c) **38**, 857 (1935); (d) **43**, 532, 557 (1940); (e)
51, 796 (1948); (f) **51**, 965 (1948).
3. HOYLE, F., Mon. Not. R.A.S. **106**, 406 (1946).
4. BERLAGE, H. P., (a) Proc. Kon. Ned. Akad. Wet. Amsterdam **B56**, 45 (1953);
(b) **B56**, 56 (1953).
5. HALM, J., Proc. Roy. Soc. Edinburgh **25**, I, 553 (1905).
6. BERLAGE, H. P., Ann. Bosscha St., Misc. Papers No. 7 (1934).
7. JEANS, Sir JAMES, Astronomy and Cosmogony, p. 406 (Camb. Univ. Press, 1929).
8. JEFFREYS, H., The Earth, p. 46 and 54 (Camb. Univ. Press, 1924).
9. KUIPER, G. P., Pub. Astron. Soc. Pac. **61**, 175 (1949).
10. ———, The atmospheres of the earth and planets, p. 308 (Univ. Chicago Press, 1952).
11. DARWIN, G. H., Scientific Papers Vol. II, Tidal friction and cosmogony (Table XV and XVI) (Camb. Univ. Press, 1908).
12. JEFFREYS, H., The Earth, p. 203 (Camb. Univ. Press, 1924).
13. BIESBROECK, G. VAN, Astron. J. **56**, 110 (1951).
14. HIMPEL, K., Kosmogonie und Erdgeschichte, p. 122 (Akad. Verl. Ges. Leipzig, 1940).
15. NÖLKE, F., Das Problem der Entwicklung unseres Planetensystems (2. Auflage, Springer Berlin, 1919).
16. LYTTLETON, R. A., Mon. Not. R.A.S. **97**, 108 (1936).
17. DAUVILLIER, A. and H. CAMICHEL, C. R. **218**, 32 (1949).
18. JEFFREYS, H., Mon. Not. R.A.S. **91**, 169 (1931).
19. BULLEN, K. E., Nature **167**, 29 (1951).
20. RAMSEY, W., Mon. Not. R.A.S. **108**, 406 (1948).
21. BEMMELEN, R. W. VAN, Geologie en Mijnbouw **11**, 1 (1949).
22. DALY, R. A., Proc. Amer. Philos. Soc. **90**, 104 (1946).
23. GRAFF, K., Die physische Beschaffenheit der Planetensystems, Handbuch der Astrophysik, Bd. 4 (1929).
24. UMBROGROVE, J. H. F., The pulse of the earth, p. 228 (Second Ed., The Hague, M. Nijhoff, 1947).
25. UREY, H. C., Geochimica et Cosmochimica Acta **1**, 209 (1951), p. 226.
26. RUBEY, W. W., Bull. Geol. Soc. Amer. **62**, 1111 (1951).
27. KUIPER, G. P., Planetary and Satellite Atmospheres, Phys. Soc. Reports on Progress in Physics **13**, 247 (1950).
28. VENING MEINESZ, F. A., (a) Proc. Kon. Ned. Akad. Wet. Amsterdam **53**, 7 (1951); (b) **54**, 212 (1951); (c) **55**, 527 (1952); Jaarboek 1951-1952.

THE HYDROLYSIS AND AMINOLYSIS OF ETHYL THIOACETATE. II. KINETICS OF THE SIMULTANEOUS HYDROLYSIS AND AMINOLYSIS

BY

J. TH. G. OVERBEEK AND V. V. KONINGSBERGER
(*Van 't Hoff Laboratory, University of Utrecht*)

(Communicated at the meeting of June 26, 1954)

1. Introduction

In a preceding paper [1] we presented the results of a kinetic analysis of the alkaline hydrolysis of ethyl-thioacetate (E.T.A.). The aminolysis in aqueous media is always accompanied by some hydrolysis. By determining the rate of disappearance of E.T.A. in aqueous glycine solutions we obtained overall reaction rates, from which the kinetic constants for the aminolysis could be calculated.

2. Experimental methods and calculation of concentrations

The measurements were carried out at 37° C. The rate of disappearance of E.T.A. in the reaction mixtures and the pH were determined according to the methods described before [1].

OH⁻ ion concentrations in borate buffer solutions were calculated approximately [1] according to:

$$(1) \quad [\text{OH}] = \frac{2.4 \times 10^{-14}}{\text{antilog}(-\text{pH})} \cdot \frac{1}{\frac{[\text{H}_2\text{BO}_3]}{[\text{HBO}_2]}}$$

Concentrations are indicated by symbols between square brackets.

For the interpretation of our measurements accurate estimates of the glycinate ($\text{R}-\text{NH}_2$) concentrations are essential. At high pH practically all the glycine was present in the glycinate form. At lower pH the ratio of glycine (RNH_3^+) to glycinate (RNH_2) has to be evaluated from the pH. As little is known about the activity coefficients of amino acids in solution glycinate concentrations were determined empirically. Glycine buffers of various concentrations with a well known ratio of glycine to glycinate were prepared. The pH of these buffers was determined at 37° C. An empirical titration constant K_{NH_3} was calculated from the measurements according to

$$(2) \quad \text{pK}_{\text{NH}_3} = \text{pH} + \log \frac{[\text{RNH}_3^+]}{[\text{RNH}_2]}$$

Table 1 shows that the pK so defined varies only very slightly with glycine concentration and somewhat more with pH .

Unknown glycinate concentrations were calculated from total glycine ($[RNH_3^+] + [RNH_2]$) and pH using the appropriate pK_{NH_3} as interpolated from the data in table 1.

TABLE 1
Determined pH and calculated pK_{NH_3} of various glycine buffers at $37^\circ C$

$\frac{[RNH_2]}{[RNH_2] + [RNH_3^+]}$	Total glycine (mol l^{-1})	pH	pK_{NH_3} calc.
0.250	1	8.92	9.40
0.250	0.1	8.93	9.41
0.143	1	8.67	9.45
0.143	0.1	8.68	9.46
0.100	1	8.51	9.46
0.100	0.5	8.52	9.47
0.100	0.1	8.53	9.48
0.05	1	8.21	9.49
0.033	1	8.03	9.49

3. Simultaneous hydrolysis and aminolysis

All reactions investigated are first order with respect to $[E.T.A.]$. The results can therefore be expressed by means of K_{obs} , defined by

$$(3) \quad -\frac{d[E.T.A.]}{dt} = K_{obs} [E.T.A.].$$

Tables 2 (low pH) and 3 (high pH) show the results obtained.

TABLE 2
Simultaneous hydrolysis and aminolysis by glycine at $37^\circ C$ of 0.0025 m E.T.A. solutions in borate buffers of various pH . In exp. 86 the measurement was carried out in a pure glycine buffer; no activity correction was used for the calculation of $[OH]$ in this experiment

Exp. No.	pH	$[OH] \times 10^9$ (mol ml^{-1})	$[total\ glycine] \times 10^4$ (mol ml^{-1})	$K_{obs} \times 10^6$ (sec^{-1})	$\{K_{obs}/[OH]\} \times 10^{-3}$ ($ml\ mol^{-1}\ sec^{-1}$)
8	7.87	2.2	1	8	3.6
12	8.10	3.6	1	13	3.6
88	8.62	12.5	1	42	3.4
70	8.25	5.3	2	33	6.2
71	8.61	12.8	2	64	5.0
87	8.94	21	2	119	5.7
67	8.05	3.4	5	56	16
66	8.22	5.0	5	91	18
32	8.28	5.7	5	107	18
33	8.43	8.2	5	144	18
22	8.45	8.6	5	146	17
51	8.99	30	5	730	24
57	8.16	4.5	10	190	42
86	8.67	11.3	10	806	71
60	8.64	13	10	880	68
56	8.88	23	10	2020	88

TABLE 3

Simultaneous hydrolysis and aminolysis by glycine of E.T.A. solutions at 37° C and high pH. [OH] concentrations were calculated from the composition of the reaction mixtures

Exp. No.	$[\text{OH}] \times 10^9$ (mol ml ⁻¹)	$\frac{[\text{glycine}]_{\text{total}} \times 10^4}{= [\text{RNH}_2] \times 10^4}$ (mol ml ⁻¹)	$C_1^*) \times 10^5$ (sec ⁻¹)	$K_{\text{obs}} \times 10^6$ (sec ⁻¹)	$\{K_{\text{obs}}/[\text{OH}]\} \times 10^{-2}$ (ml mol ⁻¹ sec ⁻¹)
73	2250	0.1	7.7	480	2.1
72	14500	0.1	7.7	2600	1.8
81	5000	0.2	10.1	1270	2.5
77	10000	0.2	10.1	2150	2.2
84	5000	0.4	16.9	1650	3.3
83	10000	0.4	16.9	2760	2.8

*) For the meaning and calculation of C_1 see the end of section 4.

Evidently, K_{obs} contains contributions from hydrolysis and from aminolysis. A provisional separation may be based upon the assumption that hydrolysis and aminolysis proceed completely independently and thus:

$$(4) \quad K_{\text{obs}} = K_{\text{H. obs}} + K_{\text{A. obs}}$$

where $K_{\text{H. obs}}$ is the rate constant of hydrolysis, determined in the previous paper [1].

An analysis of the data of tables 2 and 3 then leads in the first place to the following conclusions:

1. Extrapolation of the data at low pH (<9) to $[\text{OH}]=0$ (see fig. 1 A and 1 B) shows that the limiting rate constant of aminolysis is

$$(5) \quad (K_{\text{obs}})_{[\text{OH}] \rightarrow 0} = (K_{\text{H. obs}})_{[\text{OH}] \rightarrow 0} + K [\text{RNH}_3^+] [\text{OH}^-]$$

where $\text{RNH}_3^+ = \text{H}_3\text{N}^+ - \text{CH}_2 - \text{COO}^-$.

The value for $(K_{\text{H. obs}})_{[\text{OH}] \rightarrow 0} = 1300 \times [\text{OH}] \text{ sec}^{-1}$ follows from paper [1] of this series.

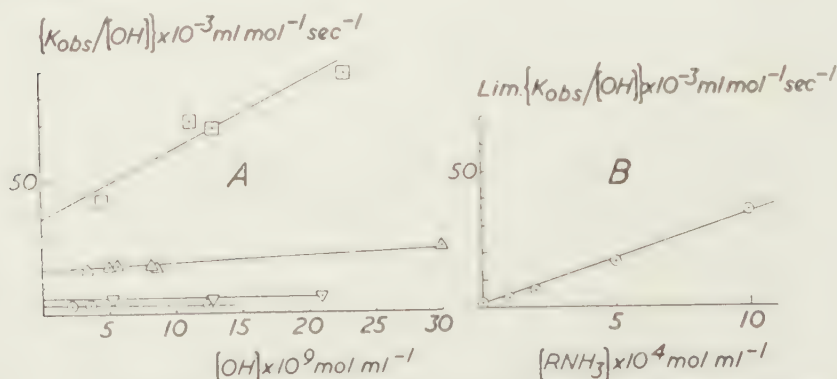


Fig. 1. Simultaneous hydrolysis and aminolysis by glycine at 37° C of 0.0025 m E.T.A. solutions under the experimental conditions described in table 2. The four curves represent the data with 0.1, 0.2, 0.5 and 1.0 m glycine

A: $K_{\text{obs}}/[\text{OH}]$ plotted against $[\text{OH}]$

B: $\lim_{[\text{OH}] \rightarrow 0} K_{\text{obs}}/[\text{OH}]$ plotted against $[\text{total glycine}] = [\text{RNH}_3]$

2. By extrapolation of the data for high pH (>10.5) it appears (see fig. 2 A and 2 B), that the rate constant approaches:

$$(6) \quad (K_{\text{obs}})_{[\text{OH}] \rightarrow \infty} = (K_{\text{H, obs}})_{[\text{OH}] \rightarrow \infty} + K''[\text{RNH}_2][\text{OH}] + f(\text{RNH}_2)$$

where $f(\text{RNH}_2)$ depends upon the concentration of glycinate but not upon the pH.

According to our previous paper [1] $(K_{\text{H, obs}})_{[\text{OH}] \rightarrow \infty} = 150 [\text{OH}] \text{ sec}^{-1}$.

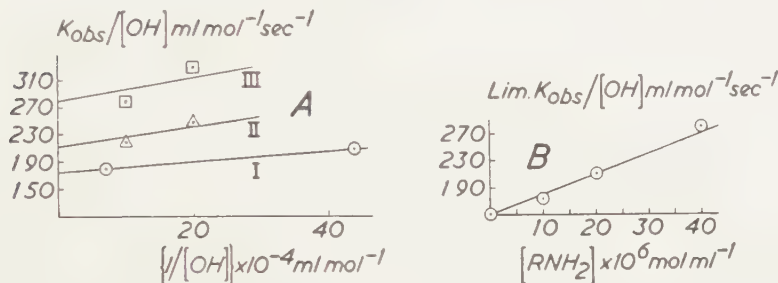


Fig. 2. Simultaneous hydrolysis and aminolysis by glycine at 37° C of E.T.A. solutions at high pH: the experimental conditions are summarized in table 3

A: $K_{\text{obs}}/[\text{OH}]$ plotted against $1/[\text{OH}]$ for:

I aminolysis by 0.01 m glycine

II " " 0.02 " "

III " " 0.04 " "

B: $\lim_{[\text{OH}] \rightarrow \infty} K_{\text{obs}}/[\text{OH}]$ plotted against $[\text{RNH}_2] = [\text{glycine}]$

According to the dissociation equation

$$(7) \quad \frac{[\text{RNH}_3^+][\text{OH}^-]}{[\text{RNH}_2]} = K_{\text{base}}$$

the rate of aminolysis at low pH (eq. (5)) can be considered to be proportional to the glycinate concentration

$$(8) \quad (K_{\text{A, obs}})_{[\text{OH}] \rightarrow 0} = K'[\text{RNH}_2].$$

Similar findings have been reported by other investigators [2, 3, 4, 5] and a reaction scheme in good harmony with the data has been proposed [4].

The data at high pH, as represented in eq. (6) are in good agreement with data published by TARBELL and HAWKINS [6]. At low pH (<9) the contribution of this reaction is not measurable because of the relatively low value of K'' .

It follows from fig. 1 A and more clearly from a plot of $K_{\text{A, obs}}/[\text{RNH}_2]$ against $[\text{OH}]$ (see table 4 and fig. 3) that eq. (5) is insufficient to describe the aminolysis at low pH.

This equation would give one straight horizontal line for all concentrations of glycine when plotted in the same way as in fig. 3. The fact that the reduced aminolysis constant $K_{\text{A, obs}}/[\text{RNH}_2]$ for small concentrations of glycine decreases with increasing $[\text{OH}]$ points to a certain competition between hydrolysis and aminolysis. The fanning out of the

TABLE 4

Aminolysis by glycine at 37°C of 0.0025 m E.T.A. solutions in borate buffers of various pH. $K_{H, obs}$ was calculated from the data on the spontaneous hydrolysis of E.T.A. [1]

Exp. No.	$[OH] \cdot 10^9$ (mol ml ⁻¹)	[Glycine] · 10 ⁴ (mol ml ⁻¹)	$[RNH_2] \cdot 10^6$ (mol ml ⁻¹)	$K_{H, obs} \cdot 10^6$ (sec ⁻¹)	$K_{A, obs} \cdot 10^6$ (sec ⁻¹)	$K_{A, obs} [RNH_2]$ (ml mol ⁻¹ sec ⁻¹)
8	2.2	1	2.2	2.8	5.2	2.4
12	3.6	1	3.8	4.6	8.4	2.2
88	12.5	1	12.5	14	28	2.2
70	5.3	2	10.8	7	26	2.5
71	12.8	2	24.4	15	49	2.0
67	3.4	5	17	4.4	52	3.0
66	5.0	5	25.5	6.4	85	3.3
32	5.7	5	29	7.2	100	3.5
33	8.2	5	41	10	134	3.3
22	8.6	5	43	10.4	136	3.2
51	30	5	138	29	701	5.1
57	4.5	10	44	5.8	184	4.2
86	11.3	10	143	14	792	5.5
60	13	10	132	15	865	6.6
56	23	10	230	24	1196	8.7

curves with increasing amounts of glycine indicates a measurable contribution of a reaction proportional to the square of the glycinate concentration.

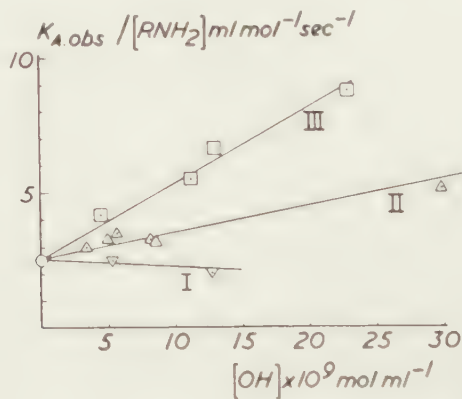


Fig. 3. Fan-shaped bundle of curves for the values of $\frac{K_{A, obs}}{[RNH_2]}$ obtained for different glycine concentrations under the experimental conditions summarized in table 4.

- I Total glycine concentration = 0.2 mol l⁻¹.
 II „ „ „ = 0.5 „ „
 III „ „ „ = 1.0 „ „

4. Discussion of a complete reaction scheme

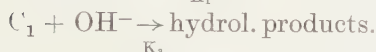
The phenomena described above can be explained by assuming the following reactions:

- a) The complex C_1 (see: [1]) reacts with both OH^- ions and RNH_2

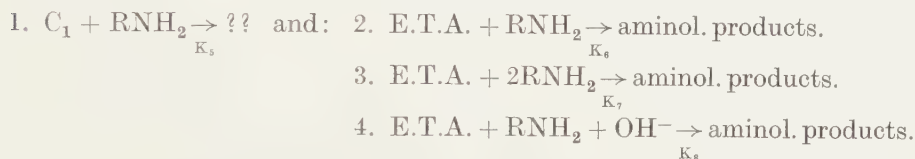
molecules. It is not certain whether acetyl glycine or hydrolysis products are formed during this reaction.

b) A reactive complex is formed by E.T.A. and glycine (RNH_2) which decomposes spontaneously but more rapidly in the presence of OH^- ions and RNH_2 molecules (base-catalysis). These reactions may yield the aminolysis product, acetyl glycine, which has been isolated [7]. Consequently, the most simple reaction scheme for the simultaneous hydrolysis and aminolysis of E.T.A. would be:

Hydrolysis: (see: [1])



Aminolysis:



A reaction kinetic analysis of this scheme gives the following equation for the disappearance of E.T.A. with the time of incubation¹⁾:

$$(9) \quad \left\{ \begin{aligned} -\frac{d[\text{E.T.A.}]}{dt} &= [\text{E.T.A.}] \left\{ \text{K}_1' \frac{\text{K}_3[\text{OH}] + \text{K}_5[\text{RNH}_2]}{\text{K}_2 + \text{K}_3[\text{OH}] + \text{K}_5[\text{RNH}_2]} + \right. \\ &\quad \left. + \text{K}_4[\text{OH}] + \text{K}_6[\text{RNH}_2] + \text{K}_7[\text{RNH}_2]^2 + \text{K}_8[\text{RNH}_2][\text{OH}] \right\} \end{aligned} \right\}$$

with $\text{K}_1' = \text{K}_1[\text{H}_2\text{O}]$.

It follows from eq. (9) that K_{obs} should be a pseudo first order rate constant if the reaction velocity measurements are carried out in buffered solutions and in the presence of an excess of glycine (and—at high pH—of OH^- ions) for:

$$(10) \quad \left\{ \begin{aligned} \text{K}_{\text{obs}} &= \text{K}_1' \frac{\text{K}_3[\text{OH}] + \text{K}_5[\text{RNH}_2]}{\text{K}_2 + \text{K}_3[\text{OH}] + \text{K}_5[\text{RNH}_2]} + \text{K}_4[\text{OH}] + \text{K}_6[\text{RNH}_2] + \\ &\quad + \text{K}_7[\text{RNH}_2]^2 + \text{K}_8[\text{RNH}_2][\text{OH}] = \text{constant.} \end{aligned} \right\}$$

After substitution of $\frac{[\text{RNH}_3][\text{OH}]}{\text{K}_b}$ for $[\text{RNH}_2]$ and expansion for small values of $[\text{OH}]$ eq. (10) can be written as:

$$(11) \quad (\text{K}_{\text{obs}})_{[\text{OH}] \rightarrow 0} = [\text{OH}] \left\{ \text{K}_1' \frac{\text{K}_3}{\text{K}_2} + \text{K}_4 + \frac{[\text{RNH}_3]}{\text{K}_b} \left(\text{K}_1' \frac{\text{K}_5}{\text{K}_2} + \text{K}_6 \right) \right\}$$

In fig. 1 B the extrapolated value of $\text{K}_{\text{obs}}/[\text{OH}]$ is plotted against the

¹⁾ For the derivation of this equation: see appendix.

total glycine concentration which for $[\text{OH}] \rightarrow 0$ is equal to $[\text{RNH}_3^+]$. The total slope of the line leads to the value:

$$\frac{1}{K_{\text{base}}} \left(K_1' \frac{K_5}{K_2} + K_6 \right) = 3.3 \pm 0.5 \text{ ml}^2 \text{ mol}^{-2} \text{ sec}^{-1}$$

K_{base} according to the data of table 1 and extrapolated to low pH ($\text{pK}_{\text{NH}_4} = 9.51$) would be

$$K_{\text{base}} = \frac{K_{\text{water}}}{\text{antilog } \text{pK}_{\text{NH}_4}} \times 10^{-3} = \frac{2.4 \times 10^{-14} \times 10^{-3}}{3.09 \times 10^{-10}} = 7.7 \times 10^{-8} \text{ mol ml}^{-1}$$

which is in reasonable agreement with the value $K_{\text{base}} = 7.16 \times 10^{-8} \text{ mol ml}^{-1}$ interpolated from OWEN's [8] data. Consequently we obtain:

$$(12) \quad K_1' \frac{K_5}{K_2} + K_6 = 2.5 \text{ ml mol}^{-1} \text{ sec}^{-1}$$

in perfect harmony with the extrapolation to $[\text{OH}] = 0$ of the fanshaped bundle of fig. 3.

No simple and direct way has been found to determine the constants K_5 , K_6 and K_7 separately. This is caused partly by the rather complicated way in which K_5 occurs in the rate equation (9), partly by the relatively strong influence of errors in experiments and calculations on the results. The constant K_8 can be determined separately from experiments at high pH. Its value is small and only of minor influence in the calculation of K_5 , K_6 and K_7 .

We determined the best set of values for K_5 , K_6 and K_7 by using successive approximations. To start with K_5 was given the largest value compatible with eq. (12) i.e.

$$K_1' \frac{K_5}{K_2} = 2.5 \text{ ml mol}^{-1} \text{ sec}^{-1} \text{ or, with } K_1' = 6 \times 10^{-5} \text{ sec}^{-1} \text{ (see [1])}$$

$$\frac{K_5}{K_2} = 4 \times 10^4 \text{ ml mol}^{-1}.$$

Rearranging eq. (10) to

$$(13) \quad \left\{ \begin{array}{l} K_{\text{obs}} - K_1' \frac{(K_3/K_2)[\text{OH}] + (K_5 \cdot K_2)[\text{RNH}_2]}{1 + (K_3/K_2)[\text{OH}] + (K_5/K_2)[\text{RNH}_2]} - K_4[\text{OH}] - K_8[\text{RNH}_2][\text{OH}] \\ \hline [\text{RNH}_2] \end{array} \right. = \frac{K_A'}{[\text{RNH}_2]} = K_6 + K_7[\text{RNH}_2]$$

and using $(K_3/K_2) = 1.9 \times 10^7 \text{ ml mol}^{-1}$, $K_4 = 150 \text{ ml mol}^{-1} \text{ sec}^{-1}$ (see [1]) and $K_8 = 3 \times 10^6 \text{ ml}^2 \text{ mol}^{-2} \text{ sec}^{-1}$ (see at the end of this section), the left hand side of eq. (13) can be plotted against $[\text{RNH}_2]$. The triangles in fig. 4 represent these points.

It is evident that a straight line through these points would not extrapolate to the origin. Consequently K_6 is at least $1-1.5 \text{ ml mol}^{-1} \text{ sec}^{-1}$ and

K_5/K_2 has to be decreased correspondingly. The circles in fig. 4 are calculated for $(K_5/K_2) = 2 \times 10^4 \text{ ml mol}^{-1}$ and $K_6 = 1.4 \text{ ml mol}^{-1} \text{ sec}^{-1}$. From the slope of the line through the circles the value $3.2 \times 10^4 \text{ ml}^2 \text{ mol}^{-2} \text{ sec}^{-1}$ for K_7 is found.

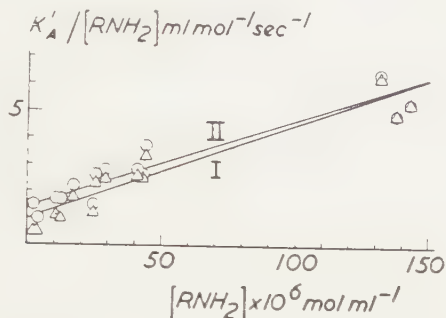


Fig. 4. Provisional and final values of $K'_A/[RNH_2]$ plotted against $[RNH_2]$:

- I Provisional values calculated with $(K_5/K_2) = 4 \times 10^4 \text{ ml mol}^{-1}$
- II Final values calculated with $(K_5/K_2) = 2 \times 10^4 \text{ ml mol}^{-1}$

The value of K_8 can only be determined from experiments at high pH. These data (table 2) are relatively inaccurate on account of the high reaction velocities.

For very high $[OH^-]$ eq. (10) may be written as:

$$(14) \quad \begin{cases} K_{\text{obs}} = K'_1 + K_4[OH^-] + K_6[RNH_2] + K_7[RNH_2]^2 + K_8[RNH_2][OH^-] \\ \hspace{20em} = C_1 + C_2[OH^-] \end{cases}$$

with

$$(14a) \quad C_1 = K'_1 + K_6[RNH_2] + K_7[RNH_2]^2$$

$$(14b) \quad C_2 = K_4 + K_8[RNH_2]$$

or

$$(15) \quad \lim_{[OH^-] \rightarrow \infty} \frac{K_{\text{obs}}}{[OH^-]} = C_1 \frac{1}{[OH^-]} + C_2.$$

The slopes C_1 have been calculated with the values of K_6 and K_7 as found above, and have been included in table 3.

In fig. 2 A straight lines corresponding to eq. (15) have been drawn and in fig. 2 B the intercepts of fig. 2 A have been plotted against $[RNH_2]$. From the slope of this line the value of

$$(16) \quad K_8 = 3 \times 10^6 \text{ ml}^2 \text{ mol}^{-2} \text{ sec}^{-1}$$

has been found.

Finally we have calculated the values of K_{obs} from the theoretical equation (10) and compared these values in table 6 to the experimental ones.

Some trial and error showed that the best fit to all the data was obtained with the values of the constants listed in table 5. The accuracy of the

TABLE 5

List of constants of hydrolysis and aminolysis by glycine of E.T.A. at 37° C

K'_1	$= 6 \times 10^{-5} \text{ sec}^{-1}$
K_3/K_2	$= 1.9 \times 10^7 \text{ ml mol}^{-1}$
K_4	$= 150 \text{ ml mol}^{-1} \text{ sec}^{-1}$
K_5/K_2	$= 2 \times 10^4 \text{ ml mol}^{-1}$
K_6	$= 1.5 \text{ ml mol}^{-1} \text{ sec}^{-1}$
K_7	$= 3 \times 10^4 \text{ ml}^2 \text{ mol}^{-2} \text{ sec}^{-1}$
K_8	$= 3 \times 10^6 \text{ ml}^2 \text{ mol}^{-2} \text{ sec}^{-1}$

constants is not very large, but it seems a fair estimate that the actual values lie within 20 % of the ones given in the table.

TABLE 6

Values of K_{obs} as calculated with the constants of table 5 from eq. (10) and as determined experimentally

Exp. No.	$[\text{OH}] \times 10^9$ (mol ml ⁻¹)	$[\text{RNH}_2] \times 10^6$ (mol ml ⁻¹)	$K_{\text{obs}} \times 10^6$ experimental (sec ⁻¹)	$K_{\text{obs}} \times 10^6$ calculated (sec ⁻¹)
73	2250	10	480	483
72	14500	10	2600	2688
81	5000	20	1270	1152
77	10000	20	2150	2202
84	5000	40	1650	1518
83	10000	40	2760	2868
8	2.2	2.2	8	8.4
12	3.6	3.8	13	13.8
88	12.5	12.5	42	45
70	5.3	10.8	33	35
71	12.8	24.4	64	82
67	3.4	17.0	56	52
66	5.0	25.5	91	81
32	5.7	29	107	95
33	8.2	41	144	144
22	8.6	43	146	153
51	30	138	730	840
57	4.5	44	190	155
86	11.3	143	806	879
60	13	132	880	772
56	23	230	2020	2001

5. Reaction products

The isolation of acetyl glycine from the reaction mixture was described in a previous paper [7]. The experimental conditions of that reaction (pH=8.4, total glycine concentration 1 molar) were such, that the main reaction paths were the spontaneous and the glycinate catalysed aminolysis (K_6 and K_7). In order to show definitely whether reactions K_8 and K_5 lead to aminolysis or hydrolysis new experiments under suitable reaction conditions are planned.

6. Kinetics at 25° C

Meanwhile the kinetic experiments have been continued at 25° C. The overall picture of the two reactions is the same as that at 37° C. The energies of activation as deduced from preliminary experiments are all low (5–15 k cal).

A discussion of the mechanism of the reaction will be postponed until the data at the lower temperature are completed.

The authors wish to thank F. BROUWER, W. P. J. D. VAN DER DRIFT, J. W. HAKEN, P. W. HENDRIKSE, Y. D. LOOPSTRA, A. H. STOUTHAMER, and A. H. WAGENAAR for their assistance in the reaction velocity measurements.

7. Appendix

Derivation of equation (9) for the velocity of simultaneous hydrolysis and aminolysis by glycine of E.T.A.:

According to the proposed reaction scheme the reaction velocity can be written as:

$$(9a) \quad \left\{ \begin{aligned} -\frac{d[\text{E.T.A.}]}{dt} &= K_1[\text{E.T.A.}][\text{H}_2\text{O}] - K_2[\text{C}_1] + K_4[\text{E.T.A.}][\text{OH}] + \\ &+ K_6[\text{E.T.A.}][\text{RNH}_2] - K_7[\text{E.T.A.}][\text{RNH}_2]^2 + K_8[\text{E.T.A.}][\text{RNH}_2][\text{OH}]. \end{aligned} \right.$$

Assuming the existence of a stationary state with respect to C_1 , we may write:

$$\frac{d[\text{C}_1]}{dt} = K_1[\text{E.T.A.}][\text{H}_2\text{O}] - K_2[\text{C}_1] - K_3[\text{C}_1][\text{OH}] - K_5[\text{C}_1][\text{RNH}_2] = 0$$

or:

$$(9b) \quad [\text{C}_1] = \frac{K_1[\text{E.T.A.}][\text{H}_2\text{O}]}{K_2 + K_3[\text{OH}] + K_5[\text{RNH}_2]}.$$

After substitution of C_1 eq. (9a) is written as:

$$\begin{aligned} -\frac{d[\text{E.T.A.}]}{dt} &= K_1[\text{E.T.A.}][\text{H}_2\text{O}] - K_2 \frac{K_1[\text{E.T.A.}][\text{H}_2\text{O}]}{K_2 + K_3[\text{OH}] + K_5[\text{RNH}_2]} + K_4[\text{E.T.A.}][\text{OH}] + \\ &+ K_6[\text{E.T.A.}][\text{RNH}_2] + K_7[\text{E.T.A.}][\text{RNH}_2]^2 + K_8[\text{E.T.A.}][\text{RNH}_2][\text{OH}] \\ &= K_1[\text{ETA}][\text{H}_2\text{O}] \frac{K_3[\text{OH}] + K_5[\text{RNH}_2]}{K_2 + K_3[\text{OH}] + K_5[\text{RNH}_2]} + K_4[\text{E.T.A.}][\text{OH}] + \\ &+ K_6[\text{E.T.A.}][\text{RNH}_2] + K_7[\text{E.T.A.}][\text{RNH}_2]^2 + K_8[\text{E.T.A.}][\text{RNH}_2][\text{OH}]. \end{aligned}$$

By substituting $K'_1 = K_1[\text{H}_2\text{O}]$ and rearranging we obtain:

$$(9) \quad \left\{ \begin{aligned} -\frac{d[\text{E.T.A.}]}{dt} &= [\text{E.T.A.}] \left\{ K'_1 \frac{K_3[\text{OH}] + K_5[\text{RNH}_2]}{K_2 + K_3[\text{OH}] + K_5[\text{RNH}_2]} + \right. \\ &\left. + K_4[\text{OH}] + K_6[\text{RNH}_2] + K_7[\text{RNH}_2]^2 + K_8[\text{RNH}_2][\text{OH}] \right\}. \end{aligned} \right.$$

8. *Summary*

The kinetics of the aminolysis of ethyl thioacetate (E.T.A.) by glycine at 37° were investigated between pH=8 and pH=12. The reaction is of the first order in E.T.A. The dependence on the pH and the concentration of glycine is complicated. Three reactions run parallel, one first order with respect to glycinate ($\text{H}_2\text{NCH}_2\text{COO}^-$), one second order with respect to glycinate and at high pH one that is first order in glycinate and in the OH^- -ion concentration. A fourth reaction in which the glycinate is involved was found at low pH. This reaction is competitive with one of the hydrolysis reactions.

BIBLIOGRAPHY

1. OVERBEEK, J. TH. G., V. V. KONINGSBERGER, *Proc. Kon. Nederl. Akad. v. Wetenschappen, Series B57*, 311 (1954).
2. LYNEN, F., E. REICHERT, L. RUEFF, *A.* **574**, 1 (1951).
3. WIELAND, TH., W. SCHÄFER, *A.* **576**, 104 (1952).
4. SCHWYZER, R., *Helv. Chim. Acta* **36**, 414 (1953).
5. ———, CH. HÜRLIMANN, *Helv. Chim. Acta* **37**, 155 (1954).
6. HAWKINS, P. J., D. S. TARBELL, *J. Am. Chem. Soc.* **75**, 2982 (1953).
7. KONINGSBERGER, V. V., J. TH. G. OVERBEEK, *Proc. Kon. Nederl. Akad. v. Wetenschappen, Series B57*, 81 (1954).
8. OWEN, B. B., *J. Am. Chem. Soc.* **56**, 24 (1934).

PLEISTOCENE VERTEBRATES FROM CELEBES. IX

ELASMOBRANCHII

BY

D. A. HOOIJER

(*Rijksmuseum van Natuurlijke Historie, Leiden*)

With plates I — II

(Communicated by Prof. H. BOSCHMA at the meeting of May 29, 1954)

In the collection of fossil vertebrates made by Mr H. R. VAN HEEKEREN at various localities in the Tjabengè area, Sopeng district, between the Walanae river and the Singkang depression, about 100 km Northeast of Macassar in Southwestern Celebes (HOOIJER, 1954, and the literature cited therein), elasmobranch fishes are represented by isolated teeth of galeoid sharks, and a few fragments of spines of sting rays. Fortunately the majority of these remains are characteristic as to genus; they will be described in the present contribution.

In contradistinction to the land vertebrate fauna (*Testudo*, *Stegodon*, *Archidiskodon*, *Celebochoerus*, (?) *Babyrousa*, and *Anoa*) the fossil fish fauna of Tjabengè contains no features that distinguish it from similar faunas in Southern and Eastern Asia. Furthermore, shark genera are rather long-lived, many of the modern genera being identifiable already down in the Cretaceous. Consequently, these fishes are less important both zoogeographically and stratigraphically than are the land vertebrates. The bone-bearing beds of Beru, Sompoh, and Tjeleko in the Tjabengè area are river deposits, which may explain the absence at these sites of certain types of sharks that are truly pelagic and do not enter rivers; indeed some of the forms identified from the present collection are closely allied to or apparently identical with modern sharks that are known to ascend rivers, some even beyond tidal influence and into fresh water.

It should be stated, too, that the Celebes fossil vertebrate remains have not been found in situ; there is no guarantee of the uniform age of these fossils. However, out of the five shark genera described below there is only one (*Hemipristis*) foreign to the region at present; the remaining genera still exist around Celebes today. Most of the fossil remains of *Galeocerdo*, *Carcharhinus*, *Isurus*, and *Carcharias* in the present collection even seem to be specifically identical with living Indo-Australian forms, while all but one or two of the land mammals of Tjabengè belong to extinct genera. Therefore, the sharks do not appear to be older geologically than the mammals, and I see no obvious reason for not dealing with these fishes under the head Pleistocene Vertebrates from Celebes just the same.

***Galeocerdo cuvier* (Lesueur) subsp.**

Galeocerdo javanus Martin, Samml. Geol. Reichsmus. Leiden, vol. 3, 1883, p. 24, pl. II fig. 15.

The tiger shark (tjutjut matjan) is represented in the Sompoh collection by two teeth (pl. I figs 1, 5, 6) that leave no doubt as to their belonging to the recent species. It is believed that there is but one living species of *Galeocerdo* in all the tropical and subtropical seas, the correct name of which is *Galeocerdo cuvier* (Lesueur) (BIGELOW and SCHROEDER, 1948, pp. 266–275).

The two fossil teeth agree closely in their highly diagnostic characters. The lingual surface is swollen near the base, the labial surface is flattened. The mesial¹⁾ margin is convex and coarsely serrate in its middle part; the serrations are rather fine in the apical portion of the mesial margin, which is straight. Distally, the crown is deeply and sharply notched; apically of the notch the margin is almost straight and finely serrate. Basal to the notch the margin is convex and denticulated, each denticle being very finely serrate itself. Both mesially and distally the serrations flatten out toward the base.

One of the fossil teeth is incomplete mesially at the base, but the other tooth is complete and shows the mesial margin to be slightly distorted at its basal end, the basal fifth of the mesial margin is S-shaped. The examination of recent jaws and isolated teeth of *Galeocerdo* in the Leiden Museum does not disclose even the slightest difference between the fossil and the recent teeth. Even the peculiar twist at the base mesially shows up in the recent teeth; it appears to provide a notch in which fits the distal extremity of the crown of the adjoining tooth, which overlaps its neighbour to a slight extent. There is no difference in general shape or in any detail of the serrated margins of the crown as described above.

Both in the upper and the lower jaws of *Galeocerdo* the teeth become lower passing from the symphysis to the corners of the mouth, and the only difference between the upper and the lower teeth is that the uppers are slightly larger than the lowers of the same serial position.

The fossil specimens from Sompoh are either of the right upper, or of the left lower jaws.

Turning now to the fossil record of *Galeocerdo* in Asia, MARTIN (1883, p. 24, pl. II fig. 15) has described an incomplete fossil tooth from Ngembak in Java as a new species, *Galeocerdo javanus*. However, the supposedly

¹⁾ In sharks, as in Man, the tooth series forms a gradual curve, without pronounced bends, which renders it convenient to refer to the sharp margins of the crowns as mesial and distal, according to the margin being toward the median line, as the teeth stand in the arch, and following its curve, or away from the median line, again following the curve of the dental arch. This is the procedure generally adopted in the description of the human dentition (see BLACK, 1902). In previous literature on sharks' teeth we find these margins being referred to either as inner and outer, or as anterior and posterior, which is confusing.

distinctive characters of the fossil Javanese shark's tooth cited by MARTIN, viz., the unevenness of the serration of the mesial margin, and the straightness of its apical part, do occur in the recent species. There is absolutely no difference between the fossil Javanese type specimen (MARTIN, l.c.) and those from my collection of Celebes (pl. I figs 1, 5, 6) and all these teeth fully conform to the recent type. A second *Galeocерdo* tooth from Java has been described by MARTIN (1883, p. 25, pl. II fig. 16) as akin to *Galeocерdo tigrinus* Müller et Henle, which is a synonym of *G. cuvier* (Lesueur) (FOWLER, 1941, p. 186; BIGELOW and SCHROEDER, 1948, p. 274).

Galeocерdo teeth occur neither in the DUBOIS collection (DUBOIS, 1907, p. 455; KOUmans, 1949) nor in the SELENKA collection (HENNIG, 1911) of fossil vertebrates from Java. DE BEAUFORT (1928, p. 4) mentions *Galeocерdo javanus* Martin from a mine at Kleripan (Djocja), Java, but these teeth have not been described or figured. DE BEAUFORT regards the Kleripan specimens as of Miocene age, as did MARTIN for the Ngembak teeth. NOETLING (1901, p. 375, pl. XXV fig. 16) reports on tooth fragments of *Galeocерdo* from Miocene beds in Burma, but these specimens are stated to be too ill-preserved to allow of a specific determination.

Tiger sharks (BIGELOW and SCHROEDER, 1948, pp. 270–271) are found indifferently far out on the high seas and in coastal waters, and they enter river mouths.

Hemipristis cf. *serra* Agassiz

As originally observed by AGASSIZ (1833–43, p. 237) *Hemipristis* teeth are, in a way, intermediate between those of *Galeocерdo* and those of certain *Carcharhinus* species. The marginal serrations do not extend quite to the tip, leaving the apical fourth or fifth of the crown smooth, and the serrations are more coarse on the concave distal margin than on the convex mesial margin. The generic type, *Hemipristis serra* Agassiz (1833–43, atlas, pl. 27 figs 18–30), which is from the Miocene Molasse of Württemberg, Germany, has been recorded from Java (MARTIN, 1883, p. 26, pl. II fig. 17) and from Burma (NOETLING, 1901, p. 374, pl. XXV figs 9–10), but the specific identity of the Javanese sample with the Württemberg types has been doubted by WOODWARD (1889, p. 450).

This is one of the rare cases in which a genus was found fossil before it was discovered in the recent state. PROBST (1878, pp. 141–146) made the discovery that the genus *Hemipristis* still lives in the Red Sea as "*Dirrhizodon*" *elongatus* Klunzinger, and this fact is adopted by WOODWARD (1889, p. 448).

None of the upper teeth of *Hemipristis* in the collection from Sompoh and Beru are complete, but their generic position is certain (pl. I figs 3, 4, 7, 8, 14). Most diagnostic is the inequality of the serrations on the mesial and distal margins, as said above. The base is swollen on the lingual surface, and the tip is gently curved distally, as in *Galeocерdo*, but the

present teeth lack the deep and sharp distal notch that is so characteristic of the last named genus. The lower teeth are more conical, higher, narrower at the base, and less recurved at the apex than the uppers; of this type there are three complete specimens in the Sompoh collection (pl. I figs 2, 9, 10).

Comparison with published figures and descriptions of fossil *Hemipristis* teeth fails to show any character by which the Celebes specimens could be differentiated. There is some, undoubtedly individual, variation in the degree of serration; five are finely serrate specimens, two are rather coarsely serrate, the remaining four teeth being intermediate. The Javanese¹⁾ and Burmese specimens are of the coarsely serrated type, as were AGASSIZ's originals. If PROBST's arrangement of the teeth of *Hemipristis* is correct, the type of tooth figured on pl. I fig. 14 is that which occurs at the distal end of the series; it could easily be mistaken for a small distal *Carcharhinus* tooth but differs in the serration being absent on the apical few mm of the tip, and in the relatively more coarse distal serrae. The larger and complete lower teeth presented on pl. I figs. 2, 9, 10 of the present paper agree with those figured by AGASSIZ (1833-43, pl. 27 figs 28-33), PROBST (1878, pl. I figs 52, 53, and 60), and NOETLING (1901, pl. XXV figs 9a-e); these are the "Uebergangszähne" (transitional teeth) of PROBST (1878, p. 145), the teeth placed between the front and the lateral teeth. As in *Galeocерdo*, there is not much difference between the recent upper teeth and the lower, the former reach greater mesio-distal lengths than the latter (PROBST, l.c.).

The variation seen in the recent species induced PROBST to unite the two Miocene species described by AGASSIZ (1833-43, pp. 237-239) as *Hemipristis serra* and *H. paucidens* respectively, but at the same time PROBST creates a new species, *H. klunzingeri*, for a number of teeth which differ from *H. serra* in being smaller (!) and somewhat less serrate;

¹⁾ Several *Hemipristis* teeth from a mine at Kleripan (Djoeja), Java, are said to agree with the tooth described by MARTIN (DE BEAUFORT, 1928, p. 4).

PLATE I

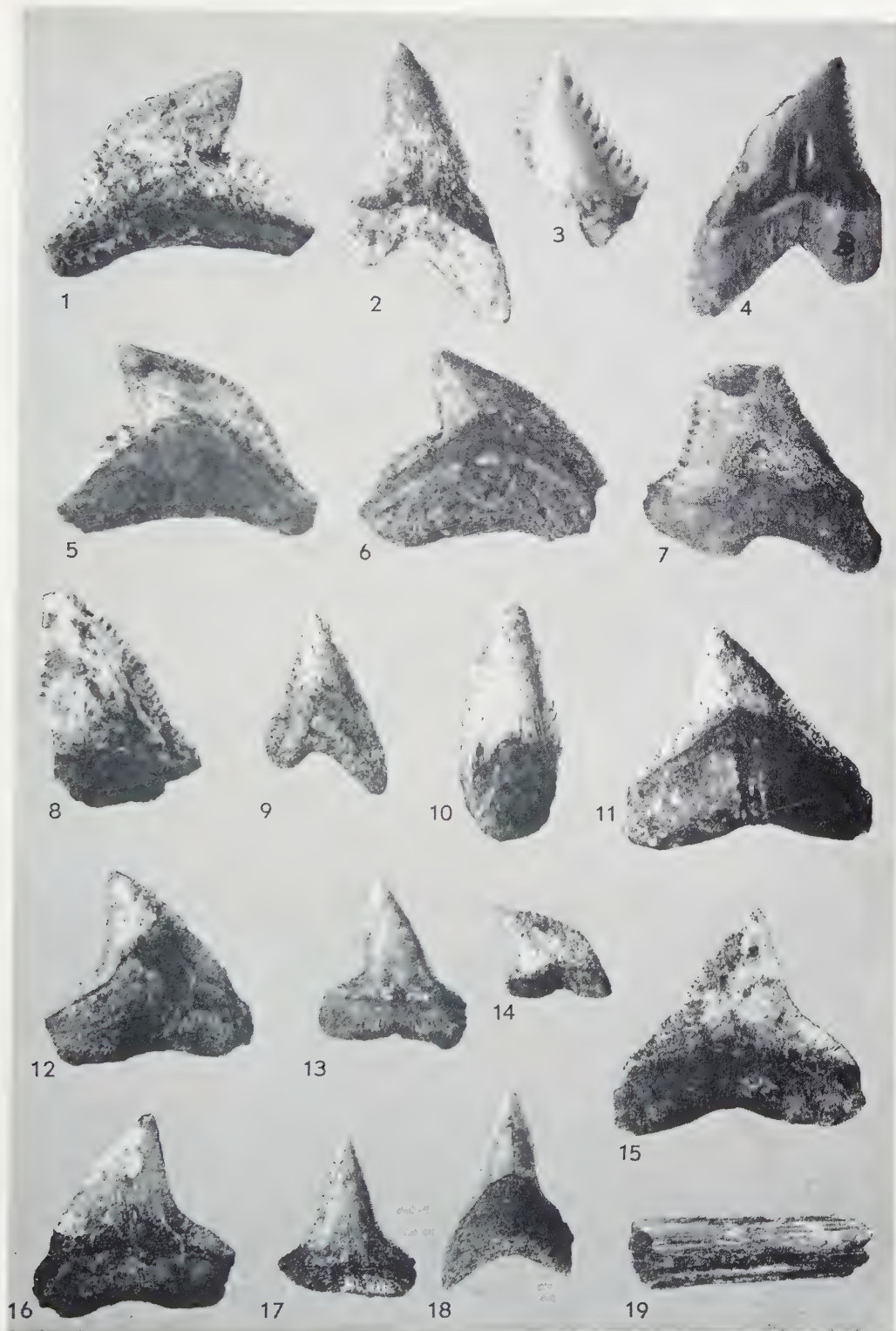
Figs 1, 5, 6. *Galeocерdo cuvier* (Lesueur) subsp., right upper or left lower teeth, Sompoh, S.W. Celebes; fig. 1, labial view; figs 5-6, lingual views

Figs 2-4, 7-10, 14. *Hemipristis* cf. *serra* Agassiz; figs 3-4, Beru, S.W. Celebes; figs 2, 7-10, 14, Sompoh, S.W. Celebes; fig. 2, right lower tooth, labial view; fig. 3, left upper tooth, lingual view; fig. 4, right upper tooth, labial view; fig. 7, left upper tooth, labial view; fig. 8, right upper tooth, lingual view; fig. 9, left lower tooth, lingual view; fig. 10, right lower tooth, lingual view; fig. 14, left upper tooth, labial view

Figs 11-13, 15-18. *Carcharhinus* cf. *brachyurus* (Günther), Sompoh, S. W. Celebes; figs 11 and 15, right upper tooth; fig. 11, lingual view; fig. 15, labial view; figs 12 and 16, right upper tooth; fig. 12, lingual view; fig. 16, labial view; figs 13, 17, 18, lower teeth; figs 13 and 17, labial views; fig. 18, lingual view

Fig. 19. *Dasyatis* (*Trygon*) spec., tail spine, Sompoh, S.W. Celebes

Figs 1-18, $1\frac{1}{2}$ natural size; fig. 19, $\frac{3}{4}$ natural size





on the transitional teeth of *Hemipristis klunzingeri* the distal serrae are from 6 to 8 in number, against 12 or more in *H. serra*, and the smooth apical part of the crown is relatively larger, the ratio of its height to that of the serrated portion of the margin being 1:2 in *H. klunzingeri* as opposed to 1:3 or 1:4 in *H. serra*. As will be seen from my figures, the Celebes teeth agree with *H. serra*, and so does the tooth figured by NOETLING (1901, pl. XXV figs 9a-e). The much better known lateral teeth of *Hemipristis* with their mesio-distally elongated bases (pl. I figs 4, 7) also closely agree with those of *H. serra* (AGASSIZ, 1833-43, pl. 27 figs 18-24; PROBST, 1878, pl. I figs 54-56). The specimens from Java (MARTIN, 1883, pl. II fig. 17) and from Burma (NOETLING, 1901, pl. XXV fig. 10) do not seem to be different from *Hemipristis serra* Agassiz either.

It is unlikely that a single species of shark should have lived in the Miocene of Württemberg and in the Pleistocene of Celebes, and it may be preferred for the present to identify the Celebes teeth as *Hemipristis* cf. *serra* Agassiz. We should keep in mind that WOODWARD (1889, p. 450), too, was reticent to identify the Javanese specimen described by MARTIN with AGASSIZ's type, a consideration that was undoubtedly based on geographical rather than morphological grounds.

Apparently nothing is known of the habits of the sole living species of the genus, *Hemipristis elongatus* (Klunzinger), but *Hemipristis* is commonly found associated with *Galeocерdo* in fossil deposits (see, e.g., JORDAN, 1907, pp. 101 and 104, figs 6 and 13¹⁾).

Carcharhinus cf. *gangeticus* (Müller et Henle)

As understood by BIGELOW and SCHROEDER (1948, pp. 320-325), ground sharks, *Carcharhinus* Blainville (*Carcharias* Cuvier, nec Rafinesque; *Eulamia* Gill) include a much larger number of species than any other genus of modern sharks, among which are many of the most familiar of the larger sharks of warm seas. The Indo-Australian *Carcharhinus gangeticus* (Müller et Henle, 1841, p. 39, pl. 13) has been recorded from the Pleistocene of Java (Trinil) by DUBOIS (1907, p. 455) and by KOUMANS (1949, p. 80, pl. II figs. 6-9), from the Miocene of Burma by NOETLING

¹⁾ Not fig. 4b, c, and e: see JORDAN and BEAL, 1913, p. 247.

PLATE II

Figs 1-12, 18-23. *Carcharhinus* cf. *gangeticus* (Müller et Henle), Sompoh, S. W. Celebes; figs 1-10, left upper teeth; figs 1-4, 9, lingual views; figs 5-8, 10, labial views; figs 11-12, right upper tooth; fig. 11, labial view; fig. 12, lingual view; figs 18-23, lower teeth; figs 18-20, labial views; figs 21-23, lingual views
Figs 13, 14, 17. *Carcharias* cf. *cuspidatus* (Agassiz), Sompoh, S.W. Celebes, teeth; figs 13 and 17, lingual views; fig. 14, mesial or distal view
Figs 15-16. *Isurus* cf. *glaucus* (Müller et Henle), Beru, S.W. Celebes, front tooth; fig. 15, lingual view; fig. 16, mesial view

All figures 1½ natural size

(1901, p. 375, pl. XXV figs 11–15), from the Neogene of Japan by ISHIWARA (1921, p. 71, pl. XII figs 22–25), and from a fossil deposit in Netherlands New Guinea by SIEMON (1929, p. 346).

It is generally accepted that *Carcharhinus japonicus* (Temminck et Schlegel) is synonymous with *C. gangeticus* (GARMAN, 1913, p. 139; FOWLER, 1941, p. 168/69), but, as already keenly observed by MARTIN (1883, p. 29), this is entirely unfounded. I have investigated this matter as we have the two cotype jaws of *C. japonicus* in the Leiden Museum. Both of these differ decidedly from *C. gangeticus* as figured by MÜLLER and HENLE (1841, pl. 13). The first specimen, *C. japonicus* cat.a, does not have broadly triangular upper teeth as *C. gangeticus* but upper teeth that narrow abruptly above the broad base, with the mesial margin obliquely straight and the distal margin deeply notched. The teeth of this specimen resemble those of *Carcharhinus melanopterus* (Quoy et Gaimard) so very closely (cf. MÜLLER and HENLE, 1841, pl. 19 fig. 5) that I can hardly doubt its specific identity with *C. melanopterus*, which, moreover, is known to occur in Japan (FOWLER, 1941, p. 161). The second cotype specimen of *C. japonicus*, Leiden Museum cat.b, has broadly triangular upper teeth, the mesial margin is convex, and the distal margin concave, increasingly so in the more distally placed teeth. This specimen is very different from *C. gangeticus*, too; it appears to belong to *Carcharhinus milberti* (Müller et Henle, 1841, p. 38, pl. 19 fig. 3), the brown or sand-bar shark that does not live anywhere near Japan at all (cf. BIGELOW and SCHROEDER, 1948, pp. 368–378). This last observation was made by MARTIN already over seventy years ago when he examined the specimen in our Museum, as shown by a signed note in his handwriting attached to the board supporting the jaws cat.b of *C. japonicus*, and I cannot but agree with MARTIN on this point. The other cotype specimen of *C. japonicus*, cat.a, has apparently not been seen by MARTIN; this specimen is even more clearly distinct from *C. gangeticus* than is cat.b.

Teeth of *Carcharhinus* are far more abundantly represented in the Sompoh collection than those of any other shark genus, and it has been possible to reconstruct almost the entire tooth series, both above and below. The best preserved specimens are represented on pl. II figs 1–12, 18–23. The upper teeth close to the symphysis are almost symmetrical, broadly triangular and finely serrate, with margins weakly convex toward the tip and weakly concave toward the base both mesially and distally. Subsequent teeth become increasingly oblique: the mesial margin remains weakly convex toward the tip and weakly concave toward the base, the distal margin is concave, most markedly so toward the base. The lower teeth are erect on broad bases with lanceolate cusps narrowing rather abruptly toward the tip. Only the apical part of the cusps is serrate on the mesial and distal margins; the basal parts are smooth.

As such, the fossil Celebes teeth agree very well with those of *Carcharhinus gangeticus* (Müller et Henle), and there seems nothing against

referring them provisionally to this species, which is known to occur in the fossil state in Java, Burma, Japan, and New Guinea as well. The species *C. gangeticus* is known to ascend rivers to above tidal influence (DAY, 1889, p. 14).

***Carcharhinus* cf. *brachyurus* (Günther)**

There is another species of *Carcharhinus* in the Celebes collection, a number of teeth of which are figured on pl. I figs 11–13, 15–18. The uppers reach a rather large size and have a swollen base as in *Galeocerdo*; the mesial margin is weakly convex toward the tip and weakly concave toward the base; the distal margin is deeply though not sharply notched, and the serrations are even and fine along both margins. The lower teeth have broad bases, are deeply notched at the base both mesially and distally, above which they narrow gradually toward the tip, and are likewise finely serrate all along the mesial and distal margins.

It seems to me that the present fossils are very close to *Carcharhinus brachyurus* (Günther). This is the very common whaler shark of Australian waters, which is placed by WHITLEY (1940, p. 97, figs 88–3, 92) in the genus *Galeolamna* Owen but which seems clearly referable to the present genus (BIGELOW and SCHROEDER, 1948, p. 320). It seems probable even that the fossil teeth from Java described by MARTIN (1883, p. 28, pl. II figs 22–23) as *Carcharias* (*Prionodon*) *dijki* belong to *C. brachyurus*. MARTIN's species has been recorded since from a mine at Kleripan, Djocja, Java, by DE BEAUFORT (1928, p. 3), and from the Lower and Middle Palembang beds of Sumatra by BURCKHARDT (1906, p. 242).

Besides the above mentioned genera and species of sharks, which belong to the family Carcharhinidae (BIGELOW and SCHROEDER, 1948, p. 262), I have a few species with teeth of a different type, even more widely known as fossils. In sand sharks, genus *Carcharias* Rafinesque (including *Odontaspis* Agassiz), the teeth in both jaws are awl-shaped and two-rooted, with or without mesial and distal basal denticles. In mackerel sharks or Makos, genus *Isurus* Rafinesque (synonym *Oxyrhina* Agassiz), and in porbeagle sharks, genus *Lamna* Cuvier (*Otodus* Agassiz), the anterior teeth are high, slender, and two-rooted just as are those of *Carcharias*. In *Isurus*, however, there are no basal denticles, while in *Lamna* most or all of the teeth do have mesial and distal basal denticles. The generic distinction is a matter requiring complete dentitions; thus, in *Carcharias* the first tooth is smaller than the second, in *Isurus* and *Lamna* the first two teeth in each jaw are similar in shape; in *Isurus* the more distal teeth tend to become triangular and labio-lingually flattened, while in *Lamna* the first two teeth are similar in shape to those succeeding distally (BIGELOW and SCHROEDER, 1948, pp. 98, 99, 111, and 123).

It would appear from this digression that, with isolated front teeth, it is well-nigh impossible to distinguish between *Carcharias* on the one

hand, and *Isurus* and *Lamna* on the other. I have studied jaws of each of these genera in the Leiden Museum, and found the anterior teeth to be very similar indeed; the only reliable differences between the anterior teeth of *Lamna* and those of *Carcharias* appear to be that in *Lamna* the basal denticles are relatively larger, and the bases of the crowns less distinctly depressed between the roots than in *Carcharias*. The teeth of *Isurus*, of course, are characterized by the total absence of basal denticles, and further by their more labio-lingually compressed crowns. The mesial and distal margins of the front teeth form sharp edges, which in *Isurus glaucus* (Müller et Henle) as well as in the fossil giant species *Isurus hastalis* (Agassiz) (PROBST, 1879, p. 129) extend from the tip down to the base of the crown, while in *Lamna* and in *Carcharias* (*Odontaspis*) the sharp edges terminate a few mm above the base, so that at this level the labial surface passes into the lingual by a smooth rounded edge (cf. PROBST, 1879, p. 143).

In my collection from Beru and Sompoh both *Isurus* and *Carcharias* are represented.

Isurus cf. *glaucus* (Müller et Henle)

A large front tooth, the apical part and one root of which are broken off, is characterized by the absence of basal denticles and by its labio-lingually compressed crown. Moreover, the sharp mesial and distal edges run down to the base of the crown (pl. II figs 15–16). This tooth, which originates from Bern, probably represents the Pacific Mako, *Isurus glaucus* (Müller et Henle, 1841, p. 69, pl. 29); it cannot be distinguished from the recent specimens in the Leiden Museum.

A much larger animal, identified as *Isurus hastalis* (Agassiz), occurs in the Pleistocene of Java (KOUmans, 1949, p. 80, pl. II fig. 5, erroneously spelled "*hastatus*"), and in the Neogene of Japan (ISHIWARA, 1921, p. 62, pl. X figs 1–32).

Carcharias cf. *cuspidatus* (Agassiz)

Seven teeth, with long and slender crowns and two roots, display tiny basal denticles mesially and distally (except in the most waterworn specimens); these denticles are smaller than those in *Lamna*. Furthermore, the sharp edges forming the mesial and distal margins do not extend to the base of the crown, and the base of the crown is more rounded, less compressed labio-lingually than in *Isurus*. It seems evident that these teeth can be referred to *Carcharias*.

The convex lingual surface of the crowns is as smooth as the flattened labial surface, without longitudinal striae. As pointed out by PROBST, the presence or absence of longitudinal striae on the lingual surface of the teeth is of systematic significance: it plays an important role in the distinction of fossil species of "*Odontaspis*" (= *Carcharias*). A delicate

longitudinal striation is seen on the lingual surface of the teeth in some of the species, such as *Carcharias macrotus* (Agassiz, 1833-43, p. 273, pl. 32 figs 29-31), including *Carcharias elegans* (Agassiz, l.c., p. 289, pl. 35 figs 1-5, pl. 37a, fig. 59), which, as pointed out by WHITE (1931, p. 62) is the young of *C. macrotus*, while in others, such as *Carcharias cuspidatus* (Agassiz, 1833-43, p. 290, pl. 37a figs 43-50), these striae are absent (PROBST, 1879, pp. 143-154; WOODWARD, 1889, pp. 360-375).

There are quite a few species of *Carcharias* (*Odontaspis* auct.) (WOODWARD, 1889, pp. 360-375; WHITE, 1931, pp. 47-65; CASIER, 1946, pp. 63-74), and our fossil Celebes teeth (pl. II figs 13, 14, 17), with their small development of basal denticles and without longitudinal striation upon the lingual surface, can be provisionally identified with *C. cuspidatus*. KOUMANS (1949, p. 80, pl. II figs 3-4) has recorded "*Odontaspis* cf. *cuspidata* (Ag.)" from the Pleistocene of Trinil, Java, but my own examination of the teeth, which form part of the DUBOIS collection (no. 11644), shows that they possess a delicate longitudinal striation upon their lingual surface (the specimens have been figured in labial view only, and thus their most diagnostic character is not visible in KOUMAN's figures), which indicates that the Javanese fossil teeth cannot possibly belong to *C. cuspidatus*. These teeth can best be identified as *Carcharias* cf. *macrotus* (Agassiz); they agree very closely with the type specimens of *Carcharias elegans* (Agassiz, 1833-43, pl. 35 figs 1-5, pl. 37a, fig. 59), which, as said above, is a synonym of *C. macrotus*.

Carcharias cuspidatus (Agassiz) is also known from the Neogene of Japan (ISHIWARA, 1921, p. 70, pl. XII figs 12-21). The living species of *Carcharias* (BIGELOW and SCHROEDER, 1948, p. 99) do not appear to have longitudinal striations upon the lingual surface of their teeth and, therefore, there is a distinct possibility that the Celebes and Japanese fossil *Carcharias* teeth actually represent one or another species of sand shark still living in the region, such as *Carcharias arenarius* Ogilby, *C. tricuspidatus* Day, or *C. owstoni* Garman.

To complete the survey of the fossil elasmobranchs of Celebes I have to mention two small and waterworn fragments of spines (pl. I fig. 19), perfectly straight and evenly barbed on both sides, compressed in cross section, with one surface convex and the other flattened with longitudinal grooves, evidently belonging to stings of *Dasyatis* (*Trygon*), the feared sting rays of the tropical Pacific and Atlantic. A great many forms have been described, both living and as fossils, and it is not well possible to allocate the species of the Sompoh specimens. Two similar fragments in the DUBOIS collection from Java (no. 11639c), mentioned by KOUMANS (1949, p. 79) as fragments of fin spines of an unidentified species of fish in reality are remains of tail spines, too. The Javanese samples are smaller than those from Celebes, the former measuring $4\frac{1}{2}$ and $8\frac{1}{2}$ mm respectively across the barbed edges against $14\frac{1}{2}$ mm in the two Sompoh fragments.

LITERATURE CITED

- AGASSIZ, L., *Recherches sur les poissons fossiles*, 3, Neuchâtel, VIII + 390 + 32 pp., 17 + 47 pls. (1833-43).
- BEAUFORT, L. F. DE, On a collection of Miocene fish-teeth from Java. *Wet. Med. Dienst Mijnb. Ned. Indië*, 8, 3-6 (1928).
- BIGELOW, B. and W. C. SCHROEDER, Sharks, in: *Fishes of the Western North Atlantic*, edited by J. TEE-VAN, C. M. BREDER, S. F. HILDEBRAND, A. E. PARR and W. C. SCHROEDER. New Haven (Sears Foundation for Marine Research), 59-546, figs 6-106 (1948).
- BLACK, G. V., *Descriptive anatomy of the human teeth*. Philadelphia (White Dental Manufacturing Co.), 4th ed., XVII + 169 pp., 143 figs (1902).
- BURCKHARDT, R., Über die sechs in den Untern und Mittlern Palembang-schichten gefundenen Selachierzähne. *Tijdschr. Kon. Ned. Aardr. Gen.*, ser. 2, 23, 241-243 (1906).
- CASIER, E., La faune ichthyologique de l'Yprésien de la Belgique. *Mém. Mus. Roy. Hist. Nat. Belg.*, no. 104, 267 pp., 6 pls., 18 figs (1946).
- DAY, F., *The Fauna of British India, including Ceylon and Burma, Fishes*, 1. London (Taylor and Francis), XVIII + 548 pp., 164 figs (1889).
- DUBOIS, E., Eenige van Nederlandschen kant verkregen uitkomsten met betrekking tot de kennis der Këndeng-fauna (fauna van Trinil). *Tijdschr. Kon. Ned. Aardr. Gen.*, ser. 2, 24, 449-458 (1907).
- FOWLER, H. W., The fishes of the groups Elasmobranchii, Holocephali, Isospondyli, and Ostariophysi, etc. *Bull. U.S. Nat. Mus.*, no. 100, 13, X + 879 pp. (1941).
- GARMAN, S., The Plagiostomia (Sharks, Skates, and Rays). *Mem. Mus. Comp. Zool. Harvard*, 36, XIII + 515 pp., 77 pls. (1913).
- HENNIG, E., Die Fischreste, in: L. SELENKA and M. BLANCKENHORN, *Die Pithecanthropus-Schichten auf Java*. Leipzig (Engelmann), 54-60, pl. XI (1911).
- HOOIJER, D. A., Pleistocene Vertebrates from Celebes. VIII. Dentition and skeleton of *Celebochoerus heekereni* Hooijer. *Zool. Verh. Museum Leiden*, no. 24, 46 pp., 6 pls. (1954).
- ISHIWARA, YOSHIO, Fossil shark teeth from the Neogene of Japan. *Sc. Rep. Tôhoku Imp. Univ.*, ser. 2 (Geol.), 5, no. 3, 61-74, pls. X-XII (1921).
- JORDAN, D. S., The fossil fishes of California with supplementary notes on other species of extinct fishes. *Univ. Calif. Publ., Bull. Dept. Geol.*, 5, no. 7, 95-144, pls. 11-12, 33 figs (1907).
- and C. H. BEAL, Supplementary notes on fossil sharks. *Ibid.*, 7, no. 11, 243-256, 5 figs (1913).
- KOUMANS, F. P., On some fossil fish remains from Java. *Zool. Med. Museum Leiden*, 30, no. 5, 77-82, pls. I-II (1949).
- MARTIN, K., *Palaeontologische Ergebnisse von Tiefbohrungen auf Java*. I. Vertebrata, Crustacea. *Samml. Geol. Reichsmus. Leiden*, 3, 1-42, pls. I-III (1883).
- MÜLLER, J. and J. HENLE, *Systematische Beschreibung der Plagiostomen*. Berlin (Veit), XXII + 200 pp., 60 pls. (1841).
- NOETLING, F., The fauna of the Miocene beds of Burma. *Mem. Geol. Surv. Ind.*, new series, 1, no. 3, 1-378, pls. I-XXV (1901).
- PROBST, J., Beiträge zur Kenntnis der fossilen Fische aus der Molasse von Baltringen. *Jahresh. Ver. nat. Nat. Württemberg*, 34, 113-154, pl. I (1878); *ibid.*, 35, 127-191, pls. II-III (1879).
- SIEMON, R., Jungtertiäre Molluskenfauna aus Niederländisch-Ost-Indien. *Ber. Naturf. Ges. Freiburg*, 29, 309-369, 4 figs, 2 maps (1929).

- WHITE, E. I., The vertebrate faunas of the English Eocene, 1, from the Thanet Sands to the basement of the London Clay. London (British Museum (Nat. Hist.)), XIV + 104 pp., 162 figs (1931).
- WHITLEY, G. P., The fishes of Australia. I. The sharks, rays, devil-fish, and other primitive fishes of Australia and New Zealand. Sydney, Roy. Zool. Soc. N.S. Wales, 280 pp., 299 figs (1940).
- WOODWARD, A. S., Catalogue of the fossil fishes in the British Museum (Natural History), Part I, Elasmobranchii. London (Taylor and Francis), XLVII + 474 pp., 17 pls., 13 figs (1889).

PALEONTOLOGY

PLEISTOCENE VERTEBRATES FROM CELEBES. X

TESTUDINATA

BY

D. A. HOOIJER

(*Rijksmuseum van Natuurlijke Historie, Leiden*)

With plate I

(Communicated by Prof. H. BOSCHMA at the meeting of May 29, 1954)

A single testudine has thus far been described from the *Archidiskodon-Celebochoerus* fauna of the Pleistocene of Southwestern Celebes, viz., a large terrestrial tortoise, *Testudo margae* Hooijer (1948). The holotype, a right scapula, has the shaft and the proscapular process more compressed anteroposteriorly, and the coracoid facet more elongated and deviating from the vertical axis of the scapula at a more acute angle than in the Galápagos, the Seychelles, and the Aldabra-Madagascar species of *Testudo*. The fossil scapula from Celebes is distinguished from that of the tortoises of the Mascarene Islands (Mauritius, Réunion, and Rodriguez) by its less slender build, and by the coracoid not being ankylosed to the scapula. The type specimen originates from Beru, Tjabengè (Sopeng district), about 100 km northeast of Macassar.

I have received evidence of gigantic species of *Testudo* from other localities in the Tjabengè area, viz., from Sompoh, 12 km North of Beru, and from Tjeleko, which is again 8 km North of Sompoh. These fossils are of interest as they belong to individuals that are much larger than that to which the type scapula of 1948 belonged. This individual must have measured already over one meter, possibly even one and one-half meters in straight carapace length (HOOIJER, 1948, p. 1179).

A proximal fragment of a huge right scapula from Tjeleko, like the type specimen, has the proscapular process broken off, and the coracoid is not preserved. As the borders of the glenoid cavity unfortunately are damaged, and as the coracoid facet is also too much injured for accurate measurement, the only measurements that can be given are the width and the anteroposterior diameter of the shaft, which are ca. 70, and 40 mm respectively, against 38, and 21 mm in the type, and further the greater and the smaller diameters of the proscapular process at its base, which are ca. 75, and 32 mm respectively, as opposed to ca. 45, and 14 mm in the type specimen. Thus, both the shaft and the proscapular process of the Tjeleko scapula appear to be less markedly compressed anteroposteriorly than those in the type specimen, but the difference is small.

The anteroposterior diameter of the shaft and the smaller diameter of

the proscapular process, the only measurements that can be exactly given and allow of a comparison between the Tjeleko fragment and the type of *Testudo margae*, both vary from 10 to 16 % of the length of the scapula (measured from glenoid cavity to distal knob) in ten gigantic specimens of *Testudo* (scapula over 200 mm in length: HOOIJER, 1948, pp. 1175-1177). The former measurement points to a scapula length of 250-400 mm, the latter to a scapula length of 200-320 mm. Accepting 300 mm as a reasonable figure for the length of the Tjeleko scapula, the straight carapace length of the individual to which the Tjeleko specimen belonged must have been somewhere between 140 and 190 cm (the length of the scapula varying from 0.16 to 0.22 of the carapace length in living specimens of *Testudo*, see HOOIJER, 1948, p. 1178), whereby the Tjeleko individual exceeds the largest living specimen of gigantic land tortoise known, and ranks among the largest fossil forms ever found. The shell of *Testudo atlas* (Falconer et Cautley) from the Upper Siwaliks of India (now Pakistan) on exhibit in the American Museum of Natural History in New York, N.Y. (BROWN, 1931) is about 180 cm long. A largely reconstructed carapace in the British Museum (Natural History) in London even is over 250 cm in length, which is probably too much (LYDEKKER, 1889, p. 75), six feet (180 cm) being a more conservative estimate.

In the collection from Sompoh there is the shaft of a left humerus, likewise referable to the present species (pl. I fig. 1). Since both extremities are missing no accurate comparison with the same bone of *Testudo atlas* (Falconer, 1868 I, pl. 31 figs 4-5, as a femur) can be made. As FALCONER (l.c. p. 374) notes, the Siwalik bone is so like the humerus of an existing *Testudo* that the outline of the fossil could pass for a magnified representation of the recent bone, done by means of the pantograph. A peculiarity of the Sompoh specimen, not noticed by FALCONER or LYDEKKER (1885, p. 160) in the humerus of *Testudo atlas*, is that there is an extensive depression on the medial surface for the insertion of the latissimus dorsi. In living species of *Testudo* this usually is merely a roughened area, but WILLIAMS (1950) notes the presence of a large and deep pit for the attachment of the latissimus dorsi in the humerus of *Testudo cubensis* Leidy, and further observes that this pit is present in a somewhat less distinct but still plainly visible form in many Galápagos tortoises. The development of the medial muscular depression in the Sompoh humerus is less marked than that in *Testudo cubensis* (cf. WILLIAMS, 1950, pl. 5 fig. 3) but nevertheless quite plainly visible, and we can be reasonably sure that if a similar development had occurred in *Testudo atlas* it would not have been left unnoticed by FALCONER or by LYDEKKER. The specific value of its occurrence in the Celebes fossil humerus of *Testudo* appears to be somewhat doubtful, and further specimens are required in order to settle whether this is a constant feature in *Testudo margae* or not.

A large bone fragment, again originating from Tjeleko, has puzzled me for some time, but I now believe it to represent a xiphiplastral cornu

(pl. I figs 2-3). FALCONER (1868 I, pl. 30 fig. 2) gave a good figure, one-sixth natural size, of the posterior portion of the plastron of *Testudo atlas*; according to LYDEKKER (1885, p. 159) the carapace of the individual to which this specimen belonged would have been about eight feet in a straight line. The Tjeleko fragment represents the left cornu, slightly damaged apically, and broken off about 10 cm from the tip, where the transverse diameter amounts to 13 cm and the dorsoventral diameter to $6\frac{1}{2}$ cm. The resemblance between the present fossil and that of FALCONER's figure is very close indeed; the upper surface is convex and grooved, the medial margin almost straight as far as preserved, the lateral margin gently convex. The lower surface (not shown in FALCONER's figure) is smooth and concave anteroposteriorly, most markedly so in its middle portion, and convex transversely. I believe, from this striking resemblance of the Celebes fossil specimen to the highly characteristic xiphiplastral cornua of the Siwalik species, that the relationships between *Testudo margae* and *Testudo atlas* may be closer than I originally thought; it has at least been shown that the Celebes form of *Testudo* is in no way inferior in size to "*Colossochelys*" *atlas* of the Asiatic continent.

The evidence of the existence of trionychoid turtles in the *Archidiskodon-Celebochoerus* fauna, however scanty, will be considered in the lines that follow.

Trionychidae, gen. et spec. indet.

Among a small number of fragments of shells of freshwater turtles, so easy to recognize because of their characteristically sculptured outer surface, there is a postero-lateral fragment of a left hypoplastron, with two processes, the anterior of which is smaller than the posterior (pl. I fig. 5). It might belong either to *Trionyx* or to *Pelochelys*, both leatherback turtles widely distributed in Southeastern Asia. It seems that *Chitra* can be excluded since in this genus the postero-lateral processes on the hypoplastron are three to four in number (SIEBENROCK, in JAEKEL, 1911, p. 79), as opposed to two in other trionychoids. It might be remarked, however, that a recent skeleton of *Chitra indica* (Gray) (Leiden Museum, herp. reg. no. 7054) and a series of fossil *Chitra* hypoplastra in the DUBOIS collection from Trinil, Java, in the Leiden Museum (Coll. Dub. nos. 2726, 2733, 2734, and 9936) show that the posterior postero-lateral process of the hypoplastron is distinctly set off from the anterior two processes, which are united to a greater or less extent, thereby simulating the

Figs 1-3. *Testudo margae* Hooijer; fig. 1, humerus sin., Sompoh, S.W. Celebes, medial view; figs 2-3, left xiphiplastral cornu, Tjeleko, S.W. Celebes; fig. 2, upper view; fig. 3, lateral view

Figs 4-5. Trionychidae, gen. et spec. indet., Sompoh, S.W. Celebes; fig. 4, costal plate, dorsal view; fig. 5, fragment of left hypoplastron, ventral view

Figs 1-2. 3/5 natural size; fig. 3, 3/4 natural size; figs 4-5, natural size



condition seen in *Trionyx* and related genera. Nothing special is to be said about the Sompoh hypoplastral fragment; it agrees with recent specimens closely.

There are further a few very fragmentary costal plates, the generic position of which is even less certain as, in addition to the genera of trionychoid turtles already mentioned above, they might belong to *Lissemys* or to *Dogania* as well (see SIEBENROCK, 1909, pp. 595-608, and SMITH, 1931, p. 154). The best specimen is presented on pl. I fig. 4.

This must bring our discussion of the evidence of fossil turtles to a close. Even more urgently than in the cases of the mammals (HOOIJER, 1954, and the literature cited therein) we do need more and better specimens of the turtles in order that we may eventually obtain a complete knowledge of the species that make up the *Archidiskodon-Celebochoerus* fauna.

LITERATURE CITED

- BROWN, B., The largest known land tortoise. *Natural History*, 31, 183-187, 5 figs (1931).
- FALCONER, H., *Palaeontological memoirs and notes*. London (Hardwicke), 2 vols. (1868).
- HOOIJER, D. A., Pleistocene Vertebrates from Celebes. II. *Testudo margae* nov. spec. *Proc. Kon. Ned. Akad. v. Wetenschappen Amsterdam*, 51, 1169-1182, 1 pl. (1948).
- , Pleistocene Vertebrates from Celebes. VIII. Dentition and skeleton of *Celebochoerus heekereni* Hooijer. *Zool. Verh. Museum Leiden*, no. 24, 46 pp., 6 pls. (1954).
- JAEKEL, O., Die fossilen Schildkrötenreste von Trinil. in: L. SELENKA and M. BLANCKENHORN, *Die Pithecanthropus-Schichten auf Java*. Leipzig (Engelmann), pp. 75-81, pls. XIV-XV (1911).
- LYDEKKER, R., Siwalik and Nerbada Chelonia. *Mem. Geol. Surv. Ind.*, ser. 10, 3, 155-208, pls. XVIII-XXVII, 1 fig. (1885).
- , *Catalogue of the fossil Reptilia and Amphibia in the British Museum (Natural History)*, part 3, containing the order Chelonia. London (Taylor and Francis), XVIII + 239 pp., 53 figs (1889).
- SIEBENROCK, F., Synopsis der rezenten Schildkröten, mit Berücksichtigung der in historischer Zeit ausgestorbenen Arten. *Zool. Jahrb., Suppl.* no. 10, 427-618 (1909).
- SMITH, M. A., *The Fauna of British India. Reptilia and Amphibia. I. Loricata, Testudines*. London (Taylor and Francis), XXVIII + 185 pp., 2 pls., 42 figs, map (1931).
- WILLIAMS, E., *Testudo cubensis* and the evolution of Western hemisphere tortoises. *Bull. Amer. Mus. Nat. Hist.*, 95, art. 1, 1-36, pls. 1-8, 2 figs (1950).

GEOLOGY

CROSS-CUTTING CHARACTER OF PLUTONS IN THE CORDILLERA BLANCA, PERU

BY

C. G. EGELER AND T. DE BOOY

(Communicated by Prof. H. A. BROUWER at the meeting of May 29, 1954)

The present paper is based on field observations made by the authors in 1952, during a geological exploration in the southern part of the Cordillera Blanca in NW Peru ¹⁾; the observations were worked out by C. G. EGELER. It is the second of a number of preliminary notes on various results of the exploration ²⁾.

The main scope of this paper is to draw attention to the fact that, contrary to the generally accepted opinion, the visible contacts of the plutonic bodies in the Cordillera Blanca are very often discordant with respect to the structure of the folded country-rock.

Before going into our own observations on this subject, some general remarks will be made on the plutonic bodies in the Andes and their distribution in relation to the general tectonic pattern, with particular reference to the Cordillera Blanca.

Plutonic rocks of the calc-alkaline suite are of considerable importance in many of the South American Cordilleras. They are chiefly represented by intermediate members of the granite-diorite series, and therefore will, when speaking in a general manner, be called granodiorites. The rocks in question are for the greater part thought to have been emplaced during the Lower to Middle Tertiary.

Two mountain ranges consisting for an important part of such plutonic rocks, stand out especially on account of their unusual height, viz. the Cordillera Blanca already mentioned and the Cordillera Real in northern Bolivia. In these two ranges ice-clad granodiorite peaks reach up to heights well above 6000 m. and find their culmination in the 6768 m high Cerro Huascaran, the highest summit of the Cordillera Blanca.

STEINMANN was the first to realize the true extent of the tertiary

¹⁾ The writers gratefully acknowledge grants from: the Netherlands Organization for Pure Research (ZWO), the Royal Netherlands Geographical Society (KNAG), the Royal Netherlands Geological and Mining Society (KNGMG), the Molengraaff Fund, the Prins Bernhard Fund, the Royal Netherlands Alpine Club (KNAV), as well as from various Dutch industrial and business concerns.

²⁾ A first note, by C. G. EGELER, entitled: "Predominance of intermediate and more acid rocks among the cretaceous volcanic products in the southern Cordillera Blanca, Peru", was published in these same Proceedings (Lit. 3).

plutonic activity in the Andes, and to discuss, in a highly interesting article (Lit. 5, see also Lit. 6), the relationship between the general structure of the Cordilleras and the distribution and shape of the granodiorite bodies. He pointed out the more or less axial position of the plutonic masses with respect to the structure of the mountain ranges, and compared their surface extension with loosely strung rows of pearls, arranged in the general trend in a setting of contact metamorphic slates. This holds good for the Cordillera Blanca, where in the trend of this range several granodiorite masses break through the folded sedimentary cover, whereas they appear to play no role of importance in the depressions which border it on both sides: In those parts of the Santa valley W of the Cordillera Blanca not covered by secondary material (approx. between 2500 and 3400 m), the rocks exposed seem to be almost exclusively mesozoic sediments (Lit. 6, p. 233), while in the east the parts of the Mosna valley visited during the 1952 exploration, though locally eroded to a level below 3000 m, were found to be devoid of granodiorite.

While the granodiorite outcrops attain their largest extension in the northern and central parts of the Cordillera, they are also exposed over considerable areas further south. In the region investigated, they were found to be almost entirely restricted to the western side of the range³).

The various granodiorite masses, as far as these are exposed in the southern part of the Cordillera, give an impression of independence, as in the trend of the range they are often separated by fairly extensive sedimentary areas. However, notwithstanding this apparent independence at the surface, the distribution of the thermal metamorphism in the sedimentary series, indicates a connection at a deeper level. The parts of the massifs that are visible may merely be considered as local culminations of a larger plutonic mass, for the main part concealed by the folded cover and with its longer axis stretched more or less parallel to the tectonic axis of the Cordillera; this is in accordance with STEINMANN's conception. It is important to state, however, that the situation may be more complicated. During our investigations in the southern part of the range, we found e.g. that the plutonic bodies—apart from the usual basic, marginal facies—are sometimes inhomogeneous, being composed of more than one rock type, differing not only in composition but also in age of emplacement. A good example of such a heterogeneous pluton is afforded by the large mass exposed in the N of the investigated region, which mass is found to be composed of three different rock types. Since this complex will be dealt with in a later publication, it need only be mentioned here that a tonalite and two different types of granodiorites can be distinguished, one of the latter of a highly leucocratic character and locally grading into granite. These separate masses were emplaced in order of increasing acidity. Although little is known about the actual

³) For the general geological setting and a geological sketch-map of the investigated area, refer to Lit. 3.

age difference, there seems no reason to doubt that these masses are closely related and that their emplacement proceeded during a single plutonic phase.

The gradual decline of the Cordillera Blanca towards its southern extension, in relation to the axial plunge, already becomes evident in the investigated region. Towards the S, the sedimentary cover gradually gains in importance, while visible plutonic masses become scarce. The same appears to be the case at the northern end of the range (Lit. 5).

While it is thus an established fact, that both shape and distribution of the plutonic masses are closely related to the major tectonic pattern of the Cordillera, it does not imply that a similar relationship exists on a smaller scale. During our investigations in the Cordillera Blanca, special attention was paid to this subject. We can state that we were repeatedly struck by the marked independence of the shape of the plutonic masses and the folded structure of the sedimentary cover, the great majority

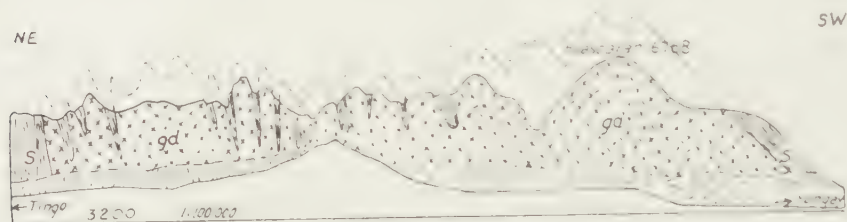


Fig. 1. Section through the Cordillera Blanca, (somewhat diagrammatic) after STEINMANN (Lit. 6, p. 230), s contactmetamorphic slates and sandstones, gd granodiorite

of the contacts being clearly cross-cutting. This observation holds good not only for the often steep contacts exposed in the walls of the deeply eroded transverse-valleys, but just as much for the contacts at higher levels, where the sedimentary cover partly closes over the upper parts of the granodiorite masses, or where only remnants of the roof are preserved. The latter fact stands in direct contrast to STEINMANN's statements, which are often cited as illustrating the relations of a more or less classical example of Andean plutons (e.g. PENCK Lit. 4, p. 361 and BEARTH Lit. 1, p. 569). While STEINMANN admits an often discordant contact relationship in the deeper parts of the plutonic bodies, he claims that their contacts with the sedimentary roof are mostly of concordant nature, the sediments forming anticlinal arches with the stratification generally parallel with the contact surface. This conception of adaptation to structure, is illustrated by his cross-section of the Cordillera Blanca, reproduced in fig. 1.

In the part of the Cordillera visited during the 1952 exploration, concordant contacts (see e.g. fig. 5), proved to be quite exceptional. In those cases where concordance was indeed observed, it was mostly only over a relatively short distance and sometimes clearly coincidental, though one must

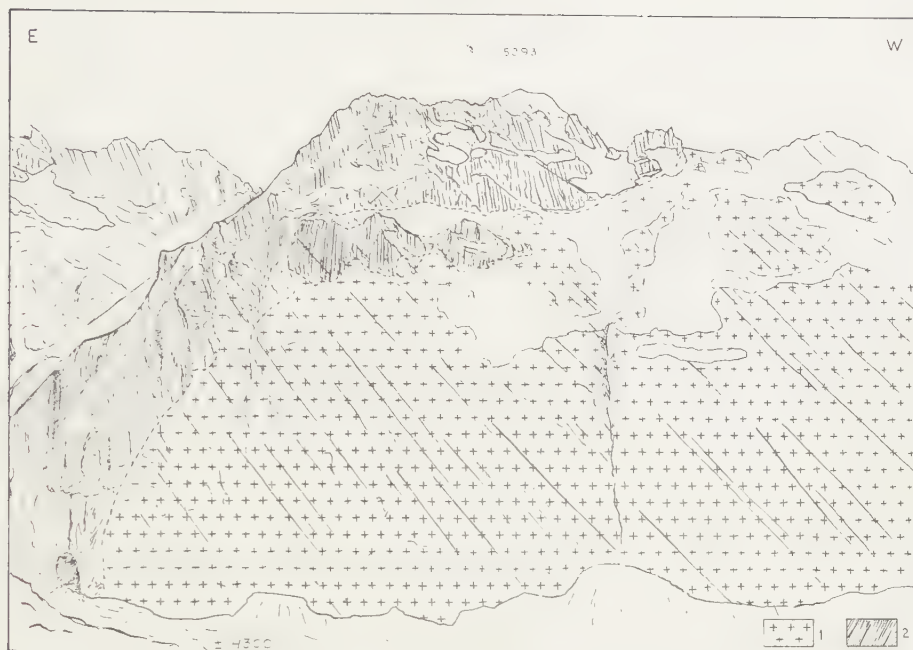


Fig. 2. Sketch of part of the southern wall of Quebrada Shallap. 1 granodiorite, 2 contact metamorphic sediments (lower neocomian slate-sandstone formation). The granodiorite abruptly cuts off the almost perpendicular sediments; the contact is irregular, with isolated roof-pendants and with abundant small apophyses (the latter not indicated in the sketch); the joints in the granodiorite (dipping ca 50° W) continue into the sedimentary cover

of course allow for a certain preference of the invading material to follow pre-existing discontinuities. It may be pointed out that in general the contacts are fairly sharp, and thus leave no doubt as to the position of the contact surface.

Examples of the usual type of contact, cross-cutting both in plan and in cross-section, are given in the figs 2-4.

Discordance is well demonstrated i.a. on the ridge S of Quebrada Shallap (fig. 2). Here the granodiorite abruptly cuts off the almost vertical sediments of the cover, without showing even the slightest tendency towards adaptation to structure.

Concordance, though over a short distance, does seem to exist directly E of Nevado Churup (fig. 3), but this only holds good for the contact of the sediments with one of the types of granodiorites represented at this locality ("grey" granodiorite). The younger "white" granodiorite, which forms the main plutonic mass, is plainly discordant.

Another example of the discordant contact relationship in the higher part of a plutonic body, if not in the roof itself, is illustrated by fig. 4, showing the contact of a tonalite mass at the junction of the Quebradas Cayesh and Quilcayhuanca.

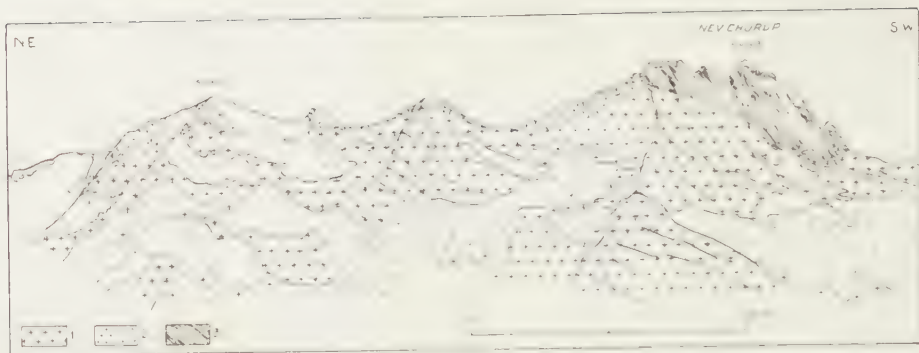


Fig. 3. Sketch of Nevado Churup, as viewed from the N. 1 "white" granodiorite, 2 "grey" granodiorite, 3 contact metamorphic sediments (lower neocomian slate-sandstone formation). Whereas the contact of the steeply inclined sediments with the "grey" granodiorite is apparently concordant, that with the younger "white" granodiorite is clearly of discordant character

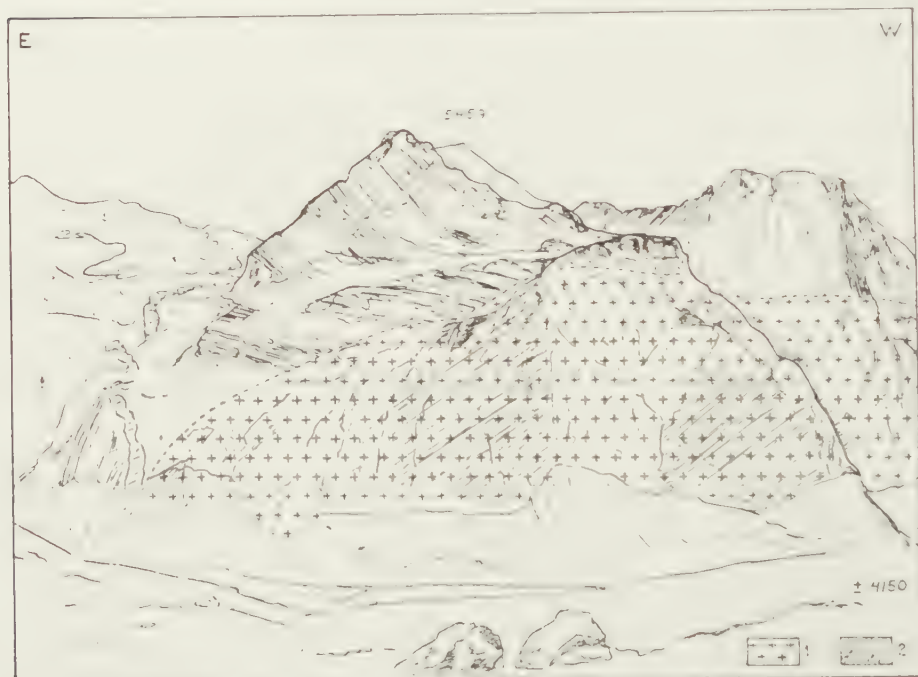


Fig. 4. Sketch of the tonalite contact at the junction of Quebrada Cayesh and Quebrada Quilcayhuanca. 1 tonalite, 2 contact metamorphic sediments (lower neocomian slate-sandstone formation)

In the foregoing it has been demonstrated that the contacts of the granodiorite masses in the investigated part of the Cordillera Blanca are generally discordant. Neither are the visible parts of the granodiorite masses confined to the anticlinal parts of the folded cover, though in a single case a small plutonic body—obviously a minor offshoot of the

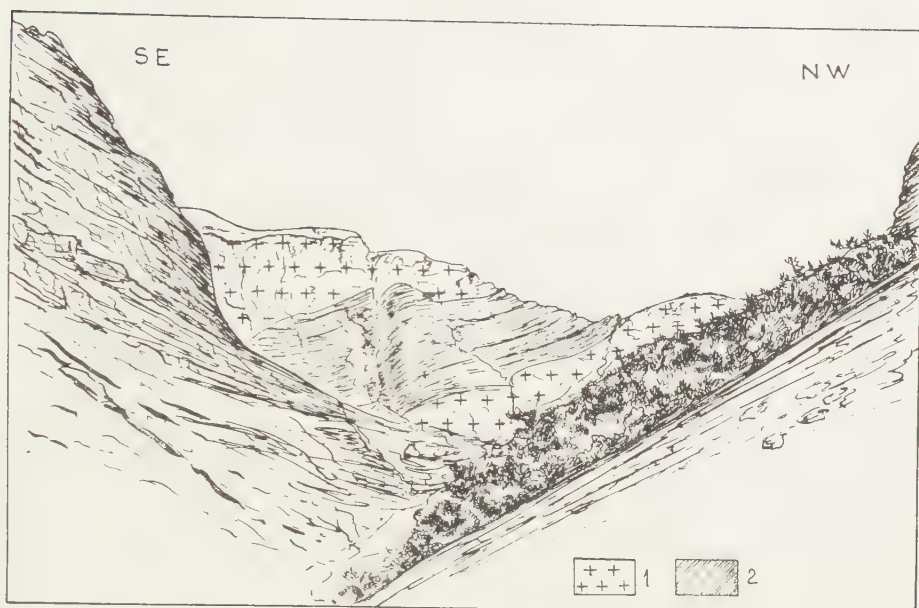


Fig. 5. Sketch of part of the Pongos Massif (ridge N of p. 5680), as viewed from the E. 1 granodiorite, 2 contact metamorphic sediments (lower neocomian slate-sandstone formation). A sedimentary mass of considerable size lies in the granodiorite body, the contacts being more or less concordant

main granodiorite body exposed further west—gave the impression of being emplaced in the core of an anticlinal fold (along the road approx. 1.5 km E of the Cahuish Pass). The majority of the apophyses of the larger bodies is, however, clearly discordant with respect to the structure.

It is clear that the prevalence of cross-cutting contacts harmonizes with the concept of post-tectonic emplacement of the granodiorites, i.e. an emplacement after the main folding. This does not imply, however, that the rocks have not been influenced by movements subsequent to their consolidation. In fact, crushed zones in the granodiorites appear to be far more common than generally realized, and microscopical study often discloses a considerable degree of mylonitization, especially in the most western parts of the plutonic masses⁴). It also seems impossible to attribute to other than tectonic causes, the intensive jointing of the type shown in fig. 2, which is generally a characteristic feature of the granodiorites. It seems obvious that these various phenomena should be attributed to a younger tertiary orogenic phase, in accordance with STEINMANN's opinion (Lit. 6).

In the Cordillera Blanca it is only the higher parts of the plutons that are exposed. Whereas the continuation of these masses towards depth thus

⁴) An intensive cataclasis of the granodiorites has been emphasized by BORR (Lit. 2), whose conclusion, however, that their intrusion took place prior to the main phase of the folding, is not consistent with the facts.

remains speculative, their visible contacts in most cases appear to diverge downwards. In any case not too much value should be attached to those rare cases where the granodiorite bodies give an impression of upward enlargement, or where large sedimentary masses are partly enclosed (fig. 5). These may, in fact, be no more than superficial phenomena and warrant no conclusions as to a possible floor. On this latter subject the deeply eroded valleys of the Cordillera Blanca, which offer such an ideal opportunity for a study of the plutonic bodies over vertical sections of more than 2 kilometers, fail to give any conclusive information.

Amsterdam, Geological Institute of the University

REFERENCES

1. BEARTH, P., Gesteine der Peruanischen Anden. Schweiz. Min. Petr. Mitt. **18**, 512-590 (1938).
2. BOIT, B., Algunas datos sobre la geología de Ancachs. Bol. Soc. Geol. Perú, **2**, 47-74 (1926).
3. EGELER, C. G., Predominance of intermediate and more acid rocks among the cretaceous volcanic products in the southern part of the Cordillera Blanca, Peru. Proc. Kon. Ned. Akad. v. Wetensch. **B57**, 329-335 (1954).
4. PENCK, W., Der Südrand der Puna de Atacama (NW-Argentinien). Abh. Math.-Phys. Kl. Sächs. Akad. d. Wiss. **I** (1920).
5. STEINMANN, G., Gebirgsbildung und Massengesteine in der Kordillere Süd-amerikas. Geol. Rundsch. **I**, 13-35 (1910).
6. ———, Geologie von Perú. (Heidelberg, 1927).

THE CRYSTAL STRUCTURES OF P_4S_{10} AND P_4S_7

BY

AAFJE VOS AND E. H. WIEBENGA

(Communicated by Prof. J. M. BIJVOET at the meeting of June 26, 1954)

Phosphorus and sulfur form the compounds P_4S_3 , P_4S_5 , P_4S_7 and P_4S_{10} [1], which are prepared [2] by melting a mixture of the elements. After solidification of the melt, crystals can be obtained by a slow continuous extraction with CS_2 .

An electron diffraction study of P_4S_3 was made by HASSEL *et al.* [3] in 1941. In the present paper our preliminary results of the structure determinations of P_4S_7 and P_4S_{10} by means of X-ray diffraction are reported. The work on P_4S_{10} is fairly complete, that on P_4S_7 is still in the stage of refinement of the atomic coordinates. Full details will be given elsewhere.

 P_4S_{10}

Optical goniometric measurements and X-ray photographs show that P_4S_{10} crystals are triclinic. With λ $CuK\alpha = 1.5418 \text{ \AA}$ the following values for the lattice constants were obtained:

$$\begin{array}{ll} a = 9.07 (\pm 0.04) \text{ \AA} & \alpha = 100^\circ.0 (\pm 0^\circ.4) \\ b = 9.07 (\pm 0.04) \text{ \AA} & \beta = 93^\circ.8 (\pm 0^\circ.4) \\ c = 9.16 (\pm 0.04) \text{ \AA} & \gamma = 108^\circ.5 (\pm 0^\circ.4) \end{array}$$

Two P_4S_{10} per unit cell.

WILSON's statistical method [4] and the absence of piezoelectricity indicate the spacegroup C_i , which was confirmed by the structure analysis.

The intensities of approximately 900 reflexions hkl were obtained from integrated oscillation photographs [5] about the b axis. The photographs were made using Zr filtered Mo radiation. No correction for absorption had to be applied.

From a three-dimensional Patterson synthesis it appeared that the atoms are arranged in molecules P_4S_{10} as shown in fig. 1. Because of their nearly equal atomic scattering factors phosphorus and sulfur atoms are difficult to distinguish by X-ray methods; as far as the distinction between phosphorus and sulfur concerns the structure given in fig. 1 is based on chemical arguments. The approximate position of the molecules relative to the centre of symmetry was determined by trial and error. The atomic coordinates were refined by computing consecutive Fourier syntheses of the [100] and [010] projections in the usual way. After applying BOOTH's "backshift" correction [6] for the finite series effect disagreement indices

$R \equiv \Sigma ||Fo| - |Fc|| / \Sigma |Fo|$ amounting to 0.10, 0.12 and 0.13 were obtained for the observed 0kl, h0l and hk0 reflexions respectively.

The bond lengths and angles are subject to estimated standard deviations

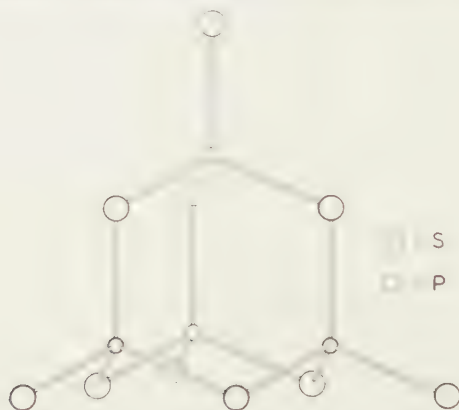


Fig. 1. Molecule of P_4S_{10}

of 0.035 Å and $1^\circ.5$. For sulfur atoms connected to two phosphorus atoms the average distance to a neighbouring phosphorus atom is 2.09 Å, for sulfur atoms connected to only one phosphorus atom this distance amounts to 1.96 Å on an average. The individual bond lengths show no significant deviations from the average values.

The bond lengths may be compared with PAULING and HUGGINS' [7] values for the length of a single (2.14 Å) and double (1.95 Å) bond between phosphorus and sulfur. None of the bond angles shows a significant deviation from $109^\circ 28'$. Short intermolecular distances range from 3.4 to 4.0 Å.

P_4S_7

P_4S_7 is monoclinic. Rotation and Weissenberg photographs about the a, b, and c axes were made using Ni filtered Cu radiation. From these the following values for the lattice constants were obtained, with $\lambda CuK\alpha = 1.5418$ Å:

$$\begin{aligned} a &= 8.87 (\pm 0.02) \text{ Å} \\ b &= 17.35 (\pm 0.03) \text{ Å} & \beta &= 92^\circ.7 (\pm 0^\circ.3) \\ c &= 6.83 (\pm 0.02) \text{ Å} \end{aligned}$$

Four P_4S_7 per unit cell.

The systematic absences are those required by the space group $P2_1/n$.

After some unsuccessful attempts to find approximate projections of the structure by the application of phase relationships between the structure factors, a three-dimensional Patterson synthesis was computed. The intensities were obtained from integrated Weissenberg photographs taken with Ni filtered Cu radiation. They were only approximately corrected for absorption. From the Patterson synthesis, it could be deduced that the atoms are arranged in molecules as shown in fig. 2. In this figure phosphorus

and sulfur atoms are again distinguished by chemical arguments only. Also the approximate position of the molecules in the cell could be found from the Patterson map. That the structure thus obtained is essentially

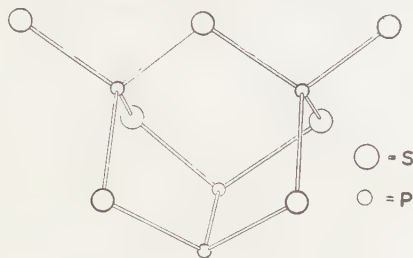


Fig. 2. Molecule of P_4S_7

correct appears from the three Fourier projections which could be computed using the signs of the structure factors as calculated from the approximate atomic positions. After one cycle of refinement by the Fourier method disagreement indices of 0.21, 0.16 and 0.18 were obtained for the observed $0kl$, $h0l$ and $hk0$ reflexions respectively. A further refinement of the atomic coordinates using Mo data is in progress. The bond lengths between phosphorus and sulfur atoms agree within the limits of error with those observed for P_4S_{10} . In the present stage of refinement the distance between the directly connected phosphorus atoms is remarkably large, namely 2.49 Å. The bond angles vary from 99° to 115° .

It is interesting that, although several structures for P_4S_7 were proposed by inorganic chemists, the structure given in fig. 2 was, as far as we know, never suggested before.

We wish to thank Mr A. P. MOSTERMAN for his assistance in many of the calculations and Messrs R. BELZ, Y. D. FEIKEMA and H. A. WESTRA for their experimental as well as computational cooperation during the work on P_4S_7 . Our thanks are also due to Professor Dr P. TERPSTRA and Dr W. G. PERDOK for their piezoelectric measurements on P_4S_{10} . We want to express our great gratitude to Theodorus Niemeijer N.V. for putting their I.B.M. equipment generously at our disposal for the summation of the Patterson and Fourier series and to Mr M. R. VAN DER VELDE and Miss G. E. VELDMAN for their assistance in operating these machines. The support of the Netherlands Organisation for Pure Scientific Research (Z.W.O.) is also gratefully acknowledged.

REFERENCES

1. PERNERT, J. C. and J. H. BROWN, *Chem. Eng. News* **27**, 2143 (1949).
TREADWELL, W. D. and CH. BEELI, *Helv. Chim. Acta* **18**, 1161 (1935).
STOCK, A. and B. HERSCOV, *Ber.* **43**, 1223 (1910).
2. *Org. Synth.* **12**, 73 (1932).
3. HASSEL, O. and ALF. PETTERSEN, *Tjids. Kjemi Bergvesen Met.* **1**, 57 (1941).
4. WILSON, A. J. C., *Acta Cryst.* **2**, 318 (1949).
5. WIEBENGA, E. H. and D. W. SMITS, *Acta Cryst.* **3**, 265 (1950).
BOSWIJK, K. H., Thesis Groningen, p. 35 (1954).
6. BOOTH, A. D., *Proc. Roy. Soc. (London)* **A188**, 74 (1946).
7. PAULING, L. and M. L. HUGGINS, *Z. Krist.* **87**, 205 (1934).

A-C OVERVOLTAGES

BY

FELIX GUTMANN *

(Van 't Hoff Laboratory, University of Utrecht)

AND

L. M. SIMMONS

*(School of Applied Chemistry, The N.S.W. University of Technology, Sydney, Australia)**(Communicated by Prof. J. TH. G. OVERBEEK at the meeting of May 29, 1954)*

We have drawn attention¹⁾ to the surprisingly large alternating potentials that can be applied to electrolytic solutions without gas being evolved, under conditions in which gases are copiously liberated on the application of the expected small direct voltage. In view of the interest in this phenomenon²⁾ we have further investigated the effect using the experimental arrangement shown in fig. 1. The source consists of a

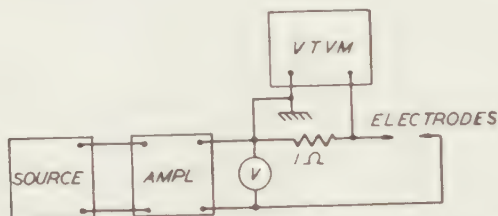


Fig. 1. Block-Diagram of Experimental Arrangement

Hewlett Packard Function Generator driving a Williamson Low Distortion Amplifier³⁾. The current through the cell was measured as the voltage drop across a 1 Ohm resistor by means of a Radiometer Vacuum Tube Voltmeter, or alternatively, by means of a Cambridge Precision Thermocouple of 9.6 Ohm heater resistance and a Leeds and Northrup type K potentiometer. The applied voltage was measured by a rectifier type voltmeter calibrated in RMS volts for sinusoidal input. The voltage and current waveforms were checked by means of an oscillograph, incorporating direct coupled amplifiers.

Platinized platinum exhibits a very low *d.c.* hydrogen overvoltage: less than 50 mV has been reported. Its *d.c.* oxygen overvoltage is approxi-

*) Permanent address: School of Applied Chemistry, The N.S.W. University of Technology, Sydney, Australia.

¹⁾ F. GUTMANN and L. M. SIMMONS, *Rev. Sci. Inst.* **20**, 674 (1949).

²⁾ R. H. MUELLER, *Anal. Chem.* **22**, 72 (1950).

³⁾ D. T. N. WILLIAMSON, *W.W.* **55**, 282, 365, 423 (1949).

mately 250 mV. In order to operate with a minimum of amplification and in a region of comparatively low *a.c.* overvoltages, platinum electrodes were therefore used after they had been allowed to become platinized by the passage of *a.c.* through the cell. They were observed through the walls of the cell by means of a low power microscope. The electrolyte was N/10 sulfuric acid.

To ensure that conditions were such that the usual *d.c.* overvoltages would cause gas evolution, a very low frequency square wave (0.1 cps) was applied and gas was evolved at a potential of about 1.0 V.

Typical values of the sinusoidal alternating voltages E_b required to liberate gas bubbles from the same system are listed in table 1 as a function of applied frequency. Up to 9 cps E_b is virtually the same as the *d.c.* overvoltage, but at higher frequencies it increases, reaching 6 times the *d.c.* value at 500 cps.

TABLE I
RMS Volts needed to produce gas evolution at a Pt — n/10 H₂SO₄ — Pt system at various frequencies. (sine-wave)

Frequency cps	RMS Volts required	Current passed mA
1	0.85	0.01
6	0.85	
9	1.1	
10	1.1	
15	1.6	
20	2.15	0.02
25	2.2	
50	3.0	
100	3.5	
250	4.5	
500	6.5	0.54

The values of E_b were reproducible to $\pm 10\%$, the variations probably being due to the difficulties in deciding when gas evolution just commences. It was noticed that on all occasions bubbles first formed on the electrode which had the smaller immersed area. When the difference between the areas of the two electrodes was considerable, quite rapid gas evolution could be observed from the smaller while no bubble formation could be detected at the larger. In one case, using a 100 cps square wave, a potential of 3 V was required to cause bubbles to form at the smaller electrode, but gas was liberated from both electrodes only when the voltage was raised to 6.5 V. This current density effect was also tested with a sinusoidal *a.c.* of 50 cps, the voltage being gradually increased from 0. Bubbles first appeared to form at the shorter electrode at 2.2 V RMS, none being visible at the longer. The longer electrode was then shortened until its immersed area was less than that of the other electrode; on the voltage again being gradually raised from 0 bubbles now appeared on the shortened

electrode before any were formed at the longer. The latter did not commence gas evolution until 5 V was reached.

When silver electrodes of unequal length were immersed in N/10 sulfuric acid, and to them is applied a gradually increasing 50 cps sinusoidal voltage, no gas was evolved until 0.5 V was reached when both electrodes appeared to be dissolving, yielding brown diffusion trails. Bubbles formed at 1 V at the shorter electrode. On increasing the frequency, dissolution ceased at 400 cps and 0.5 V, but recommenced at 2.5 V, bubbles appearing at 3.3 V at this higher frequency. The overvoltage thus appears to be considerably reduced if the electrode is capable of reacting with the electrolyte.

Fig. 2 shows that the Tafel equation ⁴⁾

$$(1) \quad \eta = a + b \log I$$

where η is the overvoltage, I the current and a and b are constants, is approximately obeyed by alternating current only at voltages less than about 2 V. However, the value of the transfer coefficient α calculated from this relationship is much too small; moreover the slopes of the Tafel

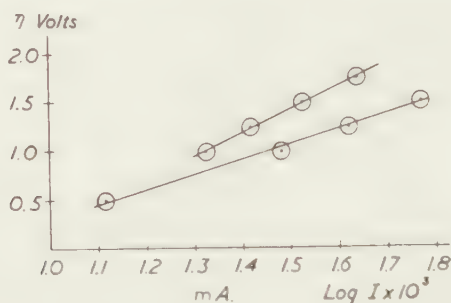


Fig. 2. Plots of the Tafel equation $\eta = a + b \log I$ for two values of current density

lines in fig. 2 depend on current density: the line corresponding to overvoltages at higher current densities *) is steeper than the line relating overvoltages at lower current densities.

A number of current vers. voltage curves were determined at frequencies between 20 and 1200 cps. The results were well reproducible (better than 3 %) and show that at voltages higher than about 2 V Ohm's law is obeyed for voltages at least up to 30 V. The cell admittance Y thus does not depend on the voltage when this exceeds about 2 V, but it varies with the frequency f according to the empirical relation

$$(2) \quad Y = a - b/\sqrt{f}$$

This is demonstrated by the straight lines obtained in plotting Y vers. $f^{-1/2}$ and shown in fig. 3. The constants for the system $Pt - N/10 \text{ H}_2\text{SO}_4 - Pt$

⁴⁾ J. TAFEL, Z. Phys. Chem. 50, 641 (1905).

*) All current densities refer to apparent (geometric) electrode areas.

used had the values $a=443$ micro-mhos and $b=795$ micro-mhos $f^{1/2}$. It is thus seen that at higher frequencies Y does indeed become frequency independent and its value approaches the conductivity of the electrolyte. This, of course, is the basis of the electrolytic tank method for the mapping

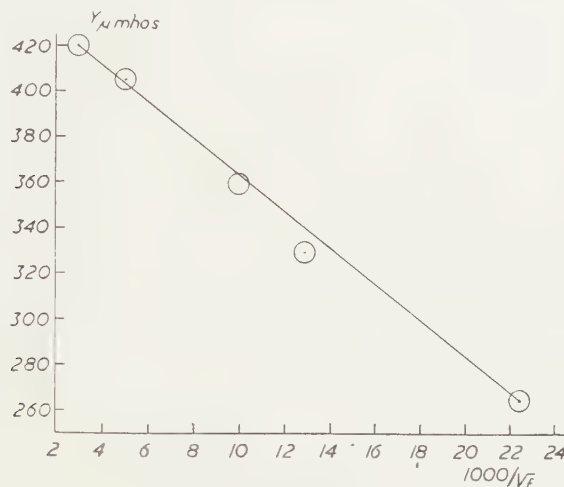


Fig. 3. Cell admittance Y plotted vers. $(\text{frequency})^{-1/2}$

of electric and other fields. Even at the comparatively high current densities which we employed, the admittance changed only from 405 to 420 micro-mhos between 405 and 1200 cps.

At a given constant current density the overvoltage decreases with

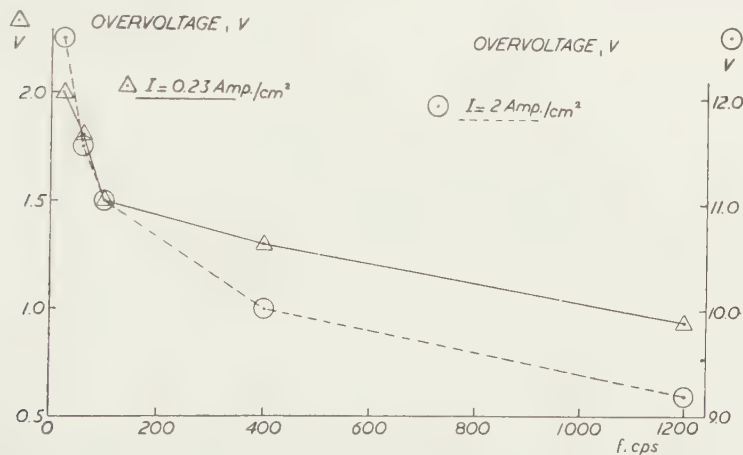


Fig. 4. Overvoltages at two values of current density vers. frequency

frequency irrespective of whether gas is evolved or not. This is in contradistinction to E_b , which rises with increasing frequency. Fig. 4 shows the overvoltages measured at the current densities (see footnote *) of 2.0 Amp/cm² and 0.23 Amp/cm², respectively, as a function of frequency.

While E_b rises with decreasing current density, the overvoltage at constant alternating current density exhibits the opposite behaviour by rising with increasing current density. A break is seen to occur in the potential vers. frequency curve for 2.0 Amp cm² at 100 cps; this is associated with the formation of visible gas bubbles, 11.0 V being applied. However, although a similar break occurs at this frequency at 0.23 Amp cm², no bubbles could be seen. This may have been due to the difficulty in observing the slow evolution of gas at the lower current density.

The fact that an equation of the form of equ. (2) cannot be derived from any finite combination of lumped circuit elements is in agreement with Grahame's theory of the Faradaic Admittance⁵), although, of course, a filter circuit could be devised to approximate as closely as desired to the behaviour of the electrochemical system. Grahame's equivalent circuit for the system $Pt-N/10\ H_2SO_4-Pt$ is shown in fig. 5, where C_{dl} is the

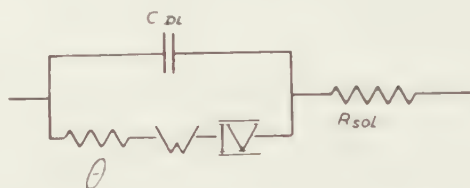


Fig. 5. Grahame's (ref. 5) equivalent circuit of the system

capacitance of the double layer, R_{soln} the resistance of the solution and the symbols $-W-$ and $-IV-$ represent complex impedances defined in Grahame's paper⁵). The resistance θ is defined by GRAHAME as the partial derivative $\partial E/\partial i$ and can be expressed in terms of the average current i_{av} as $\theta = RT/nFi_{av}$. At low frequencies, and at low voltages, the non-linear branch involving θ will produce a non-linear current-voltage relationship which may well be approximated, purely formally, by an equation of the Tafel type. At higher frequencies the series capacitance approaches the double layer capacitance and the series resistance approaches the solution resistance (GRAHAME, loc.cit.); θ will then be very large, unless gases are copiously evolved. This accounts for the ohmic behaviour of the system at higher voltages. The values of E_b , particularly at higher frequencies and at low current densities, thus appear produced by polarization resistance: the heavy capacitive current produces such a large voltage drop across R_{soln} that the potential difference which remains available across the double layer does not suffice to discharge sufficient ions to cause bubble formation. In other words, the impedance of the double layer, being predominantly capacitive, at higher frequencies becomes very small compared with the series resistance of the solution, so that the voltage drop across the double layer remains below the discharge potential. We have tested this hypothesis by doubling the electrode

⁵) D. C. GRAHAME, J. Electrochem. Soc. **99**, 370C, (1952).

spacing, thus doubling R_{soln} and find that, as expected, E_b is thereby very nearly doubled.

With the electrode system employed, viz. platinized *Pt*, the true electrode area is considerably larger than the apparent, geometric, area. The capacitance of the double layer thus reaches very large values indeed. It is seen from table 1 that at 20 cps the voltage has reached about twice its *d.c.* value; at this frequency, therefore, the impedance of the double layer is about equal to the series resistance of the solution. The total cell impedance at 2.0 V was found to be 417 Ohm, the impedance of the double layer thus being about 208 Ohm. Considering as an, admittedly coarse, approximation that this admittance is wholly capacitive, a value of about 9.6 microfarad for the double layer capacitance is obtained. Since the geometric area of the electrode in this experiment was only 0.021 cm², an apparent capacitance of 460 mF/cm² results, which is about 20 times larger than the double layer capacitance commonly encountered. The geometric electrode area thus has to be multiplied by a "roughness-factor" of about 20, which is not an unreasonable value.

Even larger overvoltages occur in poorly conducting solutions, e.g. viscous watrglass. Values in excess of 240 V at 50 cps have been observed. The admittance remains ohmic and varies with frequency according to equ.(2) even at voltages which produce copious gas evolution at one or both electrodes. However, additional damping of the current indicating device then becomes necessary.

That the large *a. c.* overvoltages are not connected with the time needed to establish or reverse the double layer was shown as follows: the circuit given in fig. 6 produces on the cathoderay-oscillograph screen a horizontal

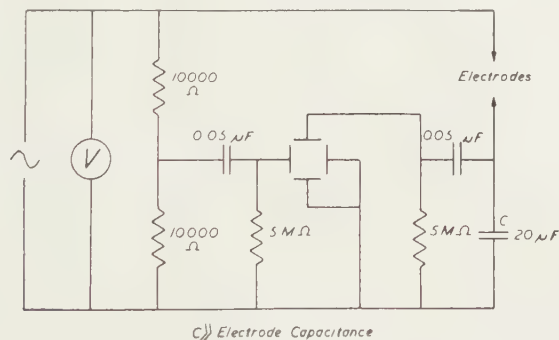


Fig. 6. Circuit producing a horizontal deflection proportional to the applied voltage and a vertical deflection proportional to the instantaneous charge on the double layer

voltage axis and a vertical deflection proportional to the instantaneous charge on the double layer. Even at the highest frequencies used by us (1200 cps) a square voltage wave produced an undistorted and square cathoderay-oscillograph pattern. Therefore, the time needed to form the double layer is estimated to be less than about 10^{-5} sec, which is small compared with the period of the alternating voltages employed.

These results have a bearing on the aforementioned method of mapping electric fields by means of the electrolytic tank. While hitherto only small voltages have been considered permissible because of the risk of causing non-ohmic behaviour and thus distorting the field, it is clear from the above that such fears are ungrounded particularly for low current densities and higher frequencies.

SANDERS and YATES ⁶⁾ claim in a report on their work with the electrolytic tank that spikes which they observed in the waveform of their probe potentials, upon application of a square voltage wave, were caused by polarization. Our results do not seem to support this. As these authors have pointed out this would require that "as a result of polarization at the electrode surfaces a small p.d. increasing with time after each reversal appears between the electrode and the bulk electrolyte". This is tantamount to a time comparable to the rise time of the square wave being required for the formation of the double layer, which time we have shown in fact to be negligible at audio frequencies.

We have observed similar spikes on the current wave pattern when applying a rectangular voltage wave. The ratio of the amplitude of the spike to the amplitude of the rectangular plateau decreases sharply with increasing frequency and increasing voltage. Whereas at 100 cps this ratio is 11 at 0.5 V, at 25 V it is only 0.3; at 1000 cps no spike could be observed at any voltage up to 25 V. These spikes are probably caused by the charging of the double layer capacitance through the high series resistance of the solution.

There is no contradiction between our results in measuring the instantaneous charge on the double layer and the appearance of spikes in the current wave, which are associated with the current passing through. According to the extension of the Debye-Hueckel Theory by BREYER and GUTMANN ⁷⁾, the structure of the double layer is largely independent of the applied voltage; the equations for the local ionic concentration do not involve the applied field, at least to the approximation employed. Even a very small field suffices to establish the double layer. The instantaneous current, however, is determined by the complex admittance of the system.

The authors wish to thank Prof. J. Th. G. OVERBEEK for his interest and most helpful discussion and criticism.

Summary

The sinusoidal alternating voltages E_b required to liberate gas bubbles from the system platinized $Pt-N/10 H_2SO_4$ —platinized Pt were determined as a function of the applied frequency f . Up to 9 cps virtually the *d. c.* value, viz. 1.0 V, was obtained, but 6.5 V were required at 500 cps. Tafel's equation was found to hold only below 2 V, the slope of the Tafel

⁶⁾ K. F. SANDERS and J. G. YATES, *Proc. I.E.E.* **100-II**, 167 (1953).

⁷⁾ B. BREYER and F. GUTMANN, *J. Chem. Phys.* **21**, 1323 (1953).

lines depending on the current density I . At higher voltages, Ohm's law is obeyed. The admittance Y of the system was found to follow the empirical law $Y = a - b/\sqrt{f}$. The overvoltage decreases with f at constant I , irrespective of gas evolution, while E_b increases with f . Values of E_b in excess of 240 V at 50 cps were observed in poorly conducting solutions, e.g. viscous waterglass.

It is shown experimentally that these large values of E_b are not related to the relaxation time of the double layer, which time was found to be less than 10^{-5} sec. It is suggested that the high *a.c.* overvoltages are caused by polarization resistance: the impedance of the double layer, being mainly capacitive, at higher frequencies becomes very small compared to the series resistance R_s of the solution. Most of the applied voltage thus appears across R_s and the potential across the double layer remains below the discharge potential. This is supported by the fact that on doubling the electrode spacing very nearly twice the previous value of E_b is required.

It is suggested that quite appreciable voltages may be safely applied to electrolytic tank measurements without causing non-ohmic behaviour or field distortion.

Spikes, similar to those already reported by other workers, were also observed on the current wave pattern when a rectangular voltage wave was applied. The relative height of the spike decreases rapidly with increasing frequency and increasing voltage. These spikes are thought to be caused by the charging of the double layer capacitance through R_s , and not to be related to the time necessary to establish the double layer itself.

Utrecht and Sydney, May 1954.

ELECTROCHEMICAL BEHAVIOUR OF ION-EXCHANGING SUBSTANCES. VIII.

ROOT POTENTIALS IN SODIUM CHLORIDE SOLUTIONS

BY

H. J. C. TENDELOO AND D. MACGILLAVRY

(Laboratory of Physical and Colloid Chemistry, Agricultural University, Wageningen)

(Communicated by Prof. C. H. MACGILLAVRY at the meeting of September 25, 1954)

Summary

It was possible to obtain stable and reproducible potentials of roots of Lucerne clover in NaCl-HCl solutions as well as in KCl-HCl solutions. Evidence was obtained indicating that the behaviour of potentials in the NaCl-HCl solutions is different from the behaviour in the KCl-HCl solutions.

The behaviour of electric potentials of young roots in electrolyte solutions has been investigated in this laboratory for a number of years ¹).

Strong evidence was adduced indicating that steady potentials may be established in KCl solutions, often within a few minutes. It was shown, furthermore, that these potentials may be interpreted in terms of a Donnan membrane equilibrium. The theoretical formula for the dependence of potential on the concentrations of K⁺ and H⁺ ions contains two constants which are characteristic of each plant species. The quotient of these two constants, it was explained in a recent article ²), may be interpreted as the effective isoionic point of the ion-exchanging material inside the membrane where the shift of electric potential occurs.

It appeared desirable to take up the study of root potentials in solutions containing other univalent cations. A comparative study of Na⁺ and K⁺ ions would be of interest. The theory of Donnan equilibria, as developed further by TENDELOO and VERVELDE, involves only the charge of permeating ions. Still, from a biological point of view, a difference in behaviour between Na⁺ and K⁺ ions might well be expected.

In this communication a short account will be given of root potentials in NaCl solutions. Seeds of Lucerne clover (Provence or Northern France) were grown from 10 to 30 days on distilled water. Then, using the whole

¹) H. J. C. TENDELOO, G. J. VERVELDE and A. J. ZWART VOORSPUY, *Rec. trav. chim.* **63**, 97 (1944); **65**, 539 (1946); *Versl. Ned. Akad. v. Wetenschappen* **53**, 169 (1944).

G. J. VERVELDE, *Proc. Koninkl. Ned. Akad. v. Wetenschappen* **51**, 308 (1948).

G. J. VERVELDE and H. J. C. TENDELOO, *Rec. trav. chim.* **72**, 62 (1953).

²) D. MACGILLAVRY and H. J. C. TENDELOO, *Rec. trav. chim.* **73**, 15 (1954).

seedlings, potentials were measured with the technique described by TENDELOO, VERVELDE and ZWART VOORSPUY¹⁾. Some modifications of apparatus and procedure were adopted. These will be described more in detail in another publication.

The following points need here be mentioned. Before starting measurements, the mounted seedlings were pretreated in a KCl or NaCl solution³⁾, usually during a whole night. Then measurements were taken first in a set of NaCl solutions and then in a similar set of KCl solutions, or sometimes in reversed order. All solutions contained also 5×10^{-5} N HCl. The potentials were measured with a Cambridge or an Electrofact electrometer.

It was possible to obtain stationary potentials in NaCl as in KCl solutions, often after a few minutes, sometimes more slowly. These potentials were reproducible and reversible with respect to variations in concentration or changes from NaCl to KCl or vice versa, as far as could be judged from available observations. The average values obtained for the potentials, averaged over all roots measured, at the different concentrations are listed in Table I.

TABLE I
Average root potentials

Molarity NaCl				Molarity KCl			
10^{-5}	10^{-4}	10^{-3}	10^{-2}	10^{-5}	10^{-4}	10^{-3}	10^{-2}
-15.5	-14.8	+ 4.2	+35.8	-41.3	-34.4	+ 3.5	+40.0

An arbitrary reference point has been chosen, as the correct location of zero potential for the effective Donnan membrane equilibrium has to be derived by further analysis.

The measurements, the averages of steady potentials for individual roots, are presented in Table II.

TABLE II

	Root	Pretreatment ¹⁾	Electro-meter ²⁾	Molarity NaCl				Molarity KCl			
				10^{-5}	10^{-4}	10^{-3}	10^{-2}	10^{-5}	10^{-4}	10^{-3}	10^{-2}
1	3-B-111	KCl	C	-12	-13	- 7	+26	(-45) ³⁾	-31	- 1	+31
2	5-B-124	NaCl	C	-30	-29	-14	+22	-52	-45	-12	+28
3	8-B-132	NaCl	C	- 9	-16	+ 6	+25	-47	-36	+11	+37
4	9-B-141	NaCl	C	-12	-11	+ 5	+34	-27	-15	+19	+43
5	19-C-29	KCl	E	-12	- 7	+10	+39	-37	-18	+ 5	+40
6	3-C-39	KCl	E	-15	-13	+ 9	+41	-32	-27	+11	+49
7	4-C-46	KCl	E	- 3	- 9	+18	+50	-60	-55	- 2	+43
8	7-C-52	KCl	E	+13	+14	+34	+58	-24	-21	+17	+50
9	8-C-59	KCl	E	-53	-48	-23	+16	-44	-55	-19	+27
10	10-C-70	KCl	C	-22	-16	+ 4	+47	-45	-41	+ 6	+52

¹⁾ All solutions contain also 5×10^{-5} N HCl.

²⁾ C: Cambridge pH-Electrometer; E: Electrofact Electrometer.

³⁾ This root was not measured in 10^{-5} M KCl; the value listed was estimated by means of the missing plot technique.

³⁾ Containing 10^{-4} M salt and 5×10^{-5} N HCl.

In general a correspondence of behaviour in NaCl and KCl solutions is evident. A variance analysis was made to account for the main effects, of concentration, medium, root mean, and "interaction". Results are given in table III.

TABLE III

Source of variation	Sum of squares	Dimension	Variance	F
Concentration	56,626.24	3	18,875.41	271.9
Medium	2,194.51	1	2,194.51	31.6
Root mean	9,770.31	9	1,085.59	15.6
Interaction (concentration \times medium)	3,145.14	3	1,048.38	15.1
Residual	4,303.99	62	69.42	$F_{.05} (1,62) = 4.00$
Total	76,040.19	78		

It may be verified with the F tables that at the 5 % level all effects are significant. Thus, the potentials in the NaCl-HCl solutions studied may not be considered identical with those in the corresponding KCl-HCl solutions. It may here be stated that the differences between the potential averages of NaCl or KCl (see Table I) at the same molarity apparently are too large to be attributed to the differences of diffusion potentials set up between the solutions and the saturated KCl bridge. The difference in behaviour between NaCl and KCl must then be attributed to the response of the roots themselves. The significance will be discussed further

TABLE IIIA

Source of variation	Sum of squares	Dimension	Variance
Differences due to pretreatment	196.80	1	196.80
Differences within groups	9,573.51	8	1,196.69
Differences between roots	9,770.31	9	

TABLE IIIB

Source of variation	Sum of squares	Dimension	Variance
Differences due to electrometer	316.02	1	316.02
Differences within groups	9,454.29	8	1,181.79
Differences between roots	9,770.31	9	

in a later publication. Other conditions not kept strictly uniform, especially pretreatment and electrometer used, apparently did not influence the potentials to any extent. This was checked by splitting up the sum of squares for the variation between roots. See Tables IIIA and IIIB.

There are no indications that differences may be ascribed to an influence caused by the pretreatments or to the use of the Electrofact electrometer instead of the Cambridge pH-electrometer.

In conclusion it may be stated that evidence was obtained indicating that the behaviour of root potentials in NaCl-HCl solutions is different from the behaviour in KCl-HCl solutions. The investigation is being continued.

We are much obliged to Prof. Dr N. H. KUIPER, Ir S. H. JUSTESEN and Ir L. C. A. CORSTEN of the Department of Mathematics for advising us about questions of statistical analysis.

CHEMISTRY

ELECTROCHEMICAL BEHAVIOUR OF ION-EXCHANGING SUBSTANCES. IX.

ROOT POTENTIALS IN POTASSIUM CHLORIDE SOLUTIONS

BY

D. MACGILLAVRY AND H. J. C. TENDELOO

(Laboratory of Physical and Colloid Chemistry, Agricultural University, Wageningen)

(Communicated by Prof. C. H. MACGILLAVRY at the meeting of September 25, 1954)

Summary

Potential measurements of Lucerne clover, *Medicago Sativa*, were taken in KCl solutions. Regression equations were derived for the dependence of potential on KCl concentration. A statistical analysis of the data showed that the potentials do not depend on the age of seedlings. The measuring precision is discussed.

In this laboratory the electric potentials of plant roots in KCl solutions have been measured for a number of plant species. Purpose of this investigation was to extend preliminary measurements ¹⁾ of Lucerne clover, Provence variety (*Medicago Sativa*).

Apparatus

The electric chain was essentially as described by TENDELOO, VERVELDE and ZWART VOORSPUY ²⁾. A few modifications were made from time to time. The final form as now used is shown in Figure 1.

On the day measurements were to be taken a whole seedling was mounted with a little isoelectric gelatin in a drawn out tube (B). From the reservoir of the holder (A) for the Ag/AgCl electrodes enough liquid (10^{-2} M KCl) to make electric contact was allowed to flow above the gelatin collar. The root itself was immersed in a series of KCl solutions (vessels C). The vessels with these solutions were placed on a microscope stage. The depth of immersion could be adjusted by raising or lowering the stage. The other electrode was a saturated calomel electrode (E). This electrode was mounted in a vessel (D) containing saturated KCl and carrying an agar bridge for making electric contact with the KCl solutions in the vessels (C).

¹⁾ Measurements performed by E. G. KLOOSTERMAN, see G. J. VERVELDE, „Salt accumulation by plant roots”, dissertation, Wageningen, 1952, page 42.

²⁾ H. J. C. TENDELOO, G. J. VERVELDE and A. J. ZWART VOORSPUY, Rec. trav. chim. 63, 97 (1944).

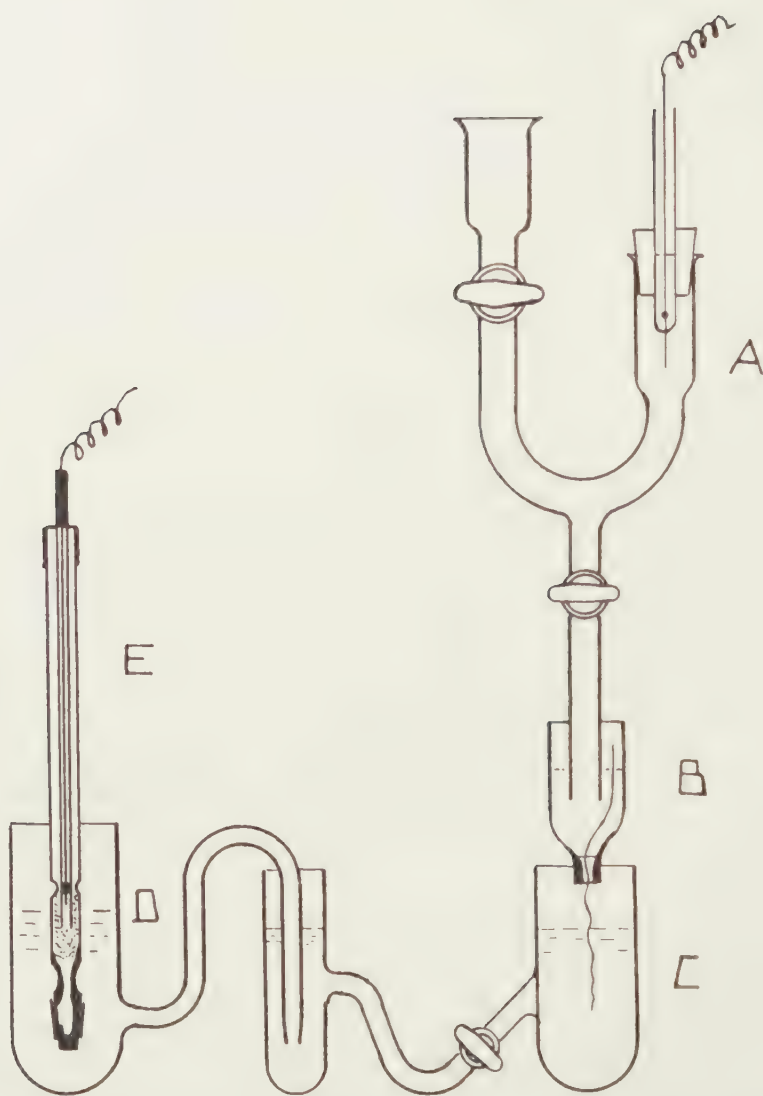


Fig. 1. Electrolytic Chain. A. Electrode holder with two Ag/AgCl electrodes (one electrode is shown). B. Tube with seedling held in place with a gelatin collar. C. Vessel containing x-molar KCl. D. Vessel containing saturated KCl solution and carrying an agar bridge. E. Saturated calomel electrode

All units were so constructed and arranged that the chain potential could be measured while keeping all stopcocks open. The electric measurements were made with a Cambridge pH-electrometer.

Experimental results. Statistical analysis of data

A first series of potential measurements was taken with 14 roots. The seeds were germinated on gauze discs. After a few days the seedlings,

when grown large enough, were transferred and placed loose in the drawn out tubes; the roots were hanging in a nutrient solution ³⁾).

Of each solution two samples were taken. Usually measurements were started in the most dilute solution. It was found possible also to start measurements in 0.1 M KCl and to go through the series of solutions in reversed order.

The measured potentials are represented in Table I. One measurement was not duplicated. The same value —99 was filled in the open space in order to have a complete rectangular set of data.

TABLE I
Root potentials. Germination started on 27 VII

root	date of measurements	Molarity KCl							
		10 ⁻⁴		10 ⁻³		10 ⁻²		10 ⁻¹	
1'	31 VII	— 60	— 63	— 30	— 30	— 2	+ 5	+ 22	+ 15
4	1 VIII	— 52	— 61	— 30	— 33	+ 6	+ 4	+ 33	+ 35
4'	1	— 54	— 60	— 30	— 33	+ 5	+ 1	+ 27	+ 23
8	3	— 67	— 79	— 45	— 49	— 9	— 9	+ 24	+ 22
8'	5	— 58	— 52	— 30	— 15	+ 7	+ 6	+ 42	+ 37
2'	5 VIII	— 61	— 59	— 30	— 31	+ 1	+ 2	+ 32	+ 39
11'	6	— 42	— 61	— 31	— 24	— 1	— 1	+ 11	+ 14
14	6	— 68	— 74	— 40	— 42	— 1	— 1	+ 13	+ 10
14'	6	— 41	— 53	— 18	— 19	+ 16	+ 16	+ 32	+ 37
13'	7	*— 99	— 99	— 68	— 68	— 27	— 26	+ 6	+ 14
18'	7 VIII	— 56	— 57	— 25	— 24	+ 3	+ 4	+ 15	+ 18
21''	7	— 75	— 77	— 38	— 37	— 1	+ 9	+ 22	+ 23
12'	12	— 72	— 72	— 37	— 36	+ 8	+ 11	+ 19	+ 17
12	12	— 68	— 75	— 35	— 36	+ 6	+ 7	+ 33	+ 31

* estimated value.

A statistical analysis of the data yielded the following results. Besides a pronounced dependence of potential on concentration, a marked difference between individual seedlings was noted. This difference is not merely a variation of general level of potentials, but also a degree of variation in response of individual roots to KCl concentration. The variance estimates for these sources of variation of potential are given in Table II.

TABLE II

Source of variation	Sum of squares	Dimension	Variance estimate
Concentration	128,329.61	3	42,776.54
Root mean	10,375.46	13	798.11
Interaction (concentration × root). . .	3,165.89	39	81.18
Differences between duplicate readings .	839.00	55	15.25

³⁾ See VERVELDE, page 86.

The last source of variation is a measure of precision, or of possible error (about 4 mV) of potential measurements for this type of electric chain comprising a seedling. The Cambridge pH-meter can be read to 0.5–1.0 mV. The third source of variation may be considered an inherent source of varying results for potential measurements on a *series* of roots. This apparently unavoidable source of variation is more marked than the chance errors of an individual measurement. Thus, the estimate 81.18 for this source is used as a basis of comparison as to significance for other variance estimates. It is seen that not only the variance due to concentration is significant, but also the variance caused by differences between roots on account of different potential levels.

The question arose whether the differences between roots might be attributed to the age of seedlings. Thus, the variance of differences between the seven different age groups was compared with the variance of potential differences within each age group (Table III). It was found that differences in age of a few days offer no explanation for the observed differences between roots. Roots show these differences regardless of age.

TABLE III

Source of variation	Sum of squares	Dimension	Variance estimate
Differences between age groups	4,117.50	6	686.25
Differences within age groups	6,257.96	7	893.99
Differences between roots	10,375.46	13	798.11

A further analysis of data showed that the measuring errors at the four different concentrations were not uniform. The estimates of variance are listed in Table IV.

TABLE IV

$\log C_{KCl}$	Sum of squares	Dimension	Variance estimates
— 4	452.50	13	34.81
— 3	159.00	14	11.36
— 2	91.50	14	6.54
— 1	136.00	14	9.71
all concentrations	839.00	55	15.25

The Bartlett test ⁴⁾, as modified by HARTLEY and PEARSON, was used. On account of this criterion, it is not permissible to use the variance estimate 15.25 as a uniform base of reference. This makes no difference with regard to the other conclusions arrived at above, as all the estimates for the different concentrations are smaller than the variance estimate 81.18, the preferred basis of reference.

⁴⁾ HARTLEY, *Biometrika* 31, 249 (1940).

With a second series the seeds were allowed to germinate in the folds of a strip of moist filter paper. This strip was supported on a slanting glass plate. The lower end of filter paper and glass plate reached in a shallow trough with distilled water. In this way the filter paper was kept moist. Seedlings were transferred to the drawn out tubes, as before, when grown large enough and before root hairs could develop too much. The roots were hanging either in distilled water or nutrient solution.

Each root after mounting was pretreated a while in a KCl solution until the potential remained reasonably constant. The depth of immersion was adjusted so as to minimize variation of potential with depth of immersion, preferably at the level where the observed potential attained an extreme value.

A greater range of concentrations was used. It was found, however, that the potentials were established more slowly in 0.4 and 1.0 M KCl and tended to become irreversible. No further measurements were taken in these high concentrations.

TABLE V

Root potentials. Set A germination started on 17 VIII. Set B germination started on 24 VIII

Root	Date of measurements	Germinating medium ¹⁾	Pretreatment ²⁾ solution	Molarity KCl									
				10 ⁻⁵	10 ⁻⁴	10 ⁻³	10 ⁻²	10 ⁻¹					
A 1'	31 VIII	+	—	*— 83	*— 83	— 40	— 59	— 38	— 40	— 7	— 5	+ 20	+ 19
A 2'	1 IX	+	— 4	— 54	— 67	— 62	*— 62	— 28	— 33	+ 7	+ 3	+ 27	+ 28
A 5'	2	+	— 5	— 87	— 87	— 71	— 75	— 47	— 56	— 15	+ 6	+ 20	+ 16
A 6'	2, 3	+	— 2										
A 7'	3	—	— 2	— 137	— 133	— 95	— 95	— 45	— 52	— 2	— 5	+ 27	+ 27
A 8'	1 IX	—	— 5	— 63	— 56	— 50	— 51	— 20	— 20	+ 19	+ 20	+ 40	+ 39
A 9'	7	+	— 3	— 78	— 81	— 69	— 70	— 28	— 30	+ 1	— 2	+ 15	+ 14
A 10'	7, 8	+	— 3	— 59	— 60	— 48	— 44	— 22	— 23	+ 1	+ 1	*+ 13	+ 13
A 11'	8	—	— 3	*— 81	— 81	— 64	— 69	— 37	— 37	— 1	— 4	+ 15	+ 13
B 2	15, 16	+	— 3	— 91	— 86	— 77	— 77	— 40	— 47	— 4	— 8	+ 4	+ 3
B 3	16 IX	—	— 3	— 64	— 62	— 48	— 48	— 17	— 17	— 1	0	+ 4	+ 5
B 4	17	—	— 4	— 80	— 71	— 73	— 73	— 38	— 37	+ 6	+ 3	+ 21	*+ 21
B 5	18	+	— 4	— 119	— 111	— 90	— 92	— 46	— 43	+ 2	+ 7	+ 36	+ 35
B 6	18	+	— 4	— 83	— 84	— 73	— 71	— 27	— 22	+ 12	+ 13	+ 19	+ 19
B 7	19	—	— 4	— 102	— 100	— 95	— 98	— 62	— 62	— 32	— 16	0*	0*
B 8	21 IX	—	— 4	— 105	— 99	— 96	— 95	— 60	— 62	— 21	— 8	+ 32	+ 21
B 9	21	+	— 4	— 77	— 78	— 72	— 77	— 36	— 36	+ 7	— 2	+ 23	+ 22
B 10	22	+	— 4	— 95	— 99	— 80	— 83	— 36	— 35	+ 6	+ 3	+ 27	+ 27
B 11	22	—	— 3	— 121	— 119	— 103	— 102	— 55	— 56	— 7	— 4	+ 27	+ 25
B 12	23	—	— 3	— 103	— 89	— 82	— 79	— 37	— 39	— 4	— 1	+ 30	+ 25

1) + indicates root grown in nutrient solution.

— indicates root grown in distilled water.

2) —*n* indicates pretreatment in 10^{-*n*} M KCl solution.

* estimated values.

This second series comprised a set of 8 seedlings measured first and another set of 11 seedlings measured later. These two sets were treated as one series of measurements. Results are listed in Table V.

The starred values were not measured, but are estimated values. Where a measurement was not duplicated, the same value as measured was filled in the open space. Where no measurements were taken suitable values were estimated by the missing plot technique. Indicated also are manner of growing the seedlings, whether in distilled water or nutrient solution, and the concentration of the pretreatment KCl solution. Again, the same main sources of variation are accounted for as shown in Table VI.

TABLE VI

Source of variation	Sum of squares	Dimension	Variance estimate
Concentration	323,400.08	4	80,850.02
Root mean	21,786.45	18	1,210.36
Interaction (concentration \times root). . .	18,154.92	70	259.36
Differences between duplicate readings .	1,334.00	89	14.99

It is seen that the variance caused by chance errors is practically the same as for the first series of measurements. The other variance estimates follow the same pattern; they are a little higher. Hence, the same conclusions hold as before.

Again, the variance estimates due to reading errors may not be considered uniform for the five different concentrations. The estimates now are as shown in Table VII.

TABLE VII

$\log C_{\text{KCl}}$	Sum of squares	Dimension	Variance estimate
- 5	338	17	19.88
- 4	241	18	13.39
- 3	129	19	6.79
- 2	537	19	28.26
- 1	89	16	5.56
all concentrations	1334	89	14.99

The same conclusion obtains as for the first series. The present pattern of estimates, it may be noted, is somewhat different from the pattern for the first series of measurements. The relatively large variance for 10^{-2} M KCl is striking. This modified pattern might be attributed to two causes, a pretreatment in a KCl solution up to an hour, and (or) a slightly modified technique with respect to depth of immersion.

As a possible means of improving the technique of measuring root potentials, the seedlings, whether grown in water or a nutrient solution, were placed in a dilute KCl solution. They were left there until an apparently stationary potential distribution along the root was obtained. In this way the roots were preconditioned so to say for the measurements in the series of KCl solutions, when mainly changes in direct response to the varying KCl concentrations will then occur.

It was noticed, as just mentioned, that a more or less pronounced distribution of potential may be found on varying the depth of immersion. In so far as true Donnan equilibria might be established at membranes showing selective permeability, more pronounced potential differences might be established than might be on account of steady diffusion. Thus, it is natural to look for a depth of immersion giving a maximal potential difference. From a more experimental point of view, adjusting the depth of immersion so as to obtain, if possible, a potential extreme has the advantage that then the exact depth of immersion would be least critical. Thus, the potentials measured might be best reproducible. Once a certain depth of immersion of a root had been decided on, all further measurements were made at this same depth.

It may be remarked further that with this second series the individual variance estimates for the different concentrations all are somewhat smaller than the corresponding estimates for the first series, excepting the variance estimate for 10^{-2} M KCl. This is still true if the two subsets of 8 and 11 roots are examined separately. In table VIII all estimates for the different concentrations are listed.

TABLE VIII
Variance estimates due to chance errors

	log KCl concentration				
	— 5	— 4	— 3	— 2	— 1
Series I	—	34.81	11.36	6.54	9.71
Series II	19.88	13.39	6.79	28.26	5.56
Series II _A	20.33	30.00	10.25	30.50	1.71
Series II _B	19.64	2.91	4.27	26.64	8.55

The estimates for the two subsets are rather different for three of the KCl concentrations used. Hence, it appeared desirable to probe a little deeper and to examine the point, whether the two subsets should be considered distinct in some manner. The seedlings of the first subset were measured from 14–22 days after they started to grow, while the roots of the second subset were measured when they were from 23–30 days old. Hence, there might be a difference between the two age groups. This was tested along analogous lines as for the first series of measurements. The variance estimates found and the dimensions are given in Table IX.

TABLE IX

Source of variation	Sum of squares	Dimensions	Variance estimate
Differences between the two periods. . .	3,154.79	1	3,154.97
Differences within the two periods . . .	18,631.48	17	1,095.97
Differences in level between roots . . .	21,786.45	18	1,210.36

The first variance estimate is larger than the second estimate. The quotient is not that large that the subsets may be considered different on account of age.

Another question has to be considered whether the seedlings grown in nutrient solution and those grown in distilled water might show different characteristics. The roots of each subset and the entire series may be divided into two groups accordingly. This gives the following results (Table X).

TABLE X

Source of variation	Sum of squares	Dimension	Variance estimate
Subset II _A			
Effect of nutrient solution	178.64	1	178.64
Differences otherwise	8,688.35	6	1,448.06
	8,866.99	7	1,266.71
Subset II _B			
Effect of nutrient solution	798.22	1	798.22
Differences otherwise	8,966.27	9	996.25
	9,764.49	10	976.45
Entire series II			
Effect of nutrient solution	1,545.61	1	1,545.61
Differences otherwise between roots . .	20,240.84	17	1,190.64
	21,786.45	18	1,210.36

As far as can be concluded from the present data, growing seedlings in nutrient solution does not contribute to the differences existing between roots.

The differences between roots, as measured, occur regardless of age of seedlings and of manner of growing them, whether in nutrient solution or distilled water. The two subsets II_A and II_B did differ with respect to precision of measurement, as we saw already.

The measurements of II_B at the KCl concentrations 10^{-4} and 10^{-3} M

were much more precise. After the pretreatment as indicated in Table I, the potentials were always measured first in the most dilute solution and then in turn in the more concentrated solutions. With several roots, after the standard series of measurements was finished, additional readings were taken in the reversed order. A selection of these data will be given elsewhere.

These check measurements gave evidence, that the potentials as measured are reversible with respect to KCl concentration. They were quickly reversible if the order was reversed after measuring in 10^{-2} M KCl. All this tends to indicate that simple, quickly established equilibria are determining the potentials, as one would expect for a Donnan equilibrium at a membrane with small inner volume. Time factors due to life processes hardly seem to interfere.

From observation of the dependence of potential on time in 0.4 and 1.0 M KCl, the conviction was already gained that Provencer Lucerne clover was adversely affected by these higher concentrations of KCl. The potentials became erratic and sluggish.

The peculiar lack of precision in 10^{-2} M KCl is considered the paradoxical result of an improved technique. It is suggested, as an explanation, that time factors are hard to avoid altogether. With the improved techniques described, it apparently was possible to reach stationary potentials quickly before time factors made themselves felt. This then was so in 10^{-4} M KCl and still in 10^{-3} M KCl. By the time measurements in 10^{-2} M KCl are taken, the experimenter is overtaken by slow but still small time factors.

Yet, the average potentials calculated from the duplicate measurements for 10^{-2} M KCl may conform reasonably close to the stationary potentials of the same simple membrane equilibrium. It is felt, that this is not true any more for the potentials in 0.1 M KCl.

The discussion presented gives an account of known experimental factors and parameters. Concentration of KCl is the dominant factor. For a theoretical interpretation of the measured potentials it is desirable to ascertain *how* the potentials vary with KCl concentration. The average potentials found are listed in Table XI A.

TABLE XI A
Potential averages

	log KCl concentration				
	- 5	- 4	- 3	- 2	- 1
First series.		- 64.8	- 34.4	+ 1.4	+ 23.8
Second series.	- 87.6	- 73.9	- 39.1	- 0.8	+ 20.3

In the beginning of this investigation, a special reference potential on the potentiometer viz. 921 and 920 mV was taken for each series.

For future reference it is desirable to adopt a common reference potential for which we took 900 mV. A Weston cell was placed in series. The revised averages for these preliminary series are given in Table XI B.

TABLE XI B
Potential averages

	log KCl concentrations				
	- 5	- 4	- 3	- 2	- 1
First series.		- 85.8	- 55.4	- 19.6	+ 2.8
Second series.	- 107.6	- 93.9	- 59.1	- 20.8	+ 0.3

The effect of KCl concentration was analyzed in the usual way by means of orthogonal polynomials in terms of linear, second and higher degree components. The relative importance for each series of measurements can be judged from the variance estimates listed in Table XII by comparison with the reference estimates as discussed above (see Tables II and V).

TABLE XII
First series

Degree components	Sum of squares	Dimension	Variance estimate
First.	127,383.78	1	127,383.78
Second.	448.00	1	449.00
Third	497.83	1	497.83
	128,329.61	3	

Second Series

Degree components	Sum of squares	Dimension	Variance estimate
First.	317,033.09	1	317,033.09
Second.	818.80	1	818.80
Third	5,548.17	1	5,548.17
Fourth.	0.02	1	0.02
	323,400.08	4	

For the first series all three possible components are significant. The linear and third degree component are significant for the second series. No fourth degree component is indicated. Statistically the second degree component is not significant. Since a second degree component is significant for the first series, such a component will be retained for the second series as well.

By means of these orthogonal components the regression equations for potential (y) on logarithm of concentration (x) were obtained. These equations are (potentials referred to the new common reference potential)

First Series	$y = -7.11 - 32.33x - 25.57x^2 - 3.14x^3$
Second series.	$y = -14.27 - 38.81x - 27.41x^2 - 3.18x^3$

In connection with a theoretical interpretation, the location of the inflection point of the empirical equations is of interest. The point of inflection is easily obtained from the regression equations.

	log molarity KCl	Potential at inflection point
First series	- 2.71	- 44.84
Second series	- 2.87	- 53.43

It should be noted that both estimates fall at nearly the same KCl concentration. To decide whether the two points of inflection could be different, the confidence intervals for each of the two series were determined. The confidence interval here is the stochastic region such that the probability that it covers the true abscissa of the inflection point is equal to 0.95. These intervals with limits x_1 and x_2 come out fairly large.

Limits of confidence ranges for abscissae of points of inflection

First series	$x_1 = -3.73$	$x_2 = -2.53$
Second series	$x_1 = -3.03$	$x_2 = -2.64$

It is seen that the confidence interval of x for the second series falls entirely inside the confidence interval of x for the first series. The two abscissae in question for the two series fall both well within the shorter confidence range for the second series.

Conclusions

1. It was found that stationary potentials are established in KCl solutions. The potentials are reasonably reproducible and reversible.
2. The potentials are not dependent on the age of young seedlings. The manner of growing, whether in nutrient solution or distilled water, appears to have no influence.
3. The regression equations for the dependence of potential on KCl concentration for the first and second series of roots agree fairly well. The KCl concentrations at the inflection points of the two graphs agree closely.

Acknowledgement

We are much obliged to Prof. Dr N. H. KUIPER and Ir L. C. A. CORSTEN of the Department of Mathematics for assisting us with the statistical analysis.

THE CRYSTAL STRUCTURE OF SOME TARTRATES AND CORRESPONDING RACEMATES

BY

A. J. J. SPRENKELS

(Communicated by Prof. J. M. BIJVOET at the meeting of October 30, 1954)

The difference in stacking of the molecules in optically active compounds and their racemates respectively, has been investigated only in a very few cases [1]. In this paper we give a preliminary account of the geometrical results in the comparison of the crystal structures of some tartrates with those of the corresponding racemates.

Details concerning the structure determinations and a possible discussion of physical properties in relation to the crystal structure will, after refinement of some of the structures using Geiger-counter-intensities, be published in due time in *Acta Crystallographica*.

Figure 1 gives the [100]- and [001]-projections of *NH₄-bitartrate*. Cell dimensions: $a=7.71$, $b=11.57$, $c=7.84$ Å, $\beta=104^\circ 47'$. Space group: $P 2_1/b$ Number of molecules per cell : 4.

When compared with the structure of the active *NH₄-bitartrate* [2], fig. 2, a striking similarity is seen. The tartrate-ions are lying between (010)-planes of kations, exactly in the way we find in the active compounds. In the racemate, however, subsequent layers are built up by *l*- and *d*-molecules respectively, by the action of the glide plane.

In the racemate a closer approach is observed between alcoholic OH and CO groups of subsequent layers. This might be the cause of the stability of the racemate.

If the free enthalpy were about equal for the respective tartrate and racemate we should expect the solubility of the racemate to be greater than that of the tartrate as a result of the entropy of mixing in the solution. The solubility of the racemate is even found to be somewhat less when compared with that of the tartrate.

For *Li-NH₄-tartrate monohydrate* a structure was deduced which in the stacking of the tartrate ions shows much resemblance to that of Rochelle salt, NaK-tartrate tetrahydrate, the main difference being a layer of 3 water molecules parallel (100) inserted in the latter structure. Figure 3 gives the [100]- and [001]-projections of *Li-NH₄-tartrate H₂O*. Cell dimensions: $a=7.89$, $b=14.74$, $c=6.42$ Å. Space group: $P 2_1 2_1 2$. Number of molecules per cell : 4.

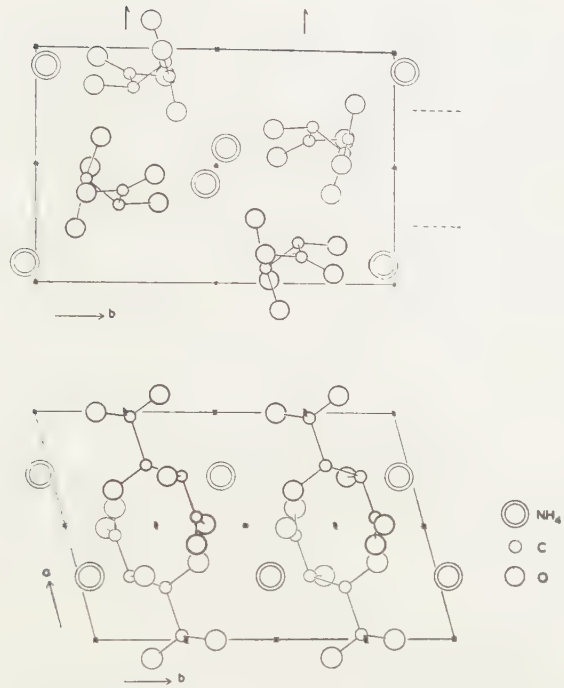


Fig. 1. [100]- and [001]-projections of NH_4 -biracetate

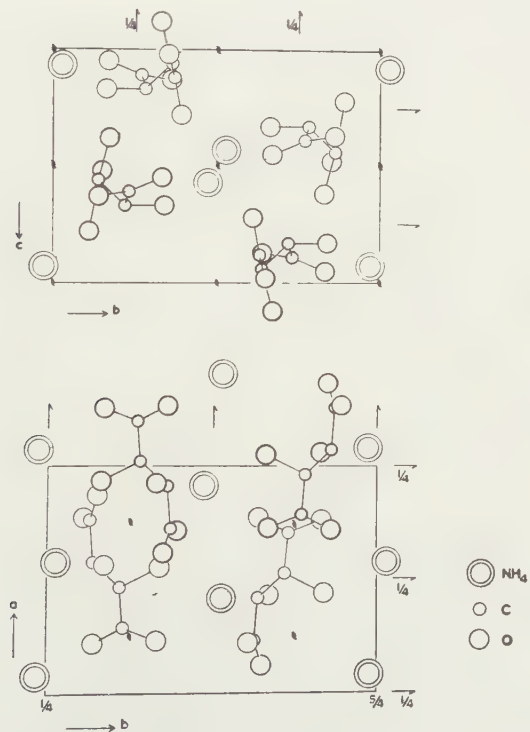


Fig. 2. [100]- and [001]-projections of NH_4 -bitartrate



Fig. 3. [100]- and [001]-projections of Li-NH₄-tartrate. H₂O

The [001]-projection may be compared with that of the Rochelle salt given in fig. 4.

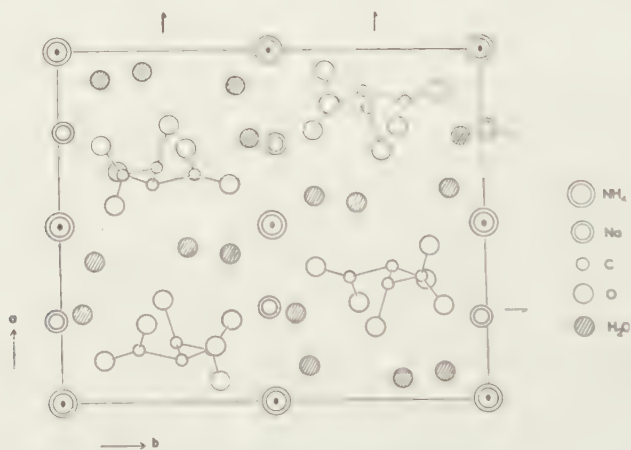


Fig. 4. [001]-projection of Rochelle-salt

The corresponding *Li NH₄-racemate monohydrate* has cell dimensions: $a=9.67$, $b=18.50$, $c=9.79$, $\beta=115^\circ$.

Space group: $A 2/a$. Number of molecules per cell : 8.

The [100] and [001] projections are given in fig. 5. In this case the translation of the glide mirror-operation is *parallel* to the (010)-plane of kations. Then, in the layer between these subsequent planes of kations, *l*- and *d*-ions now are intermixed; in the layer we find parallel to the

c-axis alternating columns of *l*- and *d*-molecules respectively. In this case the *l*- and *d*-ions around a centre of symmetry can be considered as a racemate-ion with which concept the interionic distances seem to be in accordance.

Location of the Li-ion is pending further refinement.

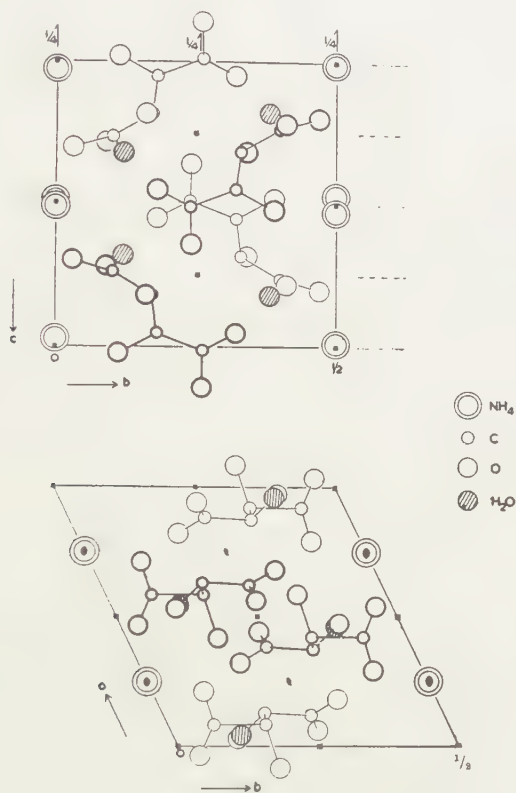


Fig. 5. [100]- and [001]-projections of Li-NH₄-racemate. H₂O

The methods used in these structure determinations were as follows: The Rb-ion is located from Patterson-projections.

The structure of Rb-bi-racemate could be determined by the heavy atom technique since Rb contributes to all reflections. Starting from this structure, the isomorphous one of NH₄-bi-racemate was refined by Fourier- and least squares methods.

In the case of Li-Rb-tartrate monohydrate the special positions of the Rubidium prohibited the application of the heavy-atom technique. A Patterson-shift implying the Rb-Rb-vector led to the [100]-projection. In the *x*-direction the molecule was located with the help of spatial- and intensity-considerations, and a first refinement was performed of the Li-NH₄-tartrate monohydrate by Fourier- and least-squares methods.

The [001]-projection of Li-Rb-racemate-monohydrate was determined by the heavy atom technique; the [100]-projection again with the help

of a model. Refinement of the structure of Li-NH₄-racemate-monohydrate is in progress.

Our thanks are due to Mr H. MATTHIJSEN bachelor of chemistry and some others who contributed to this investigation.

*Laboratorium voor Kristalchemie
der Rijks Universiteit, Utrecht*

REFERENCES

1. SADANAGA, R., The crystal structure of potassium sodium d-l-tartrate tetrahydrate $K Na C_4H_4O_6 \cdot 4H_2O$ Acta Cryst. 416-423 (1950).
2. BOMMEL, A. J. VAN, The crystal structure of d-Rb-bi-tartrate and its absolute configuration. Proc. Kon. Ned. Akad. Wetenschap. B 56, 268-271 (1953).

CHEMISTRY

INFLUENCE OF SALT ON THE SPREADING PRESSURE OF FILMS OF LONG-CHAIN WEAK ACIDS

BY

TH. A. J. PAYENS

(Communicated by Dr E. J. W. VERWEY at the meeting of October 30, 1954)

Various workers have investigated the double layer of charged monolayers spread at air/water and oil/water interfaces. DAVIES [1] especially has shown that for films of fully ionized substances like $C_{18}H_{37}N(CH_3)_3^+$ the effect of increasing the ionic strength of the water phase under the monolayer is a decrease of the film pressure. As the surface charge of this type of double layer is constant, this decrease of surface pressure is readily explained by the lowering of the surface potential, because the charges of the film become more and more screened by the counterions when the salt content of the water is increased.

The simple Gouy-theory, assuming the region of the surface charges to be homogeneous and impenetrable to the counter-ions and the counter-ions themselves to be point charges, often proved to be a good approximation for describing the behaviour of such a double layer.

For films of incompletely ionized substances, such as long-chain weak acids a lowering of the ionization constant of the film with respect to the free molecule takes place as a consequence of the electrostatic interaction of the ionized centres of the film with an H-ion to be split off. Such lowerings were observed by SCHULMAN and coworkers [2] and by DANIELLI [3] for monolayers of long-chain fatty acids and recently by DAVIES [4] in the case of films of monocetyl succinate. Such a monolayer thus behaves in a way analogous to the behaviour of a weak poly-electrolyte in solution. Like in the latter case this lowering of the dissociation constant might be written [5] [6],

$$(1) \quad K = \alpha \cdot C_{H^+} / (1 - \alpha) = K_0 \exp (-e\Psi_0/kT),$$

where K is the dissociation constant of the film, K_0 the dissociation constant of an isolated acid molecule, α the degree of ionization of the film and C_{H^+} the hydrogen ion concentration of the water phase under the monolayer. Ψ_0 is the electrical surface potential of the film due to its ionized centres.

In the following we want to mention some experiments done with monolayers of surface-active weak electrolytes spread on subphases of different ionic strength.

For such monolayers an increase of the saltcontent of the water is

followed by an increase of the film pressure, in contradistinction to what is found for films of the completely ionized octadecyltrimethylammonium chloride and sodium dodecylsulphate [7]. This increase of film pressure might be understood in the following way.

The increase of the salt content of the water brings about a lowering of the electrical surface potential, just as in the case of the double layer of $C_{18}H_{37}N(CH_3)_3^+$. From equation (1) it is seen, that this lowering of the potential is accompanied by an increase of the degree of ionization of the film and consequently of the number of surface charges.

Obviously an increase of the surface pressure means that the electrostatic repulsion between these new surface charges predominates the effect of the lowering of the electrical surface potential of the film as a whole.

In a series of experiments we investigated the behaviour of long-chain acids and amines in this respect at the petrol ether/water and at the air/water interface.

Spreading at the oil/water interface was carried out by the method of ALEXANDER and TEORELL [8] on an interface of constant area. The surface concentration was gradually increased by injection of the surface-active material into the interface with an Agla micrometer syringe.

The interfacial tension was measured by the ring method and by the hanging plate technique. Measurements were accurate to about 0.04 dyne cm^{-1} . Both methods of measurement led to the same result. From the surface-active weak electrolytes investigated only cetyl-phosphonic and stearyl-phosphonic acid¹⁾ gave stable films at the petrol ether/water interface.

For films of stearyl-phosphonic acid fig. 1 shows the increase of the spreading pressure brought about by an increase of the ionic strength of the water phase.

At the air/water interface measurements were made using a Langmuir-Adam trough.

In this case it was again found that the surface pressure increases with increasing salt content of the water, though not always to the same extent. This is probably connected with the circumstance that at the air/water interface stearyl-phosphonic acid films are of the condensed monolayer type.

Also for films of the more soluble lower fatty acids ($C_5H_{11}COOH$ and $C_7H_{15}COOH$) the effect of salt was demonstrated. We measured the concentration dependence of the surface tension on solutions of these acids under different conditions of ionic strength. With the aid of the Gibbs adsorption theorem such measurements can be used to calculate the amount of fatty acid adsorbed at the surface of the solution. The difference

¹⁾ The author is indebted to Dr K. H. KLAASSENS and Mr C. J. SCHOOT for the preparation of the long-chain acids.

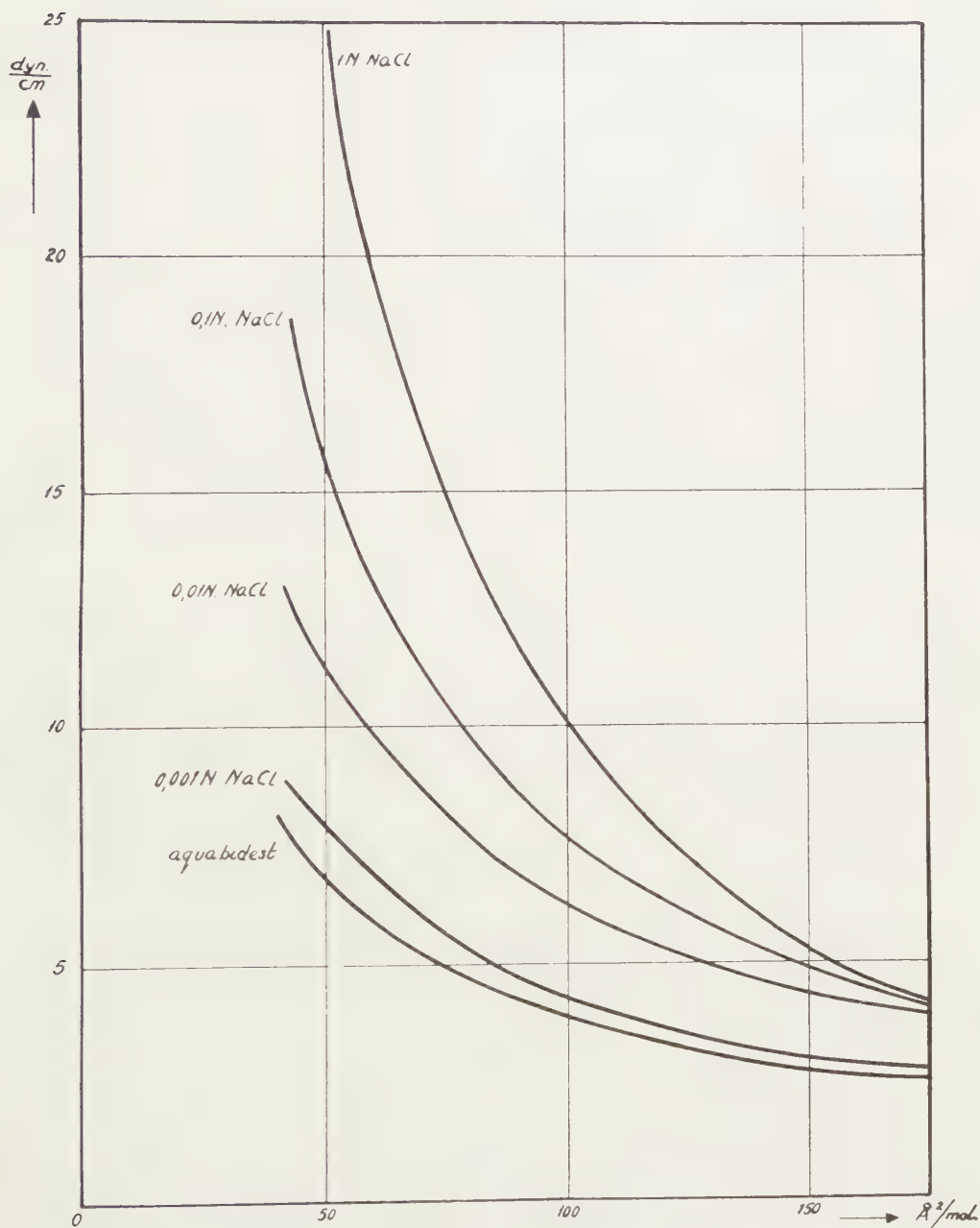
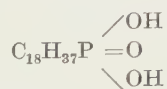


Fig. 1. Effect of neutral salt on the film pressure of films of



at the oil/water interface. pH of the subphase 5.8

in surface tension of pure water and the solution might, as is well known, be interpreted as the surface pressure of the adsorbed film. So again the measurements can be understood as surface pressure/molecular area curves.

Fig. 2 shows the result from measurements on solutions of caprylic acid

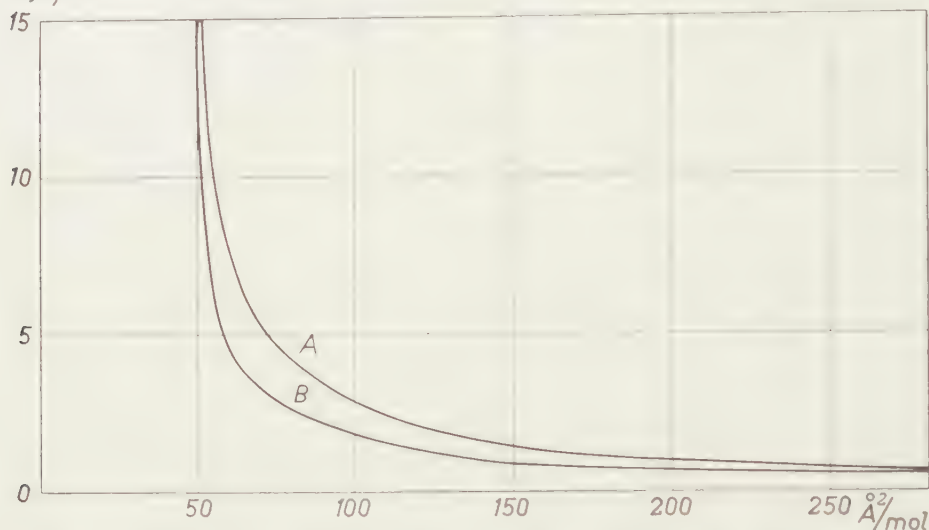


Fig. 2. Increase of the surface pressure of films of caprylic acid adsorbed at the air/water interface, due to increased ionic strength of the water.

Curve A: 0.2 molar acetate buffer, pH = 5

Curve B: without any added electrolyte

acid, once without any added electrolyte and once in the presence of 0.2 molar acetate buffer, pH=5.

Also in this case an increase of film pressure at the same molecular area is found to be the result of the increased electrolyte content. The fact that this increase is less for the fatty acid film must be accounted for by the difference between the ionization constant K_0 of the caprylic acid ($\sim 10^{-5}$) and of the phosphonic acid ($\sim 10^{-2.5}$).

Theoretically the effect of salt can be calculated with a model proposed by VERWEY [10], combining Stern's theory of specific adsorption of the counterions (e.g. of the H-ions) with the well-known Gouy equation for the capacity of the electrical double layer [11]. The equation of Stern turns out to be equivalent to equation (1). In this way it is possible to derive values of surface charge and potential at a planar interface for different conditions of pH and ionic strength. In how far such a theory can account for the experimentally observed differences in surface pressure is being investigated now.

Eindhoven, 21 October 1954

(Philips Research Laboratories
N.V. Philips' Gloeilampenfabrieken
Eindhoven-Netherlands)

REFERENCES

1. DAVIES, J. T., Proc. Roy. Soc. A 208, 224 (1951).
2. SCHULMAN, J. H. and A. H. HUGHES, Proc. Roy. Soc. A 138, 430 (1932).
3. DANIELLI, J. F., Surface Chemistry, 87 (London, 1949).
4. DAVIES, J. T., Surface Chemistry, 95 (London, 1949).
5. KATCHALSKY, A., J. Polym. Sc. VII, 393 (1951).
6. OVERBEEK, J. TH. G., Bull. Soc. Chim. Belg. 57, 252 (1948).
7. PETHICA, B. A., Trans. Farad. Soc. 50, 413 (1954).
8. ALEXANDER, A. E. and T. TEORELL, Trans. Farad. Soc. 35, 727 (1939).
9. COCKBAIN, E. G., Trans. Farad. Soc. 50, 874 (1954).
10. VERWEY, E. J. W., private communication.
11. ——— and J. TH. G. OVERBEEK, Theory of the stability of lyophobic colloids, 52 (Amsterdam, 1948).

LIMIT ANALYSIS OF SHELLS OF REVOLUTION¹). I

BY

E. T. ONAT AND W. PRAGER

(Brown University)

(Communicated by Prof. C. B. BIEZENO at the meeting of September 25, 1954)

Summary. This paper is concerned with the load carrying capacity of shells of revolution made of a plastic-rigid material that obeys Tresca's yield condition and the associated flow rule. Only axially symmetric conditions of loading and support are considered. The yield criterion is determined in terms of the stress resultants of the shell, and the associated flow rule is given in terms of the rates of extension and curvature of the middle surface. The load carrying capacity, i.e. the load intensity at which a plastic-rigid shell would begin to deform, can be determined by the use of this yield condition and flow rule.

1. *Introduction.* Plastic or limit design of structures was first advocated by KAZINCZY [1]²) in Hungary and KIST [2] in Holland. For over three decades research in this field remained restricted to structures composed of one-dimensional elements, in particular continuous beams [3], frames [4], and arches [5]. JOHANSEN's work [6] represents the first attempt to apply the concepts of limit design to plates. In the terminology of the general theory of limit design [7], JOHANSEN's "solutions" are based on kinematically admissible velocity fields and furnish therefore only upper bounds for the load carrying capacity of the considered plate. Lower as well as upper bounds for the load carrying capacity of a simply supported circular plate under uniformly distributed loading were first obtained by PELL and PRAGER [8], and complete solutions for circular plates under various rotationally symmetric conditions of loading and support were given by HOPKINS and PRAGER [9]. DRUCKER [10], ONAT [11], and HODGE [12] extended the concepts of limit analysis to cylindrical shells subjected to various types of axially symmetric loading. The present paper is concerned with the load carrying capacity of shells of revolution made of a plastic-rigid material that obeys TRESCA's yield condition and the associated flow rule. Only axially symmetric conditions of loading and support are considered. The earlier results regarding circular plates and cylindrical shells constitute special cases of the general results obtained in this paper.

¹) The results presented in this paper were obtained in the course of research sponsored by the Ballistic Research Laboratories of Aberdeen Proving Ground under Contract DA-19-020-ORD-798. The authors are indebted to the Authorities of the Ballistic Research Laboratories for the permission to publish this material.

²) Numbers in square brackets refer to the bibliography at the end of the paper.

2. *Generalized stresses and strain rates.* Figure 1 shows a shell element with the stress resultants transmitted across its boundary meridians and parallels: M_φ and M_θ are the meridional and circumferential bending moments, N_φ and N_θ the meridional and circumferential membrane forces,

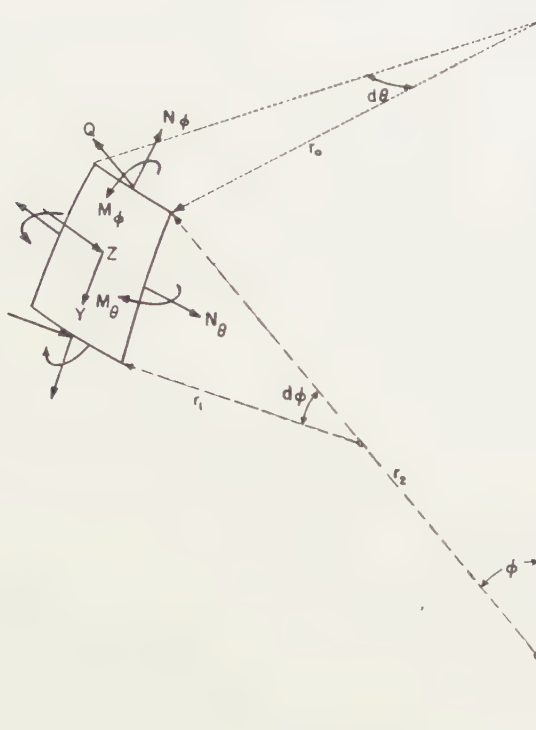


Fig. 1

and Q the shear force. The load per unit area of the middle surface of the shell has the components Y in the direction of the meridian and Z in the direction of the normal. The arrows in Fig. 1 indicate the usual conventions for positive forces and couples. The element has the distance r_0 from the axis of revolution and its principal radii of curvature are r_1 and r_2 . Note that

$$(1) \quad r_0 = r_2 \sin \varphi.$$

The equilibrium of the shell element requires that

$$(2) \quad \begin{cases} (r_0 N_\varphi)' - r_1 N_\theta \cos \varphi - r_0 Q + r_0 r_1 Y = 0, \\ r_0 N_\varphi - r_1 N_\theta \sin \varphi + (r_0 Q)' + r_0 r_1 Z = 0, \\ (r_0 M_\varphi)' - r_1 M_\theta \cos \varphi - r_0 r_1 Q = 0, \end{cases}$$

where the prime denotes differentiation with respect to φ [13].

For the velocity field of the incipient plastic flow the usual assumption will be made that the particles originally on a normal to the undeformed middle surface continue to remain on a normal to the middle surface as this is deforming.

If the meridional and normal velocity components are denoted by v and w , respectively, the positive directions being those indicated by Y and Z in Fig. 1, the principal rates of extension in the middle surface are

$$(3) \quad \varepsilon_\varphi = \frac{1}{r_1} (v' - w), \quad \varepsilon_\theta = \frac{1}{r_2} (v \cot \varphi - w).$$

The principal rates of curvature of the middle surface are

$$(4) \quad \kappa_\varphi = -\frac{1}{r_1} \left[\frac{1}{r_1} (v + w') \right]', \quad \kappa_\theta = \frac{\cot \varphi}{r_1 r_2} (v + w').$$

From the point of view of the general theory of limit design [14] the stress resultants M_φ , M_θ , N_φ , and N_θ are the generalized stresses of the present problem and κ_φ , κ_θ , ε_φ , and ε_θ are the corresponding generalized strain rates, the rate at which mechanical energy is dissipated in plastic flow being

$$(5) \quad D = M_\varphi \kappa_\varphi + M_\theta \kappa_\theta + N_\varphi \varepsilon_\varphi + N_\theta \varepsilon_\theta$$

per unit area of the middle surface. The expression for D does not contain a term with Q on account of the assumption that particles on a normal to the undeformed middle surface continue to form a normal of the bent middle surface. Accordingly, Q is not a generalized stress but has the nature of a reaction.

3. *Yield condition and flow rule.* The state of stress at a generic point of a thin shell is essentially two-dimensional. For such states of plane stress, Tresca's yield condition and the associated flow rule are conveniently summarized in Fig. 2, where the principal stresses σ_1 and σ_2 are used as rectangular coordinates. Plane states of stress at the yield limit are represented by points on the yield hexagon $ABCDEF$.

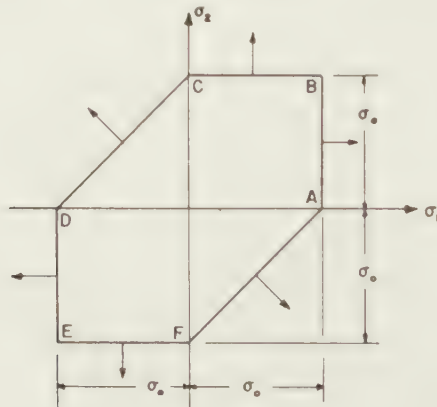


Fig. 2

For a yield state of stress represented by an interior point of a side of the yield hexagon, the flow mechanism is one of pure shear; it is represented in Fig. 2 by the vector plotted at the center of the considered side of the

hexagon, the components of this vector with respect to the coordinate axes being proportional to the principal strain rates ε_1 and ε_2 with a positive factor of proportionality. For a yield state of stress represented by a corner of the yield hexagon, the flow mechanism can be any linear combination, with positive coefficients, of the flow mechanisms corresponding to the adjacent sides.

Inspection of Fig. 2 reveals that the yield state of stress is uniquely determined by the flow mechanism provided this is not pure shear. On the other hand, the flow mechanism is uniquely determined by the yield state of stress provided that the three principal stresses, σ_1 , σ_2 , and $\sigma_3 = 0$, are distinct. In spite of the fact that there is no one-to-one correspondence between yield point states and flow mechanisms, the rate d at which mechanical energy is dissipated in plastic flow is completely determined by the flow mechanism; per unit volume this energy has the value

$$(6) \quad d = \sigma_0 \max |\varepsilon|,$$

where ε stands for ε_1 , ε_2 , or $\varepsilon_3 = -(\varepsilon_1 + \varepsilon_2)$.

The yield condition for a shell element expressed in terms of the stress resultants must be symmetric in N_φ and N_θ and in M_φ and M_θ . In the derivation of this yield condition it is therefore advisable not to identify σ_1 prematurely with either the meridional or the circumferential stress. Let ε_{10} and ε_{20} be the principal rates of extension of the middle surface and κ_1 and κ_2 the corresponding rates of curvature. The distribution of the principal strain rates over the thickness of the shell is then given by

$$(7) \quad \varepsilon_1 = \varepsilon_{10} + \kappa_1 z, \quad \varepsilon_2 = \varepsilon_{20} + \kappa_2 z, \quad \varepsilon_3 = -(\varepsilon_1 + \varepsilon_2).$$

Figures 3a, b, and c show typical distributions of ε_1 , ε_2 , and ε_3 . The zeros of these distributions (the points P , R , and Q) have the ordinates ³⁾

$$(8) \quad hp = -\varepsilon_{10}/\kappa_1, \quad hr = -\varepsilon_{20}/\kappa_2, \quad hq = -(\varepsilon_{10} + \varepsilon_{20})/(\kappa_1 + \kappa_2).$$

Since the stresses depend only on the ratios between the principal strains, the parameters p , q , r are adequate for the specification of the stress and hence the stress resultants.

Figure 3d shows the corresponding distribution of $\max |\varepsilon|$. When multiplied by σ_0 , the area bounded by the heavy lines in this figure gives the rate of energy dissipation D per unit area of the middle surface. Since the perfectly plastic solid is inviscid, D must be homogeneous of the order one in ε_{10} , ε_{20} , κ_1 , and κ_2 . By EULERS theorem on homogeneous functions we have therefore

$$(9) \quad D = \frac{\partial D}{\partial \varepsilon_{10}} \varepsilon_{10} + \frac{\partial D}{\partial \varepsilon_{20}} \varepsilon_{20} + \frac{\partial D}{\partial \kappa_1} \kappa_1 + \frac{\partial D}{\partial \kappa_2} \kappa_2.$$

³⁾ Note that a negative value of p has been assumed in Fig. 3 to achieve better separation of the points P , Q , and R , and hence greater clarity of the figure. The distance OP in Fig. 3a must therefore be labelled $-ph$.

On the other hand,

$$(10) \quad D = N_1 \epsilon_{10} + N_2 \epsilon_{20} + M_1 \kappa_1 + M_2 \kappa_2,$$

in accordance with (5). Comparison of (9) and (10) furnishes the following expressions for the stress resultants:

$$(11) \quad N_1 = \frac{\partial D}{\partial \epsilon_{10}}, \quad N_2 = \frac{\partial D}{\partial \epsilon_{20}}, \quad M_1 = \frac{\partial D}{\partial \kappa_1}, \quad M_2 = \frac{\partial D}{\partial \kappa_2}.$$

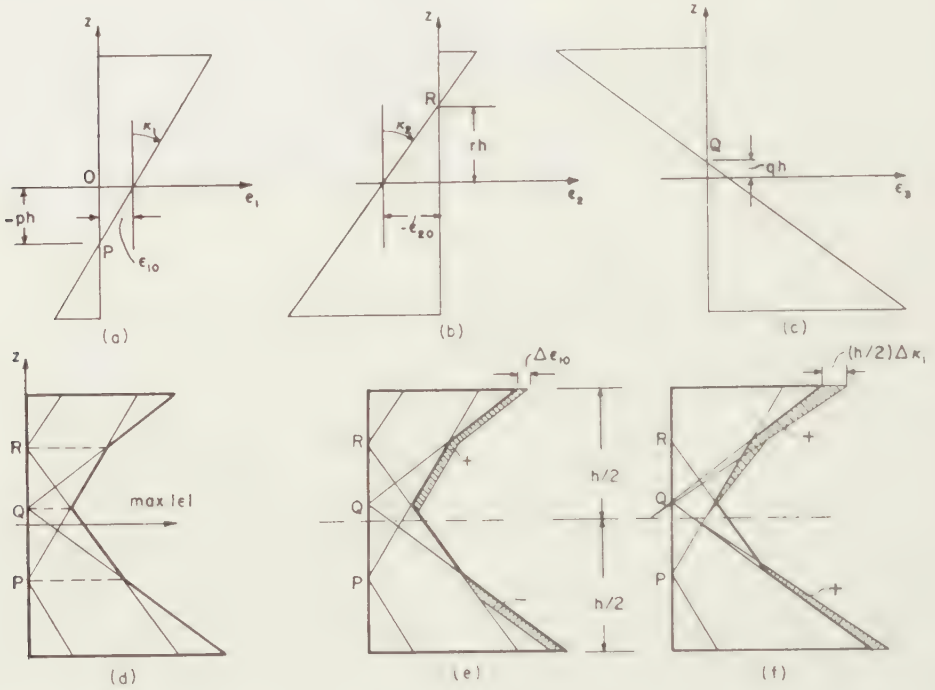


Fig. 3

These derivatives are most conveniently evaluated by considering the change of the area of the diagram of Fig. 3a when one of the parameters ϵ_{10} , ϵ_{20} , κ_1 , or κ_2 , is changed by a small amount. From the limiting value of the shaded areas in Figs. 3e and f, for instance, it is found that

$$(12) \quad \begin{cases} N_1 = \sigma_0 h \left[\frac{1}{2} - q - \left(\frac{1}{2} + p \right) \right] = -\sigma_0 h (p + q), \\ M_1 = \frac{\sigma_0 h^3}{2} \left[\frac{1}{4} - q^2 + \left(\frac{1}{4} - p^2 \right) \right] = \frac{\sigma_0 h^3}{4} [1 - 2(p^2 + q^2)]. \end{cases}$$

The remaining stress resultants are obtained in a similar manner:

$$(13) \quad \begin{cases} N_2 = -\sigma_0 h (q + r), \\ M_2 = \frac{\sigma_0 h^3}{4} [1 - 2(q^2 + r^2)]. \end{cases}$$

In the following the bending moments and membrane forces will be made dimensionless by dividing them by $M_0 = \sigma_0 h^3/4$ and $N_0 = \sigma_0 h$, respectively.

The letters m and n will be used, with appropriate subscripts, to denote the resulting dimensionless quantities. Equations (12) and (13) then take the form

$$(14) \quad \begin{cases} n_1 = -(p+q), & n_2 = -(q+r), \\ m_1 = 1 - 2(p^2 + q^2), & m_2 = 1 - 2(q^2 + r^2). \end{cases}$$

If n_1 , n_2 , m_1 , and m_2 are regarded as rectangular Cartesian coordinates in a four-dimensional stress space, Eqs. (14) constitute a parametric representation of a part of the yield surface. These equations do not represent the entire yield surface because they are derived from a figure that incorporates a definite arrangement of the points P , Q , and R . The range of validity of Eqs. (14) must therefore be explored.

In Fig. 3, the points P , Q , R fall within the interval $-h/2 \leq z \leq h/2$ and are arranged in the order P , Q , R in the direction of increasing z values; thus

$$(15) \quad -\frac{1}{2} \leq p < q < r \leq \frac{1}{2}.$$

The range of validity of Eqs. (14) would therefore seem to be specified by (15). It can be shown, however, that Eqs. (14) apply also when

$$(16) \quad -\frac{1}{2} \leq r < q < p \leq \frac{1}{2}.$$

Indeed, if Figs. 3a and b are assumed to represent the distributions of ϵ_2 and ϵ_1 , respectively, Figs. 3c and d remain unchanged except that the labels P and R have to be interchanged in the latter. The same change of labels has to be made in Figs. 3e and f, which then indicate the effects of small increments in ϵ_{20} and κ_2 . This means that N_2 and M_2 are now obtained from Eqs. (12) provided that p is replaced by r . The resulting expressions, however, are identical with Eqs. (13).

If Figs. 3a and b are redrawn so as to correspond to the opposite signs of the quantities ϵ_{10} , ϵ_{20} , κ_1 , and κ_2 , the values of the parameters p , q , and r defined by (8) remain unchanged, and the only modification needed in Figs. 3e and f is a change of the sign of each shaded area. When p , q , and r satisfy either (15) or (16), Eqs. (14) may therefore be considered to furnish n_1 , n_2 , m_1 , m_2 or $-n_1$, $-n_2$, $-m_1$, $-m_2$.

Let us now investigate the possibility that one or more of the points P , Q , and R fall outside the interval $-h/2 \leq z \leq h/2$. If, for example, $p < -1/2 \leq q < r \leq 1/2$, examination of the modified Figs. 3e and f reveals that Eqs. (12) remain valid provided that p is replaced by $-1/2$. Since this value of p is admitted by (15), no new points of the yield surface are obtained by letting P fall outside the thickness of the shell. Another way of looking at this situation is the following. By setting $p = -1/2$ in Eqs. (14), we express the four stress resultants in terms of two parameters, q and r . The modified Eqs. (14) therefore represent the two-dimensional boundary of the part of the three-dimensional yield surface that is defined by the original Eqs. (14). Similar remarks apply when more than one of the points P , Q , and R fall outside the thickness of the shell.

The preceding discussion shows that Eqs. (14) apply as long as the points P , Q , and R are distinct and Q lies between P and R , provided that p , q , and r are replaced by $1/2$ or $-1/2$ whenever the corresponding point leaves the interval $-1/2 \leq z \leq 1/2$ by crossing the boundary $z = 1/2$ or the boundary $z = -1/2$. Two further cases are obtained by letting P or R be the central point. The corresponding formulas are assembled in Table I.

TABLE I
Distinct points P , Q , R .

Central Point	Stress resultants			
	$\pm n_1$	$\pm n_2$	$\pm m_1$	$\pm m_2$
P	$-(p+q)$	$-(q-r)$	$1-2(p^2+q^2)$	$2(r^2-q^2)$
Q	$-(p+q)$	$-(q+2)$	$1-2(p^2+q^2)$	$1-2(q^2+r^2)$
R	$-(q-r)$	$-(q+r)$	$2(p^2-q^2)$	$1-2(q^2+r^2)$

Flow rule for all cases

$$N_0\epsilon_{10}:N_0\epsilon_{20}:M_0\kappa_1:M_0\kappa_2 = -4p(q-r):-4r(p-q):(q-r):(p-q)$$

Note: The given expressions for the stress resultants presuppose that all of the points P , Q , and R fall within the thickness of the shell. If, for instance, $p > 1/2$, the parameter p in the formulas for the stress resultants must be replaced by $1/2$. No such change should be made in the flow rule.

TABLE II
Coincident points P , Q , R .

Coin- cidence	Yield Surface	Flow Rule
		$N_0\epsilon_{10}:N_0\epsilon_{20}:M_0\kappa_1:M_0\kappa_2$
$P=Q$	$m_1 = \pm(1-n_1^2)$	$+2n_1:0:1:0$
$Q=R$	$m_2 = \pm(1-n_2^2)$	$0:\pm 2n_2:0:1$
$P=R$	$m_1-m_2 = \pm[1-(n_1-n_2)^2]$	$\pm 2(n_1-n_2):\mp 2(n_1-n_2):1:-1$

A separate investigation becomes necessary when two or all of the points P , Q , and R coincide. If $p=q=r$, the quantity $\max |\epsilon|$ is one of the quantities $|\epsilon_1|$, $|\epsilon_2|$, or $|\epsilon_3|$ over the entire thickness of the shell. An examination of the possible cases along the lines of the preceding discussion reveals that the formulas in the rows P , Q , or R of Table I should be used in this case depending on whether $\max |\epsilon| = |\epsilon_1|$, $\max |\epsilon| = |\epsilon_3|$, or $\max |\epsilon| = |\epsilon_2|$. It is possible, however, that only two of the quantities p , q , and r have the same value while the third is indeterminate. To discuss this case, let us assume that $\epsilon_{10}=\kappa_1=0$. Then $q=r$, while p is indeterminate. For a generic value of z we have $\epsilon_1=0$ from the first Eq. (7). It follows that the state of stress is represented by a point on the sides CB or EF of the yield hexagon of Fig. 2. Accordingly, $\sigma_2=\sigma_0$ where $\epsilon_2>0$ and $\sigma_2=-\sigma_0$ where $\epsilon_2<0$. The stress resultants m_2 and n_2 therefore depend on the single para-

meter $q=r$, while the remaining stress resultants are not uniquely determined. When this parameter is eliminated between the equations for m_2 and n_2 , the following yield condition is obtained:

$$(17) \quad m_2 = \pm (1 - n_2^2).$$

The cases $p=q$ and $p=r$ furnish other parts of the yield surface. The relevant equations are assembled in Table II.

(To be continued)

LIMIT ANALYSIS OF SHELLS OF REVOLUTION. II

BY

E. T. ONAT AND W. PRAGER

(Brown University)

(Communicated by Prof. C. B. BIEZENO at the meeting of September 25, 1954)

4. *Special cases.* Tables I and II define a closed convex hypersurface in the four-dimensional stress space with the rectangular Cartesian coordinates m_1 , m_2 , n_1 , and n_2 . Each point of this hypersurface represents a combination of stress resultants under which plastic flow is possible. The flow mechanisms corresponding to the various types of yield state of stress are indicated in Tables I and II.

Important special cases of the yield condition represented by Tables I and II are obtained by setting one or more of the stress resultants equal to zero. For instance, an important special case is obtained by setting $n_2=0$. Figure 4 shows three views and an axonometric sketch of the intersection of the yield hypersurface and the hyperplane $n_2=0$. The resulting yield surface in the three-dimensional stress space with the rectangular coordinates m_1 , m_2 , and n_1 is symmetric with respect to the coordinate origin. For clarity only the front half of this surface is shown in Fig. 4d. Table III indicates the columns of Table I or rows of Table II from which the various parts of this front half are obtained, the choice of sign being indicated in the last column of Table III.

TABLE III
Yield surface of Fig. 4d

Part	Equations of		Choice of Sign
	Table	Row	
$\frac{ABC,}{A'B'C}$	I	Q	+
$\frac{ABF,}{A'FB'}$	I	R	+
$AFA'C$	II	$Q = R$	+
$B'CBH$	II	$P = Q$	+
$B'IBF$	II	$P = R$	-

The rate of energy dissipation D per unit area of the middle surface is readily evaluated, as function of ϵ_{10} , ϵ_{20} , κ_1 , and κ_2 , from Eq. (10) and the information in Tables I and II. For instance, if the points P , Q , and R fall

within the shell thickness and Q lies between P and R , the expressions (12) and (13), which are summarized in row Q of Table I, must be substituted into (10), and p , q , and r must then be expressed in terms of ε_{10} , ε_{20} , κ_1 , and κ_2 by means of Eqs. (8). On the other hand, if $P=Q$ and R is indeter-

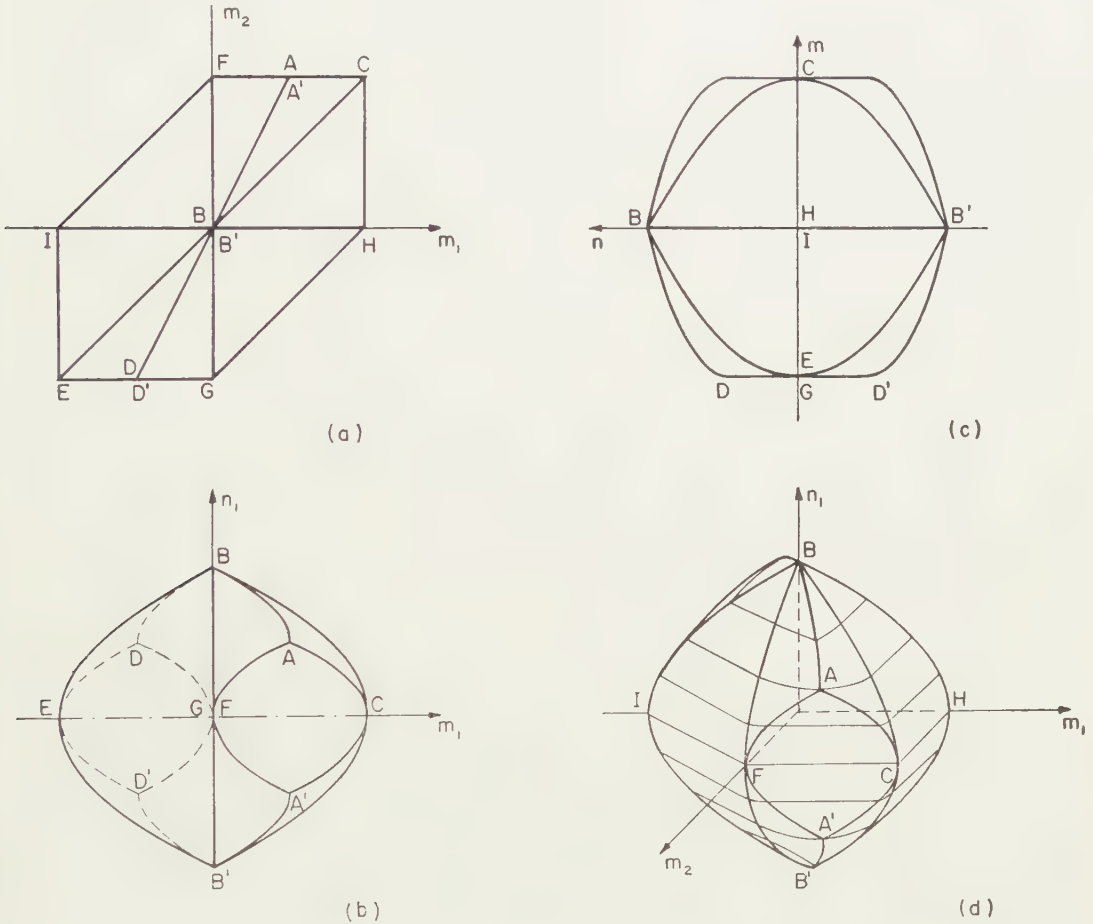


Fig. 4

minate, the row $P=Q$ of Table II applies. Since $\varepsilon_{20}=\kappa_2=0$ in this case, $D=N_0 n_1 \varepsilon_{10} + M_0 m_1 \kappa_1$. The yield condition given in the second column of Table II furnishes m_1 in term of n_1 , and the flow rule in the third column of Table II identifies n_1 with $\pm N_0 \varepsilon_{10} / (2M_0 \kappa_1)$, so that D can be expressed in terms of ε_{10} and κ_1 .

5. *Limit analysis.* As HILL [15] has pointed out, the general concepts of limit analysis first formulated by GREENBERG and PRAGER [4] and DRUCKER, GREENBERG, and PRAGER [16] with reference to elastic-plastic solids, are most readily explained with reference to plastic-rigid solids. This point of view will therefore be adopted in the following.

Consider a shell of revolution made of a plastic-rigid material and subjected to an axially symmetric type of loading. As the intensity of this loading is raised gradually, starting from zero, the shell at first remains rigid. Only when the load intensity reaches a critical value can the plastic-rigid shell begin to deform. Limit analysis is concerned with the determination of this critical load intensity. The incipient plastic flow developing under the critical load is treated as quasistatic, i.e. inertia effects are neglected.

In the accepted terminology of the theory of perfectly plastic solids a "complete" solution of our problem consists in the specification of the critical load intensity and associated fields of stress and incipient plastic flow. These fields are specified by giving the stress resultants M_φ , M_θ , N_φ , and N_θ , and the velocity components v and w , as functions of the angle φ or the arc length s along the meridian.

The stress resultants must satisfy the equations of equilibrium (2) in which the components Y and Z of the exterior load are given only to within a common factor λ that defines the unknown critical load intensity. Moreover, the state of stress at a generic point of the shell must be represented by a point on or inside the yield hypersurface discussed in the preceding section. All these conditions impose considerable restrictions on the stress field but do not suffice to define a unique stress field and a unique value of λ . Any stress field satisfying these conditions will be called "statically admissible" and the associated value of λ will be called a "statically admissible multiplier".

When the velocities v and w of an assumed incipient plastic flow are given, the flow mechanism at any point of the shell is determined by means of (3) and (4). The values of p , q , r then follow from (8) and the rate of energy dissipation D is evaluated from the expressions given in Tables I and II. Since no energy can be stored in the plastic-rigid shell, the total rate of energy dissipation must equal the rate at which the applied loads (multiplied by λ) do work. This condition is satisfied if λ is determined from

$$(18) \quad \lambda \int (vY + wZ)r_0 r_1 d\varphi = \int D r_0 r_1 d\varphi,$$

where the integration is extended over the entire meridian. Any factor λ determined in this manner from a velocity field v , w will be called a "kinematically admissible multiplier". Equation (18) furnishes such a multiplier for an assumed velocity field, but does not single out any particular velocity field.

It has been seen that neither the purely statical nor the purely kinematical approach leads to a unique solution. To achieve such a degree of uniqueness as is possible within the framework of the theory of perfectly plastic solids⁴⁾ the statical and kinematical points of view must be combined by using the flow rule. Plastic deformation can develop only in

⁴⁾ For a discussion of the uniqueness problem see HILL [15].

those parts of the shell where the state of stress is represented by a point on the yield hypersurface; the other parts of the shell remain at rest or perform rigid body motions. At any point where plastic deformation occurs, the state of stress and the flow mechanism must satisfy the flow rule.

As can be seen from the preceding discussion, the construction of a complete solution is not an easy task. The importance of the fundamental theorem of limit analysis stems from the fact that this theorem allows us to extract useful information from statically admissible stress fields on one hand, and velocity fields, on the other hand, without imposing the cumbersome condition that the stress and velocity fields should be related to each other by the flow rule. The fundamental theorem compares the factor λ defining the critical load intensity to statically or kinematically admissible multipliers and states that λ is the largest statically admissible multiplier and the smallest kinematically admissible multiplier (see, for instance, [7]). Any statically admissible stress field therefore furnishes a lower bound for λ , and any velocity field yields an upper bound for λ . The stress and velocity fields of a complete solution furnish, of course, coincident bounds. The price paid for this coincidence of the upper and lower bounds is the time spent in reconciling the stress and velocity fields by means of the flow rule. It is frequently possible to arrive rapidly at sufficiently close bounds without completely reconciling these fields.

6. *Example.* As an example, consider a built-in spherical cap subjected to uniformly distributed pressure (Fig. 5). If the given pressure is

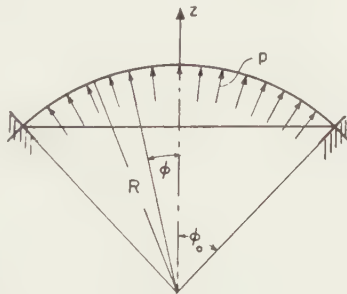


Fig. 5

assumed to have unit intensity, the factor λ bounded by the fundamental theorems of limit analysis represents the critical pressure under which the plastic-rigid shell begins to deform.

To obtain an upper bound for this critical pressure, consider the velocity field

$$(19) \quad v = 0, \quad w = \cos \varphi_0 - \cos \varphi.$$

The velocity vector (19) is directed along the exterior normal of the sphere; it vanishes at the support and has the intensity $1 - \cos \varphi_0$ at the pole.

The velocity field (19) does not satisfy the clamping condition: $w' = 0$ for $\varphi = \varphi_0$. This means that the parallel $\varphi = \varphi_0$ must be considered as a hinge circle (see [9]).

From Eqs. (19) the principal rates of extension and curvature of the middle surface are obtained by means of Eqs. (3) and (4):

$$(20) \quad \varepsilon_\varphi = \varepsilon_\theta = \frac{1}{R} (\cos \varphi - \cos \varphi_0),$$

$$(21) \quad \kappa_\varphi = \kappa_\theta = -\frac{1}{R^2} \cos \varphi.$$

Equations (8) then furnish

$$(22) \quad p = q = r = \frac{R}{h} \frac{\cos \varphi - \cos \varphi_0}{\cos \varphi}.$$

The points $P=Q=R$ will fall within the shell thickness if the non-negative right-hand side of (22) is smaller than $1/2$, i.e. if $\varphi^* < \varphi < \varphi_0$, where φ^* is given by

$$(23) \quad \cos \varphi^* = \frac{2 \cos \varphi_0}{2 - h/R}.$$

Since h/R is much smaller than 2 Eq. (23) indicates that $p=q=r > 1/2$ except in a zone close to the support. For a fixed value of h/R the relative importance of this zone increases with decreasing φ_0 because the same percentage change in the cosine corresponds to a larger change in angle when the angle is small.

Where $p=q=r > 1/2$, the dimensionless stress resultants are obtained from the row Q of Table I by setting $p=q=r=1/2$ and using the negative sign because $\max |\varepsilon| = |\varepsilon_3|$ and $\varepsilon_3 < 0$. Thus,

$$(24) \quad n_1 = n_2 = 1, \quad m_2 = m_1 = 0.$$

The corresponding rate of energy dissipation per unit area is

$$(25) \quad D_1 = \sigma_0 h (\varepsilon_\varphi + \varepsilon_\theta) = 2 \sigma_0 \frac{h}{R} (\cos \varphi - \cos \varphi_0), \quad (0 \leq \varphi < \varphi^*).$$

On the other hand, where $0 \leq p=q=r < 1/2$, the stress resultants are found from the row Q of Table I by using the common value (22) for $p=q=r$ and the negative sign. Thus,

$$(26) \quad \begin{cases} n_1 = n_2 = 2 \frac{R}{h} \frac{\cos \varphi - \cos \varphi_0}{\cos \varphi}, \\ m_1 = m_2 = -1 + 4 \frac{R^2}{h^2} \frac{(\cos \varphi - \cos \varphi_0)^2}{\cos^2 \varphi}. \end{cases}$$

The corresponding rate of energy dissipation per unit area is found to be

$$(27) \quad D_2 = 2 \sigma_0 \frac{(\cos \varphi - \cos \varphi_0)^2}{\cos \varphi} + \frac{\sigma_0 h^2}{2 R^2} \cos \varphi, \quad (\varphi^* < \varphi < \varphi_0).$$

The rate of flexure at the hinge circle $\varphi = \varphi_0$ is given by w'/R evaluated

at $\varphi = \varphi_0$. Thus, the rate at which energy is dissipated per unit arc length of the hinge circle is

$$(28) \quad D_3 = \frac{\sigma_0 h^2}{4} \frac{\sin \varphi_0}{R}.$$

The total rate of energy dissipation Δ for the entire shell is given by

$$(29) \quad \Delta / (2\pi R^2) = \int_0^{\varphi^*} D_1 \sin \varphi d\varphi + \int_{\varphi^*}^{\varphi_0} D_2 \sin \varphi d\varphi + D_3 \frac{\sin \varphi_0}{R}.$$

The rate W at which the applied unit pressure does work on the velocities (19) is found from

$$(30) \quad W / (2\pi R^2) = \int_0^{\varphi_0} (\cos \varphi - \cos \varphi_0) \sin \varphi d\varphi.$$

The kinematically admissible multiplier corresponding to the assumed velocities is found from $\lambda W = \Delta$. In view of (25), the first integrand in (29) is proportional to the integrand in (30). The multiplier λ can therefore be written as follows:

$$(31) \quad \lambda = 2\sigma_0 \frac{h}{R} + \frac{\int_{\varphi^*}^{\varphi_0} (D_2 - D_1) \sin \varphi d\varphi + (D_3/R) \sin \varphi_0}{\int_0^{\varphi_0} (\cos \varphi - \cos \varphi_0) \sin \varphi d\varphi}.$$

Now, the yield state of balanced bi-axial tension defined by (24) is statically admissible for the pressure $2\sigma_0 h/R$. The first term on the right-hand side of (31) is therefore a lower bound for the critical pressure, so that the second term represents the gap between the lower and upper bounds. Evaluation of the integrals appearing in Eq. (31) leads to the following expression for this gap:

$$(32) \quad \left\{ \begin{aligned} \lambda - 2\sigma_0 \frac{h}{R} = & \frac{2\sigma_0}{(1 - \cos \varphi_0)^2 (1 - h/2R)} \left\{ \frac{h^2}{4R^2} \left(1 - \frac{h}{2R}\right)^2 \sin^2 \varphi_0 + \right. \\ & + \frac{h^3}{16R^3} \left(1 - \frac{h}{2R} - 4 \cos \varphi_0\right) \cos \varphi_0 + \\ & \left. + \frac{h}{4R} \left(3 \frac{h}{R} - 4\right) - 2 \left(1 - \frac{h}{2R}\right)^2 \log \left(1 - \frac{h}{2R}\right) \right\}. \end{aligned} \right.$$

Figure 6 shows the ratio ρ between the upper and lower bounds found from Eq. (32). As is to be expected from the nature of the considered

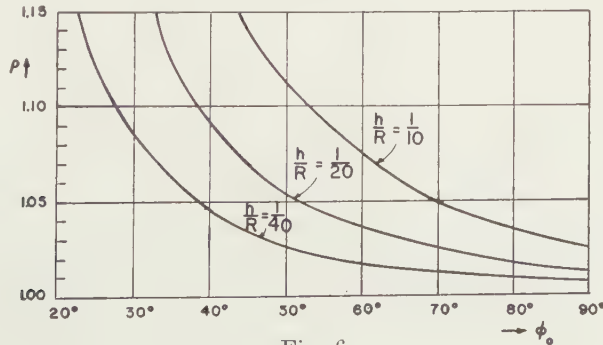


Fig. 6

statically admissible stress field. the gap between the bounds decreases with h/R . For a fixed value of h/R , the gap increases with decreasing φ_0 , because the bending moments disregarded in the statically admissible stress field gain in relative importance as φ_0 decreases.

BIBLIOGRAPHY

1. G. KAZINCZY, *Betonszemele* (Budapest), 2, 68, 83, 101 (1914).
2. N. C. KIST, Inaugural Dissertation, Technical University, Delft, Holland (1917).
3. See, for instance, J. A. VAN DEN BROEK, *Trans. ASCE* 105, 638 (1940).
4. See, for instance, J. F. BAKER, *J. Instn. Civ. Engrs.* 27, 188 (1949); H. J. GREENBERG and W. PRAGER, *Proc. ASCE* 77, Separate No. 59 (1951); B. G. NEAL and P. S. SYMONDS, *Proc. Instn. Civ. Engrs.* 1, III, 58 (1952).
5. See, for instance, A. W. HENDERSON, *Civ. Engg. Publ. Works Review* 47, 38 (1952); E. T. Onat and W. Prager, *J. Mech. Phys. Solids* 1, 77 (1953) and *Proc. 1st Midwestern Conf. Solid Mech.* (Urbana, Ill., 1953).
6. K. W. JOHANSEN, *Brudlinieteorier*, J. GJELLERUP (Copenhagen, 1943).
7. See, for instance, W. PRAGER and P. G. HODGE, Jr., *Theory of Perfectly Plastic Solids*, Sects. 33 and 39 (J. WILEY, New York, 1951).
8. W. H. PELL and W. PRAGER, *Proc. 1st Nat. Congr. Appl. Mech.* (Chicago, Ill., 1951).
9. H. G. HOPKINS and W. PRAGER, *J. Mech. Phys. Solids* 2, 1 (1953).
10. D. C. DRUCKER, *Proc. 1st Midwestern Conf. Solid Mech.* (Urbana, Ill., 1953).
11. E. T. ONAT, Report DA-798/9, Brown University, (Providence, R. I., 1954), to appear in *Q. Appl. Math.*
12. P. G. HODGE, Jr., Pibal Report 242, Polytechn. Inst., (Brooklyn, 1954).
13. See, for instance, W. FLÜGGE, *Statik und Dynamik der Schalen*, p. 148 (J. SPRINGER, Berlin, 1934).
14. W. PRAGER, Sectional Address, 8th Internat. Congress Theor. Appl. Mech. (Istanbul, 1952).
15. R. HILL, *Phil. Mag.* (7) 42, 868 (1951).
16. D. C. DRUCKER, H. J. GREENBERG and W. PRAGER, *J. Appl. Mech.* 18, 371 (1951); *Q. Appl. Math.* 9, 381 (1951/2).

ON THE BENDING OF CANTILEVER, RECTANGULAR
PLATES. III ¹⁾

BY

W. T. KOITER AND J. B. ALBLAS

(Communicated by Prof. C. B. BIEZENO at the meeting of September 25, 1954)

4. *The semi-infinite strip*

4.1. An ineffective attempt

Our first attempt was directed at the solution of the problem of a semi-infinite strip, loaded by an equilibrium system of bending moments and shear forces along its root section $x=0$ in such a way that the anticlassic curvature at this section, due to a primary solution for the plate considered as a beam, is compensated (cf. part I, paras. 1 and 2 and eq. (6)). Obviously, this problem is equivalent to the problem of an *infinite* strip, loaded by an equilibrium system of *forces* normal to the plane of the plate at the section $x=0$ in such a way that the prescribed anticlassic curvature at this section is obtained. The unknown load distribution along $x=0$ was assumed in a FOURIER-series

$$(79) \quad q(y) = \sum_{n=1}^{\infty} q_n \cos n\pi y.$$

The resulting deflection along $x=0$ was also obtained in the form of a FOURIER-cosine series (with coefficients depending on all q_n 's) and this deflection was equated to the prescribed deflection (6)

$$(80) \quad w_{x=0} = \frac{1}{2} \frac{\nu}{1-\nu^2} m_{xp} y^2 = \frac{\nu}{1-\nu^2} m_{xp} \left[\frac{1}{6} + \frac{2}{\pi^2} \sum_{n=1}^{\infty} \frac{(-1)^n}{n^2} \cos n\pi y \right].$$

The resulting infinite system of equations proved insoluble. The usual procedure of approximation by solving the first k equations in which all q_j ($j > k$) are put zero did not show acceptable convergence. In fact, this system of equations did not satisfy any of the available convergence criteria for infinite systems (ref. 13).

It is now clear that this failure is due to the singularities in the corners of the plate, where the reduced shear force (which is half the external load $q(y)$) is unbounded as $(1 \pm y)^{-0.92}$ (cf. eq. (77)). The series (79) may still be convergent (except in the corners) but its convergence will be *extremely slow* and truncation of this series cannot result in a satisfactory approximation unless a prohibitive number of terms is retained.

¹⁾ For parts I and II of these Proceedings, 57, 250 and 259.

4.2. Solution by means of eigenfunctions

A general method of solution of problems in plate bending with *homogeneous* boundary conditions along two opposite edges has been indicated by CARRIER and SHAW (ref. 14). This solution is obtained in the form of an expansion in eigenfunctions which, in the examples treated by CARRIER and SHAW, is rapidly convergent.

If our problem is approached from the beam solution by superposition of a solution of the biharmonic equation (1) which satisfies the boundary conditions (6) and (7)

$$(6) \quad x = 0: w = \frac{1}{2} \frac{\nu}{1-\nu^2} m_{xy} y^2, \quad \frac{\partial w}{\partial x} = 0,$$

$$(7) \quad \begin{cases} |y| = 1: \frac{\partial^2 w}{\partial y^2} + \nu \frac{\partial^2 w}{\partial x^2} = 0, \\ \frac{\partial^3 w}{\partial y^3} + (2-\nu) \frac{\partial^3 w}{\partial x^2 \partial y} = 0. \end{cases}$$

the latter boundary conditions are homogeneous.

The eigenfunctions in our problem are defined as solutions of the biharmonic equation of the type $e^{\lambda x} f(y)$ which satisfy (7). The function $f(y)$ must satisfy the equation

$$(81) \quad \frac{d^4 f}{dy^4} + 2\lambda^2 \frac{d^2 f}{dy^2} + \lambda^4 f = 0$$

and the boundary conditions at $y = \pm 1$

$$(82) \quad \begin{cases} \frac{d^2 f}{dy^2} + \nu \lambda^2 f = 0, \\ \left(\frac{d^3 f}{dy^3} + (2-\nu) \lambda^2 \frac{df}{dy} \right) = 0. \end{cases}$$

The general solution of (81) which is symmetric in y is

$$(83) \quad f(y) = A \cos \lambda y + B \lambda y \sin \lambda y,$$

where A and B are constants of integration. The boundary conditions (82) yield the homogeneous equations

$$(84) \quad \begin{cases} A \cos \lambda - \left[\frac{2}{1-\nu} \cos \lambda - \lambda \sin \lambda \right] B = 0 \\ A \sin \lambda + \left[\frac{1+\nu}{1-\nu} \sin \lambda - \lambda \cos \lambda \right] B = 0, \end{cases}$$

which have non-trivial solutions only if the determinant is zero. This condition leads to the eigenvalue equation

$$(85) \quad \sin 2\lambda = \frac{1-\nu}{3+\nu} 2\lambda.$$

For any root λ_k of (85) the ratio of A and B is determined by (84) and the eigenfunction is obtained in the form

$$(86) \quad w_k(x, y) = e^{\lambda_k x} \left[\left(-\frac{1+\nu}{1-\nu} + \lambda_k \cot \lambda_k \right) \cos \lambda_k y + \lambda_k y \sin \lambda_k y \right].$$

Taking $\nu = \frac{1}{4}$ we have calculated the two real roots of (85)

$$(87) \quad \lambda = \pm 1,2604$$

and the first five sets of complex roots

$$(88) \quad \begin{cases} \lambda = \pm 3,8345 \pm 0,5966 i, \\ \lambda = \pm 6,9996 \pm 0,9255 i, \\ \lambda = \pm 10,1542 \pm 1,1163 i, \\ \lambda = \pm 13,3042 \pm 1,2530 i, \\ \lambda = \pm 16,4518 \pm 1,3597 i, \end{cases}$$

For $k > 5$ the roots of the k^{th} set are readily approximated by the asymptotic formula

$$(89) \quad \lambda = \pm \left[\frac{\pi}{4} + k\pi - \frac{1}{(4k+1)\pi} \ln \left((4k+1) \pi \frac{1-\nu}{3+\nu} \right) \right] \pm \frac{1}{2} i \ln \left((4k+1) \pi \frac{1-\nu}{3+\nu} \right).$$

The accuracy of this approximation may be assessed from its application to $k=5$, yielding the approximation $\lambda = \pm 16,4521 \pm 1,3614 i$, in excellent agreement with the correct values.

Because the stresses must vanish for $x \rightarrow \infty$ the eigenvalues with a positive real part can be dropped. Denoting the negative real eigenvalue by λ_0 and an eigenvalue with negative real and positive imaginary part by λ_k , its conjugate by $\bar{\lambda}_k$, the solution is assumed in the form

$$(90) \quad \begin{cases} w = A + Bx + a_0 w_0 + \sum_{k=1}^{\infty} (a_k w_k + \bar{a}_k \bar{w}_k) = \\ = A + Bx + a_0 w_0 + 2 \operatorname{Re} \sum_{k=1}^{\infty} a_k w_k, \end{cases}$$

where w_k is given by (86), \bar{w}_k is its conjugate, a_0 is a real constant and the a_k 's are complex constants with conjugates \bar{a}_k . The first two terms represent a rigid body motion; they do not affect the stress distribution.

The constants a_0, a_k are to be determined from the boundary conditions (6), which are replaced by the equivalent conditions

$$(91) \quad x=0: \quad \frac{\partial^2 w}{\partial y^2} - \frac{\nu}{1-\nu^2} m_{xp} = 0, \quad \frac{\partial w}{\partial x} = 0.$$

An *approximate* solution is now achieved by retaining only the first n a_k 's and by orthogonalizing the left-hand members of (91) with respect to $\cos m\pi y$ ($m=0, 1, 2, \dots n$). The resulting system of equations is for $m_{xp}=1$

$$(92) \quad a_0 \lambda_0 \sin \lambda_0 + 2 \operatorname{Re} \sum_{k=1}^n a_k \lambda_k \sin \lambda_k = \frac{\nu}{2(1+\nu)}.$$

$$(93) \quad \begin{cases} a_0 \lambda_0^3 \sin \lambda_0 \frac{\lambda_0^2 - (2-\nu)m^2\pi^2}{(\lambda_0^2 - m^2\pi^2)^2} + 2 \operatorname{Re} \sum_{k=1}^{\infty} a_k \lambda_k^3 \sin \lambda_k \frac{\lambda_k^2 - (2-\nu)m^2\pi^2}{(\lambda_k^2 - m^2\pi^2)^2} = 0, \\ m = 1, 2, \dots n; \end{cases}$$

$$(94) \quad \left\{ \begin{aligned} a_0 \lambda_0^2 \sin \lambda_0 \frac{\nu \lambda_0^2 - m^2 \pi^2}{(\lambda_0^2 - m^2 \pi^2)^2} + 2 \operatorname{Re} \sum_{k=1}^{\pi} a_k \lambda_k^2 \sin \lambda_k \frac{\nu \lambda_k^2 - m^2 \pi^2}{(\lambda_k^2 - m^2 \pi^2)^2} &= 0, \\ m &= 1, 2, \dots, n; \end{aligned} \right.$$

where the single equation which contains B has been omitted.

Taking $n=5$, we have solved this system for one real constant a_0 and five complex constants a_k . It will appear from the discussion in section 4.4 (part IV of this paper) that the accuracy is only moderate. An improvement may, of course, be obtained by retaining a larger number of constants a_k but the required numerical work would increase considerably. However, a more satisfactory solution is obtained in the next paragraph.

4.3. Solution by FOURIER-transforms

We now consider the strip problem formulated by eq. (1)

$$(1) \quad \Delta \Delta w = 0$$

with boundary conditions (4) and (5)

$$(4) \quad x = 0: w = 0, \quad \frac{\partial w}{\partial x} = 0;$$

$$(5) \quad \left\{ \begin{aligned} |y| = 1: \frac{\partial^2 w}{\partial y^2} + \nu \frac{\partial^2 w}{\partial x^2} &= -\nu m_{xp}, \\ \frac{\partial^3 w}{\partial y^3} + (2 - \nu) \frac{\partial^3 w}{\partial x^2 \partial y} &= 0, \end{aligned} \right.$$

where m_{xp} is the primary bending moment in a plate of infinite width (cf. para. 2). This problem is the counterpart of para. 3.

The deflection and slope $\partial w / \partial x$ will not vanish at infinity. In order to apply the FOURIER sine transform (10) we first subtract a linear function $A + Bx$, obtaining

$$(96) \quad w^*(x, y) = w(x, y) - A - Bx,$$

where w^* and its derivatives are assumed to vanish at infinity. Putting

$$(97) \quad W^*(\lambda, y) = \int_0^{\infty} w^*(x, y) \sin \lambda x dx$$

the biharmonic equation is transformed into

$$(98) \quad \frac{d^4 W^*}{dy^4} - 2\lambda^2 \frac{d^2 W^*}{dy^2} + \lambda^4 W^* = -\lambda p(y) - \lambda^3 A,$$

where

$$(12) \quad p(y) = \left(\frac{\partial^2 w^*}{\partial x^2} \right)_{x=0} = (m_x)_{x=0}$$

is the root bending moment. The boundary conditions along $|y|=1$ are transformed into

$$(13) \quad \frac{d^2 W^*}{dy^2} - \nu \lambda^2 W^* = M_\nu(\lambda) + \nu \lambda A,$$

$$(14) \quad \frac{d^3 W^*}{dy^3} - (2 - \nu) \lambda^2 \frac{dW^*}{dy} = 0,$$

where $M_y(\lambda)$ is the sine transform of $-vm_{xp}$

$$(99) \quad M_y(\lambda) = \int_0^{\infty} -vm_{xp} \sin \lambda x \, dx.$$

The ordinary differential equation (98) is solved by means of the finite cosine transform

$$(100) \quad W_k^*(\lambda) = \int_{-1}^1 W^*(\lambda, y) \cos k\pi y \, dy, \quad k = 0, 1, 2, \dots,$$

Introducing the auxiliary unknown function

$$(101) \quad q(\lambda) = \left(\frac{dW^*}{dy} \right)_{y=1},$$

and using (14) the differential equation is transformed into

$$(102) \quad \lambda^4 W_0^* = -2\lambda^3 A + 2\nu\lambda^2 q(\lambda),$$

$$(103) \quad (k^2\pi^2 + \lambda^2)^2 W_k^* = -\lambda p_k + 2(-1)^k (k^2\pi^2 + \nu\lambda^2) q(\lambda), \quad k = 1, 2, \dots,$$

where

$$(104) \quad p_k = \int_{-1}^1 p(y) \cos k\pi y \, dy.$$

Because $p(y)$ is an *equilibrium* system of root bending moments $p_0 = 0$.

In the inversion formula for finite cosine transforms

$$(105) \quad W^*(\lambda, y) = \frac{1}{2} W_0^* + \sum_{k=1}^{\infty} W_k^* \cos k\pi y$$

the terms involving $q(\lambda)$ may be summed in virtue of the formula

$$(106) \quad \sum_{k=1}^{\infty} (-1)^k \frac{k^2\pi^2 + \nu\lambda^2}{(k^2\pi^2 + \lambda^2)^2} \cos k\pi y = \frac{1-\nu}{4} \frac{1}{\lambda \sinh \lambda} \left[\left(\frac{1+\nu}{1-\nu} - \lambda \coth \lambda \right) \cosh \lambda y + \lambda y \sinh \lambda y \right] - \frac{\nu}{2\lambda^2},$$

which is easily verified. The resulting expression for $W^*(\lambda, y)$ reads

$$(107) \quad \left\{ W^*(\lambda, y) = -\frac{A}{\lambda} - \sum_{k=1}^{\infty} \frac{\lambda}{(k^2\pi^2 + \lambda^2)^2} p_k \cos k\pi y + \right. \\ \left. + \frac{1-\nu}{2} \frac{q(\lambda)}{\lambda \sinh \lambda} \left[\left(\frac{1+\nu}{1-\nu} - \lambda \coth \lambda \right) \cosh \lambda y + \lambda y \sinh \lambda y \right] \right\}.$$

The series in (107) may be differentiated twice and the boundary condition (13) yields the equation

$$(108) \quad \sum_{k=1}^{\infty} (-1)^k \frac{(k^2\pi^2 + \nu\lambda^2)\lambda}{(k^2\pi^2 + \lambda^2)^2} p_k + \frac{(3+\nu)(1-\nu)}{4} \frac{\lambda q(\lambda)}{\sinh^2 \lambda} \left[\sinh 2\lambda - \frac{1-\nu}{3+\nu} 2\lambda \right] = M_y(\lambda),$$

which may serve to eliminate $q(\lambda)$.

Applying the FOURIER sine inversion formula (24) and using (26) and the well-known formula

$$\int_0^{\infty} \frac{\sin \lambda x}{\lambda} \, d\lambda = \frac{\pi}{2} \quad (x > 0),$$

the deflection $w(x, y)$ is obtained from (96) and (107)

$$(109) \quad \left\{ \begin{aligned} w(x, y) &= Bx - \frac{1}{2} x \sum_{k=1}^{\infty} \frac{p_k}{k\pi} e^{-k\pi x} \cos k\pi y + \\ &+ \frac{1-\nu}{\pi} \int_0^{\infty} \frac{q(\lambda)}{\lambda \sinh \lambda} \left[\left(\frac{1+\nu}{1-\nu} - \lambda \coth \lambda \right) \cosh \lambda y + \lambda y \sinh \lambda y \right] \sin \lambda x d\lambda. \end{aligned} \right.$$

The slope at the root is now obtained in the form

$$(110) \quad \left\{ \begin{aligned} \left(\frac{\partial w}{\partial x} \right)_{x=0} &= B - \frac{1}{2} \sum_{k=1}^{\infty} \frac{p_k}{k\pi} \cos k\pi y + \\ &+ \frac{1-\nu}{\pi} \int_0^{\infty} \frac{q(\lambda)}{\sinh \lambda} \left[\left(\frac{1+\nu}{1-\nu} - \lambda \coth \lambda \right) \cosh \lambda + \lambda y \sinh \lambda y \right] d\lambda = \\ &= B + \frac{2\nu}{\pi} \int_0^{\infty} \frac{q(\lambda)}{\lambda} d\lambda + \\ &+ \sum_{k=1}^{\infty} \left\{ -\frac{1}{2} \frac{p_k}{k\pi} + \frac{4}{\pi} (-1)^k \int_0^{\infty} \frac{k^2 \pi^2 + \nu \lambda^2}{(k^2 \pi^2 + \lambda^2)^2} \lambda q(\lambda) d\lambda \right\} \cos k\pi y. \end{aligned} \right.$$

Equating this expression to zero yields the equations

$$(111) \quad B + \frac{2\nu}{\pi} \int_0^{\infty} \frac{q(\lambda)}{\lambda} d\lambda = 0,$$

$$(112) \quad -\frac{p_k}{2k\pi} + (-1)^k \frac{4}{\pi} \int_0^{\infty} \frac{k^2 \pi^2 + \nu \lambda^2}{(k^2 \pi^2 + \lambda^2)^2} \lambda q(\lambda) d\lambda = 0.$$

Although the system of equations (108) and (112) is very similar to its counterpart (28) and (29) in the wedge problem, we have not been able to obtain a solution in closed form. However, if $q(\lambda)$ is eliminated by means of (108), an infinite system of linear equations in the FOURIER coefficients p_k is obtained

$$(113) \quad \frac{(1-\nu)(3+\nu)}{16} (-1)^k \frac{p_k}{k} + \sum_{h=1}^{\infty} (-1)^h a_{kh} p_h = b_k, \quad k = 1, 2, \dots,$$

where

$$(114) \quad a_{kh} = \int_0^{\infty} \frac{k^2 \pi^2 + \nu \lambda^2}{(k^2 \pi^2 + \lambda^2)^2} \frac{h^2 \pi^2 + \nu \lambda^2}{(h^2 \pi^2 + \lambda^2)^2} \frac{\cosh 2\lambda - 1}{\sinh 2\lambda - c \cdot 2\lambda} \lambda d\lambda,$$

$$(115) \quad b_k = \int_0^{\infty} \frac{k^2 \pi^2 + \nu \lambda^2}{(k^2 \pi^2 + \lambda^2)^2} \frac{\cosh 2\lambda - 1}{\sinh 2\lambda - c \cdot 2\lambda} M_{\nu}(\lambda) d\lambda,$$

$$(116) \quad c = \frac{1-\nu}{3+\nu}.$$

Unfortunately, the infinite system of equations (113) does not satisfy any of the simple convergence criteria (ref. 13). On the other hand, from a practical point of view a satisfactory approximate solution is obtained if

all unknowns p_k for $k > m$ are put zero and only the first m equations are retained. By taking m successively equal to 5, 6, ... 10 we have shown that the first few coefficients do not change appreciably if the number of retained unknowns and equations is increased, i.e. we have established a satisfactory stability (see para. 4.4). Moreover the coefficients p_k alternate and decrease with increasing k approximately as $1/k$, thereby ensuring convergence of the series for the root bending moment.

$$(117) \quad (m_x)_{x=0} = p(y) = \sum_{k=1}^{\infty} p_k \cos k\pi y.$$

In order to evaluate the bending and torsional moments for $x > 0$ we have to compute the second derivatives of $w(x, y)$. Eliminating $q(\lambda)$ from (109) by means of (108) we obtain

$$(118) \quad \left\{ \begin{aligned} w(x, y) = & Bx - \frac{1}{2} x \sum_{k=1}^{\infty} \frac{p_k}{k\pi} e^{-k\pi y} \cos k\pi y + \\ & + \frac{4}{\pi(3+\nu)} \int_0^{\infty} \frac{M_y(\lambda)}{\lambda^2} \frac{\sinh \lambda}{\sinh 2\lambda - c.2\lambda} \left[\left(\frac{1+\nu}{1-\nu} - \lambda \coth \lambda \right) \cosh \lambda y + \right. \\ & + \left. \lambda y \sinh \lambda y \right] \sin \lambda x d\lambda + \\ & - \frac{4}{\pi(3+\nu)} \sum_{k=1}^{\infty} (-1)^{k+1} p_k \int_0^{\infty} \frac{k^2 \pi^2 + \nu \lambda^2}{(k^2 \pi^2 + \lambda^2)^2} \frac{\sinh \lambda}{\lambda (\sinh 2\lambda - c.2\lambda)} \\ & \left[\left(\frac{1+\nu}{1-\nu} - \lambda \coth \lambda \right) \cosh \lambda y + \lambda y \sinh \lambda y \right] \sin \lambda x d\lambda, \end{aligned} \right.$$

where c is given by (116). We may now obtain the derivatives by differentiation under the integral signs.

The foregoing analysis presupposes the convergence of the integral in (111). In view of (108) it is therefore required that $M_y(\lambda) \rightarrow 0$ for $\lambda \rightarrow 0$. Assuming $m_{xy} = e^{-\alpha x}$, we obtain from (99)

$$(119) \quad M_y(\lambda) = \frac{-\nu \lambda}{\alpha^2 + \lambda^2},$$

satisfying the above requirement. The solution for a *constant* primary bending moment is now obtained for $\alpha \rightarrow 0$. Because (115) remains convergent for $\alpha = 0$ no difficulties occur with respect to the FOURIER coefficients p_k . Moreover, although (118) diverges for $\alpha = 0$, the expressions for the second derivatives remain convergent if (118) is first differentiated twice and the limit $\alpha \rightarrow 0$ is taken subsequently.

The numerical evaluation is facilitated by contour integration and the theorem of residues. It is convenient to evaluate first the last integral in (118). The integrand is even in λ and has *double* poles $\pm ik\pi$, *simple* poles $i\lambda_n$, where λ_n is any non-zero root of the eigenvalue equation (85), and finally a simple pole in $\lambda = 0$. It appears after a straight-forward but tedious calculation that the terms involving the residues in the double poles $\pm ik\pi$ cancel the second term in (118).

The result is

$$(120) \quad \left\{ \begin{aligned} w(x, y) = & \frac{\nu}{1-\nu^2} \sum_{k=1}^{\infty} (-1)^{k+1} \frac{p_k}{k^2 \pi^2} + Bx + \\ & \frac{4}{\pi(3+\nu)} \int_0^{\infty} \frac{M_y(\lambda)}{\lambda^2} \frac{\sinh \lambda}{\sinh 2\lambda - c} \left[\left(\frac{1+\nu}{1-\nu} - \lambda \coth \lambda \right) \cosh \lambda y + \right. \\ & \left. + \lambda y \sinh \lambda y \right] \sin \lambda x d\lambda + \\ & + \frac{2}{3+\nu} \sum_{k=1}^{\infty} (-1)^k p_k \sum_{\operatorname{Re}(\lambda_n) < 0} \frac{k^2 \pi^2 - \nu \lambda_n^2}{(k^2 \pi^2 - \lambda_n^2)^2} \frac{\sin \lambda_n}{\lambda_n (\cos 2\lambda_n - c)} w_n(x, y), \end{aligned} \right.$$

where $w_n(x, y)$ are the eigenfunctions (86), corresponding with the eigenvalues λ_n .

Differentiating this expression and applying contour integration and the theorem of residues for $M_y(\lambda) = -\nu/\lambda$ we obtain finally

$$(121) \quad \frac{\partial^2 w}{\partial x^2} = \sum_{\operatorname{Re}(\lambda_n) < 0} \{a_n \lambda_n^2 w_n(x, y)\} + \frac{\nu^2}{1-\nu^2},$$

$$(122) \quad \frac{\partial^2 w}{\partial x \partial y} = \sum_{\operatorname{Re}(\lambda_n) < 0} a_n \lambda_n \frac{\partial w_n(x, y)}{\partial y},$$

$$(123) \quad \frac{\partial^2 w}{\partial y^2} = \sum_{\operatorname{Re}(\lambda_n) < 0} \left\{ a_n \frac{\partial^2 w_n(x, y)}{\partial y^2} \right\} - \frac{\nu}{1-\nu^2},$$

where w_n are again the eigenfunctions (86) and the coefficients a_n are given by

$$(124) \quad a_n = -\frac{2}{3+\nu} \left[\frac{\nu}{\lambda_n^2} - \sum_{k=1}^{\infty} (-1)^k p_k \frac{k^2 \pi^2 - \nu \lambda_n^2}{(k^2 \pi^2 - \lambda_n^2)^2} \right] \frac{\sin \lambda_n}{\lambda_n (\cos 2\lambda_n - c)}.$$

The last terms in (121) and (123) are due to the fact that the secondary loading system by a constant bending moment $m_{y0} = -\nu$ along the longitudinal edges of the strip does not vanish at infinity. They arise in the evaluation of (120) by contour integration because the line of integration must be shifted from the real axis in the λ -plane to a parallel line slightly above or below the real axis in order to avoid a pole on the line of integration when $\sin \lambda x$ is written as $1/2i (e^{i\lambda x} - e^{-i\lambda x})$.

An interesting feature of the solution in this form is that it is an expansion in eigenfunctions of para. 4.2. It may be observed that the solution of the problem considered in para. 4.2 is obtained from the present solution by adding the simple function

$$(125) \quad w = -\frac{1}{2} \frac{\nu^2}{1-\nu^2} x^2 + \frac{1}{2} \frac{\nu}{1-\nu^2} y^2.$$

representing the deflection of an infinite free strip, loaded by bending moments $m_y = -\nu$ along both longitudinal edges. On the assumption that the infinite system of equations (113) has a solution our present result justifies the eigenfunction expansion of para. 4.2. Moreover the series

involving p_k in (124) is rapidly convergent; the first few coefficients a_n are readily computed from a limited number of FOURIER-coefficients p_k . The main advantage of the present method over the eigenfunction expansion in para. 4.2 lies in the accuracy by which the coefficients a_n are obtained. The comparative inaccuracy of these coefficients as determined from the eigenfunction method itself is due to the fact that the eigenfunctions are far from being mutually orthogonal.

The detailed discussion of the numerical results will be given in part IV of this paper.

(To be continued)

REFERENCES ¹⁾

13. RIESZ, F., Les systèmes d'équations linéaires à une infinité d'inconnues (Gauthier-Villars, Paris, 1913).
14. CARRIER, G. F. and F. S. SHAW, Some problems in the bending of thin plates. Proc. of Symposia in Appl. Math. 3, 125 (McGraw-Hill, New York, 1950).

¹⁾ For ref. 1-8 and 9-12 of these Proceedings, 57, 258 and 269.

APPROXIMATE SOLUTION OF WIENER-HOPF TYPE INTEGRAL EQUATIONS WITH APPLICATIONS

I. GENERAL THEORY

BY

W. T. KOITER

(Communicated by Prof. C. B. BIEZENO at the meeting of September 25, 1954)

1. Introduction

A number of problems in the theory of elasticity and in other branches of mathematical physics may be reduced to a non-homogeneous integral equation of the first kind of the WIENER-HOPF type

$$(1) \quad \int_0^{\infty} m(\xi) h(x - \xi) d\xi = \varphi(x),$$

where $h(x - \xi)$ is the kernel of the equation, $\varphi(x)$ is given for $x > 0$ (but unknown for $x < 0$) and $m(x)$ is to be found for $x > 0$. This type of integral equation may be solved by means of FOURIER-transforms (ref. 1, art. 11.17).

On the assumptions that $e^{\lambda|x|}h(x)$ belongs to $L^2(-\infty, \infty)$ for all $\lambda < b$, $e^{-\lambda x}m(x)$ and $e^{-\lambda x}\varphi(x)$ belong to $L(0, \infty)$ for all $\lambda < c$, and $e^{\lambda x}\varphi(x)$ belongs to $L(-\infty, 0)$ for all $\lambda < c$, where $0 < c < b$, the FOURIER-transforms

$$(2) \quad \frac{1}{\sqrt{2\pi}} \int_{-\infty}^{\infty} h(x) e^{iwx} dx = H(w), \text{ regular for } -b < v = \text{Im } w < b,$$

$$(3) \quad \frac{1}{\sqrt{2\pi}} \int_0^{\infty} \varphi(x) e^{iwx} dx = \phi_+(w), \text{ regular for } v > c,$$

$$(4) \quad \frac{1}{\sqrt{2\pi}} \int_{-\infty}^0 \varphi(x) e^{iwx} dx = \phi_-(w), \text{ regular for } v < -c,$$

$$(5) \quad \frac{1}{\sqrt{2\pi}} \int_0^{\infty} m(x) e^{iwx} dx = M_+(w), \text{ regular for } v > c$$

exist and are regular in the strip and half-planes indicated with each transform.

Applying the convolution theorem for FOURIER-transforms to the left-hand member of (1), and rewriting the right-hand member by means of its inverse FOURIER-transform, equation (1) may be written in the equivalent form

$$(6) \quad \left\{ \begin{aligned} \int_{ia-\infty}^{ia+\infty} M_+(w) H(w) e^{-iwx} dw &= \frac{1}{\sqrt{2\pi}} \int_{ia-\infty}^{ia+\infty} \phi_+(w) e^{-iwx} dw + \\ &+ \frac{1}{\sqrt{2\pi}} \int_{-ia-\infty}^{-ia+\infty} \phi_-(w) e^{-iwx} dw, \end{aligned} \right.$$

where $c < a < b$. It now follows from a general theorem given by TITCHMARSH (ref. 1, art. 9.9) that $\phi(w)$ is regular in the extended half-plane $v < b$ and that in this half-plane

$$(7) \quad \sqrt{2\pi} M_+(w) H(w) - \phi_+(w) = \phi_-(w),$$

where $H(w)$ and $\phi_+(w)$ are known functions.

The solution is obviously complete if either $M_+(w)$ or $\phi_-(w)$ has been obtained. Its uniqueness usually requires an additional investigation; however, in problems of elasticity and in many other fields it is ensured by a general uniqueness theorem.

In some problems an integral equation of type (6) occurs in a somewhat more general form

$$(8) \quad \left\{ \begin{aligned} \int_{ia_2-\infty}^{ia_2+\infty} M_+(w) H(w) e^{-iwx} dw &= \frac{1}{\sqrt{2\pi}} \int_{ia_2-\infty}^{ia_2+\infty} \phi_+(w) e^{-iwx} dw + \\ &+ \frac{1}{\sqrt{2\pi}} \int_{ia_1-\infty}^{ia_1+\infty} \phi_-(w) e^{-iwx} dw, \end{aligned} \right.$$

where $H(w)$ is regular in the strip $b_1 < v < b_2$, $\phi_+(w)$ and $M_+(w)$ are regular in the half-plane $v > c_2$, $\phi_-(w)$ is regular in the half-plane $v < c_1$ and $b_1 < a_1 < c_1 < c_2 < a_2 < b_2$. This equation is sometimes obtained directly, i.e. without recourse to an integral equation of type (1), by means of FOURIER-transforms applied to the differential equation and boundary conditions which govern the particular problem under consideration. It then follows from (8) that $\phi_-(w)$ is regular in the extended half-plane $v < b_2$ and in this half-plane eq. (7) holds again.

The essential feature of the WIENER-HOPF technique consists of the *factorization* of $H(w)$, by means of which it is written in the form

$$(9) \quad H(w) = (w - w_1) \dots (w - w_n) \frac{H_+(w)}{H_-(w)},$$

where $H_+(w)$ and $H_-(w)$ are regular, free from zeros and of algebraic order at infinity in the half-planes $v > b_1$ and $v < b_2$ respectively, and w_1, w_2, \dots, w_n are the zeros of $H(w)$ in the strip $b_1 < v < b_2$. Although a general method is available under fairly weak assumptions on the behaviour of $H(w)$ in its strip of regularity (ref. 1, art. 11.17 and ref. 2, art. 8.5), it is extremely cumbersome in most cases. Therefore it is not surprising that very few solutions of integral equations of the WIENER-HOPF type have actually been obtained in a manageable form and evaluated numerically.

However, a comparatively simple and entirely satisfactory *approximate solution* may be obtained if the FOURIER-transform $H(w)$ of the kernel $h(x)$ allows a sufficiently close approximation by a *simple function* $H^*(w)$ in a strip inside the strip of regularity of $H(w)$, viz. $b_1 < v < b_2$. The approximate solution is then obtained by applying the WIENER-HOPF method to the modified transformed kernel $H^*(w)$. This approximate

method has already given excellent results in several problems, some of which will be discussed in part II of this paper.

At first sight this approximation may seem highly suspect from the mathematical point of view. In fact, the WIENER-HOPF method is based on the behaviour of the transforms concerned in the entire w -plane and the behaviour of $H^*(w)$ may be radically different from the behaviour of $H(w)$. On the other hand, it may be contended that the original integral equation (1) or the equivalent differential equation and boundary conditions involve only real quantities and the WIENER-HOPF technique for its solution, by which the complex w -plane is introduced, is no more than an extremely ingenious artifice. If $H^*(w)$ closely approximates $H(w)$ in a strip inside the strip of regularity of the latter transform, it may be expected that its inverse transform $h^*(x)$ is a good approximation to the original kernel $h(x)$, and the solution of (1), modified by replacing $h(x-\xi)$ by $h^*(x-\xi)$, should afford a useful approximation to the exact solution. A more detailed discussion of this aspect will be given in the next paragraphs. From a practical point of view the comparison to be given in part II of this paper is probably even more significant because it shows by means of a rather critical example how close an approximation may be achieved by a function $H^*(w)$ which approximates $H(w)$ in a strip but behaves radically different in the complex plane.

2. Solution of modified problem

A mathematical justification may be given, starting either from the solution to the original problem or from the solution to the modified problem. The latter approach is preferred here because the modified problem will be actually solved in the applications and the assumptions introduced in this justification may therefore be verified.

The factorization of the modified transformed kernel $H^*(w)$ is assumed to be known in the form

$$(10) \quad H^*(w) = (w - w_1^*) \dots (w - w_m^*) \frac{H_+^*(w)}{H_-^*(w)},$$

where w_1^*, \dots, w_m^* are the zeros of $H^*(w)$ in its strip of regularity $b_1^* < v < b_2^*$, and $H_+^*(w)$ and $H_-^*(w)$ are regular, free from zeros and of algebraic order in the half-planes $v > b_1^*$ and $v < b_2^*$ respectively.

Denoting the corresponding approximate solution by $M_+^*(w)$ and $\phi_-^*(w)$, eq. (7) for the modified problem reads

$$(11) \quad \sqrt{2\pi} M_+^*(w) (w - w_1^*) \dots (w - w_m^*) H_+^*(w) - \phi_+^*(w) H_-^*(w) = \phi_-^*(w) H_-^*(w),$$

holding for $c_2^* < v < b_2^*$ if $M_+^*(w)$ and $\phi_+^*(w)$ are assumed to be regular for $v > c_2^*$, where $b_1^* < c_2^* < b_2^*$. The first term in the left-hand member in (11) is regular in the half-plane $v > c_2^*$, the right-hand member in the overlapping half-plane $v < b_2^*$.

The second term in the left-hand member is regular in the strip $c_2^* < v < b_2^*$

and it may be decomposed into two functions which are regular in overlapping half-planes. If we assume that

$$(12) \quad \Psi^*(w) = \phi_+(w) H_-^*(w) = O(|w|^{-\mu}) \text{ for } |w| \rightarrow \infty$$

in the strip $c_2^* < v < b_2^*$ for some $\mu > 0$, this decomposition reads

$$(13) \quad \Psi^*(w) = \frac{1}{2\pi i} \int_{i\alpha_1^* - \infty}^{i\alpha_1^* + \infty} \frac{\Psi^*(z)}{z-w} dz - \frac{1}{2\pi i} \int_{i\alpha_2^* - \infty}^{i\alpha_2^* + \infty} \frac{\Psi^*(z)}{z-w} dz = \Psi_+^*(w) - \Psi_-^*(w),$$

holding for $c_2^* < \alpha_1^* < v < \alpha_2^* < b_2^*$, where $\Psi_+^*(w)$ and $\Psi_-^*(w)$ are regular in the half-planes $v > \alpha_1^*$ and $v < \alpha_2^*$ respectively. For $|w| \rightarrow \infty$ in these half-planes $\Psi_+^*(w)$ and $\Psi_-^*(w)$ are $O(|w|^{-\mu})$ if $\mu < 1$ and $O(|w|^{-1})$ if $\mu \geq 1$. If $\phi_+(w)$ is a rational function $\Psi_+^*(w)$ and $\Psi_-^*(w)$ may be evaluated by contour integration in the lower half-plane; in this case $\Psi_+^*(w)$ is always $O(|w|^{-1})$ for $|w| \rightarrow \infty$, even if $0 < \mu < 1$.

Eq. (11) may now be written in the form

$$(14) \quad \sqrt{2} \pi M_+^*(w) (w-w_1^*) \dots (w-w_m^*) H_+^*(w) - \Psi_+^*(w) = \phi_-^*(w) H_-^*(w) - \Psi_-^*(w),$$

where the left-hand member is regular for $v > \alpha_1^*$ and the right-hand member is regular in the overlapping half-plane $v < \alpha_2^*$. Therefore they are each other's analytic continuation and both members represent the same *integral function*; it must be a polynomial $P^*(w)$ by the generalization of LIOUVILLE's theorem on account of the algebraic order of $H_+^*(w)$, assumption (12), and the fact that $M_+^*(w)$ is a FOURIER transform and therefore tends to zero for $|w| \rightarrow \infty$. The solution of (14) is now

$$(15) \quad M_+^*(w) = \frac{1}{\sqrt{2\pi}} \frac{\Psi_+^*(w) + P^*(w)}{(w-w_1^*) \dots (w-w_m^*) H_+^*(w)},$$

$$(16) \quad \phi_-^*(w) = \frac{1}{\sqrt{2\pi}} \frac{\Psi_-^*(w) + P^*(w)}{H_-^*(w)},$$

if these expressions tend to zero for $|w| \rightarrow \infty$.

The solution is obviously *unique* if $P^*(w)$ must be zero on account of this asymptotic requirement, i.e. if one of the expressions

$$(17) \quad \frac{1}{(w-w_1^*) \dots (w-w_m^*) H_+^*(w)}, \quad \frac{1}{H_-^*(w)}$$

does *not* tend to zero for $|w| \rightarrow \infty$. Henceforward we shall make this assumption thereby ensuring the uniqueness of our approximate solution. Furthermore we may observe that we must have in general

$$(18) \quad c_2^* \geq \text{Max} (v_1^*, v_2^*, \dots, v_m^*),$$

where $v_j^* = \text{Im}(w_j^*)$, in order that (15) is analytic for $v > c_2^*$; this requirement can only be circumvented in exceptional cases where the given function $\phi_+(w)$ is such that $\Psi_+^*(w)$ is zero for the zero of $H^*(w)$ in its strip of regularity with the largest imaginary part.

The final approximate solution is now obtained by means of the inverse FOURIER-transforms of (15), (16)

$$(19) \quad m^*(x) = \frac{1}{\sqrt{2\pi}} \int_{i\alpha_1^* - \infty}^{i\alpha_2^* + \infty} M_+^*(w) e^{-iwx} dw, \quad x > 0,$$

$$(20) \quad \varphi^*(x) = \frac{1}{\sqrt{2\pi}} \int_{i\alpha_2^* - \infty}^{i\alpha_1^* + \infty} \phi_-^*(w) e^{-iwx} dw, \quad x < 0,$$

where $\alpha_1^* < a^* < \alpha_2^*$.

This approximate solution still seems fairly complicated because the FOURIER-transforms (15), (16) involve the functions $\Psi_+^*(w)$ and $\Psi_-^*(w)$, defined by the infinite integrals in (13). However, if $\phi_+(w)$ is a *rational* function the integrals need not be evaluated; the solution may then be written down simply by *inspection* of eq. (11). Some examples will be given in part II of this paper.

3. Justification of the approximate method

The modified transformed kernel $H^*(w)$ is assumed to be a "good" approximation to the original transformed kernel in a strip

$$(21) \quad \beta_1^* < v < \beta_2^*, \text{ where } \text{Max}(v_1^*, \dots, v_m^*) < \beta_1^* < \beta_2^* < b;$$

moreover we assume without loss of generality that $\phi_+(w)$ is regular for $v > \beta_1^*$. Our assumption is stated more precisely by the formula

$$(22) \quad H(w) = H^*(w) e^{\varepsilon f^*(w)},$$

where ε is a (small) positive number, and $f^*(w)$ is regular and $O(|w|^{-1})$ for $|w| \rightarrow \infty$ in the strip (21). This assumption obviously implies that $H(w)$ is regular and has no zeros in this strip.

The function $f^*(w)$ may be written in the form

$$(23) \quad f^*(w) = \frac{1}{2\pi i} \int_{i\gamma_1^* - \infty}^{i\gamma_1^* + \infty} \frac{f^*(z)}{z-w} dz - \frac{1}{2\pi i} \int_{i\gamma_2^* - \infty}^{i\gamma_2^* + \infty} \frac{f^*(z)}{z-w} dz = f_+^*(w) - f_-^*(w),$$

holding for $\beta_1^* < \gamma_1^* < v < \gamma_2^* < \beta_2^*$, where $f_+^*(w)$ and $f_-^*(w)$ are regular and $O(|w|^{-1})$ for $|w| \rightarrow \infty$ in the half-planes $v > \gamma_1^*$ and $v < \gamma_2^*$ respectively. The factorization of (22) may now be written in the form

$$(24) \quad H(w) = (w-w_1^*) \dots (w-w_m^*) \frac{H_+^*(w) \exp[\varepsilon f_+^*(w)]}{H_-^*(w) \exp[\varepsilon f_-^*(w)]},$$

holding for $\gamma_1^* < v < \gamma_2^*$. It will be noted that this factorization is not identical with (9); in fact, (24) only holds in an interior strip of $b_1 < v < b_2$ which does not contain any zero of $H(w)$, whereas (9) holds in the entire strip $b_1 < v < b_2$.

The solution of the original problem may now be obtained along the same lines as the approximate solution, the only difference being that $H_+^*(w)$ and $H_-^*(w)$ are multiplied everywhere by $\exp[\varepsilon f_+^*(w)]$ and

$\exp [\varepsilon f_{\pm}^*(w)]$ respectively. The asymptotic behaviour of (12) and (17) is not affected by these factors and the rigorous solution is therefore also unique. It is given by the inverse transforms of

$$(25) \quad M_+(w) = \frac{1}{\sqrt{2\pi}} \frac{\bar{\Psi}_+(w) \exp [-\varepsilon f_+^*(w)]}{(w-w_1^*) \dots (w-w_m^*) H_+^*(w)},$$

$$(26) \quad \phi_-(w) = \frac{\bar{\Psi}_-(w) \exp [-\varepsilon f_-^*(w)]}{H_-^*(w)},$$

where the functions $\bar{\Psi}_+(w)$ and $\bar{\Psi}_-(w)$, defined by

$$(27) \quad \bar{\Psi}_+(w) = \frac{1}{2\pi i} \int_{i\delta_1^* - \infty}^{i\delta_1^* + \infty} \frac{\Psi^*(z) \exp [\varepsilon f_+^*(z)]}{z-w} dz,$$

$$(28) \quad \bar{\Psi}_-(w) = \frac{1}{2\pi i} \int_{i\delta_2^* - \infty}^{i\delta_2^* + \infty} \frac{\Psi^*(z) \exp [\varepsilon f_-^*(z)]}{z-w} dz,$$

where $\gamma_1^* < \delta_1^* < \delta_2^* < \gamma_2^*$, are analytic in the half-planes $v > \delta_1^*$ and $v < \delta_2^*$ respectively.

We may now prove that the differences between the rigorous solution and the approximate solution, i.e. $m(x) - m^*(x)$ and $\varphi(x) - \varphi^*(x)$ are *small of the order ε* for $x > 0$ and $x < 0$ respectively. On account of our assumption (12) and the asymptotic behaviour of $f_{\pm}^*(w)$ we may write

$$(29) \quad \bar{\Psi}_+(w) = \Psi_+^*(w) + \varepsilon g_+^*(w), \quad \bar{\Psi}_-(w) = \Psi_-^*(w) + \varepsilon g_-^*(w),$$

where $g_+^*(w)$ and $g_-^*(w)$ are analytic and $O(|w|^{-1})$ for $|w| \rightarrow \infty$ in the half-planes $v > \delta_1^*$ and $v < \delta_2^*$ respectively. The numerators in (25) and (26) may now be written in the form

$$(30) \quad \bar{\Psi}_+(w) \exp [-\varepsilon f_+^*(w)] = \Psi_+^*(w) + \varepsilon G_+^*(w),$$

$$(31) \quad \bar{\Psi}_-(w) \exp [-\varepsilon f_-^*(w)] = \Psi_-^*(w) + \varepsilon G_-^*(w),$$

where $G_+^*(w)$ and $G_-^*(w)$ are analytic and $O(|w|^{-1})$ for $|w| \rightarrow \infty$ in the half-planes $v > \delta_1^*$ and $v < \delta_2^*$ respectively. Hence we may write

$$(32) \quad m(x) - m^*(x) = \frac{1}{2\pi} \int_{a^* - i\infty}^{a^* + i\infty} \frac{\varepsilon G_+^*(w)}{(w-w_1^*) \dots (w-w_m^*) H_+^*(w)} e^{-iwx} dw, \quad x > 0,$$

$$(33) \quad \varphi(x) - \varphi^*(x) = \frac{1}{\sqrt{2\pi}} \int_{a^* - i\infty}^{a^* + i\infty} \frac{\varepsilon G_-^*(w)}{H_-^*(w)} e^{-iwx} dw, \quad x < 0,$$

where $\delta_1^* < a^* < \delta_2^*$. The convergence of (32) and (33) is ensured by the convergence of (19) and (20) because the integrands in the latter integrals approach to zero more slowly (or at least not more rapidly) for $|w| \rightarrow \infty$. This completes our proof that the solution of the modified problem deviates from the rigorous solution by a function that is small of order ε .

Some of the assumptions introduced in this discussion are unnecessarily restrictive. E.g. our assumption (12) may be dropped and replaced by a

much weaker assumption. On the other hand, more precise results can only be obtained by the introduction of additional assumptions on the behaviour of $\phi_+(w)$ and $f^*(w)$. However, we shall not pursue the general theory any further here but turn to some practical problems in part II.

Acknowledgment

The author is indebted to his colleagues Prof. Dr L. J. F. BROER, who drew his attention to this class of problems by mentioning a particular problem in hydrodynamics (the approximate solution of which will be discussed in part II), and Prof. Dr R. TIMMAN, who suggested the possibility of a mathematical justification of our approximative method by a perturbation analysis.

REFERENCES

1. TITCHMARSH, E. C., Theory of Fourier integrals (Oxford University Press, Oxford, 1937).
2. MORSE, P. M. and H. FESHBACH, Methods of theoretical physics (McGraw-Hill, New York, 1953).

APPROXIMATE SOLUTION OF WIENER-HOPF TYPE INTEGRAL
EQUATIONS WITH APPLICATIONS. IIASOME PLATE BENDING PROBLEMS AND AN EXAMPLE FROM
HYDRODYNAMICS *)

BY

W. T. KOITER

(Communicated by Prof. C. B. BIEZENO at the meeting of September 25, 1954)

1. *Plate strips with discontinuous boundary conditions*

Consider an infinite plate strip of unit width with uniform boundary conditions along one edge AB ($y=1$), which is assumed to be *simply supported* in the first problem (fig. 1) and *clamped* in the second problem (fig. 2), but with *discontinuous* boundary conditions along the other edge

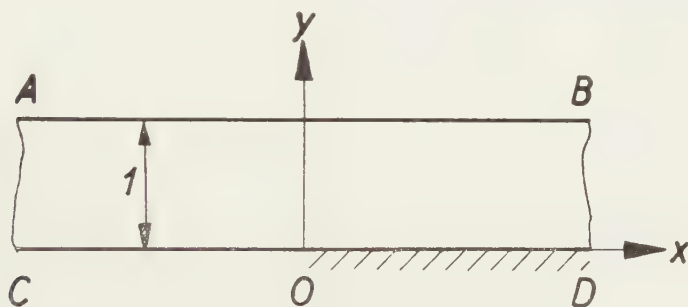


Fig. 1

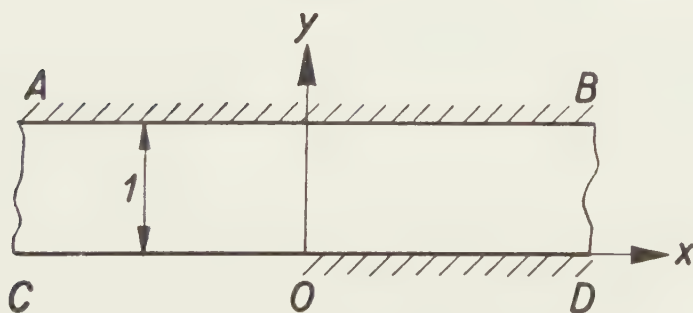


Fig. 2

CD . Along the half-edge CQ ($y=0$, $x<0$) the strip is assumed to be *simply supported* and along the half-edge OD ($y=0$, $x>0$) the strip is *clamped*. The strip is loaded perpendicular to its plane.

*) For part I (General theory) cf. these Proceedings 57, 558 (1954).

The stress distribution might be obtained by well-known methods (e.g. straight forward FOURIER-transforms) if the half-edge OD were also simply supported. The solution to the present problem may be found from this *primary* solution if a suitable *secondary* solution for the strip, loaded by *edge moments along OD* , is superimposed in such a way that the transverse slope along OD , due to the primary solution, is neutralized.

In the *first* problem (fig. 1) it is therefore required to obtain a solution of the biharmonic equation

$$(1) \quad \Delta \Delta \zeta = 0$$

for the (non-dimensional) deflection ζ with boundary conditions

$$(2) \quad y = 1 : \zeta = 0, \frac{\partial^2 \zeta}{\partial y^2} = 0,$$

$$(3) \quad y = 0, x < 0 : \zeta = 0, \frac{\partial^2 \zeta}{\partial y^2} = 0,$$

$$(4) \quad y = 0, x > 0 : \zeta = 0, \frac{\partial^2 \zeta}{\partial y^2} = -m(x),$$

where $m(x)$ is an *unknown* function, to be determined from the condition that along OD the transverse slope

$$(5) \quad y = 0, x > 0 : \frac{\partial \zeta}{\partial y} = \varphi(x)$$

is a *prescribed* function $\varphi(x)$ for $x > 0$. In the *second* problem (fig. 2) the boundary condition (2) should be replaced by

$$(6) \quad y = 1 : \zeta = 0, \frac{\partial \zeta}{\partial y} = 0.$$

Introducing the FOURIER-transform (ref. 1)

$$(7) \quad Z(w, y) = \frac{1}{\sqrt{2\pi}} \int_{-\infty}^{\infty} \zeta(x, y) e^{iwx} dx,$$

and assuming that $\zeta e^{-\lambda x}$ is $L(-\infty, \infty)$ for all values of λ in a range $0 < a_1 < \lambda < a_2$ (thus ensuring the regularity of $Z(w, y)$ in a strip $a_1 < v = \text{Im } w < a_2$), the biharmonic equation (1) is transformed into the ordinary differential equation

$$(8) \quad \frac{d^4 Z}{dy^4} - 2w^2 \frac{d^2 Z}{dy^2} + w^4 Z = 0.$$

Transformation of the boundary conditions (2), (3) and (4) for the *first* problem (fig. 1) yields the following boundary conditions for Z

$$(9) \quad y = 1 : Z = 0, \frac{d^2 Z}{dy^2} = 0,$$

$$(10) \quad y = 0 : Z = 0, \frac{d^2 Z}{dy^2} = -M_+(w),$$

where

$$(11) \quad M_+(w) = \frac{1}{\sqrt{2\pi}} \int_0^{\infty} m(x) e^{iwx} dx$$

is the transform of the unknown edge moment. If $e^{-\lambda x}m(x)$ is assumed to be $L(0, \infty)$ for all $\lambda > a_1$, the transform $M_+(w)$ is regular for $v = \text{Im}(w) > a_1$.

The solution of (8), (9) and (10) reads

$$(12) \quad Z(w, y) = \frac{M_+(w)}{2w \sinh^2 w} [- (1 + y \sinh^2 w) \sinh wy + y \sinh w \cosh w \cosh wy]$$

and its derivative along $y=0$ is

$$(13) \quad \left(\frac{dZ}{dy} \right)_{y=0} = M_+(w) \frac{\sinh w \cosh w - w}{2w \sinh^2 w}.$$

The slope along the edge $y=0$ is now obtained by means of the inverse FOURIER-transform

$$(14) \quad \begin{cases} \left(\frac{\partial \zeta}{\partial y} \right)_{y=0} = \frac{1}{\sqrt{2\pi}} \int_{ia-\infty}^{ia+\infty} \left(\frac{dZ}{dy} \right)_{y=0} e^{-iwx} dw = \\ \quad = \frac{1}{\sqrt{2\pi}} \int_{ia-\infty}^{ia+\infty} M_+(w) \frac{\sinh w \cosh w - w}{2w \sinh^2 w} e^{-iwx} dw, \end{cases}$$

where $a_1 < a < a_2$.

On the other hand, this slope $\varphi(x)$ is prescribed for $x > 0$. Introducing the F_+ transform

$$(15) \quad \phi_+(w) = \frac{1}{\sqrt{2\pi}} \int_0^\infty \varphi(x) e^{iwx} dx$$

and the *unknown* F_- transform

$$(16) \quad \phi_-(w) = \frac{1}{\sqrt{2\pi}} \int_{-\infty}^0 \varphi(x) e^{iwx} dx,$$

which are assumed to be regular in the overlapping halfplanes $v > a_1$ and $v < a_2$ respectively, and applying the inverse transformation, we obtain

$$(17) \quad \left(\frac{\partial \zeta}{\partial y} \right)_{y=0} = \varphi(x) = \frac{1}{\sqrt{2\pi}} \int_{ia-\infty}^{ia+\infty} \phi_+(w) e^{-iwx} dw + \frac{1}{\sqrt{2\pi}} \int_{ia-\infty}^{ia+\infty} \phi_-(w) e^{-iwx} dw.$$

Equating expressions (14) and (17) yields the integral equation

$$(18) \quad \begin{cases} \int_{ia-\infty}^{ia+\infty} M_+(w) H_1(w) e^{-iwx} dw = \frac{1}{\sqrt{2\pi}} \int_{ia-\infty}^{ia+\infty} \phi_+(w) e^{-iwx} dw + \\ \quad + \frac{1}{\sqrt{2\pi}} \int_{ia-\infty}^{ia+\infty} \phi_-(w) e^{-iwx} dw, \end{cases}$$

where

$$(19) \quad H_1(w) = \frac{1}{\sqrt{2\pi}} \frac{\sinh w \cosh w - w}{2w \sinh^2 w}.$$

It is easily recognized that (18) is of the type of eq. (6) of Part I if the strip $a_1 < v < a_2$ overlaps the strip of regularity of $H_1(w)$, viz. $-\pi < v < \pi$. On this assumption (18) is equivalent to

$$(20) \quad \sqrt{2\pi} M_+(w) H_1(w) - \phi_+(w) = \phi_-(w),$$

where both members are regular in the half-plane $v \leq a$.

The solution of the *second* problem proceeds entirely similar. The resulting equation is again (20), where $H_1(w)$ is replaced by

$$(21) \quad H_2(w) = \frac{1}{2\pi} \frac{\sinh^2 w - w^2}{2w(\sinh w \cosh w - w)}.$$

It may be worthwhile to observe that (20) is obtained without recourse to an explicit integral equation of the WIENER-HOPF type (Eq. (1) of part I). In fact, even although the poles of $H_1(w)$, viz. $\pm k\pi i$ ($k=1, 2, \dots$) are distributed in a simple way, the corresponding kernel in eq. (1) of part I

$$(22) \quad \left\{ \begin{aligned} h_1(x) &= \frac{1}{2\pi} \int_{-\infty}^{\infty} H_1(w) e^{-iwx} dw \\ &= \frac{1}{2} |x| \frac{e^{-\pi|x|}}{1 - e^{-\pi|x|}} - \frac{1}{2\pi} \log [1 - e^{-\pi|x|}], \end{aligned} \right.$$

evaluated by contour integration and summing of the series of residues, is already a rather complicated function. For the second problem it does not seem possible to give an expression for $h_2(x)$ in closed form because the poles of the transformed kernel (21) are complex.

Factorization of both $H_1(w)$ and $H_2(w)$ appears to be troublesome, if at all possible in a useful form. In $H_1(w)$ the numerator with its complex zeros causes the difficulty whereas in $H_2(w)$ the zeros of both numerator and denominator are complex. A rigorous solution of (20) therefore appears to be impracticable. A satisfactory approximate solution will be given in para. 3.

2. An example from hydrodynamics¹⁾

We consider the problem of slow steady flow of a viscous fluid between two infinite and one semi-infinite parallel plates (fig. 3).

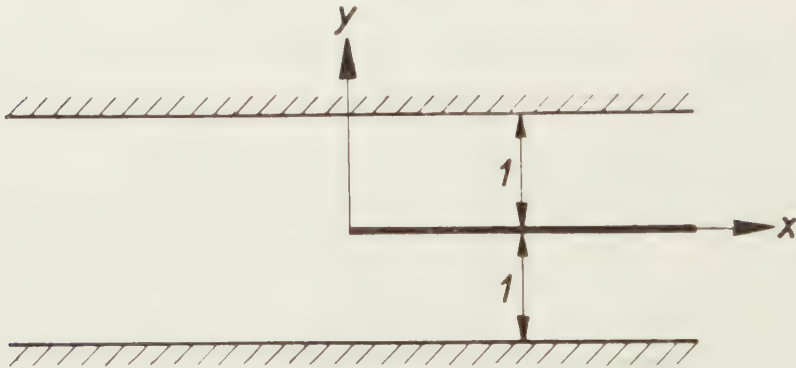


Fig. 3

The velocity components u_x and u_y are expressed by means of a stream function (ref. 1, art. 341)

$$u_x = -\frac{\partial \psi}{\partial y}, \quad u_y = \frac{\partial \psi}{\partial x},$$

¹⁾ The author is indebted to his colleague Prof. Dr L. J. F. BROER, who drew his attention to this problem.

where ψ satisfies the biharmonic equation with boundary conditions $\partial\psi/\partial x=0$ and $\partial\psi/\partial y=0$ on the boundaries $y=\pm 1$ and $y=0, x>0$. The problem is solved by first considering the problem without an intermediate semi-infinite plate with the simple primary solution

$$\psi = \frac{3}{2} u_m \left(y - \frac{1}{3} y^3 \right),$$

where u_m is the average velocity u_x . A secondary solution in the upper half region $0 < y < 1$ is now superimposed (and continued antimetrixally with respect to the x -axis) with boundary conditions $\psi=0, \partial\psi/\partial y=0$ along $y=1$, and $\psi=0, \partial^2\psi/\partial y^2=0$ along $y=0$ for $x<0$ and $\psi=0, \partial^2\psi/\partial y^2=-m(x)$ for $y=0, x>0$, where $m(x)$ is an unknown function, to be determined from the condition that the sum of the values of $\partial\psi/\partial y$ for the primary and secondary solutions vanishes along $y=0, x>0$. It is obvious that this problem is *formally identical* with the second problem of para. 1 (fig. 2).

3. Approximate solution

Both $H_1(w)$ and $H_2(w)$, as given by eqs. (19) and (21), may be approximated by a simple function of the same type

$$(23) \quad H^*(w) = \frac{1}{\sqrt{2\pi}} \frac{A}{w^2 + B^2}$$

where the constants, A_1 and B_1 for $H_1^*(w)$, A_2 and B_2 for $H_2^*(w)$, are chosen such that $H_1^*(w)$ and $H_2^*(w)$ take the same values as $H_1(w)$ and $H_2(w)$ for $w=0$ and that $H_1^*(w)$ and $H_2^*(w)$ show the same asymptotic behaviour for $w \rightarrow \pm \infty$ as $H_1(w)$ and $H_2(w)$; these constants are therefore $A_1=1/2, B_1=3/2; A_2=1/2, B_2=2$. The accuracy of this approximation may be assessed from table I; the largest error amounts to some 10 percent.

TABLE I

w	$\sqrt{2\pi}H_1^*(w)$ eq. (23)	$\sqrt{2\pi}H_1^{**}(w)$ eq. (24)	$\sqrt{2\pi}H_1(w)$ eq. (19)	$\sqrt{2\pi}H_2^*(w)$ eq. (23)	$\sqrt{2\pi}H_2^{**}(w)$ eq. (24)	$\sqrt{2\pi}H_2(w)$ eq. (21)
0	0,3333	0,3333	0,3333	0,2500	0,2500	0,2500
1	0,2775	0,2931	0,2940	0,2236	0,2347	0,2343
2	0,2000	0,2208	0,2213	0,1768	0,1974	0,1965
4	0,1170	0,1248	0,1244	0,1118	0,1221	0,1229
10	0,0494	0,0501	0,0500	0,0490	0,0501	0,0500
$\rightarrow \infty$	$\rightarrow \frac{1}{2w}$	$\rightarrow \frac{1}{2w}$	$\rightarrow \frac{1}{2w}$	$\rightarrow \frac{1}{2w}$	$\rightarrow \frac{1}{2w}$	$\rightarrow \frac{1}{2w}$

Although it will appear from a numerical example in the next paragraph that this accuracy is adequate for all practical purposes, a much better approximation may be achieved if a suitable rational factor is added to (23), i.e. by a function of the type

$$(24) \quad H^{**}(w) = \frac{1}{\sqrt{2\pi}} \frac{A}{w^2 + B^2} \frac{w^4 + Cw^2 + D}{w^4 + Ew^2 + D},$$

the constants (C_1, D_1 and E_1 for $H_1^{**}(w)$; C_2, D_2 and E_2 for $H_2^{**}(w)$) being

adjusted in order to make the error approximately as small as possible. The accuracy of this second approximation may again be judged from table I, where the numerical values $C_1=6,9$, $D_1=20$, $E_1=5,4$ and $C_2=7,6$, $D_2=38$, $E_2=5,4$ have been used. The largest error has now been reduced to around 0,7 percent.

The solution will be obtained for the second approximation (24). The solution corresponding with the first approximation (23) follows easily from this result by taking $C=E$. Denoting the complex zeros of the rational factor by $\pm \alpha \pm i\beta$ ($\alpha > 0$, $\beta > 0$) and the complex poles by $\pm \mu \pm i\nu$ ($\mu > 0$, $\nu > 0$), where

$$(25) \quad (\alpha^2 + \beta^2)^2 = (\mu^2 + \nu^2)^2 = D,$$

the factorization of (24) reads

$$(26) \quad H^{**}(w) = \frac{1}{\sqrt{2\pi}} \frac{A}{\sqrt{w-iB} \sqrt{w+iB}} \frac{(w-\alpha-i\beta)(w-\alpha+i\beta)(w+\alpha-i\beta)(w+\alpha+i\beta)}{(w-\mu-i\nu)(w-\mu+i\nu)(w+\mu-i\nu)(w+\mu+i\nu)},$$

where the square roots indicate the principal values in the complex w -plane, cut from $-iB$ to $-i\infty$ for $\sqrt{w+iB}$ and from iB to $i\infty$ for $\sqrt{w-iB}$ (fig. 4).

The modified equation

$$(27) \quad \sqrt{2\pi} M_+^{**}(w) H^{**}(w) - \phi_+(w) = \phi_-^{**}(w),$$

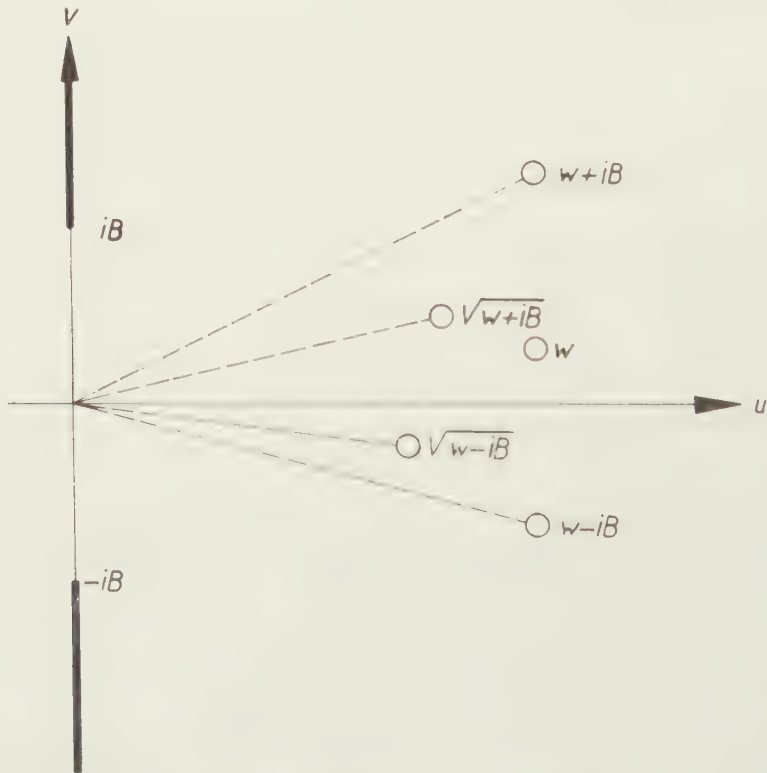


Fig. 4. Principal values of square roots

where $M_+^{**}(w)$ is the FOURIER-transform of the approximate solution $m^{**}(x)$ for $x > 0$, and $\phi_-^{**}(w)$ the corresponding transform of the slope $\varphi^{**}(x)$ for $x < 0$, is now readily soluble by the WIENER-HOPF technique. If $\phi_+(w)$ is a simple function, the solution may sometimes even be written down by simple inspection of eq. (27) and the factorization (26). E.g., if the plate strips in figs. 1 and 2 are loaded *uniformly* with respect to x , the prescribed slope $\varphi(x)$ for $x > 0$ for the secondary solution is a constant; the same condition applies to the hydrodynamical problem of para. 2. Taking this constant equal to *unity*, its F_+ -transform is

$$(28) \quad \phi_+(w) = \frac{1}{\sqrt{2\pi}} \frac{i}{w}.$$

The solution of (27) is now determined from the requirements

- (a) $M_+^{**}(w)$ is regular for $v > a_1$, where $0 < a_1 < v$ and $0 < a_1 < B$;
- (b) $\phi_-^{**}(w)$ is regular for $v < a_2$, where $a_1 < a_2 < v$ and $a_1 < a_2 < B$;
- (c) $M_+^{**}(w)$ and $\phi_-^{**}(w)$ tend to zero for $|w| \rightarrow \infty$ in their half-planes of regularity.

It is immediately obvious from (26) and (27) that $M_+^{**}(w)$ must have the factors $\sqrt{w+iB}$, $(w-\mu+iv)$ and $(w+\mu+iv)$ in order to satisfy requirement (b); moreover $M_+^{**}(w)$ must contain a factor $1/w$ with such a cofactor for $w=0$, that $w=0$ is *not* a pole of $\phi_-^{**}(w)$. In order to satisfy condition (c) $M_+^{**}(w)$ must have in its denominator such regular and non-zero factors for $v > a_1$ that $M_+^{**}(w) \rightarrow 0$ for $|w| \rightarrow \infty$. In view of requirement (b) on $\phi_-^{**}(w)$ these factors must be $(w-\alpha+i\beta)$ and $(w+\alpha+i\beta)$. The solution is now obviously *unique*: it is expressed by

$$(29) \quad \left\{ \begin{aligned} M_+^{**}(w) &= \frac{1}{\sqrt{2\pi}} \frac{i}{Aw} \sqrt{-iB} \sqrt{w+iB} \frac{(w-\mu+iv)(w+\mu+iv)}{(w-\alpha+i\beta)(w+\alpha+i\beta)} = \\ &= \frac{1}{\sqrt{2\pi}} \frac{i}{Aw} \sqrt{-iB} \sqrt{w+iB} \left[1 + \frac{2i(v-\beta)w}{w^2+2i\beta w-\sqrt{D}} \right], \end{aligned} \right.$$

$$(30) \quad \left\{ \begin{aligned} \phi_-^{**}(w) &= \frac{1}{\sqrt{2\pi}} \frac{i}{w} \left[\frac{\sqrt{-iB}}{\sqrt{w-iB}} \frac{(w-\alpha-i\beta)(w+\alpha-i\beta)}{(w-\mu-iv)(w+\mu-iv)} - 1 \right] = \\ &= \frac{1}{\sqrt{2\pi}} \frac{i}{w} \left[\frac{\sqrt{-iB}}{\sqrt{w-iB}} - 1 + \frac{\sqrt{-iB}}{\sqrt{w-iB}} \frac{2i(v-\beta)w}{w^2-2i\beta w-\sqrt{D}} \right]. \end{aligned} \right.$$

The approximate solution for the edge moment $m^{**}(x)$ for $x > 0$ is now obtained by means of the inverse FOURIER-transform

$$(31) \quad m^{**}(x) = \frac{1}{\sqrt{2\pi}} \int_{ia-\infty}^{ia+\infty} M_+^{**}(w) e^{-iwx} dw,$$

and the approximate solution for the slope $\varphi^{**}(x)$ for $x < 0$ is

$$(32) \quad \varphi^{**}(x) = \frac{1}{\sqrt{2\pi}} \int_{ia-\infty}^{ia+\infty} \phi_-^{**}(w) e^{-iwx} dw.$$

It may be noted that the solution $m^*(x)$, $\varphi^*(x)$, corresponding with the

first approximation of the transformed kernel (23) is obtained from this result by putting $\beta = \nu$.

In order to evaluate (31) conveniently the path of integration in the complex w -plane is deformed into the contour Γ (fig. 5), taking due



Fig. 5. Deformation of the path of integration into Γ for (31) and into Γ' for (32)

account of the residues in the poles $w = 0$, $w = \alpha - i\beta$ and $w = -\alpha - i\beta$. Remembering the cuts in the w -plane in our definition of the square roots, we have

$$\sqrt{-i} = e^{-\pi i/4}, \quad \sqrt{i} = e^{\pi i/4},$$

$$\sqrt{\alpha + i(B - \beta)} = \varrho e^{i\theta}, \quad \sqrt{-\alpha + i(B - \beta)} = \varrho e^{i((\pi/2) - \theta)},$$

where ϱ and θ are given by

$$(33) \quad \varrho^4 = \alpha^2 + (B - \beta)^2, \quad \tan 2\theta = \frac{B - \beta}{\alpha}, \quad 0 < |2\theta| < \frac{\pi}{2}.$$

After some elementary algebra expression (31) is now reduced to

$$(34) \quad \left\{ \begin{aligned} m^{**}(x) = & \frac{B}{A} + \frac{1}{2\pi} e^{\pi i/4} \frac{\sqrt{B}}{A} \int_{\Gamma} \frac{\sqrt{w + iB}}{w} e^{-i\omega x} dw + \\ & + 2(\nu - \beta) \frac{\sqrt{B}}{A} \left\{ \frac{\varrho}{\alpha} e^{-\beta x} \cos\left(\alpha x - \frac{\pi}{4} - \theta\right) + \right. \\ & \left. + \frac{i}{2\pi} e^{\pi i/4} \int_{\Gamma} \frac{\sqrt{w + iB}}{w^2 + 2i\beta w - \sqrt{D}} e^{-i\omega x} dw \right\}. \end{aligned} \right.$$

¶ If the contour Γ is approached from the half-plane $u = \operatorname{Re}(w) > 0$, the square root is

$$\sqrt{w + iB} = e^{-\pi i/4} \sqrt{v' - B},$$

where $v' = -v = -\operatorname{Im}(w)$. On the opposite bank of the cut the square root has the opposite sign. Introducing the substitution $v' = B + \eta^2$, the solution may now be written in real form

$$(35) \quad \left\{ \begin{aligned} m^{**}(x) &= \frac{B}{A} + \frac{2}{\pi} \frac{\sqrt{B}}{A} e^{-Bx} \int_0^\infty \frac{\eta^2}{\eta^2 + B} e^{-\eta^2 x} d\eta + \\ &+ 2(\nu - \beta) \frac{\sqrt{B}}{A} \left\{ \frac{\varrho}{\alpha} e^{-\beta x} \cos\left(\alpha x - \frac{\pi}{4} - \theta\right) + \right. \\ &\left. - \frac{2}{\pi} e^{-Bx} \int_0^\infty \frac{\eta^2 e^{-\eta^2 x}}{\eta^4 + 2(B - \beta)\eta^2 + (B - \beta)^2 + \alpha^2} d\eta \right\}. \end{aligned} \right.$$

In order to evaluate the first integral in (35) we observe that the integral

$$(36) \quad I(x) = \int_0^\infty \frac{1}{\eta^2 + B} e^{-\eta^2 x} d\eta$$

satisfies the ordinary differential equation

$$(37) \quad \frac{dI}{dx} - BI = - \int_0^\infty e^{-\eta^2 x} d\eta = - \frac{1}{2} \sqrt{\frac{\pi}{x}}.$$

The solution of (37) which tends to zero for $x \rightarrow \infty$ is

$$(38) \quad I(x) = \frac{\pi}{2} \frac{1}{\sqrt{B}} e^{Bx} [1 - E_2(\sqrt{Bx})],$$

where $E_2(s)$ is the error function

$$(39) \quad E_2(s) = \frac{2}{\sqrt{\pi}} \int_0^s e^{-t^2} dt.$$

The first integral in (35) is now obtained in the expression

$$(40) \quad \int_0^\infty \frac{\eta^2}{\eta^2 + B} e^{-\eta^2 x} d\eta = -\frac{dI}{dx} = \frac{1}{2} \sqrt{\frac{\pi}{x}} - \frac{\pi}{2} \sqrt{B} e^{Bx} [1 - E_2(\sqrt{Bx})]$$

and the final result for our approximate solution, holding for $x > 0$, is

$$(41) \quad \left\{ \begin{aligned} m^{**}(x) &= \frac{\sqrt{B}}{A} \frac{e^{-Bx}}{\sqrt{\pi x}} + \frac{B}{A} E_2(\sqrt{Bx}) + \\ &+ 2(\nu - \beta) \frac{\sqrt{B}}{A} \left\{ \frac{\varrho}{\alpha} e^{-\beta x} \cos\left(\alpha x - \frac{\pi}{4} - \theta\right) + \right. \\ &\left. - \frac{2}{\pi} e^{-Bx} \int_0^\infty \frac{\eta^2 e^{-\eta^2 x}}{\eta^4 + 2(B - \beta)\eta^2 + (B - \beta)^2 + \alpha^2} d\eta \right\}, \end{aligned} \right.$$

where the remaining integral has to be evaluated by numerical integration. The corresponding first approximation obtained by putting $\beta = \nu$, has the particularly simple form

$$(42) \quad m^*(x) = \frac{B}{A} \left[\frac{e^{-Bx}}{\sqrt{\pi Bx}} + E_2(\sqrt{Bx}) \right].$$

Expression (32) is evaluated in an entirely similar way by deforming the path of integration into the contour Γ' (fig. 5), taking due account of the poles $w = -\mu + i\nu$ and $w = \mu + i\nu$. The result, holding for $x < 0$, is

$$(43) \quad \left(\begin{aligned} \varphi^{**}(x) &= 1 - E_2(\sqrt{-Bx}) + \\ &- 2(\nu - \beta) \sqrt{B} \left\{ \frac{1}{\mu \varrho'} e^{\nu x} \cos\left(\mu x - \frac{\pi}{4} - \theta'\right) + \right. \\ &\left. - \frac{2}{\pi} e^{Bx} \int_0^\infty \frac{e^{\eta^2 x} d\eta}{\eta^4 + 2(B - \nu)\eta^2 + (B - \nu)^2 + \mu^2} \right\}, \end{aligned} \right.$$

where ϱ' and θ' are defined by

$$(44) \quad \varrho'^4 = \mu^2 + (B - \nu)^2, \tan 2\theta' = \frac{B - \nu}{\mu}, \quad 0 < |2\theta'| < \frac{\pi}{2}.$$

The corresponding first approximation is again extremely simple

$$(45) \quad \varphi^*(x) = 1 - E_2(\sqrt{-Bx}).$$

It will be observed that the difference between the first and second approximations contains the factor $\nu - \beta$, which is fairly small because the roots of numerator and denominator of the rational factor in (24) are not widely different. *Therefore it may be expected that the first approximation is already fairly accurate*, the more so because the difference between the first and second approximations approaches to zero rapidly for $x \rightarrow \infty$ and $x \rightarrow -\infty$ respectively on account of the factors $e^{-\beta x}$, e^{-Bx} and $e^{\nu x}$, e^{Bx} , whereas this difference is *exactly zero* for $x = 0$. The latter statement is seen to be correct when the expressions (29) and (30) are examined more closely. The difference between the second and first approximation arises from the *last term* between brackets in (29) and (30). The corresponding *parts* of the inverse transforms (31) and (32) are *continuous* functions of x for $x \geq 0$ and $x \leq 0$ respectively because the integrals converge *uniformly*. For $x = 0$ these integrals may be evaluated by contour integration in the *upper* half-plane for (31) and in the *lower* half-plane for (32) and these integrals are therefore zero because the integrands are regular in these half-planes.

An interesting feature of the first approximation is that it is a function of the single variable Bx . The distribution of the edge moment along $x > 0$ and of the slope along $x < 0$ is *entirely similar* for a strip with a simply-supported edge AB (fig. 1) and for a strip with a clamped edge AB (fig. 2): the strip with clamped edge AB acts in this respect like a strip with simply-supported edge AB of width $3/4$ because the values of B in these cases are 2 and $3/2$ respectively, whereas A has the same value $1/2$ in the two problems.

(To be continued)

APPROXIMATE SOLUTION OF WIENER-HOPF TYPE INTEGRAL
EQUATIONS WITH APPLICATIONS. II_BSOME PLATE BENDING PROBLEMS AND AN EXAMPLE FROM
HYDRODYNAMICS *)

BY

W. T. KOITER

(Communicated by Prof. C. B. BIEZENO at the meeting of September 25, 1954)

4. *Comparison of rigorous and approximate solutions in a similar problem*

It would be very cumbersome to obtain the rigorous solutions to the problems considered in sections 1 and 2 because the zeros of $H_1(w)$ (19) and both the zeros and poles of $H_2(w)$ (21) are complex and their distribution over the w -plane is rather complicated. However, the behaviour of these transformed kernels is very similar to the behaviour of the simpler function

$$(46) \quad H_3(w) = \frac{1}{\sqrt{2\pi}} \frac{1}{w} \tanh w.$$

For this transformed kernel with purely imaginary zeros and poles the rigorous solution can be obtained without serious difficulty. On the other hand, (46) allows approximation by functions of the type (23) and (24) with an accuracy that is comparable with the approximations of (19) and (21). Comparison of the rigorous and approximate solutions for the transformed kernel (46) should therefore provide a sufficiently critical test for the accuracy of our approximate method, the more so because the behaviour of the transformed kernel (46) and its approximations is entirely different in the complex w -plane. Whereas $H_3(w)$ has an infinite number of zeros and poles on the imaginary axis, $H_3^*(w)$ has only two branch points and $H_3^{**}(w)$ has in addition to these branch points only four complex zeros and poles.

The approximations to (46) of type (23) and (24) are

$$(47) \quad H_3^*(w) = \frac{1}{\sqrt{2\pi}} \frac{1}{\sqrt{w^2+1}}$$

$$(48) \quad H_3^{**}(w) = \frac{1}{\sqrt{2\pi}} \frac{1}{\sqrt{w^2+1}} \frac{w^4+3,6w^2+4}{w^4+3w^2+4},$$

i.e. $A=1$, $B=1$, $C=3,6$, $D=4$ and $E=3$ in our general formulae. The errors are about 9 percent for $H_3^*(w)$ and 0,5 percent for $H_3^{**}(w)$, cf. table II.

*) For part I (General theory) cf. these Proceedings, 57, 558 (1954).

TABLE II

w	$\sqrt{2\pi}H_3^*(w)$ eq. (47)	$\sqrt{2\pi}H_3^{**}(w)$ eq. (48)	$\sqrt{2\pi}H_3(w)$ eq. (46)
0	1,000	1,000	1,000
0,2	0,981	0,987	0,987
0,5	0,894	0,923	0,924
1,0	0,707	0,760	0,762
1,5	0,554	0,601	0,603
2,0	0,447	0,480	0,482
3,0	0,316	0,331	0,332
5,0	0,196	0,200	0,200
$\rightarrow\infty$	$\rightarrow\frac{1}{w}$	$\rightarrow\frac{1}{w}$	$\rightarrow\frac{1}{w}$

The factorization of $H_3(w)$ is achieved by means of the well-known gamma function formula

$$(49) \quad \Gamma(z) \Gamma(1-z) = \frac{\pi}{\sin \pi z}.$$

The result is

$$(50) \quad H_3(w) = \frac{1}{1-2\pi} \frac{1}{\pi} \frac{\Gamma\left(\frac{1}{2} + \frac{iw}{\pi}\right) \Gamma\left(\frac{1}{2} - \frac{iw}{\pi}\right)}{\Gamma\left(1 - \frac{iw}{\pi}\right) \Gamma\left(1 + \frac{iw}{\pi}\right)}.$$

Taking the prescribed function $\varphi(x)$ for $x > 0$ again equal to unity, its F_+ -transform is given by (28) and the unique solution of (20) (where $H_1(w)$ is replaced by $H_3(w)$) which satisfies the requirement that $M_+(w)$ and $\phi_-(w)$ tend to zero for $|w| \rightarrow \infty$ in their half-planes of regularity is

$$(51) \quad M_+(w) = \frac{1}{1-2\pi} \frac{i\Gamma(1/2)}{w} \frac{\Gamma\left(1 - \frac{iw}{\pi}\right)}{\Gamma\left(\frac{1}{2} - \frac{iw}{\pi}\right)}.$$

$$(52) \quad \phi_-(w) = \frac{1}{1-2\pi} \frac{i}{w} \left[\frac{1}{\Gamma(1/2)} \frac{\Gamma\left(\frac{1}{2} + \frac{iw}{\pi}\right)}{\Gamma\left(1 + \frac{iw}{\pi}\right)} - 1 \right].$$

The rigorous solution is now obtained by the inverse transforms

$$(53) \quad m(x) = \frac{i\Gamma(1/2)}{2\pi} \int_{ia-\infty}^{ia+\infty} \frac{1}{w} \frac{\Gamma\left(1 - \frac{iw}{\pi}\right)}{\Gamma\left(\frac{1}{2} - \frac{iw}{\pi}\right)} e^{-iwx} dw, \quad x > 0,$$

$$(54) \quad \varphi(x) = \frac{i}{2\pi} \int_{ia-\infty}^{ia+\infty} \frac{1}{w} \left[\frac{1}{\Gamma(1/2)} \frac{\Gamma\left(\frac{1}{2} + \frac{iw}{\pi}\right)}{\Gamma\left(1 + \frac{iw}{\pi}\right)} - 1 \right] e^{-iwx} dw, \quad x > 0,$$

where $0 < a < \pi/2$.

The integrals (53) and (54) are evaluated by contour integration and the theorem of residues. The poles of $\Gamma(1-iw/\pi)$ are $w = -ik\pi$ ($k = 1, 2, \dots$)

and its residues are $(-1)^{k+1} (\pi i)/\Gamma(k)$. The solution $m(x)$ for $x > 0$ is now written in the form

$$(55) \quad \left\{ \begin{aligned} m(x) &= 1 + \Gamma(1/2) \sum_{k=1}^{\infty} \frac{(-1)^k e^{-k\pi x}}{k\Gamma(k)\Gamma(\frac{1}{2}-k)} = \\ &= \sum_{k=0}^{\infty} \frac{\Gamma(1/2)}{\Gamma(k+1)\Gamma(\frac{1}{2}-k)} (-e^{-\pi x})^k = \frac{1}{\sqrt{1-e^{-\pi x}}} \end{aligned} \right.$$

by the binominal theorem.

The poles of $\Gamma(1/2 - iw\pi)$ are $w = (k - 1/2)\pi i$ ($k = 1, 2, \dots$) and its residues are $(-1)^k (\pi i)/\Gamma(k)$. The solution $\varphi(x)$ for $x < 0$ is now obtained in the form

$$(56) \quad \left\{ \begin{aligned} \varphi(x) &= - \sum_{k=1}^{\infty} \frac{(-1)^k}{\Gamma(1/2) (k - \frac{1}{2}) \Gamma(k) \Gamma(\frac{3}{2} - k)} e^{(k-1)\pi x} = \\ &= - \int_{-\infty}^x \sum_{k=0}^{\infty} \frac{(-1)^k \Gamma(1/2)}{\Gamma(k+1) \Gamma(\frac{1}{2} - k)} e^{(k+1)\pi \xi} d\xi = \\ &= - \int_{-\infty}^x e^{i\pi \xi} \frac{1}{1 - e^{\pi \xi}} d\xi = \frac{2}{\pi} \arcsin(e^{1/2\pi x}). \end{aligned} \right.$$

The approximate solutions, corresponding with the modified kernels $H_3^*(w)$ and $H_3^{**}(w)$ are given by (42) and (45), and by (41) and (43) respectively, where $A = B = 1$, and $\alpha = 0,3162$, $\beta = 1,3784$, $\mu = 0,5000$, $\nu = 1,3229$ are the real and imaginary parts of the zeros of $w^4 + 3,6w^2 + 4$ and $w^4 + 3w^2 + 4$ in the first quadrant. The approximate solutions $m^*(x)$ and $m^{**}(x)$ are compared with the rigorous solution in table III and fig. 6.

TABLE III

x	$m^*(x)$ eq. (42)	$m^{**}(x)$ eq. (41)	$m(x)$ eq. (55)
0	$\frac{1}{\sqrt{\pi x}}$	$\frac{1}{\sqrt{\pi x}}$	$\frac{1}{\sqrt{\pi x}}$
0,1/ π	3,255	3,232	3,242
0,3/ π	1,997	1,956	1,967
0,25	1,399	1,347	1,356
1,00	1,050	1,023	1,022
$\rightarrow \infty$	$\rightarrow 1,000$	$\rightarrow 1,000$	$\rightarrow 1,000$

The accuracy of $m^{**}(x)$ is such (error less than 0,7 percent) that the difference between rigorous and approximate solution disappears in the graph. Even the error of the first approximation $m^*(x)$ does not exceed 3 percent.

The approximate solution $\varphi^*(x)$ is compared with the rigorous solution in table IV and also in fig. 6. This first approximation is excellent in the region where $\varphi(x)$ is not small. For larger values of $-x$ a better approximation would, of course, be achieved by the second approximation $\varphi^{**}(x)$, but the improvement can only be very small in the most interesting region

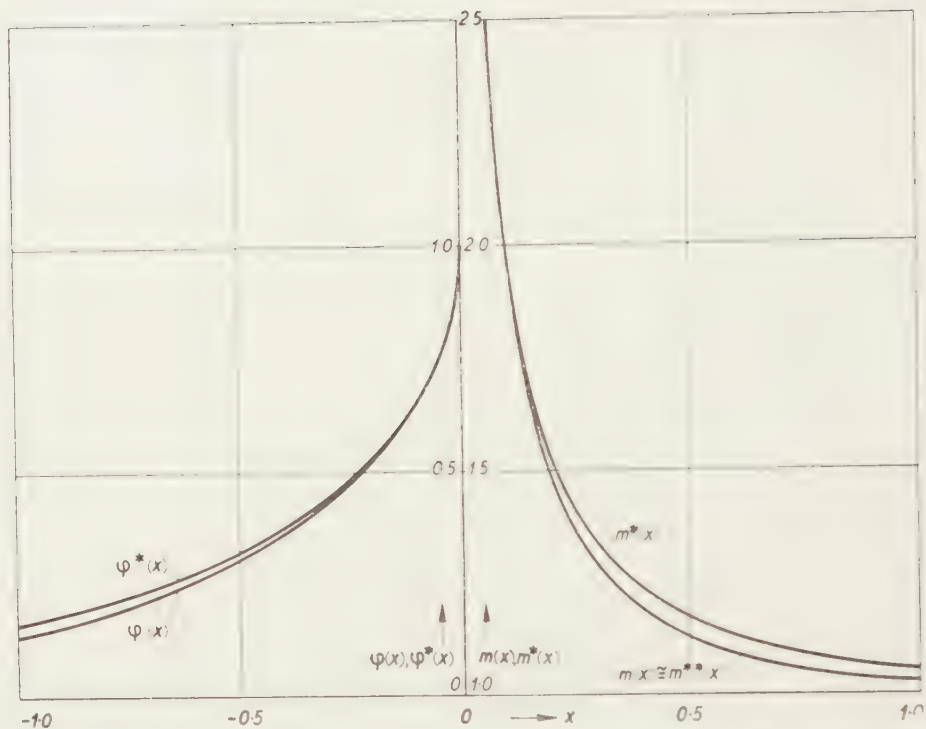


Fig. 6. Comparison of rigorous and approximate solution for example of para. 4

TABLE IV

$-x$	$\varphi^*(x)$ eq. (45)	$\varphi(x)$ eq. (56)
$\rightarrow 0$	$1 - 2 \left \frac{-x}{\pi} \right $	$1 - 2 \left \frac{\sqrt{-x}}{\pi} \right $
$1/16$	0,7237	0,7226
$1/8$	0,6171	0,6139
$1/4$	0,4795	0,4719
$1/2$	0,3175	0,3040
1	0,1573	0,1333
2	0,0455	0,0275
$\rightarrow \infty$	$\rightarrow \frac{e^x}{\sqrt{-\pi x}}$	$\rightarrow \frac{2}{\pi} e^{\frac{\pi}{2} x}$

$-1/2 < x < 0$. Therefore it was not deemed worthwhile to evaluate the integral in (43) by numerical integration.

Finally, it may be observed that the difference in asymptotic behaviour (cf. the last line in table IV) is explained by the kernels, corresponding with the transforms $H_3(w)$ and $H_3^*(w)$. The first kernel, evaluated by contour integration and summing of the resulting series of residues, is

$$(57) \quad h_3(x) = \frac{1}{2\pi} \int_{-\infty}^{\infty} \frac{1}{w} \tanh w e^{-iwx} dw = \frac{1}{\pi} \log \frac{1 + e^{-(\pi/2)|x|}}{1 - e^{-(\pi/2)|x|}};$$

the second kernel is by a well-known Bessel function formula (ref. 2, p. 172)

$$(58) \quad h_3^*(x) = \frac{1}{2\pi} \int_{-\infty}^{\infty} \frac{1}{\sqrt{w^2+1}} e^{-iwx} dw = \frac{1}{\pi} K_0(|x|).$$

The first kernel approaches to zero for

$$|x| \rightarrow \infty \text{ as } \frac{2}{\pi} e^{-\frac{\pi}{2}|x|} \text{ and the modified kernel as } \frac{1}{|2\pi|x|} e^{-|x|}.$$

5. *Concluding remarks*

The problems considered in this part prove that an entirely satisfactory approximate solution may indeed sometimes be obtained by suitable modification of the transformed kernel of the WIENER-HOPF equation. Moreover, it should be noted that the numerical work required in the evaluation of this approximate solution is negligible for the first approximation and only moderate for the second approximation. It seems likely that a similar approach to other problems of elasticity, which are intractable by other methods, e.g. shrink-fit problems and some stress-diffusion problems in plane stress, will also lead to useful results.

REFERENCES

1. LAMB, H., *Hydrodynamics* (6th edition, Cambridge University Press, Cambridge 1932).
2. WATSON, G. N., *Theory of Bessel functions* (2nd edition, Cambridge University Press, Cambridge, 1944).

MIOGYPSINA IN NORTHWESTERN MOROCCO

BY

C. W. DROOGER

(Communicated by Prof. G. H. R. VON KOENIGSWALD at the meeting of Oct. 30, 1954)

Abstract. Peculiar associations of several *Miogypsina* species at some levels of the Moroccan Tertiary are emphasized. It is supposed that these associations are of secondary origin, caused by Miocene drifting of earlier deposited sediments. As a consequence, some deposits in the Ouezzane area, hitherto considered to be of Oligocene age, are shifted into the Miocene.

INTRODUCTION

Our knowledge of the Miogypsinidae from northwestern Morocco comes from the papers of BOURCART and DAVID (1933), SENN (1935) and especially from the detailed study of BRÖNNIMANN (1940).

From both earlier papers it appears that the authors observed the frequent association of representatives of the subgenera *Miogypsinoides* and *Miogypsina* s.str. Unfortunately, the specific determinations are too simplistic for our present classification; mostly the described taxonomic units cannot be fitted in, because of a lack of sufficient data.

On the other hand, BRÖNNIMANN's reports on the important taxonomic features of the encountered Miogypsinae fully enable a reliable evaluation of the various assemblages. The descriptions in BRÖNNIMANN's paper are accompanied by numerous photographs. This author made a detailed study of the larger Foraminifera from some of the samples taken by SENN in the region between Souk el Arba and Ouezzane. For the Miogypsinidae he investigated SENN's sections of the Djebel Rihaiene (Chattian) and of the Si Ameur-el-Hadi (= grande vallée de Basra; Burdigalian), localities that are at a distance of about 10 km from one another. Again it appears that several, up to four, *Miogypsina* species were found together in a single sample. These coexisting species partly belong to one morphological series, which series is considered to consist elsewhere of successive stages of one phylogenetic lineage. So the frequently noted coexistence in Morocco, of representatives of the subgenera *Miogypsinoides* and *Miogypsina* s.str., is extremely rare or doubtful in other parts of the world. Since outside Morocco no more than two species were ever found together—and then always species that clearly belong to different lineages—the queer associations require some special explanation.

Before accepting any complicated evolution- and (or) migration-pattern of the *Miogypsinidae*, it has to be checked whether the remarkable associations can be accounted for by some geological cause. For this reason new observations in the field were made.

In 1952 I visited Basle where BRÖNNIMANN's collections are being stored. In the spring of 1954 I went to Morocco to see the outcrops where SENN had made his collections. These journeys were possible through ample grants of the Netherlands Organisation for Pure Scientific Research (Z.W.O.) and the Molengraaff Foundation, respectively. In Basle a few additional thin-sections could be made of free specimens in BRÖNNIMANN's material. In Morocco I was enabled to study the original notes of SENN's, as well as his thin-sections. For this magnificent support and collaboration I am glad to acknowledge my sincere thanks to the institutions and persons involved: the Netherlands Organisation for Pure Scientific Research (Z.W.O.) at The Hague and the Molengraaff Foundation at Delft for their financial support; Prof. M. REICHEL and Dr E. A. RITTER for their ready authorization to study the original collections in Basle; Mr R. LÉVY, managing director of the exploration, Mr M. REY, chief stratigrapher, and Mr M. DARDENNE and Mr P. L. ALLARD, paleontologists, all of the Société Chérifienne des Pétroles at Petitjean, for the many facilities they gave me in Morocco. Most of all, I wish to thank Dr P. BRÖNNIMANN (Havana, Cuba) for his friendly discussion of my manipulations with the work he had so admirably carried out.

In the following paragraphs the various lithologic and paleontologic features of the stratigraphic sections of Djebel Rihaiene and Si-Ameur-el-Hadi, will be discussed. They are mainly adopted from the data (partly unpublished) gathered by SENN and BRÖNNIMANN, with a number of personal additions.

LITHOLOGY

Since the origin of the sediments will appear to have an important influence on the foraminiferal contents of the samples, the lithology will be dealt with at some length, and separately.

SENN reported from the Djebel Rihaiene some 200 meters of Upper Oligocene deposits (samples 88-102B; see BRÖNNIMANN, p. 5), which he considered to be of Chattian age because of the association of *Nummulites*, *Lepidocyclina* and *Miogypsina*. On the basis of the lithology he subdivided (in his unpublished report) the series into a lower and an upper part that each mainly consists of calcareous sandstones to limestone microbreccias with an occasional conglomeratic layer, and a middle part of predominantly sandy marls.

At the Djebel Si Ameur-el-Hadi, SENN ascribed a complex of sediments (samples 232-262, 277/78) of about 500 meters thickness to the Burdigalian, since he considered the indigenous fauna of these beds to consist of numerous *Miogypsina irregularis* with rare *Lepidocyclina tournoueri*.

The series consists of sandy marls, more or less calcareous sandstones and conglomerates.

The sediments of both sections show many similarities. Not only do they both contain numerous derived Foraminifera, such as *Asterocyclina* individuals, but also in lithologic features there is much resemblance.

A peculiar characteristic in both series was not described by SENN, though in his unpublished notes he often referred to it. He observed that the so-called sandstones as well as the sandy marls often contain clay fragments, which he recorded as "enclaves et mouches d'argile (verte)". Because of the deep weathering of the exposed rocks usually only the empty hollows are to be found. This occurrence of clay bodies is a common phenomenon in the Oligo-Miocene sediments of the region involved. BOURCART and DAVID described them as "vides en forme d'amande remplies par des "marnes" vertes".

In the section of Si Ameur there is at present a quarry in one of the "sandstone" zones, in which exposure the fresh rock can be seen. It is an arenaceous elastic limestone with minute clay particles and interstitial calcite. Some of the beds contain numerous green clay fragments that range in size from the tiny flakes up to boulders of some decimeters' length. They are mostly flattened bodies with one dimension much shorter than the others, with straight longer axis, with more or less rounded angles and in which occasionally distinct traces of lamination parallel to the longer axis, could be observed. In the quarry these clay bodies are rather irregularly scattered in the thick beds, in which they are embedded under various angles with the bedding planes. In some other outcrops, however, it appeared, especially from the hollows, that the clay bodies (up to 1 cm in size) are oriented with their shorter axis perpendicular to the bedding planes. Here it was sometimes observed, that the clay fragments show distinct grading. Where such graded bedding was observed, it always appears in narrow bands of up to 1 dm thickness, which bands are part of much thicker massive layers (up to 1 m). The clay lumps are generally of bigger size than the other clastic particles at the same horizontal level. A mainly parallel position of the embedded fragments without sorting was observed as well, but in that case the bodies are usually scattered in broader bands. Observations of graded bedding are scarce, which may be partly due to the weathered state of the outcrops: but this phenomenon is distinctly absent in many instances. In fact, no differences in grain size were observed in the majority of the "sandstones" during the rapid survey in the field.

One more observation, of obscure significance, on the calcareous sandstones may be mentioned. Mainly in the upper parts of the sections, and especially in that of the Djebel Rihaiene, some of the massive beds show, by means of colour differences on their weathered surface, a fine banding of a constant thickness of but a few millimeters. These bands do not correspond to parting planes within the beds. Their nature could not be

established, since the structures near the surface seem to have been completely wiped out by recrystallization of the calcareous material.

In addition to the frequent occurrence of sand grains and small clay slabs in the marls, SENN observed the presence of pebbles in some of these marly beds. I also found some pebbles, when digging at two places in the so-called "marnes de la cuvette", a series of marls that lie on top of the Burdigalian at Si Ameur.

The third component of the sedimentary complex of Si Ameur consists of the conglomerates that occur throughout the series, but especially in its lower part, where they alternate with "sandstones" and mostly unexposed marls. These conglomeratic beds with a thickness of up to some meters, contain unsorted blocks of all sizes (up to 1 m in diameter) and of Jurassic to Tertiary age. These elements are enclosed in a finely breccious to argillaceous, more or less cemented, matrix. SENN observed among others blocks of Eocene *Asterocyclina*-marls. The series of Si Ameur, considered to be transgressive on the Eocene, has some layers of calcareous sandstone at its base. The first conglomerate appears some ten meters higher up in the section. According to SENN the series of Djebel Rihaiens has a conglomerate at its base, where it is in contact with Middle Oligocene beds with a fault in between. In the field I failed to find such an anomalous contact; the beds on top of, as well as under, the observed conglomerate are similar calcareous sandstones with clay fragments. So it is likely that none of the two series has a basal conglomerate in a strict sense.

As to the mode of formation of the Si Ameur series, SENN thought of sediments deposited in a torrential delta. No doubt this was in 1935 the most plausible explanation for the enumerated observations. However, a difficulty in it is the frequent occurrence of clay fragments up to considerable size. It is very unlikely that such soft pebbles and particles could endure transport by traction in currents, over more than extremely short distances without being completely destroyed. Evidently, the mechanisms, based on experiments and much field work, which have been proposed by KUENEN and others (lit. 8-12) offer a much better explanation for the observed phenomena.

Hence, it is considered more likely that much of the sedimentary material moved from a shallow environment to deeper parts of the sea through submarine sliding, with more or less turbulent flow, of earlier deposited sediments. Such simultaneous displacements of great quantities of material may keep the detached clay fragments in suspension till the moment of settling. The absence of distinct grading in many of the layers may be due to displacement without much turbulence, and to but slight variation in grain size of the unconsolidated material of the slid masses. This may also account for the haphazard arrangement of the clay fragments in some thick beds. The original rock probably accumulated as a sequence of sediments of various fore-reef facies with the admixture of changing amounts of detrital material from the hinterland. This concept

corresponds best with the composition of the clastic sediments of medium grain size. The repeated occurrence of beds with mixtures of faunal elements of a rather variable age (? Early Eocene to ?Middle Miocene; see below) may point to a relatively long and quiet accumulation period, after which numerous slides caved in, probably raised by some orogenic cause.

Sliding and turbidity currents are considered to be responsible for the pebbles and possibly also for the numerous sand grains in the marls, as well as for the many conglomeratic beds. The constituents of the conglomerates, mainly hinterland material, were probably for the greater part derived from torrential deltas. While sliding down into the deeper sea, the mass may have locally eroded Eocene *Asterocyclina*-marls from outcrops on the sea floor. A greater erosion capacity of the descending masses that consisted of much conglomeratic material, gives a reasonable explanation for the frequent occurrence of lumps of *Asterocyclina*-marl in the conglomerates of Si Ameur, whereas only some free *Asterocyclinae* occur scattered in the finer sediments of this section.

PALEONTOLOGY

Si Ameur-el-Hadi

Altogether, the records of 21 samples of the Si Ameur section were found in SENN's notes. The reports of the fauna are usually restricted to the mentioning of genera. The specific determinations are too poorly based for our present demands.

Asterocyclina is reported from seven samples. It is most common in and near the conglomerates of the basal part of the section (233) and in those of the uppermost beds (277/78); occasional specimens were found in sandstones and marls of other levels. Representatives of *Nummulites*, mostly small individuals, are commonly associated with the *Asterocyclina* specimens and they show about an identical frequency distribution. *Lepidocyclinae* are rare; in his paper SENN reported no more than seven specimens, which appear to occur scattered over the entire section. Some of them are determinable (*Nephrolepidina tournoueri*); the others are indistinct. In nearly all the samples *Miogypsinidae* have been found. They mostly belong to the subgenus *Miogypsina*, but representatives of *Miogypsinoides* occur throughout the section as well. The relative proportion of individuals of both subgenera varies considerably and unsystematically in the section. Commonly *Miogypsina* s.str. predominates, but in some samples (e.g. 259) the *Miogypsinoides* individuals strongly outnumber a few specimens of *Miogypsina* s.str..

As to the *Miogypsinidae* specific determinations were re-made for the distinct thin-sections in the collections of SENN and BRÖNNIMANN. Determinations of less than 5 specimens ($N < 5$) must be considered more or less approximative. For the used symbols one is referred to lit. 5, pp. 4-14.

Per sample, from bottom to top of the stratigraphic series the following data are available.

233B: *M. tani* (N=2) and *M. complanata* (N=1; X=17).

240B: The Miogypsinae of this sample have been carefully analyzed by BRÖNNIMANN. He recognized four species: *Miogypsina* (*Miogypsinoidea*) *complanata* SCHLUMBERGER var. *mauretanica* BRÖNNIMANN, *M. (Miogypsina) basraensis* BRÖNNIMANN, *M. (Miogypsina) irregularis* (MICHELOTTI) and *M. (Miolepidocyclina) burdigalensis* (GÜMBEL). This group of species forms a highly remarkable association. The coexistence of *M. irregularis* and *M. burdigalensis* offers no difficulties, since both species are known to belong to different lineages, which were also found together in the basal Burdigalian of southwestern France. But if the frequently proved principle of nepionic acceleration for the evolution of the Miogypsinidae is also accepted for the Moroccan representatives of the family, we have to consider both *M. complanata* var. *mauretanica* and *M. basraensis* as older species than *M. irregularis*.

In SENN's material I found no thin-sections that belong to this sample. I made some additional thin-sections of the Basle material (deposited in the Naturhistorischem Museum of Basle). Combined with most of BRÖNNIMANN's thin-sections, measured according to my own methods, I disposed of 53 individuals that were of a satisfactory quality. For these I arrived at the same ultimate conclusions as did BRÖNNIMANN. The main difficulty is the extremely wide range of variation of the number of spiral chambers in the group of specimens with a peripheral position of the early stages. Calculating the coefficient of variation ($V = 100 \sigma/M$) for the

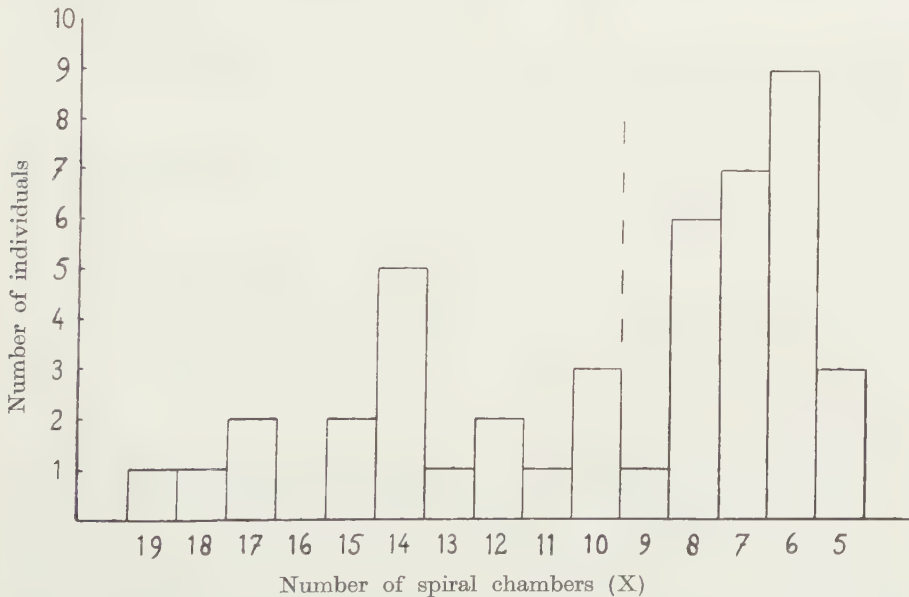


Fig. 1. Frequency distribution for X in 44 *Miogypsina* individuals with peripheral position of the embryonic-nepionic stage. Sample 240B

entire assemblage we arrive at a value ($V=41.5$) more than double the value achieved for eight, arbitrarily chosen, homogeneous assemblages from other parts of the world ($V=9$ to 18). The heterogeneous character of the Moroccan assemblage also appears as likely from the frequency distribution of X (see fig. 1). If we subdivide the group into two parts between $X=9$ and $X=10$, we get two artificial groups each having a more probable frequency distribution for X . These groups are then determinable as *M. basraensis* ($V=19.3$) and *M. irregularis* ($V=16.0$), respectively. Probably a few specimens of *M. complanata* are mixed with the individuals of *M. basraensis*, but they cannot be clearly separated; BRÖNNIMANN evidently had the same impression. Specimens of *M. gunteri* and *M. tani* may also be present, disguised among the individuals of *M. basraensis* and *M. irregularis*. The fourth species in sample 240B is *M. burdigalensis*, the specimens of which are easily distinguishable from those of the other species by the non-peripheral position of the early ontogenetic stages. The data of the various recognized groups of individuals of this sample are as follows:

M. basraensis and *M. complanata*: $N=18$; $R_X=19-10$, $M_X=13.8 \pm 0.63$; $R_Y=20^\circ$ (via γ or 180°) $\pm 70^\circ$, $M_Y=179 \pm 29.5$. None of the specimens has a second primary auxiliary chamber.

M. irregularis: $N=26$; $R_X=9-5$, $M_X=6.7 \pm 0.21$; $R_{200\alpha/\beta}=0-63$, $M_{200\alpha/\beta}=30 \pm 4.5$. Eighteen of the specimens clearly show the presence of two principal auxiliary chambers. $R_Y=-50^\circ - +65^\circ$, $M_Y=12^\circ \pm 5.2^\circ$.

M. burdigalensis: $N=9$, Π_p : $R_X=10-7$, $M_X=8.6 \pm 0.39$; Π_d : $R_X=5-8$, $M_X=6.0 \pm 0.51$; Π'' : $R_{X''}=0-3$, $M_{X''}=1.1 \pm 0.35$; Π''' : $R_{X'''}=0-3$, $M_{X'''}=1.3 \pm 0.41$; $R_{200\alpha/\beta}=0-56$, $M_{200\alpha/\beta}=24 \pm 7.4$. In three of the specimens the presence of a second principal auxiliary chamber could not be ascertained.

241: BRÖNNIMANN's collection contains one distinct thin-section of *M. complanata* or *M. basraensis* with $X=13$ or 14, and one clear section of *M. irregularis* ($200 \alpha/\beta=35$; $\gamma=65^\circ$).

246/47: In SENN's collection there is one specimen attributable to *M. irregularis* and another that belongs to *M. burdigalensis*.

249/50: In SENN's collection one specimen was found with $200 \alpha/\beta=75$ (*M. cushmani*).

260/61: In BRÖNNIMANN's collection one distinct individual occurs with $200 \alpha/\beta=56$ and $\gamma=75^\circ$ (*M. intermedia*).

277/78: From this uppermost sample of the Si Aneur series BRÖNNIMANN analysed a homogeneous assemblage of high-developed Miogypsinae. In addition to individuals with *Miogypsina* s.str. features (type of *Miogypsina mediterranea* BRÖNNIMANN), many others have the embryonic-nepionic stages slightly removed from the periphery (*M. mediterranea* var. *excentrica* BRÖNNIMANN). As to the $200 \alpha/\beta$ values this assemblage has the height of development of *M. antillea*. It is further characterized by the frequent

occurrence of accessory auxiliary chambers, especially on the deuteroconch. The angle γ is usually high, mostly about 90° . The data for 53 specimens are:

$$R_{200\alpha/\beta} = 56-100; M_{200\alpha/\beta} = 88 \pm 1.3; R_\gamma = 0^\circ-160^\circ, M_\gamma = 69^\circ \pm 3.4^\circ$$

(based on 58 individuals). 29 out of 53 specimens have $200 \alpha/\beta$ values greater than 90° . Slightly less than fifty percent of the sectioned individuals have the early stages distinctly, but slightly removed from the periphery. In eleven specimens one or two accessory auxiliary chambers on the deuteroconch were distinctly visible; such a chamber on the protoconch could be clearly observed in but one individual. The greater frequencies of individuals with such chambers, given by BRÖNNIMANN, are probably due to observations during the grinding which are lost afterwards.

In the morphological classification it is very hard to find a suitable name for the assemblage. For one thing it is comparable to *M. antillea* of the *Miogypsina* s.str. series of species. On the other hand it shows intergradation to highly developed populations of *M. (Miogypsinita) mexicana*. Similar assemblages have recently become known from at least two other places in the western Mediterranean area (Algeria (see DAVID and FLANDRIN) and Majorca (unpublished observations)), whereas assemblages attributable to *M. mexicana* are unknown so far in this region. So it seems best to maintain as yet for these assemblages with the enumerated intermediate features in between *M. antillea* and *M. mexicana*, a distinct specific name: *M. mediterranea* BRÖNNIMANN (thus including the type of *M. mediterranea* var. *excentrica* BRÖNNIMANN, which latter name moreover cannot be recognized, since it is a homonym of *Miogypsina (Miolepidocyclina) excentrica* TAN SIN HOK, 1937 that was described from the island of Madura). This is not yet the end of the nomenclatorial difficulties, however. Morphologically very similar assemblages have been described as *Miogypsina* ex. interc. *cushmani-mexicana* from Venezuela (lit. 5, pp. 41-43, 59). If we give such intermediate assemblages a separate specific name, *M. mediterranea* might be a younger synonym of *M. staufferi* KOCH, 1926 or *M. venezuelana* HODSON, 1926, which are insufficiently known, however. As yet I will retain the name of *M. mediterranea* for the assemblages of the Mediterranean area, pending further investigations.

Sample 277/78 in SENN's collection finally contains the section of an individual of *M. complanata* or *M. basraensis* ($X=10$).

According to SENN only the individuals of *Asterocyclina* and *Nummulites* in the sediments of Si Ameur had been reworked from older strata. It has been shown above, however, that the composition of the sediments allows of any degree of reworking among the faunal components. So, in my opinion, also the Lepidocyclinae, *Miogypsina complanata* and *M. basraensis* must be considered as derived elements. The remaining Miogypsinae that are considered to be autochthonous, form a morphological series that is in

accordance with the principle of nepionic acceleration, as well as with the stratigraphic succession of species, established in other regions of the world (see fig. 2). In the Moroccan succession within the subgenus *Miogypsina*, the presence of *M. irregularis* (MICHELOTTI) and *M. mediterranea* BRÖNNI-MANN are well-established points. Stratigraphically in between the levels of these two species there are indications of the presence of *M. intermedia*

RUPELIAN-CHATTIAN		AQUITANIAN		BURDIGALIAN		HELVETIAN	
complanata	basraensis	gunteri	tani	irregularis	intermedia	cushmani	mediterranea

Fig. 2. Probable succession of *Miogypsina* species in Morocco, based on the principle of nepionic acceleration

DROOGER and *M. cushmani* VAUGHAN, which are both morphologically and phylogenetically, intermediate. Possibly, the series of Si Ameur begins at the level of *M. tani* DROOGER, of which species an indication was found in sample 233B. The occurrence of *M. burdigalensis* (GUMBEL) in the section, at the level of *M. irregularis* is in good accordance with the data from southwestern France, where the association of both species marks the early Burdigalian.

If the series from *M. tani* to *M. mediterranea* does represent the autochthonous succession of species, and if we correlate this series with the sequence of species in southwestern France, we get the following stratigraphic results. The basal part of the Si Ameur section belongs to the (Upper) Aquitanian, while on top of the Burdigalian the upper beds with *M. cushmani* and *M. mediterranea* have to be placed in the Vindobonian. The latter conclusion follows from the fact that in the uppermost beds of the typical Burdigalian near Bordeaux the Miogypsinidae had not yet developed beyond the morphologic level of early *M. intermedia*.

Djebel Rihaiene

In SENN's notes there are records of 16 samples (88/89-102B) of the "Chattian" series of Djebel Rihaiene. *Nummulites* is recorded from three samples, in two of which it is accompanied by *Asterocyclina*. *Lepidocyclina* occurs throughout the section, mostly in small numbers. As far as could be ascertained most of the individuals of the latter genus approach the type of *L. (Nephrolepidina) tournoucri*, but occasional individuals of the subgenus *Eulepidina* were also observed. The Miogypsinidae are the most common larger Foraminifera. Mostly representatives of *Miogypsinoides* predominate, but at a few levels (e.g. in the lowest sample 88/89) *Miogypsina* s.str. is at least as common. The detailed data as to the specifically determined Miogypsinae are as follows:

88/89: A thin-section of SENN's contains distinct transverse sections of many individuals of *Miogypsina* s.str. and *Miogypsinoides*. Two fairly

good horizontal sections of the latter show *M. complanata* with 17 and 16 spiral chambers respectively.

90/91: This is a sample that was analyzed in detail by BRÖNNIMANN. He recognized two species in it: *Miogypsina* (*Miogypsinoidea*) *complanata* SCHLUMBERGER var. *mauretana* BRÖNNIMANN and *M. (Miogypsina) irregularis* (MICHELOTTI). During the grinding of additional individuals I observed in one, which had a long nepionic spiral, the presence of lateral chambers. So it is likely that specimens of the *M. basraensis* group of species occur mixed up with the *M. complanata* individuals. For practical reasons BRÖNNIMANN's variety of *M. complanata* is not used here: the various encountered assemblages of *Miogypsinoidea* are so widely diverging in characters that they could better be attributed to *M. complanata* in its wide sense. BRÖNNIMANN's thin-sections of *M. irregularis* were not sufficiently clear. After making a number of new thin-sections of the *Miogypsina* s.str. group of individuals, I disposed of five sections that enabled the determination *M. cushmani* for them. The coexistence of *M. complanata* and *M. cushmani* is indeed the most remarkable of all observed aberrant associations.

The detailed features for both groups of individuals in sample 90/91 are:

M. complanata: $N=31$; $R_X=15-9$, $M_X=11.4 \pm 0.29$; $R_Y=-30^\circ$ (via + or -180°) till $+160^\circ$, $M_Y=-118^\circ \pm 7.1^\circ$.

M. cushmani: $N=5$; $R_{200\alpha/\beta}=64-85$; $M_{200\alpha/\beta}=76 \pm 3.9$, $R_Y=10^\circ-110^\circ$, $M_Y=38^\circ \pm 18.5^\circ$.

93: In SENN's collection there is one distinct individual of *Miogypsina* s.str. with $200\alpha/\beta=55$ (*M. intermedia*).

95: In BRÖNNIMANN's collection were found:

M. complanata: $N=6$; $R_X=15-11$, $M_X=13.3 \pm 0.58$; $R_Y=-130^\circ$ (via + or -180°) — $+170^\circ$, $M_Y=-160^\circ \pm 8.2^\circ$.

M. intermedia or *M. cushmani*: $N=1$; $200\alpha/\beta=67$; $\gamma=25^\circ$.

96A: In SENN's collection there is one specimen of *M. complanata* with $X=11$.

102A: Again in the collection SENN two individuals occur of *M. complanata* both with $X=17$.

102B: One rock-section of SENN's contains numerous *Miogypsinoidea* specimens. In 9 of them the number of spiral chambers could be counted more or less accurately ($R_X=22-12$, $M_X=\text{about } 17$).

Among the individuals of the Rihaiene section, attributed to *M. complanata*, some may belong to the *M. basraensis* — *M. tani* group. This may be concluded for some specimens from the relative size of the spiral chambers and the shape of the equatorial chambers, but these are unreliable features for a clear distinction.

It must be further pointed out that the *M. complanata* assemblages of

samples 90/91, 95 and 102B in this order show differences in their M_x values that clearly favour the principle of nepionic retardation. The two observations of sample 88/89 might contradict such a general trend, but the data are insufficient. This conclusion of nepionic retardation is not opposed by the field observations. Only two or three examples of graded bedding were noted during the rapid survey of the beds of the Djebel Rihaiene, but they contradict the supposition that the strata are upside down. Conclusions on the development of Moroccan *Miogypsinoides* are nevertheless premature, as may be seen from the following.

With the exception of the Asterocyclinae, which are not reported in his paper, SENN considered the entire fauna of larger Foraminifera as contemporaneous with the deposition of the sediments. On the association of few *Nummulites* with *Lepidocyclina* and *Miogypsina* he based his determination of the Chattian age. In my opinion the *Nummulites*, commonly occurring with the Asterocyclinae, have also been derived from older beds. The association of *Lepidocyclina tournoueri* and *Miogypsina complanata* s.l. is a common feature of the Chattian of southwestern France (Saint Etienne-d'Orthe, etc., see lit. 7). As such SENN's age determination might still be correct but for the presence of *Miogypsina* s.str.. Moreover, the latter are of such unexpected high level of development that the species involved were not even yet present in France at the end of the Burdigalian. This association of Eocene, Oligocene and Miocene components in the fauna leads to the conclusion that only the youngest (*M. cushmani*) are autochthonous, however small their relative amount may be. This explanation requires that most of the coarser sediment belonged to unconsolidated deposits of Upper Oligocene age that were carried down into the deeper parts of the sea during Vindobonian time. The nature of the sediments certainly allows of such an explanation.

As a consequence the sediments involved of the Djebel Rihaiene would be of about the same age as part of the series of Si Ameur-el-Hadi. Their distinct differences in relative amounts of the various reworked and autochthonous components are probably due to different proportions of derived material in the beds, as well as to somewhat different sources for this drifted material among the earlier deposited sediments.

Possibly the "Aquitanian" sediments of the Djebel Chlouche (see SENN, p. 90) are also of about the same age. A rock section of a sample in SENN's collection (S436) revealed the distinct presence of representatives of both the subgenera *Miogypsinoides* and *Miogypsina* s.str..

Just one more point may be raised. Since the work of SENN, it has become known that the region between Souk el Arba and Ouezzane is not only tectonically highly complicated by fracturing, but also that it belongs as a whole to the "nappe pré-rifaine". It has been established that the orogenetic movements arrived at a climax during the Miocene (lit. 3, pp. 70-71). So it is not surprising that marine Miocene sediments of flysch

character within this mobile zone show such numerous examples of submarine sliding and turbidity currents. This is a strong support of the viewpoint that the peculiar faunal associations must be accounted for by combined tectonic-sedimentary actions instead of complicated and astounding evolution patterns and migration ways. Unfortunately, no undisturbed marine Oligo-Miocene series with larger Foraminifera have so far become known in Morocco outside this tectonic belt. Possible finds in such series may reveal the regular succession of faunas again.

REFERENCES

1. BOURCART, J. and E. DAVID, Étude stratigraphique et paléontologique des Grès à Foraminifères d'Ouezzan au Maroc. Mém. Soc. Sc. Nat. Maroc, 37 (1933).
2. BRÖNNIMANN, P., Über die tertiären Orbitoiden und die Miogypsiniden von Nordwest-Marokko. Schweiz. Pal. Abh., 63 (1940).
3. CHOUBERT, G. and J. MARÇAIS, Géologie du Maroc; Aperçu structural. Monogr. région. XIXe Congr. géol. intern., sér. 3, no. 6, fasc. 1, 1re part. (1952).
4. DAVID, L. and J. FLANDRIN, Sur la présence de Miocène à Miogypsinides dans les Monts de la Haute-Merdjeda. Bull. Soc. géol. France, in the press (1954).
5. DROOGER, C. W., Study of American Miogypsinidae. Acad. thesis Utrecht (1952).
6. ———, Miogypsinids in northern Italy. Proc. Kon. Ned. Ak. Wetensch., ser. B, 57, 227-249 (1954).
7. ———, J. P. H. KAASSCHIEP and A. J. KEY, The microfauna of the Aquitanian-Burdigalian of southwestern France. Verh. Kon. Ned. Ak. Wetensch., in the press (1954).
8. KUENEN, PH. H., Properties of turbidity currents of high density. Spec. Publ. Soc. Ec. Paleont. and Mineral., 2, 14-33 (1951).
9. ———, Significant features of graded bedding. Bull. Am. Ass. Petr. Geol., 37, 1044-1066 (1953).
10. ——— and A. CAROZZI, Turbidity currents and sliding in geosynclinal basins of the Alps. Journ. Geol., 61, 363-373 (1953).
11. ——— and H. W. MENARD, Turbidity currents, graded and non-graded deposits. Journ. Sed. Petrol., 22, 83-96 (1952).
12. KUENEN, PH. H. and C. I. MIGLIORINI, Turbidity currents as a cause of graded bedding, Journ. Geol., 58, 91-127 (1950).
13. SENN, A., Die stratigraphische Verbreitung der tertiären Orbitoiden mit spezieller Berücksichtigung ihres Vorkommens in Nord-Venezuela und Nord-Marokko. Ecl. géol. Helv., 28, 51-113, 369-373 (1935).

THERMOELECTRIC PHENOMENA IN GALVANIC CELLS ¹⁾

BY

HANS HOLTAN JR ²⁾

(*Institute for Theoretical Physics, The University, Utrecht, Netherlands*)

(Communicated by Prof. J. M. BIJVOET at the meeting of September 25, 1954)

Abstract

The expression for the potential difference of galvanic cells containing also temperature gradients is derived. It is shown that there is a simple relationship between this potential difference and the potential differences of the corresponding isothermal cell and the corresponding pure thermocells (Soret effects hindered). These new relations may easily be tested experimentally.

In systems of electrolytic conductors thermoelectric forces exist just as in metallic thermocouples. In current textbooks of electrochemistry and physical chemistry the treatment of galvanic cells has been limited to the isothermal state. It is of considerable theoretical interest to include also temperature gradients and to derive an expression for the thermoelectric part of the potential difference. It is also of practical importance since for instance the calomel electrode during pH measurements is often (out of practical reasons) kept at room temperature while the other electrode is submerged in solutions of temperatures different from room temperature.

The expressions for the potential difference of pure thermocells (identical electrodes kept at different electrodes) have recently been derived by applying [1-4] the thermodynamical theory of irreversible processes [5]. Some experimental work on thermocells has also recently been reported by the author [1, 6].

A theoretical relationship between the temperature coefficient of an isothermal cell and the thermopotentials of the corresponding pure thermocells has recently been derived [7]. According to this relation the temperature coefficient of the isothermal cell (German sign convention was used for the temperature coefficient)

$$(1) \quad E_1 ; \text{Electrolyte} ; E_2 ,$$

¹⁾ In part abstracted from the author's thesis, presented to the University, Utrecht, Netherlands, April 1953.

²⁾ Present address: Det Norske Zinkkompani A/S, Eitheim pr. Odda, Norway.

where E_1 and E_2 stand for electrodes (with ion reversible to the electrolyte), equals the differential thermopotential of the thermocell

$$(2) \quad E_1 \underset{T}{;} \text{Electrolyte} \underset{T+\Delta T}{;} E_1,$$

minus the differential thermopotential of the thermocell

$$(3) \quad E_2 \underset{T}{;} \text{Electrolyte} \underset{T+\Delta T}{;} E_2,$$

plus the differential thermopotential of the metallic thermocouple

$$(4) \quad M_2 \underset{T}{;} M_1 \underset{T+\Delta T}{;} M_2,$$

where M_1 and M_2 stand for the metals of electrode 1 and 2 respectively.

The extension of the theory of pure thermocells to cells of the general type

$$(5) \quad E_A \underset{T}{;} \text{Electrolyte} \underset{T+\Delta T}{;} E_B,$$

is simple, and may be carried out as follows.

The cell represented by (5) has three junctions. The junction between metal M_A and M_B may be kept at the temperature T or at the temperature $T + \Delta T$.

The total potential difference of the cell is given by

$$(6) \quad \Delta\varphi_t = \Delta\varphi_{ele} - \Delta\varphi_{met} + \Delta\varphi_{het},$$

where *ele*, *met* and *het* refer to the electrolyte, the metallic phase and the heterogeneous potential jumps respectively.

If the junction between the two metals in the external part of the circuit is kept at temperature T , we have [1, 2] for the homogeneous potential difference in this phase

$$(7) \quad \Delta\varphi'_{met} = ({}_B Q_{el}'^* / FT) \Delta T,$$

where ${}_B Q_{el}'^*$ is the molar heat of transfer of the electrons in metal B .

If the junction is kept at temperature $T + \Delta T$, we have correspondingly

$$(8) \quad \Delta\varphi''_{met} = ({}_A Q_{el}'^* / FT) \Delta T.$$

The electric potential difference at each heterogeneous interface may be calculated from the condition

$$(9) \quad \tilde{A} = 0,$$

where \tilde{A} is the electrochemical affinity.

For the heterogeneous electrode reactions between the electrodes and the electrolyte, we have

$$(10) \quad F(\varphi_1 - \varphi_2) = \Delta G,$$

where G is Gibbs' function. ΔG is calculated for the passage of 1 Faraday of electricity through the interphase from the electrode to the electrolyte. Subscript 1 refers to the metallic phase and 2 to the electrolyte.

We then have for the two heterogeneous junctions between electrode and electrolyte

$$(11) \quad F(\varphi_A - \varphi_2)_T = \Delta G'_{A,T}.$$

and

$$(12) \quad F(\varphi_B - \varphi_2)_{T+\Delta T} = \Delta G_{B,T+\Delta T}.$$

For the heterogeneous junction in the external part of the circuit we have simply

$$(13) \quad F(\varphi_A - \varphi_B) = {}_A\mu_{\text{el}} - {}_B\mu_{\text{el}}.$$

μ being the chemical potential.

For the net heterogeneous potential difference we obtain

1. when the external junction is kept at temperature T (Soret effect hindered)

$$(14) \quad \begin{cases} F \Delta \varphi'_{\text{het}} = \Delta G_{B,T+\Delta T} - \Delta G_{A,T} + ({}_A\mu_{\text{el}} - {}_B\mu_{\text{el}})_T = \\ = \Delta G_{B,T} - \Delta S_B \Delta T - \Delta G'_{A,T} + ({}_A\mu_{\text{el}} - {}_B\mu_{\text{el}})_T, \end{cases}$$

S being the entropy.

2. when the external junction is kept at temperature $T + \Delta T$

$$(15) \quad \begin{cases} F \Delta \varphi''_{\text{het}} = \Delta G_{B,T+\Delta T} - \Delta G_{A,T} + ({}_A\mu_{\text{el}} - {}_B\mu_{\text{el}})_{T+\Delta T} = \\ = \Delta G_{B,T+\Delta T} - \Delta G_{A,T+\Delta T} - \Delta S_A \Delta T + ({}_A\mu_{\text{el}} - {}_B\mu_{\text{el}})_{T+\Delta T}. \end{cases}$$

For the isothermal cell corresponding to (5) we have

$$(16) \quad F \Delta \varphi_{\text{is}} = \Delta G_B - \Delta G_A + ({}_A\mu_{\text{el}} - {}_B\mu_{\text{el}}).$$

We see that

$$(17) \quad \Delta \varphi'_{\text{het}} = \Delta \varphi_{\text{is},T} - \Delta S_B \Delta T / F,$$

and

$$(18) \quad \Delta \varphi''_{\text{het}} = \Delta \varphi_{\text{is},T+\Delta T} - \Delta S_A \Delta T / F.$$

As the thermopotential of the pure thermocell

$$(19) \quad \begin{matrix} E \\ T \end{matrix} ; \text{Electrolyte} ; \begin{matrix} E \\ T+\Delta T \end{matrix},$$

is given by [1]

$$(20) \quad \Delta \varphi_{\text{th}} = \Delta \varphi_{\text{ele}} - Q'_{\text{el}} / FT - \Delta S \Delta T / F,$$

we see that when

1) the external junction is kept at temperature T

$$(21) \quad \Delta \varphi_t = {}_B\Delta \varphi_{\text{th}} + \Delta \varphi_{\text{is},T},$$

where ${}_B\Delta \varphi_{\text{th}}$ is the thermopotential difference of the pure thermocell

$$(22) \quad \begin{matrix} E_B \\ T \end{matrix} ; \text{Electrolyte} ; \begin{matrix} E_B \\ T+\Delta T \end{matrix},$$

2) the external junction is kept at the temperature $T + \Delta T$

$$(23) \quad \Delta\varphi_t = {}_A\Delta\varphi_{th} + \Delta\varphi_{is, T+\Delta T},$$

where ${}_A\Delta\varphi_{th}$ is the thermopotential difference of the pure thermocell

$$(24) \quad E_A \underset{T}{;} \text{Electrolyte} \underset{T+\Delta T}{;} E_A.$$

We thus see that the potential difference of a galvanic cell containing also temperature gradients may be expressed in quite general terms by means of the potential difference of the corresponding isothermal cell and the potential differences of the corresponding pure thermocells.

These new relations may easily be tested experimentally.

We realize that the difference between the potentials (23) and (21) equals the thermoelectric force of the metallic thermocouple

$$(25) \quad Me_A \underset{T}{;} Me_B \underset{T+\Delta T}{;} Me_A.$$

We see that it is also equal to

$$(26) \quad {}_A\Delta\varphi_{th} + \frac{\partial \Delta\varphi_{is}}{\partial T} \Delta T - {}_B\Delta\varphi_{th}.$$

We thus get a confirmation of the relation already referred to [7] between the temperature coefficient of an isothermal cell and the thermopotentials of the corresponding pure thermocells. Note that the temperature coefficient in (26) is defined according to American sign convention, whereas in reference [7] the German sign convention was used.

Remark

In the derivations concentration gradients (the Soret effect) has been supposed to be absent in the electrolyte as it is in most experimental cases. The influence of the Soret effect on the thermopotential difference of pure thermocells has recently been discussed [8].

REFERENCES

1. HOLTAN JR., H., Electric Potentials in Thermocouples and Thermocells, Thesis, Utrecht, April 1953.
2. ———, P. MAZUR and S. R. DE GROOT, *Physica* **19**, 1109 (1953).
3. ———, *Proc. Kon. Ned. Ak. v. Wet.*, Amsterdam **B 56**, 498 (1953).
4. ———, *ibid.* **B 56**, 510 (1953).
5. DE GROOT, S. R., *Thermodynamics of Irreversible Processes* (North Holland Publ. Company, Amsterdam and Intersc. Publ., New York, 1951).
6. HOLTAN JR., H., *Tidsskr. Kjemi, Bergvesen, Met.*, **12**, 5 (1952).
7. ———, *Proc. Kon. Ned. Ak. v. Wet.*, Amsterdam **B 57**, 138 (1954).
8. HAASE, R., *Trans. Far. Soc.* **49**, 724 (1953).

ASTRONOMY

PRELIMINARY REPORT CONCERNING THE ECLIPSE OF JUNE 30, 1954 AND THE DUTCH EXPEDITION TO GOTLAND

BY

A. C. S. VAN HEEL, J. HOUTGAST AND M. G. J. MINNAERT

(Communicated at the meeting of September 25, 1954)

A systematic series of eclipse observations by Dutch astrophysicists began in 1901 and was continued in 1905, 1912, 1914, 1925, 1927, 1929, 1932 and 1936. This tradition was interrupted by the war and there was a danger that valuable experience of many years would be lost. However, due to the active support of the Organization for Pure Scientific Research (Z.W.O.), it proved possible already in 1952 to organize an expedition so that the Dutch astronomers, who have always taken such an active part in solar research, were again represented among the observing groups. It was obvious that efforts had to be made also in view of the eclipse of 1954, which could be observed in regions easily accessible and favorable from the meteorological point of view.

The Eclipse Committee of the Royal Academy assembled on January 22, 1953 and took a definitive decision, after a thorough discussion concerning the location of the camp, the program of the observations and the financial questions involved.

The selection of the camp

The zone of totality extended from Canada over the South point of Greenland, one of the Shetlands, southern Norway, southern Sweden, Poland, the Soviet Union unto Iran and India. Through the care of the International Astronomical Union and the Swedish astronomers, a precise description was available of the astronomical and meteorological conditions along the zone of totality ¹⁾. The greatest solar altitude and the longest duration of totality were to be found in Scandinavia, and there also were the best chances of a clear sky, especially at the south-eastern coast and on the islands Öland and Gotland. The meteorologist of the Eclipse Committee, Professor W. BLEEKER, analyzed carefully the situation and made further enquiries in Norway and Sweden. He concluded, that the southern point of Gotland seemed especially favourable: first, because it was relatively distant from the continent; secondly, because the observations there would not be hampered by cumulus formation, which is of general occurrence over islands when the weather

¹⁾ H. O. GRÖNSTRAND, Stockholms Annaler 16, Nr. 2 (1950).

is fair. It was of minor importance that this site was not located on the central line, and that the duration of totality would be only 136^s instead of 151^s on the central line. An excellent survey of the local circumstances was obtained by the kind help of Dr ÅKE WALLENQUIST, observer at the Uppsala Observatory, who explored the island already in the summer of 1953 and sent us an extensive report, illustrated with snapshots of the regions of interest. Professor B. LINDBLAD had also the kindness to collect the necessary information on the spot, and confirmed entirely what we had deduced from the report of Dr WALLENQUIST.

It seemed unpracticable to locate the camp at the very south point of the island, where there are hardly any trees nor shelter from the seawind and where it would have been difficult to find accommodation. But slightly farther to the northeast there was a boarding-house for holiday guests at Holmhällar, near Hamra, surrounded by sparse fir trees, where the members of the expedition could find simple but comfortable rooms, good meals and all kinds of practical help. Holmhällar is connected by an automobile road with Hamra, at 4 km distance, and with the railway station of Burgsvik at 10 km.

From the ordnance map and from the general information available, the following fundamental data for the observation were derived:

geographical position: N.lat. $56^{\circ}56'$; E.long. $18^{\circ}17'30''$;

moment of 1st contact: 11^h37^m UT;

moment of 2nd contact: $12^h50^m10^s$;

moment of 3rd contact: $12^h52^m26^s$;

moment of 4th contact: 14^h01^m ;

altitude of sun at mid-totality: $49^{\circ}45'$;

azimuth of sun at mid-totality: $45^{\circ}47'$.

The program of the observations

1. From the start it was clear, that the investigations concerning *the structure of the chromosphere*, commenced in 1952 by Dr J. HOUTGAST, would have to be continued and completed. The general method may be summarized as follows: at the precise moment when totality begins, the extremely narrow chromospheric crescent, not yet covered by the moon, is photographed by means of a prismatic camera. A spectrum of bright flash arcs is obtained, of which the intensity is determined by the total radiation of the chromosphere, for so far it is still left free. This is repeated a number of times, with intervals of a couple of seconds, while the moon gradually advances and covers the successive layers. From such exposures, by differentiation, the emission in each individual spectral line may be derived as a function of the height. The data obtained are of fundamental importance for all considerations on the stratification of the chromosphere and for the determination of temperatures and densities. In 1952, only a few exposures could be taken at each contact and special attention was

paid to the numerous metal lines of the lower chromosphere. This time it would be necessary to follow especially the strong lines of hydrogen, helium and calcium and to make exposures in quick succession.

The prismatic camera with a Cooke triplet, belonging to the Commission since 1901, was well suited for this kind of observations; but we intended to use only one prism, in order to obtain a great part of the spectrum at each exposure. The principal data concerning this instrument are:

focal distance 260 cm;
 diameter objective 15 cm;
 size of the prism 15 cm \times 18 cm;
 dispersion H_{α} —K 9,8 cm.

The objective was subjected to a careful revision by Professor VAN HEEL, at the Laboratory for Technical Physics, Delft. The rear end of the instrument was equipped with a camera for aerial survey, procured from the K.L.M. Air Lines; the chief technician of the Utrecht Observatory N. VAN STRATEN and the technician J. VAN DEN BROEK modified this camera in such a way, that the film was moved entirely automatically and that two exposures were made every 3 seconds, with exposures times of 0,1 sec. each. The prismatic camera would be fed by a coelostat of the Commission, constructed already for the 1940 eclipse by the engineering works "Jaffa" at Utrecht and now mounted on a slanting support in view of the relatively high latitude.

2. Secondly it was decided to observe also *the continuous spectrum of the inner corona*, which is due to sunlight, scattered by the free electrons of these intensely hot gases. It is well-known that a spectrum of the inner corona shows no Fraunhofer lines, because of the considerable Doppler shifts, due to the high thermal motion. In 1931 GROTRIAN noticed a broad depression in the spectrum, which he explained as the half obliterated, heavy H and K lines, together with other ultraviolet groups of strong Fraunhofer lines¹⁾. On the other hand neither SHAJN²⁾ nor MENZEL were able to find again this depression. It seemed interesting to obtain a decision, the more so because such an observation could yield valuable data on the coronal temperature.

We intended to record this spectrum with a spectrograph of moderate size but high lightgathering power, which was also constructed already in 1901. However, it was found necessary to change most of the optical parts. The Rutherford prisms absorbed too much of the ultraviolet light; the solar image was too small. In the optical laboratory of Prof. VAN HEEL two new prisms of light flint, a new objective and a new collimating lens were ground. The data for the instrument, thus modified, are as follows:

¹⁾ Zs. Aph. 3, 199 (1931).

²⁾ Izv. Krymsk. Ap. Obs. 1, 102 (1947).

objective diameter 9,2 cm; focal distance 80,2 cm;
 collimator diameter 3,7 cm; focal distance 28,5 cm;
 camera lens diameter 3,6 cm; focal distance 13 cm;
 size of prisms 8,4 cm \times 6 cm;
 dispersion 35 Å/mm near H and K.

In order to record simultaneously the spectrum of different parts of the corona, a threefold slit was constructed (fig. 1); the two outer slits would be placed radially and would yield the spectrum near the poles;

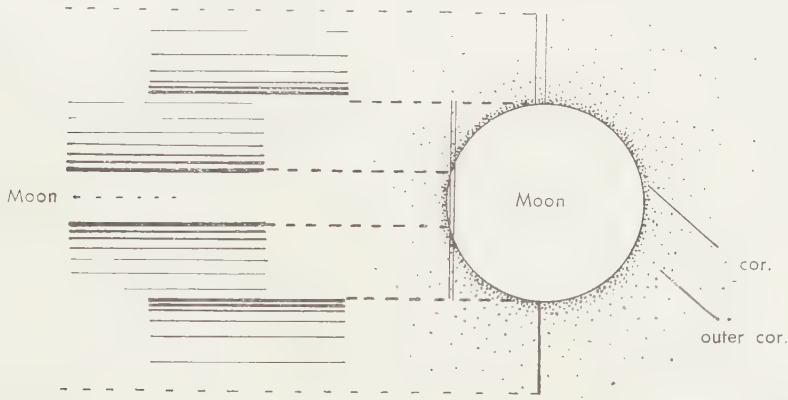


Fig. 1. Slit system for the corona spectrograph.

the central slit would be placed tangentially, or rather slightly inside the sun's limb, and would yield the spectrum of the equatorial parts of the inner corona on a less compressed scale. By regulating the width of each separate slit in the proper way, three spectra of different density would be obtained; so that each part of the coronal spectrum would be into the well measurable range. The spectrograph was fed by a small coelostat, equipped with a 20 cm mirror; this very practical instrument, divided by N. VAN STRATEN, was constructed in the workshop of the observatory.

3. As a third point on the program, Prof. VAN HEEL proposed to study the *shadow bands*, which appear just before and just after totality and which are due to temperature inhomogeneities in the atmosphere of the earth, carried along by the wind. A cinematographic record of this phenomenon would furnish valuable information on the atmospheric turbulence. From the rather superficial and partly contradictory descriptions of this phenomenon it seemed probable that the shadowbands have a considerable speed and that the exposure times ought to be less than 1/100 sec. It was estimated that the illumination would be so low, that photographs of a white screen could not be successful. For these reasons the following set-up was devised and constructed at the Laboratory for Technical Physics, Delft (fig. 2).

Sunlight falls on an off-axis parabolic mirror S , of which the axis AB intersects the objective O of the camera. The composite mirror of $80\text{ cm} \times 100\text{ cm}$ is formed by 40 assembled facets, each of these being a concave

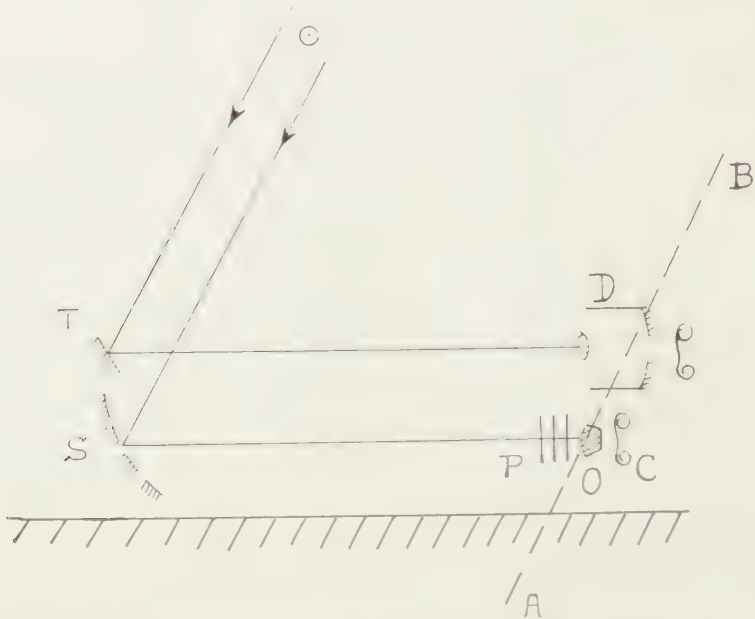


Fig. 2. Apparatus for the cinematography of the shadow bands.

spherical mirror of $10\text{ cm} \times 20\text{ cm}$, aluminized at the frontside and so adjusted that it osculates the paraboloid. The unsharp solar image in O has considerable aberrations, but is entirely included within the objective of the film camera if this has a wide aperture. The focal distance of the paraboloid is 4.2 m ; the solar image would have a diameter of 4 cm if there were no aberrations, actually an 8 cm objective is necessary. The great advantage is thus obtained, that almost the whole of the light which reaches the mirror S takes part in the image formation.

The film camera OC is focussed on the surface of the parabolic mirror S and records any uneven distribution of light in this plane. A 16 mm film camera had to be used, because such an instrument reaches almost immediately its normal speed, so that the exposure can be easily interrupted and started again. This, however, obliged to reduce the size of the image. A photographic objective with an aperture of 80 mm and a focal distance of 150 mm was equipped with several auxiliary lenses, by which the focal distance was reduced to 70 mm , the image remaining sufficiently sharp over the whole field. The relative aperture thus became $1/0.86$. This camera was handdriven with a speed of 60 images per second. By a wedge in front of the film a brightness gradient was produced, the intensity at one side of the image being reduced by a factor 10 with respect to that at the other side. This would allow to make an estimate of the

contrast in the shadow bands. During the exposures, in order to compensate for the considerable variations in the illumination, several half-aluminized plates P in front of the objective could be inserted or removed, so that there would be some parts of the film overexposed, other parts underexposed, and in between some sections with the right exposure times.

The Gevaert factories most kindly presented 300 meter of Gevapan film for these purposes. We are most grateful to Mr PLASMEYER, representative of this firm at The Hague, for this important gift.

In top of the mirror S, a plane mirror T reflected the sunlight into a second film camera, synchronous with the first one, equipped with a mirror objective "Fototel" of "de Oude Delft" (diameter 8 cm, focal distance 50 cm). This camera recorded the solar creseent itself on a positive film, also presented by the Gevaert factories. The light was reduced by a partly aluminized plate of yellow glass and a ring diaphragm.

The mirrors were mounted on a frame which was rotated by hand around the polar axis, in order to keep the reflected beam in a fixed direction.

The preparations

The members of the expedition were selected among the astrophysicists available in view of the requirements of the program. They were:

Prof. M. G. J. MINNAERT	spectrum of the corona.
Dr J. HOUTGAST }	spectrum of the chromosphere.
H. HEINTZE }	
Prof. A. C. S. VAN HEEL }	shadow bands.
Ir G. J. BEERNINK }	
W. G. EINTHOVEN }	

Mr N. VAN STRATEN, technician, was added to the expedition in general but would assist more particularly for the corona exposures. Mrs T. J. HOUTGAST-HOINKES and Mr C. VAN DER VALK also joined the group; they both did very useful work by helping with automobile transportation and by co-operating to the eclipse observations.

July 10, 1953, the Eclipse Commission sent a petition to the Organization for Pure Scientific Research, with full particulars concerning the expedition and its purposes, and a request for the necessary money grants. In January 1954 we were informed that this subsidy had been granted. Fortunately, due to the kind help of Mr BANNIER, director of Z.W.O., means had been found already earlier in order to start the preparations. As mentioned before, the instruments for the two first points of the program were constructed or renovated in the workshop of the Utrecht Observatory, while the apparatus for the third point were constructed at Delft. It was also at the Delft Technical University that all mirrors were aluminized.

The organization of the journey was in hands of the Nederlandse Reisvereniging. Through the intermediary of this agency, the "Stockholms

Rederiaktiebolag Svea" shipped our 1400 kg of instruments free of charge to Stockholm. The s.s. company "Gotland" granted an important reduction of the freight costs from Stockholm to Gotland. We also are grateful to the Statens Järnvägar for a reduction of 50 % on the railway fares in Sweden.

The Utrecht members of the expedition reached Stockholm along various routes and met there on May 31; the Delft members were expected to arrive later. Present were also a group of Uppsala astronomers and shortly afterwards a small expedition from the Liège Institute of Astrophysics. The co-operation with these foreign colleagues has been most pleasant and stimulating. Dr Å. WALLENQUIST, with his perfect knowledge of the local circumstances and the scientific requirements, helped in the most kind way for all practical questions.

After arrangements had been made for the accommodation of the expedition members, a site for the observations was selected on the grounds of the pension, at 200 meters from the coast, with a free view over the sea in southern directions. Small groups of fir trees gave a good protection against the rather strong wind. A lighthouse on the small island Heligholmen, at about 1 km from the coast, was used as an azimuth mark.

In the meantime the instruments and other implements had arrived. By the kind help of the Dutch military authorities the expedition was equipped with a big officers tent, size 8 m \times 6 m, which was used as a general store house for the expedition and which also protected the apparatus for the flash spectrum. The installation for the coronal spectrum was set up at some distance outside the tent and protected against rain by tarpaulin. A small darkroom under a tree in direct proximity of the instruments proved very useful. Since Holmhällar is not connected to the main electric current, six batteries of storage cells of 6 V each were hired from a garage at Burgsvik; they could be charged by means of our petrol motor and a dynamo.

On former occasions, the instruments of the Dutch expeditions were ordinarily mounted on concrete pillars. We decided to try another method: wooden poles were driven into the ground to a depth of 50 cm and strongly cross-connected. This solution was not only much cheaper but saved also time, since it was not necessary to wait till the concrete had dried.

The azimuth of our landmark was determined for each separate instrument with a surveyor's transit, lent to the expedition by Prof. A. KRUIDHOF at Wageningen. There was no difficulty with the time, which was checked by the radio signals from Motala and from the B.B.C.; on the eclipse day there were special signals emitted during several hours by the short wave stations, which facilitated considerably the time service. First the coelostats were adjusted by observing in autocollimation with the surveyors transit and checking azimuth and height of the mirror normal. For the corona, the coelostat reflected the beam horizontally into the spectrograph and a second mirror was unnecessary. We also could do with one mirror for the

chromosphere; the reflected beam in this case was directed upwards, under such an inclination that it was refracted by the prism in a horizontal plane or thereabout.

Next several series of exposures were taken for comparison and for calibration, which were of great importance in view of the investigation of the eclipse spectra. In fact, for both parts of the solar program it was necessary to carry out an exact photometric comparison between the eclipse records and these of the normal solar radiation, reduced in brightness by a very great but known factor, without change in its distribution over the wavelengths. The method used (fig. 3) was based on the

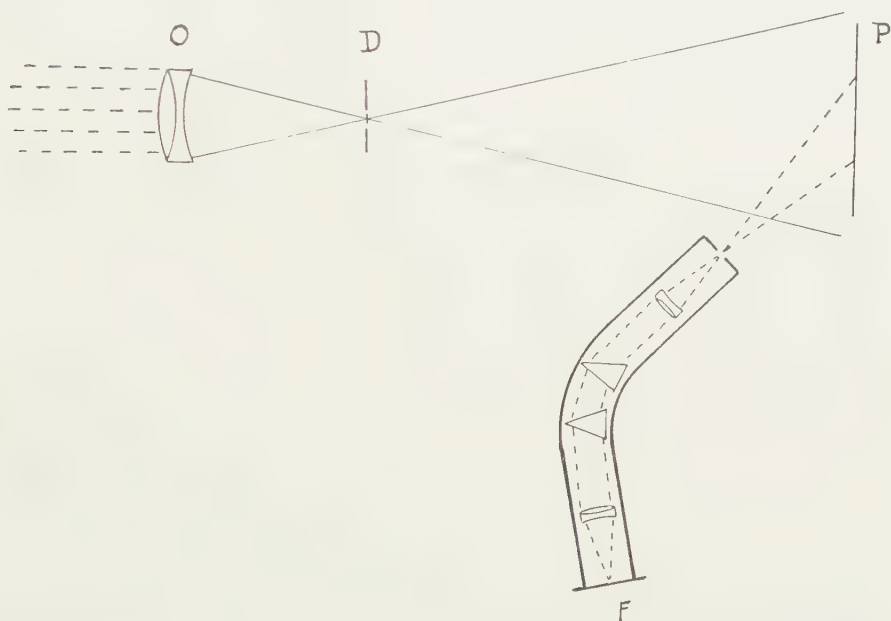


Fig. 3. Principle of the standardization for corona and chromosphere spectra.

properties of an ideal white screen, which diffuses the light uniformly in all directions according to Lambert's law. A polished aluminum plate, covered by the smoke of burning magnesium, is known to have almost exactly these properties. The radiance of such a plate, illuminated by the sun, compares to the mean radiance of the solar disc in the proportion $\pi(1/216)^2 : \pi = 1/46,600$ (one solar radius = $1/216$ radians). However, it is necessary to avoid that the screen should catch radiation from the blue sky around the sun. We therefore with a lens form an image of the sun precisely inside the hole of a diaphragm; behind this diaphragm the rays diverge and finally illuminate the white screen. All parts of the solar disc co-operate equally to the illumination, except at the periphery of the cone of light. By varying the distance DO/DP the illumination of the white screen may be varied within considerable limits, so that the reduction factor may be increased easily to 250,000. If for the calibration the same

lens is used which during the eclipse makes an image of the corona on the slit, we have the advantage that the glass absorption is the same in both cases. A still further reduction of the illumination was finally obtained by inserting a perforated nickel screen. — By this method the calibration of the chromospheric and coronal spectra was easy; moreover the selection of plate, slitwidth, exposure time etc. could be made with perfect safety in view of the eclipse.

Such comparison spectra for the corona were obtained on several clear days before the eclipse, the altitude of the sun being the same; they were taken on plates of the same box and developed later, together with the eclipse plates. A high speed rotating sector before the slit yielded the calibration scale. Similar spectra were also taken on the film which was to be used for the chromosphere; in this case it was of course necessary to dispose a collimator with a slit before the prismatic camera.

On June 21 the Delft physicists arrived in the camp. The steel mountings for their apparatus were brought ready made on a spot near the other Dutch instruments, and were mounted and adjusted in a relatively short time.

During the preparations the weather had been in general excellent; in this whole month there were only two days of rain and one thunderstorm overnight. However, the last week was rather cloudy and the Delft party had only just enough sunshine for the necessary adjustments.

The camp received the visit of the Governor of Gotland and of the Bishop of Visby. On Wednesday 23 a press conference was arranged, followed by a demonstration. On Sunday 27 the instruments were shown to the general public, about 3000 visitors showing their interest in the eclipse preparations. In order to avoid a similar affluence on the eclipse day, the public was directed through the newspapers to another point of observation; moreover, thanks to the kind help of the authorities, an extended area around the camp was surrounded by ropes and guarded by soldiers.

The eclipse day

On the morning of June 30th the sky was entirely overcast. Around 11 o'clock the clouds were breaking and at 12 o'clock the sky was almost entirely blue. Totality was observed at 13h50 MET in a perfectly clear sky, except for a bank of clouds, low in the SW. At 14h15 some light clouds passed already over the sun and at 15h the sky was clouded all over again.

The plate for the coronaspectra was exposed at the calculated times with respect to the theoretical moments of second and third contact. For the chromospheric spectra the exposures were timed after the direct visual observation of the disappearing last crescent. It was rather a surprise that the observed second contact was at least 3 seconds late compared to the data from the almanacs. The same was also noticed by the Uppsala party at Holmhällar. It is not impossible that photospheric

light was still visible through some deep valleys of the moon, while the *mean* lunar limb had already reached the point of contact.

During totality the darkness was not complete, still we were obliged to use flashlights in reading our chronometers. The corona was strikingly regular and symmetric, as it could be expected in this year of exceptionally small solar activity; at each side of the sun the aureole contracted into a long streamer, the two of them being exactly opposite to each other and extending over 5 or 6 solar diameters. It was found that the corona was visible already before the beginning of totality and even 21 seconds after the end of it. In the Delft group, Messrs. VAN HEEL, BEERNINK and VAN DER VALK observed visually the phenomenon of the shadow bands.

Directly after the totality was over, the different observers reported that they had worked almost without any failure, as far as this could be said at that moment. The labour of months was rewarded and there was a deep satisfaction and exuberant happiness. The Swedish and Belgian parties had been equally successful. However, when gloomy messages came from the big Dutch amateur group at Figeholm and from the numerous, perfectly equipped expeditions on Öland; later when we heard of the almost general failure all along the eclipse belt, the feelings became more subdued and we realized how exceptional our good luck had been.

The results

On July 3 the instruments had already been packed and were dispatched to Holland in the same way as they had come to Sweden. They arrived undamaged. The development of the plates and films could not take place on Gotland because of the dust which is blown around by the wind there and because of the lack of technical facilities. It was carried out directly after our return. It is a pleasure to pay our thanks to the section Aero-Carto of the K.L.M., where the chromosphere films were developed; and to the Gevaert Laboratories at Scheveningen, where the positive film and pan-films for the shadow-bands were carefully processed.

The results in general come up to the expectations. Figure 4, (a)(b)(c) is a small selection out of the very rich results concerning the chromosphere. The flash spectrum was filmed from 10^s before till 40^s after second contact, and from 40^s before till 10^s after third contact. Altogether there are about 20 meters of film with 133 spectra. They show in full detail the intensity variation of about 10 strong chromospheric lines during the flash. Suitable diaphragms had been inserted before the prism, so that the lines remain easily measurable everywhere, notwithstanding their strong intensity variation. These films will yield a very valuable complement to the results, obtained in 1952 at Khartoum.

Fig. 4(d) shows some of the photographs of the continuous coronal spectrum. The strips (e) are spectra of the normal sun, of which the Fraunhofer lines can be used as a wavelength scale. The strips (d) are spectra of the inner corona with exposure times of 70^s; the Fraunhofer

lines of the outer corona are apparent. No emission lines of the corona are visible, the excitation of the corona being apparently very low in this minimum period. The plate is very suitable for the measurements. Combined with a number of comparison plates, it will allow an exact photometry of the continuous coronal spectrum.

Figure 4, (f) and (g), shows two images of the film with the shadow bands, which have now been for the first time recorded by cinematography. Due to uncertainty about the illumination, considerable sections of the film are under- or overexposed. A sufficient part, however, is well-suited for measurements. Broad dark and bright bands are clearly seen to move over the fixed mosaic of the rectangular mirrors. A provisional measurement shows that the wavelength is of the order of 10 cm and that the speed is between 1 and 3 m/sec. The contrast is small, the bands are only visible in the range of medium densities. The photographic record corresponds very well with the visual observations made by Mr VAN DER VALK, as to wavelength, speed and direction of drift. They are found to move in the direction of the local wind, which came from WSW, as well near the ground as at the level of the clouds (probably about 1500 m). The images, recorded during totality, do not show the shadow bands (fig. 4g).

The complete photometric investigation of the plates and films will of course take many months; only then will the results properly be reached.

The members of the expedition acknowledge with feelings of deep gratitude their indebtedness towards the Dutch Organisation for Pure Scientific Research, which granted the financial means for the expedition. They also return thanks to all official bodies and to all persons, partly already mentioned in the course of this report, who contributed to the success by their help and interest. They especially remember the help and kindness of the Swedish authorities, the Swedish colleagues and the Swedish people, which made our stay on Gotland a real pleasure.

Fig. 4.

- a. Spectrum of the chromosphere near 2d contact. The streak of continuous spectrum is due to photospheric light, shining through a valley of the moon.
- b, c. Spectra of the chromosphere near 3rd contact, with continuous spectrum of corona, red coronal line, and prominence spectra; the interval between (b) and (c) is about 1 sec.
- d. Continuous spectrum of the corona; the chromospheric lines *H* and *K* in emission; on the first strip they are seen as absorption lines in the outer corona.
- e. Comparison spectrum of the photosphere.
- f. Shadow bands on the mosaic mirror.
- g. The same mirror during totality.

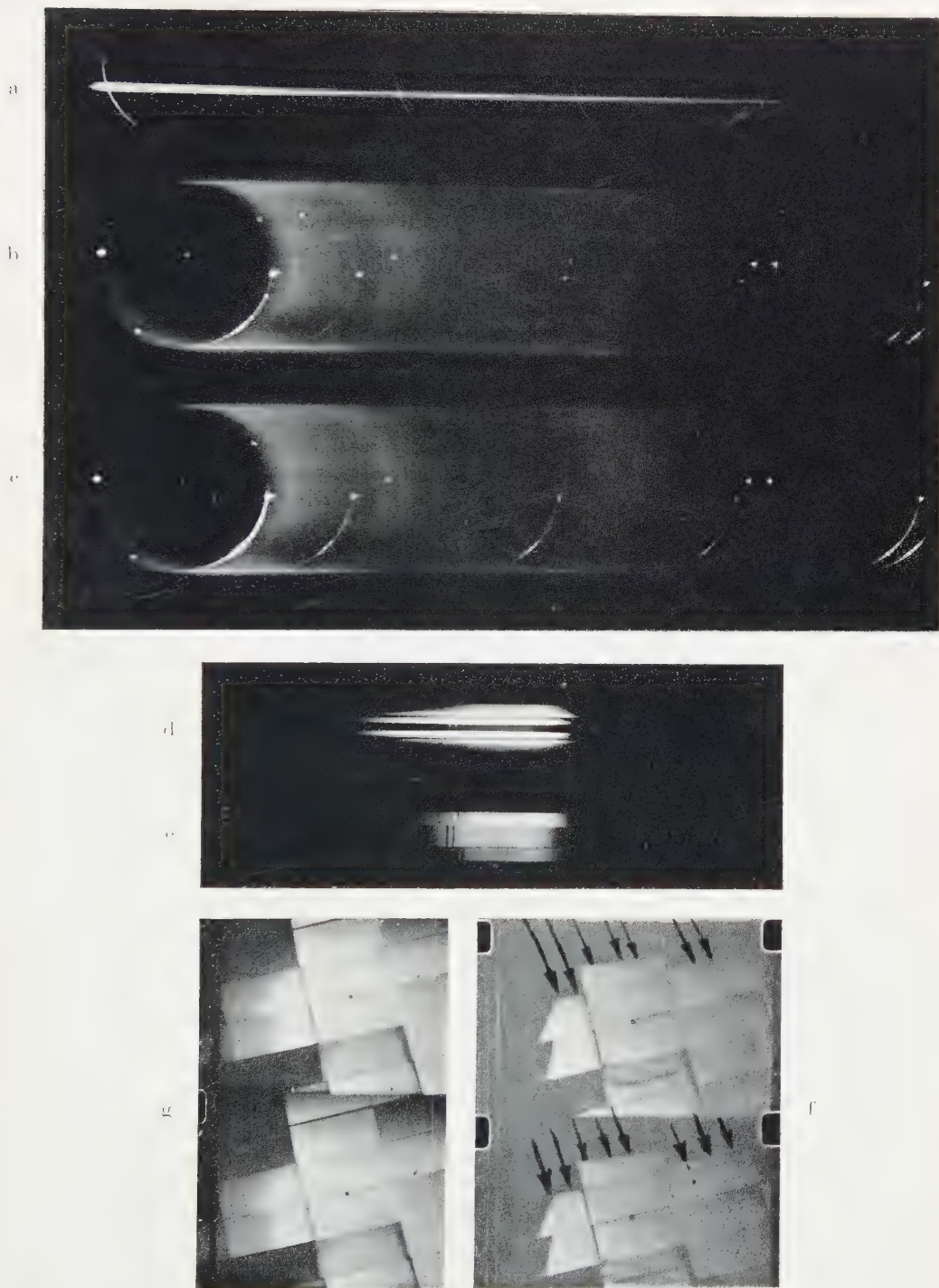


Fig. 4

INDEX

(*Proceedings, Series B, Vol. LVII, 1954*)

Astronomy

- BERLAGE, H. P.: Remarks on the origin of satellites in general and on the metamorphosis of the systems of Neptune and the earth in particular, p. 452.
HEEL, A. C. S. VAN, J. HOUTGAST and M. G. J. MINNAERT: Preliminary report concerning the eclipse of June 30, 1954 and the Dutch expedition to Gotland, p. 596.

Chemistry

- ARENS, J. F. and TH. R. RIX: The chemistry of acetylenic ethers. VI, p. 270.
ARENS, J. F. and TH. R. RIX: The chemistry of acetylenic ethers. VII, p. 275.
ARENS, J. F. and TH. R. RIX: The chemistry of acetylenic ethers. VIII, p. 281.
BOER, J. H. DE, J. M. H. FORTUIN and J. J. STEGGERDA: The dehydration of alumina hydrates. II, p. 434.
BOOIJ, H. L., H. KWESTROO-VAN DEN BOS and J. H. BLEKKINGH: Influence of organic compounds on soap and phosphatide coacervates. XX, p. 215.
BOOIJ, H. L., J. H. BLEKKINGH and H. KWESTROO-VAN DEN BOS: Influence of organic compounds on soap and phosphatide coacervates. XXI, p. 340.
BUNGENBERG DE JONG, H. G., C. R. VAN SOMEREN and F. KLEIN: Contributions to the problem of the association between proteins and lipids. VIA, p. 1.
BUNGENBERG DE JONG, H. G., C. R. VAN SOMEREN and F. KLEIN: Contributions to the problem of the association between proteins and lipids. VIB, p. 13.
BUNGENBERG DE JONG, H. G. and W. W. H. WEIJZEN: Contributions to the problem of the association between proteins and lipids. VII, p. 192.
BUNGENBERG DE JONG, H. G. and A. RECOURT: Contributions to the problem of the association between proteins and lipids. VIII, p. 204.
BUNGENBERG DE JONG, H. G. and W. W. H. WEIJZEN: Contributions to the problem of the association between proteins and lipids. IXA, p. 285.
BUNGENBERG DE JONG, H. G. and W. W. H. WEIJZEN: Contributions to the problem of the association between proteins and lipids. IXB, p. 297.
GUTMANN, FELIX and L. M. SIMMONS: A-C overvoltages, p. 500.
KONINGSBERGER, V. V. and J. TH. G. OVERBEEK: The hydrolysis and aminolysis of ethylthioacetate, p. 81.
MACGILLAVRY, D. and H. J. C. TENDELOO: Electrochemical behaviour of ion-exchanging substances. IX, p. 513.
OVERBEEK, J. TH. G. and V. V. KONINGSBERGER: The hydrolysis and aminolysis of ethyl thioacetate. I, p. 311.
OVERBEEK, J. TH. G. and V. V. KONINGSBERGER: The hydrolysis and aminolysis of ethyl thioacetate. II, p. 464.
PAYENS, TH. A. J.: Influence of salt on the spreading pressure of films of long-chain weak acids, p. 529.
SPRENKELS, A. J. J.: The crystal structure of some tartrates and corresponding racemates, p. 524.
TENDELOO, H. J. C. and D. MACGILLAVRY: Electrochemical behaviour of ion-exchanging substances. VIII, p. 509.
TROMMEL, J.: Crystal structure of d(-)-isoleucine hydrochloride monohydrate. II, p. 364.
VOS, AAFJE and E. H. WIEBENGA: The crystal structures of P_4S_{10} and P_4S_7 , p. 497.

Chemistry, Organic

- BON, W. F.: Ultraviolet spectrophotometric research of the proteins of the eye lens, p. 400.
- VERKADE, P. E. and L. J. STEGERHOEK: Esters and phosphatidic acids derived from batyl alcohol, p. 444.

Chemistry, Physical

- BOER, J. H. DE, J. M. H. FORTUIN and J. J. STEGGERDA: The dehydration of alumina hydrates, p. 170.
- BOER, J. H. DE and A. B. C. VAN DOORN: Graphitic oxide. I, p. 181.
- BRUIN, F.: Theory and application of high resolution interferometers. III, p. 125.
- BURGERS, W. G. and G. W. TICHELAAR: Occurrence of preferred orientations on decomposition of KCl-NaCl mix-crystals, p. 73.
- GROEN, L. J.: On the accelerating influence of tin-ions on the transition of white into gray tin, p. 122.
- GROEN, L. J. and W. G. BURGERS: Formation of compact pieces of gray tin, p. 79.
- HOLTAN JR, HANS: The relation between the temperature coefficient of isothermal cells and the thermopotentials of the corresponding thermocells, p. 138.
- LEEDEN, P. VAN DER: Optical rotation of organic liquids, p. 99.

Geology

- EGELER, C. G.: Predominance of intermediate and more acid rocks among the cretaceous volcanic products in the southern part of the Cordillera Blanca, Peru, p. 329.
- EGELER, C. G. and T. DE BOOY: Cross-cutting character of plutons in the Cordillera Blanca, Peru, p. 490.
- POPOL, SULTAN ACHMAD and S. W. TROMP: The stratigraphy and main structural features of Afghanistan. I, p. 370.
- POPOL, SULTAN ACHMAD and S. W. TROMP: The stratigraphy and main structural features of Afghanistan. II, p. 384.

Geophysics

- HOSPERS, J.: Reversals of the main geomagnetic field. III, p. 112.
- VENING MEINESZ, F. A.: Earth-crust movements in the Netherlands resulting from Fennoscandian postglacial isostatic readjustment and Alpine foreland rising, p. 142.
- VENING MEINESZ, F. A.: Correlation between geomagnetic field and tectonic movements?, p. 395.

Hystory of Science

- CITTERT, P. H. VAN: On the use of glass globules as microscope-lenses, p. 103.

Hydro- and Aerodynamics

- BURGERS, J. M.: On the coalescence of wave like solutions of a simple non-linear partial differential equation. I, p. 45.
- BURGERS, J. M.: On the coalescence of wave like solutions of a simple non-linear partial differential equation. II, p. 57.
- BURGERS, J. M.: On the coalescence of wave like solutions of a simple non-linear partial differential equation. III, p. 67.
- BURGERS, J. M.: Further statistical problems connected with the solution of a simple non-linear partial differential equation, p. 159.
- BURGERS, J. M.: Statistical problems connected with the solution of a simple non-linear partial differential equation. — Continuation. I, p. 403.

BURGERS, J. M.: Statistical problems connected with the solution of a simple non-linear partial differential equation. — Continuation. II, p. 414.

BURGERS, J. M.: Statistical problems connected with the solution of a simple non-linear partial differential equation. — Continuation. III, p. 425.

Mechanics

KOITER, W. T.: Approximate solution of Wiener-Hopf type integral equations with applications. I, p. 558.

KOITER, W. T.: Approximate solution of Wiener-Hopf type integral equations with applications. IIA, p. 565.

KOITER, W. T.: Approximate solution of Wiener-Hopf type integral equations with applications. IIB, p. 575.

KOITER, W. T. and J. B. ALBLAS: On the bending of cantilever, rectangular plates. I, p. 250.

KOITER, W. T. and J. B. ALBLAS: On the bending of cantilever, rectangular plates. II, p. 259.

KOITER, W. T. and J. B. ALBLAS: On the bending of cantilever, rectangular plates. III, p. 549.

ONAT, E. T. and W. PRAGER: Limit analysis of shells of revolution. I, p. 534.

ONAT, E. T. and W. PRAGER: Limit analysis of shells of revolution. II, p. 542.

Necrology

BAAS BECKING, L. G. M.: Henri George Derx †, p. 157.

Paleontology

DROOGER, C. W.: *Miogypsina* in northern Italy. I, p. 227.

DROOGER, C. W.: *Miogypsina* in northern Italy. II, p. 240.

DROOGER, C. W.: *Miogypsina* in northwestern Morocco, p. 580.

HOOLJER, D. A.: Pleistocene Vertebrates from Celebes. IX, p. 475.

HOOLJER, D. A.: Pleistocene Vertebrates from Celebes. X, p. 486.

KEY, A. J.: Some recent Ostracoda of Manila (Philippines), p. 351.

KOENIGSWALD, G. H. R. VON: The Australopithecinae and Pithecanthropus. III, p. 85.

REGTEREN ALTENA, C. O. VAN: The status of *Hasseltides primigenius* Weyenbergh, 1869, p. 336.

Petrology

BODENHAUSEN, J. W. A.: The mineral assemblage of some residual monazite- and xenotime-rich cassiterite deposits of Banka (Indonesia), p. 322.

Philosophy, Natural

CLAY, J.: Intuitive and discursive thought, a comparison, p. 20.

Physics

BOER, J. H. DE and S. KRUYER: Entropy and mobility of adsorbed molecules. V, p. 92.

CLAY, J.: Second and higher maxima in the shower curve of cosmic radiation, p. 29.

CLAY, J. and M. BRUIN: On the neutral horizontal component of cosmic radiation, p. 33.

HOLTAN JR, HANS: Thermoelectric phenomena in galvanic cells, p. 592.

LEEDEN, P. VAN DER: The thermal resistances of cubic metals at intermediate temperatures, p. 317.

AUTHOR-INDEX

A

ALBLAS, J. B., 250, 259, 349.
ARENS, J. F., 270, 275, 281.

B

BAAS BECKING, L. G. M., 157.
BERLAGE, H. P., 452.
BLEKKINGH, J. H., 215, 340.
BODENHAUSEN, J. W. A., 322.
BOER, J. H. DE, 92, 170, 181, 434.
BON, W. F., 400.
BOONJ, H. L., 215, 340.
BOOY, T. DE, 490.
BRUIN, F., 125.
BRUIN, M., 33.
BUNGENBERG DE JONG, H. G., 1, 13,
192, 204, 285, 297.
BURGERS, J. M., 45, 57, 67, 159, 403,
414, 425.
BURGERS, W. G., 73, 79.

C

CITTERT, P. H. VAN, 103.
CLAY, J., 20, 29, 33.

D

DOORN, A. B. C. VAN, 181.
DROOGER, C. W., 227, 240, 580.

E

EGELER, C. G., 329, 490.

F

FORTUIN, J. M. H., 170, 434.

G

GROEN, L. J., 79, 122.
GUTMANN, FELIX, 500.

H

HEEL, A. C. S. VAN, 596.
HOLTAN JR, HANS, 138, 592.
HOOIJER, D. A., 475, 486.
HOSPERS, J., 112.
HOUTGAST, J., 596.

K

KEY, A. J., 351.
KLEIN, F., 1, 13.
KOENIGSWALD, G. H. R. VON, 85.

KOITER, W. T., 250, 259, 349, 558,
565, 575.
KONINGSBERGER, V. V., 81, 311, 464.
KRUYER, S., 92.
KWESTROO-VAN DEN BOS, H., 215, 340.

L

LEEDEN, P. VAN DER, 99, 317.

M

MACGILLAVRY, D., 509, 513.
MINNAERT, M. G. J., 596.

O

ONAT, E. T., 534, 542.
OVERBEEK, J. TH. G., 81, 311, 464.

P

PAYENS, TH. A. J., 529.
POPOL, SULTAN ACHMAD, 370, 384.
PRAGER, W., 534, 542.

R

RECOURT, A., 204.
REGISTEREN ALTENA, C. O. VAN, 336.
RIX, TH. R., 270, 275, 281.

S

SIMMONS, L. M., 500.
SOMEREN, C. R. VAN, 1, 13.
SPRENKELS, A. J. J., 524.
STEGGERHOEK, L. J., 444.
STEGGERDA, J. J., 170, 434.

T

TENDELOO, H. J. C., 509, 513.
TICHELAAR, G. W., 73.
TROMMEL, J., 364.
TROMP, S. W., 370, 384.

V

VENING MEINESZ, F. A., 142, 395.
VERKADE, P. E., 444.
VOS, AAFJE, 497.

W

WIEBENGA, E. H., 497.
WELJZEN, W. W. H., 192, 285, 297.



3 8198 305 321 471

UNIVERSITY OF ILLINOIS AT CHICAGO

